Investigation of Quinazoline Derivatives as Inhibitors of Breast Cancer Resistance Protein (BCRP/ABCG2)

Dissertation

zur

Erlangung des Doktorgrades (Dr. rer. nat.)

der Mathematisch-Naturwissenschaftlichen Fakultät

der

Rheinischen Friedrich-Wilhelms-Universität Bonn

vorgelegt von

Michael Krapf

aus Würzburg / Bayern

Bonn 2017

Angefertigt mit Genehmigung der Mathematisch-Naturwissenschaftlichen Fakultät der
Rheinischen Friedrich-Wilhelms-Universität Bonn

1. Referent: Prof. Dr. Michael Wiese

2. Referent: Prof. Dr. Christa Elisabeth Müller

Tag der Promotion: 19.12.2017

Erscheinungsjahr: 2018

Die vorliegende Arbeit wurde in der Zeit von 2012 bis 2017 am Pharmazeutischen Institut der Rheinischen Friedrich-Wilhelms-Universität unter der Leitung von Herrn Prof. Dr. Michael Wiese durchgeführt.

The most beautiful we can experience is the mysterious.
It is the source of all true art and science.
-Albert Einstein

Dedicated to

Tracy and my parents.

Abstract

The treatment of cancer with chemotherapeutic drugs is strongly limited by intrinsic or aquired resistance of the cancer cells. This is the main reason of a failure of the therapy. The cellular resistance mostly originates from an overexpression of ABC transport proteins that efflux many structurally diverse molecules, including several chemotherapeutic drugs, out of the cells. Due to the reduced concentration of cytostatic drugs in the resistant cancer cells higher doses of the cytostatic agent are required, leading to systemic toxic effects, and may render the therapy ineffective. A possible way to overcome this so-called multidrug resistance (MDR) is to target the efflux transport proteins with suitable inhibitors.

In this study several inhibitors of ABCG2 - one of three major ABC transport proteins that are associated with MDR - were synthesized. To date, only few potent, selective and nontoxic inhibitors have been discovered for ABCG2. For this reason a library of 219 novel compounds based on a quinazoline scaffold or closely related structures was developed and investigated in several functional assays. The investigations comprise the determination of the inhibitory potency and selectivity toward ABCG2 as well as the cytotoxicity of the compounds. Further studies aimed to explore the ability of a compound to reverse the MDR toward common cytostatic drugs such as SN-38 and mitoxantrone (MX). Other studies were used to help shed some light on the function of the protein. Thus, enzyme kinetic investigations of several compounds were carried out in the presence of the substrate Hoechst 33342 to gain insights into the different binding modes of the inhibitors. Complementary to that, a conformation sensitive 5D3 antibody binding assay was conducted to find patterns among the inhibitors to provide a meaningful classification. The investigation of the ATPase activity obtained some information related to the transport activity of the protein in co-administration of inhibitors.

Overall, this work yielded 40 highly potent inhibitors of ABCG2, with IC_{50} values below 100 nM in the Hoechst 33342 acumulation assay. For comparison, Ko143, which is considered as one of the most potent inhibitors of ABCG2 in literature, possessed an IC_{50} value of 227 nM. Important molecular features that are vital for the activity of the corresponding quinazoline derivatives could be deduced *via* a SAR analysis. Moreover, the crucial factors regarding the selectivity of a compound could be determined, which can be beneficial for the specific synthesis of either selective or broadspectrum inhibitors. Also, the cytotoxicity of the quinazoline derivatives could be modulated, either by modification of the scaffold or specific substitution patterns, leading to several nontoxic compounds. The multidrug resistance toward commercial chemotherapeutic drugs was successfully reversed and the potency of the reversal could thereby be determined. Additionally, strong evidence for the existance of several binding sites in ABCG2 and possibly different modes of interaction of the inhibitors with the protein was provided by the different results in the investigation of the interaction type with Hoechst 33342, 5D3 shift, and ATPase assays. The collected data could contribute to the synthesis of further potent inhibitors with the desired characteristics and lead to a better understanding of the function of ABCG2. Owing to the excellent properties of some of the synthesized compounds the transfer of the *in vitro* experiments to *in vivo* studies is a promising prospect for continuative studies.

Contents

1 Introduction

1.1 The occurrence of multidrug resistance (MDR) and chemotherapy

An estimate of roughly 1,700,000 new cases and 600,000 cancer deaths were predicted in the United States for the year 2016.[1] The majority of these deaths are most likely attributed to the resistance of the cancer cells toward the chemotherapeutic treatment.[2]

In many cases this resistance is associated with the expression of ATP binding cassette (ABC) transport proteins, most notably P-glycoprotein (P-gp, ABCB1), the multidrug resistance-associated protein 1 (MRP1, ABCC1) and the breast cancer resistance protein (BCRP, ABCG2).[3] These transport a wide variety of structurally unrelated substrates, including many chemotherapeutic drugs, against a concentration gradient out of the cell, using ATP hydrolysis as a source of energy.[4] In such cases a chemotherapeutic cancer treatment may result in failure, owing to the decreased intracellular drug concentration in resistant cancer cells. [5,6]

The resistance of the cells can either be preexisting (intrinsic) or induced by the drugs (acquired resistance), following a chemotherapeutic treatment or after a change in therapy by a relapse of resistant cells.[7] This phenomenon of cellular resistance against various xenobiotics is termed multidrug resistance (MDR). Although there are also other mechanisms for cancer cells to become resistant to anticancer drugs, such as activation of DNA repair, decreased influx, activation of detoxifying systems, or blocked apoptosis, the increased efflux by transport proteins is by far of greatest importance.[8]

1.2 ATP-binding cassette transport proteins

The ATP-binding cassette transport proteins comprise one of the largest superfamily of proteins in eukaryotic and prokaryotic organisms.[9] These integral membrane proteins transport structurally diverse substrates across the membrane using hydrolysation of ATP to ADP and orthophosphate (P_i) as a source of energy.[10] ABC transporters can be classified as importers or exporters that mediate the cellular uptake of nutrients (e.g. amino acids, sugars, essential metals) or excretion of various molecules (e.g. lipids, toxins, cholesterol, chemotherapeutic drugs).[11] Importers and exporters are both present in prokaryotes, whereas in eukaryotes almost exclusively exporters are found.[12]

By definition, ABC transport proteins contain an ATP binding cassette, referred to as the nucleotide-binding domain (NBD), which contains the highly conserved motifs Walker A and Walker B sequences, the ABC signature motif, the H loop and the Q loop.[13] In its smallest functional form they consist of at least two transmembrane domains (TMDs) and two nucleotide-binding domains (NBDs), of which the NBDs are highly conserved in structure and sequence among all ABC transporters.[14]

For the transport of substrates at least 12 membrane spanning α-helices are required, and a large binding-pocket is suggested to be located at the TMDs.[15] Besides full transporters such as ABCB1 (P-gp) possessing the mentioned core requirements for transport, there also exist half-transporters such as ABCG2 (BCRP). These half transporter must form dimers or oligomers to achieve a fully functioning transport protein and are reviewed in more detail for ABCG2 in chapter 1.2.4.2.

In the human genome 48 ABC genes were identified that could be arranged in the seven subfamilies ABC-A to ABC-G, based on phylogenetic similarity.[6] The subfamily **ABCA** contains 12 genes that are mostly related to lipid trafficking in various organs.[16] Some genes have been associated with several diseases, such as Alzheimer's (mutation in ABCA2), Tangier disease (mutation in ABCA1), familial high-density cholesterol deficiency syndrome (mutation in ABCA1) or harlequin ichthyosis congenital skin disease (mutation in ABCA12).[17,18]

The subfamily **ABCB** contains 11 genes and is the only group containing both full- and half-transport proteins.[19] Here, the most prominent member is ABCB1 which is related to multidrug resistance in cells with an overexpression of this gene. Mutations in the

ABCB family have been implicated for instance in diabetes type 2, coeliac disease or cholestatic liver diseases.[13]

The subfamily **ABCC** contains 13 members of which 9 are associated with MDR. Similar to ABCB and ABCG this subfamily complies a protective function by effluxing toxins and other harmful molecules out of cells. In this regard, ABCC1 is the most notorious member associated with MDR and is able to efflux mostly glutathione and other conjugates of many toxic compounds.[19]

The subfamily **ABCD** contains four genes where the function of ABCD2, ABCD3 and ABCD4 is not yet clear. Mutation in ABCD1 however was associated with the X-linked form of Adrenoleukodystrophy (ALD) resulting in neurodegeneration and adrenal deficiency.[20] Moreover, ALD patients often exhibited an accumulation of fatty acids in cells leading to the assumption that ABCD1 and possibly the other genes of this subfamily play a role in fatty acid metabolism.[19]

The subfamily **ABCE** consist only of the gene ABCE1 which is an organic anion binding protein. It is associated with the inhibition of 2-5A/RNase L system, the assembly of HIV-1 capsids, and eukaryotic translation fields and carcinogenesis. However, the involved processes are not fully elucidated and no diseases have been attributed to ABCE1, yet.[21]

Interestingly, ABCE1 and the **ABCF** members contain ATP-binding domains, but no TMDs, assuming that they are unable to transport substrates. The ABCF subfamily contains three different genes which could play a role in inflammatory processes, but have not been associated with any diseases so far.[13]

The subfamily **ABCG** consists of 5 genes and shows a reversed orientation regarding the sequence of NBD and TMD, where the NBD is at the N-terminus and the TMD at the C-terminus. Being half-transporters, they must at least dimerize to form a functional transporter. Most notably, the gene ABCG2 confers cellular resistance toward many cytostatic drugs and other structurally unrelated molecules that can lead to MDR. ABCG5 and ABCG8 mediate the transport of sterols and can lead to sitosterolaemia in the case of mutation in one of these genes. [13,22] More detailed information regarding ABCG2 is provided in chapter 1.2.4.

1.2.1 Suggested transport mechanisms

Most eukariotic ABC transport proteins are ATP denpendend exporters, that effectuate the active transport of various molecules across membrane lipid bilayers, even against a concentration gradient. Unfortunately, the exact mechanism that is involved in the transport of substrates is not fully understood in the various systems.

Initial evidence regarding the transport mechanism was collected by investigating different crystal structures in importers and exporters.[23] In the year 2002, the first crystal structure of an intact ABC importer was published for the *E. coli* vitamin B_{12} importer BtuCD.[7] Four years later, the first reliable crystal structure of an exporter, namely the multidrug efflux pump Sav1866, was published after purification from *Staphylococcus aureus*.[24] Unfortunately, all crystal structures lacked a high diffraction resolution which could lead to wrong assessments and had to be handled with caution.[11]

The NBDs of ABC transport proteins displayed a high identity in the amino acid sequence and also in some characteristic motifs.[25] It was found, that the NBDs undergo a considerable conformational change due to ATP binding and also after the hydrolysis of ATP.[26] As depicted in Figure 1, each of the two NBDs is coupled with a single TMD *via* flexible coupling helices. In the ATP-unbound form, the TMDs are facing inward, providing binding pockets for substrates. According to the ATP-Switch-Model, binding of substrates to the TMDs induce a conformational change in the initial open dimer form of the disengaged NBDs, by which their binding affinity to ATP increases. Subsequent binding of two ATP molecules induces a putative nucleotide „sandwich dimer“ leading to a closed NBD-ATP complex. During this binding process, the TMDs change from the inward facing to the outward facing arrangement, releasing the substrate in the extracellular space.[27] Sequential hydrolysis of ATP to ADP and P_i resets the tranport protein to the initial state with a inward facing high affinity drug-binding cavity at the TMDs and an open low affinity nucleotid binding site at the NDBs.

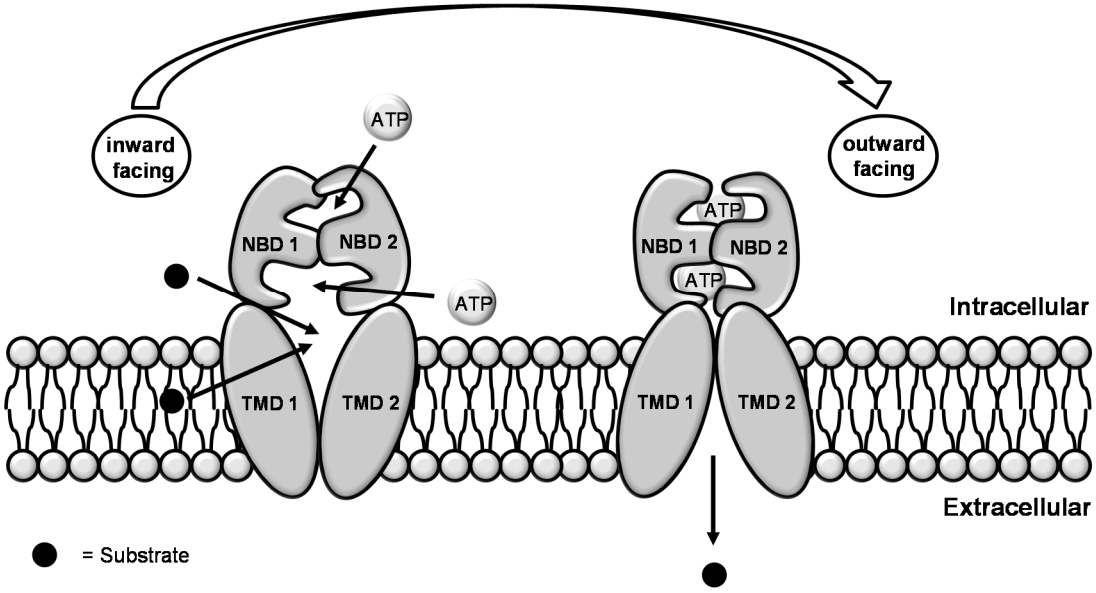

Figure 1: Schematic model of the transport mechanism of substrates by ABC transport protein exporters modified from S. Wilkens.[12] Hydrolysis of the bound ATP in the NBDs on the right hand side resets the transport protein to its initial inward facing state illustrated on the left hand side. In the ATP-Switch-Model the two NBDs are found in a disengaged open form, while they stay engaged in the Constant-Contact-Model.

Based on the work of Senior *et al.* a similar model termed Constant-Contact-Model was proposed.[28] Here, an alternating process of ATP binding and hydrolysis is proposed, where one site opens due to ATP hydrolysis while the corresponding other site remains closed by bound ATP. This induces the formation of the inward facing form (binding of substrates) followed by the outward facing form (release of the substrate), completing the cycle. Although both models can be involved in the transport mechanism, different crystal structures of several exporters provided substantial evidence that is in good accordance with the ATP-Switch-Model.[29]

1.2.2 P-glycoprotein (P-gp) / ABCB1

In the year 1976, Juliano *et al.* published the discovery of a colchicine selected Chinese hamster ovary cell line that displayed resistance toward a wide range of amphiphilic drugs.[30] Owing to the altered drug permeability, they named this cell surface glycoprotein P-glycoprotein. Among the three most important MDR-associated ABC transport proteins (ABCB1, ABCC1 and ABCG2), P-glycoprotein (P-gp/ABCB1/MDR1) was

discovered first and is probably the best studied member. It is widely expressed on the plasma membrane, Golgi membrane, and intracellular canaliculus of normal human tissues, including the liver, kidney, colon, adrenal gland, intestine, placenta, hematopoietic precursor cells and endothelial cells at the blood-brain, blood-testis and blood-placenta barriers.[31] ABCB1 functions as a protective cellular unit by effluxing xenobiotics, including chemotherapeutic drugs. Since the transport protein is often also widely expressed in drug resistant tumors, a chemotherapeutic cancer treatment can result in failure owing to the MDR of the cancer cells toward the chemotherapeutic drugs.

1.2.2.1 Structure and function

ABCB1 is a 170 kDa glycoprotein, encoded by the MDR1 gene, and consists of 1280 amino acids.[32,33] The transport protein contains two symmetrical NBDs and TMDs, where the TMDs consist of six membrane spanning α-helical domains each (see Figure 2).[8] The two homolog halves are joined by a linker region and the N- and C-termini are located in the cytoplasm.[34] Rosenberg *et al.* suggested by cryoelectron microscopy that the two TMDs form a funnel-shaped aqueous "pore" in the membrane that is probably involved in the transport of substrates.[35]

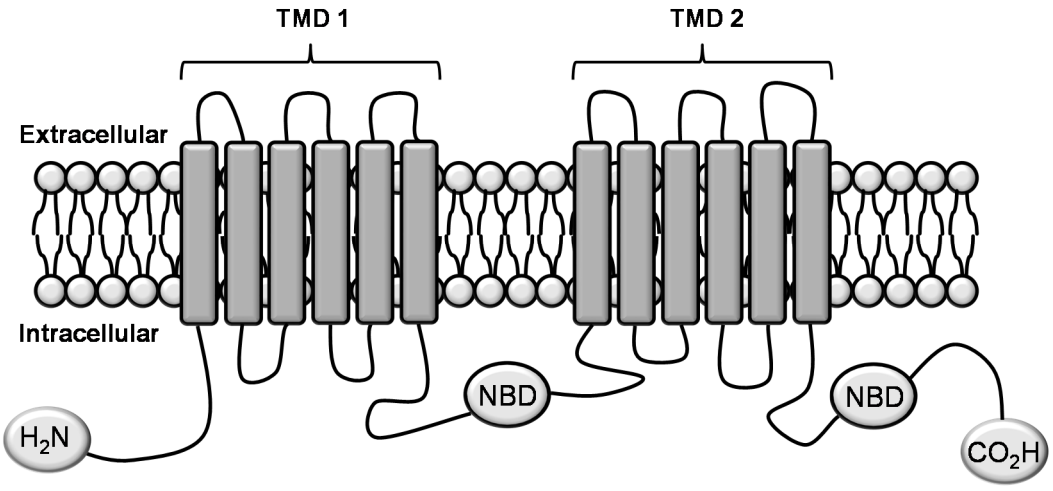

Figure 2: Topology model of ABCB1 (P-gp).

As mentioned before, the transport protein is able to efflux a wide variety of substrates by ATP consumption. In this regard, lipophilic, uncharged or (weakly) basic species are

transported most efficiently and an amphophilic nature was identified as a common feature of many substrates.[36] This finding is in accordance with the proposed transport mechanism for ABCB1: the "vacuum cleaner"- and the "flippase"-models, that are illustrated in Figure 3.

Raviv *et al.* discovered in a fluorescence resonance energy transfer (FRET) study with the lipophilic photolabelled probe iodonaphthalene-1-azide that the substrate doxorubicin was located within the membrane close to ABCB1.[37] Based on this and other studies as well, it was proposed, that ABCB1 interacts with its substrates within the membrane and subsequently effluxes them directly to the extracellular medium.[38] This transport process was termed hydrophobic "vacuum cleaner" and is depicted on the left hand side in Figure 3.

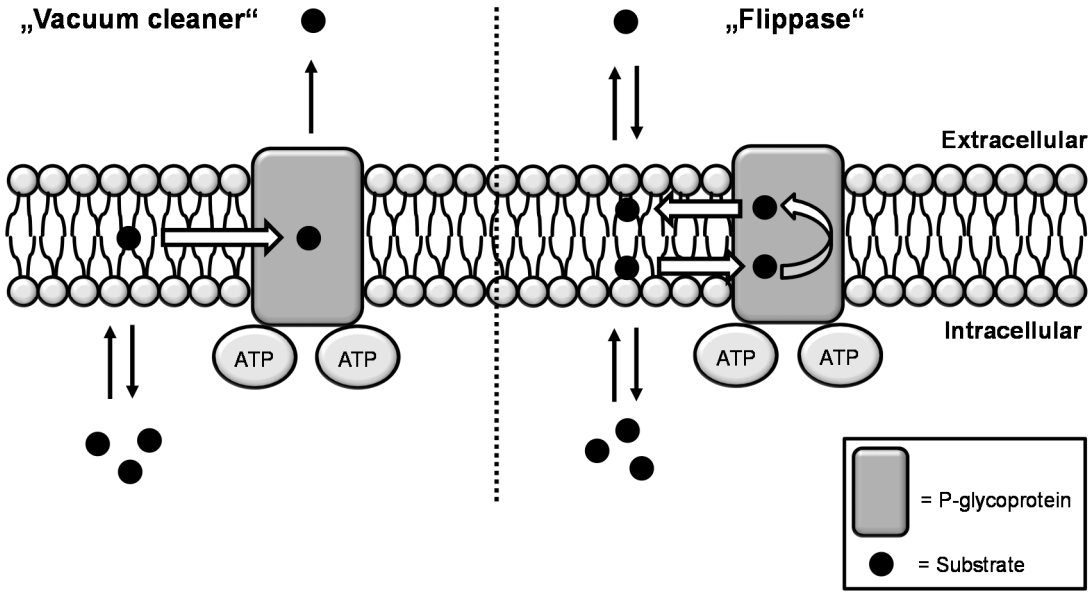

Figure 3: Schematic model of the "Vacuum cleaner" and "Flippase" transport mechanism of substrates by P-glycoprotein (P-gp/ABCB1) modified from Sharom.[39]

Also, NMR studies revealed that (amphiphilic) substrates enter the lipid bilayer of the membrane and frequently accumulate in the inner or outer leaflet near to the headgroup of the lipid chain.[40] The "Flippase" model (right hand side in Figure 3) describes the translocation of a substrate by the transport protein from the inner leaflet of the lipid bilayer to the outer leaflet. From here, the substrate exits the membrane by passive diffusion into the extracellular medium. Indeed, the majority of the scientific evidence

points to the suggestion that the efflux takes place in a flippase-like manner although both models could be involved in the transport process.[38]

1.2.2.2 Substrates and inhibitors of ABCB1

The spectrum of transported substrates of ABCB1 is broad and includes compounds preferably with lipophilic and amphiphilic properties. The molecular weight of transported molecules ranges from less than 200 to almost 1900 Da comprising aromatic groups, but also non-aromatic linear or circular molecules.[36] It effluxes several chemotherapeutic agents, fluorescent dyes, natural products, TKIs, HIV protease inhibitors, steroids and other substances (compare Table 1). Fluorescent dyes like calcein can be co-administered with modulators to monitor the efflux activity of the transport protein which can be correlated to the inhibitory potency of the test compounds. Most notably, ABCB1 was called multidrug resistance protein 1 (MDR1) as its expression is associated with the cellular resistance toward several cytotoxic drugs, which can be a major obstacle in chemotherapy.

In silico analysis revealed, that the number and the strength of the hydrogen bonds formed between a compound and ABCB1 is a crucial determinant for the distinction between substrates and inhibitors: compounds with a pronounced ability to form hydrogen bonds are more likely to be inhibitors than substrates of ABCB1.[41]

Table 1: Selection of Substrates of ABCB1.[36,39]

Compound-class	**Compound**
CHEMOTHERAPEUTIC AGENTS	
Anthracyclines	Daunorubicin
	Doxorubicin
Camptothecins	Topotecan
Taxanes	Doxotacel
	Paclitaxel
Vinca alkaloides	Vinblastine
	Vincristine
FLUORESCENT DYES	
	Calcein AM (calcein acetoxymethylester)
	Hoechst 33342
	Rhodamine 123
NATURAL PRODUCTS	
	Flavonoides
	Curcuminoides
	Colchicine
TYROSINE KINASE INHIBITORS	
	Imatinib
	Gefitinib
STEROIDS	
	Corticosterone
	Aldosterone

Inhibitors of ABCB1 were classified in three generations according to specificity, affinity and toxicity (see Table 2). Many of the first generation inhibitors like the calcium channel blocker verapamil or the immunosuppressive cyclosporine A, were found to be transported substrates themselves and act as competitive inhibitors. Unfortunately, serious toxic effects resulted owing to the high doses that were needed for an effective inhibition of ABCB1.[42] In the first clinical trials using inhibitors of the first and partly of the second generation, mostly poor results were achieved which were due to the mentioned toxic effects, unwanted pharmacokinetic drug interactions and a poor potency and selectivity of the inhibitors toward the transport protein.[43]

Table 2: Selection of Inhibitors of ABCB1.[44,45]

Inhibitors	**Compound**
FIRST GENERATION	
	Verapamil
	Cyclosporine A
	Reserpine
	Quinidine
	Tamoxifen
SECOND GENERATION	
	Dexverapamil
	Valspodar (PSC833)
	Dofequidar fumarate (MS-209)
	Biricodar (VX-710)
THIRD GENERATION	
	Elacridar (GF120918)
	Tariquidar (XR9576)
	Zosuquidar (LY336979)
	Mitotane (NSC-38721)

The second generation inhibitors were often deduced from the structures of the first generation inhibitors. These derivatives frequently displayed a higher specificity and a reduced toxicity. However, several compounds were found to be substrates of cytochrome P450 3A4 (CYP450 3A4) and influenced the metabolism of co-administered anticancer drugs which led to unpredictable pharmacokinetics.[46]

Third generation inhibitors did not exhibit the described downsides of the first two generations. For instance, Tariquidar or Zusoquidar were found to be potent and specific inhibitors of ABCB1 with a low cytotoxicity. Some of them even achieved promising results in clinical trials.[47,48,49] Nevertheless, the transfer from successful *in vitro* experiments to *in vivo* led to the rise of unexpected difficulties that must to be addressed in future studies.[43]

1.2.3 Multidrug Resistance associated Protein 1 (MRP1) / ABCC1

ABCC1 was first discovered in 1992 by Cole *et al.* and cloned from the multidrug-resistant small cell lung cancer cell line H69AR.[50] This cell line exhibited resistance toward the cytostatic drug doxorubicin which could be attributed to the expression of the multidrug resistance associated protein 1 (MRP1) later termed ABCC1. Similar to ABCB1 and ABCG2, ABCC1 is able to efflux a wide spectrum of molecules, including several anticancer drugs, highlighting ABCC1 as an important target in terms of MDR. Subsequent work showed, that ABCC1 performs important pharmacological and toxicological functions:[36] a study conducted by Wijnholds *et al.* concluded that the sensitivity of mice towards treatment with the cytostatic drug Etoposide was highly increased in Abcc1 knockout mice.[51] Other studies with Abcc1 knockout mice resulted in the same conclusion, correlating the expression of the transport protein to an increased cellular resistance toward some toxic compounds.[52] ABCC1 is expressed in almost all human tissues, most notably in lung, spleen, testis, kidney, placenta, thyroid, bladder and adrenal gland.[53] In contrast to the apical membrane location of other ABC transporters, ABCC1 is predominantly located in the basolateral membrane of polarized cells where it most likely effluxes its substrates into the interstitial space, rather than excreting them into bile, urine or gut.[54]

1.2.3.1 Structure and function

ABCC1 consists of 1531 amino acid residues and adds up to a molecular weight of 190 kDa.[55] Within the ABCC subfamily, ABCC1 exists in a „long“ form, meaning that it contains two TMDs with 6 membrane spanning α-helices each, two NBDs and an additional TMD 0 with 5 membrane spanning α-helices (see Figure 4).[56] The function of this additional TMD 0 is not yet clear. Mutational studies in this region have shown that it could influence the folding of the protein.[57] Other studies suggest that it can contribute to the ABCC1 homo-dimerization.[58] However, complete removal of TMD 0 did not affect the transport function or its proper routing to the plasma membrane.[59]

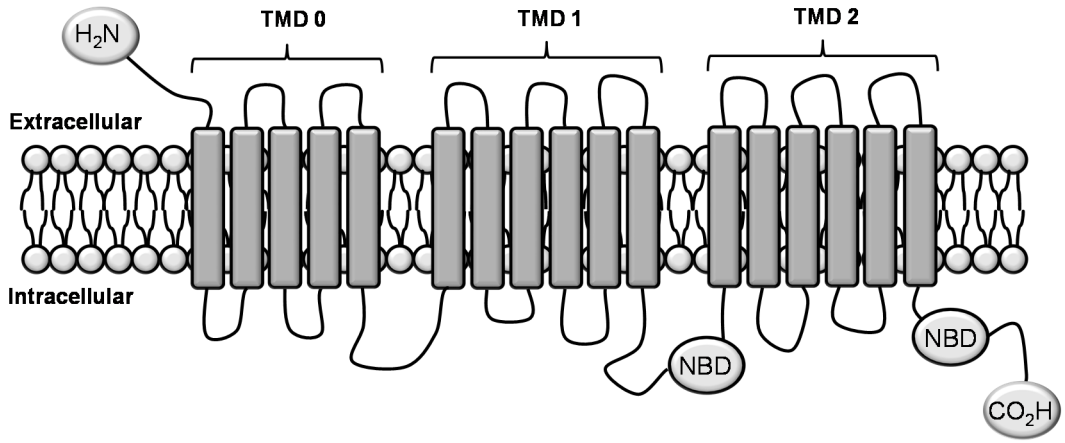

Figure 4: Topology model of ABCC1 (MRP1).

The transport is accomplished by TMD 1 and 2 forming a „pore“ through which the substrates are effluxed.[55] A similar phenomenom was described in chapter 1.2.2.1 for ABCB1, that shares the same functional core (two TMDs and two NBDs) and also forms a „pore“ which is involved in the transport of substrates.

1.2.3.2 Substrates and inhibitors of ABCC1

The substrate spectrum of ABCC1 comprises several anticancer drugs such as anthracyclines, mitoxantrone, methotrexate or camptothecines and also *Vinca* alkaloids. This can affect the response of cancer patients toward chemotherapeutic treatment and may lead to failure of the therapy. Interestingly, it was found that for some substrates, which do not form GSS-conjugates, GSH is required for the transport. Substrates depending on the co-transport with GSH are for instance the *Vinca* alkaloid Vincristine or the anthracyclines Daunorubicin and Doxorubicin.[60] In this regard, ABCC1 mostly (co-)transports amphipathic organic anions including hydrophobic drugs or other compounds that are conjugated or complexed to either the anionic tripeptide glutathione (GHS), glucuronic acid, or to sulfate.[36,61] Also heavy metal ions, such as arsenite or antimony are subject to transport by ABCC1, most likely as a complex with GSH.[62,63] A selection of ABCC1 substrates is illustrated in Table 3.

Table 3: Selection of Substrates of ABCC1.[36,54]

Compound class	**Compound**
CHEMOTHERAPEUTIC AGENTS	
Vinca alkaloids	Vinblastine Vincristine
Camptothecins	Topotecan Irinotecan SN-38
Anthracyclines	Doxorubicin Daunorubicin Epirubicin
Others	Methotrexate Mitoxantrone
GLUTATHIONE CONJUGATES (-GS)	Dinitrophenyl-GS, Doxorubicin-GS, Cyclophosphamide-GS, Hydroxynonenal-GS, Glutathione (GSH, GSSG)
GLUCURONIDE CONJUGATES (-G)	Bilirubin-G, Estradiol 17βD-G, Etoposide-G, NS-38-G
SULFATE CONJUGATES (-S)	Estrone-3-S, Taurocholate-3-S, Sulfatolithocholyl taurine
OTHERS	Curcuminoides Calcein

Owing to the affinity of the transporter toward anionic molecules, there have been difficulties in finding effective inhibitors that are able to permeate the lipophilic cell membrane and so far only few inhibitors of ABCC1 as compared to ABCB1 have been identified.[64] The first compounds included general organic anion transport inhibitors, such as probenecid, sulfinpyrazole, benzbromarone or indomethacin. Unfortunately, these compounds modulated the activity of most of the ABC-related organic anion efflux transporters and also the activity of some of the pharmacological relevant solute carrier

family organic anion importers.[55] Another problem was the low affinity and poor specificity of some inhibitors like cyclosporine A or PSC833.[65]

Later, more specific inhibitors of ABCC1 were developed. Most notably, the quinoline derivative MK-571 (a LTC_4 analog), which is used as a specific standard inhibitor and possesses a carboxyl function which is deprotonated in physiological conditions. The compound was originally developed as a cysteinyl leukotriene receptor 1 (CysLTR1) antagonist for the purpose of treating asthma.[55] In the class of LTC4 derivatives the compound ONO-1078 was found to be potent and specific toward ABCC1. Moreover, the tricyclic isoxazoles LY465803 and LY475776 exhibited a considerable potency and selectivity toward the transport protein. Nevertheless, there is a persistent need for more potent and specific inhibitors displaying a low cytotoxicity.

1.2.4 Breast Cancer Resistance Protein (BCRP) / ABCG2

The human breast cancer resistance protein is the second member of the G subfamily of the ATP-binding cassette (ABC) efflux transporter superfamily, and hence also designated as ABCG2.[66] It was first discovered in 1998 by the research group of Doyle *et al.* in MCF-7/AdrVp human breast cell carcinoma cells that displayed a resistance toward anticancer drugs even in the absence of known multidrug resistance transporters such as P-gp and MRP.[67] The newly discovered transport protein was then termed breast cancer resistance protein (BCRP). Shortly after, Allikmets *et al.* reported the cloning of a nearly identical transporter that was widely expressed in the placenta and thus named it ABCP.[68] Later, Miyake *et al.* reported multiple distinct mitoxantrone-resistant sublines, pointing to the existence of another major transport protein conferring drug resistance.[69] Here, the transport protein was named MXR or mitoxantrone resistance protein, due to its discovery in co-administration of mitoxantrone in the colon carcinoma cell line S1-M1-80. Owing to the different terms for the newly discovered gene (BCRP, ABCP and MXR), the Gene Nomenclature Committee officially named it ABCG2, reflecting that it is the second member of the human ABCG subfamily. [2, 70]

To date, the subfamily G comprises the six members ABCG1, ABCG2, ABCG3, ABCG4, ABCG5 and ABCG8 which are extensively reviewed in the work of Moitra *et*

al. and Kusuhara and Sugiyama.[71,72] Among those, ABCG3 has not been detected in humans so far.

1.2.4.1 Distribution and physiological role of ABCG2 in human tissues

Increased expression of ABCG2 is often found in human tissues comprising important physiological functions such as the protection of the organism against harmful xenobiotics. The research group of Doyle *et al.* reported high levels of ABCG2 in the placenta, brain, prostate, small intestine, testis, ovary, liver, adrenal gland, uterus, and central nervous system, using the northern blot analysis.[73] ABCG2 was also found to be widely expressed in stem cells and is recognized as a marker in cancer stem cells.[74] Some of these functional tissues are discussed in more detail in the following paragraph.

Significant expression levels of ABCG2 were found in the syncitiotrophoblasts of the **placenta**, giving rise to the assumption that the transport protein is vital for the protection of the fetus from toxins.[75] Experiments carried out by Jonker *et al.* substantiated this hypothesis as they administered the cytostatic drug topotecan, which is a substrate of ABCG2, together with the ABCG2-inhibitor elacridar to pregnant P-gp deficient mice. As a result, the relative fetal penetration of topotecan was two-fold higher than in the vehicle-treated control group.[76] Similar results were found in a study conducted by Zhang *et al.* where the administration of the antibiotic nitrofurantoin to ABCG2 knockout mice and wild-type mice showed that the knockout mice lacked the protective function of the placenta toward the drug.[77] In this regard it is not surprising that ABCG2 has been reported to transport substrates from the fetal to the maternal space, even against a concentration gradient.[78,79]

A considerable induction of ABCG2 expression has also been found in the **mammary gland** in the breast of lactating mice, cows and humans. The physiological role of ABCG2 in the lactating breast was investigated by van Hervaarden *et al.* in a study on ABCG2-deficient and wild type mice. A 60-fold higher concentration of riboflavin (vitamin B_2) was found in the milk of wild-type mice leading to the conclusion that ABCG2 can accumulate important nutrients into milk.[80] However, the active secretion of clinically and toxicologically important substrates, such as PhIP (2-Amino-1-methyl-6-phenylimidazo[4,5-b]pyridine), the cytostatic drug topotecan or the anti-ulcerative

cimetidine, also led to an accumulation of the harmful substances in mouse milk.[81] A similar outcome resulted for other dietary carcinogens and antibiotics which accumulated in the milk of animals with an expression of ABCG2 in the mammarial gland.[82,83,84] Hence, the diet of a breastfeeding mother plays an important role in reducing the excretion of harmful doses of toxins into the milk.

The **blood brain barrier** (BBB) exhibits high levels of ABCG2 that are mainly located at the luminal cell surface of the microvessel endothelium.[85,86,87] It was found that ABCG2 works together with ABCB1 in the BBB and is responsible for restricting the entry of numerous xenobiotics into the brain.[6] However, many therapeutic agents are thereby restrained from reaching their intracerebral targets which leads to the requirement of higher drug doses and therefore can often result in a systemic toxicity.[88] An increased brain uptake of chemotherapeutic drugs was achieved by inhibition of both, ABCB1 and ABCG2, by dual-inhibitors like Elacridar. Several results comprising different studies were summarized by Agarwal *et al.* and demonstrated, that MDR caused by ABC transport proteins can be overcome by direct inhibition.[89]

More details regarding the expression of ABCG2 in different tissues are provided in the reviews of Robey *et al*. (2009) and Stacy *et al*. (2013). [4,90]

1.2.4.2 Structure and function of ABCG2

ABCG2 is a 72 kDa integral membrane protein consisting of 655 amino acids.[91] It comprises only one cytosolic N-terminal nucleotide-binding domain (NBD) and one C-terminal transmembrane domain (TMD) with six transmembrane helices, as depicted in Figure 5.[92] Unlike ABCB1 and ABCC1, ABCG2 is a half-transporter that exhibits a reversed TMD-NBD arrangement of which the relevance is still unknown.[93] Among ABC transport proteins, the formation of composite ATP binding sites, based on the interaction of two NBDs, is postulated as the fundamental functional unit.[94,95] With regard to ABCG2, the full function can be achieved by dimerization or the formation of higher oligomers.

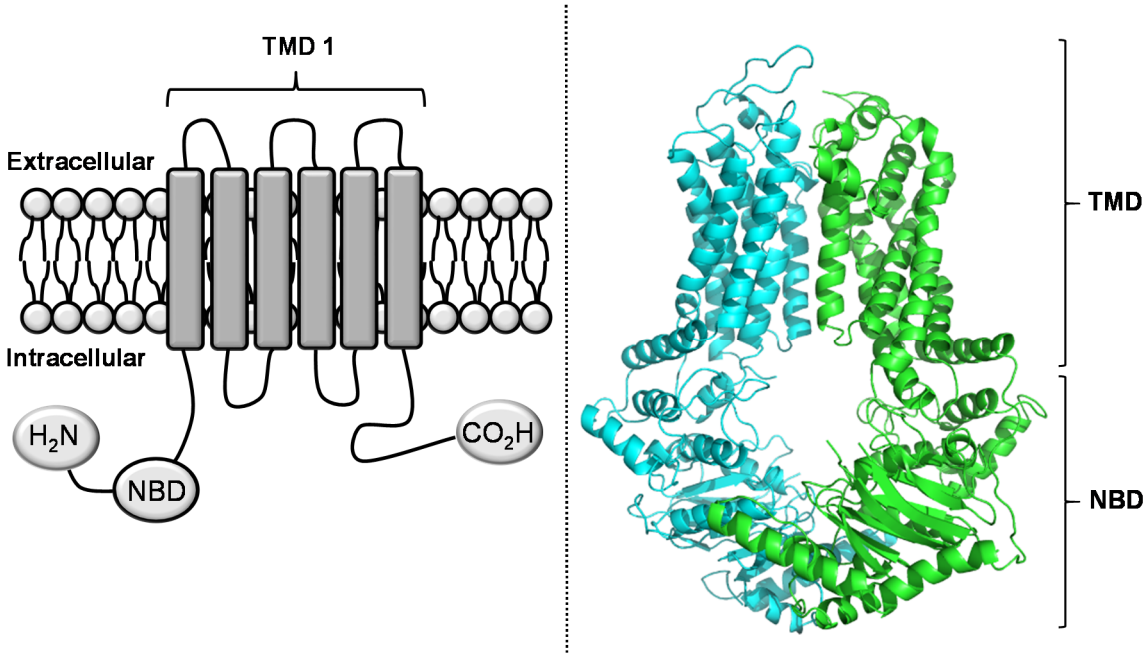

Figure 5: Topology model of ABCG2 (BCRP), a). Protein 3D structure of the ABCG5/ABCG8 heterodimer, b).

Current studies revealed, that the formation of tetramers is preferred in the presence or absence of transported substrates. This has been demonstrated by a combination of fluorescence correlation spectroscopy, photon counting histogram analysis, and stepwise photobleaching.[96,97] Moreover, it is suggested that one functional tetrameric complex is composed of four BCRP homodimers which could form *via* linkages by intermolecular disulfide bridges at cysteine 603.[98,99,100,101] However, there is also contradicting evidence to this hypothesis described by some mutation studies in C603.[99,102]

For a better clarity, a schematic topology of the membrane is illustrated in Figure 6, highlighting the residues or mutations that affect the functioning of the transport protein. Here, C603 is highly conserved at the extracellular loop between TMD 5 and 6 in proximity to C592 and C608. According to mutagenesis data, all mentioned cysteine residues probably provide stability to the protein by formation of intramolecular disulfide bonds.[100] In this regard, the mutation of C592 or C608 in ABCG2 expressing Flp-In-293 cells resulted in a significant decrease in protein levels of the transporter.

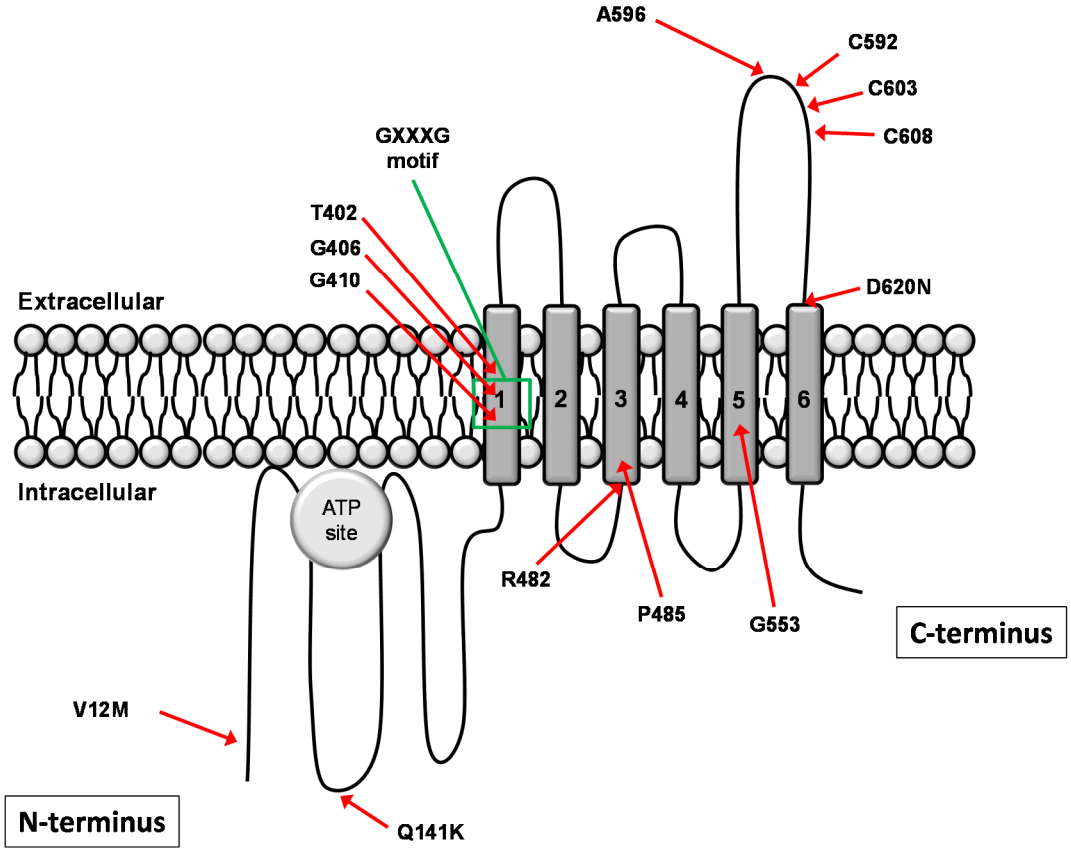

Figure 6: Schematic illustration of the membrane topology of ABCG2 and highlights of residues or mutations that affect the functioning of the transporter. The graphic was modified from Stacy et al. (2013).[90]

Further mutational studies of Wakabayashi *et al.* and Polgar *et al.* identified two more regions that could be involved in the formation of dimers:[103,104] this regards the amino acids T402, G406, G410, G553 and the GXXXG motif in general, comprising the amino acid chain G406-G410. One or several mutations at the mentioned regions could result in a reduced protein expression, decreased drug efflux, alterations in glycosylations and retention of ABCG2 in the endoplasmatic reticulum (ER).

The glycosylation of ABCG2 was found to play a vital role in the function of ABCG2 as it confers stability to the protein structure. Altered glycosylation could lead to an increased degradation of the protein and thereby regulates the expression of the transport protein.[105]

In this regard, the N-linked glycosylation site at amino acid 596 was found to play a crucial role as demonstrated by mutagenesis studies.[106]

Moreover, a so-called "gain of function" was observed in a single nucleotide polymorphism (SNP) at amino acid 482 where substitution of arginine by threonine or glycine led to a broadened substrate spectrum of ABCG2.[107,108] The dye rhodamine 123, for instance, is transported by the R482T and R482G mutants, but not by wild-type cells. Also, these mutants exhibited a higher affinity to several anthracyclines such as doxorubicin, daunorubicin, epirubicin and also bisanthrene, fluorescene and lysotracker green. Some substrates of the ABCG2 wild-type and the R482G variant are depicted in Figure 7. Photoaffinity labelling studies with the substrate-analog [I^{125}]iodoarylazidoprazosine (IAAP) and the investigation of the ATPase activity revealed in several of the R482 mutants that most of the variants have a high impact on the substrate transport and ATP turnover, but might not be necessary for substrate recognition and binding.[109, 110]

In proximity to amino acid 482 in TM3 a P485A variant exhibited a considerable reduction (70%) of the efflux of BODIPY-prazosin, but had no effect on the transport of MX and Hoechst 33342.[111] It is known that Pro residues are able to form flexible hinges in TM α-helices that can be accountable for dynamic conformational changes in the protein which can affect the binding of drugs and the transport activity of the protein.[112]

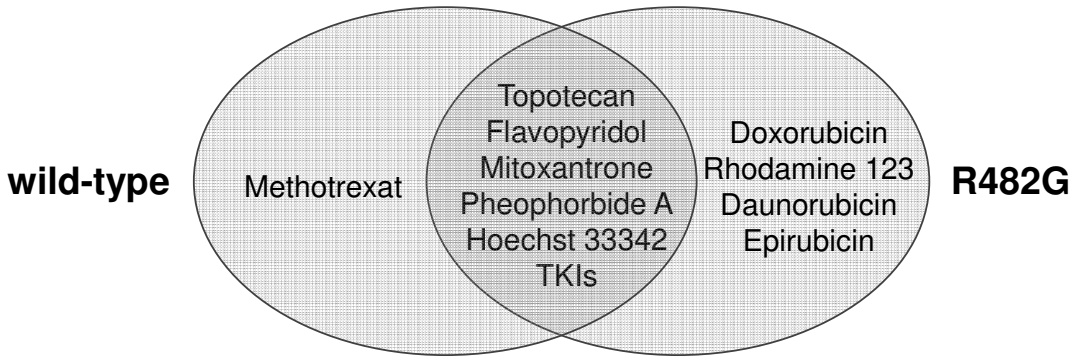

Figure 7: Substrate specificity of the ABCG2 wild-type form and the mutant R482G isoform.[113]

Other SNPs studies of the ABCG2 gene targeted the amino acid changes at V12M, Q141K and D620N.[114] Regarding the Q141K ABCG2 variant, cytotoxicity assays revealed a considerable effect on the transport activity of substrates like MX, topotecan, SN-38 and diflomotecan: HEK-293 cells exhibited a significant lower transport activity in the Q141 variant than in wild-type cells. On the contrary, the V12M and D620N

variants displayed no significant impact on the transport activity compared to ABCG2 wild-type cells. The altered transport function in the Q141K variant needs to be considered in chemotherapeutic treatment, since it has important implications for the pharmacokinetics and drug-resistance profiles of chemotherapeutics and is one of the most frequently observed SNP variants of ABCG2 in the human population.[90]

1.2.4.3 Substrates and inhibitors of ABCG2

The first **substrates** were discovered as ABCG2 overexpressing cells exhibited resistance toward several chemotherapeutics, such as methotrexate, mitoxantrone, anthracyclines and camptothecin derivates (see Table 4). Fluorescent dyes like Hoechst 33342 were found to be useful tools to investigate the transport activity of the protein in functional assays.[115] This includes the porphyrine derivative pheophorbide A that can also be used as a photosensitizer in photodynamic therapy.[116] The flavonoid derivative quercetin for instance is often used as standard activator in studies of the ATPase activity of ABCG2. Interestingly, TKIs like gefitinib or imatinib exhibit concentration dependent properties, as they act as substrates at low concentrations and as inhibitors at higher concentrations. But also other drugs like sulfasalazine or omeprazole are transported by ABCG2 which should be considered to avoid possible unwanted side-effects in medicated patients since they are frequently prescribed.

The selection of substrates in Table 4 illustrates that ABCG2 is able to transport a broad diversity of structurally unrelated compounds. Notably, single nucleotide polymorphisms can alter the substrate spectrum considerably. In particular mutations at amino acid 482 were found to broaden the spectrum (gain-of-function mutation) of ABCG2.

Table 4: Selection of Substrates of ABCG2.

Compound-class	Compound	Reference
CHEMOTHERAPY AGENTS		
Antifolates	Methotrexate**	117, 118
	Tomudex	119
Anthracenes	Mitoxantrone	120, 121
	Bisantrene	121
	Aza-anthrapyrazole	122, 123
Anthracyclines	Daunorubicin*	120
	Doxorubicin*	120
	Epirubicin*	120
	Flavopiridol	124
Camptothecin derivatives	Topotecan	121
	SN-38	125
	Irinotecan	126, 127
FLUORESCENT DYES		
	Rhodamine 123*	121
	Lysotracker green*	121
	BODIPY-prazosin	121
	Hoechst 33342	115
	6-carboxy-2´,7´-dichlorofluoresceine	128
PORPHYRINES		
	Pheophorbide A	129
	Protoporphyrine IX	129
	Phytoporphyrine	130
FLAVONOIDES		
	Genistein	131
	Quercetin	132
TYROSINE KINASE INHIBITORS		
	Imatinib	90, 133
	Gefitinib	90, 133
	Nilotinib	90, 133
OTHER DRUGS		
	Omeprazole	134
	Pantoprazole	134
	Prazosin	121
	Indolocarbazole	135
	Sulfasalazine	136
	Abacavir	137

**: Subject to transport by the ABCG2 SNP482 mutants only*

***: Subject to transport by the ABCG2 wild-type only*

But there is also a significant overlap of substrates between ABCG2, ABCB1 and ABCC1, as depicted in Figure 8. Mitoxantrone for instance is tranported by all three transport proteins. Topotecan, Rifamipicine and Hoechst 33342 are subject to transport by ABCG2 and ABCB1.

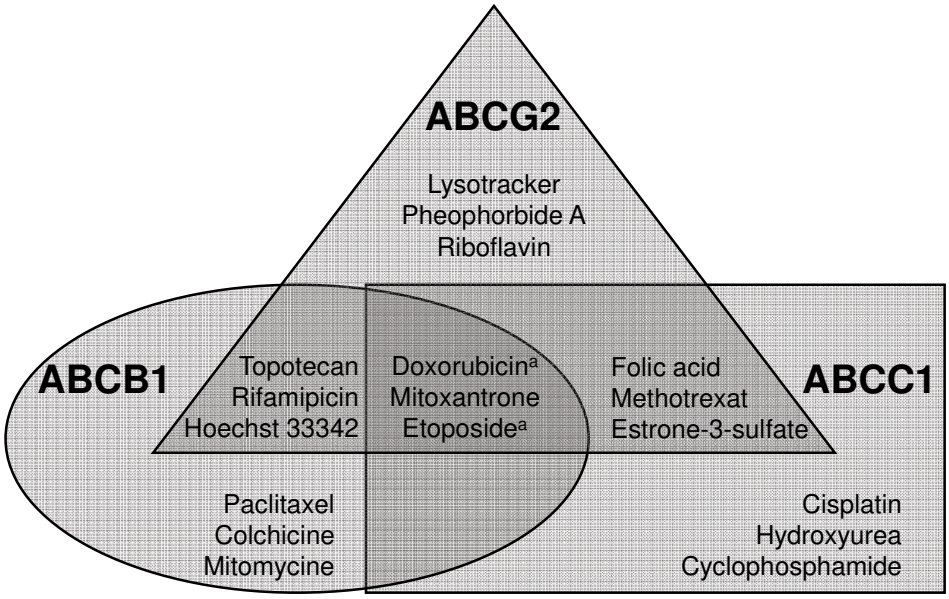

Figure 8: Substrate overlap between ABCG2, ABCB1 and ABCC1. Substrates that are marked with an "a" are subject to transport by the ABCG2 R482G isoform but not the wild-type form.[90]

Further overlap in substrates was detected among ABCG2 and ABCC1, where both transport folic acid, methotrexate and estrone-3-sulfate. This is in particular important in terms of chemotherapeutic treatment of cancer by drugs that are transported by one or more tranport proteins. Tissues or barriers like the BBB, that is simultaneously expressing ABCG2 and ABCB1, can be addressed by broadband inhibitors to reduce the resistance of the cells toward cytostatics with overlapping substrate specificity, such as topotecan.
Several inhibitors of ABCG2 also displayed an overlap of selectivity with ABCB1 and ABCC1, which indeed is more pronounced between the transport proteins ABCG2 and ABCB1. Like the substrates, the inhibitors of ABCG2 comprise molecules of different structural features that can be compared in Table 5. To date, only few selective and potent inhibitors, active in the submicromolar range have been reported, and further research is required.[138]

Table 5: Selection of Inhibitors of ABCG2.

Compound-class	Compound	Reference
DIKETOPIPERAZINES		
	Fumitremorgin C	[123]
	Ko143	[139]
	Indolyl diketopiperazines	[140]
STEROIDS AND STEROID-LIKE		
	Corticosterone	[141]
	Digoxin	[141]
	Mometasone	[142]
IMMUNOREPRESSANTS		
	Cyclosporine A (CsA)	[143]
	Sirolimus	[143]
	Tacrolimus	[143]
TYROSINE KINASE INHIBITORS		
	Gefitinib	[144]
	Imatinib	[144]
	Nilotinib	[144]
ABCB1/ABCG2 DUAL-INHIBITORS		
	Elacridar (GF-120918)	[145]
	Tariquidar (XR-9576)	[129]
	WK-X24 (XR-9577)	[146]
FLAVONOIDES		
	Chrysin	[147]
	Benzoflavone	[148]
	Kaempferol	[131]
	Genistein	[131]
AZOLES		
	Pantoprazole	[134]
	Omeprazole	[134]
	Ketoconazole	[149]
CALCIUM CHANNEL BLOCKERS		
	Dipyridamole	[150]
	Nicardipine	[150]
	Nitrendipine	[150]
OTHER DRUGS		
	PZ compounds	[151, 152]
	Curcumine	[153, 154]
	Xanthine	[155]

The first specific inhibitor of ABCG2 was the diketopiperazine fumitremorgin C (FTC), which was isolated from *Aspergillus furmigatus* but displayed severe neurotoxicity. Later, a less toxic and 10-fold more potent FTC analog, namely Ko143, was developed. It exhibited a high selectivity toward ABCG2 up to 1 µM and was established as one of

the standard inhibitors of the transport protein.[156] More inhibitors were discovered in the class of steroides and immunosupressants: the immunosupressant CsA for instance was used as standard inhibitor in the screenings with ABCB1 and ABCC1 overexpressing cells, to determine the selectivity toward ABCG2 of selected compounds in this work. The immunosupressants CsA and Sirolimus were both able to reverse the MDR of ABCG2 expressing HEK cells toward the cytostatic agents topotecan and MX.[143]

The class of TKIs take a particular role among inhibitors of ABCG2. Several are inhibitors of ABCG2 and ABCB1 and some were found to have an extraordinarily high affinity to ABCG2.[144,157,158] Imatinib for instance has already been successfully applied in the treatment of chronic myeloid leukemia (CML).[159] Also epidermal growth factor receptor (EGFR)-directed TKIs, such as gefitinib, erlotinib and afatinib demonstrated to be approved treatments for non-small lung cancers by activating the mutations in the EGFR kinase.[160] Lung cancers with EGFR mutations have shown to be dependent on EGFR signalling for survival and proliferation, making them highly sensitive to treatment with EGFR TKIs such as gefitinib or erlotinib.[161]

The broadspectrum inhibitor elacridar (GF120918) is a potent inhibitor of both, ABCG2 and ABCB1. It has demonstrated to increase the oral bioavailability of cytotoxic agents and increased brain and CNS levels of anti-HIV drugs.[162,163] elacridar is particularly beneficial in tissues with expression of both transport proteins, ABCG2 and ABCB1, as found in the BBB.

Moreover, several compounds in the class of flavonoides, azoles and calciumchannel blockers have been discovered to exhibit some inhibitory potency toward ABCG2. In the section “other drugs” of Table 5 the compound class curcumines and PZ-compounds were listed. Like FTC, curcumines are “static” inhibitors which only inhibit the function of ABCG2. The PZ-compounds contain a benzothiazol structure and were found to be “dynamic” inhibitors that inhibit the ABCG2 function and induce lysosome-dependent degradation of ABCG2 protein.[151,152] For illustration of the broad structural variety of different inhibitors of ABCG2 a selection is presented in Table 6. Although the list of inhibitors of ABCG2 is constantly growing, only a few have been found to be highly potent, selective and nontoxic.

Table 6: Structural Formulas of Selected Inhibitors of ABCG2.

SPECIFIC INHIBITORS
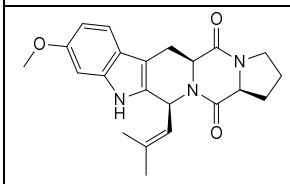 FTC 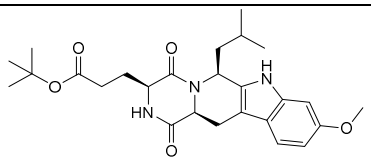 Ko143 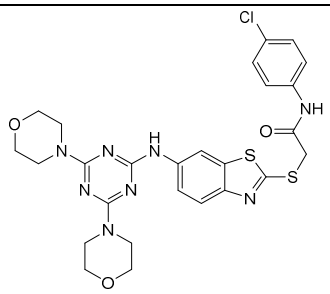 PZ-39
BROADSPECTRUM INHIBITORS
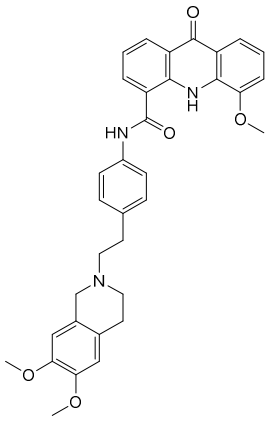 Elacridar (GF120918) 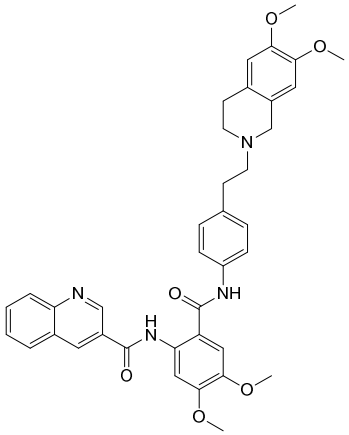 Tariquidar (XR-9576) 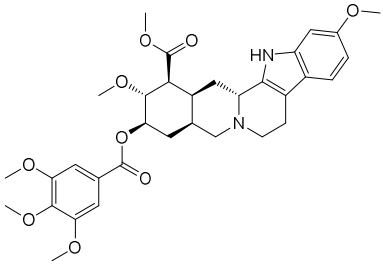 Reserpine
TYROSINE KINASE INHIBITORS (TKIs)
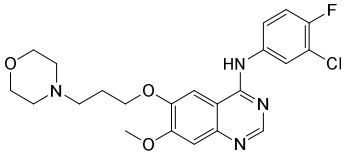 Gefitinib 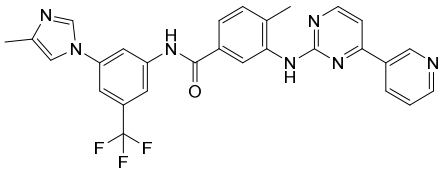 Nilotinib 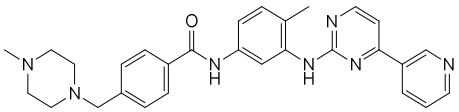 Imatinib

Further research is necessary to develop more compounds with the desired properties that might be suitable for application *in vivo*. Moreover, it is necessary to shed some light on the complex interaction of inhibitors of ABCG2 with the transport protein.

1.2.4.4 Drug binding in ABCG2

To date, only few studies have investigated the drug binding interaction with ABCG2, mostly by mutational experiments (see chapter 1.2.4.2), functional kinetic assays as well as photoaffinity labelling and radioligand studies. The bulk of the data presented in these studies pointed to the existence of several binding sites in ABCG2 that could partially overlap. For instance, Shukla *et al.* performed photoaffinity labelling of ABCG2 by IAAP and [^{3}H]azidopine, that were both found to be transported substrates of the protein.[164] Here, the photolabelling as well as the transport of the photoaffinity analogs could be inhibited by 1,4-dihydropyridines, such as nicardipine and nifedipine. A concentration dependent inhibition of the labelling was determined in co-administration of different substrates and inhibitors providing a valuable tool for distinguishing substrates from inhibitors and studying the drug-binding site(s) of the transporter.

Additional information about the binding pockets that are occupied by the photo-labelling agents could be derived from purified photo-labelled ABCG2. Subsequent investigations by trypsin digestion and mass spectrometrical analysis of the peptide fragments might yield crucial information about the localization of binding pockets in ABCG2, but have not yet been carried out successfully.[66]

The research group of Clark *et al*. performed direct binding kinetic studies with [3H]daunomycin leading to the assumption that the found results cannot be described by a simple single site binding process.[165] They showed that there are at least two binding sites in each ABCG2 monomer unit, one for mitoxantrone and Hoechst 33342 and another for prazosin. Between the two protein units, negative allosteric interactions and a positive cooperativity were found among different bound substrates. Unfortunately, it could not be determined if the two Rhodamine 123 sites interact with each other as well.

Another study conducted by Takenaka *et al.* revealed different binding sites for prazosine (here: IAAP) and some other substrates of ABCG2 based on a purine scaffold.[166] In a similar fashion, Giri *et al.* suggested different binding sites for the nucleotide analog

substrates zidovudine and abacavir that seem not to overlap with those of prazosine or imatinib.[167] The inhibitor Ko143 takes a peculiar role, as it is thought to interact with both binding sites mentioned above.

There have also been some *in silico* studies comprising homology modeling of ABCG2 either based on a crystal structure of mouse ABCB1 or, more recently, an ABCG5/ABCG8 heterodimer.[168,169] An atomic model for the human ABCG5/ABCG8 heterodimer was generated by X-ray crystallography in a nucleotide-free state at a resolution of 3.9 Å. In docking studies with different substrates and non-substrates László *et al.* identified several binding sites. Binding site 1 allows the entry of all drugs. Subsequent entry to a proposed site 2 was restricted for non-substrates of ABCG2 like verapamil or calcein which may serve as a selectivity filter for toxic molecules from natural metabolites. This hypothesis is substantiated by the localization of amino acid R482 in this binding region which has a great impact on the substrate selectivity. The same applies to the mutations of T402 or P485 that have been reported to have a considerable impact on the transport of substrates.[170] Unfortunately, the mechanism of the binding of substrates and inhibitors to the protein is still not clear and awaits further investigation.

1.2.4.5 Relevance of ABCG2 in cancer therapy

The role of ABCG2 in cancer therapy is controversially discussed, since early expectations of promising *in vitro* results for inhibitors of P-gp were not met by the subsequent *in vivo* studies.[171] However, several clinical studies have found some indication that a higher expression of ABCG2 correlates with a lower survival rate in small cell lung cancer, non-small cell lung cancer, pancreatic cancer, mantle cell lymphoma, acute myeloid leukemia, ovarian cancer and breast cancer.[172,173,174,175,176,177,178,179,180,181]

Also, it is known that overexpression of ABCG2 can be a significant obstacle in the chemotherapeutic treatment of cancer with cytostatic drugs, since many of the agents are substrates of ABCG2. Hence, an intrinsically or developed resistance in cancer cells toward those drugs induced by this overexpression, might be overcome by direct inhibition of the transport protein. Unfortunately, only a few clinical studies targeting to

reverse this MDR in chemotherapy by inhibition of ABCG2 *via* co-administration of inhibitors have been conducted to date. Out of five clinical studies only two completed the dose-finding phase and only one is currently actively running (see Table 7).

Regarding the terminated phase II trial of the TKI lapatinib in co-administration with topotecan, no clinical benefit was detected in epithelial ovarian cancer in comparison to the use of the cytostatic agent only. Lheureux *et. al* suggested that the absence of correlation between ABCG2 expression and clinical outcome pointed to other mechanisms of resistance to topotecan.[182]

Table 7: Clinical Trials with ABCG2 Inhibitors, Adapted from Ricci et al.[172]

Clinical trials with ABCG2 inhibitors (clinical trial title and phase)	**Status**	**Cancer**	**Chemo-therapy**	**Conjunctive therapy**
Erlotinib Hydrochloride and Irinotecan Hydrochloride in Treating Patients With Advanced Solid Tumors (Phase I)	Active, not recruiting	Advanced Solid Tumors	Irinotecan	Erlotinib
A Phase I Study of Oral Topotecan and Lapatinib in Subjects with Advanced Solid Tumors (Phase I) [183]	Withdrawn	Advanced Solid Tumors	Topotecan	Lapatinib
Dosage-finding and PK Study of IV Topotecan and Erlotinib with Refractory Solid Tumors (Phase I, Dose-finding) [184]	Completed	Metastatic, Refractory Solid Tumors	Topotecan	Erlotinib
A Phase I, Randomized Open-label, Parallel-cohort, Dose-finding Study of elacridar (GF120918) and Oral Topotecan in Cancer Patients (Phase I, Dose-finding) [49]	Completed	Cancer	Topotecan	Elacridar (GF120918)
Phase II trial of Lapatinib and Topotecan (LapTop) in Patients with Platinum-refractory/resistant Ovarian and Primary Peritoneal Carcinoma (Phase II) [182,185]	Terminated	Platinum-refractory/ resistant Ovarian and Primary Peritoneal Carcinoma	Topotecan	Lapatinib

Indeed, there have also been several animal models that aimed to reverse the ABCG2 induced MDR by inhibition of the protein. Although many first generation inhibitors such

as FTC exhibited a high *in vitro* efficacy, they could not meet the expectations *in vivo* owing to significant toxic effects.[126,186] In the case of FTC, a severe neurotoxicity prevented any further clinical use and led to the development of considerably less toxic structural analogs like Ko143.[187] This FTC analog was able to inhibit the intestinal Abcg2 in mice which led to an increased oral availability of topotecan.[139] However, Ko143 has not been tested in clinical trials to date.

Other inhibitors of ABCG2 have been investigated as well: curcumines for instance increased the relative bioavailability of sulfasalazine by selectively inhibiting the ABCG2 function.[188] Moreover, the broadspectrum inhibitor elacridar was able to restore sensitivity of a doxorubicin resistant C-26 tumor toward the cytostatic agent doxorubicin.[189] Certainly, a spotlight was put on the investigation of tyrosine kinase inhibitors as they were frequently used in animal models.

The class of TKIs was found to be very promising, since several inhibitors have already been tested in the clinic (compare Table 7) or even found application in cancer treatment. Many TKIs like gefitinib, erlotinib, sunitinib or imatinib have proven to reverse the MDR toward cytostatic agents induced by ABCG2 expression *in vitro*.[190] Interestingly, they act as substrates at low concentrations, probably competing for the same binding site as other substrates, such as SN-38, prazosin or topotecan, but inhibit the ABCG2 function at higher concentrations.[191,192,193] Moreover, some TKIs could interact with the PI3K-Akt pathway leading to a downregulation of the ABCG2 expression in K562/BCRP-MX10 cells.[194] These properties were exploited in an animal model by co-administering the TKI imatinib and the photosensitizer pheophorbide A, which is a substrate of ABCG2. The presence of the inhibitor imatinib led to an increased accumulation of the photosensitizer in the ABCG2 expressing cells resulting in considerably enhanced results of the photodynamic therapy (PDT).[195] But TKIs have also shown mixed outcomes as ABCG2 inhibitors when co-administered with cytotoxic agents that are substrates of ABCG2.

Unfortunately, it seems that some other mechanisms involved *in vivo* could contribute to MDR, making the transfer from *in vitro* more complex than expected. Inhibitors with little side-effects, high selectivity and potency as well as a low toxicity can increase the chances for a successful outcome regarding *in vivo* studies.

2 Aim the work

Since ABCG2 is one of three major transmembrane ABC transport proteins associated with the occurrence of multidrug resistance (MDR), several research groups have focused on finding potent, selective and nontoxic inhibitors as a possible way to overcome MDR. Although ABCG2 was discovered in the year 1998, to this date only little is known about the function of the transport protein and its interaction with inhibitors on a molecular level.

A main objective of this work was to build a comprehensive library of different inhibitors of ABCG2 based on a quinazoline scaffold, including some closely related structures. From the data an extensive **structure-activity-relationship** (SAR) is targeted that could pave the way for the development of novel potent inhibitors. In this regard, emphasis was put on the **inhibitory potency** and **selectivity** of a compound toward ABCG2. Hence, accumulation assays were carried out using the dyes Hoechst 33342 and pheophorbide A and the inhibitory potencies toward ABCB1 and ABCC1, the two other major ABC transport proteins, were investigated in a calcein AM assay.

Further studies concerned the **intrinsic cytotoxicity** of selected compounds aiming to gather information about the structure-toxicity-relationship and highlighting promising compounds for future clinical trials.

One central objective of this study was to investigate the ability of a compound to reverse MDR in ABCG2 overexpressing cells toward commercial cytostatic drugs like SN-38 and mitoxantrone that are also substrates of the transport protein. Therefore a **MDR reversal assay** was carried out investigating selected compounds in co-administration with cytostatic drugs and monitoring the impact on the viability of ABCG2 overexpressing cells. Since inhibition of ABCG2 leads to a reduced efflux of the cytostatic drug out of the cell a stronger decrease in the cell viability results than in absence of an inhibitor. A reversal of MDR can be observed if the corresponding inhibitor is able to increase the sensitivity of an ABCG2 overexpressing cell toward the cytostatic agent considerably. This *in vitro* investigation is important for continuative *in vivo* studies with promising compounds to enhance the outcome of chemotherapeutic cancer treatment that is often restricted by intrinsic or acquired MDR related to overexpression of ABCG2.

In addition, the inhibitory potencies obtained in the Hoechst 33342 accumulation assay

were compared to the derived **potency of a compound to reverse MDR**, given as an IC_{50} value.

Inhibitory enzyme kinetics were carried out for a better understanding of the interaction between an inhibitor and the ABCG2 substrate Hoechst 33342. Different modes of binding to ABCG2 could be identified with help of the obtained data and compared to other well-known inhibitors like Ko143, gefitinib and elacridar.

The interaction data analysis was complemented with further studies including the **conformation sensitive binding of the 5D3 antibody** to an epitope of ABCG2. Hereby, the conformational impact of different inhibitors on ABCG2 was classified and compared to other functional assays to elucidate the interaction with the transport protein.

Another building block was the investigation of the **ATPase activity** providing information about the consumption of ATP through hydrolysis in the presence of an inhibitor. The so-called vanadate sensitive ATPase activity is closely related to the transport activity of the protein giving further details of the interaction and binding in presence of an inhibitor.

In summary, this study can contribute to the development of new potent, selective and nontoxic inhibitors of ABCG2, containing a scaffold based on quinazoline and related structures and provide a comprehensive SAR for future studies. Also, their ability to reverse MDR in ABCG2 overexpressing cells by restoring the sensitivity toward cytostatic drugs is investigated to find promising candidates for clinical trials. Finally, the new data collected in several functional assays can provide new insights into the function of ABCG2 in presence of inhibitors which is barely understood and still lacks significant scientific publications.

2.1 Concept for synthesis of inhibitors of ABCG2 derived from a quinazoline scaffold

Keynote for the synthesis and design of inhibitors of ABCG2 was to modify a quinazoline scaffold as lead-structure that has previously been used for some potent inhibitors such as TKIs gefitinib, PD158780 and, with small modifications, PD153035 (Figure 9). The

named inhibitors all contain a substituted aniline linker at position 4 as a common characteristic, this feature was also adopted for the compounds in this work.

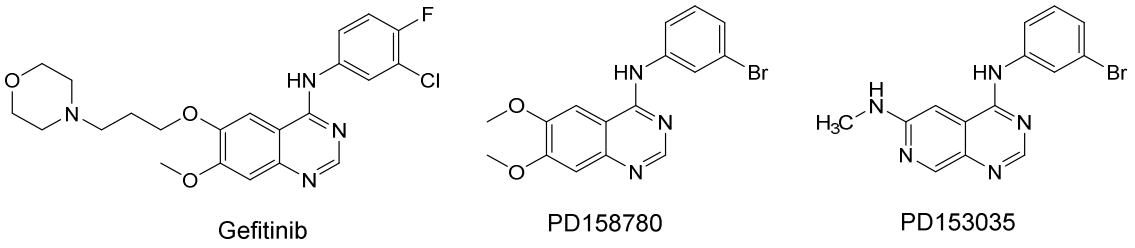

Figure 9: Tyrosine kinase inhibitors (TKIs) based on a quinazoline scaffold or related structures.

Based on the investigations of Juvale *et al*. it was discovered that substitution with a phenyl moiety at position 2 of the quinazoline scaffold led to a considerable increase of the inhibitory potency toward ABCG2.[196, 197, 198] Besides the basic quinazoline scaffold, there are several other positions that can be modified conveniently such as substitution at positions 2, 4, 6 and 7 as well as the introduction of nitrogen atoms at the aromatic core of the quinazoline scaffold. These modifications have already in part been carried out and investigated in other studies. The current problem is that most of the existing inhibitors containing a quinazoline scaffold lack inhibitory potency toward ABCG2 or comprise other downsides like high intrinsic cytotoxicity, low solubility or a decreased selectivity. The basic variations introduced in this study are grouped into projects I to VI and are briefly described in the following paragraphs. An overview of all modifications is illustrated in Figure 10.

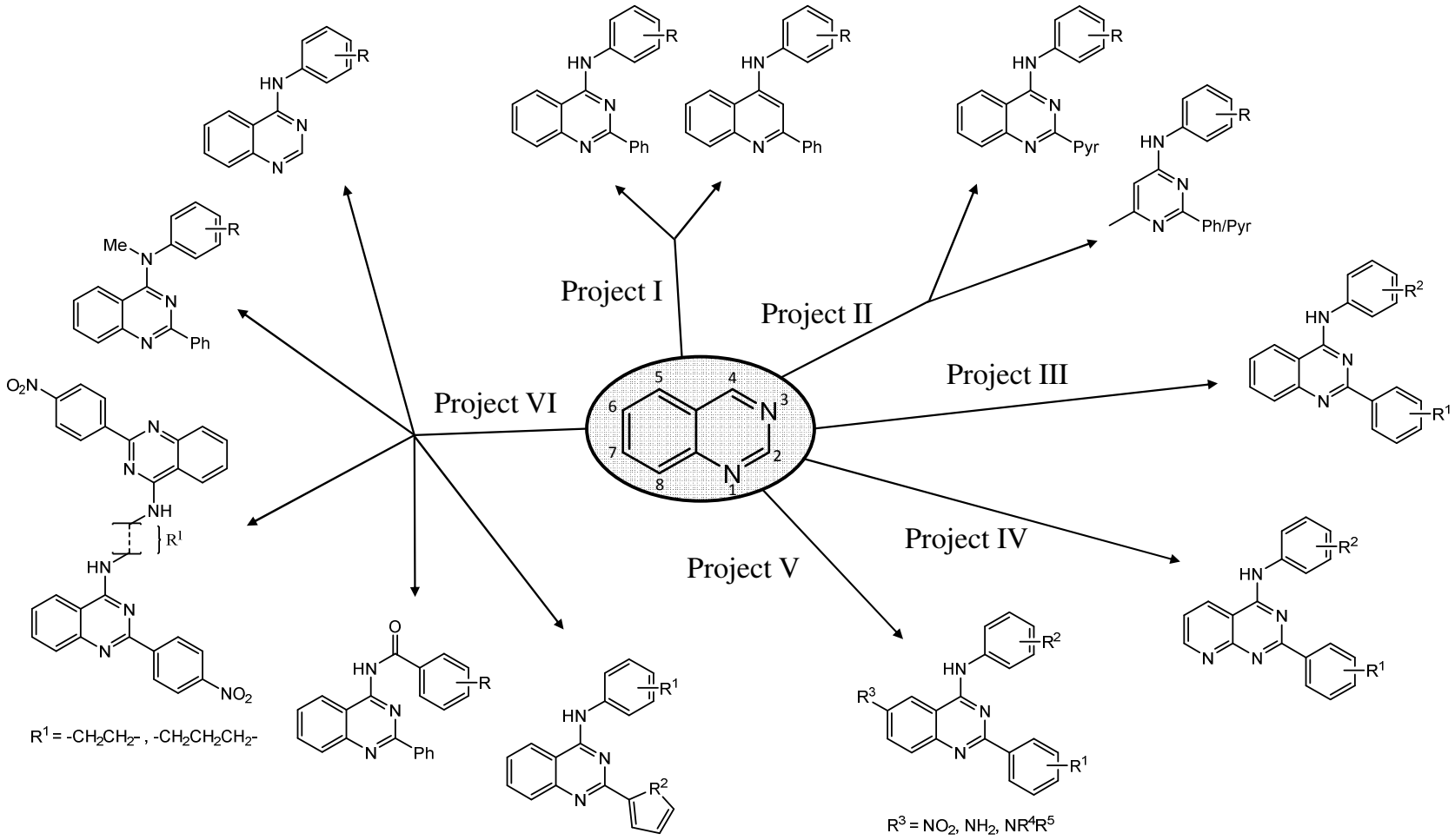

Figure 10: Overview of the structural variations carried out in project I to VI.

In **project I**, the importance of a nitrogen atom at position 3 of the quinazoline scaffold for the inhibitory activity toward ABCG2 was investigated (R^1 = C or N). Substitution was only carried out in *meta* and *para* position at R^2 since earlier results exhibited low potencies of *ortho* substitution. In order to provide a distinct interpretation of the SAR, all derivatives were synthesized with a phenyl moiety at position 2 of the scaffold (see Figure 11). Herby an easy comparison with the compounds synthesized in other projects was possible providing a meaningful interpretation of the corresponding modifications.

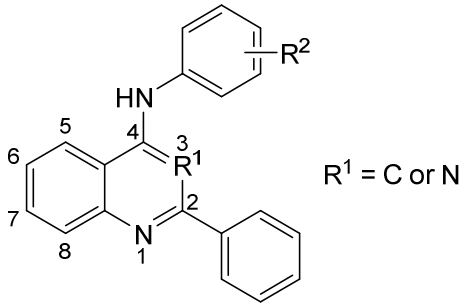

Figure 11: Substitution pattern for the compounds of Project I.

In **project II**, the phenyl moiety at position 2 was replaced by different pyridyl residues to investigate the impact of *ortho*, *meta* and *para* pyridyl substitution at this position. Moreover, the importance of the non-heteroaromatic condensed core of the quinazoline scaffold was investigated by replacing it with a methyl residue. The small methyl residue was necessary due to a convenient synthetic preparation but is unlikely to have any considerable impact on the inhibitory properties of the compound.

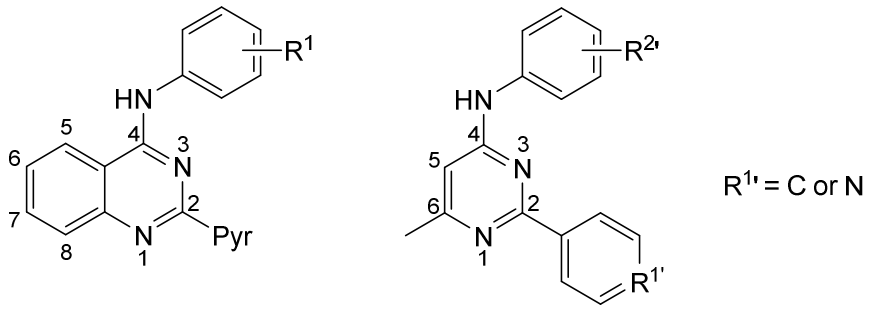

Figure 12: Substitution pattern for the compounds of Project II.

For **project III** substitution was carried out at the aniline linker at position 4 and also at the phenyl moiety at position 2 of the quinazoline scaffold. This allows the investigation of cumulative effects of R^1 and R^2 including the interchangeability of both functions. In comparison to project I a broader spectrum of substitution patterns could be covered adding to the SAR of this investigation.

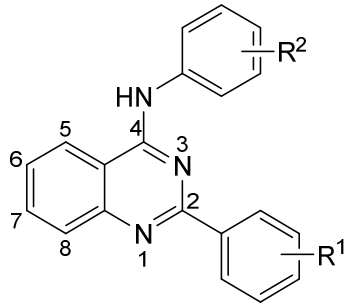

Figure 13: Substitution pattern for the compounds of Project III.

In **project IV** modification was carried out at the quinazoline scaffold by introducing a nitrogen atom at position 8. The resulting pyrido[2,3-d]pyrimidine scaffold was further functionalized by a substituted aromatic function at position 2 and a substituted aniline linker at position 4. Hence, the compounds could easily be compared to those of project I-III.

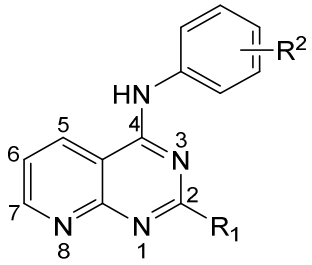

Figure 14: Substitution pattern for the compounds of Project IV.

In **project V** a nitro group was introduced at R^3 making amino and amido functions accessible after reduction of the nitro residue. Additionally, the quinazoline scaffold contains a phenyl residue at R^1, which in some cases was further substituted, and also a substituted aniline group at position 4. This allows an easy comparison between the

corresponding derivatives of project I-III (R^3 = H) and also among the nitro, amino and amido derivatives of this project.

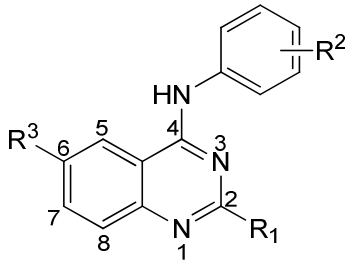

Figure 15: Substitution pattern for the compounds of Project V.

In **project VI** several modifications at the quinazoline scaffold were investigated. In one case a 5-membered heteroaromatic residue like thiophene and pyrrole was introduced at position 2 (scaffold A). Another modification was the methylation of the amino function at the aniline linker replacing the hydrogen atom with a methyl group (scaffold B) investigating the importance of an H-donor function at this position. Moreover, the amino linker at position 4 was replaced by an amido function (scaffold C) including both, an H-donor and H-acceptor function. In scaffold D the aromatic moiety at position 2 was replaced by hydrogen and is therefore closely related to TKIs like gefitinib. Additional substitution was carried out at R^1. Finally, a dimer was synthesized containing a 4-nitrophenyl moiety at position 2 of a quinazoline scaffold (scaffold E). Two molecules were then linked by two diamines of different chain length obtaining the corresponding dimer.

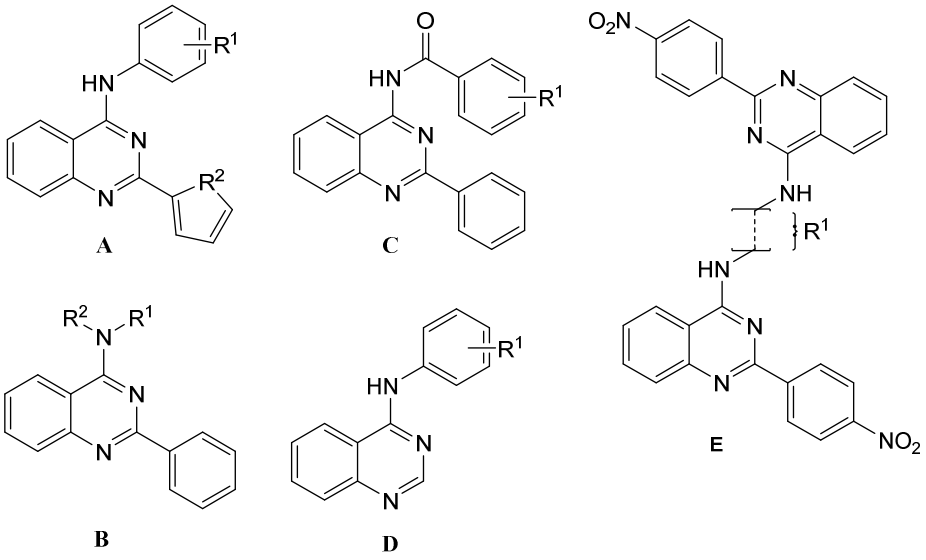

Figure 16: Substitution pattern for the compounds of Project VI. Different scaffolds are marked with the capital letters A-E.

A more detailed discussion of the modifications and the corresponding results from the investigations is provided in the following text.

3 Project I: 4-Substituted-2-phenylquinazolines and -quinolines

Synthesis of the substituted 4-anilino-2-phenylquinazolines was performed using a fast and convenient method involving microwave radiation. Commercially available aniline derivatives and 4-chloro-2-phenylquinazoline were used to create a comprehensive substance library. Substitution was only carried out at the aniline linker at position 4 and only comprised *meta* and *para* substituted 2-phenylquinazoline derivatives since *ortho* substitution was found to be unfavorable in former studies.[196] Moreover, the gaps in previous studies were filled and the spectrum broadened with new substituents to provide a meaningful discussion of the SAR. Furthermore, two fluorescent conjugates with a 4-anilino-2-phenylquinazoline scaffold were introduced to investigate the distribution of the compounds between the cells and the aqueous medium.

Additionally, the importance of the nitrogen atom at position 3 of the quinazoline scaffold was investigated by synthesizing several quinoline analogues for comparison. It is notable that the 4-anilino-2-phenylquinazoline scaffold is more planar than the 4-anilino-2-phenylquinoline structure, since some studies presuppose that planarity of an inhibitor is crucial for a high inhibitory potency.[112, 66] Furthermore, the nitrogen atom at position 1 of aforementioned structures exhibits a more basic character for the quinoline derivative with a calculated pK_a of 8.4 vs. 5.6 of the quinazoline derivative. Due to the fact that membrane permeability correlates approximately with the logP value of a compound calculations were carried out for the unsubstituted 4-anilino-2-phenylquinazoline and -quinoline scaffold resulting in a calculated logP of 4.08 and 5.63, respectively.

3.1 Reaction mechanism

The synthesis route and a detailed reaction mechanism is provided in this chapter. Scheme 1 illustrates the reaction conditions and Scheme 2 the reaction mechanism.

*Scheme 1: General synthesis scheme for the preparation of compounds **1-32**.[a]*

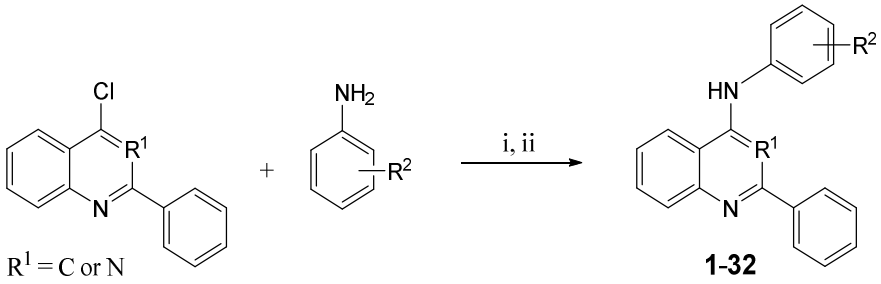

[a]: Reagents and conditions for compounds **1-27** (R^1 = N): (i) *i*-PrOH, 100 watt microwave irradiation, 110 °C, 30 min. Reagents and conditions for compounds **28**-**32** (R^1 = C): (ii) *i*-PrOH, 100 watt microwave irradiation, 110 °C, 15 min.

Reaction mechanism:

Final compounds were synthesized *via* nucleophilic aromatic substitution of a 4-chloro-2-phenylquinazoline or -quinoline precursor by a substituted aniline derivative. The reaction mechanism is illustrated below, starting with the nucleophilic attack at position 4 of the corresponding 4-chloro derivative by the amine.

*Scheme 2: Reaction mechanism for compounds **1-32**.*

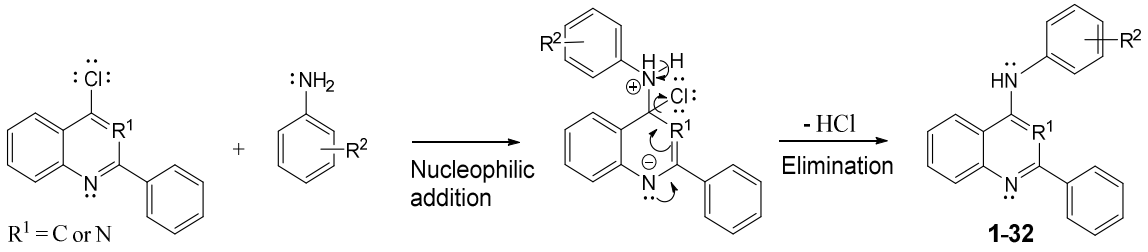

Synthesis of the compounds was carried out as described in section 10.1.1.1. In the first step the substituted aniline performs a nucleophilic attack at the carbon atom at position 4 due to its low electron density induced by the chlorine atom. After addition of the aniline derivative to the aromatic ring, the electrons of the double bond shift to position 1 since nitrogen is capable of stabilizing negative charges. In the last step, hydrochloric acid is eliminated restoring the aromatic character of the quinazoline/quinoline scaffold. In the

case of an incomplete reaction, triethylamine was added to the mixture to react with hydrochloric acid generated during the reaction. This prevents the protonation of the substituted aniline molecule which would result in a significantly decreased nucleophilic character.

3.2 Investigation of the inhibitory potency toward ABCG2 in the Hoechst 33342 and Pheophorbide A accumulation assay

The Hoechst 33342 accumulation assay was carried out with the MDCK II ABCG2 overexpressing and parental cell line to investigate the inhibitory potency of the compounds. The principle of this assay is based on the significant increase in fluorescence of the Hoechst 33342 dye when embedded in a lipophilic environment like a cell membrane or bound to DNA. Since it is also a substrate of ABCG2 the active efflux of the dye by the transport protein leads to a decrease of the total fluorescence. Inhibition of the transport protein on the other hand leads to lower efflux of the dye. Detection of the fluorescence is carried out at different inhibitor concentrations over a time-period of two hours. Representative curves of the measured fluorescence in the presence of the standard inhibitor Ko143 are illustrated in Figure 17 a). Measured fluorescence values at each inhibitor concentration increase until a steady-state equilibrium for Hoechst 33342 is reached.

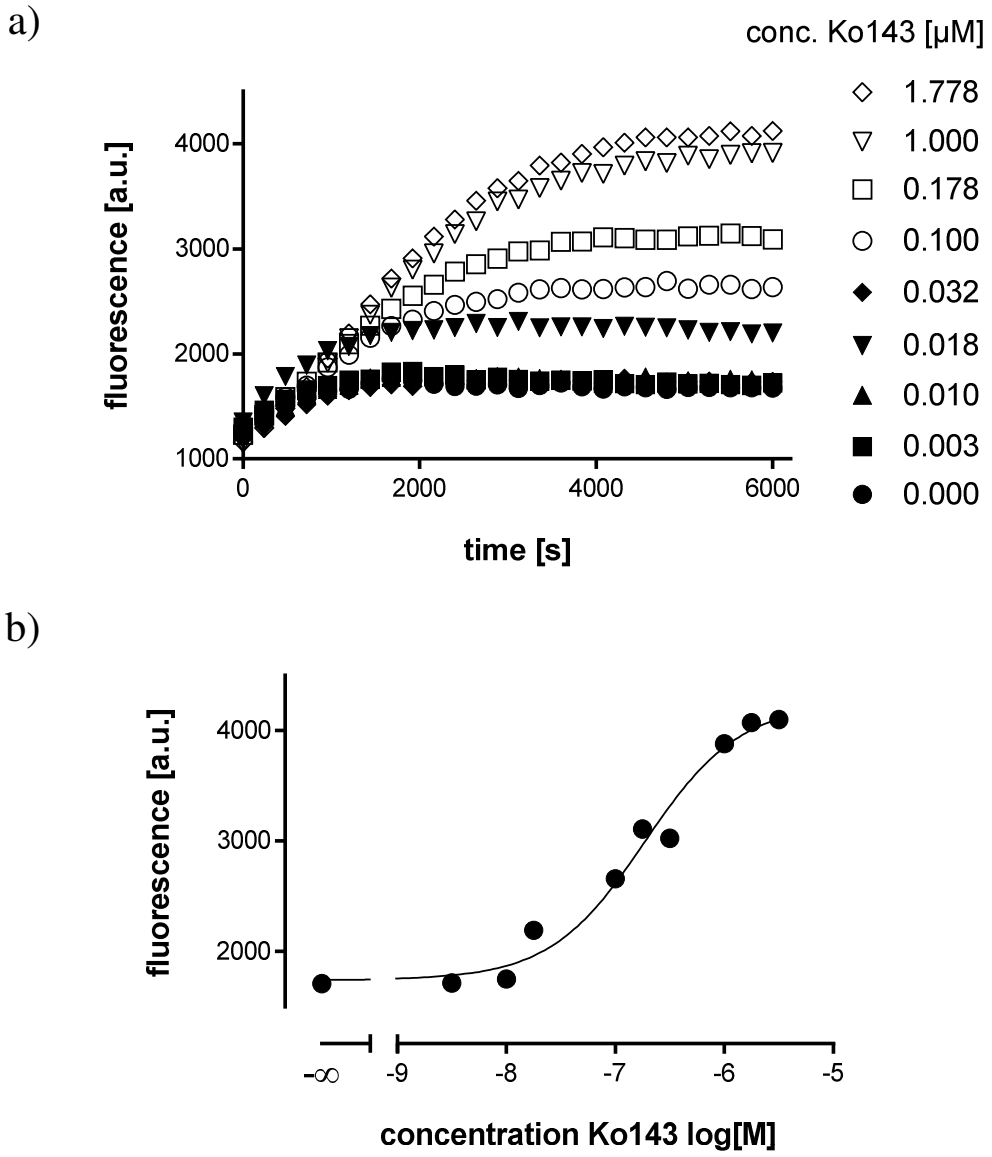

Figure 17: Plot of the fluorescence intensity over time at various concentrations of the standard inhibitor Ko143 in a Hoechst 33342 accumulation assay (a). Corresponding concentration-response-curve (IC_{50}: 226 nM) obtained at various concentrations of Ko143 in a Hoechst 33342 accumulation assay (b).

At steady state only negligible changes in the fluorescence intensity can be observed and it is reached after approximately 100 minutes. From the average fluorescence value acquired in the steady-state for each Ko143 concentration a sigmoidal concentration-response curve is fitted using the 4-parameter logistic equation or the 3-parameter logistic equation with a fixed Hill-slope depending on statistical preference. A representative concentration-response curve of Ko143 is illustrated in Figure 17 b). After a successful curve-fit, characteristic parameters like the inflection point of the concentration-response

curve (IC_{50}) can be calculated in order to compare the inhibitory potency of the compounds. More details regarding the procedure are provided in chapter 10.2.2.2.

A second method to determine IC_{50} values was additionally applied to confirm the results of the Hoechst 33342 accumulation assay. For this purpose, a pheophorbide A accumulation assay was carried out. Here, the fluorescence of pheophorbide A is measured directly in the cells on a FACSCalibur cell analyzer (see chapter 10.2.2.3). The advantage of this accumulation assay is that pheophorbide A is a specific substrate of ABCG2 whereas Hoechst 33342 is also transported by ABCB1. Therefore, a comparison between both assays is used to validate the obtained results, excluding substrate specific effects as source of error.

The steady-state fluorescence is measured individually in selected cells and can be correlated to the degree of inhibition of the ABCG2 efflux transporter. Corresponding sigmoidal concentration-response curves are generated as described for the Hoechst 33342 accumulation assay. Furthermore, this method allows the measurement of fluorescence only in healthy cells after gating them according to their size and granularity given by the FSC and SSC detected on the FACS (Figure 18).

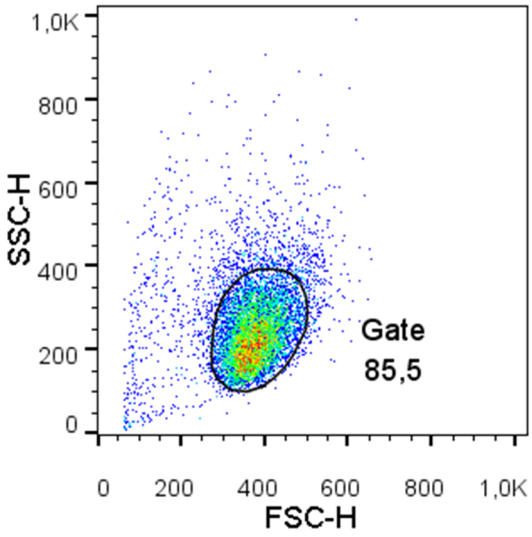

Figure 18: Cell population obtained as a dot plot from forward scatter (FSC) versus side scatter (SSC) measured by FACSCalibur cell analyzer. Circled subpopulation (85.5% of total population) was used for the measurement while non-circled cells represent unhealthy cells/debris and were excluded. For the evaluation the FlowJo V10 data analysis software package was used.[199]

The results from the Hoechst 33342 accumulation assay are discussed first. A summary of the obtained IC_{50} values from the Hoechst 33342 accumulation assay and the pheophorbide A assay is depicted in Table 8. The substitution pattern for all compounds is depicted above the table.

Table 8: Inhibitory Activities Determined in the Hoechst 33342 Accumulation Assay Using ABCG2 Overexpressing MDCK II BCRP Cells. Molecular Formula of the Substitution Patterns are Depicted Above the Table.

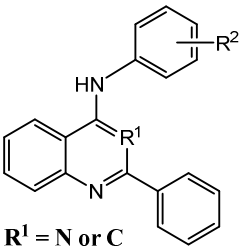

R^1 = N or C

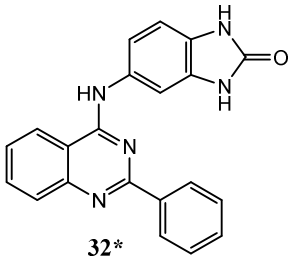

32*

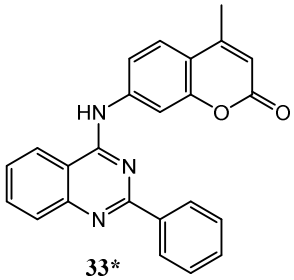

33*

Compound	R^1	R^2	Hoechst 33342 IC_{50} ± SD [nM][a]	Pheophorbide A IC_{50} ± SD [µM][a]
1[c]	N	H	882 ± 157	n.d.
2[b]	N	3-NO_2	130 ± 30	n.d.
3	N	3-NO_2-4-OH	81.1 ± 9.1	113 ± 17
4[b]	N	3-CN	140 ± 40	n.d.
5	N	4-CN	70.0 ± 10.0	84.5 ± 17.0
6	N	4-OH	204 ± 37	304 ± 82
7	N	4-SO_2F	556 ± 68	n.d.
8	N	3-NHCOMe	278 ± 33	224 ± 43
9	N	4-NHCOMe	539 ± 112	n.d.
10	N	3-SMe	1190 ± 30	n.d.
11[b]	N	3-OMe	1320 ± 100	n.d.
12[b]	N	4-OMe	1930 ± 110	n.d.
13[c]	N	3,4-OMe	152 ± 19	n.d.
14	N	3,5-OMe	2500 ± 500	n.d.
15	N	3-F-4-OMe	872 ± 200	689 ± 149
16	N	3-OMe-4-Br	289 ± 34	202 ± 44
17	N	3-Me-4-I	1460 ± 70	n.d.
18	N	3-F	355 ± 53	405 ± 66
19	N	4-F	1060 ± 170	n.d.
20[c]	N	3-Cl	1930 ± 280	n.d.
21	N	4-Cl	830 ± 118	n.d.
22	N	3-I	791 ± 199	n.d.
23	N	4-I	612 ± 62	n.d.
24	N	4-COOMe	944 ± 164	n.d.

Table continues on the next page

25	N	4-COO*t*-Bu	5650 ± 920	n.d.
26	N	4-COOH	6380 ± 1390	n.d.
27	N	3-CCH	672 ± 96	513 ± 136
28	N	3-Me	1150 ± 160	n.d.
29	N	4-Me	1480 ± 230	n.d.
30	N	3-*t*-Bu	1070 ± 110	n.d.
31	N	4-*t*-Bu	1060 ± 200	n.d.
32*	N	[e]	295 ± 55	n.d.
33*	N	[e]	654 ± 131	n.d.
34	C	3-NO_2-4-OH	712 ± 124	n.d.
35	C	3-CN	1680 ± 283	n.d.
36	C	4-CN	846 ± 169	n.d.
37	C	3-NHCOMe	1630 ± 330	n.d.
38	C	3-OMe	951 ± 296	n.d.
39	C	3-SMe	1900 ± 130	n.d.
40	C	3-F	2130 ± 460	n.d.
Gefitinib			1730 ± 270	n.d.
XR9577[d]			740 ± 80	718 ± 105
Ko143[d]			227 ± 14	n.d.

[a]: *IC_{50} values are means of three independent experiments.*
[b]: *IC_{50} value taken from literature.* [196]
[c]: *Compound was synthesized previously.* [196]
[d]: *Used as reference in the corresponding assay.*
[e]: *See substitution pattern above.*
n.d.: Not determined.

According to the results in the Hoechst 33342 accumulation assay cyano, nitro, hydroxy, acetamido and fluoro functions were found to be very potent single substituents at the aniline moiety of the 2-phenylquinazoline scaffold. Highest potency resulted for compound **5**, containing a 4-cyano group leading to an excellent IC_{50} value of 70.0 nM. Interestingly, substantial differences in a two-fold range between the IC_{50} values of compounds containing either the same substituent in *meta* or a *para* position were observed (e.g. compound pairs **4/5**, **8/9**, **11/12**, **18/19**).

The electronic effect (electron withdrawing or electron donating) of the substituent on the aromatic residue in general played a minor role for the inhibitory potency of a compound (e.g. IC_{50} of compounds **5**-**12**). Indeed, the position of the substituent had a significant impact on the potency of a compound. Electron withdrawing groups like cyano and nitro were in particular beneficial in *para* position (e.g. compound **4/5**, **2/89**; see chapter 4.2 for **89**, IC_{50}: 70 nM) whereas electron donating groups like methoxy and acetamide

exhibited a decreased inhibitory potency at this position (e.g. compound **8/9**, **11/12**). On the contrary most electron donating groups had a more favorable effect at *meta* position. A distinct correlation was found among the compounds containing halogen atoms: Halogens of lower atomic numbers like fluorine exhibited a considerably higher inhibitory potency in *meta* than in *para* position. Increasing atomic numbers reversed this trend, favoring the *para* substitution slightly as demonstrated by iodine (e.g. compounds **18**-**23**).

Moreover, some disubstitutions in *meta* and *para* position were investigated. The potency of compound **2** (R^1: 3-nitro) for instance could be increased from an IC_{50} of 130 nM to 81.1 nM by addition of a hydroxy function in *para* position, obtaining compound **3**. Concentration-response curves of the most potent compounds **3** and **5** together with Ko143 are depicted in Figure 19.

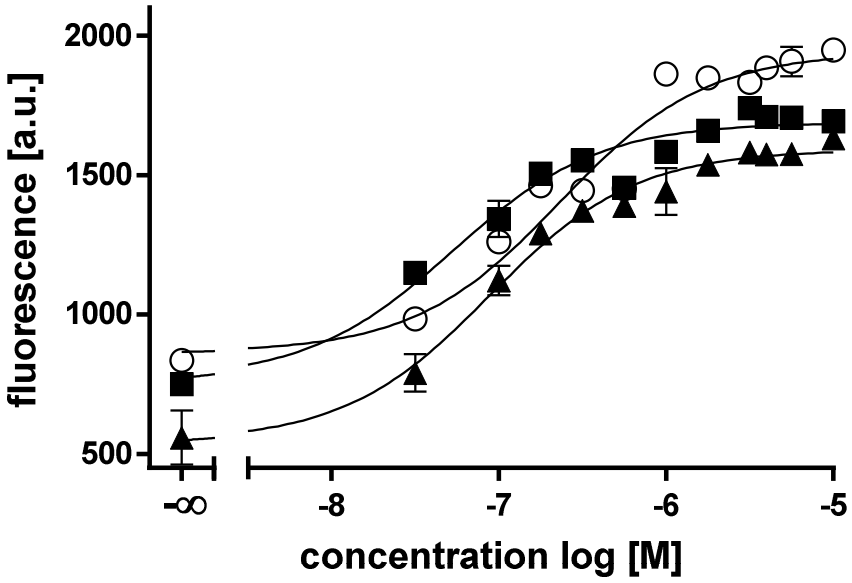

*Figure 19: Concentration-response curve of compound **5** (■, IC_{50}: 70.0 nM) and **3** (▲, IC_{50}: 81.1 nM) in the Hoechst 33342 accumulation assay with Ko143 (○, IC_{50}: 227 nM) as reference, using the ABCG2 overexpressing MDCK II BCRP cell line.*

Considerably high potencies were also determined for the 3,4-disubstituted compounds **13** and **16**. Compound **13** containing a 3,4-dimethoxy group (IC_{50}: 152 nM) was significantly more potent in comparison to the 3,5-dimethoxy analogue **14** (IC_{50}: 2500 nM).

Although the calculated logP values of all compounds showed no correlation with the inhibitory potency, considerably low values may lead to inactivity due to the loss of membrane permeability of a compound. This is probably a reason for the low potency of compound **26** (IC_{50}: 6380 nM) containing a carboxylic acid moiety which undergoes deprotonation at pH 7.4 and thereby exhibits a much lower logP value and possesses a negative charge. Formation of carboxylic acid groups from some ester functions by cellular esterases is not uncommon. However, cleavage of the methyl ester group in compound **24** is not likely due to the relatively high IC_{50} of 944 nM.

Investigation of the sterical effects on the inhibitory potency comprising different functions of varying bulkiness exhibited no clear correlation as illustrated by the similar IC_{50} values of compounds **28**-**31**. The sterically demanding substituents of compounds **32** and **33** confirmed this assertion, exhibiting rather high inhibitory potencies of 295 nM and 654 nM, respectively. Based on these results, the potency of a compound appears subject to the nature and positioning of a function at the aniline moiety rather than its sterical effects.

With regard to the inhibitory potency of the quinoline derivatives **34**-**40** a significant decrease was detected in comparison to their quinazoline analogues emphasizing the importance of a nitrogen atom at position 3 of the scaffold. Of the quinolines only compounds **36** and **38** possessed moderate activities in the submicromolar range containing a 4-cyano and 3-methoxy substituent, respectively.

For some compounds the IC_{50} values were additionally determined in a pheophorbide A accumulation assay, described in chapter 10.2.2.3. Obtained pIC_{50} values led to a very good correlation with the pIC_{50} values determined in the Hoechst 33342 accumulation assay (r^2 = 0.91). The scatterplot of the pIC_{50} values determined in both assays is illustrated in Figure 20.

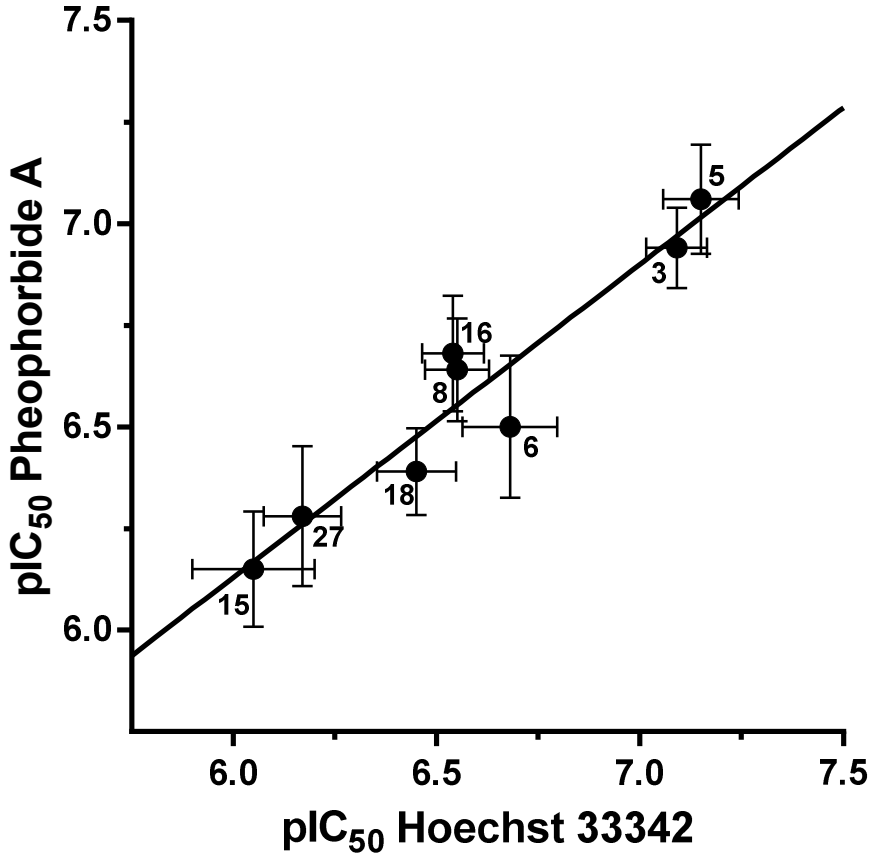

Figure 20: Scatterplot of pIC_{50} values obtained in the Hoechst 33342 assay versus the pheophorbide A assay of selected compounds. Each dot represents the mean pIC_{50} value obtained from at least three independent experiments and is labelled accordingly by compound number. Error bars indicate the standard deviation of the corresponding assay. The squared correlation coefficient $r^2 = 0.91$.

The concentration-response curves of the most potent compounds, **3** and **5**, determined in the pheophorbide A accumulation assay are depicted in Figure 21. XR9577 was used as standard inhibitor in this assay. The tariquidar analog is known to inhibit ABCG2 as well as ABCB1 with different potencies and has been established as an internal standard in our working group.

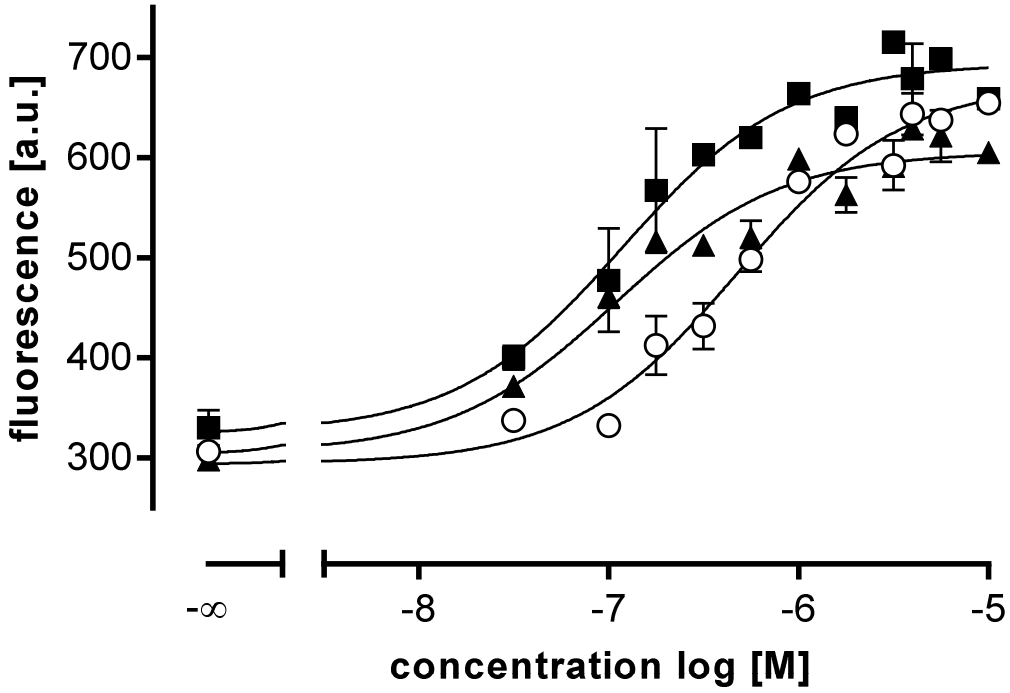

*Figure 21: Concentration-response curve of compounds **5** (■, IC_{50}: 0.0700 µM) and **3** (▲, IC_{50}: 0.0800 µM) in the pheophorbide A accumulation assay with XR9577 (○, IC_{50}: 0.740 µM) as reference. The ABCG2 overexpressing MDCK II BCRP cell line was used.*

The Hoechst 33342 and the pheophorbide A accumulation assay both exhibited a good correlation giving no indication of different substrate specifities of ABCG2 toward both compounds.

3.3 Investigation of the inhibitory potency toward ABCB1 and ABCC1 in the calcein AM assay

The inhibitory potency of the compounds toward ABCB1 and ABCC1 was determined in a calcein AM assay (see chapter 10.2.2.4). The assay is based on the intracellular accumulation of calcein which is formed in the cell by unspecific esterases. After cleavage of the acetoxymethyl esters, negatively charged calcein molecules accumulate

in the cell and can be measured fluorometrically. The intracellular concentration of calcein AM on the other hand depends on the efflux rate by the corresponding transport protein which can be modulated by inhibitors of ABCB1 and ABCC1. Thus, the measured fluorescence can be correlated to the inhibitory potency of a compound.

A screening was conducted with the ABCB1 overexpressing cell line A2780adr and the ABCC1 overexpressing cell line H69AR. The inhibitory potency in comparison to a standard inhibitor of both transport proteins, namely cyclosporine A (CsA), was determined at a concentration of 10 µM for each compound. In the case of inhibitory potencies of more than 25% relative to CsA, complete concentration-response curves were determined and the IC_{50} values calculated. The results of the screening with both cell lines are depicted in Figure 22 and the IC_{50} values in Table 9.

Among the quinazoline derivatives only compounds **13**, **14** und **28** exhibited more than 25% of inhibition relative to the standard CsA with the ABCB1 overexpressing A2780adr cell line. In particular, substitution with methoxy groups led to increased inhibitory potencies whereas other substitutions resulted in only negligible activity. However, almost all quinoline derivatives **34**-**40** displayed a relatively high inhibitory potency toward ABCB1 mostly exceeding the 25% mark.

a)

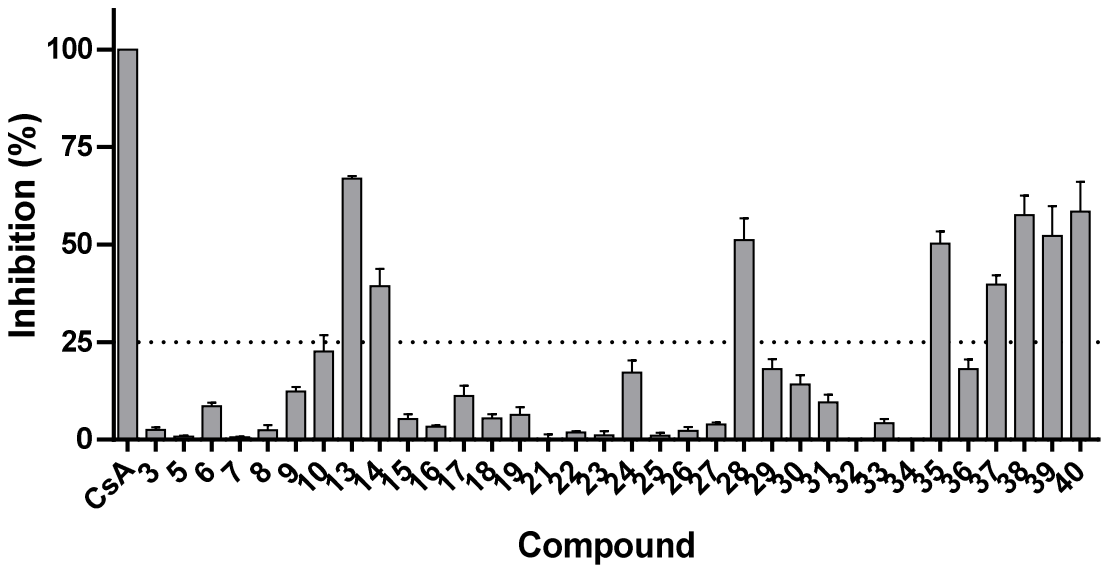

Figure continues on the next page

b)

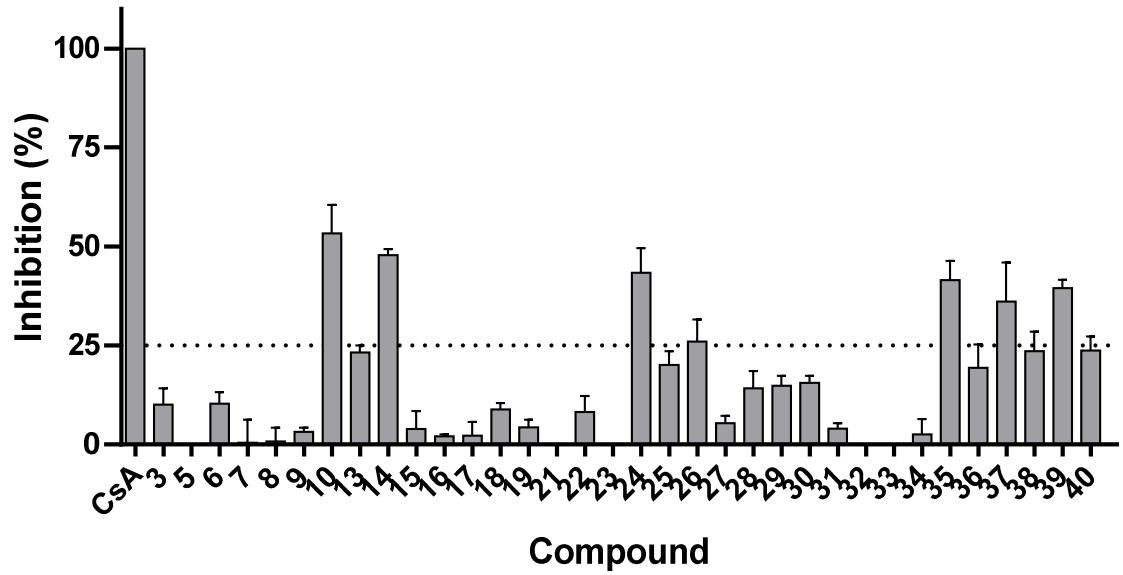

Figure 22: Inhibitory effect of screened compounds toward P-gp overexpressing cell line A2780adr (a) and MRP1 overexpressing cell line H69AR (b) in the calcein AM assay at a concentration of 10 µM. Cyclosporine A (CsA) was used as positive control, indicating complete inhibition. The inhibitory effect of each compound is expressed by the length of the bars, representing the inhibition compared to the positive control in percent. For each compound, three independent experiments were performed and the standard deviation is expressed by error bars.

Similar results were observed in the screening of the inhibitory potency toward ABCC1. Compounds **10**, **14**, **24**, **26**, **35**, **37** and **39** were found to possess more than 25% inhibition relative to CsA. Again, the quinoline derivatives obtained higher rates of inhibition in comparison to the quinazoline derivatives. A possible explanation for this phenomenon could be the basic character of the nitrogen atom in the quinoline structure with a calculated pK_a of 8.4 vs 5.6 for the quinazoline structure. Meaning that the quinoline derivatives would be mostly protonated while the quinazolines were mostly neutral under physiological pH.

Table 9: Inhibitory Activity of Compounds Exhibiting an Inhibition of more than 25% in Comparison to the Reference Cyclosporine A (CsA) in the Calcein AM Assay at a Concentration of 10 µM.

	R^1	R^2	Calcein AM (ABCB1) IC_{50} ± SD [µM][a,b]	Calcein AM (ABCC1) IC_{50} ± SD [µM][a,c]
10	N	3-SMe	n.d.	3.73 ± 0.51
13[d]	N	3,4-OMe	1.86 ± 0.30	n.d.
14	N	3,5-OMe	2.43 ± 0.44	6.91 ± 0.97
24	N	4- COOMe	n.d.	8.13 ± 1.40
26	N	4- COOH	n.d.	8.77 ± 0.77
28	N	3-Me	3.00 ± 0.26	n.d.
35	C	3-CN	5.06 ± 0.70	6.52 ± 0.91
36	C	4-CN	4.74 ± 0.32	n.d.
37	C	3-NHCOMe	0.664 ± 0.17	5.80 ± 0.94
38	C	3-OMe	2.87 ± 0.20	n.d.
39	C	3-SMe	1.42 ± 0.14	2.98 ± 0.38
CsA[e]			1.17 ± 0.17	3.77 ± 1.03

[a]: IC_{50} values were determined by three independent experiments.
[b]: The P-gp overexpressing cell line A2780adr was used.
[c]: The MRP1 overexpressing cell line H69AR was used.
[d]: Compound was synthesized previously.[198]
[e]: CsA is used as reference for both assays.
n.d.: Not determined, due to low effect in the initial screening.

Moreover, it is known that ABCC1 is capable of transporting anionic molecules which have sufficient lipophilicity to enter the membrane.[50] Interestingly, compound **26** containing a carboxylic acid function demonstrates some inhibitory potency toward ABCC1 but not ABCB1. This could be due to deprotonation of the carboxylic acid function at pH 7.4, forming an anionic species. Moreover, there is evidence that compound **24** undergoes cleavage of the methoxy ester by intracellular esterases forming a carboxylate function. This theory is substantiated by the very similar IC_{50} values of compounds **24** and **26** but is in contrast to the results from the Hoechst 33342 accumulation assay. A possible explanation for this is the use of different cell lines in both assays.

In comparison a higher inhibitory potency resulted toward ABCB1 than ABCC1 for the majority of compounds.

3.4 Investigation of the intrinsic cytotoxicity with the MDCK II cell lines in a MTT assay

The intrinsic cytotoxicity of selected compounds was investigated in a MTT assay using MDCK II parental and ABCG2 overexpressing cells. Toxic effects were measured after 72 h incubation of the cells in the presence of different compound concentrations using 3-(4,5-dimethylthiazol-2-yl)-2,5-diphenyltetrazolium bromide (MTT) as indicator of the cell viability. Due to the fact that living cells are capable of reducing MTT via mitochondrial and other unspecific reductases to a purple formazan species cell viability can be correlated with the spectrometrically measured absorption of the dye. Further details regarding the assay are provided in chapter 10.2.2.5.

From the obtained absorption values a concentration-response curve could be fitted yielding characteristic values like the GI_{50}. This determinant describes the corresponding compound concentration which reduces the cell survival to 50% of the control. Due to the fact that small amounts of MeOH (≤1.8%) and DMSO (≤1%) were used for the preparation of the compound dilutions, a control was carried out giving the toxic effect in the absence of a compound (GI_{50}: 96.1 µM; BCRP). Moreover, a therapeutic ratio (TR) was calculated from GI_{50}/IC_{50} providing information about possible benefits, for instance regarding application of a compound in clinical trials.

The obtained GI_{50} values and the corresponding TRs are depicted in Table 10. For better comparison, the TR is also illustrated as bar chart in Figure 23.

Table 10: Intrinsic Toxicity and Therapeutic Ratio of Selected Compounds on MDCK II ABCG2 Overexpressing and Parental Cells.

Compound	R^1	R^2	GI_{50} [µM][a] BCRP	GI_{50} [µM][a] Parental	Therapeutic ratio (GI_{50}/IC_{50}) [b]
1	N	H	27	26	30
3	N	3-NO_2-4-OH	52	150	660
5	N	4-CN	8.0	17	110
6	N	4-OH	12	27	60
8	N	3-NHCOMe	13	31	46
13[c]	N	3,4-OMe	23	17	150
18	N	3-F	17	28	49
19	N	4-F	29	26	27
21	N	4-Cl	6.8	15	8.1
22	N	3-I	15	17	19
23	N	4-I	9.3	8.9	15
28	N	3-Me	13	24	11
Gefitinib			1.4	2.1	0.80
Ko143			11	11	49
Quercetin			46	33	
MeOH/DMSO			96[d]	140[d]	

[a]: *Concentration leading to 50% of cell survival of MDCK II BCRP and parental cells. The data was obtained from at least two independent experiments as mean values.*

[b]: *The therapeutic ratio of selected compounds is calculated from the ratio of GI_{50} to IC_{50} values, derived from MTT viability assay and Hoechst 33342 accumulation assay with ABCG2 overexpressing MDCK II BCRP cells.*

[c]: *Compound was previously synthesized.*[198]

[d]: *Positive control of the cytotoxicity from dilution with DMSO/MeOH without compound.*

Among all test compounds a moderate intrinsic cytotoxicity was found which was mostly lower than that of Ko143 (GI_{50}: 11.1 µM). To ponder the benefit of a compound for further studies, its IC_{50} value must also be taken into account yielding a TR. In this regard the potent standard inhibitor Ko143, often described in literature as “nontoxic”, obtained a TR of 49 with MDCK II ABCG2 overexpressing cells.

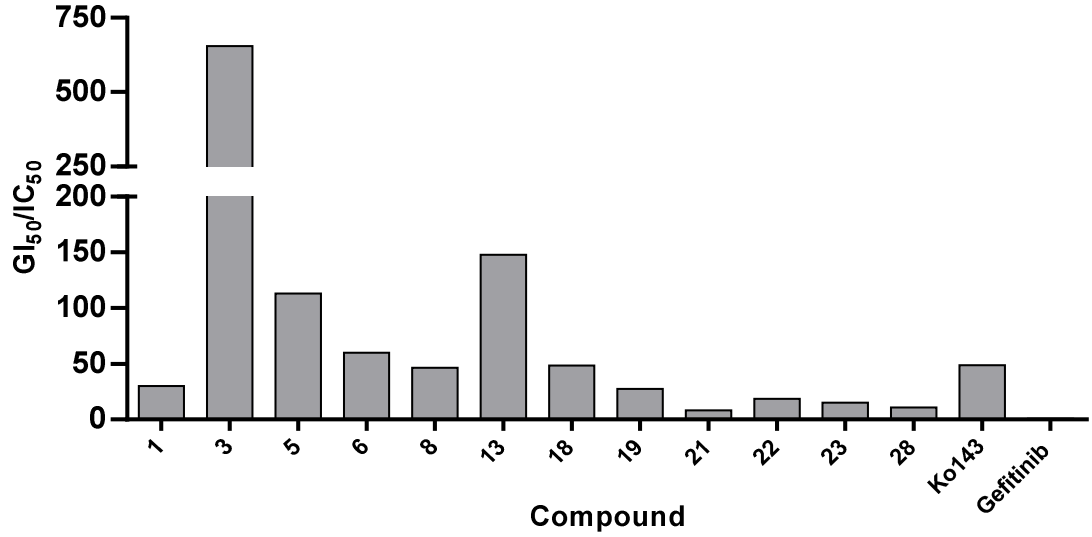

Figure 23: Therapeutic ratio of selected compounds, calculated from the ratio of GI_{50} to IC_{50}-values, derived from MTT viability assay and Hoechst 33342 accumulation assay with ABCG2 overexpressing MDCK II BCRP cells. The highest score was obtained with compound ***3*** *(GI_{50}/IC_{50} = 655), while the reference compound Ko143 yielded GI_{50}/IC_{50} = 48.9.*

Interestingly, the most potent compounds from the Hoechst 33342 accumulation assay, namely **3** and **5**, exhibited significant differences in their toxicities obtaining GI_{50} values of 52.4 µM and 7.96 µM, respectively. Corresponding concentration-response curves of both compounds including the determined toxicity of MeOH/DMSO without compound are illustrated in Figure 24.

The disubstitution with 3-nitro and 4-hydroxy carried out for compound **3** led to the highest TR of 655 in this subset. This finding is particularly startling, since compound **6**, containing a monosubstitution with 4-hydroxy, exhibited a considerably higher cytotoxicity (GI_{50}: 12.2 µM). Although it is known that nitro and cyano functions can contribute to increased toxic effects, this is not the case for the disubstituted compound **3**.

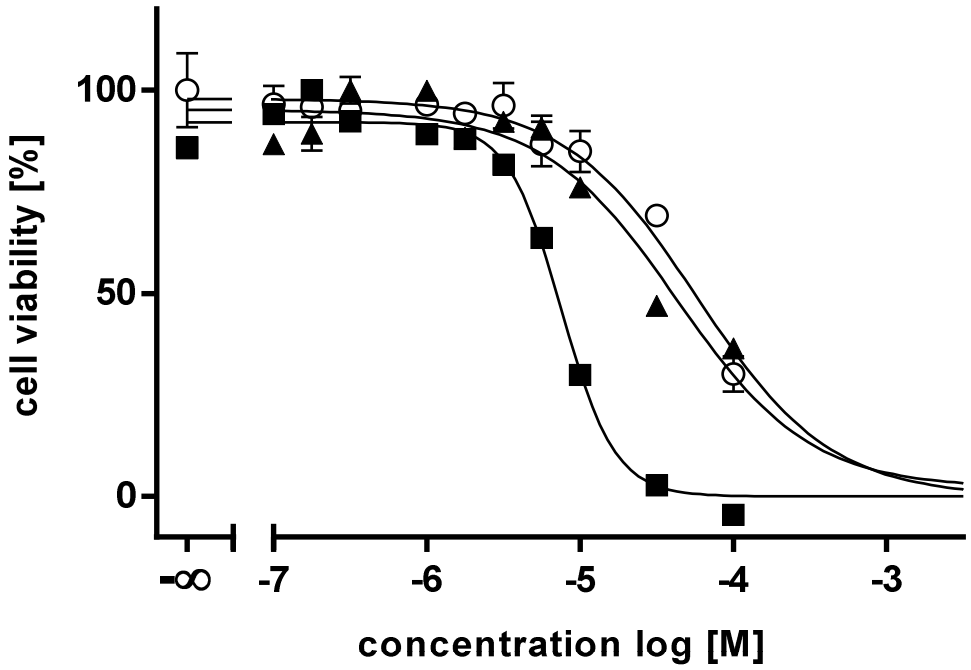

*Figure 24: MTT viability assay of compound **3** (▲, GI_{50} = 52.4 µM) and **5** (■, GI_{50} = 7.96 µM) using the ABCG2 overexpressing cell line MDCK II BCRP. A control with the same concentration of MeOH and DMSO (○, GI_{50} = 71.5 µM), analogue to the dilution of the compounds, was carried out for comparison. The amount of MeOH and DMSO used for the dilution was ≤ 1.8% and ≤ 1.0%, respectively.*

Regarding *meta* and *para* substituents, distinct differences in cytotoxicity were observed for some compound pairs like **18/19** or **22/23**. Similar differences between the *meta* and *para* derivatives have already been discussed in terms of the inhibitory potency investigated in the Hoechst 33342 accumulation assay. It is likely that these derivatives occupy different binding pockets at ABCG2 or exhibit a different interaction with the transport protein. More evidence to this suggestion is provided in the following chapters.

3.5 Investigation of the reversal of multidrug resistance

Multidrug resistance toward cytostatic drugs like SN-38 or MX is often related to an overexpression of ABCG2, which facilitates the active efflux of the drugs out of the cell.

Since some cytostatic drugs are substrates of ABCG2 the cellular resistance to these drugs can be overcome by co-administration with potent inhibitors. Inhibition of the transport protein leads to a reduced efflux of cytostatic drugs resulting in an increased intracellular accumulation and lower cell viability. The measured cell viability can then be correlated to the inhibitory efficacy of the co-administered compound.

For this subset the cytostatic agents Hoechst 33342 and SN-38 were investigated, since they are both substrates of ABCG2. The assay was carried out with the ABCG2 overexpressing MDCK II BCRP and parental cell line. Due to the lack of transport proteins, parental cells show no resistance toward the cytostatic drugs and were used as control indicating "total inhibition" of ABCG2. In contrast the ABCG2 overexpressing MDCK II BCRP cell line exhibits resistance toward the drugs, which can be reduced by co-administering different concentrations of an inhibitor. More details regarding the execution of the assay are provided in chapter 10.2.2.6. The investigation was carried out with the most potent compounds, **3** and **5**. Both compounds were able to achieve a full reversal of the MDR in MDCK II BCRP cells toward SN-38 and Hoechst 33342 at low concentrations of about 5 µM. Corresponding concentration-cell viability curves for compound **3** and **5** in the presence of Hoechst 33342 and SN-38 are depicted in Figure 25.

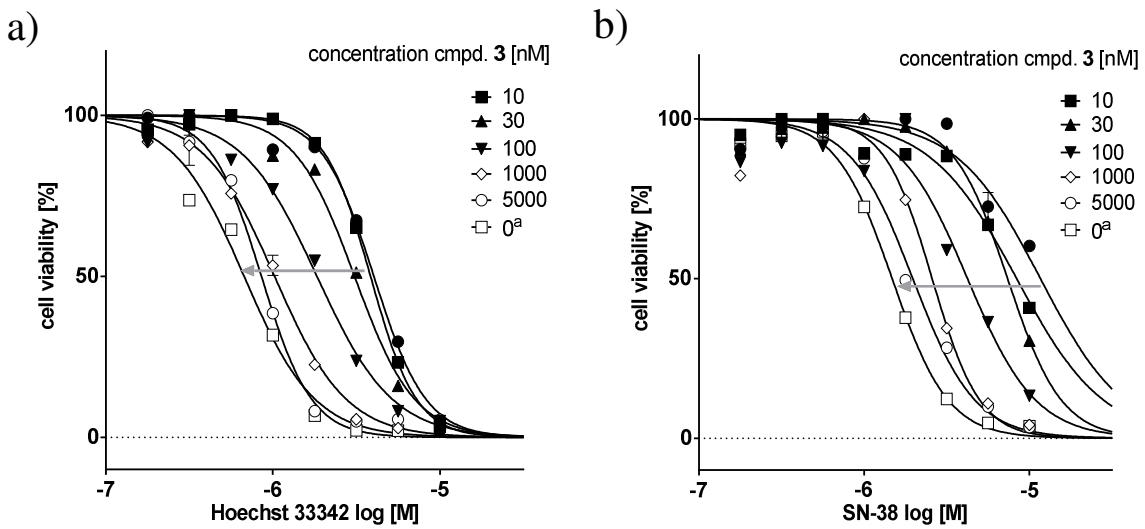

Figure continues on the next page

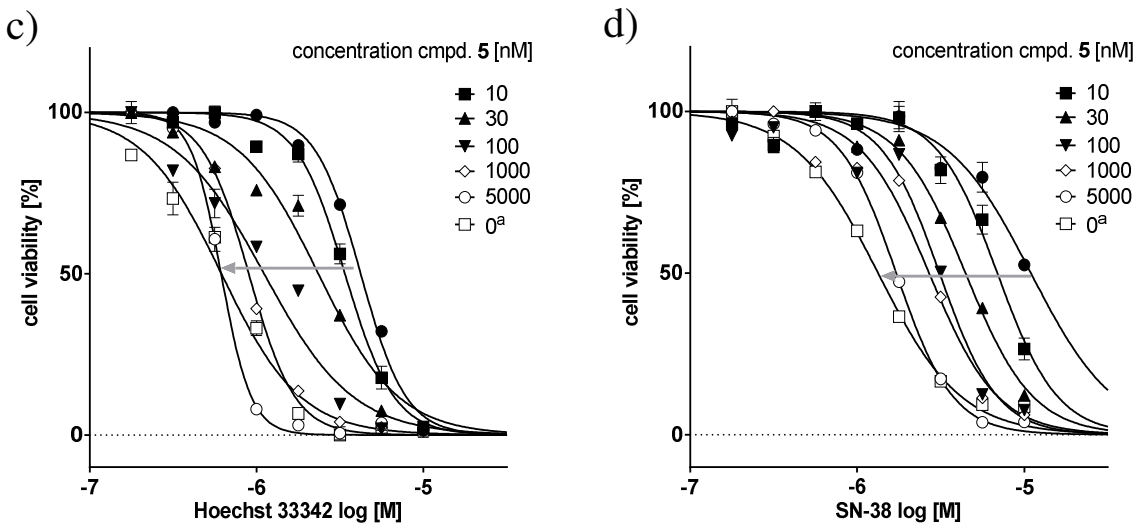

*Figure 25: MDR reversal assay of compound **3** (a, b) and **5** (c, d), demonstrating the ability to reverse the MDR toward the cytostatic drugs Hoechst 33342 (a, c) and SN-38 (b, d), using parental MDCK II and ABCG2 overexpressing cell lines. The grey arrows indicate the increasing sensitization of the ABCG2 overexpressing cells with higher compound concentrations (see legend). At a compound concentration of 5 µM, full reversal is achieved, indicated by a similar IC_{50} value as the parental cells.*
a: parental MDCK II cells.

A full reversal of MDR is indicated by the concentration-response curves with similar GI_{50} values of the parental cells and the ABCG2 overexpressing cells in the presence of the corresponding inhibitor. The grey arrows indicate the increased sensitization toward the corresponding cytostatic drug with increasing compound concentration. This can also be visualized by plotting the pGI_{50} values from the concentration-effect curves obtained in the MDR reversal assay against the logarithm of the compound concentration. Hereby, concentration-efficacy curves can be fitted with the logistic equation yielding EC_{50} values that characterize the extent of MDR reversal by a compound. The resulting sigmoidal curves are depicted in Figure 26.

According to the plot, a very similar efficacy was obtained for both inhibitors in the presence of Hoechst 33342 and also SN-38. For compound **3** an EC_{50} value of 132 nM for Hoechst 33342 and 161 nM for SN-38 were calculated. In comparison to the Hoechst 33342 accumulation assay (IC_{50}: 81.1 nM) the derived EC_{50} values obtained from the MDR reversal assay are slightly higher. Compound **5** on the other hand obtained IC_{50} values of 52.9 nM and 46.5 nM in the MDR reversal assay in co-administration of

Hoechst 33342 and SN-38, respectively. Hence, the efficacy of compound **5** is estimated slightly higher than suggested by the Hoechst 33342 accumulation assay (IC_{50}: 70.0 nM).

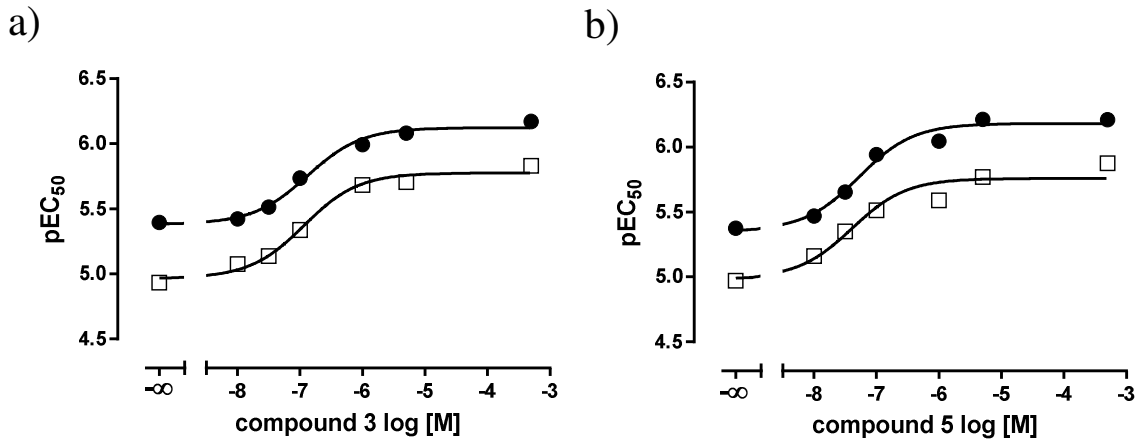

*Figure 26: Plot of the pGI_{50} values, determined in the MDR reversal assay (Figure 25), against the corresponding concentration of compound **3** and **5**, respectively. The efficacy of sensitization toward the corresponding cytostatic is indicated by the pEC_{50} value corresponding to a reversal of MDR by 50%. The pGI_{50} of the parental cells defines "total sensitization" of ABCG2, while the pGI_{50} of the resistant cell line defines "no sensitization", depicted in the figure by –∞ and -3, respectively. For compound **3** (a) IC_{50} values of 132 nM (● Hoechst 33342) and 161 nM (□ SN-38) were determined. Compound **5** (b) yielded IC_{50} values of 52.9 nM (● Hoechst 33342) and 46.5 nM (□ SN-38).*

Investigation of the factor of resistance (F_r), given by the ratio of the GI_{50} in the resistant cell line to the GI_{50} of the sensitive cells in the presence of a cytostatic drug, obtained a mean value of 6.40 for Hoechst 33342 and 7.95 for SN-38. Hence, the ABCG2 expressing cell line exhibits a slightly decreased sensitivity toward SN-38 compared to Hoechst 33342.

Additionally, the sensitization of the ABCG2 overexpressing MDCK II BCRP cell line toward the cytostatic drug MX, which is also a substrate of ABCG2, was investigated in the presence of compound **3** and **5**. Similar to SN-38, co-administration of an inhibitor of ABCG2 leads to increased intracellular concentrations of MX owing to a reduced efflux out of the cell. As a result a greater decrease in cell viability is observed than in absence of an inhibitor. The assay was carried out at different compound concentrations in the presence and absence of 0.5 µM MX. Further details of the assay are provided in chapter 10.2.2.7.

The bar charts in Figure 27 illustrate that both compounds were able to reverse the resistance of the ABCG2 overexpressing cells toward MX.

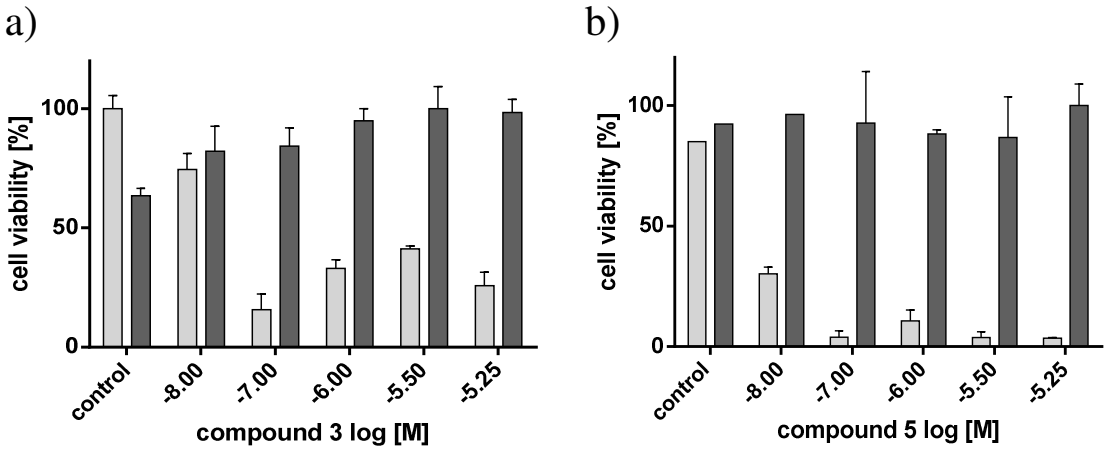

*Figure 27: MDR reversal assay of compounds **3** (a) and **5** (b), demonstrating their ability to reverse MDR toward the cytostatic mitoxantrone (MX), in the ABCG2 overexpressing cell line MDCK II BCRP. The bars represent the cell viability at a given modulator concentration in the presence (light grey) and absence (dark grey) of 0.5 µM mitoxantrone. Control shows viability of cells without modulator. The standard deviation is expressed by error bars.*

Half-maximal growth inhibition (GI_{50}) was achieved for compound **3** at 68.4 nM and for **5** at 4.41 nM. Due to few measurements, the determined values in the MDR reversal assay with MX are more susceptible to error than with SN-38, but still provide a good estimation of the efficacy of a compound.

Overall, compound **5** demonstrated a considerably high potency in MDR reversal assays using SN-38, Hoechst 33342 and MX, suggesting a somewhat higher inhibitory potency than determined in the Hoechst 33342 accumulation assay. The inhibitory potency of compound **3** in the MDR reversal assays concurs very well with the results of the Hoechst 33342 accumulation assay. Also, the differences between the calculated IC_{50} values obtained with Hoechst 33342 and SN-38 exhibit a good correlation for both compounds, meaning there is probably no significant difference regarding the substrate specificity of ABCG2 toward both cytostatic drugs.

3.6 Investigation of the interaction with Hoechst 33342

The interaction of selected compounds with Hoechst 33342 was investigated using ABCG2 overexpressing MDCK II BCRP cells. Varying compound concentrations were combined with varying concentrations of Hoechst 33342 and the interaction type could be determined using the Lineweaver-Burk double reciprocal plot, described in chapter 10.2.2.8. This method provides information about the compound interacting with Hoechst 33342 either in a competitive, non-competitive or uncompetitive manner using a relatively simple graphical method.

Although the Lineweaver-Burk method can be susceptible to experimental errors due to the double reciprocal plot, it provides preliminary results that can be compared to other methods like the Cornish-Bowden direct linear plot. A summary of the results obtained with the Lineweaver-Burk method is presented in Table 11 listing the intersection of the straight lines together with the corresponding interpretation. A selection of the corresponding plots is depicted in Figure 28.

Table 11: Interaction with Hoechst 33342 According to the Lineweaver-Burk Double Reciprocal Plot.

Compound	**Substituent R^2 (R^1 = N)**	**Intersection**	**type of interaction with Hoechst 33342**
3	3-NO_2-4-OH	2. Quadrant	Non-competitive mixed type
4	3-CN	X-axis	Non-competitive
5	4-CN	2. Quadrant	Non-competitive mixed-type
17	3-Me-4-I	Y-axis	Competitive
18	3-F	2. Quadrant	Non-competitive mixed-type
19	4-F	X-axis	Non-competitive
20	3-Cl	2. Quadrant	Non-competitive mixed-type
21	4-Cl	Y-axis	Competitive
22	3-I	X-axis	Non-competitive
23	4-I	3. Quadrant	Non-competitive mixed-type
Ko143		3. Quadrant	Non-competitive mixed-type

Since a non-competitive interaction with Hoechst 33342, mostly of the "mixed type", was found to be the predominant mechanism, compounds **17** and **21** take a peculiar role due to their competitive interaction. It is likely that both compounds bind to the same pocket or at least have a high impact on the binding of Hoechst 33342. Further studies with the conformational sensitive 5D3 antibody binding (see chapter 3.7) and the ATPase activity assay (see chapter 3.8) substantiated the differences that were observed in the interaction type investigation, distinguishing non-competitive inhibitors from those of the "mixed type" and the competitive inhibitors.

Another striking point is the distinction of compounds by the position of their substituent (*meta* or *para*) according to their interaction with Hoechst 33342 (e.g. compounds **4** and **5**; **18** and **19**; **20** and **21**; **22** and **23**). The same observation was mostly made for the IC_{50} values in the Hoechst 33342 accumulation assay resulting in different inhibitory potencies of the *meta* and *para* derivatives.

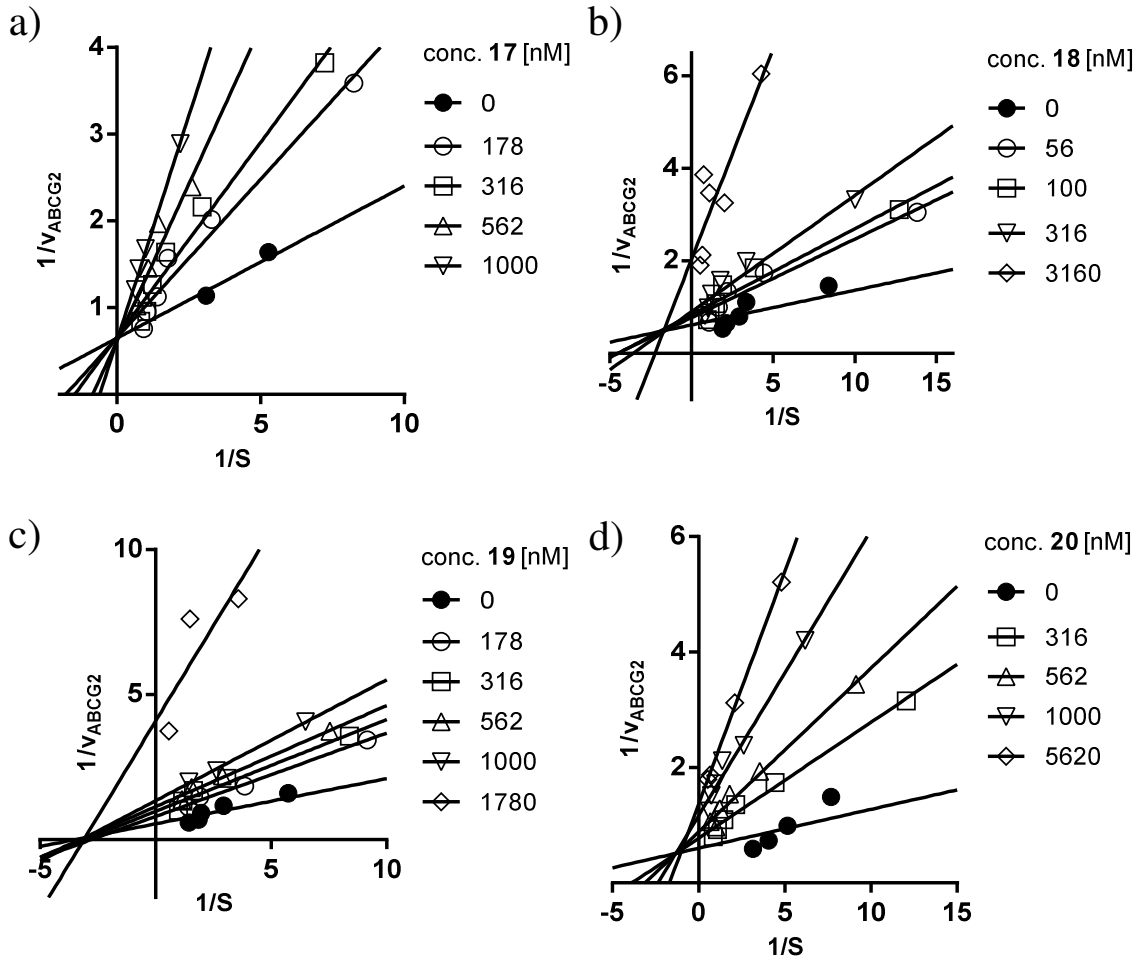

Figure continues on the next page

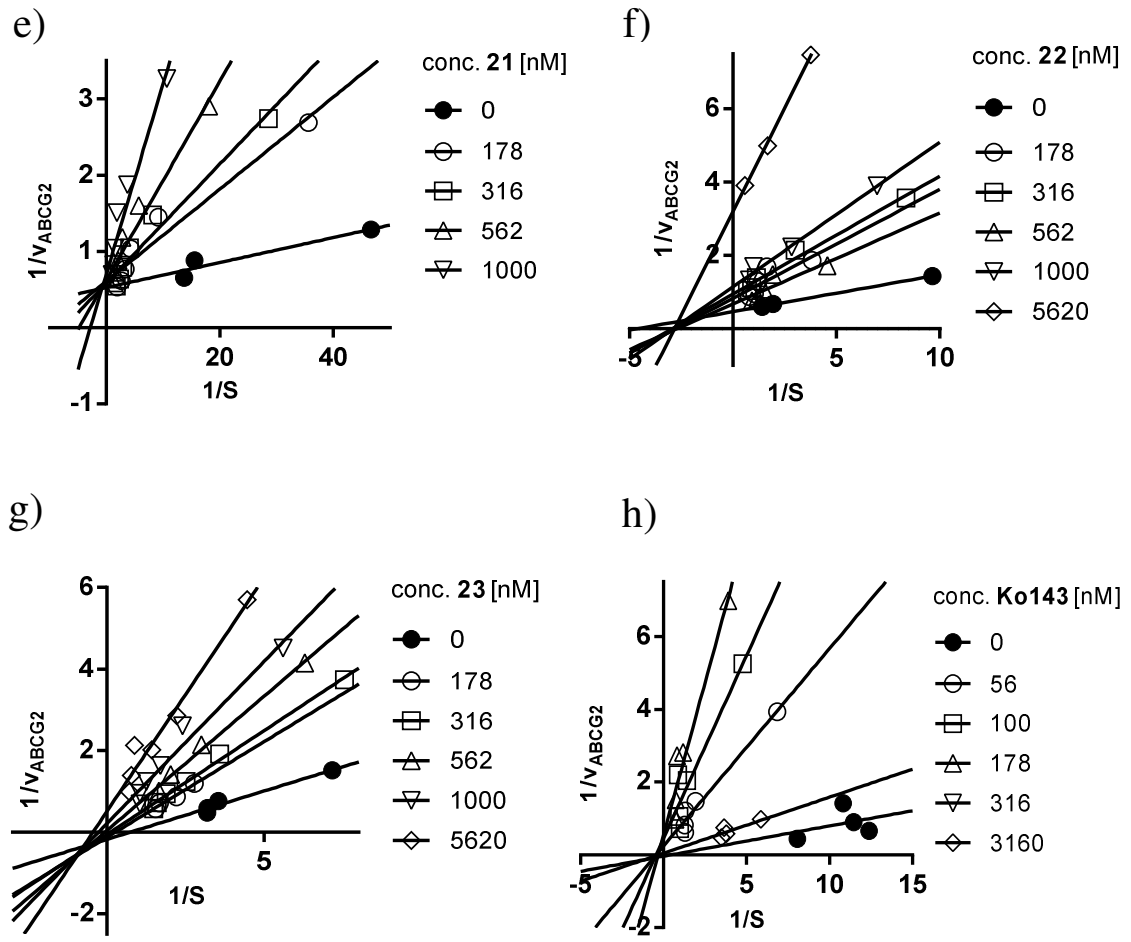

*Figure 28: Double-reciprocal plot according to Lineweaver-Burk for selected compounds **17** (a), **18** (b), **19** (c), **20** (d), **21** (e), **22** (f), **23** (g) and **Ko143** (h). Compound concentrations are specified in the legend.*

In order to validate the results from the Lineweaver-Burk double reciprocal plot, the Cornish-Bowden method was applied (see chapter 10.2.2.8). A direct linear plot of the data produces the corresponding V_{max} and K_M values for each inhibitor concentration. By means of the trend regarding the values toward increasing compound concentration a non-competitive (V_{max} ↓, K_M ↔), competitive (V_{max} ↔, K_M ↑) or "mixed-type" (V_{max} ↓, K_M ↑) interaction with Hoechst 33342 is suggested. For better comparison, linear regression of the V_{max} and K_M values was performed and the obtained slopes summarized as scatter plot in Figure 29.

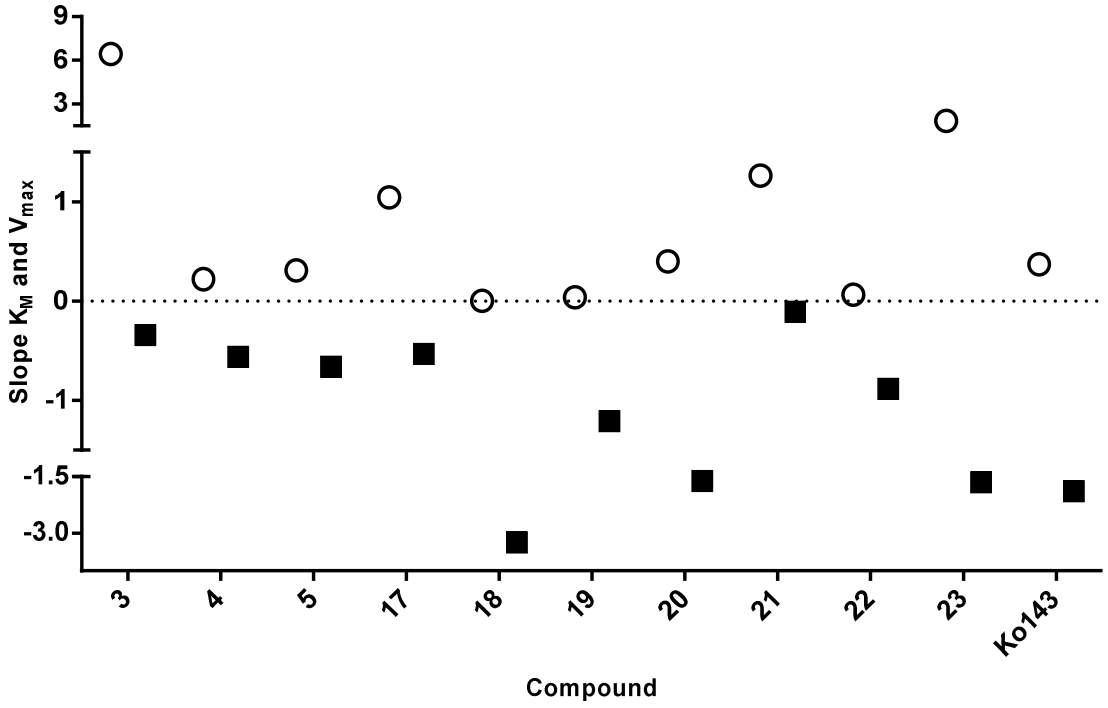

Figure 29: Scatter plot of the calculated slopes obtained from the linear regression of K_M (○) and V_{max} (■) values according to the Cornish-Bowden direct linear plot.

Obtained results are in accordance with the type of interaction determined from the Lineweaver-Burk double reciprocal plot. Corresponding Cornish-Bowden plots of selected compounds are depicted in Figure 30. Compounds with considerably high competitive character like **3**, **17**, **21** and **23** obtained high positive slopes for K_M. On the other hand, compound **18**, **19**, **20**, **22**, **23** possess a high negative slope for V_{max} which is characteristic for compounds with a non-competitive interaction. Interestingly, all of the compounds showing a high portion of competitive interaction contain a *para* substitution, mostly with lipophilic halogen atoms of a high atomic number like chlorine and iodine. In contrary, an increased non-competitive character was frequently observed for *meta* substituted derivatives.

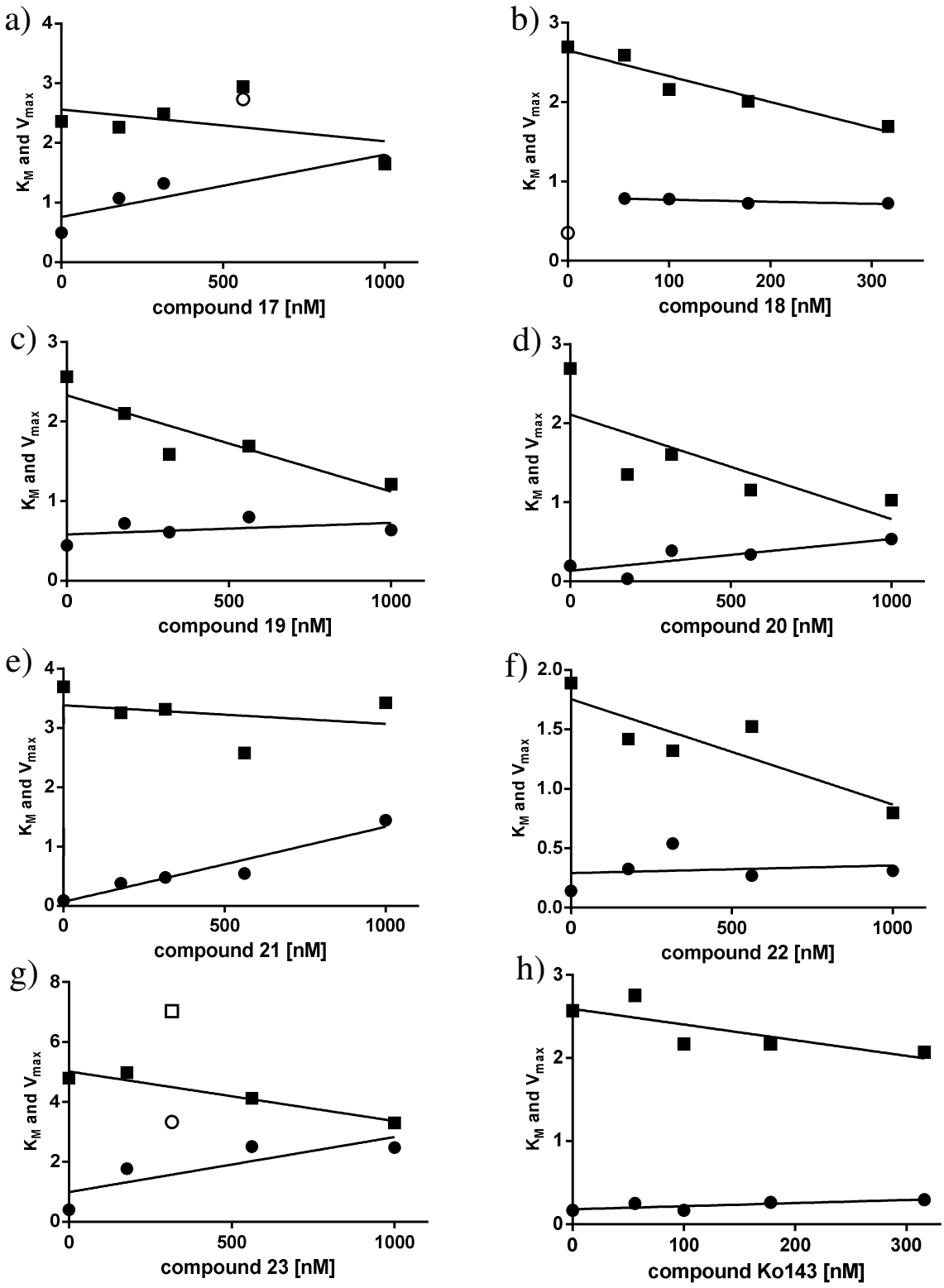

*Figure 30: Direct linear plot for compound **17** (a), **18** (b), **19** (c), **20** (d), **21** (e), **22** (f), **23** (g) and **Ko143** (h) according to Cornish-Bowden. For better visualization of the slopes linear regression of the V_{max} (■) and K_M (●) values was performed. Excluded values are depicted as open symbols of the corresponding shape.*

The change of the interaction type observed for several compounds like the 3-chloro and 4-chloro derivatives **20** and **21** is particularly interesting, as it suggests different binding pockets for those derivatives. According to the Lineweaver-Burk plot and the Cornish-Bowden plot, the phenomenon of different types of interaction of *meta* and *para* derivatives containing the same substituent was observed for most of the investigated compounds.

3.7 Investigation of the conformation sensitive 5D3 antibody binding to an epitope of ABCG2

The investigations of the conformational impact of a compound on ABCG2 was carried out with the conformation sensitive 5D3 antibody using the ABCG2 overexpressing PLB-985 cell line. This antibody binds specifically to an epitope of ABCG2 indicating intramolecular changes. The fluorescence measured by a FACSCalibur flow cytometer originating from the bound 5D3 antibody-fluorophore conjugate correlates with the conformational change of ABCG2. A shift in fluorescence, called a "5D3-shift", is observed when the co-administration of a compound produces a different rate of labelling in ABCG2 than without compound. Additional information about the assay is provided in chapter 10.2.2.9.

Prior studies suggested that the monoclonal antibody can serve as a sensitive tool to study intramolecular changes but also reflects ATP binding, the formation of a catalytic intermediate, or substrate inhibition within the transport cycle of the ABCG2 protein.[200] It was found that substrates often induced a smaller shift than inhibitors of ABCG2.[201]

Some compounds exhibit concentration dependent properties, they can act as substrates at low concentrations and as inhibitors at high concentrations as asserted for ABCB1.[202] Hence, this assay can also be used to detect a change in a concentration dependent binding mode (e.g. binding pocket, substrate/inhibitor) of a compound indicated by a significant change in the 5D3-shift.

Some 5D3-shifts of selected commercially available drugs are depicted as a bar chart in Figure 31 (black bars). The amount of labelling obtained by the standard inhibitor of ABCG2, namely Ko143, was set to 100%. Both concentrations of 10 µM and 25 µM

yielded a comparable degree of labelling with 5D3 antibody. A considerably lower shift was found for Hoechst 33342 at 10 µM which is known to be a substrate of ABCG2. The flavonoid quercetin, which is also a substrate of ABCG2, gives comparable results to Hoechst 33342, and exhibits only a small shift at the concentrations of 10 and 25 µM, which was also found in other studies.[203, 204] In contrast, the TKIs and inhibitors of ABCG2 gefitinib and elacridar show an increased shift at 10 µM. Interestingly, the shift caused by elacridar is very similar to Ko143.

For better comparison, a dotted line was introduced in the bar chart (Figure 31) indicating the amount labelling obtained by Hoechst 33342 at 10 µM.

Highest shifts were obtained with compounds **17** (1 µM: 88%) and **23** (10 µM: 82%) both containing a 4-iodo substituent. Notably, both compounds exhibited an exclusively competitive interaction with Hoechst 33342. In contrary, compounds with a high non-competitive character (**3**, **4**, **18**, **19**, **20**, **22**) predominantly resulted in shifts lower than the average of 61% at a concentration of 10 µM. Noticeable differences for instance between a *meta* iodo (**22**) and *para* iodo (**23**) derivatives that have already been observed in the interaction type investigation (see chapter 3.6), were also found in the 5D3 antibody binding assay: both compounds exhibit an increasing shift toward higher compound concentrations. However, this effect is much more pronounced for compound **23**, resulting in increasingly higher shifts than **22** at equivalent concentrations. This indicates that both compounds bind to a different site on ABCG2 or possibly to several binding pockets of different affinities, which could depend on the compound concentration. The substantially different effects of both compounds, including other *meta*/*para* derivatives, on the ATPase activity is discussed in chapter 3.8.

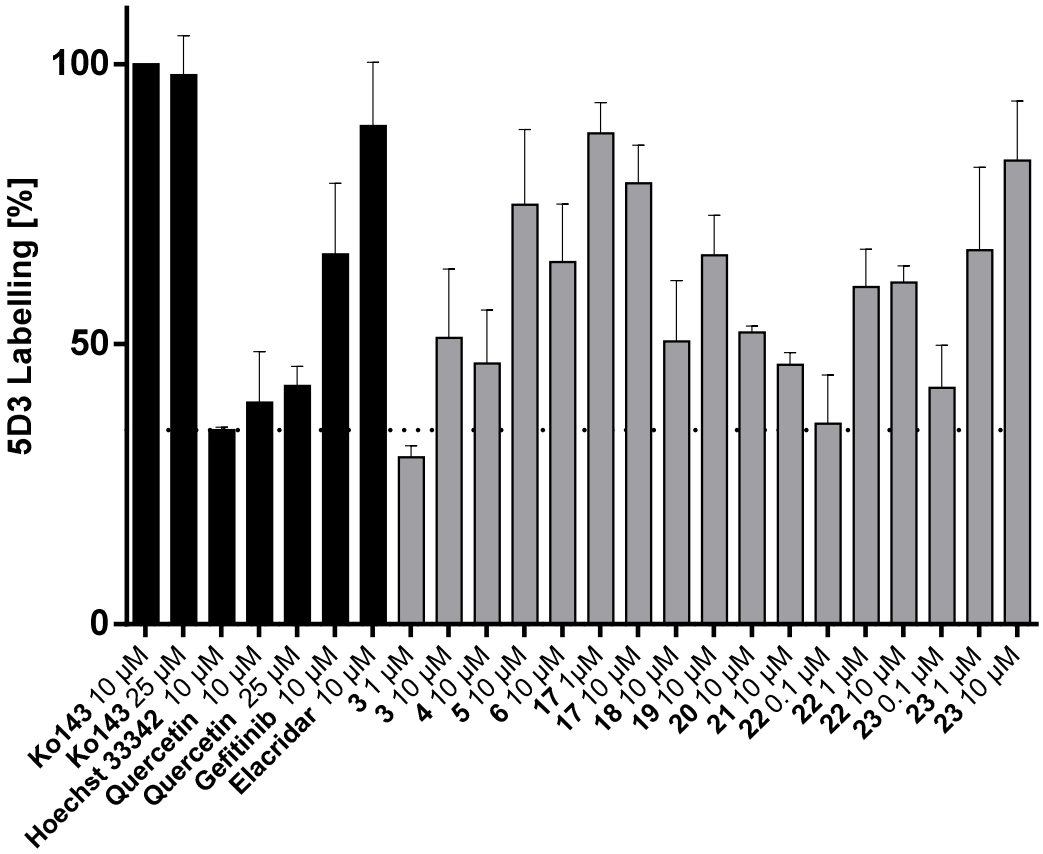

Figure 31: 5D3 immunoreactivity modulation of ABCG2 by commercial compounds (black bars) and various compounds at different concentrations (grey bars). Fluorescence detected by the 5D3-labeling of ABCG2 in the presence of 10 µM Ko143 was set to 100% and the fluorescence measured in the absence of any compound taken as 0%. The dotted line represents the labelling obtained with 10 µM of Hoechst 33342.

Compound **3** with the second highest inhibitory potency among all compounds yielded only a moderate shift of 51% with regard to Ko143. However, the majority of the compounds exhibited a rate of labelling far above that of the substrate Hoechst 33342 (35%, dotted line) or quercetin (40%). According to the results, there was no correlation between the observed 5D3-shifts and the IC_{50} values determined in the Hoechst 33342 accumulation assay. Representative histograms of compound **3, 17** and Ko143 at 10 µM are illustrated in Figure 32.

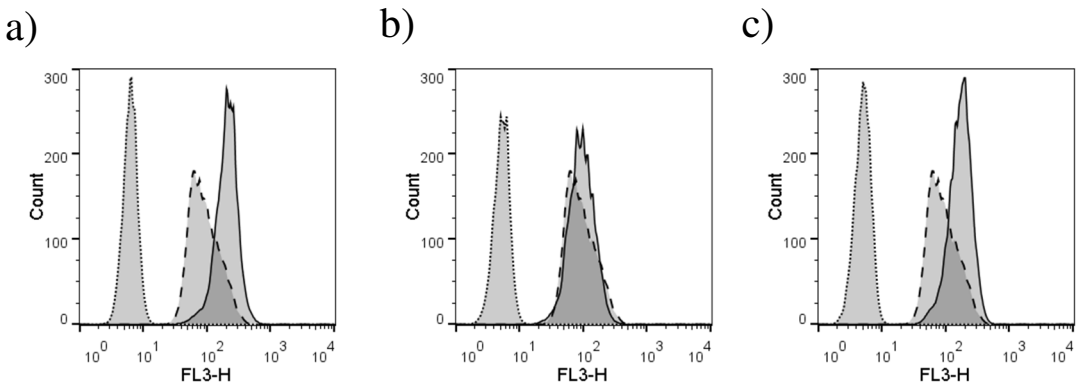

Figure 32: Histogram of the measured fluorescence at the FL3-H detector (X-axis) and the cell-count gated according to the fluorescence. Depicted is the fluorescence of the isotype-control (dotted curve) as well as of 5D3 antibody in the absence of a compound (dashed curve) and in the presence of a compound (continuous curve). Investigated compounds with the highest and lowest 5D3 shifts: ***Ko143*** *(a),* ***3*** *(b) and* ***17*** *(c) at a concentration of 10 µM.*

Fluorescence of the isotype-control in presence of the corresponding compound is given as a dotted line. This is necessary to exclude an unspecific staining, which was considerably low for all compounds. Also, the obtained fluorescence with 5D3 antibody in the absence (dashed curve) and presence (continuous curve) of a compound is illustrated in the figure. High shifts were found for Ko143 and **17**, whereas **3** resulted in a minor shift.

3.8 Investigation of the ATPase activity

The study of the ATPase activity in presence of a compound provides important information about the transport activity or related processes in ABCG2 leading to hydrolysis of ATP. In the simplest instance ATP consumption is associated with an active transport of substrates by ABCG2. Cleavage of ATP forms inorganic phosphate (Pi) that can be measured colorimetrically giving an estimation of the transport activity of the protein. But first, the transport unspecific ATP hydrolysis must be taken into account by adding orthovanadate that is able to efficiently inhibit the activity of ABC transport proteins. Subtraction of this so-called insensitive vanadate ATPase activity from the total ATPase activity yields the specific ATPase activity that is solely associated with the

transport protein. Moreover, the basal activity detected for the basic function of the protein in the absence of a compound was measured. For the assay Ko143 was used as the standard ATPase inhibitor and quercetin as the standard stimulator using High Five insect cell membrane preparations. The ATPase activity assays were performed by Jennifer Gallus. Further details are provided in chapter 10.2.2.10.

The investigation was carried out with selected compounds, including the most potent ones, at three concentrations (0.1, 1 and 10 µM). A clear relation between the substitution pattern and the ATPase activity was observed for most compounds. The obtained results are presented as a bar chart in Figure 33.

Stimulation was found for the unsubstituted compound **1** and most of the *meta* substituted derivatives like **4**, **18**, **20** and **22**. All compounds containing a *para* substituent exhibited an ATPase activity at the basal level or below, except for compound **6** containing a *para* hydroxy substituent. It is particularly striking that the observed differences between *meta* and *para* derivatives with the same substituent have such a substantial impact on the ATPase activity, as illustrated by the *meta*/*para* compound pairs **4/5**, **18/19**, **20/21** and **22/23**. It is very likely that a different mode of binding to ABCG2 is responsible for this result. This suggestion is also in accordance with the results of other assays presented above.

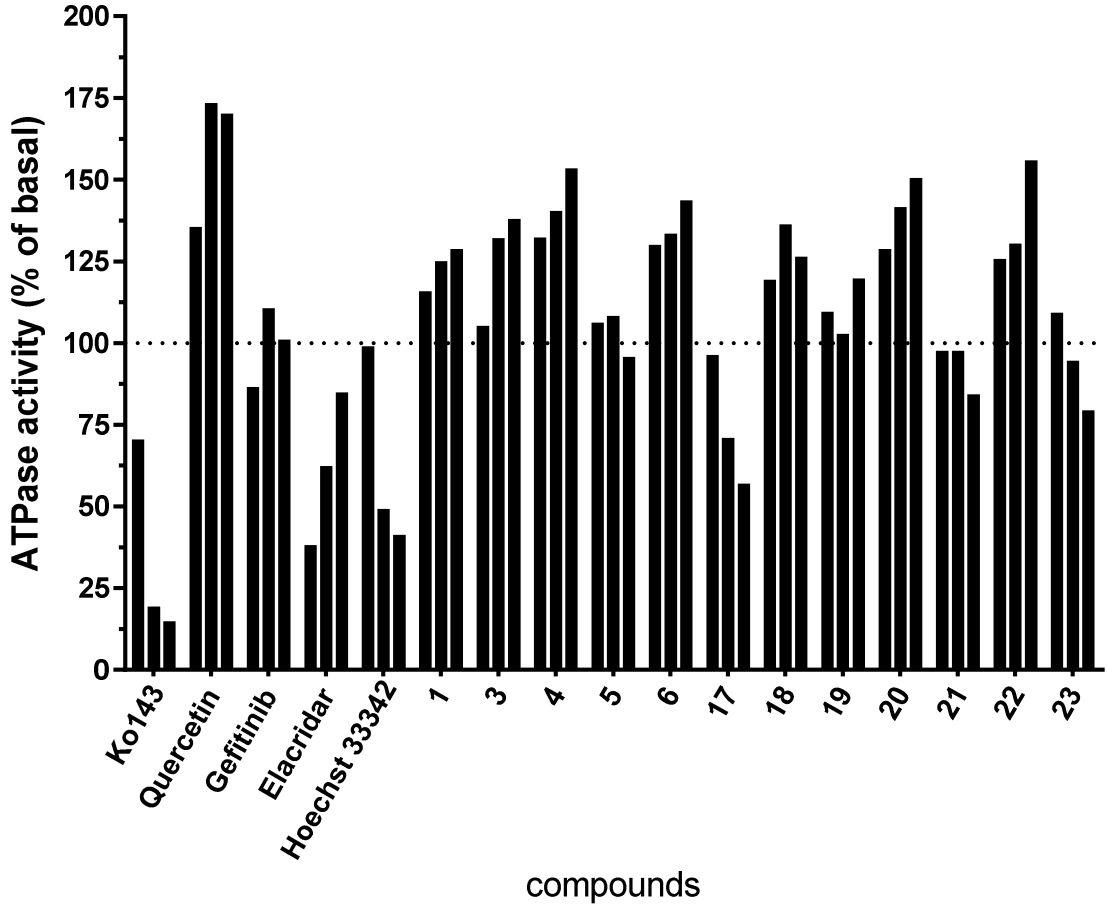

Figure 33: Screening of ATPase activity of selected compounds at three different concentrations. From left to right the bars correspond to 0.1, 1 and 10 µM final concentration of compound. Quercetin was used as a standard for activation of ABCG2 ATPase activity. All values are relative vanadate-sensitive ATPase activities in relation to the basal activity, which is set to 100%.

Concentration-response curves using several compound concentrations are depicted in Figure 34. Regarding the *meta* and *para* iodo derivatives **22** and **23** a very different effect on the ATPase activity was found: Compound **22** showed a strong stimulation whereas **23** inhibited the ATPase activity with increasing compound concentrations below basal level.

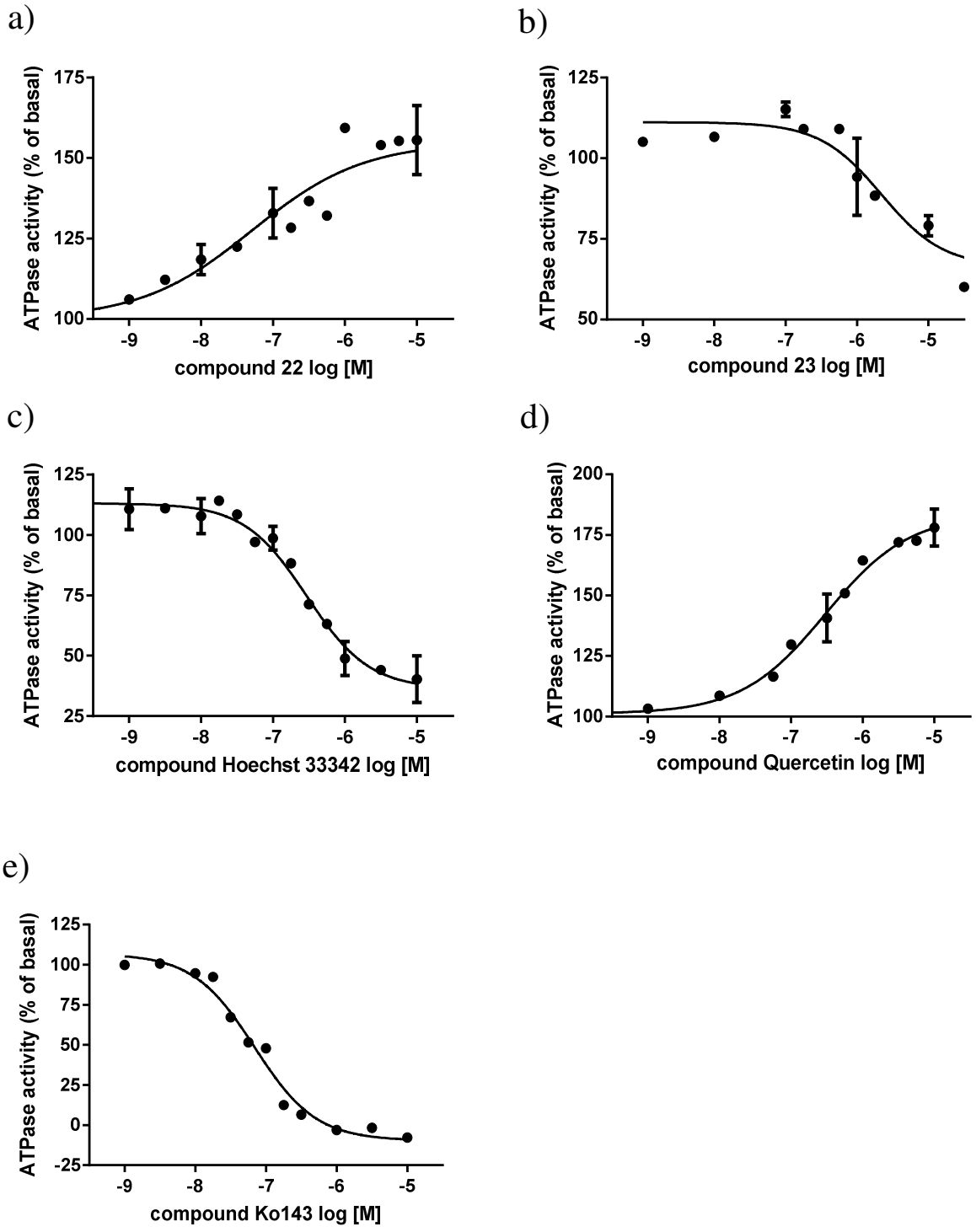

*Figure 34: Concentration-response curves for compounds **22** (a, EC_{50}: 2350 nM), **23** (b, EC_{50}: 8270 nM), **Hoechst 33342** (c, EC_{50}: 295 nM), **Quercetin** (d, EC_{50}: 302 nM) and **Ko143** (e, EC_{50}: 69 nM) in the ATPase assay. All values are relative vanadate-sensitive ATPase activities in relation to the basal activity, which is set to 100%.*

As mentioned before, this finding is not very surprising, since considerable differences between *meta* and *para* substituted derivatives have already been noticed in the investigation of the inhibitory potency toward ABCG2, the type of interaction with Hoechst 33342 and the binding studies with the conformation sensitive 5D3 antibody.

A biphasic trend of the concentration dependent ATPase activity was found for the substrate Hoechst 33342. Although most substrates are expected to stimulate the ATPase activity due to an active transport by ABCG2, relatively strong deactivation was found in the case of Hoechst 33342. Similar results for Hoechst 33342 were also reported in other studies.[214] As expected, highest inhibition was achieved with the standard inhibitor Ko143 whereas the standard stimulator quercetin exhibited a substantially increased stimulation of the ATPase activity with increasing compound concentrations.

4 Project II: 4-Substituted-2-pyridylquinazolines and -pyrimidines

Synthesis of the 4-substituted-2-pyridylquinazolines and –pyrimidines was carried out in a similar fashion as described for the compounds of project I. In comparison to project I, the phenyl moiety at position 2 was replaced by a pyridyl group. Since *ortho*, *meta* and *para* pyridyl substitutions were carried out in the final compounds, three different 4-chloro-2-pyridylquinazoline precursors were synthesized. Further modification was achieved by introducing a substituted anilino linker at position 4 *via* a nucleophilic aromatic substitution under microwave radiation. This enables an easy comparison between the different *ortho*, *meta* and *para* pyridyl derivatives and also to the corresponding phenyl derivatives of project I.

Calculation of the mean logP of all three unsubstituted 4-anilio-2-pyridyl derivatives resulted in a value of 2.94 that is about 1 log unit lower than with phenyl at position 2. Low logP values are in particular beneficial for a good watersolubility but need to be high enough to ensure a sufficient membrane permeability.

Another approach was to remove the non-heteroaromatic core of the quinazoline scaffold in order to evaluate the molecular building blocks that are crucial for the inhibitory potency toward ABCG2. Consequently, the quinazoline scaffold was reduced to a 4-methylpyrimidine structure. The small methyl residue was necessary due to a convenient synthetic preparation and is unlikely to impact the properties of the compound considerably. Substitution was carried out at position 2 with phenyl and *para* pyridyl. Further modification was achieved by introducing a substituted aniline moiety at position 4. The logP value with the unsubstituted 4-anilino linker was calculated for both structures to be 3.53 (2-phenyl) and 2.27 (2-pyridyl).

It was observed that a few compounds like **89,** containing a *para* nitro substituent at position 4, exhibited a decreased solubility. This phenomenon was investigated by detecting the change in absorbance of a compound solution over time. An absorbance spectrum of compound **89** at a final concentration of 10 µM is illustrated in Figure 35. According to the result, no precipitation was observed within a time period of 2 h, using the highest final concentration applied in the Hoechst 33342 accumulation assay.

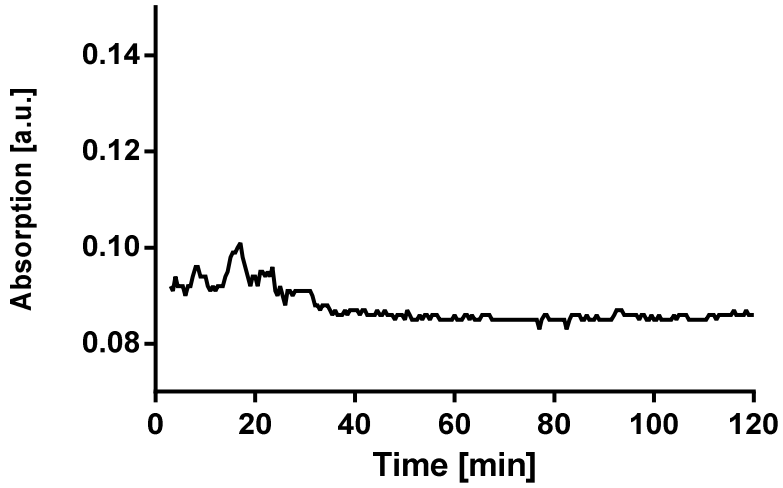

*Figure 35: Absorption spectrum measured at the excitation maximum of compound **89** for a time period of 2h. The compound was diluted to 10 µM in KHB and the measurement carried out at room temperature.*

Hence, precipitation is most likely to occur during the preparation of the dilution series, since they contain higher concentrations than used for the measurement of the plates. This problem could be overcome by heating the KHB used for the dilution series to 37 °C and/or adjusting the methanol content to ≤1.8% in the final concentration. Hereby three IC_{50} values determined in a prior study by Juvale *et al.* were corrected by this method and are marked accordingly in the tables.[198]

4.1 Reaction mechanism

A schematic synthesis route and a detailed reaction mechanism is provided above.

*Scheme 3: General synthesis scheme for the preparation of compounds **41**-**88**.* [a]

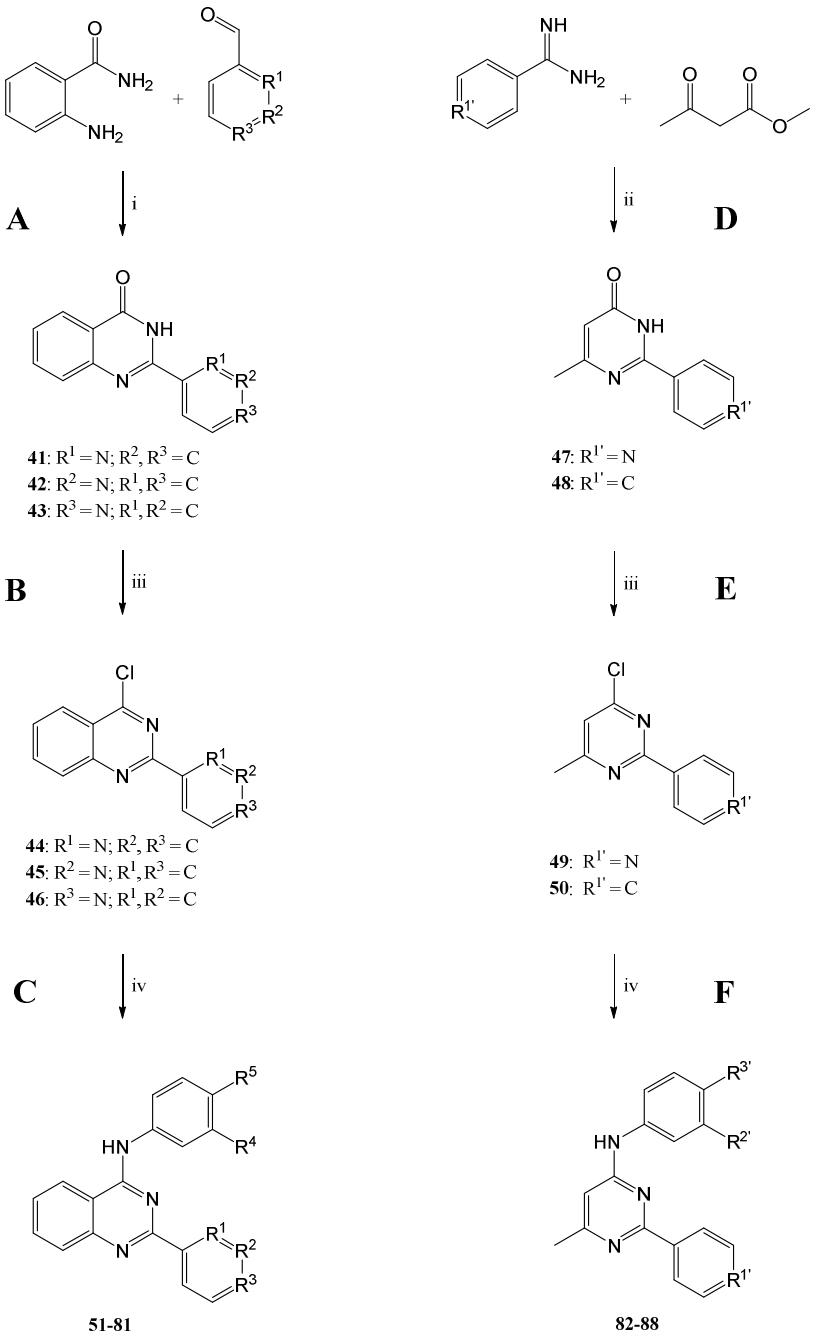

[a]: Reagents and conditions: (i) DMF, I_2, K_2CO_3, 70-90 °C, 4-8 h. (ii) MeOH, NaOMe, 60 watt microwave irradiation, 70 °C, 4 h. (iii) $POCl_3$, reflux, 4-12 h. (iv) Substituted aniline, 100 watt microwave irradiation, 110 °C, 15 - 30 min.

Reaction mechanism **A**:

In the first step, anthranilamide attacks the carbonyl function of the aldehyde derivative with its amino function *via* a nucleophilic addition followed by elimination of H_2O. Ring-closure is achieved *via* a nucleophilic addition of the amido-nitrogen atom at the initially formed imine double bond depicted below. In the last step, a double bond between position 1 and 2 is formed by oxidation with elemental iodine.

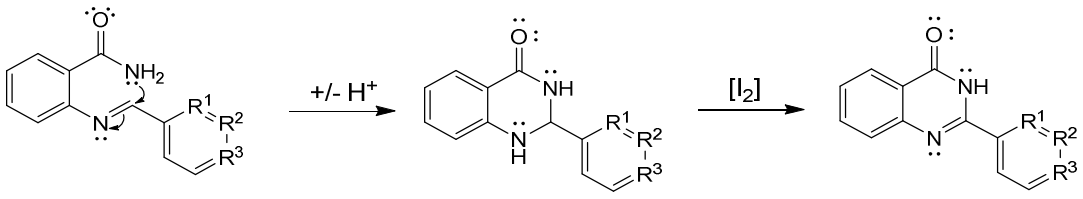

Reaction mechanism **B/E**:

The carbonyl function at position 4 is substituted by chlorine *via* a chlorination reaction using $POCl_3$. The reaction mechanism for **B** is illustrated below and applies analogously to **E**.

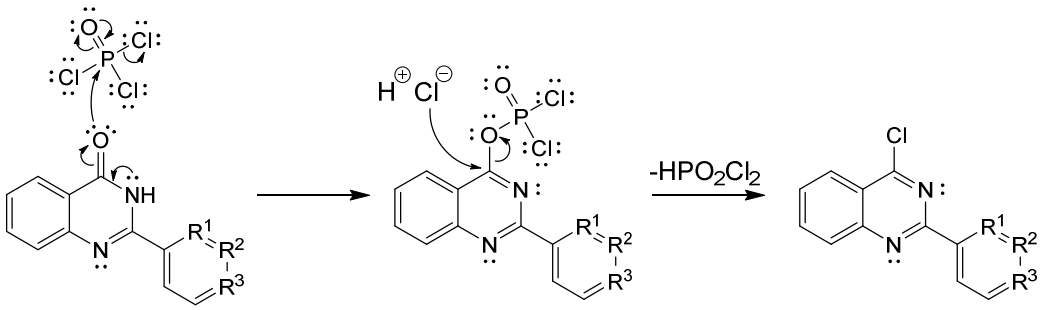

Reaction mechanism **C/F**:

A nucleophilic aromatic substitution of the corresponding 4-chloro precursor by a substituted aniline derivative was carried out to obtain the final compounds. The reaction mechanism is analogous to that used for the compounds in project I and can be reviewed in chapter 3.1. If the reaction was not complete, triethylamine was added to the mixture to react with hydrochloric acid generated during the reaction to prevent the protonation of the substituted aniline molecule.

Reaction mechanism **D**:

Initially, the amino function performs a nucleophilic attack at the carbonyl group eliminating H_2O, illustrated below. Ring-closure is achieved *via* an addition-elimination mechanism; releasing methanol. In the last step a re-arrangement of H^+ occurs leading to the desired precursor.

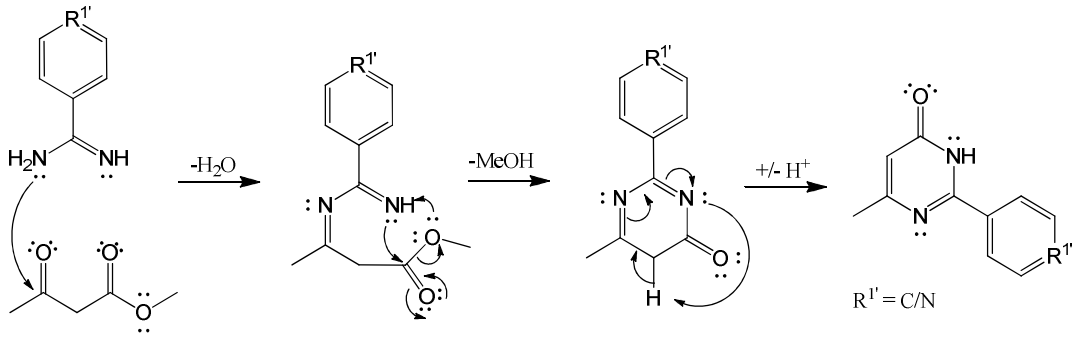

4.2 Investigation of the inhibitory potency toward ABCG2 in the Hoechst 33342 accumulation assay

Investigation of the inhibitory potency of the compounds was carried out in a Hoechst 33342 accumulation assay using the ABCG2 overexpressing MDCK II BCRP and parental cell line. More information to the Hoechst 33342 accumulation assay as is provided in chapter 3.2 and 10.2.2.2. A summary of the associated activity data is given in Table 12.

Table 12: Inhibitory Activities Determined in the Hoechst 33342 Accumulation Assay Using ABCG2 Overexpressing MDCK II BCRP Cells. Structural Formulas of the Substitution patterns of Scaffold A and B are Depicted Above the Table.

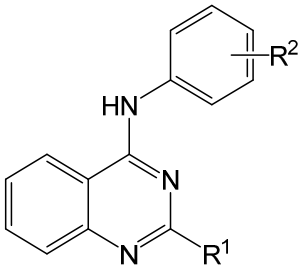

Scaffold A: Quinazoline

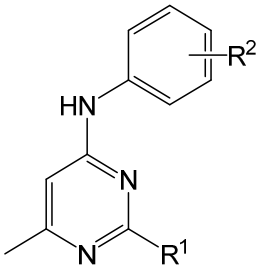

Scaffold B: 4-Methylpyrimidine

Compound	R^1	R^2	Scaffold	Hoechst 33342 IC_{50} ± SD [nM][a]
51	2-Pyr	3-NO_2	A	376 ± 91
52	3-Pyr	3-NO_2	A	105 ± 35
53	4-Pyr	3-NO_2	A	117 ± 29
54	3-Pyr	4-NO_2	A	64.1 ± 8.5
55	2-Pyr	3-CN	A	507 ± 61
56	3-Pyr	3-CN	A	108 ± 21
57	4-Pyr	3-CN	A	134 ± 10
58	3-Pyr	4-CN	A	166 ± 29
59	2-Pyr	3-OMe	A	1630 ± 320
60	3-Pyr	3-OMe	A	1020 ± 180
61	4-Pyr	3-OMe	A	558 ± 111
62	4-Pyr	4-OMe	A	742 ± 21
63	2-Pyr	3,4-OMe	A	1060 ± 80
64	3-Pyr	3,4-OMe	A	753 ± 151
65	4-Pyr	3,4-OMe	A	545 ± 113
66	4-Pyr	3-CF_3	A	216 ± 40
67	4-Pyr	4-CF_3	A	488 ± 38
68	4-Pyr	3-CF_3,4-OMe	A	146 ± 23
69	3-Pyr	3-F	A	156 ± 37
70	4-Pyr	3-SO_2F	A	1380 ± 184
71	3-Pyr	3-$N(Me)_2$	A	1200 ± 210
72	4-Pyr	3-OH	A	1070 ± 190
73	4-Pyr	4-OH	A	4260 ± 1220
74	3-Pyr	3-CH_2OH	A	810 ± 239
75	4-Pyr	3-CH_2OH	A	921 ± 216

Table continues on the next page

76	3-Pyr	3-NO_2,4-OH	A	245 ± 21
77	3-Pyr	3-CO_2Me	A	362 ± 74
78	4-Pyr	3-CO_2Me	A	405 ± 98
79	4-Pyr	3-CO_2*t*Bu	A	299 ± 97
80	4-Pyr	3-CO_2H	A	60000 ± 14800
81	4-Pyr	4-CO_2H	A	9640 ± 2
82	4-Pyr	3-CN	B	132 ± 24
83	4-Pyr	3-OMe	B	271 ± 28
84	4-Pyr	4-OMe	B	874 ± 181
85	Ph	3-CN	B	122 ± 24
86	Ph	4-CN	B	128 ± 32
87	Ph	3-NO_2,4-OH	B	98.8 ± 17.4
88	Ph	H	B	648 ± 149
3	Ph	3-NO_2,4-OH	A	81.1 ± 9.2
2[b]	Ph	3-NO_2	A	130 ± 30
89[c]	Ph	4-NO_2	A	69.6 ± 8.2
4[b]	Ph	3-CN	A	140 ± 40
5	Ph	4-CN	A	71.4 ± 10.1
90[b]	Ph	3-OH	A	150 ± 30
6	Ph	4-OH	A	211 ± 38
18	Ph	3-F	A	363 ± 54
1	Ph	H	A	882 ± 157
Ko143[d]				227 ± 14

[a]: IC_{50} values are means of three independent experiments.
[b]: IC_{50} value taken from literature.[198]
[c]: Compounds synthesized in earlier study.[198]
[d]: Used as reference in the assay.

First, the inhibitory potency of *ortho*, *meta* and *para* pyridyl residues was compared at R^1 together with different substituents at R^2 such as nitro, cyano, methoxy or 3,4-dimethoxy. The evidence that was gathered pointed to a low inhibitory potency of the compounds substituted with an *ortho* pyridyl moiety. In contrast, *meta* and *para* pyridyl residues yielded compounds of considerably higher potency, both at a comparable level. The relation between *ortho*, *meta* and *para* pyridyl is exemplified in compounds **51-53**, **55-57**, **59-61** and **63-65.** These results led to the synthesis of only *meta* and *para* pyridyl derivatives in the following compounds.

Interestingly, a significant similarity regarding the IC_{50} values was found for most of the *meta* and *para* pyridyl derivatives and their phenyl analogues discussed in project I. Hence it is not surprising that the combination with nitro, cyano, trifluoromethyl and fluoro at R^2 resulted in high inhibitory potencies. Only a few instances like the 3- and 4-

hydroxy derivatives **72** and **73** exhibited a pronounced difference in comparison to their corresponding phenyl analogues **90** and **6**.

The highest inhibitory potency was obtained by compound **54** with an IC_{50} of 64 nM, containing a 3-pyridyl group at R^1 and 4-nitro at R^2. The compound is about 4-fold more potent than one of the most potent inhibitors of ABCG2, namely Ko143. The corresponding 2-phenyl analogue **89** possessed a very similar IC_{50} of 70 nM containing 4-nitro at R^2. Again, the *para* nitro substitution at R^2 in compound **54** turned out to be more potent than the *meta* nitro substitution present in compound **52** (IC_{50}: 105 nM).

Moreover, a few compounds containing methoxy and butoxy esters were investigated and resulted in increased inhibitory potency (see compound **77**-**79**).

Subsequently, several compounds containing a considerably smaller 4-methyl pyrimidine scaffold were investigated using pyridyl or phenyl groups as substituents at position 2. In comparison to their quinazoline analogues, very similar IC_{50} values were obtained for the 4-methyl pyrimidine derivatives (see compounds **82/57**, **83/61**, **84/62**, **85/4**, **86/5**, **87/3** and **88/1**). Concentration-response curves of the most potent compounds containing a quinazoline (compound **54**) or a 4-methyl pyrimidine scaffold (compound **87**) together with the standard inhibitor Ko143 is depicted in Figure 36.

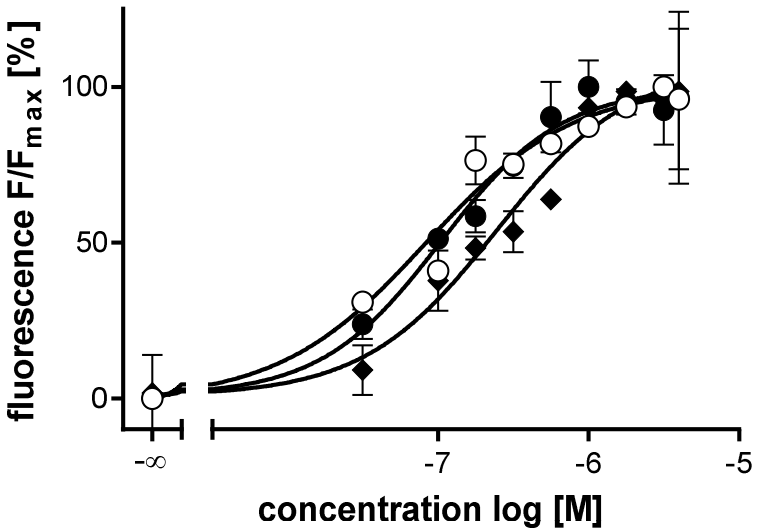

*Figure 36: Concentration-response curve of compound **54** (■, IC_{50}: 64.1 nM) and **87** (▲, IC_{50}: 98.8 nM) in a Hoechst 33342 accumulation assay with Ko143 (○, IC_{50}: 227 nM) as reference, using the ABCG2 overexpressing MDCK II BCRP cell line.*

The substituted 4-methyl pyrimidine scaffold is particular interesting since it represents a very small molecule consisting of only three aromatic moieties but reveals significantly

high inhibitory potencies similar to a quinazoline scaffold. Besides the high ligand efficiency in comparison to the quinazoline derivatives, it also exhibits a decreased calculated logP value in the range of half a log unit. This is interesting since a certain degree of lipophilicity is required for membrane permeability but must also not be too high due to a reduced solubility of the compound under physiological conditions. However, a rather poor correlation ($r^2 = 0.21$) between the pIC_{50} value and the calculated logP value was observed for the compounds of this subset (Figure 37). Here the two carboxyl groups containing compounds **80** and **81** were omitted, as the logP is calculated for the neutral form, which is not present under the assay conditions.

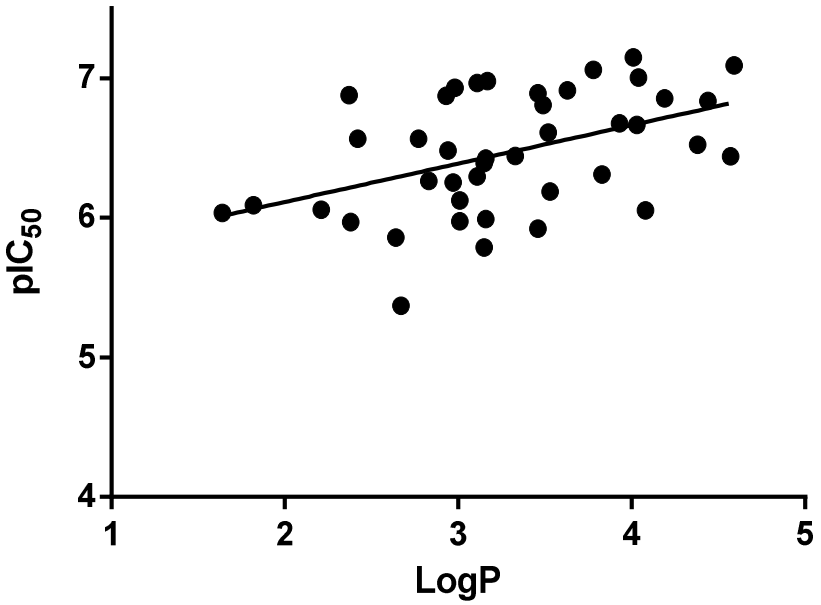

Figure 37: Correlation of calculated logP values with the corresponding pIC_{50} values. For the calculation of the logP values a software package from ACD/Labs was used (see experimental section).

4.3 Investigation of the inhibitory potency toward ABCB1 and ABCC1 in the calcein AM assay

A calcein AM assay was conducted to screen the selectivity of several compounds toward ABCG2. Therefor the ABCB1 overexpressing cell line A2780 adr and the ABCC1 overexpressing cell line H69 AR were used and the assay was carried out as described in

chapters 3.3 and 10.2.2.4. The corresponding screenings were carried out at a compound concentration of 10 µM and CsA was used as positive control, indicating total inhibition of both transporters. In the cases where compounds exhibited an inhibitory potency of more than 25% relative to the control, additional tests were carried out with more dilutions to generate concentration-response curves allowing calculation of IC_{50} values. A summary of the calculated IC_{50} values of the compounds showing more than 25% of inhibition in the screening is given in Table 13. Screening results for the inhibitory activity toward ABCB1 and ABCC1 are depicted as bar charts in Figure 38.

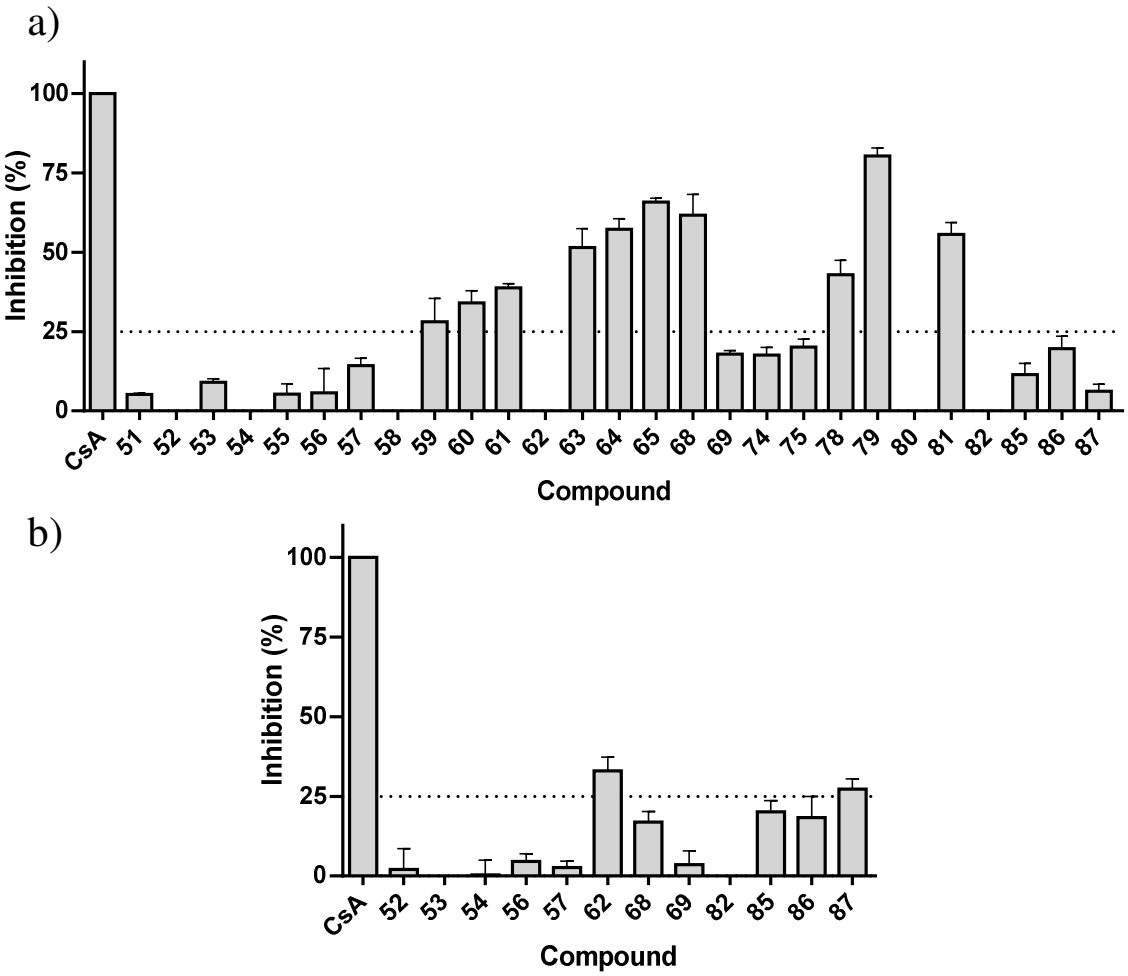

Figure 38: Inhibitory effect of screened compounds toward ABCB1 overexpressing cell line A2780 adr (a) and ABCC1 overexpressing cell line H69 AR (b) in a calcein AM assay at a concentration of 10 µM. Cyclosporine A (CsA) was used as positive control, indicating complete inhibition. The height of the bars represents the inhibition compared to the positive control in percent. For each compound, three independent experiments were performed and the standard deviation expressed as error bars.

Compounds with nitro and cyano functions at R^2 exhibited a high selectivity toward ABCG2 which is advantageous with respect to their significantly high inhibitory potency in the Hoechst 33342 accumulation assay. Increased potencies toward ABCB1 and, to a lesser extent, toward ABCC1 was observed in the presence of methoxy and ester functions. These observations were in good accordance with the results of project I and prior studies.[198, 205]

Interestingly, compound **79** containing a 4-pyridyl residue at R^1 and *tert*-butyl 3-aminobenzoate at R^2 obtained a higher inhibitory potency toward ABCB1 than the standard CsA (IC_{50}: 1.21 µM) with an excellent IC_{50} of 0.334 µM. Because compound **79** also has a high inhibitory potency toward ABCG2, it could be used as an interesting drug for inhibiting both, ABCB1 and ABCG2 which are simultaneously expressed in some important tissues like the BBB.

Table 13: Inhibitory Activity of Compounds Exhibiting an Inhibition of more than 25% in Comparison to the Reference CsA in a Calcein AM Assay at 10 µM.

Compound	R^1	R^2	Scaffold	Calcein AM (ABCB1) IC_{50} ± SD [µM][a]	Calcein AM (ABCC1) IC_{50} ± SD [µM][b]
59	2-Pyr	3-OMe	A	12.7 ± 1.83	n.t.
60	3-Pyr	3-OMe	A	4.78 ± 0.57	n.t.
61	4-Pyr	3-OMe	A	5.43 ± 0.83	n.t.
62	4-Pyr	4-OMe	A	n.d.	17.9 ± 2.1
63	2-Pyr	3,4-OMe	A	6.30 ± 0.36	n.t.
64	3-Pyr	3,4-OMe	A	3.11 ± 0.21	n.t.
65	4-Pyr	3,4-OMe	A	2.08 ± 0.36	n.t.
68	4-Pyr	3-CF_3,4-OMe	A	2.78 ± 0.50	n.d.
78	4-Pyr	3-CO_2Me	A	6.37 ± 0.12	n.t.
79	4-Pyr	3-CO_2*t*Bu	A	0.334 ± 0.056	n.t.
81	4-Pyr	4-CO_2H	A	3.67 ± 0.10	n.t.
87	Ph	3-NO_2,4-OH	B	n.d.	15.9 ± 2.9
CsA[c]				1.21 ± 0.16	2.97 ± 0.38

[a]: *The ABCB1 overexpressing cell line A2780 adr was used.*
[b]: *The ABCC1 overexpressing cell line H69 AR was used.*
[c]: *Cyclosporine A is used as reference for both assays.*
n.d.: Not determined, due to low effect in the initial screening.
n.t.: Not tested

A concentration-response curve of compound **79** including the positive control CsA is depicted in Figure 39.

Moreover, the inhibitory potency toward ABCB1 was found to correlate with the position of the nitrogen atom at the pyridyl moiety in R^1, showing increasing activities from *ortho* to *meta* to *para* (see compound **51**-**53**, **55**-**57**, **59**-**61** and **63**-**65**).

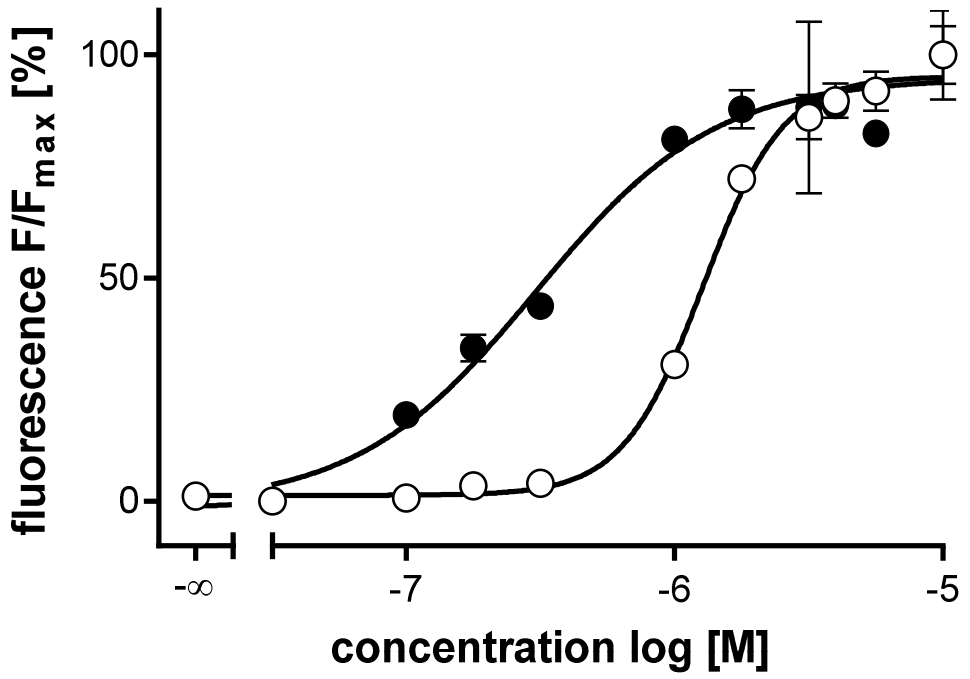

*Figure 39: Concentration-response curve of compound **79** (●, IC_{50}: 0.334 µM) in a calcein AM assay with cyclosporine A (○, IC_{50}: 1.21 µM) as reference, using the ABCB1 overexpressing cell line A2780 adr. Results were obtained in at least three independent experiments and the standard deviation is expressed by error bars.*

The screening of the inhibitory potency of selected compounds toward ABCC1 resulted in only two compounds giving slightly more than 25% of inhibition relative to the positive control CsA (IC_{50}: 2.97 µM). Only compounds **62** and **87** obtained an increased inhibitory potency but resulted in poor IC_{50} values of 18 and 16 µM when tested with several compound dilutions. Although the selection included the most potent compounds, the test set was smaller than in the screening performed with ABCB1 overexpressing cells. This was due to prior results from project I identifying the inhibition of ABCC1 as less important.

4.4 Investigation of the intrinsic cytotoxicity with the MDCK II cell lines in a MTT assay

The intrinsic cytotoxicity of selected compounds was investigated in a MTT assay with MDCK II parental and ABCG2 overexpressing cells. Toxic effects were measured after 72 h incubation of the cells in the presence of different compound concentrations using MTT as indicator of the cell viability. Further details of the procedure are provided in chapters 3.4 and 10.2.2.5. A summary of the obtained GI_{50} values and the corresponding therapeutic ratios is depicted in Table 14.

Table 14: Intrinsic Toxicity of Selected Compounds toward MDCK II ABCG2 Overexpressing and Parental Cells.

Compound	R^1	R^2	Scaffold	GI_{50} [µM][a] BCRP	GI_{50} [µM][a] Parental	Therapeutic ratio (GI_{50}/IC_{50}) [b]
52	3-Pyr	3- NO_2	A	71	65	620
54	3-Pyr	4- NO_2	A	73	74	1100
56	3-Pyr	3-CN	A	75	91	700
57	4-Pyr	3-CN	A	88	110	660
58	3-Pyr	4-CN	A	79	100	240
66	4-Pyr	3-CF_3	A	13	12	58
67	4-Pyr	4-CF_3	A	120	170	240
68	4-Pyr	3-CF_3,4-OMe	A	2.9	2.5	20
69	3-Pyr	3-F	A	47	130	300
71	3-Pyr	3-$N(Me)_2$	A	10	14	8.3
72	4-Pyr	3-OH	A	9.2	12	8.6
73	4-Pyr	4-OH	A	55	120	13
82	4-Pyr	3-CN	B	6.9	9.3	52
86	Ph	4-CN	B	18	28	140
87	Ph	3-NO_2,4-OH	B	49	58	500
88	Ph	H	B	110	140	170
3	Ph	3-NO_2,4-OH	A	52	150	650
4	Ph	4-CN	A	10	14	150
6	Ph	4-OH	A	15	23	69

Table continues on the next page

16	Ph	3-F	A	18	28	50
1[c]	Ph	H	A	27	26	30
Ko143				13	13	49
MeOH/DMSO				96[d]	140[d]	

[a]: *Concentration leading to 50% of cell survival of MDCK II BCRP and parental cells. The data was obtained from at least two independent experiments as mean values.*

[b]: *The therapeutic ratio of selected compounds is calculated from the ratio of GI_{50} to IC_{50}-values, derived from MTT viability assay and Hoechst 33342 accumulation assay with ABCG2 overexpressing MDCK II BCRP cells.*

[c]: *Compound was previously synthesized.* [197, 198]

[d]: *Positive control of the cytotoxicity from dilution with DMSO/MeOH without compound.*

Resulting GI_{50} values of the quinazoline derivatives (scaffold A) **52**, **54**, **56**-**58**, **66**-**69** and **71**-**73** containing a pyridyl moiety illustrate a substantial benefit of this group regarding their intrinsic cytotoxicity. Only compounds containing *meta* substitutions with trifluoromethyl, dimethylamino or hydroxy exhibited increased toxic effects (see compound **66**, **68**, **71** and **72**). A possible mechanism for increased toxic effects could be associated with ATP depletion in the cell due to increased stimulation of the ATPase activity by a compound. For several instances, high stimulation of the ATPase activity was found in *meta* substituted compounds at the anilino linker and deactivation in case of *para* substitution. Moreover, for several compounds significant differences in the GI_{50} values between the *meta* and *para* derivatives at R_2, were observed, as for instance in compounds **72/73** and **66/67**.

Numerous pyridyl derivatives led to negligible or low cytotoxic effects in comparison to their phenyl analogues, including compounds with substitution at R^2 by either 4-cyano (compounds **58/4**: GI_{50} = 79.4/10.4 µM), 4-hydroxy (compounds **73/6**: GI_{50} = 55.0/14.6 µM) or 3-fluoro (compounds **69/16**: GI_{50} = 46.8/18.0 µM).

Concentration-response curves of highly potent compounds (IC_{50} < 140 nM) containing scaffold A or B (compound **54**, **56**, **57**, **82** and **87**) and a control (only DMSO/MeOH) are depicted in Figure 40.

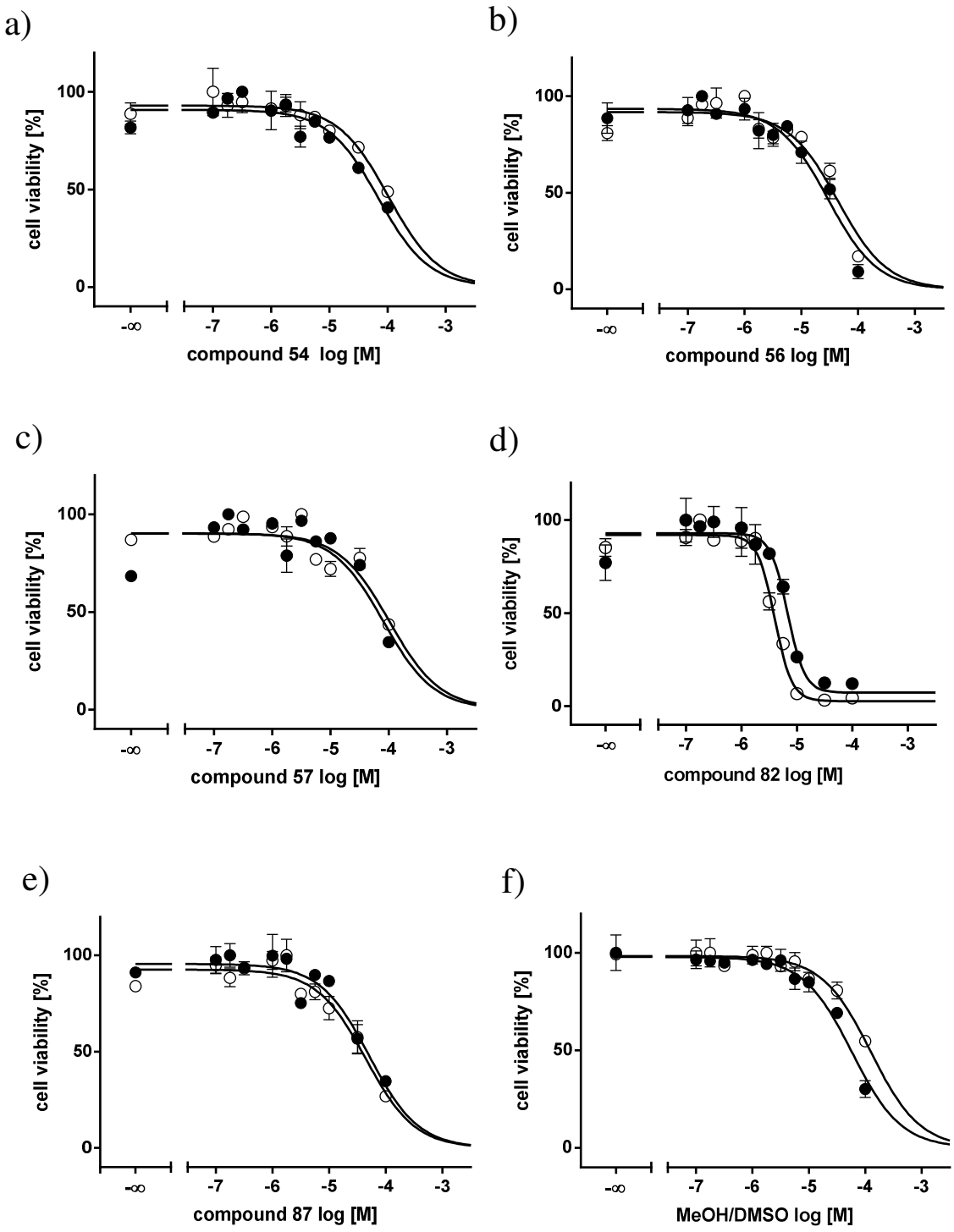

*Figure 40: MTT viability assay of compounds **54**, **56**, **57**, **82** and **87** using the ABCG2 overexpressing MDCK II BCRP(closed circle) and parental MDCK II cell line (open circle). The following GI_{50}-values were determined in the ABCG2 overexpressing cell line: compound **54** GI_{50}: 73.3 µM, **56**: 75.3 µM, **57**: 88.1 µM, **82**: 6.92 µM and **87**: 49.0 µM. A control with the same concentration of MeOH and DMSO used in the dilution of the compounds, was carried out for comparison (■, GI_{50} = 96.1 µM). The final concentration of MeOH and DMSO used for the dilution was ≤ 1.8% and ≤ 1.0%, respectively.*

Derivatives containing a 4-methyl pyridyl scaffold yielded varying GI_{50} values. Besides the 4-pyridyl derivative **82**, all other investigated derivatives containing phenyl at R^1 exhibited similar or lower cytotoxic effects than their analogues with a quinazoline scaffold. Due to the limited amount of investigated compounds, further derivatives have to be synthesized and investigated in order to provide a more comprehensive conclusion.

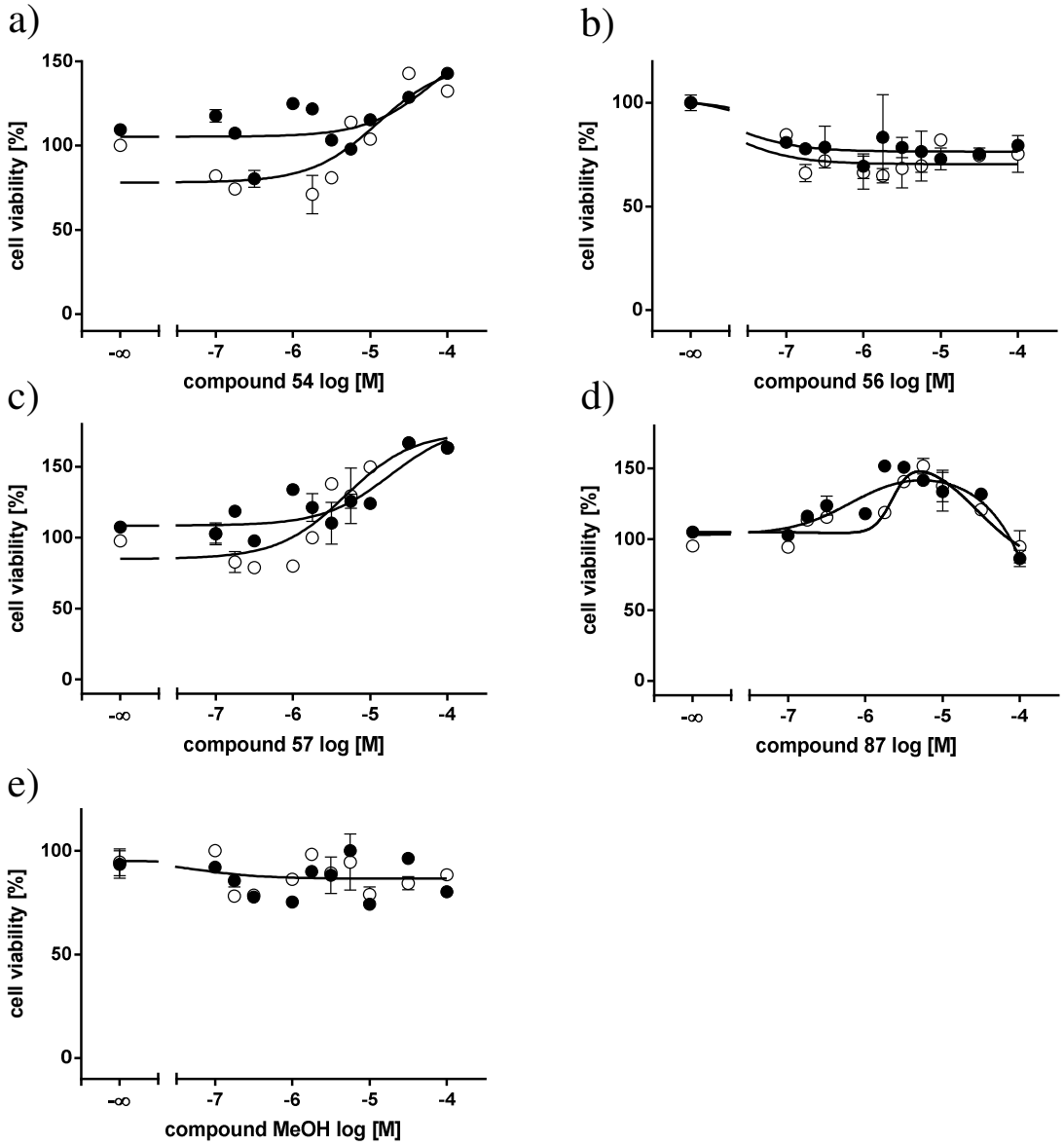

*Figure 41: MTT viability assay of compounds **54** (a), **56** (b), **57** (c), **87** (d) and a control (e) was carried out using the MDCK II ABCG2 overexpressing (closed circle) and parental MDCK II cell line (open circle). The control contains the same concentration of MeOH used in the dilution of the compounds. The final concentration of MeOH used for the dilution was ≤ 1.0%. No DMSO was used in this assay.*

Since a few compounds such as **54**, **56**, **57** and **87** exhibited no cytotoxic effects, a modified MTT viability assay was carried out without DMSO and less than 1% MeOH in the highest concentration and the remaining parameters in the MTT assay were kept the same. This modification was possible due to the increased water solubility of the compounds. Corresponding concentration-response curves of the cell viability are depicted in Figure 41.

Stimulation of the cell proliferation was often observed at low concentrations which is probably accounted to a defensive cellular mechanism. Further increase of the concentration eventually reversed this effect leading to a decreasing cell viability.

All tested compounds showed no significant cytotoxic effects in the range of 0.1 to 30 µM. On the contrary, stimulation of the cell proliferation is observed within a certain concentration range for compounds **54**, **57** and **87**. Only **87** exhibited a negative trend in the cell viability at a concentration of roughly 100 µM or higher. Compound **56** and the control, containing only MeOH, exhibited a constant cell viability at all concentrations.

Due to a restricted solubility, higher compound concentrations could not be used. Thus it was not possible to create sigmoidal concentration-viability curves and determining a GI_{50} value. In comparison to the first method using DMSO together with an increased amount of MeOH, the GI_{50} of the nontoxic compounds is very likely higher than 96 µM, resulting from the cytotoxic effects of the solvents only.

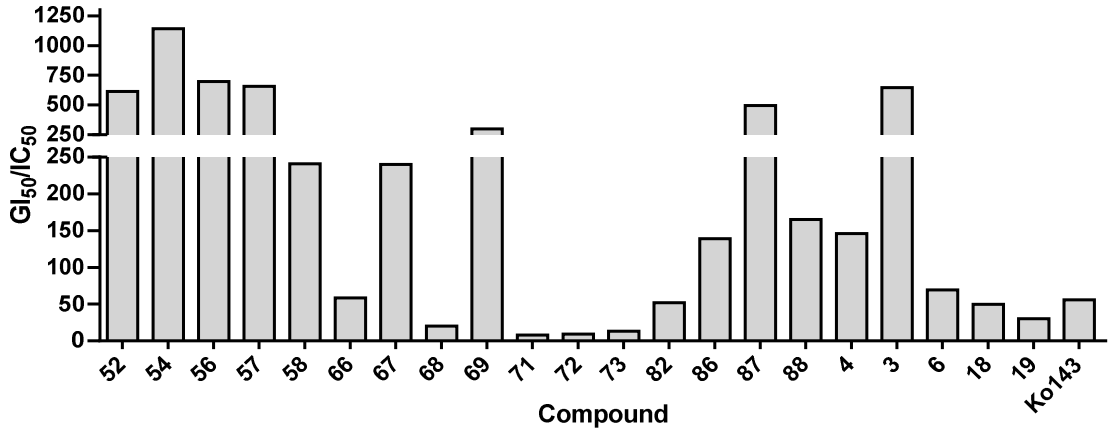

*Figure 42: Therapeutic ratios of selected compounds, calculated from the ratio of GI_{50} to IC_{50} derived from MTT cytotoxicity assay and Hoechst 33342 accumulation assay, respectively. The highest score was obtained for compound **54** (GI_{50}/IC_{50} = 1143), while the reference compound Ko143 yielded GI_{50}/IC_{50} = 48.9.*

The highest TR of 1140 resulted for compound **54** containing a substitution with 3-pyridyl at R^1 and 4-nitro at R^2. In comparison the potent inhibitor Ko143 obtained a TR of only 48.9. The benefit of the high inhibitory potency together with the low intrinsic cytotoxicity within this class of compounds leads to considerably high TRs that summarized in Figure 42. In particular, substitution with pyridyl at R^1 and nitro or cyano at R^2 resulted in selective compounds with extraordinarily high TRs that are promising candidates for *in vivo* studies.

4.5 Investigation of the reversal of multidrug resistance

The ability to reverse MDR in ABCG2 overexpressing MDCK II BCRP cell line toward SN-38 by co-administration of potent inhibitors **54**, **56** and **87** was investigated in a MDR reversal assay. Further details are provided in chapters 3.5 and 10.2.2.6.
Concentration-viability curves obtained with parental and ABCG2 expressing MDCK II cell lines are depicted in Figure 43.

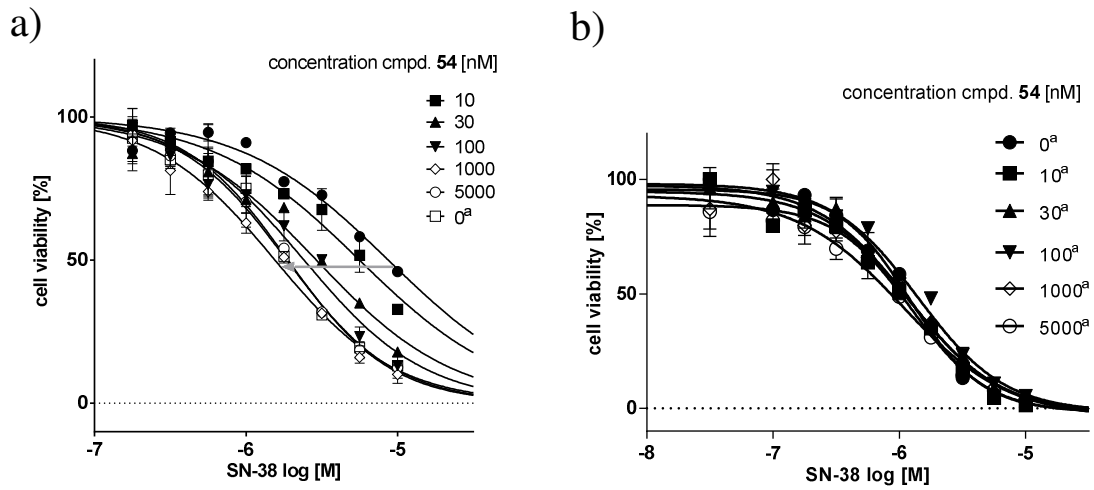

Figure continues on the next page

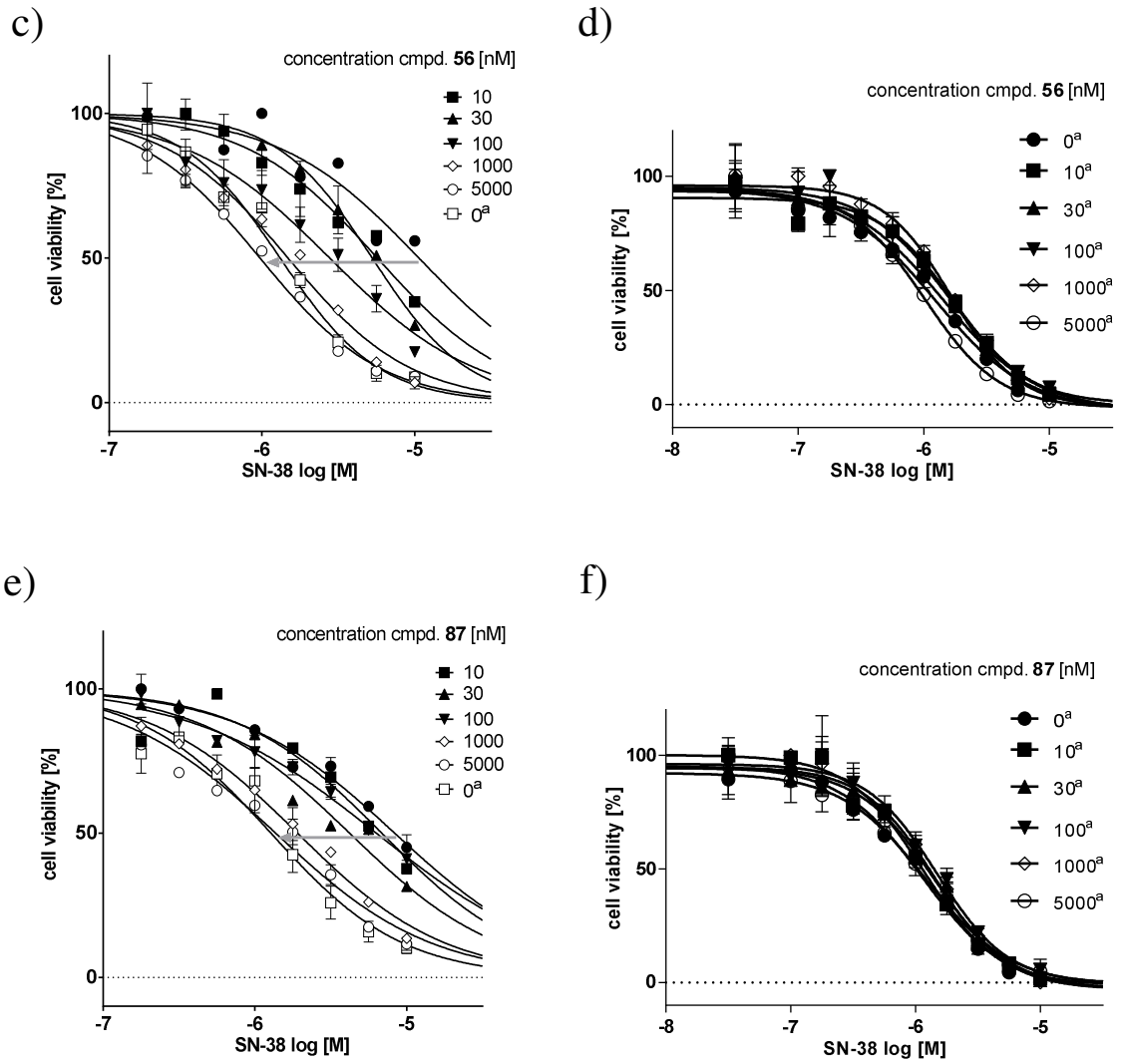

*Figure 43: MDR reversal assay of compound **54** (a, b), **56** (c, d) and **87** (e, f) demonstrating the ability to reverse the MDR toward the cytostatic SN-38, using parental MDCK II and ABCG2 overexpressing cell lines. The grey arrows indicate the increasing sensitization of the ABCG2 overexpressing cells with higher compound concentrations (see legend). At a compound concentration of 5 µM, full reversal is achieved, indicated by a similar IC_{50} value as the parental cells.*
a: Parental MDCK II cells.

The investigated compounds all led to a full reversal of the cell-resistance toward SN-38 at a concentration of 5 µM or less, indicated by similar pGI_{50} values of the parental cells and the ABCG2 expressing cells. Reversal of MDR due to increasing inhibition of ABCG2 is indicated by the grey arrow in Figure 43 a), c) and e). Repetition of the assay using parental cells resulted in comparable pGI_{50} values demonstrating no compound

concentration dependent effects on the viability of the cells, as can be seen from the concentration-viability curves presented in Figure 43 b), d) and f). Additionally, the pGI_{50} values from the MDR reversal assay were plotted against the logarithm of the corresponding compound concentration for a better visualization of the obtained results. Hereby, a sigmoidal concentration-effect curve could be fitted using the logistic equation to yield EC_{50} values that characterize the extent of MDR reversal by a compound (illustrated in Figure 44).

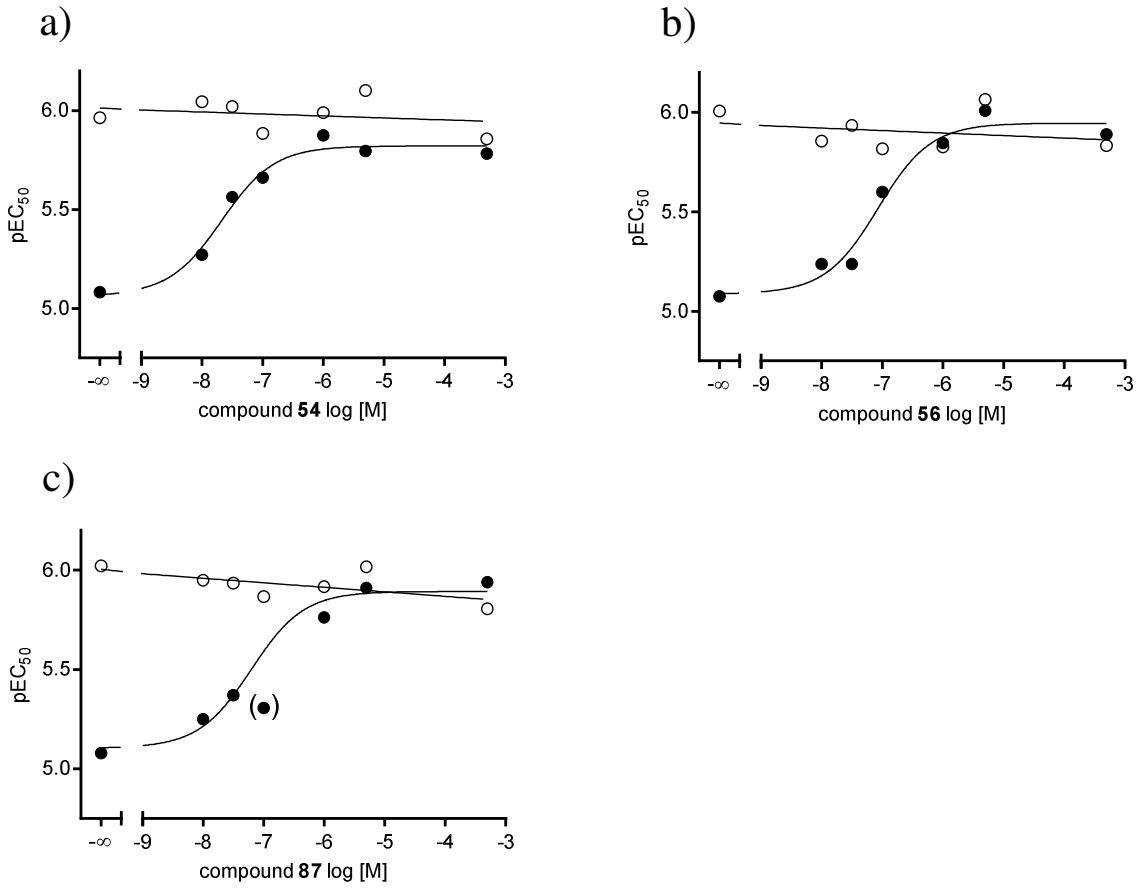

*Figure 44: Nonlinear regression of the pGI_{50} values determined in the efficacy assay (Figure 43 a, c and e) against the corresponding concentrations of compounds **54**, **56** and **87**. pEC_{50} is the concentration that reduces resistance of the ABCG2 overexpressing cells to 50 percent. The following EC_{50} values were calculated: 21.2 nM (**54**), 85.0 nM (**56**) and 62.3 nM (**87**). The pGI_{50} values of the parental cells determined in an analogous efficacy assay (Figure 43 b, d and f) are depicted by open circles. The point in parenthesis at 0.1 µM in (c) was excluded.*

Thereby EC_{50} values of 21.2, 85.0 and 62.3 nM were determined for compound **54**, **56** and **87**, respectively. According to the results in the MTT assay, the efficacy of the most potent compound **54** is about three-fold higher than the calculated IC_{50} value obtained in

the Hoechst 33342 accumulation assay. Regarding compound **56** and **87**, a good correlation was found in the determined EC_{50} values derived from the efficacy assay and the results from the Hoechst 33342 accumulation assay (IC_{50}: 108 nM, **56**; and 98.8 nM, **87**).

An additional MDR reversal assay with compound **54** and **87** was carried out to investigate the sensitization of the MDCK II ABCG2 overexpressing cell line toward the cytostatic drug MX. The assay was carried out with different compound concentrations in the presence and absence of 0.5 µM MX. Further details to the assay are provided in chapters 3.5 and 10.2.2.7. Both compounds were able to fully reverse the resistance of the cells toward MX at a concentration of about 0.1 µM as illustrated in Figure 45.

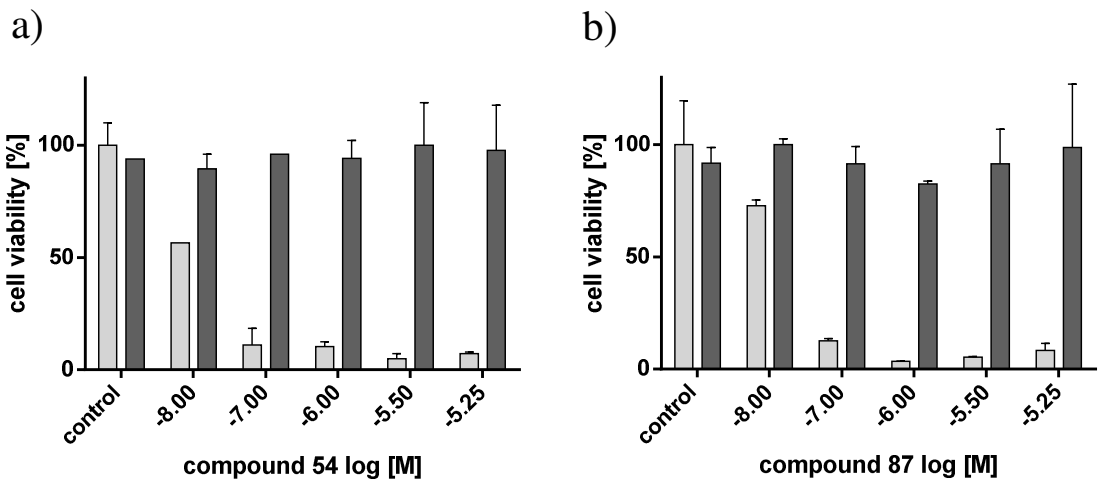

*Figure 45: MDR reversal assay of compound **54** (a, EC_{50}: 12.6 nM) and **87** (b, EC_{50}: 22.0 nM), demonstrating the ability to reverse the MDR toward the cytostatic MX, using ABCG2 overexpressing cell line MDCK II BCRP. The bars represent the cell viability at a given modulator concentration in the presence (light grey) and absence (dark grey) of 0.5 µM MX. The control shows cell viability of cells without modulator in the presence and absence of 0.5 µM MX. Standard deviation is expressed by error bars.*

Half-maximal growth inhibition was calculated for compound **54** as 12.6 nM and for **87** as 22.0 nM. The most potent compound, **54**, exhibited a high potency in both MDR reversal assays with SN-38 and MX, suggesting a somewhat higher inhibitory potency than determined in the Hoechst 33342 accumulation assay. A possible reason for this could be different affinities of the substrates to ABCG2 accounting for this result.

4.6 Investigation of the interaction with Hoechst 33342

The interaction of selected compounds with Hoechst 33342 was investigated using ABCG2 overexpressing MDCK II BCRP cells. Varying compound concentrations were combined with varying concentrations of Hoechst 33342 and the interaction type could be determined by employing the Lineweaver-Burk double reciprocal plot, described in chapters 4.6 and 10.2.2.8. A summary of the results obtained with the Lineweaver-Burk method is presented in Table 15 listing the intersection of the straight lines together with the corresponding interpretation. A selection of the corresponding plots is depicted in Figure 46.

Table 15: Interaction with Hoechst 33342 According to the Lineweaver-Burk Double Reciprocal Plot.

Compound	R^1	R^2	Scaffold	Intersection	type of interaction with Hoechst 33342
54	3-Pyr	4-NO_2	A	X-axis	Non-competitive
58	3-Pyr	4-CN	A	3. Quadrant	Non-competitive mixed type
61	4-Pyr	3-OMe	A	Y-axis	competitive
66	4-Pyr	3-CF_3	A	2. Quadrant	Non-competitive mixed type
67	4-Pyr	4-CF_3	A	3. Quadrant	Non-competitive mixed type
82	4-Pyr	3-CN	B	2. Quadrant	Non-competitive mixed type
84	4-Pyr	4-OMe	B	3. Quadrant	Non-competitive mixed type
Ko143				3. Quadrant	Non-competitive mixed-type

According to the Lineweaver-Burk double reciprocal plot the selected compounds mostly exhibited a non-competitive interaction of the "mixed type" with the substrate Hoechst 33342. The most potent compound **54** led to a clear non-competitive interaction, indicating that it binds differently from Hoechst 33342. Solely compound **61** exhibited a competitive interaction suggesting that it occupies the same binding pocket as Hoechst 33342.

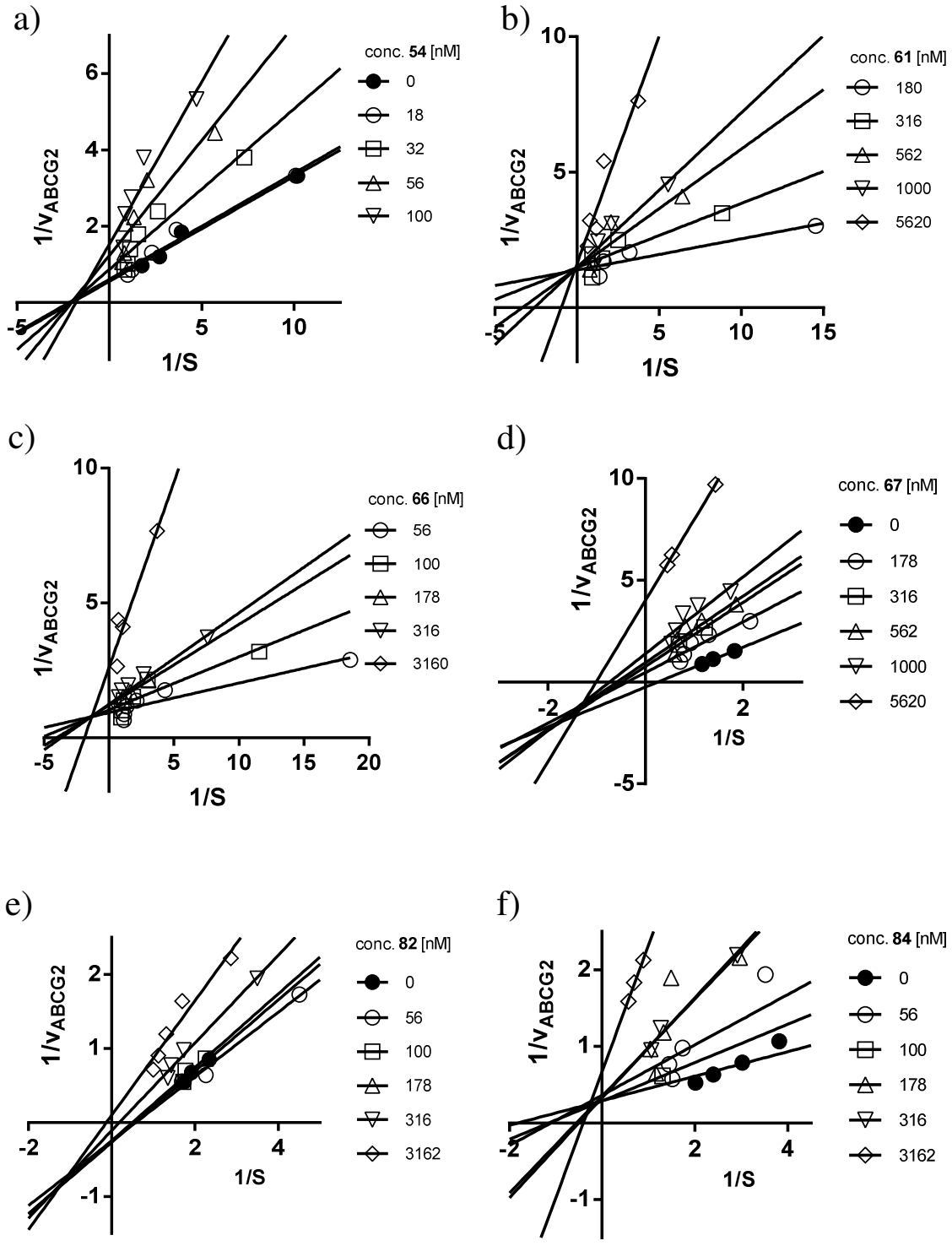

*Figure 46: Double-reciprocal plot according to Lineweaver-Burk for selected compounds **54** (a), **61** (b), **66** (c), **67** (d), **82** (e), **84** (f).Compound concentrations are specified in the legend.*

In order to validate the results from the Lineweaver-Burk double reciprocal plot, the Cornish-Bowden method was applied. Additional information is provided in chapters 3.6 and 10.2.2.8. Additionally a linear regression of the V_{max} and K_M values was performed and the obtained slopes summarized as scatter plot in Figure 47. Corresponding linear regression are depicted in Figure 48 (for Ko143 see chapter 3.6).

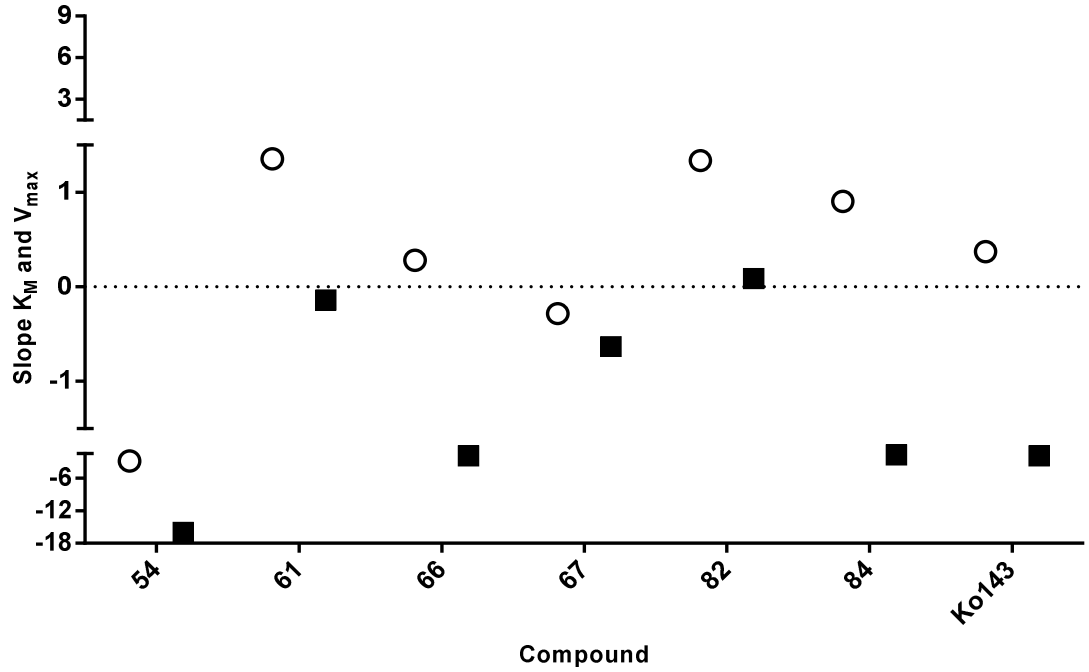

Figure 47: Scatter plot of the slopes obtained from the linear regression of K_M (○) and V_{max} (■) values calculated from the Cornish-Bowden direct linear plot.

The non-competitive interaction of compound **54** was confirmed by the Cornish-Bowden method showing decreasing V_{max} and the constant K_M values. Compound **61** on the other hand yielded a high positive slope for K_M and a roughly constant, slightly negative slope for V_{max} which is characteristic for a competitive interaction.

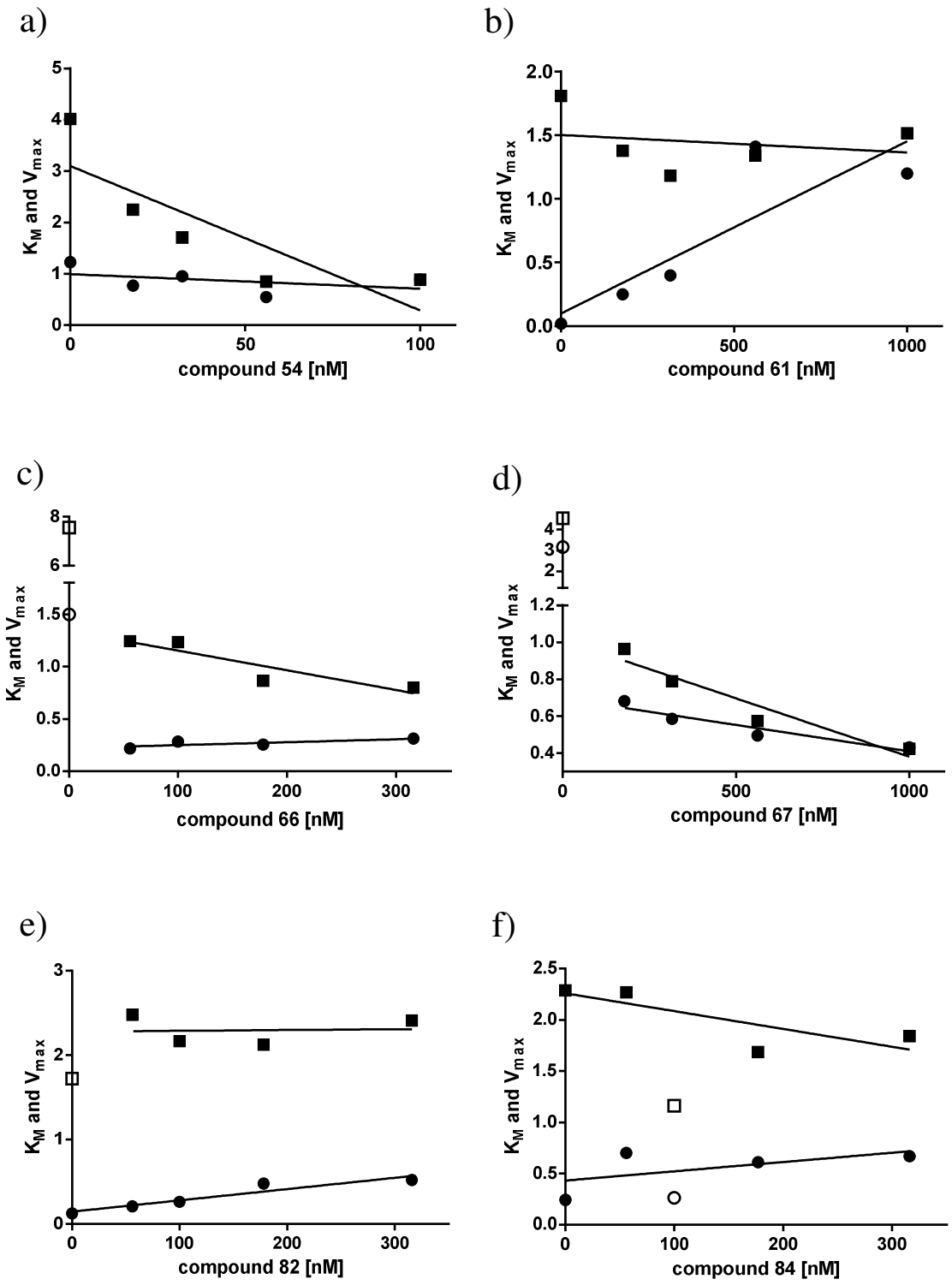

*Figure 48: Direct linear plot of **54** (a), **61** (b), **66** (c), **67** (d), **82** (e) and **84** (f) according to Cornish-Bowden resulting in compound-concentration dependent lines after linear regression of the V_{max} (■) and K_M (●) values. Excluded values are depicted as open symbols of the corresponding shape.*

For the compounds that were classified as non-competitive of the "mixed type" in the Lineweaver Burk plot, the Cornish-Bowden plot suggests a pronounced non-competitive character for compounds **66**, **67** and **84**. On the contrary, a considerably high competitive character was found for compound **82**. Overall a non-competitive interaction, mostly of the "mixed type", resulted for the majority of the investigated compounds. Similar findings were made for the 4-substituted-2-phenylquinazolines of project I. Moreover, no contradiction in the kinetic interpretation was found between the Lineweaver-Burk and the Cornish-Bowden method.

4.7 Investigation of the conformation sensitive 5D3 antibody binding to an epitope of ABCG2

The conformational impact of selected compounds on ABCG2 was investigated with the conformation sensitive 5D3 antibody which binds specifically to an epitope of the transport protein. Measurement of the fluorescence emitted by the bound antibody was carried out with a FACSCalibur flow cytometer using ABCG2 overexpressing PLB-985 cells. Additional information about the assay is provided in chapters 3.7 and 10.2.2.9. The results from this assay are summarized as a bar-chart in Figure 49 using Ko143 as positive control representing 100% labelling with the antibody.

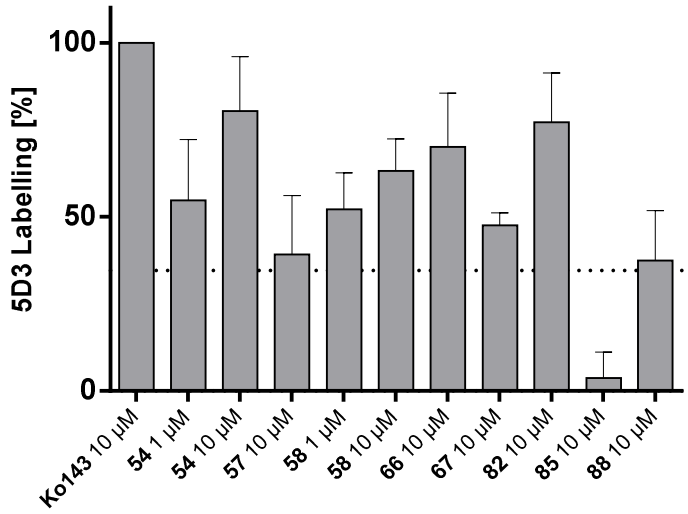

Figure 49: 5D3 immunoreactivity modulation of ABCG2 by various compounds at a concentration of 1 and 10 µM. Fluorescence detected by the 5D3-labeling of ABCG2 in the presence of 10 µM Ko143 was set to 100% and the fluorescence measured in the absence of any compound taken as 0%. The dotted line represents the labelling obtained with Hoechst 33342.

Highest labelling with the antibody was observed for the most potent compound **54** (80%) followed by **82** (77%) and **66** (70%) at a compound concentration of 10 µM. Although all three compounds exhibited a high inhibitory potency in the Hoechst 33342 accumulation assay, the IC_{50} does not necessarily correlate with the rate of staining. This is illustrated by the compounds **57** and **85** possessing high inhibitory potencies but showing low labelling with the 5D3 antibody. Moreover, some compounds presented in chapter 3.7 with relatively low inhibitory potencies (e.g. **17** and **19**) gave a high rate of labelling with the antibody.

A significant difference in the degree of labeling was found among the *meta* and *para* trifluoromethyl derivatives **66** and **67**. Here, an increased rate of labelling (70%) resulted for the *meta* derivative whereas the *para* derivative yielded a lower rate (48%). Both compounds had shown a mixed interaction type with Hoechst 33342, whereas only compound **66** exhibited a notable increase of K_M with increasing concentration in the Cornish-Bowden plot, which is characteristic for a competitive interaction.

An increase of the compound concentration from 1 µM to 10 µM led to a higher labelling with the antibody in case of compounds **54** and **58**, where the increase of labelling was considerably higher for compound **54**.

Representative histograms of the compounds Ko143, **54** and **85** at 10 µM are illustrated in Figure 50.

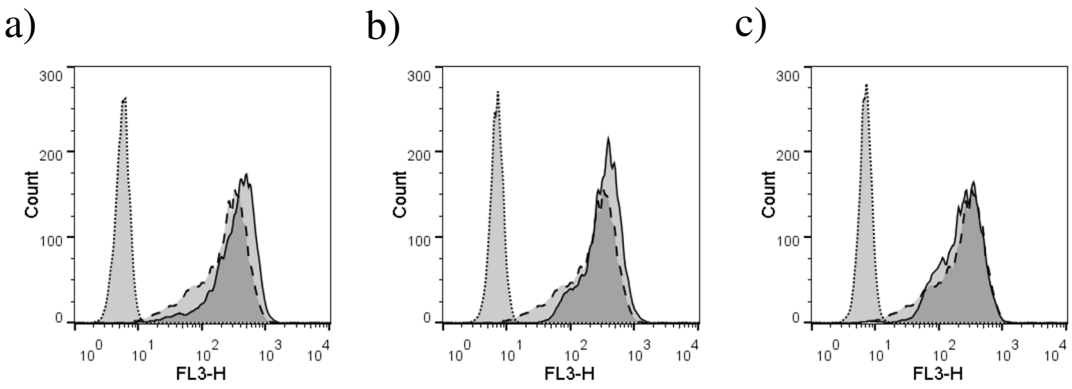

Figure 50: Histogram of the measured fluorescence at the FL3-H detector (X-axis) and the cell-count gated according to the fluorescence. Depicted is the fluorescence of the isotype-control (dotted curve) as well as of 5D3 antibody in the absence of a compound (dashed curve) and in the presence of a compound (continuous curve). Compounds with the highest and lowest 5D3 shifts: ***Ko143*** *(a),* ***54*** *(b) and* ***85*** *(c) at a concentration of 10 µM.*

Fluorescence of the isotype-control in presence of the corresponding compound is shown as a dotted line. This is necessary to exclude any unspecific staining. Also, the obtained fluorescence with 5D3 antibody in the absence (dashed curve) and presence (continuous curve) of a compound is provided. Here, high shifts were observed with Ko143 and compound **54**, while **85** results in a minor shift comparable to the fluorescence obtained with the antibody alone.

4.8 Investigation of the ATPase activity

Again Ko143 was used as the standard ATPase inhibitor and quercetin as the standard stimulator. The ATPase activity assays were performed by Jennifer Gallus. Further details are provided in chapters 3.8 and 10.2.2.10.

The screening was conducted at three different concentrations (1, 10 and 25 µM) including only the most potent compounds. A summary of the results is provided as bar chart in Figure 51.

The majority of the compounds showed high stimulation of the ATPase activity and only few a moderate stimulation near basal level. Indeed, the substitution pattern of the pyridyl at R_1 had a measurable impact on the ATPase activity. For instance, a considerably greater increase of the stimulatory effect resulted for the *para* pyridyl derivatives in comparison to their *meta* pyridyl analogues. This is exemplified in the *meta*/*para* compound pair **52/53** and **56/57**. Interestingly, compound **57** containing a 3-cyano function at R^2 led to a higher ATPase stimulation than the standard stimulator quercetin. This is in accordance with the results of project I where the 2-phenylquinazoline analogue **4** containing 3-cyano caused a considerably high activation. Almost no stimulation was found for compound **58** with a 4-cyano substituent. A similar result had already been observed for its 2-phenylquinazoline analogue **5** (see chapter 3.8). The different impact between a *meta* and a *para* substitution at the aniline linker at position 4 of the quinazoline scaffold confirmed the results of previous assays.

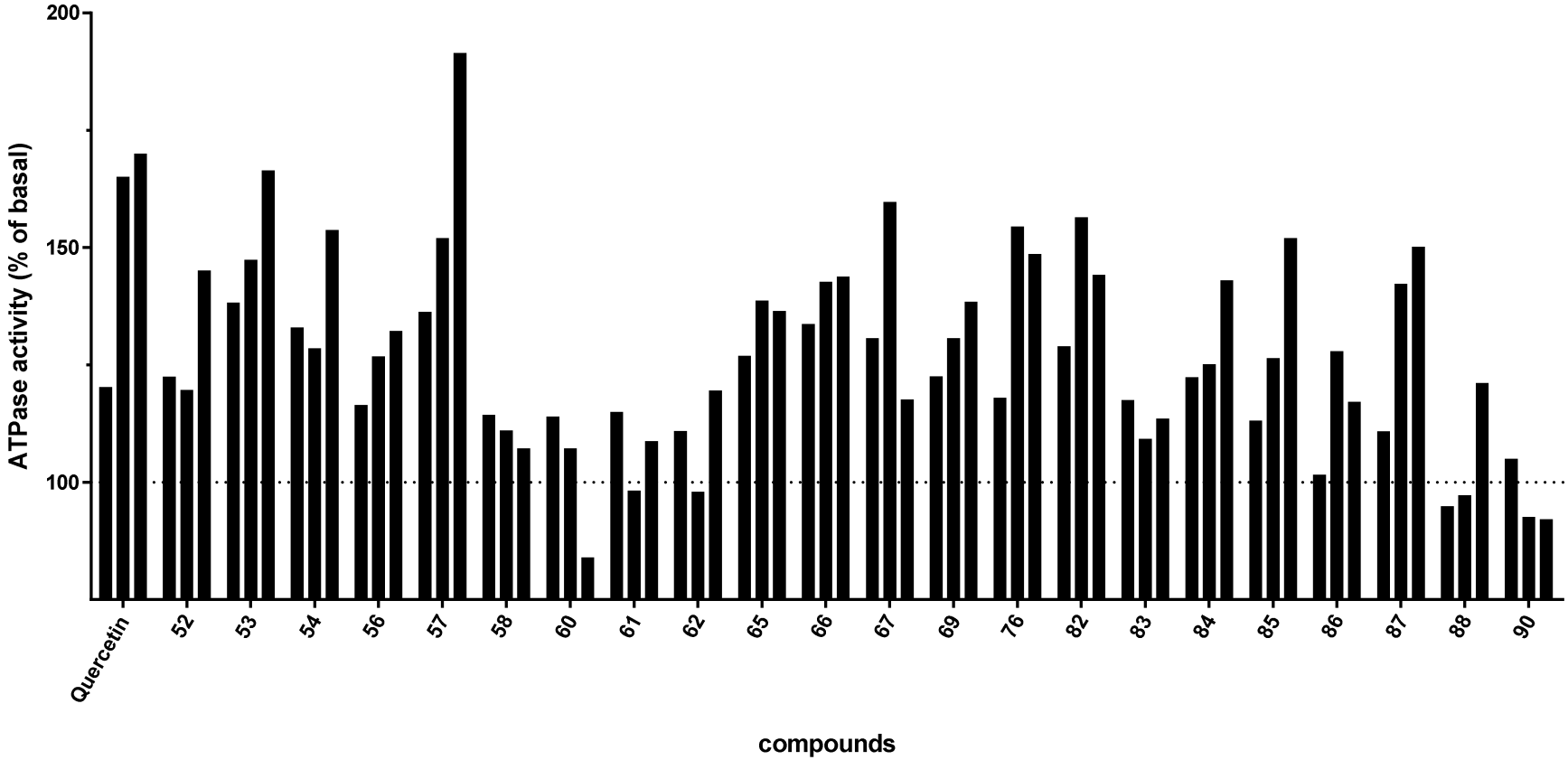

Figure 51: Screening of ATPase activity of selected compounds at three different concentrations. From left to right the bars correspond to 1, 10 and 25 µM final concentration of compound. Quercetin was used as a standard for activation of ABCG2 ATPase activity. All values are relative vanadate-sensitive ATPase activities in relation to the basal activity, which is set to 100%.

Only low stimulation near the basal level was observed for compounds **60-62** containing a *meta* or *para* methoxy group at R^2. In the previous enzyme kinetic investigation compound **61** was found to possess a distinct competitive interaction with Hoechst 33342 (see chapter 4.6). According to the collected data, a connection between a near basal or even subbasal ATPase activity and a pronounced competitive kinetic interaction with Hoechst 33342 can be drawn. Moreover, compounds with a decreased ATPase activity frequently caused high conformational changes in ABCG2 like the standard Ko143, as investigated in the 5D3 antibody binding assays.

Regarding the 4-methyl pyrimidine derivatives **82**-**88**, the trends of the ATPase activity were quite similar to their quinazoline analogues. In Figure 52 the concentration-response curves of selected compounds **54**, **61, 66** and **79** are depicted.

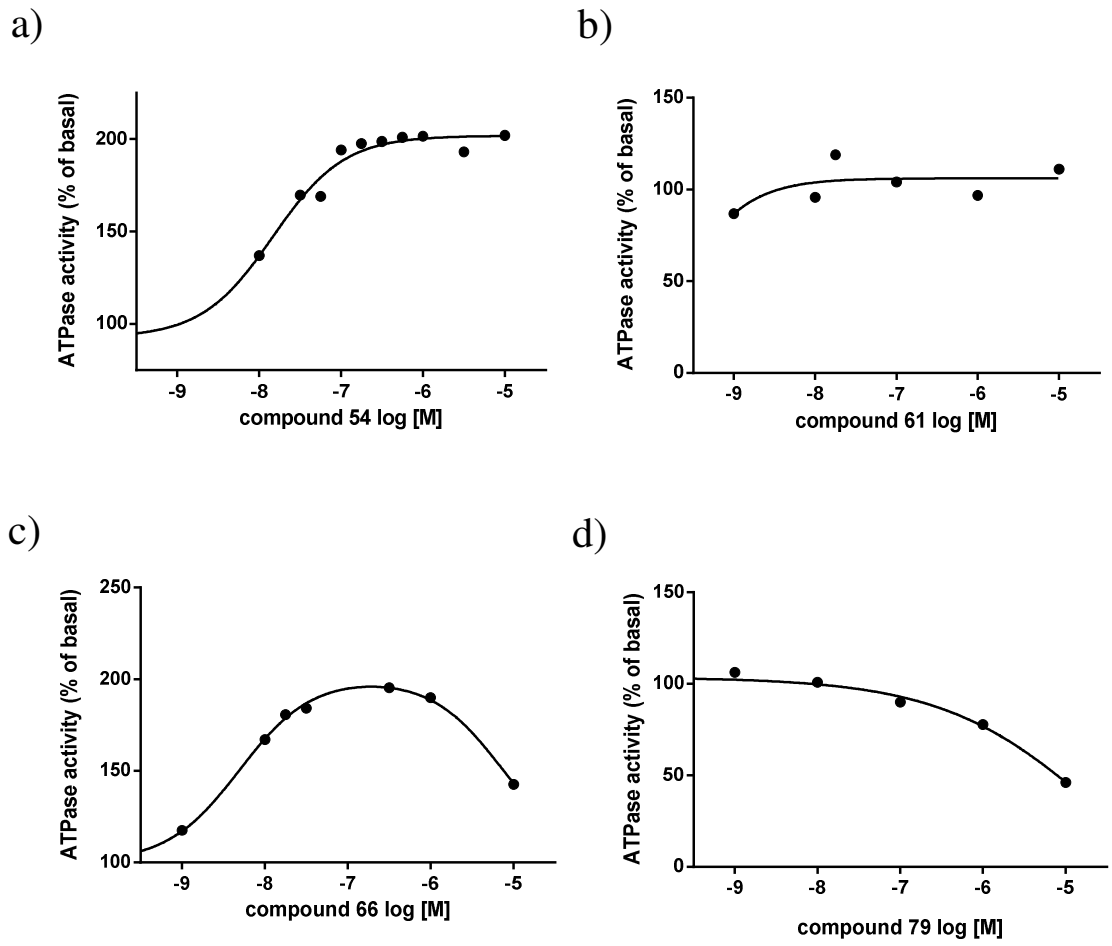

*Figure 52: Concentration-response curves for compounds **54** (a, EC_{50}: 26.7 nM), **61** (b), **66** (c) and **79** (d) in the ATPase assay. All values are relative vanadate-sensitive ATPase activities in relation to the basal activity, which is set to 100%.*

Most potent compound **54** caused a considerable stimulation of the ATPase activity, resulting in a sigmoidal concentration-response curve. The maximum value of the curve was similar to the standard activator quercetin obtaining an EC_{50} value of 26.7 nM in comparison to 302 nM of quercetin. Almost no stimulation was found for compound **61**. Interestingly a bell-shaped curve resulted for compound **66**. This is presumed to be due to an activating high-affinity and a deactivating low-affinity binding site. At low compound concentration predominantly the activating binding site is occupied whereas high concentrations lead to binding to the deactivating site triggering a reversal of the ATPase activity.[206] A strong inhibition of the ATPase activity resulted for compound **79** containing a bulky 3-*tert*-butyl ester group.

5 Project III: 2,4-Substituted quinazolines

In this project substitution was carried out on corresponding aromatic cores at position 2 and 4 of the quinazoline scaffold. Hence, precursors of differently substituted 4-chloro-2-phenylquinazoline derivatives were synthesized and reacted with differently substituted aniline derivatives *via* nucleophilic substitution under microwave radiation. In comparison to the compounds of project I this modification increased the number of possible substituent combinations and provides additional information on the reciprocal effects among the functions at positions 2 and 4 of the quinazoline scaffold. This is in particular interesting in terms of cumulative effects and also the interchangeability of substituents at positions 2 and 4 with respect to the inhibitory potency of a compound.
Decreased solubility, which was observed in only a few *para* nitro derivatives like compound **89** (see chapter 4) and **144** was reviewed by measuring the absorption over a period of 2 h.

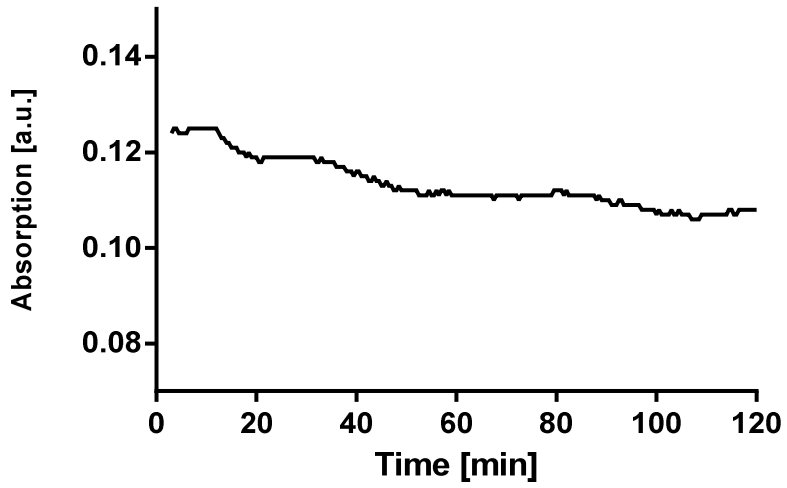

*Figure 53: Absorption spectrum measured at the excitation maximum of compound **144** over a time period of 2 h. The compound was diluted in KHB to 10 µM and the measurement carried out at room temperature.*

According to Figure 53 no precipitation occurs at a final concentration of 10 µM of compound **144**. Questionable IC_{50} values published in former work of Juvale *et al.* were re-determined and corrected.[198]

5.1 Reaction mechanism

A schematic synthesis route and a detailed reaction mechanism is provided in this chapter.

*Scheme 4: General synthesis scheme for the preparation of compounds **91-152**.[a]*

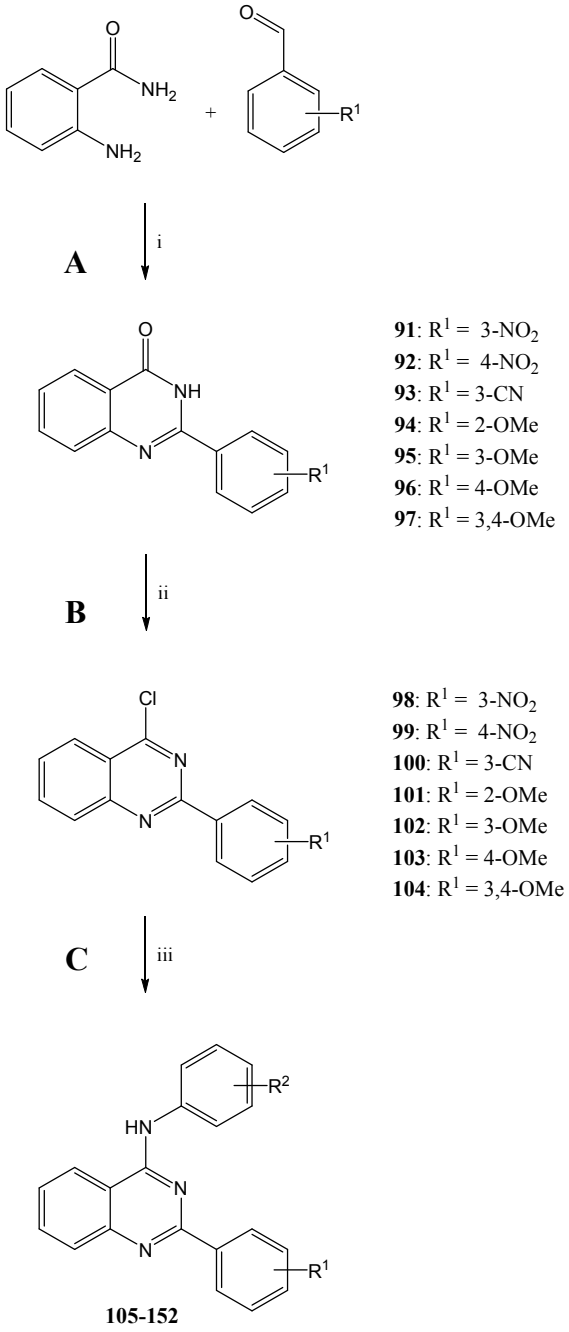

[a]: Reagents and conditions: (i) DMF, I_2, K_2CO_3, 70-90 °C, 4-8 h. (ii) $POCl_3$, reflux, 4-12 h. (iii) Substituted aniline, 100 watt microwave irradiation, 110 °C, 15 - 30 min.

Reaction mechanism **A**:

The reaction mechanism is analogue to that used for the compounds in project II and can be reviewed in chapter 4.1 (reaction mechanism **A**).

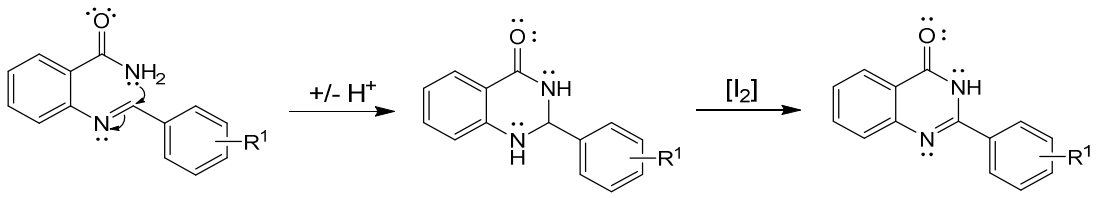

Reaction mechanism **B**:

The carbonyl function at position 4 is substituted by chlorine *via* a chlorination reaction using $POCl_3$. The mechanism is analogously to that presented in chapter 4.1.

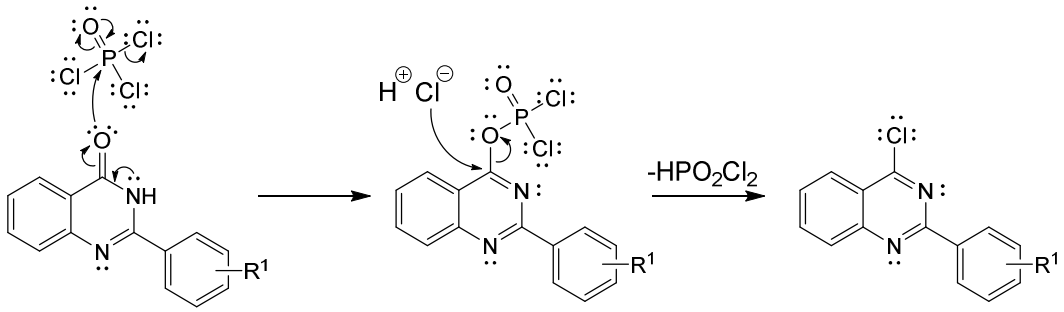

Reaction mechanism **C**:

Synthesis of the final compounds follows the mechanism explained in chapter 3.1 and can be reviewed there.

5.2 Investigation of the inhibitory potency toward ABCG2 in the Hoechst 33342 accumulation assay

The inhibitory potency of the compounds was investigated in a Hoechst 33342 accumulation assay using the ABCG2 overexpressing MDCK II BCRP and parental cell

line. Additional information to the Hoechst 33342 accumulation assay as is presented in chapter 3.2 and 10.2.2.2. The associated activity data is summarized in Table 16.

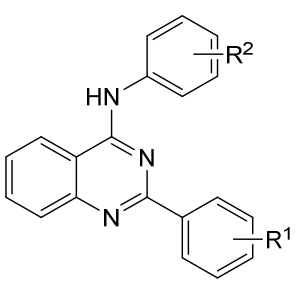

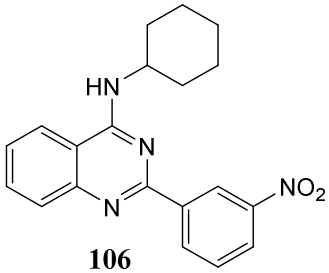

106

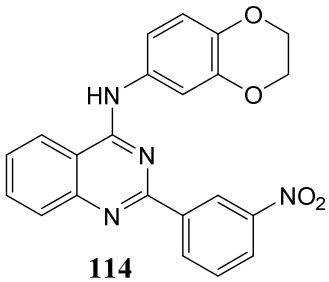

114

Table 16: Inhibitory Activities Determined in the Hoechst 33342 Accumulations Assay Using ABCG2 Overexpressing MDCK II BCRP Cells. Structural Formulas of the Substitution Pattern are Depicted Above the Table.

Compound	R^1	R^2	Hoechst 33342 IC_{50} ± SD [nM][a]
105	3-NO_2	H	108 ± 21
106	3-NO_2	[d]	2780 ± 660
107	3-NO_2	3-NO_2	236 ± 16
108	3-NO_2	3-NO_2,4-OH	151 ± 7
109	3-NO_2	3-CN	120 ± 27
110	3-NO_2	3-OCH_3	121 ± 14
111	3-NO_2	3,4-OCH_3	55.6 ± 3.1
112	3-NO_2	3-OCH_3,4-Br	801 ± 257
113	3-NO_2	3,4-Oet	210 ± 41
114	3-NO_2	[d]	263 ± 53
115	3-NO_2	3-SCH_3	94.8 ± 17.2
116	3-NO_2	4-SCH_3	88.6 ± 15.9
117	3-NO_2	3-NH_2	284 ± 40
118	3-NO_2	3-N(-CH_3)$_2$	221 ± 15
119	3-NO_2	3-N(-CH_2CH_3)$_2$	230 ± 43
120	3-NO_2	3-$NHCOCH_3$	127 ± 7
121	3-NO_2	3-CF_3	10700 ± 900
122	3-NO_2	3-CF_3,4-OCH_3	16200 ± 4900
123	3-NO_2	4-I	1770 ± 380
124	4-NO_2	3-NO_2	166 ± 19
125	4-NO_2	3-CN	336 ± 20
126	4-NO_2	3-OCH_3	107 ± 17

Table continues on the next page

127	4-NO_2	3,4-OCH_3	86.7 ± 8.0
128	3-CN	3-OH,4-OCH_3	297 ± 53
129	3-CN	3-$NHCOCH_3$	225 ± 18
130	2-OCH_3	3-NO_2	642 ± 134
131	3-OCH_3	3-NO_2	139 ± 34
132	3-OCH_3	4-NO_2	68 ± 13
133	3-OCH_3	3,5-NO_2	291 ± 54
134	3-OCH_3	3-NO_2,4-F	1190 ± 340
135	3-OCH_3	3-CN	359 ± 66
136	3-OCH_3	3-F	1640 ± 310
137	3-OCH_3	3-OCH_3	811 ± 178
138	3-OCH_3	3,4-OCH_3	480 ± 29
139	4-OCH_3	3-NO_2	183 ± 19
140	4-OCH_3	3-CN	2120 ± 310
141	4-OCH_3	3-OCH_3	2140 ± 380
142	4-OCH_3	3,4-OCH_3	418 ± 13
143[b]	3,4-OCH_3	3-NO_2	82.5 ± 6.2
144[b]	3,4-OCH_3	4-NO_2	44.2 ± 8.6
145	3,4-OCH_3	3,5-NO_2	610 ± 54
146	3,4-OCH_3	3-NO_2,4-OH	305 ± 21
147	3,4-OCH_3	3-CN	136 ± 16
148	3,4-OCH_3	3-CF_3,4-OCH_3	795 ± 190
149	3,4-OCH_3	3-OCH_3	365 ± 57
150	3,4-OCH_3	3-OCH_3,4-Br	47.5 ± 7.1
151	3,4-OCH_3	3-F	462 ± 93
152	3,4-OCH_3	3-SO_2F	570 ± 116
Ko143[c]			227 ± 14
Elacridar			361 ± 48

[a]: *IC_{50} values are means of three independent experiments.*
[b]: *Compounds synthesized in earlier study.*[198]
[c]: *Used as reference in the assay.*
[d]: *See substitution pattern above.*

According to the results of project I and II compounds with nitro in *meta* or *para* position at the anilino linker exhibit an excellent inhibitory potency (e.g. compounds **2** and **90**) often favouring the *para* substitution as more beneficial. As little was known about the effects of substitutions at the aromatic core in position 2 of the quinazoline scaffold the interchangeability of several different functions between R^1 and R^2 was investigated. In the case of 3-nitro only a negligible difference was found after interchange of the substituents leading to comparable IC_{50} values of 130 nM and 108 nM for the corresponding compound **2** and **105**. The phenomenon of interchangeability of

substituents between R^1 and R^2 was also observed for several other compounds which are summarized in Figure 54.

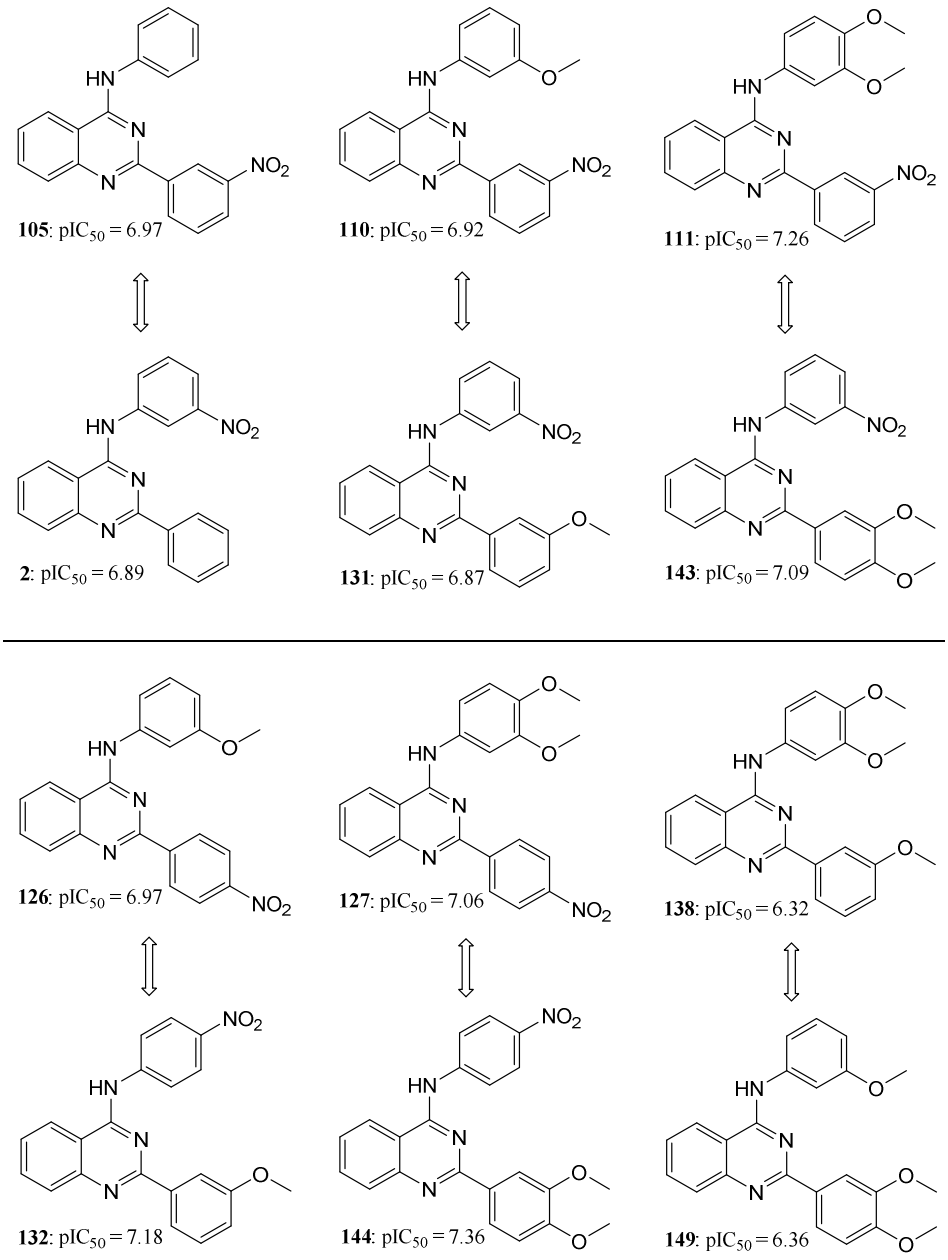

Figure 54: Comparison of the pIC50 values of structurally related compounds with interchanged substituents at R1 and R2.

Also the importance of an aromatic residue at position 4 of the quinazoline scaffold was investigated. Hence, the potent compound **105** containing 3-nitro at R^1 and an anilino moiety at position 4, was compared to compound **106** with a cyclohexylamino function

at position 4 instead of anilino. Interestingly, the loss of the aromaticity resulted in a considerable decrease of inhibitory potency of more than 25-fold.

Extraordinarily potent compounds resulted from combination of a nitro group together with a methoxy or 3,4-dimethoxy substitution at R^1 and R^2. The highest inhibitory potency was determined for compound **144**, containing a 3,4-dimethoxy group at R^1 and 4-nitro at R^2 with an IC_{50} of 44.2 nM. It was found that disubstitution with 3,4-dimethoxy led to higher potencies than a mono-methoxy function in combination with nitro groups. Examples are compounds **111**, **127**, **143** and **144**, all of which are highly potent inhibitors possessing an IC_{50} value below 100 nM.

Also the combination of 3,4-dimethoxy at R^1 and 3-methoxy,4-bromo at R^2 in compound **150** yielded a rather low IC_{50} of 47.5 nM. The 3-methoxy,4-bromo substitution had already proven its benefit in project I exhibiting a high inhibitory potency in the 4-substituted 2-phenylquinazoline derivative **16** (IC_{50}: 289 nM). Concentration-response curves of the three most potent compounds **111**, **144** and **150** in the Hoechst 33342 accumulation assay are depicted in Figure 55.

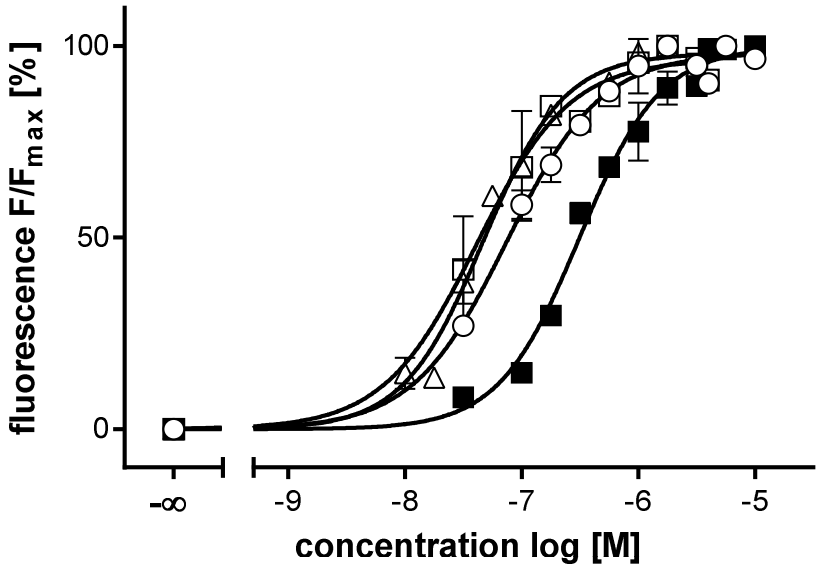

*Figure 55: Concentration-response curve of compound **111** (○, IC_{50}: 55.6 nM), **144** (□, IC_{50}: 44.2 nM) and **150** (Δ, IC_{50}: 47.5 nM) in the Hoechst 33342 accumulation assay with Ko143 (■, IC_{50} : 227 nM) as reference, using the ABCG2 overexpressing MDCK II BCRP cell line.*

Since the combination of 3,4-dimethoxy groups and nitro functions yielded extraordinarily high inhibitory potencies, further modifications at the methoxy functions

were carried out. Unfortunately, replacement of the 3,4-dimethoxy group by a 3,4-diethoxy or a 1,4-dioxane function resulted in a decreased inhibitory potency of about 4-fold illustrated in the 3-nitro (R^1) derivatives **111**, **113** and **114**. This could be due to the increased sterical demand of the ethoxy function and the restrained flexibility in the dioxane derivative.

Although some evidence was found that substituents like nitro and cyano which exhibit a negative mesomeric effect (-M) on the aromatic rings at position 2 and 4, led to high inhibitory potencies, other groups like dimethoxy with a positive mesomeric effect on the aromatic moiety also led to increased inhibitory potencies.

More important could be the formation of H-bonds by functions like nitro, cyano or methoxy that could be pivotal for interaction with the transport protein. Hydrogen bond donor functions in *meta* position of the anilino linker (R^2) are most likely not crucial for the potency of a compound as demonstrated by **117**, **118** and **119**: here, the free amine yielded a very similar IC_{50} as the dimethylamino and the diethylamino derivative, indicating that the free electron pair of the nitrogen is important for activity.

Regarding *ortho* substitutions at R^2, that have been found to lead to low inhibitory activities, one compound was synthesized with an *ortho* substitution at R^1 for comparison. As expected, it possessed the lowest inhibitory potency as illustrated by the three methoxy derivatives **130**, **131** and **139**. Again, this might be due to steric requirements of the substituent as mentioned in chapter 3.

5.3 Investigation of the inhibitory potency toward ABCB1 and ABCC1 in the calcein AM assay

The selectivity of several compounds toward ABCG2 was screened in a calcein AM. For this purpose, the ABCB1 overexpressing cell line A2780 adr and the ABCC1 overexpressing cell line H69 AR were used and the assay carried out as described in chapters 3.3 and 10.2.2.4. For the screenings a compound concentration of 10 µM was chosen and CsA was used as positive control, indicating total inhibition of both transporters. For compounds showing an inhibitory potency of more than 25% relative to the control, additional dilutions were prepared to generate a concentration-response curve

resulting in an IC_{50} value. A summary of the calculated IC_{50} values of the compounds showing more than 25% of inhibition in the screening is given in Table 17. Screening results for the inhibitory activity toward ABCB1 and ABCC1 are depicted as bar charts in Figure 56. A clear correlation was observed between the number of methoxy functions present in a compound and the inhibitory potency toward ABCB1 and, although to a lower extent, also toward ABCC1.

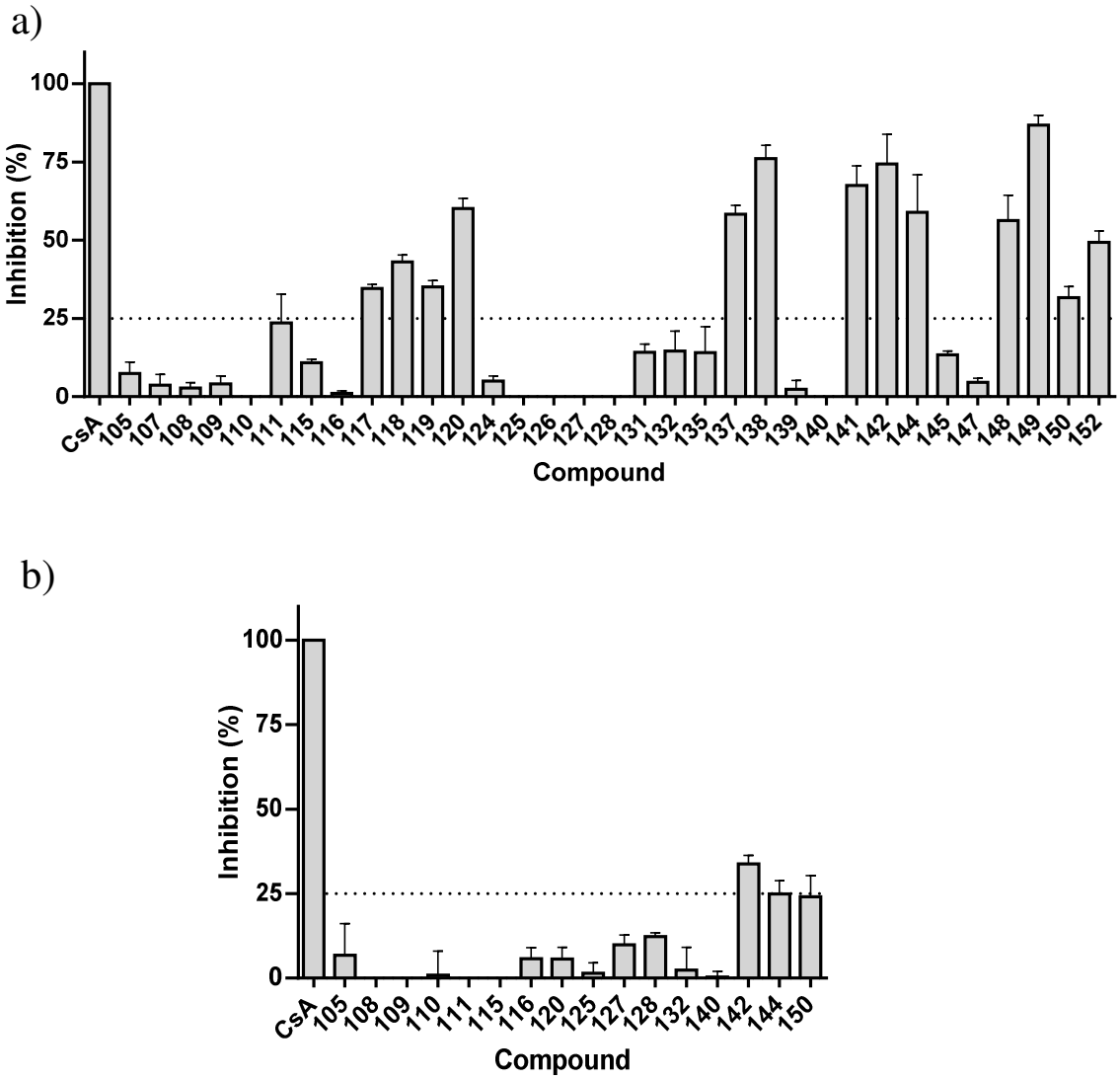

Figure 56: Inhibitory effect of screened compounds toward ABCB1 overexpressing cell line A2780 adr (a) and MRP1 overexpressing cell line H69 AR (b) in the calcein AM assay at a concentration of 10 µM. Cyclosporine A (CsA) was used as positive control, indicating complete inhibition. The inhibitory effect of each compound is expressed by the length of the bars, representing the inhibition compared to the positive control in percent. For each compound, three independent experiments were performed and the standard deviation is expressed by error bars.

Among the compounds that exceed the 25% mark in the calcein AM assay solely compound **120** with an amido group and the amino-derivatives **117**-**119** contain no methoxy group. Compounds capable of inhibiting more than one target transport protein are of particular interest with regard to tissues that express several different ABC transport proteins like ABCG2 and ABCB1 that are for instance overexpressed in the BBB.
In this context, broadspectrum inhibitors like elacridar have been successfully tested *in vivo* in tissues showing an overexpression of ABCG2 and ABCB1. Promising candidates of broadspectrum inhibitors are for instance compound **138**, **142**, **144** and **149** that were found to be highly potent inhibitors of ABCG2 and also ABCB1, some possessing comparable or even better inhibitory activities toward ABCB1 than the standard CsA.

Table 17: Inhibitory Activity of Compounds Showing an Inhibition of more than 25% in Comparison to the Reference Cyclosporine A (CsA) in the calcein AM Assay at a Concentration of 10 µM.

Compound	R^1	R^2	Calcein AM (ABCB1) IC_{50} ± SD [µM][a,b]	Calcein AM (ABCC1) IC_{50} ± SD [µM][a,c]
117	3-NO_2	3-NH_2	13.10 ± 1.02	n.t.
118	3-NO_2	3-$N(CH_3)_2$	6.30 ± 0.71	n.t.
119	3-NO_2	3-$N(CH_2CH_3)_2$	9.36 ± 1.28	n.t.
120	3-NO_2	3-$NHCOCH_3$	1.81 ± 0.58	n.d.
137	3-OCH_3	3-OCH_3	1.87 ± 0.36	n.t.
138	3-OCH_3	3,4-OCH_3	1.10 ± 0.22	n.t.
141	4-OCH_3	3-OCH_3	2.46 ± 0.23	n.t.
142	4-OCH_3	3,4-OCH_3	1.22 ± 0.17	7.72 ± 0.99
144[d]	3,4-OCH_3	4-NO_2	2.45 ± 0.42	40.6 ± 12.9
148	3,4-OCH_3	3-CF_3,4-OCH_3	1.67 ± 0.46	n.t.
149	3,4-OCH_3	3-OCH_3	1.04 ± 0.09	n.t.
150	3,4-OCH_3	3-OCH_3,4-Br	3.15 ± 0.66	44.2 ± 4.4
152	3,4-OCH_3	3-SO_2F	3.26 ± 0.06	n.t.
Cyclosporine A[e]			1.21 ± 0.17	3.53 ± 0.61

[a]: *IC_{50} values were determined by at least three independent experiments.*
[b]: *The ABCB1 overexpressing cell line A2780 adr was used.*
[c]: *The ABCC1 overexpressing cell line H69 AR was used.*
[d]: *Compound was synthesized previously.*[198]
[e]: *Cyclosporine A is used as reference for both assays.*
n.d.: Not determined, due to low effect in the initial screening.
n.t.: Not tested

Representative concentration-response curves of compound **149** and CsA are depicted in Figure 57.

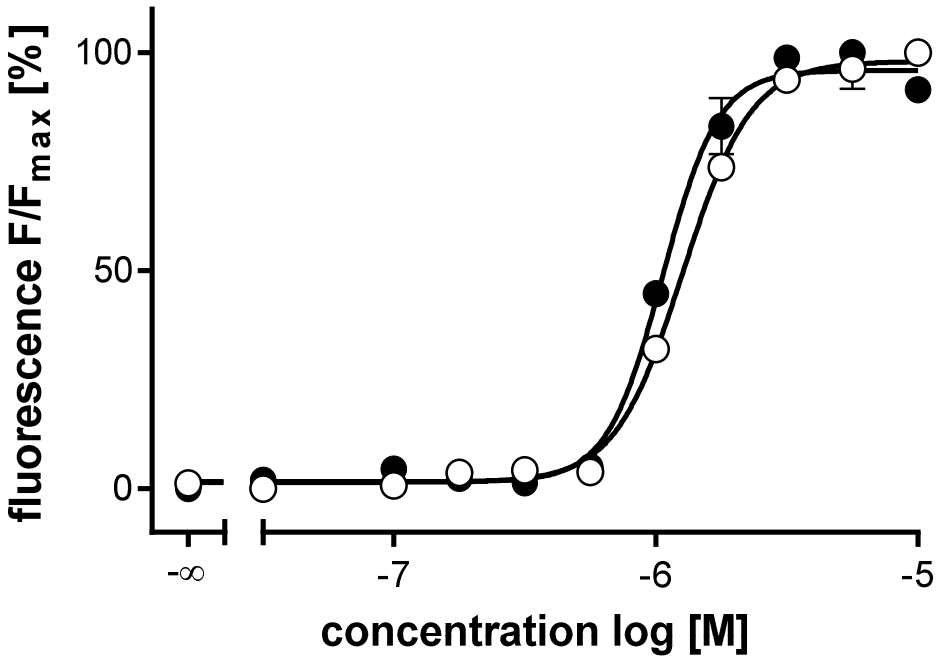

*Figure 57: Concentration-response curve of compound **149** (■, IC_{50}: 1.04 µM) in a calcein AM assay with CsA (○, IC_{50}: 1.21 µM) as reference, using the ABCB1 overexpressing cell line A2780 adr.*

The inhibitory potency toward ABCC1 was screened with fewer compounds since compounds from project I and II exhibited a lower activity. This was substantiated by the compounds of project III. One compound (**142**) was similar active against ABCB1 and ABCC1.

Only three compounds in the test set, including the most potent, barely exceeded the 25% mark in the CsA assay with ABCC1 overexpressing cells. This resulted in considerably high IC_{50} values derived from the corresponding dose response curves that had to be fitted to the top fluorescence value of CsA.

Indeed, it has to be pointed out that the majority of the substances, in particular those containing nitro functions, exhibited an excellent selectivity toward ABCG2. Some examples are the highly potent compounds **105**, **108**, **111**, **124**, **126**, **127**, **131**, **132**, **139**, and **147**.

5.4 Investigation of the intrinsic cytotoxicity with the MDCK II cell lines in a MTT assay

The determination of the intrinsic cytotoxicity of selected compounds was performed in a MTT assay using MDCK II parental and ABCG2 overexpressing cells. For this purpose, the toxic effects were measured after 72 h incubation of the cells in the presence of different compound concentrations using MTT as indicator of the cell viability. More details regarding the assay are provided in chapters 3.4 and 10.2.2.5. The obtained GI_{50} values and the corresponding therapeutic ratios are depicted in Table 18.

Table 18: Intrinsic Toxicity of Selected Compounds on MDCK II ABCG2 Overexpressing and Parental Cells.

Compound	R^1	R^2	GI_{50} [µM][a] BCRP	GI_{50} [µM][a] Parental	Therapeutic ratio (GI_{50}/IC_{50})
107	3-NO_2	3-NO_2	4.6	4.9	19
109	3-NO_2	3-CN	4.9	4.3	41
110	3-NO_2	3-OCH_3	7.3	9.1	60
111	3-NO_2	3,4-OCH_3	15	16	270
120	3-NO_2	3-$NHCOCH_3$	26	84	210
121	3-NO_2	3-CF_3	8.5	9.8	0.80
122	3-NO_2	3-CF_3,4-OCH_3	1.5	0.92	0.094
123	3-NO_2	4-I	3.2	4.4	1.8
127	4-NO_2	3,4-OCH_3	8.7	13	49
131	3-OCH_3	3-NO_2	20.9	33	150
132	3-OCH_3	4-NO_2	8.0	11	120
134	3-OCH_3	3-NO_2,4-F	99	78	83
138	3-OCH_3	3,4-OCH_3	8.7	9.3	18
143[b]	3,4-OCH_3	3-NO_2	23	17	150
144[b]	3,4-OCH_3	4-NO_2	6.4	6.9	140
147	3,4-OCH_3	3-CN	20	73	150
149	3,4-OCH_3	3-OCH_3	15	14	33
150	3,4-OCH_3	3-OCH_3,4-Br	10	11	210
Ko143			13	13	49
MeOH/DMSO			96[c]	140[c]	

[a]: *Concentration leading to 50% of cell survival of MDCK II BCRP and parental cells. The data was obtained from at least two independent experiments as mean values.*

[b]: *Compound was synthesized previously.*[198]

[c]: *Positive control of the cytotoxicity from dilution with DMSO/MeOH without compound.*

Investigation of the intrinsic cytotoxicity of selected compounds showed that GI_{50} values were either comparable or slightly worse than those in project I. This could be due to the presence of more functional groups leading to an accumulation of toxic effects. However, this suggestion does not apply to every substitution pattern. For instance the disubstitution with 3-nitro-4-hydroxy at the anilino linker was found to be considerably beneficial (see project I, compound **3**). Corresponding monosubstitutions in compound **6** and **131** often led to increased cytotoxic effects.

Another crucial factor for the cytotoxicity of a compound was found to be the position of the substitution at the aromatic ring as shown by comparing the *meta* and *para* derivatives **131/132** and **143/144**.

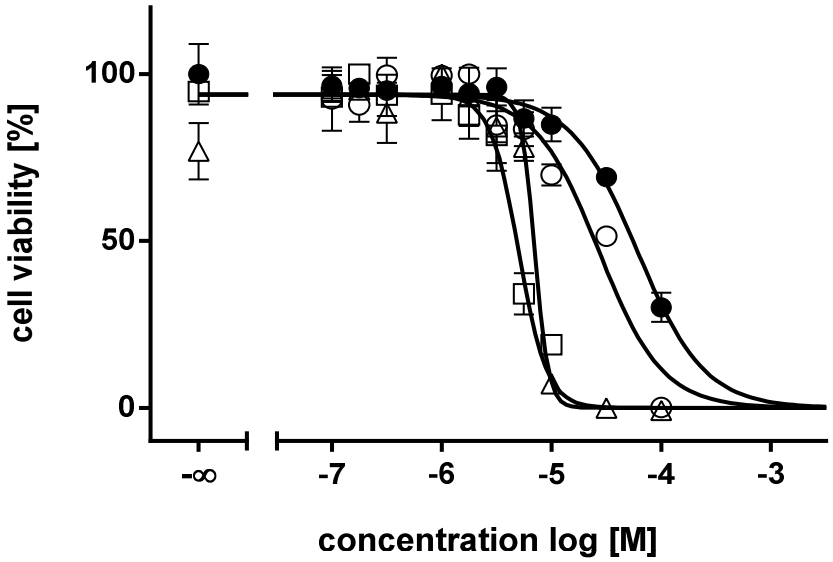

*Figure 58: MTT viability assay of compounds **111** (○), **144** (□), and **150** (Δ) using the MDCK II ABCG2 overexpressing cell line. The GI_{50} values were determined as 15.1 µM (○), 6.40 µM (□) and 10.0 µM (Δ), respectively. A control with the same concentration of MeOH and DMSO as used for the dilution of the compounds, was carried out for comparison (●, GI_{50} = 96.1 µM). The amount of MeOH and DMSO used for the dilution was ≤ 1.8% and ≤ 1.0%, respectively.*

The highest TR among the investigated compounds was found for compound **111** with a GI_{50}/IC_{50} ratio of 270. As a comparison, Ko143 had a TR of only 48.9.

Concentration-cell-viability curves for compounds **111**, **144** and **150**, which possessed the highest inhibitory potencies in the Hoechst 33342 accumulation assay, are illustrated in Figure 58. Despite their increased intrinsic cytotoxicity, the compounds yielded relatively high TRs owing to their high potency.

An overview of the TRs of selected compounds is provided as a bar chart in Figure 59.

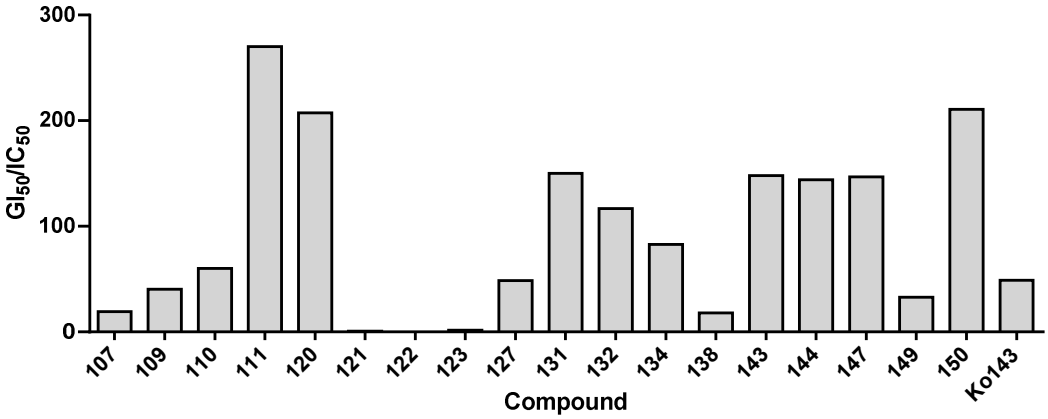

*Figure 59: Therapeutic ratios of selected compounds, calculated from the ratio of GI_{50} and IC_{50} values determined in MTT viability assay and Hoechst 33342 accumulation assay, respectively. The highest value was calculated for compound **111** (GI_{50}/IC_{50} = 270), while the reference compound Ko143 yielded GI_{50}/IC_{50} = 48.9.*

5.5 Investigation of the reversal of multidrug resistance

The Reversal of the MDR in ABCG2 overexpressing MDCK II BCRP cell line toward SN-38 was investigated by co-administration of the most potent compounds **144** and **150**. Further details are provided in chapters 3.5 and 10.2.2.6. Concentration-viability curves obtained by parental and ABCG2 expressing MDCK II cell lines are depicted in Figure 60.

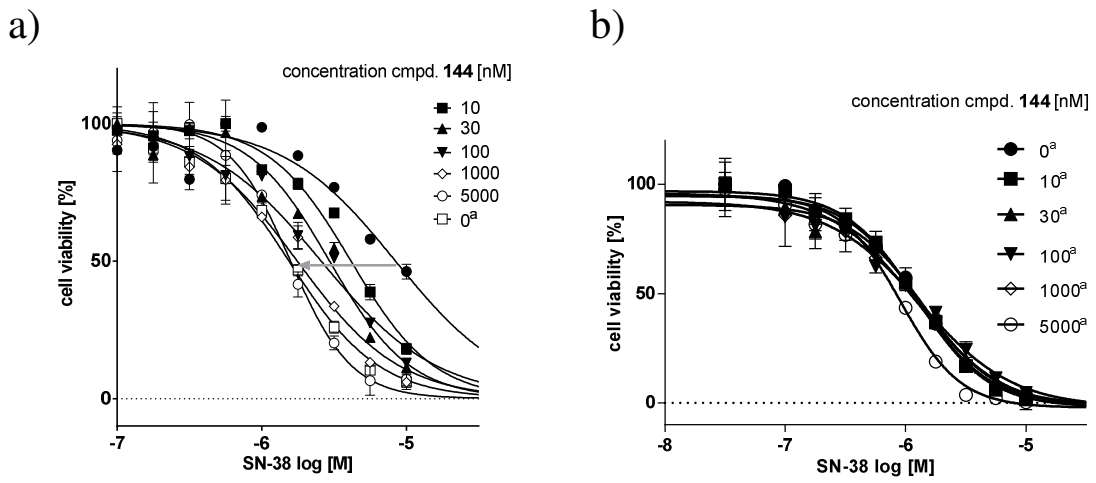

Figure continues on the next page

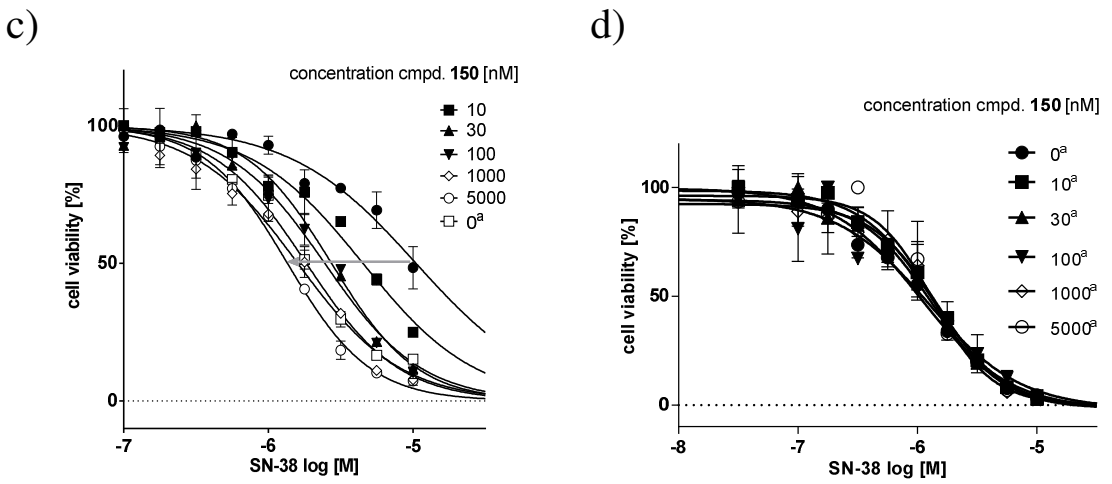

*Figure 60: MDR reversal assay of compound **144** and **150** demonstrating the ability to reverse the MDR toward the cytostatic SN-38, using parental MDCK II and ABCG2 overexpressing cell lines (a, c). The grey arrow indicates the increasing sensitization of the ABCG2 overexpressing cells with higher compound concentrations (see legend). At a compound concentration of 1 µM, full reversal is achieved, indicated by a similar pGI_{50} as the parental cells. For comparison an analogue assay was performed using only parental MDCK II cells (b, d).*
a: Parental MDCK II cells.

Compounds **144** and **150** both produce a full reversal of the resistance toward SN-38 at a concentration of 1 µM, as indicated by comparable GI_{50} values of the parental cells and the ABCG2 expressing cells in the presence of a compound. Reversal of MDR is illustrated by the grey arrow in Figure 60 a) and c) and shows the shift of the GI_{50} values toward higher compound concentration.

An analogous assay was carried out with only parental cells leading to comparable pGI_{50} values for each compound concentration (Figure 60 b) and c)). Hence, the shift in the ABCG2 overexpressing cells is caused by the inhibition of the transporter but not due to cytotoxic or other unspecific effects.

For a clear visualization of the obtained results, the pGI_{50} values from the MDR reversal assay were plotted against the logarithm of the corresponding compound concentration. And a sigmoidal concentration-effect curve was fitted with the logistic equation yielding EC_{50} values characterizing the extent of MDR reversal by a compound as depicted in Figure 61. Hereby, EC_{50} values of 12.7 and 15.6 nM were determined for compound **144** and **150**, respectively. According to the results, the efficacy of both compounds is about 3 to 3.5-fold higher than the calculated IC_{50} value obtained in the Hoechst 33342

accumulation assay. This result is similar to the most potent compounds of project I and II, namely **5** and **54** that also possessed a higher efficacy than the result of the Hoechst 33342 accumulation assay suggested.

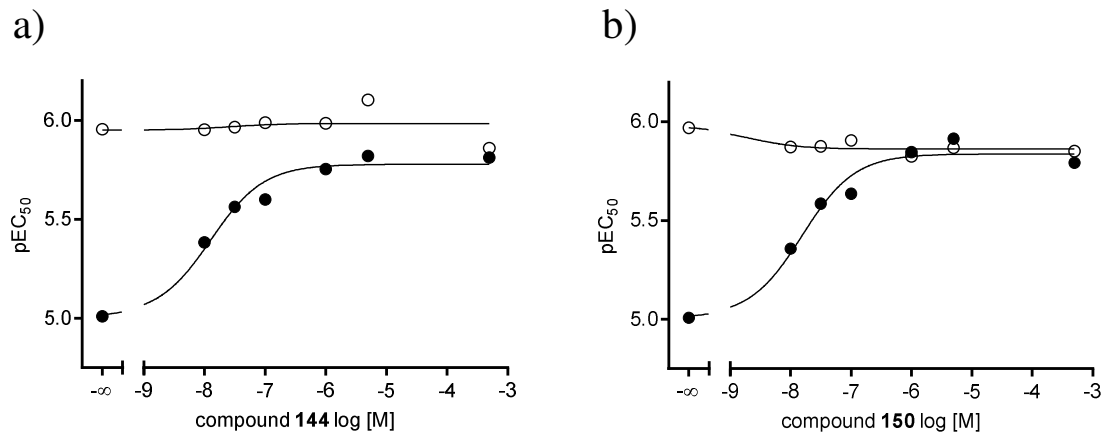

*Figure 61: Nonlinear regression of the pGI_{50} values determined in the MDR reversal assay Figure 60 a) and c) with the corresponding concentration of compound **144** and **150**. The EC_{50} value characterising half-maximal sensitization toward SN-38, was calculated as 12.7 nM (**144**) and 15.6 nM for compound **150** (●). For compounds **144** and **150** IC_{50} values of 44.2 nM and 47.5 nM in the Hoechst 33342 accumulation assay were obtained, respectively. A nonlinear regression of the pGI_{50} values determined in an analogous reversal assay (Fig. 7 b and d), but using only parental MDCK II cells, is depicted with open circles (○).*

Moreover, the sensitization of the ABCG2 overexpressing MDCK II BCRP cell line toward the cytostatic drug MX was investigated by co-administration of compound **144** and **150**. The assay was carried out at different compound concentrations in the presence and absence of 0.5 µM MX. Further details to the assay are provided in chapters 3.5 and 10.2.2.7. Both compounds were able to reverse the resistance of the cells toward MX as illustrated in Figure 62.

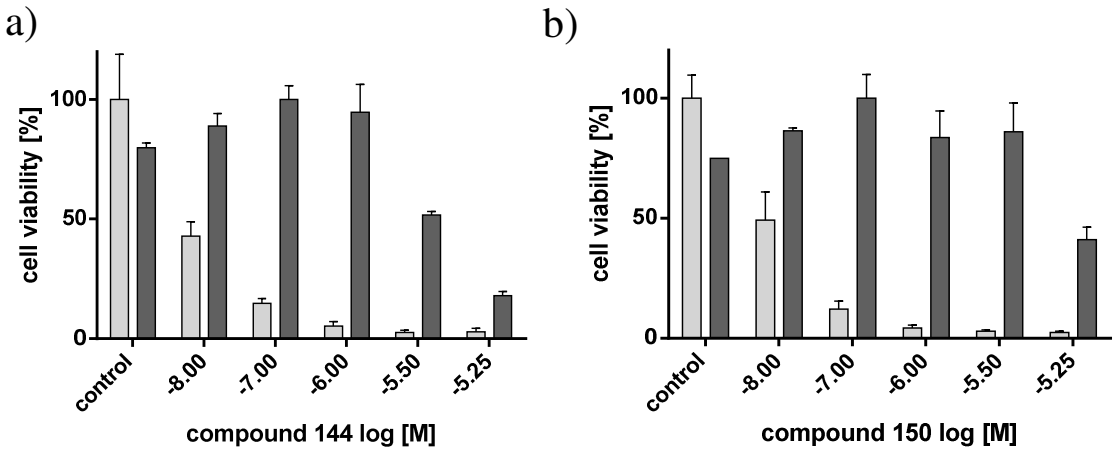

*Figure 62: MDR reversal assay of compounds **144** (a) and **150** (b), demonstrating their ability to reverse MDR toward the cytostatic drug mitoxantrone, in the ABCG2 overexpressing cell line MDCK II BCRP. The bars represent the cell viability at a given modulator concentration in the presence (light grey) and absence (dark grey) of 0.5 µM mitoxantrone. Control shows viability of cells without modulator. The standard deviation is expressed by error bars.*

Both compounds produced full reversal of the MDR at a concentration of about 1 µM. Half-maximal growth inhibition was reached for compound **144** at 7.4 nM and for **150** at 9.7 nM. The EC_{50} values determined in the MDR reversal assay with MX reflect the results of the MDR reversal assay with SN-38 very well.

5.6 Investigation of the interaction with Hoechst 33342

The interaction of selected compounds with Hoechst 33342 was investigated with ABCG2 overexpressing MDCK II BCRP cells using varying compound concentrations combined with varying concentrations of Hoechst 33342. The Lineweaver-Burk double reciprocal plot was used to determine the interaction type, described in chapters 4.6 and 10.2.2.8.

A summary of the results obtained with the Lineweaver-Burk method can be found in Table 19 listing the intersection of the straight lines with the corresponding interpretation.

Table 19: Interaction with Hoechst 33342 According to the Lineweaver-Burk Double Reciprocal Plot.

Compound	R^1	R^2	Intersection	type of interaction with Hoechst 33342
111	3-NO_2	3,4-OCH_3	2. Quadrant	Non-competitive mixed type
130	2-OCH_3	3-NO_2	2. Quadrant	Non-competitive mixed type
139	4-OCH_3	3-NO_2	Y-axis	competitive
144	3,4-OCH_3	4-NO_2	Y-axis	competitive
149	3,4-OCH_3	3-OCH_3	3. Quadrant	Non-competitive mixed type
150	3,4-OCH_3	3-OCH_3, 4-Br	3. Quadrant	Non-competitive mixed type
Ko143			3. Quadrant	Non-competitive mixed-type

Corresponding plots obtained according to the Lineweaver-Burk method are depicted in Figure 63. Evaluation of the intersections by the straight lines resulted in a non-competitive "mixed type" interaction with Hoechst 33342 for compound **111**, **130**, **149** and **150** and a competitive interaction for **139** and **144**. Interestingly, the competitive compounds both contain a single *para* substitution which was frequently found as a common pattern in previous chapters.

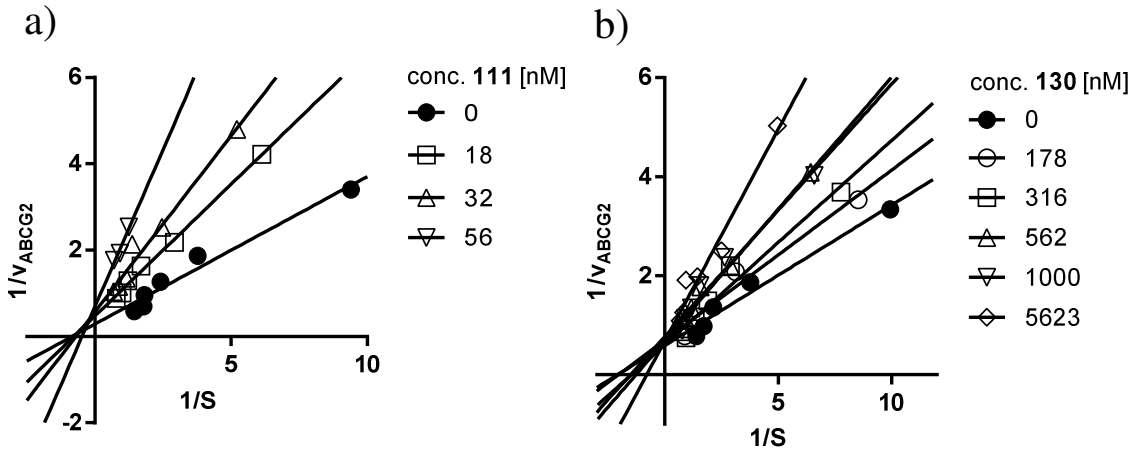

Figure continues on the next page

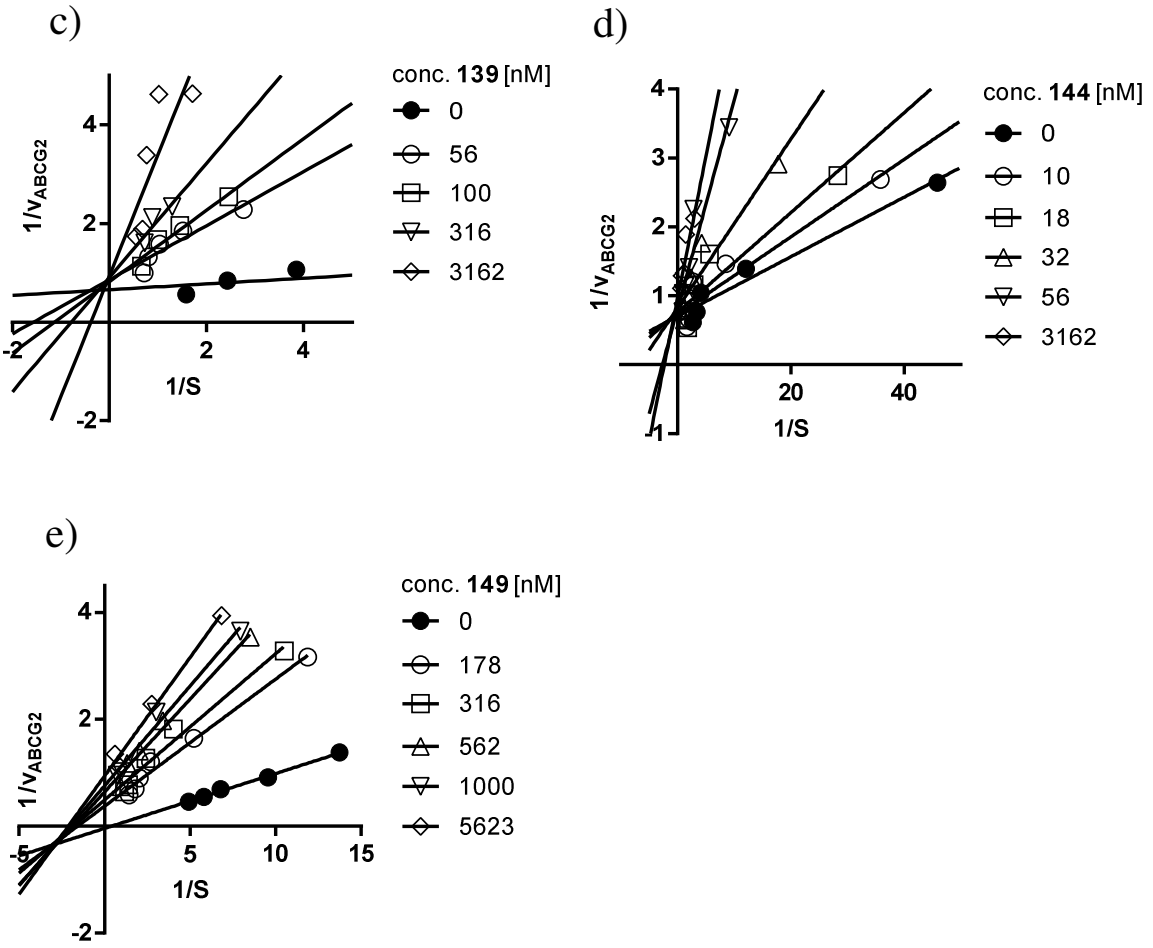

*Figure 63: Lineweaver–Burk plot for compounds **111** (a), **130** (b), **139** (c), **144** (d) and **149** (e) using various concentrations together with the ABCG2 substrate Hoechst 33342. Compound concentrations are specified in the legend.*

The results from the Lineweaver-Burk double reciprocal plot were validated using the Cornish-Bowden method, which is described in chapters 3.6 and 10.2.2.8. By linear regression of the V_{max} and K_M values the obtained slopes were summarized as scatter plot in Figure 64. Corresponding linear regression plots are illustrated in Figure 65 (for Ko143 see chapter 3.6).

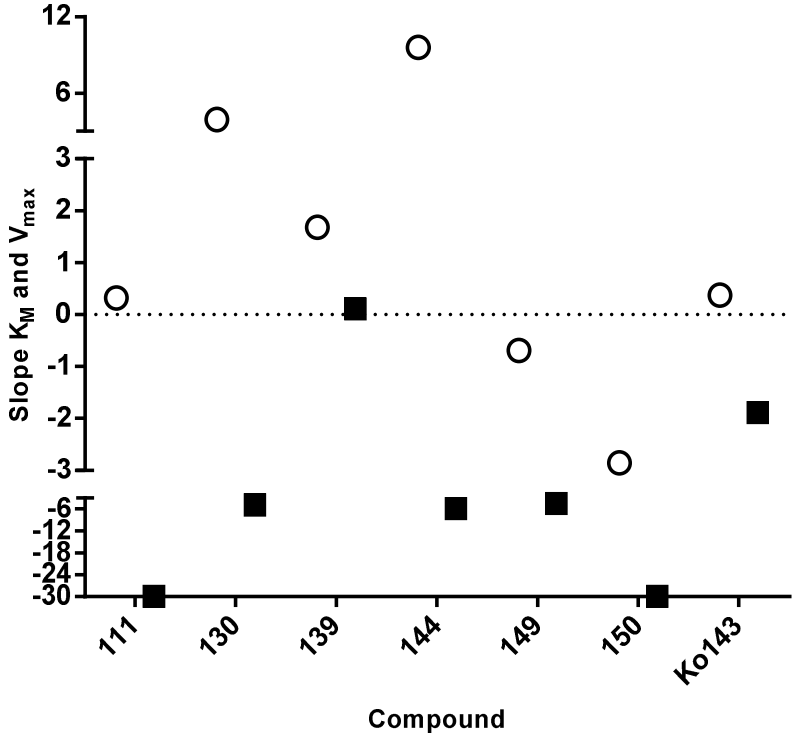

Figure 64: Scatter plot of the slopes obtained from the linear regression of K_M (○) and V_{max} (■) values calculated from the Cornish-Bowden direct linear plot.

The results from the Lineweaver-Burk plot were found to be in good accordance with the Cornish-Bowden plot: A high competitive character was found for compounds **130**, **139** and **144** indicated by the pronounced increase of the K_M values with increasing compound concentration. Compounds **130** and **144** also showed decreasing V_{max} values indicating a non-competitive interaction of the "mixed type". For compound **111**, **149** and **150** on the other hand a considerable decrease of the V_{max} values with increasing compound concentration was found that is typical for a non-competitive inhibitor. In summary, a clear competitive interaction was found for compound **139** (V_{max} ↔, K_M ↑), a purely non-competitive interaction for **111**, **149** and **150** (V_{max} ↓, K_M ↔) and a non-competitive interaction of the "mixed-type" for compounds **130** and **144**.

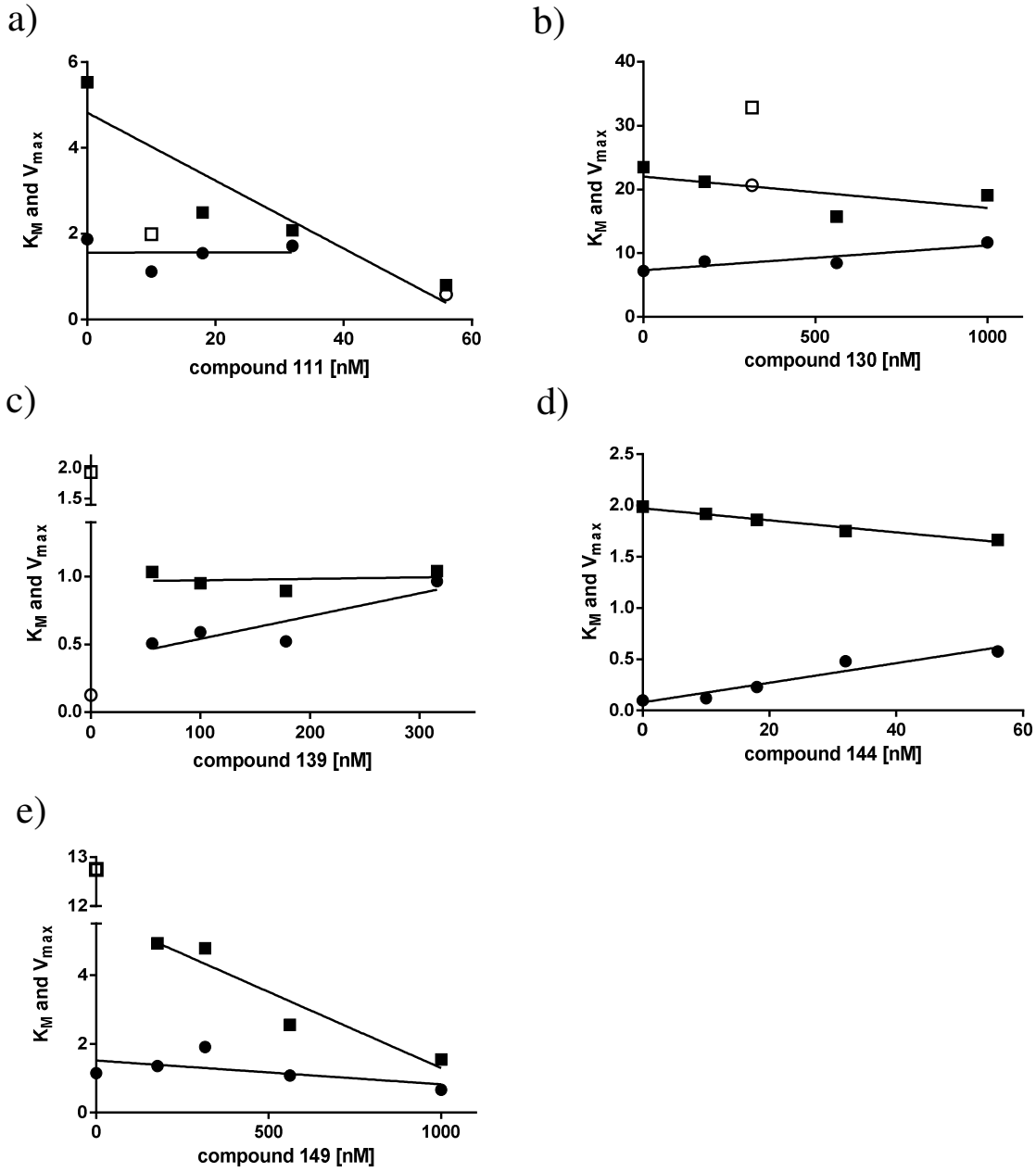

*Figure 65: Linear regression of the V_{max} (■) and K_M (●) values determined from the direct linear plot according to Cornish-Bowden for compounds **111** (a), **130** (b), **139** (c), **144** (d) and **149** (e). Excluded values are depicted as open symbols of the corresponding shape.*

Interestingly, the findings from the kinetic investigation are in agreement with those from 5D3 antibody assay (chapters 5.7) and even more pronounced from the ATPase assay (chapter 5.8).

5.7 Investigation of the conformation sensitive 5D3 antibody binding to an epitope of ABCG2

Selected compounds were investigated with the conformation sensitive 5D3 antibody, which binds specifically to an epitope of the transport protein, to explore their conformational impact on ABCG2. Emitted fluorescence by the bound antibody was measured with a FACSCalibur flow cytometer using ABCG2 overexpressing PLB-985 cells. More information about the assay is provided in chapters 3.7 and 10.2.2.9. The results are presented as a bar-chart depicted in Figure 66 including Ko143 as positive control representing 100% labelling with the antibody.

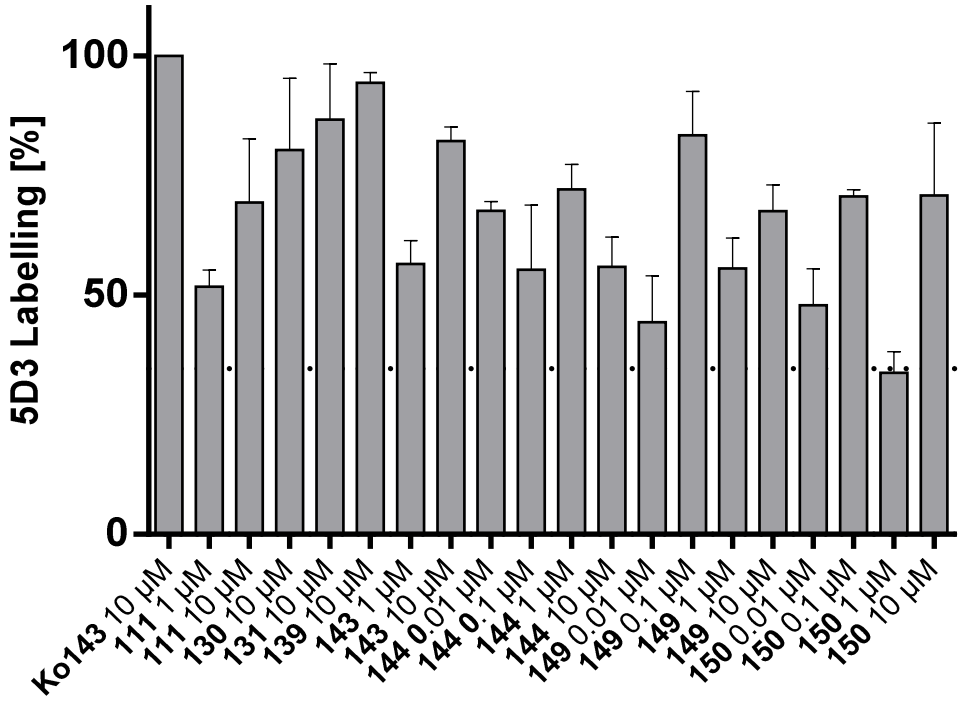

Figure 66: 5D3 immunoreactivity modulation of ABCG2 by various compounds at different concentrations. Fluorescence detected by the 5D3-labeling of ABCG2 in the presence of 10 µM Ko143 was set to 100% and the fluorescence measured in the absence of any compound taken as 0%. The dotted line represents the labelling obtained with Hoechst 33342.

Highest staining with 5D3 antibody was obtained for compound **139** at 10 µM resulting in 94% of the labelling of Ko143 at the same concentration. As presented in the previous chapter, **139** exhibited a clear competitive interaction with Hoechst 33342. A correlation

between a competitive interaction with Hoechst 33342 and the observation of high conformational change in the 5D3 antibody assay has already been found for several other compounds like **17** which was discussed in chapter 3. However, also few non-competitive compounds showed a similarly high amount of labelling by the antibody like **54** which was discussed in chapter 4.

Moreover, compounds **130** and **131** led to an increased immunostaining with 5D3 antibody obtaining 87% and 80% respective labelling with in comparison to Ko143. In the interaction investigation a highly competitive character was found for compound **130**. Further differences were identified for the *meta* and *para* derivatives **143** and **144** obtaining considerably different 5D3 shifts at 10 µM.

Additionally, several dilutions of compound **144**, **149** and **150** were prepared to investigate the concentration dependency of the rate of the bound 5D3 antibody. All three compounds gave an undulating rate of labelling with increasing concentrations. This might point toward the existence of more than one binding pocket with different affinities for those compounds. This hypothesis is substantiated by the results of the ATPase investigation discussed in the following chapter.

Representative histograms of compounds yielding the highest and the lowest 5D3 shift in the assay as well as the standard Ko143 are depicted in Figure 67. Histograms of compounds Ko143, **139** and **150** were obtained at a compound concentration of 10, 10 and 1 µM, respectively.

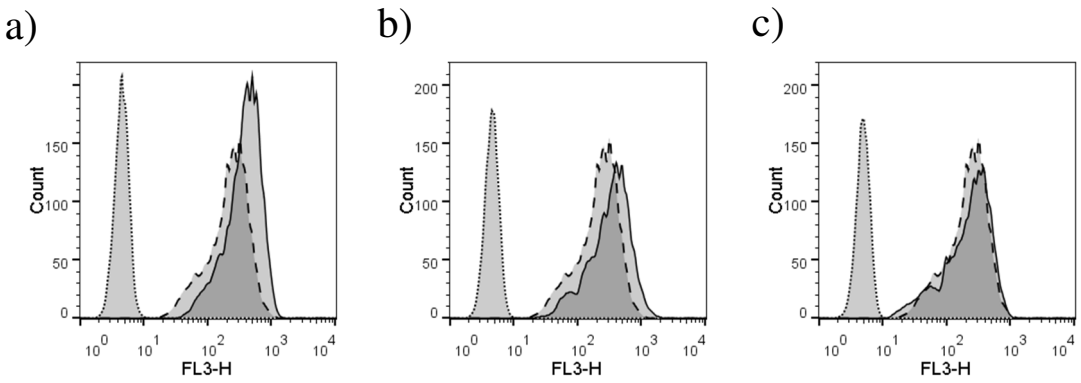

Figure 67: Histogram of the measured fluorescence at the FL3-H detector (X-axis) and the cell-count gated according to the fluorescence. Depicted is the fluorescence of the isotype-control (dotted curve) as well as of 5D3 antibody in the absence of a compound (dashed curve) and in the presence of a compound (continuous curve).Compounds with the highest and lowest 5D3 shifts: ***Ko143*** *(a),* ***139*** *(b) and* ***150*** *(c) at a concentration of 10, 10 and 1 µM, respectively.*

5.8 Investigation of the ATPase activity

The assay was performed with Ko143 as standard ATPase inhibitor and quercetin as standard stimulator using High Five insect cell membrane preparations. The ATPase activity assays were carried out by Jennifer Gallus. Further details are provided in chapters 3.8 and 10.2.2.10.

For the screening three different concentrations (1, 10 and 25 µM) were used and only the most potent compounds were selected. A summary of the results is depicted as bar chart in Figure 68.

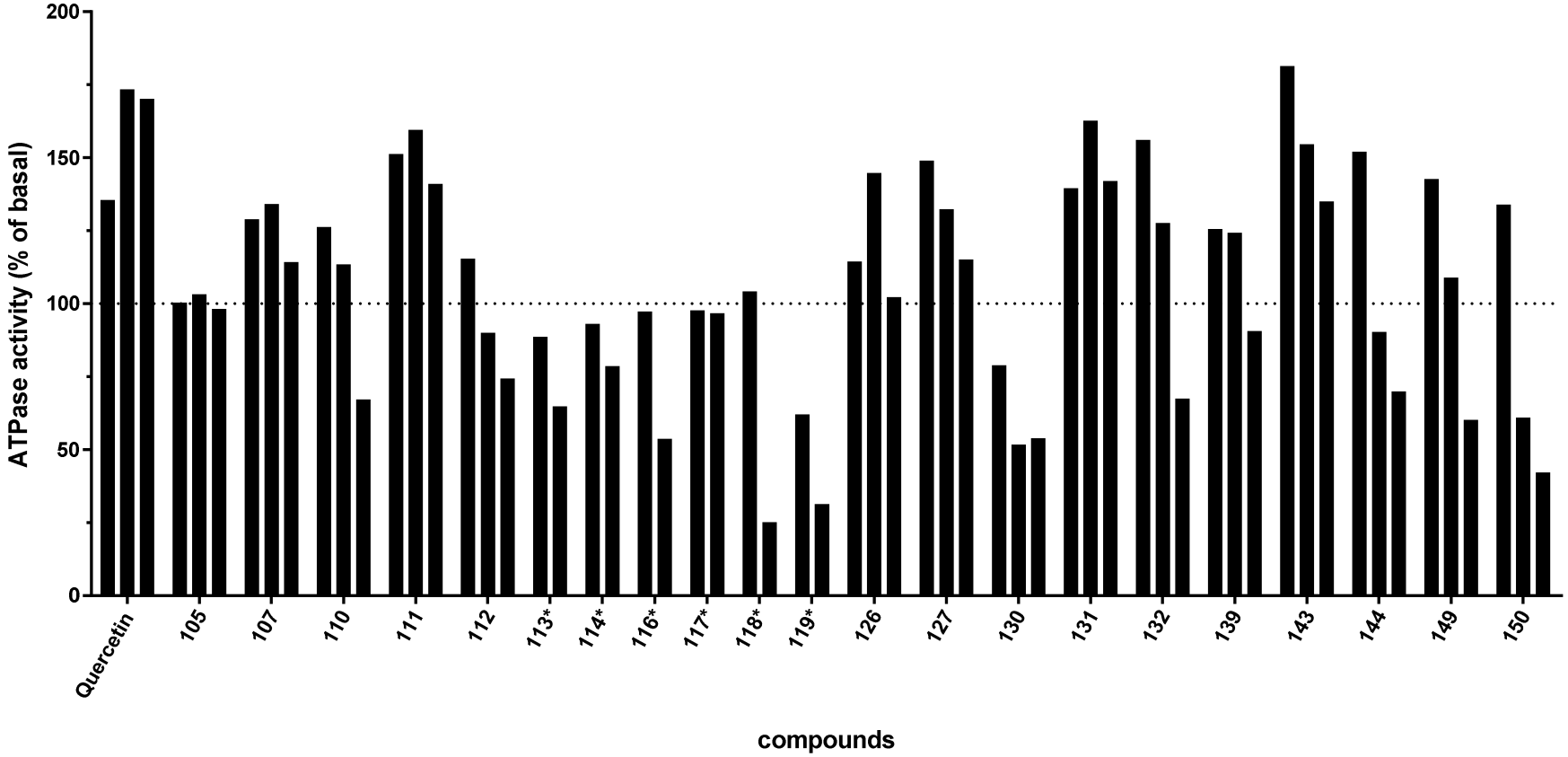

*Figure 68: Screening of ATPase activity of selected compounds at three different concentrations. From left to right the bars correspond to 1, 10 and 25 µM final concentration of compound. All values are relative vanadate-sensitive ATPase activities in relation to the basal activity, which is set to 100%. *Compounds **113 -119** were investigated at a final concentration of 1 and 10 µM. Quercetin was used as a standard for activation of ABCG2 ATPase activity.*

Investigated compounds were able to activate and also inhibit ATPase activity depending on the substitution pattern. The ATPase activity was modulated by *meta* and *para* nitro derivatives like **111/127**, **131/132** and **143/144** very differently: A strong activation was detected for the *meta* derivatives comparable to quercetin. The *para* derivatives on the other hand showed increasing deactivation with higher compound concentration leading to a biphasic progression in the screening (see compound **112**, **126**, **132**, **144** and **150**). Similar effects regarding *meta* and *para* derivatives have already been observed in the compounds of project I and II. Additionally it was found that ether and amino functions containing larger alkyl residues shift the ATPase activity considerably to the deactivating phase. This was observed for compounds **113**, **114**, **116**, **118** and **119** that yielded between 80 and 25% of the basal activity at a concentration of 10 µM. The corresponding analogues containing smaller alkyl chains exhibited high stimulation (compound **111**) or no effect in the case of **117**, which contains a free amine group. It is possible that lipophilic properties of the substituents at R^2 are responsible for the deactivating effect in the ATPase assay.

A more detailed investigation of compounds **144**, **149** and **150** at several different concentrations resulted in bell-shaped concentration-effect curves (see Figure 69). As mentioned before, this is an indication for distinct high affinity and low-affinity binding sites. A biphasic concentration-effect curve resulted for compound **130** (EC_{50}: 1.03 µM), showing ATPase stimulation at low concentration and strong inhibition at higher concentration as depicted in Figure 69 a).

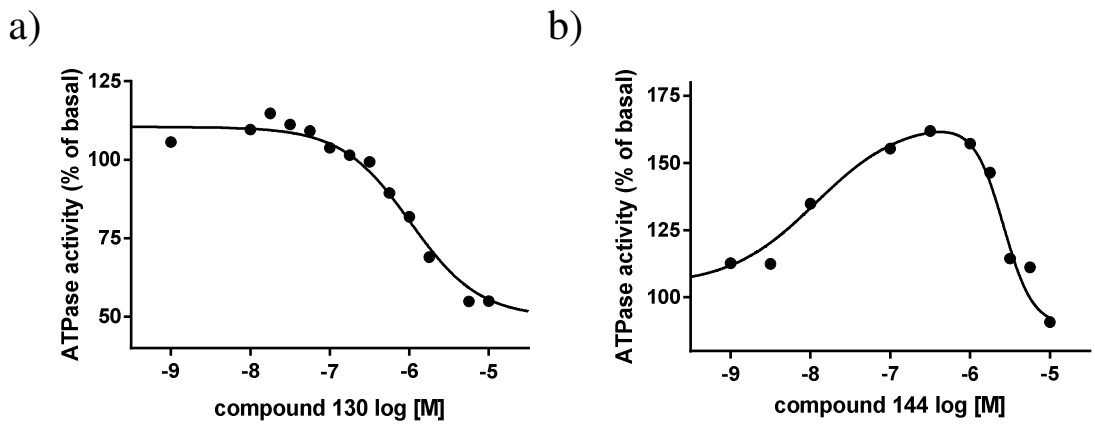

Figure continues on the next page

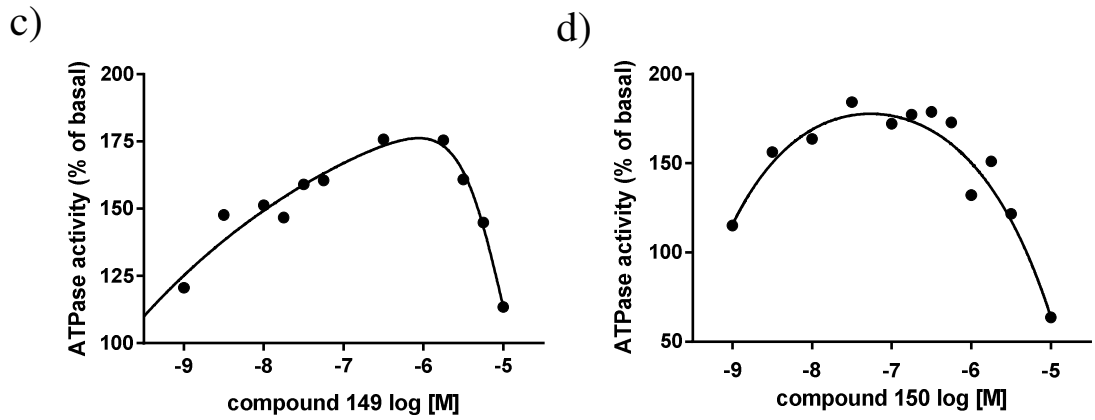

*Figure 69: Concentration-response curves for compounds **130** (a, EC_{50}: 1030 nM), **144** (b), **149** (c) and **150** (d) in the ATPase assay. All values are relative vanadate-sensitive ATPase activities in relation to the basal activity, which is set to 100%.*

6 Project IV: 2,4-Substituted pyrido[2,3-d]pyrimidines

In this project the quinazoline scaffold was modified by replacing the carbon atom at position 8 with nitrogen resulting in a pyrido[2,3-d]pyrimidine scaffold. Substitution was carried out at position 2 by introducing different aromatic functions and also at position 4 using a substituted anilino moiety. These derivatives can easily be compared to the compounds investigated in projects I, II and III, since they differ only in the basic scaffold but not in most of the substitution patterns used at the aromatic cores.

This class of compounds was prepared by a convenient synthesis presented in the following chapter. It includes several substituted acid chlorides and anilines that are readily available, facilitating a broad variety of quick modifications of the scaffold.

For the unsubstituted basic scaffold a logP value of 2.48 was calculated which is 1.60 log units lower than the quinazoline analogue. This increases the watersolubility of the 2,4-substituted pyrido[2,3-d]pyrimidines and renders precipitation under assay conditions less likely.

6.1 Reaction mechanism

A schematic synthesis route and a detailed reaction mechanism is provided below.

*Scheme 5: General synthesis scheme for the preparation of compounds **153-197**.*[a]

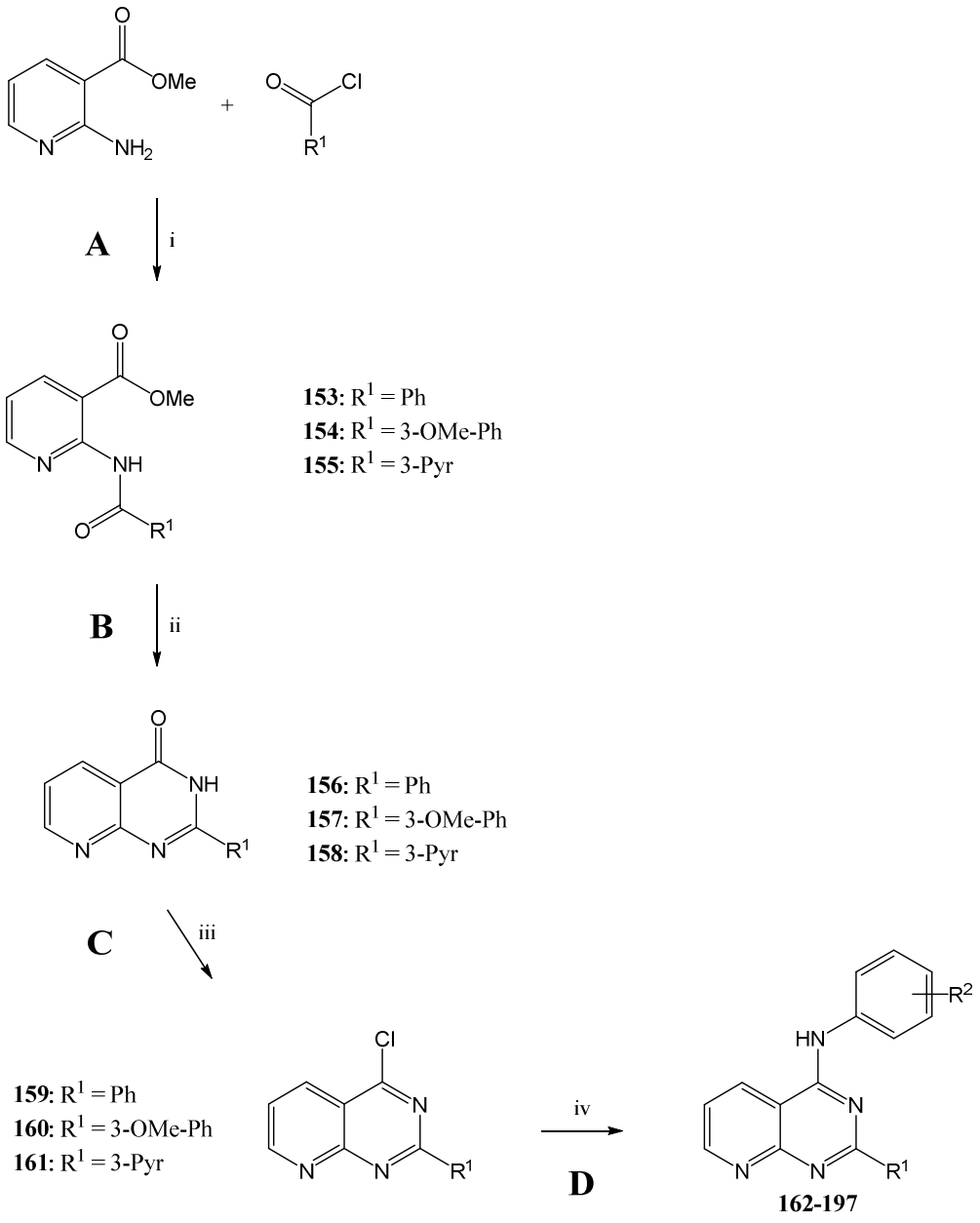

[a]: Reagents and conditions: (i) R^1COCl, Et_3N, THF. (ii) 28% aq NH_3, MeOH. (iii) $POCl_3$, reflux, 4-12 h. (iv) Substituted aniline, 100 watt microwave irradiation, 110 °C, 2 - 10 min.

Reaction mechanism **A**:

In the first step methyl 2-aminonicotinate performs a nucleophilic attack at the carbonyl function of the substituted acid chloride using the electron pair of the nitrogen atom. Nucleophilic addition is followed by elimination of hydrochloric acid restoring the carbonyl function and also compensating the formal positive charge at the nitrogen atom. After formation of the amide function, hydrochloric acid is precipitated with triethylamine as salt to prevent protonation of the amino group in the 2-aminonicotinate and thereby preserve its nucleophilic character.

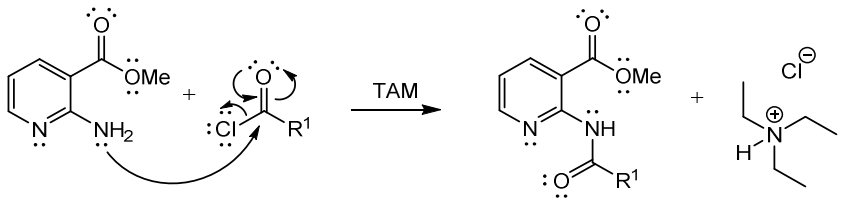

Reaction mechanism **B**:

The methoxy residue of the ester function is then substituted by ammonia, attacking the carbonyl function. Subsequently, ring closure is accomplished by an intramolecular condensation reaction: The electron pair of the previously formed amide nitrogen attacks the carbonyl function releasing water under formation of a N-C double bond at position 1.

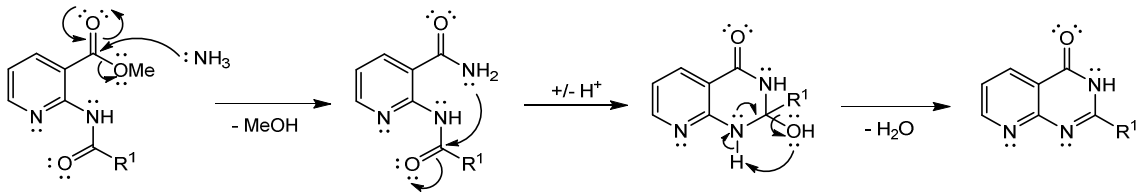

Reaction mechanism **C**:

The carbonyl function at position 4 is substituted in the presence of $POCl_3$ *via* a chlorination reaction. The corresponding reaction mechanism follows that of chapter 4.1 and is illustrated below.

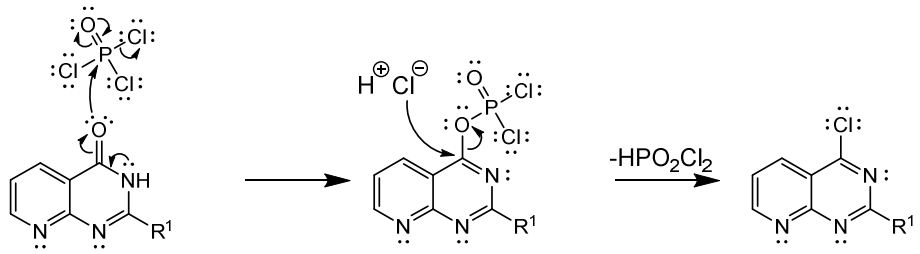

Reaction mechanism **D**:

Synthesis of the final compounds was conducted *via* nucleophilic aromatic substitution of the corresponding 4-chloropyrido[2,3-d]pyrimidine precursor by a substituted aniline derivative. The reaction mechanism is analogous to that used for the compounds in project I and can be reviewed in chapter 3.1.

6.2 Investigation of the inhibitory potency toward ABCG2 in the Hoechst 33342 accumulation assay

Inhibitory potency of the compounds was investigated in a Hoechst 33342 accumulation assay using the ABCG2 overexpressing MDCK II BCRP and parental cell line. More detailed information to the Hoechst 33342 accumulation assay as is given in chapter 3.2 and 10.2.2.2. A summary of the activity data can be reviewed in Table 20.

In the first series a phenyl moiety was introduced at R^1 in combination with different substituted anilines at R^2 yielding compounds **162 – 177**. The obtained IC_{50} values were compared to their 2-penylquinazoline analogues of project I providing information about the influence of the nitrogen atom at position 8.

Table 20: Inhibitory Activities Derived from the Hoechst 33342 Accumulations Assay Toward ABCG2 Overexpressing MDCK II BCRP Cell Line. The Substitution Pattern is Illustrated Above the Table.

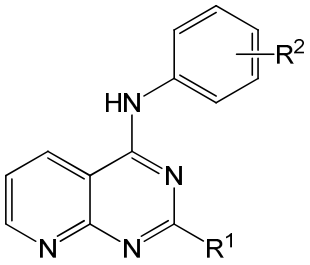

Scaffold A

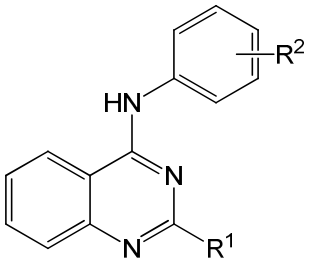

Scaffold B

Compound	R^1	R^2	Scaffold	Hoechst 33342 IC_{50} ± SD [nM][a]
162	Ph	H	A	149 ± 13
163	Ph	3-NO_2	A	519 ± 90
164	Ph	3-NO_2-4-OH	A	528 ± 94
165	Ph	4-NO_2	A	19500 ± 4200
166	Ph	3-CN	A	400 ± 56
167	Ph	4-CN	A	1210 ± 80
168	Ph	3-OMe	A	150 ± 20
169	Ph	4-OMe	A	238 ± 18
170	Ph	3,4-OMe	A	343 ± 28
171	Ph	3-SMe	A	206 ± 36
172	Ph	3-OH	A	1230 ± 58
173	Ph	4-OH	A	2040 ± 160
174	Ph	3-$NHCOCH_3$	A	5270 ± 940
175	Ph	3-CF_3	A	177 ± 18
176	Ph	3-F	A	164 ± 19
177	Ph	3-Cl	A	454 ± 149
178	3-OMe-Ph	3-NO_2	A	747 ± 168
179	3-OMe-Ph	3-NO_2-4-OH	A	1260 ± 140
180	3-OMe-Ph	3-CN	A	348 ± 51.6
181	3-OMe-Ph	4-CN	A	876 ± 172
182	3-OMe-Ph	3-OH	A	963 ± 220
183	3-OMe-Ph	4-OH	A	1300 ± 20
184	3-OMe-Ph	3,4-OMe	A	572 ± 8
185	3-OMe-Ph	4-SMe	A	910 ± 135
186	3-OMe-Ph	3-$NHCOCH_3$	A	6400 ± 2120
187	3-OMe-Ph	3-CF_3	A	264 ± 48
188	3-OMe-Ph	4-CF_3	A	425 ± 35
189	3-OMe-Ph	3-F	A	163 ± 30
190	3-OMe-Ph	4-F	A	539 ± 99

Table continues on the next page

191	3-OMe-Ph	3,4-F	A	621 ± 80
192	3-OMe-Ph	3-Cl	A	628 ± 58
193	3-OMe-Ph	3-Br	A	1530 ± 240
194	3-Pyr	3-NO_2	A	n.a.
195	3-Pyr	4-NO_2	A	n.a.
196	3-Pyr	3-F	A	1230 ± 50
197	3-Pyr	3-OH	A	16900 ± 3470
1[c]	Ph	H	B	882 ± 157
2[b]	Ph	3-NO_2	B	130 ± 30
3[c]	Ph	3-NO_2-4-OH	B	80.0 ± 9.2
89[c]	Ph	4-NO_2	B	69.6 ± 8.2
4[b]	Ph	3-CN	B	140 ± 40
5	Ph	4-CN	B	71.4 ± 10.1
11[b]	Ph	3-OMe	B	1320 ± 100
12[b]	Ph	4-OMe	B	1930 ± 110
6	Ph	4-OH	B	204 ± 37
8	Ph	3-$NHCOCH_3$	B	278 ± 33
20[b]	Ph	3-Cl	B	1930 ± 280
Ko143[d]				227 ± 14

[a]: *IC_{50} values are means of three independent experiments.*
[b]: *IC_{50} value taken from literature.*[198]
[c]: *Compounds synthesized in earlier study.*[198]
[d]: *Used as reference in the assay.*
n.a.: not active

Among the first series, the most potent compound **162** yielded an IC_{50} of 149 nM containing a phenyl group at R^1 and hydrogen at R^2. In contrast, the corresponding quinazoline analogue **1** possessed a relatively low inhibitory potency with an IC_{50} of 882 nM. Interestingly, substitution patterns that had resulted in poor IC_{50} values at a quinazoline scaffold turned out to be beneficial at the pyrido[2,3-d]pyrimidine scaffold. Examples are compounds **168** and **169** containing a *meta* and *para* methoxy substitution at R^2 with high inhibitory potencies of 150 and 238 nM, respectively. In comparison their quinazoline analogues **11** and **12** had IC_{50} values of only 1320 and 1930 nM. Concentration-response curves of highly potent compound **162** and **169** together with the standard inhibitor Ko143 are depicted in Figure 70.

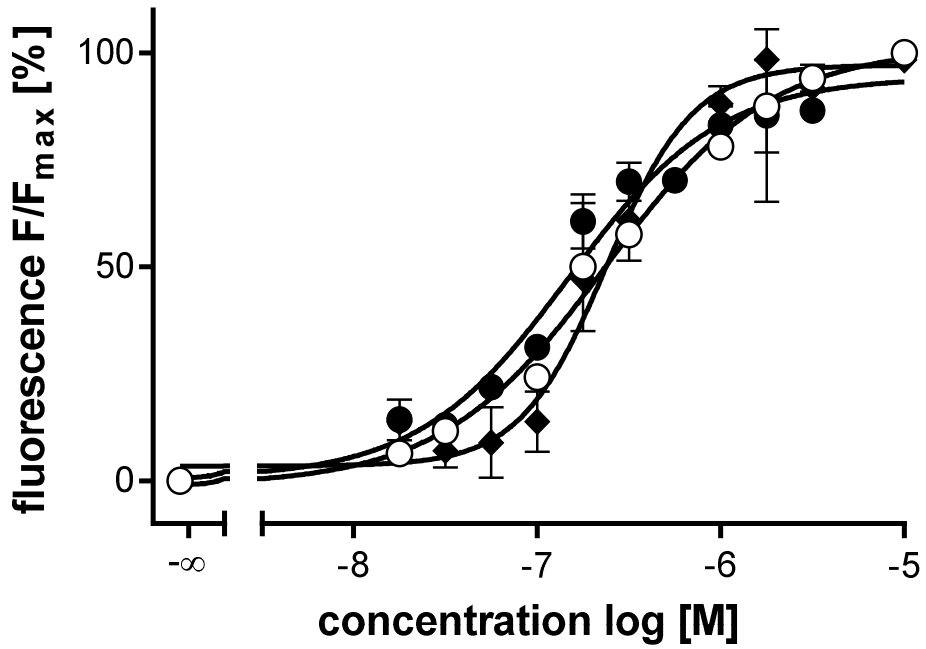

*Figure 70: Concentration-response curve of compound **162** (▲, IC_{50}: 149 nM) and **169** (■, IC_{50}: 238 nM) in a Hoechst 33342 accumulation assay with Ko143 (○, IC_{50}: 227 nM) as reference, using the ABCG2 overexpressing MDCK II BCRP cell line.*

Further potent compounds resulted from substitution with 3-trifluoro and 3-trifluoromethyl groups, yielding compounds **175** and **176** which had IC_{50} values of 177 and 164 nM, respectively.

On the other hand nitro, cyano and hydroxy functions that resulted in high potencies using a quinazoline scaffold (see compound **2**, **3**, **89**, **4**, **5** and **6**) decreased the inhibitory potency considerably for the 2-phenylpyrido[2,3-d]pyrimidine analogues. The observed inverse correlation of the inhibitory activity between most of the 2-phenylquinazoline and 2-phenylpyrido[2,3-d]pyrimidine derivatives is illustrated in Figure 71.

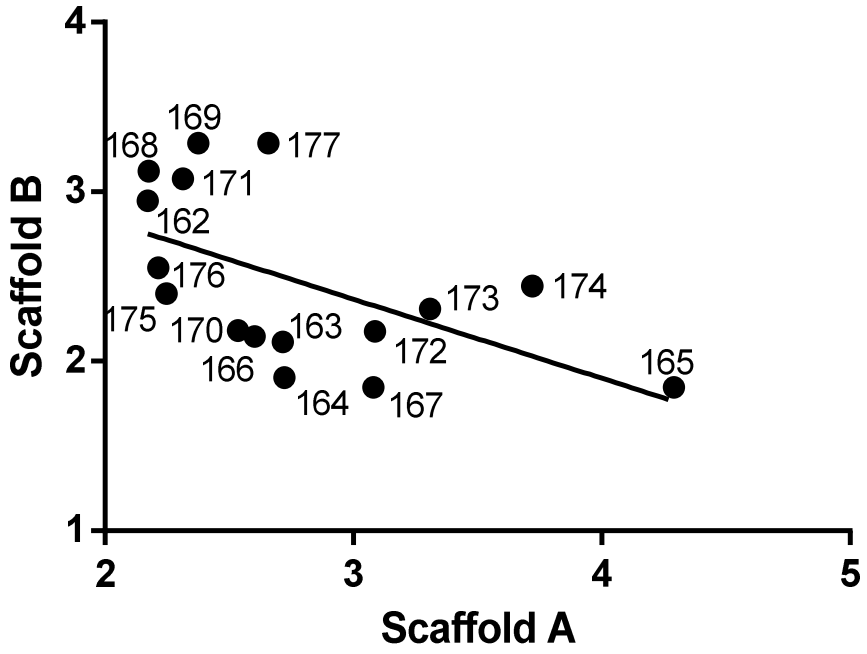

*Figure 71: Linear regression of pIC_{50} values determined in the Hoechst 33342 accumulation assay for derivatives containing the 2-phenylpyrido[2,3-*d*]pyrimidine scaffold A and the corresponding analogue containing the 2-phenylquinazoline scaffold B.*[a]

[a]*: The values of some 4-substituted-2-phenylquinazolines were taken from literature, at which the IC_{50} value of the 4-nitroanilino-2-phenylquinazoline derivative was re-determined and corrected.*[198]

In the next series a 3-methoxyphenyl moiety was introduced at R^1. Among those, the highest potencies were achieved by substitution with 3-trifluoro and 3-trifluoromethyl groups at R^2 leading to compound **187** (IC_{50}: 264 nM) and **189** (IC_{50}: 163 nM). A great resemblance in potency was found between the subsets using phenyl and the 3-methoxyphenyl groups at R^1, yielding very similar IC_{50} values for the corresponding analogues.

A significantly decreased inhibitory potency resulted in derivatives containing 3-pyridyl residues at R^1. Even substitution with 3-fluoro at R^2, which had proven to be very beneficial in the previous series, led to a rather poor IC_{50} of 1230 nM in compound **196**.

6.3 Investigation of the inhibitory potency toward ABCB1 and ABCC1 in the calcein AM assay

The selectivity toward ABCG2 was screened for several compounds in a calcein AM assay. For this purpose, the ABCB1 overexpressing cell line A2780 adr and the ABCC1 overexpressing cell line H69 AR were used and the assay carried out according to the description in chapters 3.3 and 10.2.2.4. Screening results for the inhibitory activity toward ABCB1 and ABCC1 are illustrated as bar charts in Figure 72.

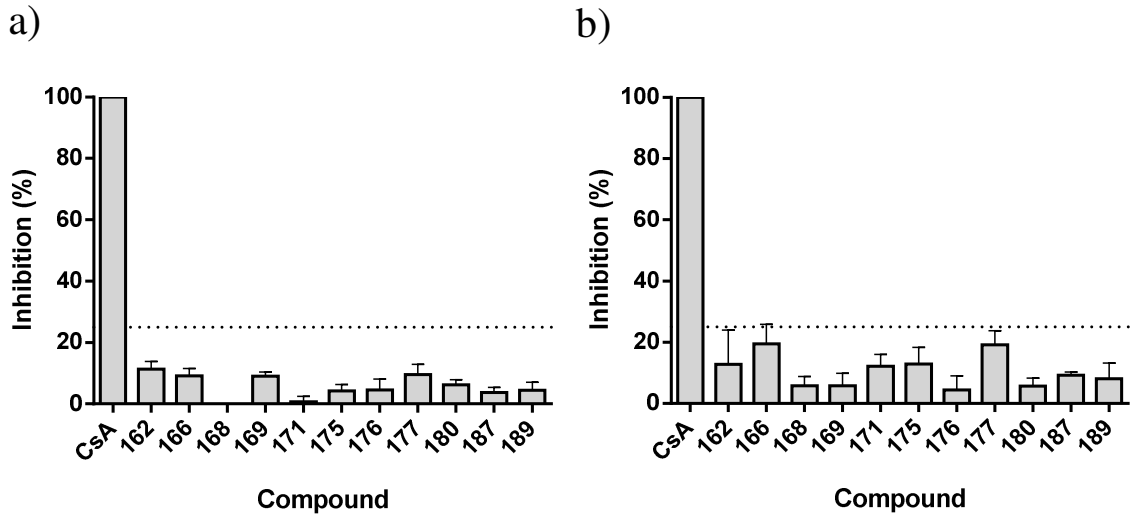

Figure 72: Inhibitory effect of screened compounds toward P-gp overexpressing cell line A2780adr (a) and MRP1 overexpressing cell line H69AR (b) in a calcein AM assay at a concentration of 10 µM. Cyclosporine A (CsA) was used as positive control, indicating complete inhibition. The inhibitory effect of each compound is expressed by the height of the bars, representing the inhibition compared to the positive control in percent. For each compound, 3 independent experiments were performed and the standard deviation expressed by error bars.

The screening of a selection of compounds, including the most potent ones, exhibited no activity toward ABCB1 and ABCC1. With regard to projects I-III the presence of one or more methoxy functions was found to correlate with increased inhibitory potency toward ABCB1 and ABCC1. Although some compounds of this test set contain methoxy functions at R^1 and R^2 the selectivity toward ABCG2 was not affected. Also a slightly higher activity toward ABCB1 was found in comparison to ABCC1. Nevertheless, none

of the selected compounds exceeded the 25% inhibition-mark using both cell lines with respect to the standard inhibitor CsA.

6.4 Investigation of the intrinsic cytotoxicity with the MDCK II cell lines in a MTT assay

A MTT assay was conducted with MDCK II parental and ABCG2 overexpressing cells to investigate the intrinsic cytotoxicity of selected compounds. Measurement of the toxic effects was performed after 72 h incubation of the cells in the presence of different compound concentrations utilizing MTT as indicator of the cell viability. The procedure is described in more detail in chapters 3.4 and 10.2.2.5. A summary of the obtained GI_{50} values together with the corresponding therapeutic ratios is depicted in Table 21.

Table 21: Intrinsic Toxicity of Selected Compounds on MDCK II ABCG2 Overexpressing and Parental Cells

Compound	R^1	R^2	Scaffold	GI_{50} [µM][a] BCRP	GI_{50} [µM][a] Parental	Therapeutic ratio(GI_{50}/IC_{50})
162	Ph	H	A	92	67	620
167	Ph	4-CN	A	75	140	62
168	Ph	3-OMe	A	84	120	590
169	Ph	4-OMe	A	47	47	200
170	Ph	3-SMe	A	86	110	420
173	Ph	4-OH	A	46	61	22
175	Ph	3-CF_3	A	97	120	680
177	Ph	3-Cl	A	62	98	360
187	3-OMe-Ph	3-CF_3	A	99	92	560
189	3-OMe-Ph	3-F	A	97	110	600
1[b]	Ph	H	B	27	26	30
5	Ph	4-CN	B	8.0	17	110
6	Ph	4-OH	B	12	27	60
Ko143				13	13	49
MeOH/DMSO				96[c]	140[c]	

[a]: *Concentration leading to 50% of cell survival of MDCK II BCRP and parental cells. The data was obtained from at least two independent experiments as mean values.*

[b]: *Compound was first synthesized elsewhere.*[198]

[c]: *Positive control of the cytotoxicity from dilution with DMSO/MeOH without compound.*

The cytotoxic investigation made clear the advantage of the compounds containing a 2,4-substituted pyrido[2,3-d]pyrimidine scaffold. They exhibited a considerably lower intrinsic cytotoxicity than compounds with a quinazoline scaffold as illustrated by the compound pairs **162/1**, **167/5** and **173/6**. Interestingly, some *para* substituents at R^2 led to slightly decreased GI_{50} values in scaffold A as observed in compounds **169** and **173**. Almost no toxic effects were detected for the *meta* derivatives **168**, **170**, **175** and **177**. According to the high GI_{50} values of the compounds, which were very similar to the control containing only MeOH and DMSO, the observed toxic effects must mostly be due to the toxic effects of the solvents.

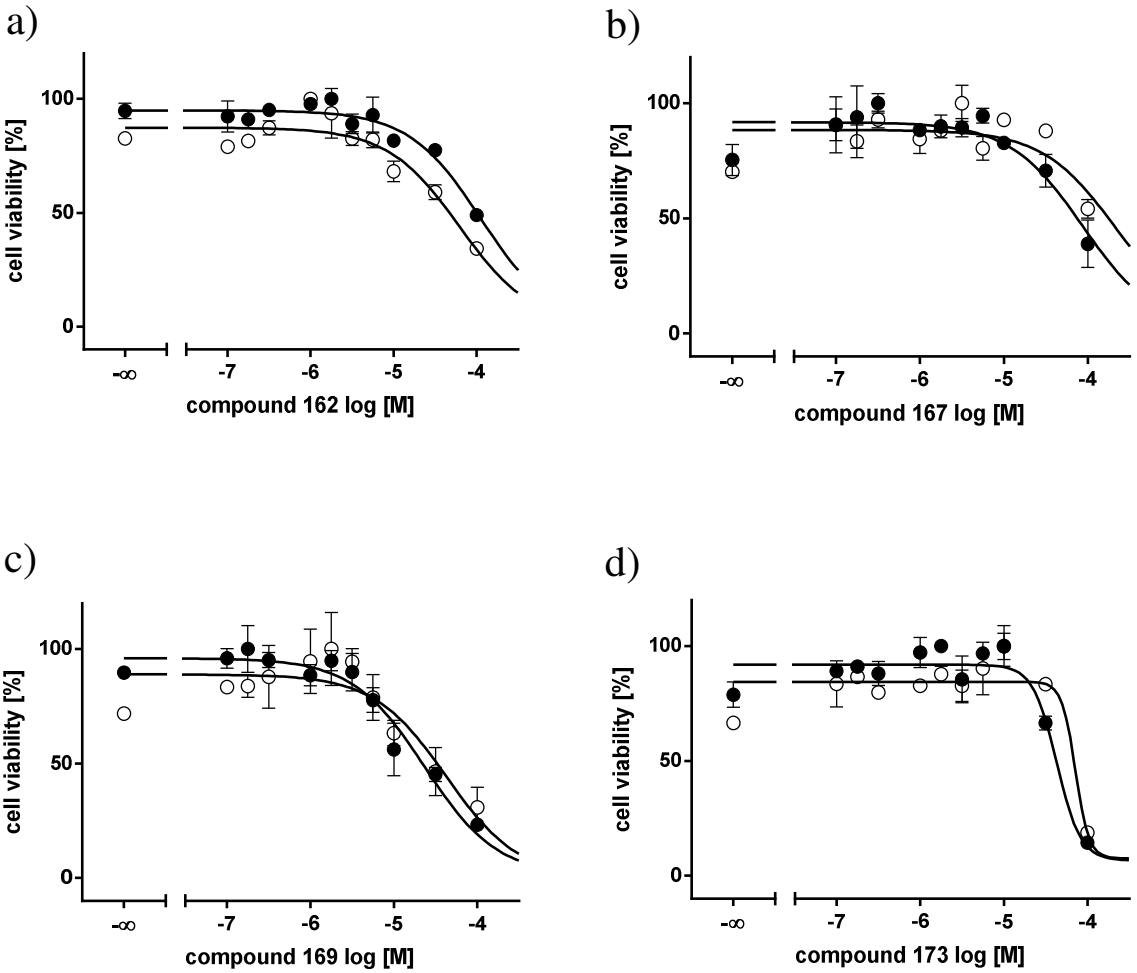

*Figure 73: MTT viability assay of compound **162**, **167**, **169** and **173** using the ABCG2 overexpressing MDCK II BCRP (■) and parental MDCK II cell line (Δ). For ■ a GI_{50} of 91.6 µM (a), 75.3 µM (b), 46.7 µM (c) and 45.5 µM (d) was determined. A control with the same concentration of MeOH and DMSO analogous to the dilution of the compounds, was carried out for comparison (■, GI_{50} = 96.1 µM). The amount of MeOH and DMSO used for the dilution was ≤ 1.8% and ≤ 1.0%, respectively.*

Therefore, the GI_{50} can probably be increased even further by reducing the amount of solvents which has already been demonstrated for some compounds of project II (see chapter 4.4). Concentration-viability curves of selected compounds **162**, **167**, **169** and **173** are depicted in Figure 73. Owing to the low cytotoxic effects of compound **175**, significantly high TRs were calculated resulting in the highest ratio of 676. A similarly high TR of 615 was determined for the unsubstituted compound **162**. Seven out of ten investigated compounds based on scaffold A resulted in TRs higher than 250 making them promising compounds for *in vivo* studies. On the contrary the standard inhibitor Ko143 has a TR of only 48.9. An overview of the TRs is given in Figure 74.

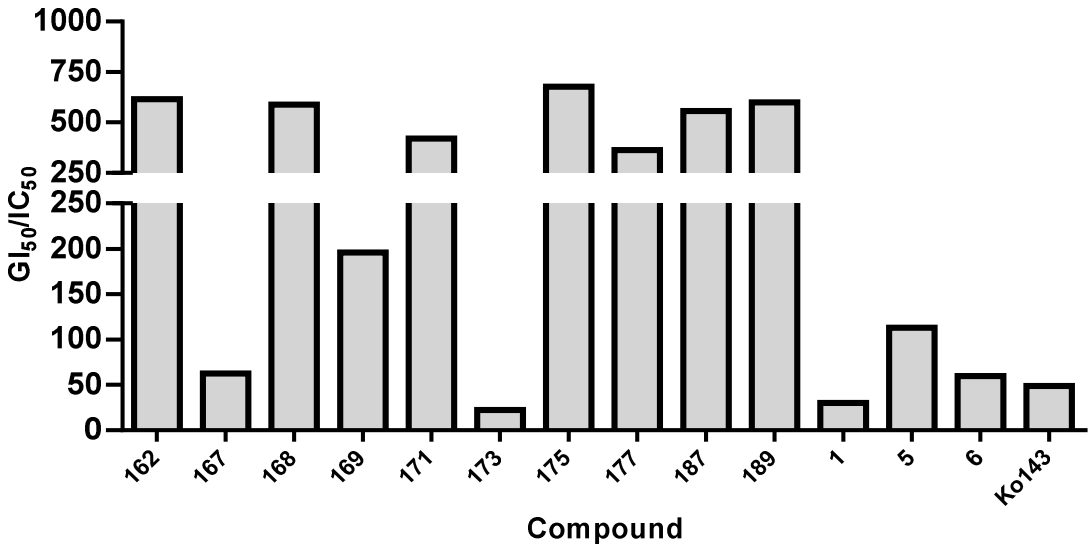

*Figure 74: Therapeutic ratio of selected compounds, calculated from the ratio of GI_{50} to IC_{50} derived from MTT viability assay and Hoechst 33342 accumulation assay, respectively. The highest value was calculated for compound **175** (GI_{50}/IC_{50} = 676), while the reference compound Ko143 yielded GI_{50}/IC_{50} = 48.9.*

6.5 Investigation of the reversal of multidrug resistance

The ability to reverse MDR in ABCG2 overexpressing MDCK II BCRP cell line against SN-38 by co-administration of the potent compounds **162**, **167** and **169** was investigated in a MDR reversal assay. Further details are provided in chapters 3.5 and 10.2.2.6. Concentration-viability curves obtained for parental and ABCG2 expressing MDCK II cell lines are depicted in Figure 75.

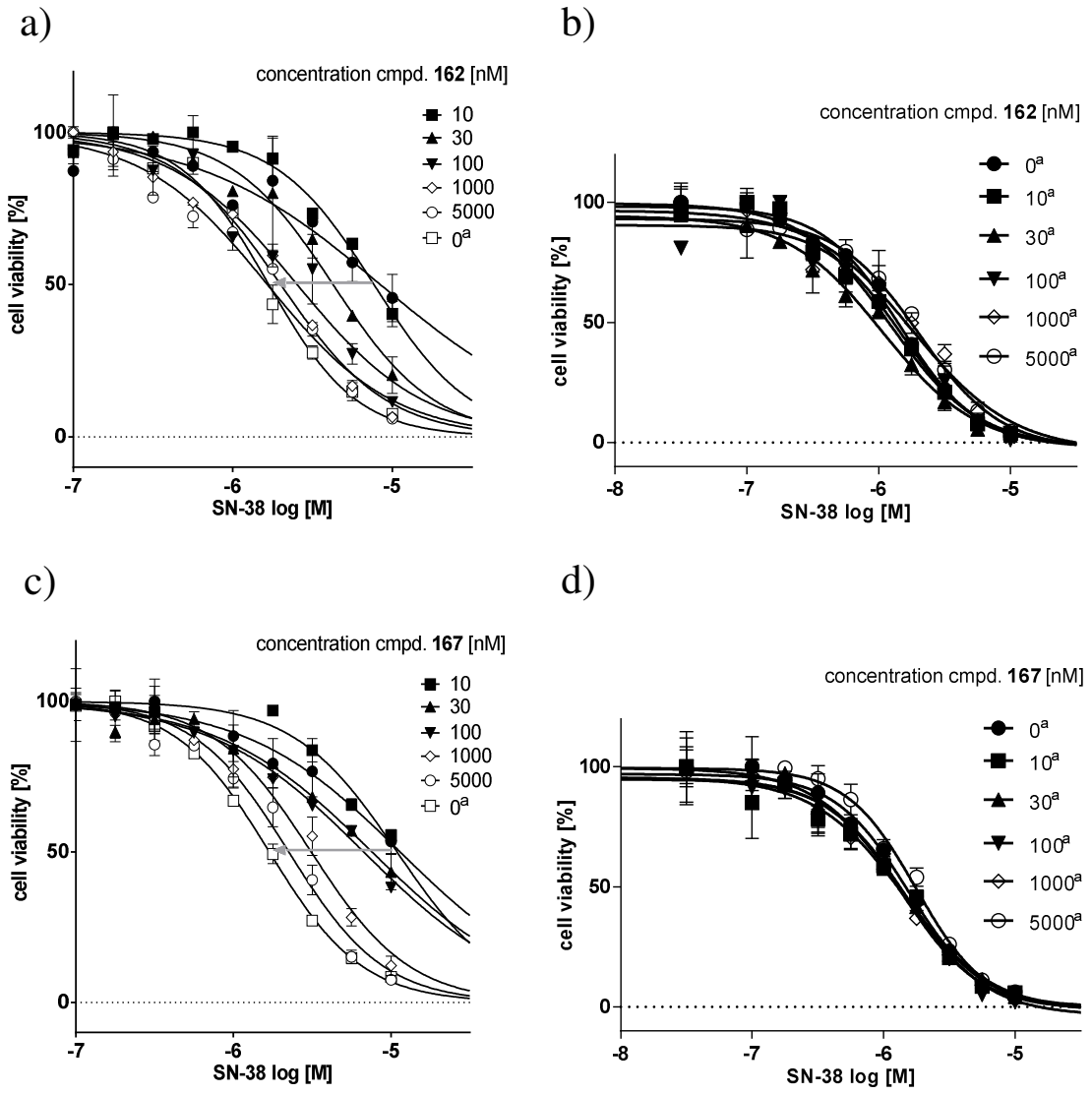

Figure continues on the next page

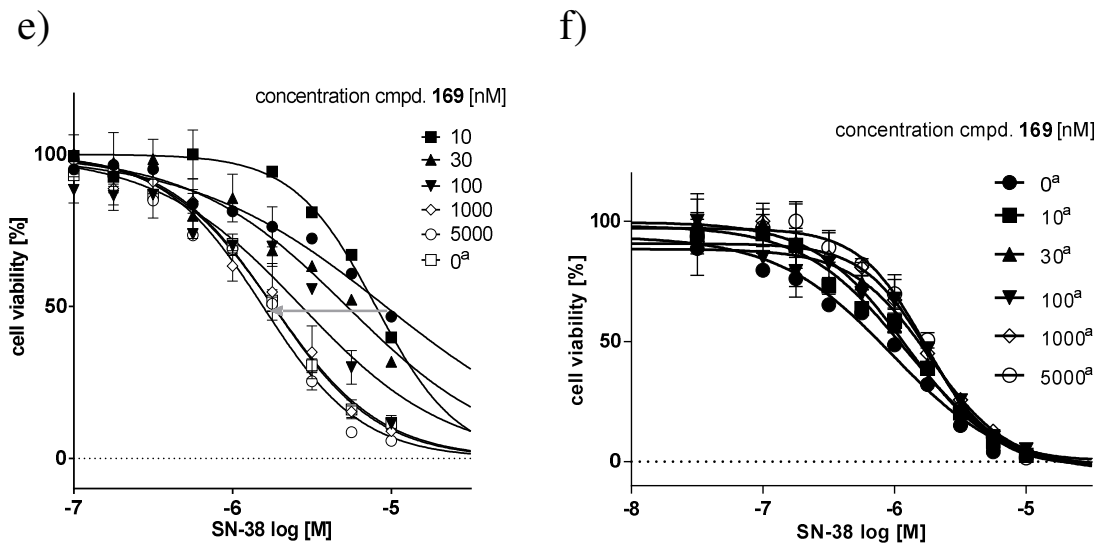

*Figure 75: MDR reversal assay of compound **162**, **167** and **169** demonstrating the ability to reverse the MDR toward the cytostatic SN-38, using parental MDCK II and ABCG2 overexpressing cell lines (a, c and e). The grey arrow indicates the increasing sensitization of the ABCG2 overexpressing cells with higher compound concentrations (see legend). At a compound concentration of 1 µM, full reversal is achieved, indicated by a similar pEC_{50} as the parental cells. For comparison an analogous assay was performed using only parental MDCK II cells (b, d and f).*
a: Parental MDCK II cells.

Full reversal of the resistance toward SN-38 was produced by selected compounds **162**, **167** and **169** at a concentration below 10 µM, indicated by comparable EC_{50} values of the parental cells and the ABCG2 expressing cells. The increasing sensitization of the ABCG2 expressing cells is visualized by the grey arrow in Figure 75 a), c) and e).

An analogous assay using only parental cells was carried out to consider possible side effects that might influence the reversal of MDR. Indeed, no such effects could be observed in the parental cell line obtaining comparable EC_{50} values from the concentration-viability curves in Figure 75 b), d) and f).

Determination of the extent of reversal by the compounds was carried out by plotting the pGI_{50} values from the MDR reversal assay against the logarithm of the corresponding compound concentration. Hereby, sigmoidal curves were fitted with the logistic equation and the EC_{50} calculated for each compound. Maximum inhibition is given by the top value of the parental cells which should be comparable to the top value obtained with the ABCG2 expressing cells indicating the state "total inhibition". The corresponding plot is illustrated in Figure 76.

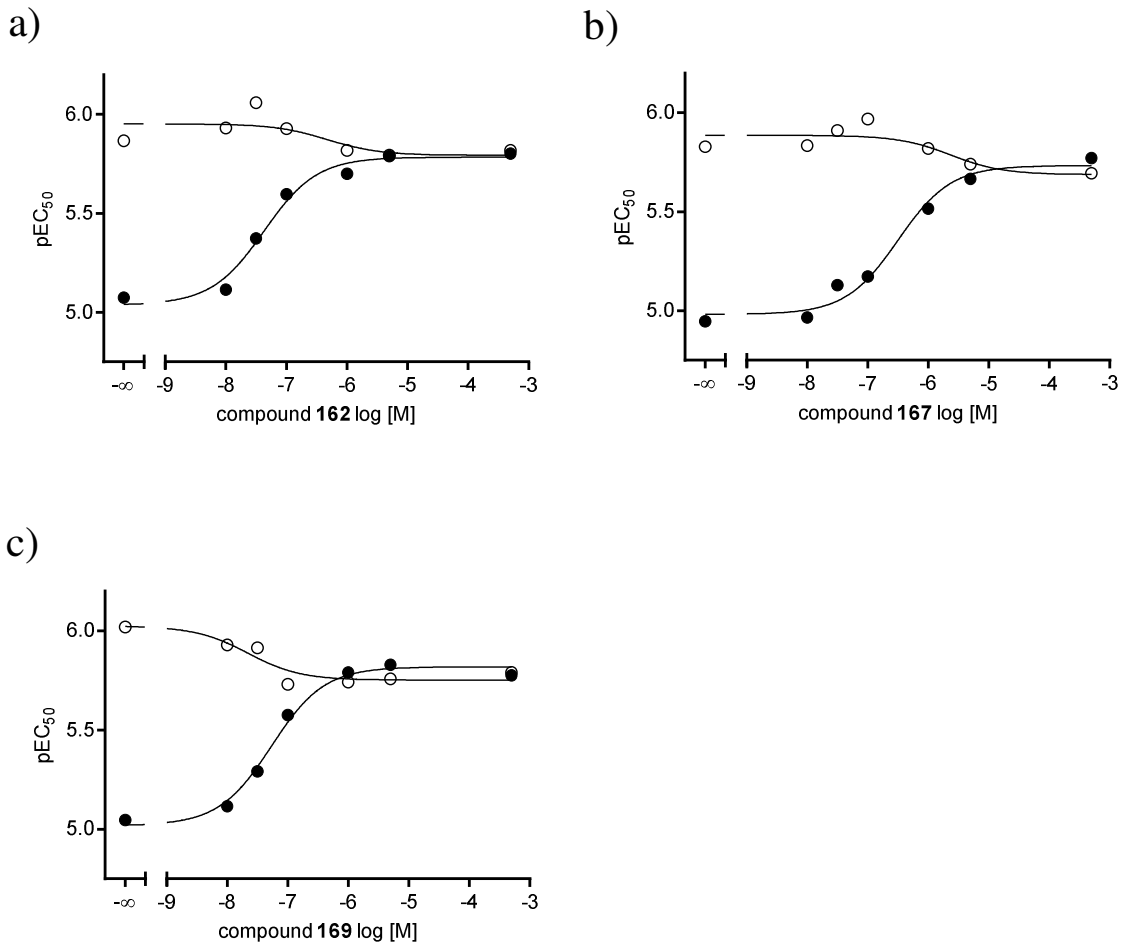

Figure 76: Nonlinear regression of the pGI50 values determined in the viability assay (Figure 75 a), c) and e)) and the corresponding concentration of compound 162, 167 and 169. Correlation of the degree of sensitization toward SN-38, indicated by the pEC50 value, an EC50 of 42.9 nM (162), 319 nM (167) and 53.8 nM (169) was determined (●). Compound 162, 167 and 169 yielded IC50 values of 149 nM, 1206 nM and 238 nM in the Hoechst 33342 accumulation assay, respectively. A nonlinear regression of the pEC50 values determined in an analogous efficacy assay Figure 75 b), d) and f)), but using only parental MDCK II cells, is depicted with open circles (○).

According to the plot EC_{50} values of 42.9, 319 and 53.8 nM resulted for compound **162**, **167** and **169**, respectively. Indeed, the inhibitory potency derived from the MDR reversal is about 4-fold higher than determined in the Hoechst 33342 accumulation assay. Yet, the tendency of the inhibitory potency obtained in both assays is in excellent accordance. Higher inhibitory activities in the MDR reversal assay in comparison to the Hoechst 33342 accumulation assay have also been observed for other compounds discussed in project I-III and could be due to a lower affinity of SN-38 to ABCG2.

Moreover, the sensitization of ABCG2 overexpressing MDCK II BCRP cell line toward the cytostatic drug MX was investigated in co-administration of compound **144** and **150**. The assay was carried out at different compound concentrations in the presence and absence of 0.5 µM MX. Further details of the assay are provided in chapters 3.5 and 10.2.2.7. Both compounds were able to reverse the resistance of the cells toward MX, as illustrated in Figure 77.

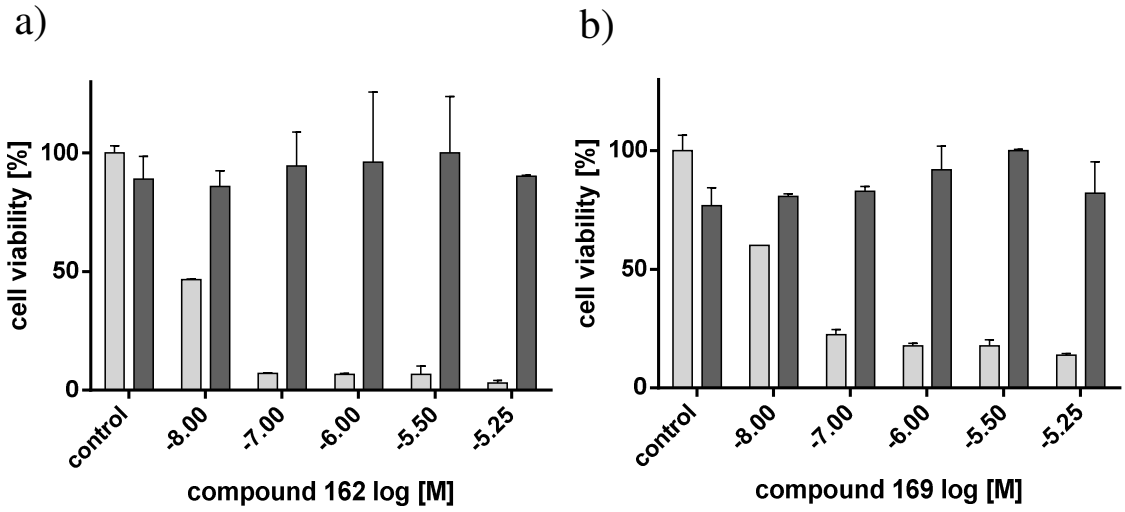

*Figure 77: MDR reversal assay of compounds **162** (a) and **169** (b), demonstrating their ability to reverse MDR toward the cytostatic mitoxantrone (MX), in the ABCG2 overexpressing cell line MDCK II BCRP. The bars represent the cell viability at a given modulator concentration in the presence (light grey) and absence (dark grey) of 0.5 µM mitoxantrone. Control shows viability of cells without modulator. The standard deviation is expressed by error bars.*

Full reversal of the resistance toward MX was resulted with both compounds at a concentration between 0.1 and 1 µM. The half-maximal growth inhibition was obtained by compound **162** and **169** at a concentration of 8.61 and 20.9 nM, respectively. Due to fewer measurements, the determined values in the MDR reversal assay with MX are more susceptible to error than with SN-38, but still provide a good estimation of the efficacy of a compound. Compound **162** was distinguished as more potent than **169**, which is in agreement to the Hoechst 33342 accumulation assay and the MDR reversal assay with SN-38.

6.6 Investigation of the interaction with Hoechst 33342

Investigation of the interaction of selected compounds with Hoechst 33342 was carried out with ABCG2 overexpressing MDCK II BCRP cells. For this purpose, varying compound concentrations were combined with varying concentrations of Hoechst 33342 and the interaction type could be determined by using the Lineweaver-Burk double reciprocal plot, described in chapters 4.6 and 10.2.2.8.

The results obtained with the Lineweaver-Burk method is depicted in Table 22, providing the intersection of the straight lines together with the corresponding interpretation. Corresponding plots obtained according to the Lineweaver-Burk method are depicted in Figure 78.

Table 22: Interaction with Hoechst 33342 According to the Lineweaver-Burk Double Reciprocal Plot.

Compound	R^1	R^2	Intersection	type of interaction with Hoechst 33342
162	Ph	H	X-axis	Non-competitive
166	Ph	3-CN	3. Quadrant	Non-competitive mixed type
167	Ph	4-CN	3. Quadrant	Non-competitive mixed type
168	Ph	3-OMe	X-axis	Non-competitive
169	Ph	4-OMe	Y-axis	Competitive
178	3-OMe-Ph	3-NO_2	X-axis	Non-competitive
181	3-OMe-Ph	4-CN	2. Quadrant	Non-competitive mixed type
188	3-OMe-Ph	4-CF_3	2. Quadrant	Non-competitive mixed type
Ko143			3. Quadrant	Non-competitive mixed-type

By evaluation of the intersections of the straight lines a non-competitive "mixed type" interaction with Hoechst 33342 was determined for compounds **166**, **167**, **181** and **188**. A pure non-competitive interaction was found for compounds **162**, **168** and **178** and a competitive interaction exclusively for compound **169**. According to the results obtained for the test set, this class of compounds, except one compound, does not compete for the same binding pocket with Hoechst 33342. Indeed, the majority exhibits a non-competitive of the "mixed-type" meaning that they are able to influence the active site but bind apart from Hoechst 33342.

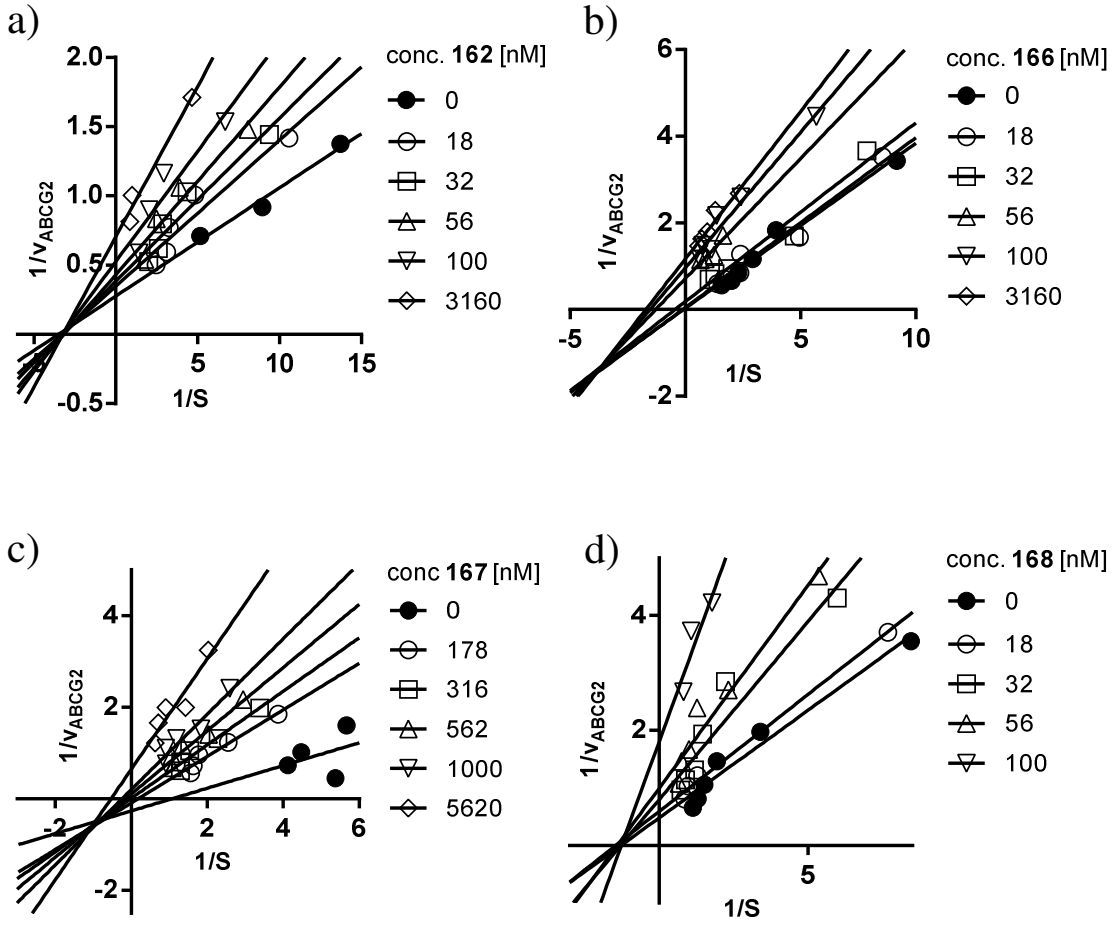

Figure continues on the next page

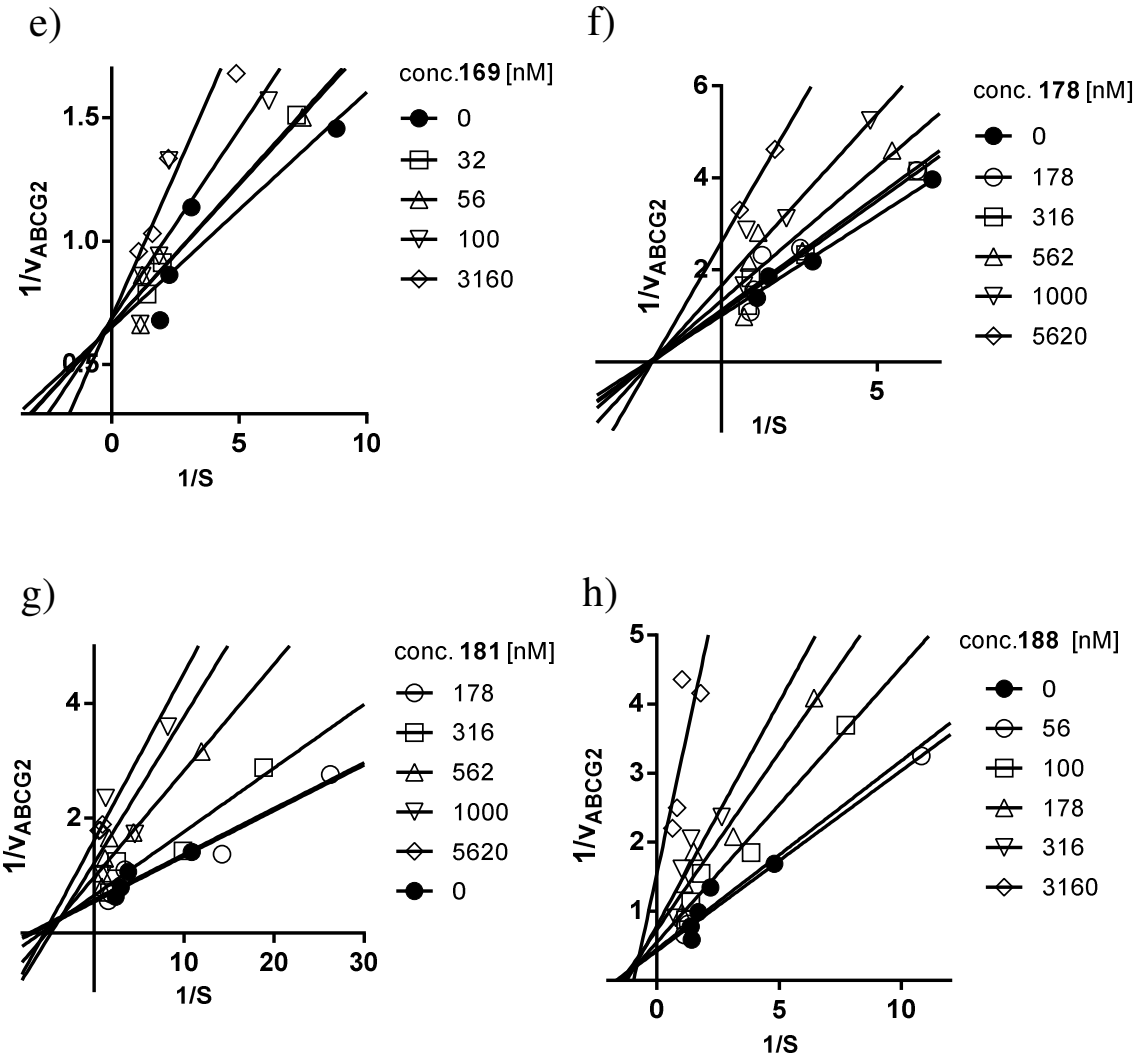

*Figure 78: Lineweaver–Burk plot for compounds **162** (a), **166** (b), **167** (c), **168** (d), **169** (e), **178** (f), **181** (g) and **188** (h) using various concentrations together with the ABCG2 substrate Hoechst 33342. Compound concentrations are specified in the legend.*

Additionally, the results from the Lineweaver-Burk double reciprocal plot were validated using the Cornish-Bowden method. Information regarding this procedure is provided in chapters 3.6 and 10.2.2.8. The linear regression of the V_{max} and K_M values resulted in slopes that were summarized as scatter plot in Figure 79. Corresponding linear regression plots are illustrated in Figure 80 (for Ko143 see chapter 3.6).

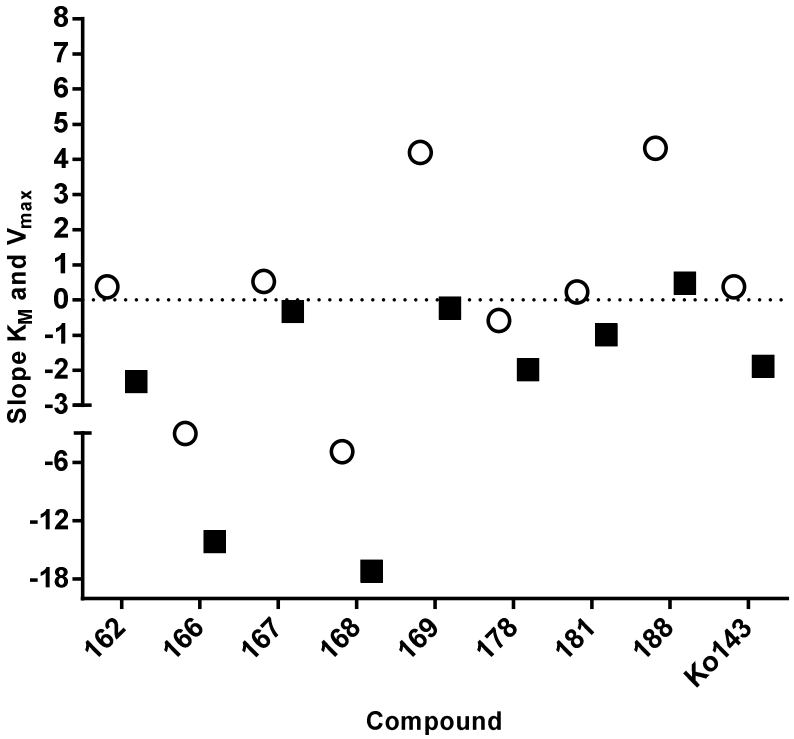

Figure 79: Scatter plot of the slopes obtained from the linear regression of K_M (○) and V_{max} (■) values calculated from the Cornish-Bowden direct linear plot.

Results obtained with the Cornish-Bowden method are consistent with the corresponding Lineweaver-Burk plots. Thus, compound **162**, **166**, **168**, **178**, **181** exhibit a more pronounced non-competitive interaction (V_{max} ↓) and **167**, **169** and **188** a rather competitive interaction (K_M ↑), as indicated by the slopes of the regression of the K_M and V_{max} values in the Cornish-Bowden plot.

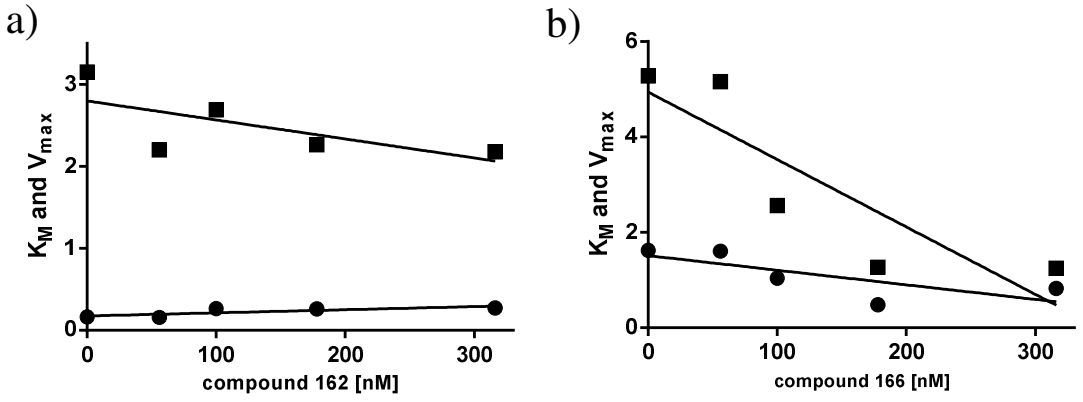

Figure continues on the next page

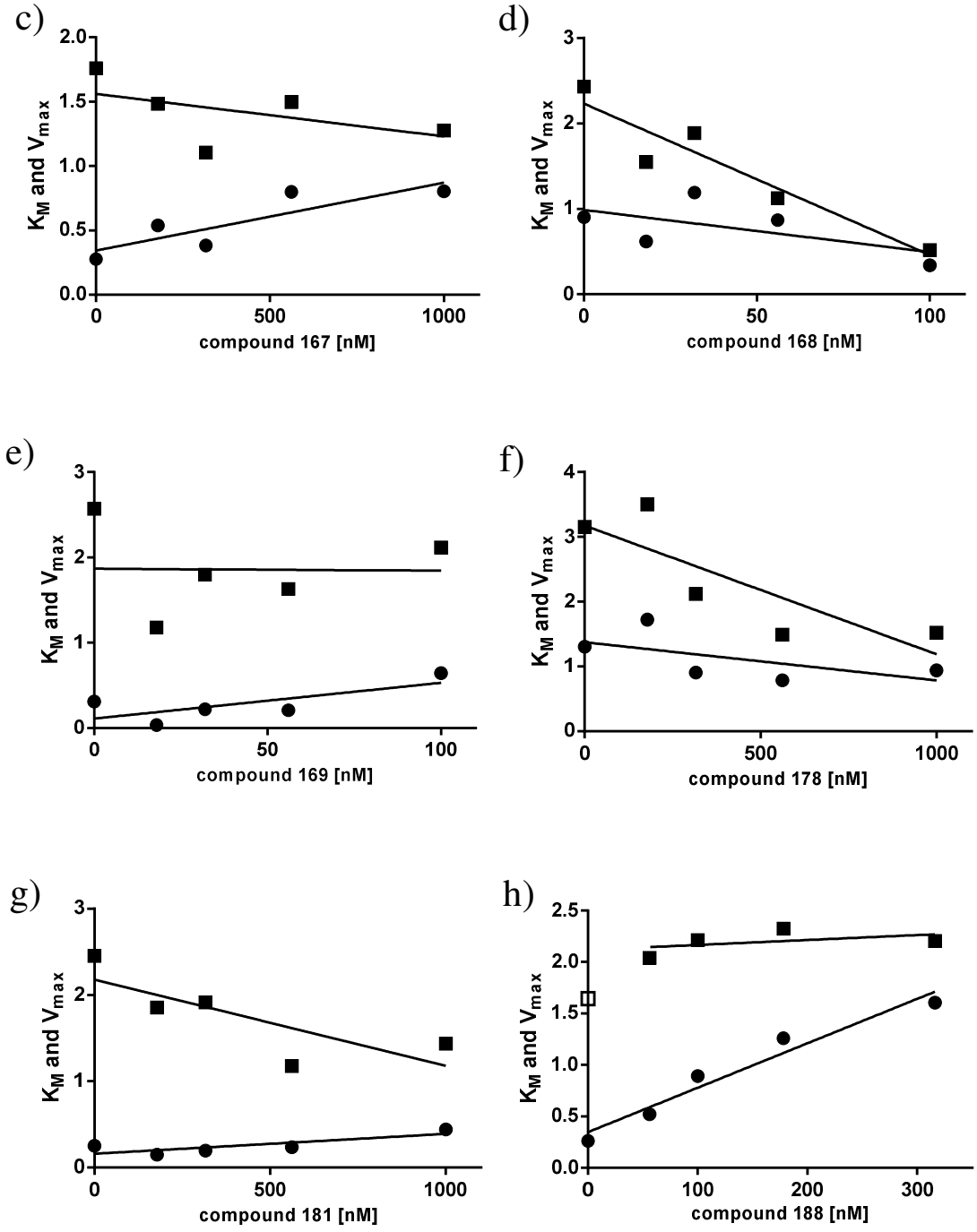

*Figure 80: Linear regression of the V_{max} (■) and K_M (●) values determined from direct linear plot for compounds **162** (a), **166** (b), **167** (c), **168** (d), **169** (e), **178** (f), **181** (g), and **188** (h). Excluded values are depicted as open symbols of the corresponding shape.*

The *para* cyano analogues **167** and **5** (see chapter 3.6) contain different scaffolds but both exhibited a noticeable competitive portion whereas the corresponding *meta* derivatives **166** and **4** showed a rather non-competitive interaction with Hoechst 33342. Another example is compound pair **168** and **169** containing 3-OMe and 4-OMe at R^1. Here the *meta* derivative shows a non-competitive and the *para* derivative a competitive interaction with Hoechst 33342. This points to the extraordinary impact of the choice of substitution and position at R^1 (*meta* vs. *para*) influencing the inhibitory potency, the binding to ABCG2, and other aspects as well.

6.7 Investigation of the conformation sensitive 5D3 antibody binding to an epitope of ABCG2

The conformational impact on ABCG2 of selected compounds was investigated using the conformation sensitive 5D3 antibody. The antibody binds specifically to an epitope of the transport protein and the emitted fluorescence by the bound antibody was measured with a FACSCalibur flow cytometer utilizing ABCG2 overexpressing PLB-985 cells. Further information is provided in chapters 3.7 and 10.2.2.9. A bar-chart summarizes the results of this assay using Ko143 as positive control representing 100% labelling with the antibody, as depicted in Figure 81.

Among selected compounds the highest labelling was observed for compound **167** containing 4-cyano at R^1 with a labelling-rate of 93% compared to the standard Ko143. In contrast, the 3-cyano derivative **166** possesses a labelling of 63% with the 5D3 antibody pointing out the distinction between *meta* and *para* derivatives. Also, a high labelling resulted for compound **181**, another 4-cyano derivative. This is in accordance to the observations in project I where compound **5** exhibited a high rate of labelling containing a 4-cyano substituent on a 2-phenylquinazoline scaffold.

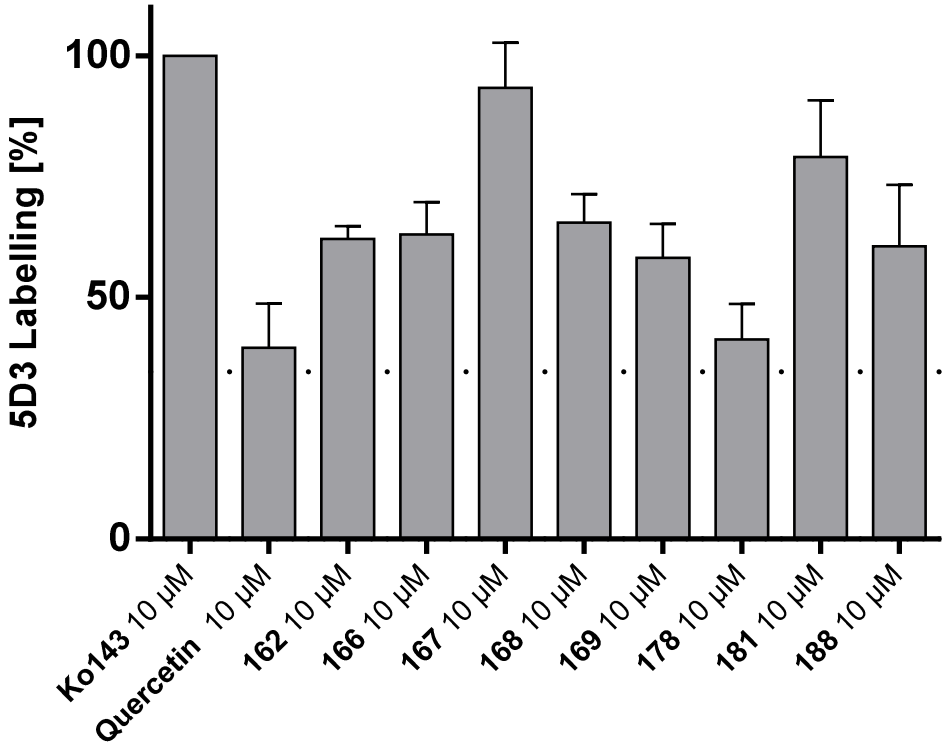

Figure 81: 5D3 immunoreactivity modulation of ABCG2 at a compound concentration of 10 µM. Fluorescence detected by the 5D3-labeling of ABCG2 in the presence of 10 µM Ko143 was set to 100% and the fluorescence measured in the absence of any compound taken as 0%. The dotted line represents the labelling obtained with Hoechst 33342.

However, only a minor difference was observed for the *meta* and *para* methoxy derivatives **168** and **169**. Interestingly, the difference in the Hoechst 33342 accumulation assay was also less pronounced, although both compounds showed different interactions with Hoechst 33342.

Very little labeling of only 41% was found for compound **178** containing 3-methoxy at R^1 and 3-nitro at R^2. Due to the fact that the obtained labelling is similar to that of Quercetin and Hoechst 33342 it is possible that compound **178** could be transported by ABCG2, at least to some extent. To substantiate this claim some more data would have to be collected from different assays. According to the cytotoxicity data and the conducted fluorescence experiments, no indication was found that the compounds are substrates of ABCG2.

Furthermore, representative histograms of compounds with the highest and the lowest 5D3 shift in the assay as well as the standard Ko143 are depicted in Figure 82. Histograms of compounds Ko143, **166** and **167** were obtained at a compound concentration of 10 µM, respectively.

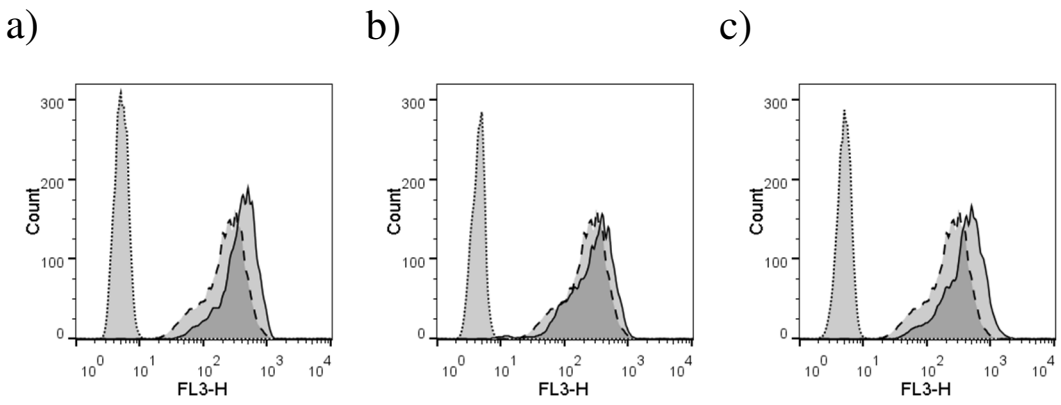

Figure 82: Histogram of the measured fluorescence at the FL3-H detector (X-axis) and the cell-count gated according to the fluorescence. Depicted is the fluorescence of the isotype-control (dotted curve) as well as of 5D3 antibody in the absence of a compound (dashed curve) and in the presence of a compound (continuous curve).Compounds with the highest and lowest 5D3 shifts: Ko143 (a), ***166*** *(b) and* ***167*** *(c) at a concentration of 10 µM.*

6.8 Investigation of the ATPase activity

For this purpose Ko143 was used as standard ATPase inhibitor and quercetin as standard stimulator using High Five insect cell membrane preparations. The ATPase activity assays were performed by Jennifer Gallus. Further details are provided in chapters 3.8 and 10.2.2.10. Three different compound concentrations (1, 10 and 25 µM) were used in the screening, including the most potent compounds. A summary of the results is illustrated as bar chart in Figure 83.

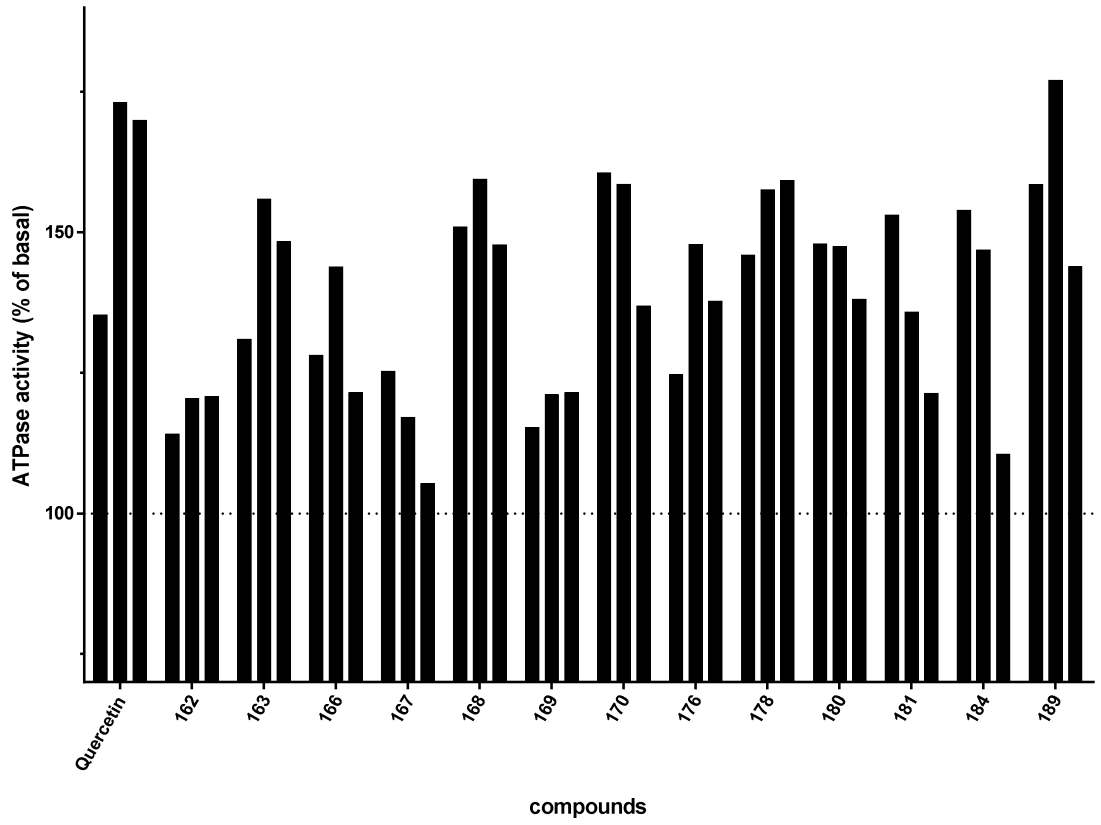

Figure 83: Screening of ATPase activity of selected compounds at three different concentrations. From left to right the bars correspond to 1, 10 and 25 µM final concentration of compound. Quercetin was used as a standard for activation of ABCG2 ATPase activity. All values are relative vanadate-sensitive ATPase activities in relation to the basal activity, which is set to 100%.

All investigated compounds led to either medium or strong activation of the ATPase activity. Differences were in particular noticeable for the *meta* and *para* compound pairs containing the same substituent. This is illustrated by compound **166/167** and **168/169** containing either a cyano or methoxy group at R^2. Both substituents led to a considerably higher ATPase stimulation when present in *meta* position compared to the *para* substitution.

Considerably higher rates of ATPase stimulation resulted for substitution with 3-methoxy than with hydrogen at R^1, as illustrated in the compound pairs **163/178**, **180/166**, **167/181** and **176/189**. Among those, compound **178** and **189** led to an extraordinary strong stimulation of the ATPase activity, in part even stronger than the standard stimulator quercetin. Corresponding concentration-response curves of compound **168**, **169** and **178** carried out with more concentrations each led to a sigmoidal curve progression illustrated

in Figure 84. Here, EC_{50} values for compound **168**, **169** and **178** were calculated as 118, 9.28 and 18.0 nM where the standard stimulator quercetin obtained an EC_{50} of only 302 nM.

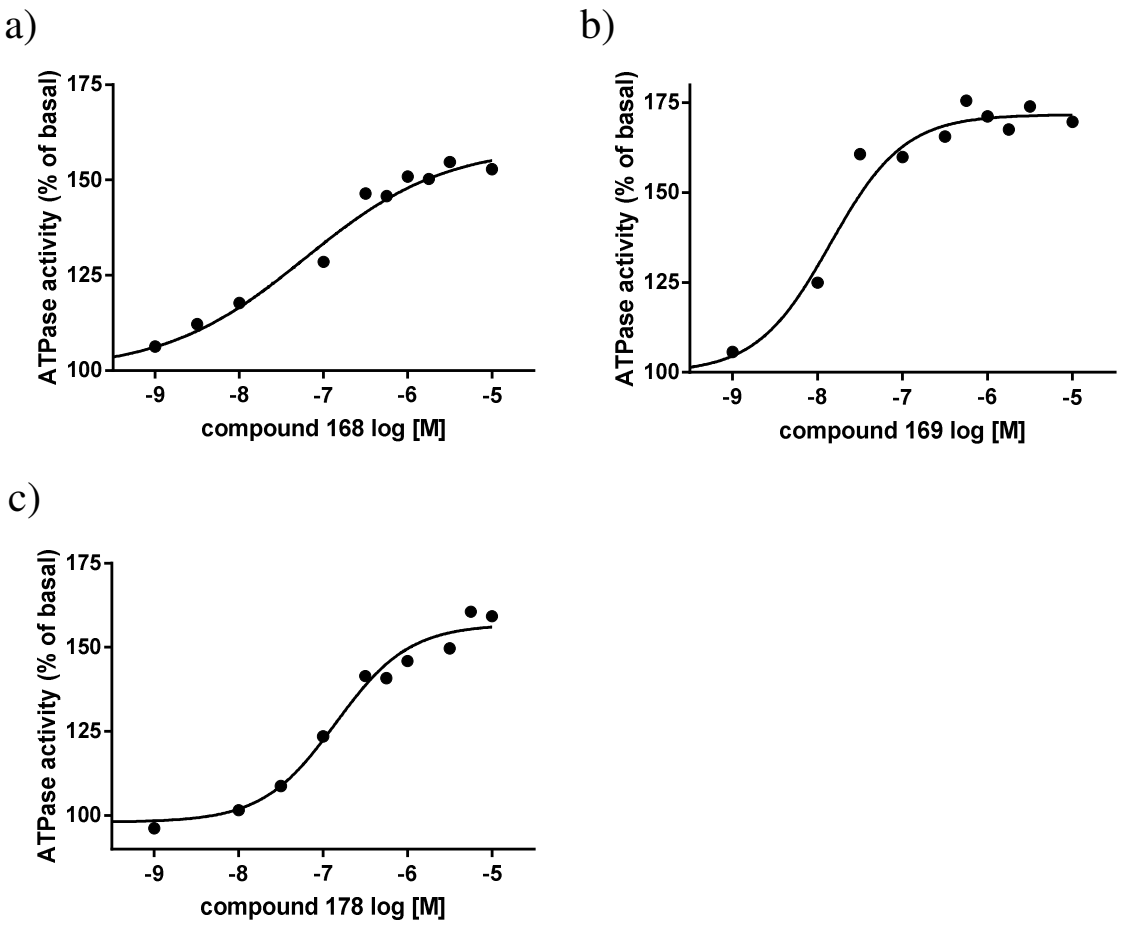

*Figure 84: Concentration-response curves for compounds **168** (a, EC_{50}: 118 nM), **169** (b, EC_{50}: 9 nM) and **178** (c, EC_{50}: 18 nM) in the ATPase assay. All values are relative vanadate-sensitive ATPase activities in relation to the basal activity, which is set to 100%.*

Compound **167**, **181** and **184** on the other hand exhibited a strong decrease of the activity with higher compound concentrations. Previous investigation of the conformation sensitive 5D3 antibody binding resulted in the highest labelling for compounds **167** and **181** (see chapter 6.7). Moreover, these two compounds were also found to possess high portions of competitive interaction with Hoechst 33342 (see chapter 6.6). In many cases, low ATPase activity levels correlated with a high rate of labelling by 5D3 antibody and a pronounced competitive character of interaction with Hoechst 33342.

7 Project V: 2,4-Substituted 6-nitroquinazolines

In this project a nitro function was introduced at position 6 of a 2,4-substituted quinazoline scaffold. The impact of this modification can easily be compared to the previously discussed compounds of project I-III. The introduced nitro group is a HBA function and decreases the electron density at the quinazoline moiety. For better insights into the SAR, reduction of the nitro moiety was carried out yielding an amino function at position 6. This aromatic amine on the other hand is a HBD function and increases the electron density at the quinazoline scaffold. Due to the large conjugated pi-system a strong fluorescence could be observed in some amino derivatives after excitation. In contrary, compounds containing nitro functions showed no fluorescence owing to quenching effects. Fluorescence measurements of compound **244** are provided in chapter 8.10, discussing the possibility of a substrate character. Further modification was achieved by reacting the amino function with aromatic acid chlorides. Formed amides contain both, a HBD and HBA function and also a bulky aromatic residue.
Although a relatively low logP value of 3.81 was calculated for the unsubstituted 6-nitro derivative **211**, some compounds showed a reduced solubility during preparation of the dilution series. Hence, the amount of MeOH was increased for some compounds, but kept below 5% in the final concentration to prevent damage of the cells.

7.1 Reaction mechanism

A schematic synthesis route and a detailed reaction mechanism is provided on the following page.

*Scheme 6. General synthesis scheme for the preparation of compounds **198-248**.*[a]

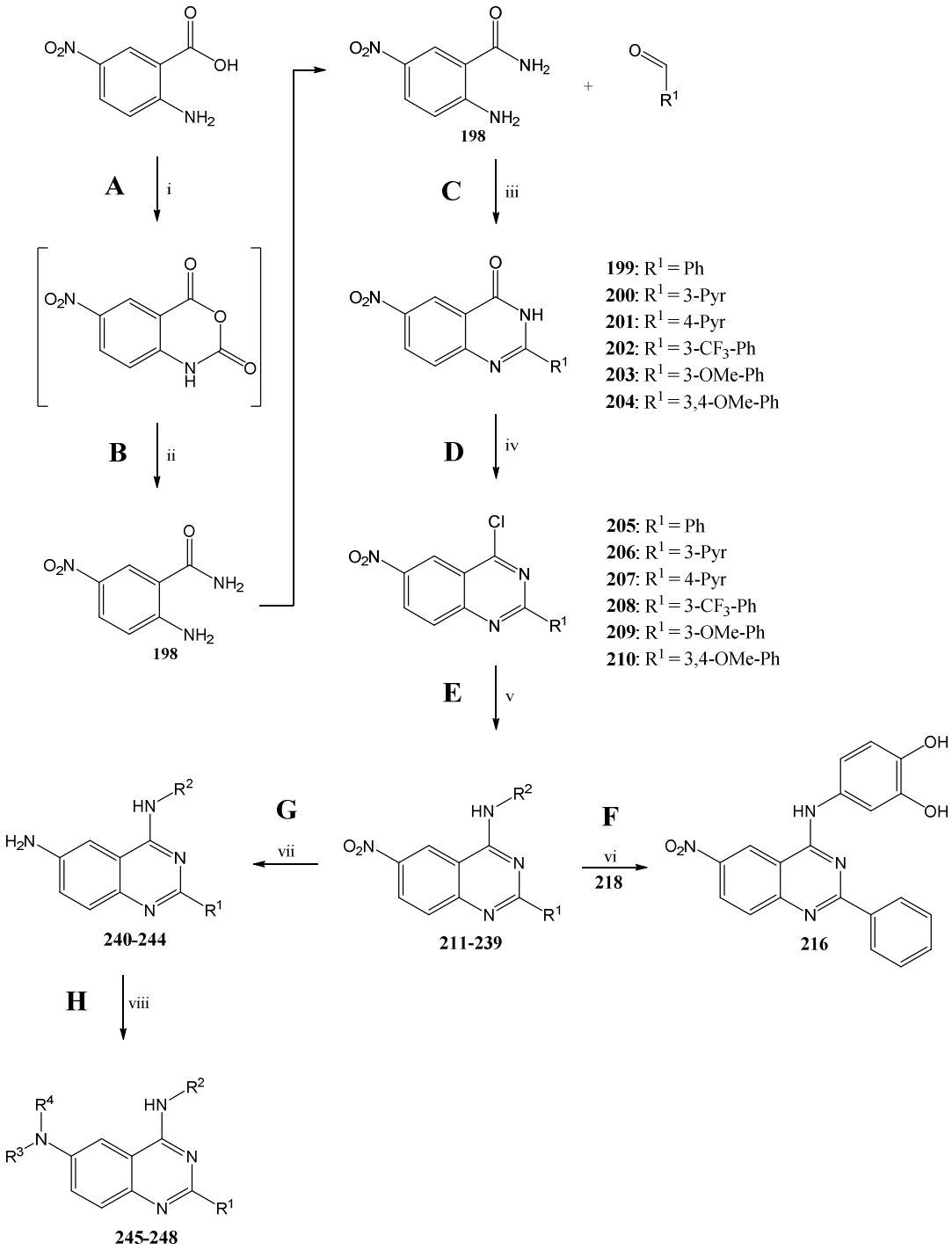

[a]: Reagents and conditions: (i) Triphosgene, THF, reflux, 3h. (ii) NH_3, 50 °C, 30 min. (iii) I_2, K_2CO_3, DMF, 90-110 °C, 8-12 h (iv) $POCl_3$, reflux, 4-12 h. (v) Substituted aniline, 100 watt microwave irradiation, 110 °C, 20-40 min. (vi) BBr_3, DCM, -60°C → RT, 12 h. (vii) THF, 4 bar H_2, Pd/C, RT, 24 h. (viii) RCOCl, THF, 0 °C → RT, 6-12 h.

Reaction mechanism **A**:

Initially, triphosgene dissociates in phosgene molecules at high temperature that react as electrophiles. The amino and the hydroxy function of the 2-amino-5-nitrobenzoic acid perform a nucleophilic attack at the positively polarized carbon atom of the phosgene molecule performing an intramolecular ring-closure and releasing hydrochloric acid. The underlying mechanism is an addition-elimination reaction.

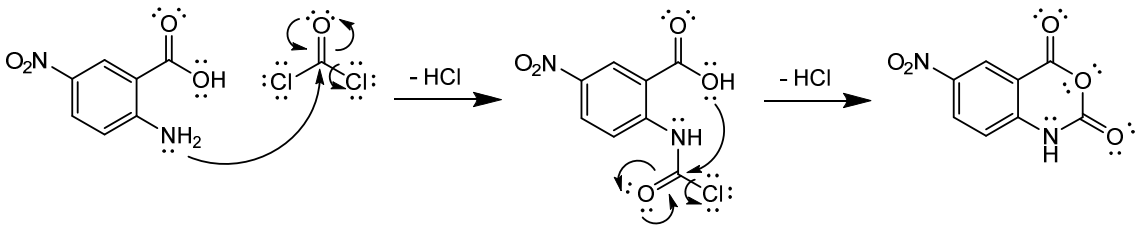

Reaction mechanism **B**:

The cyclic organic acid anhydride reacts *in situ* with ammonium gas opening the ring by nucleophilic attack at the carbonyl function at position 4. Due to the instability of the N-substituted carbamic acid group it reverts to carbon dioxide forming an amino function and yielding 2-amino-5-nitrobenzamide.

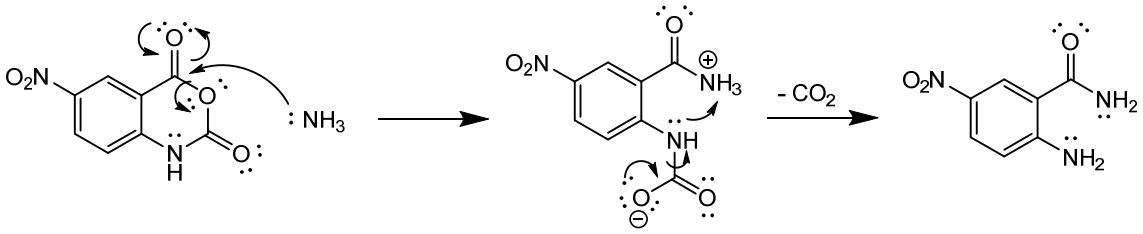

Reaction mechanism **C**:

In the first step, 2-amino-5-nitrobenzamide attacks the carbonyl function of the aldehyde derivative with its amino function *via* nucleophilic addition followed by elimination of H_2O. Ring-closure is achieved *via* nucleophilic addition by the amide nitrogen atom at the initially formed imine double bond depicted below. In the last step, a double bond between position 1 and 2 is inserted by oxidation with elemental iodine.

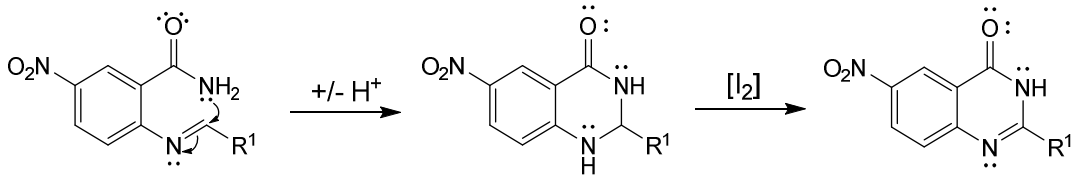

Reaction mechanism **D**:

The carbonyl function at position 4 undergoes chlorination in the presence of $POCl_3$. The corresponding reaction mechanism is illustrated below and can be reviewed in chapter 4.1.

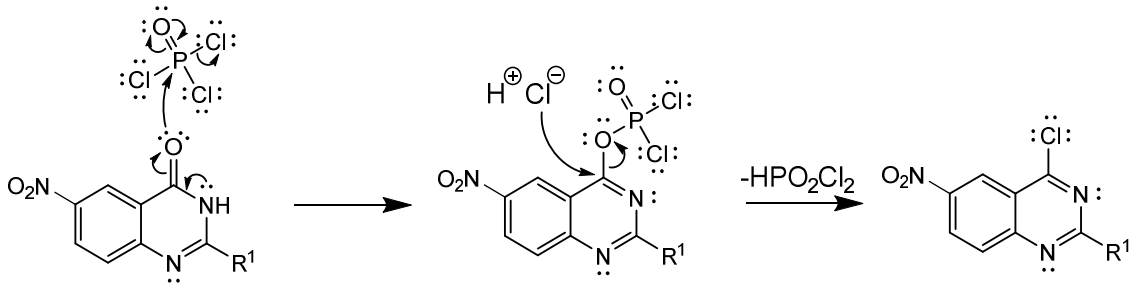

Reaction mechanism **E**:

Final compounds were synthesized *via* nucleophilic aromatic substitution of the corresponding 4-chloro-6-nitroquinazoline precursor by a substituted aniline derivative. The reaction mechanism is analogous to that used for the compounds in project I and can be reviewed in chapter 3.1.

Reaction mechanism **F**:

Boron tribromide reacts with the methyl ether functions of compound **20** as an electrophile which is attacked by the free nucleophilic electron pairs of the oxygen atom leading to an elimination of a bromine atom. The released bromide ions attack the methyl residues of the ether functions in a nucleophilic substitution reaction forming bromomethane and O-dibromoborane. Work up with water results in the formation of an aromatic hydroxy function.

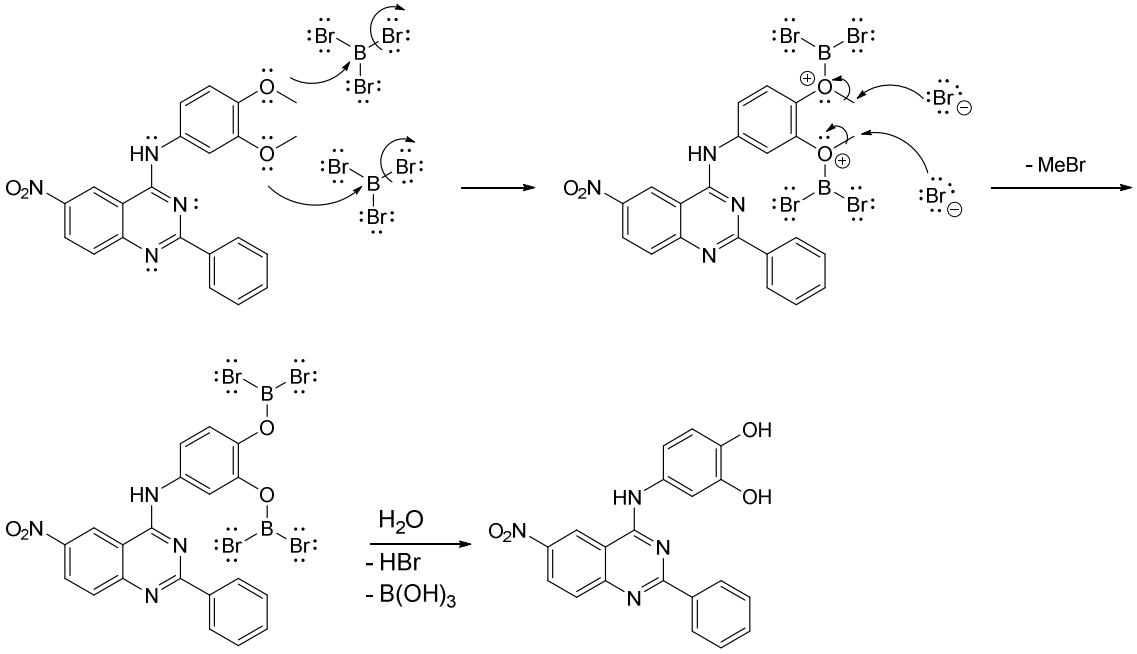

Reaction mechanism **G**:

The nitro function at position 6 can be reduced using palladium on carbon as a catalyst in the presence of hydrogen gas in a catalytic hydrogenation reaction. Hereby, the nitro function is reduced to an amino function.

Reaction mechanism **H**:

Previously formed amino function at position 6 performs a nucleophilic attack at the carbonyl function of the substituted acid chloride. Nucleophilic addition is followed by elimination of hydrochloric acid to restore the carbonyl function and compensate formal charges at the nitrogen atom to obtain an amide function. In the case of compound **245** a second addition-elimination reaction occurred yielding an iminoethyl acetate function. Hydrochloric acid was precipitated as salt formed with triethylamine.

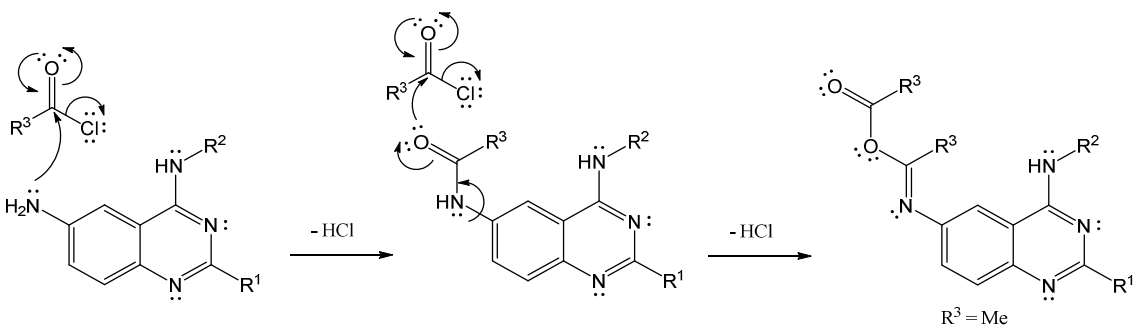

7.2 Investigation of the inhibitory potency toward ABCG2 in the Hoechst 33342 accumulation assay

Investigation of the inhibitory potency of the compounds was carried out in a Hoechst 33342 accumulation assay using the ABCG2 overexpressing MDCK II BCRP and parental cell line. Additional information to the Hoechst 33342 accumulation assay as is provided in chapter 3.2 and 10.2.2.2. The resulting activity data is given in Table 23.

Table 23: Inhibitory Activities Derived from the Hoechst 33342 Accumulations Assay Toward ABCG2 Overexpressing MDCK II BCRP Cell Line. The Substitution Pattern is Illustrated Above the Table.

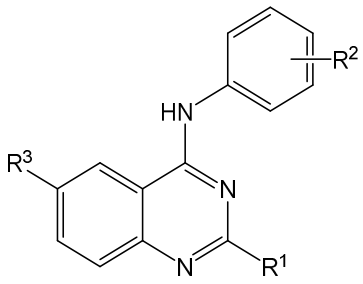

Compound	R^1	R^2	R^3	Hoechst 33342 IC_{50} ± SD [nM][a]
211	Ph	H	NO_2	106 ± 15
212	Ph	3-NO_2-4-OH	NO_2	37.4 ± 5.0
213	Ph	3-CN	NO_2	48.2 ± 7.7
214	Ph	4-CN	NO_2	48.1 ± 9.2
215	Ph	3-OH	NO_2	65.3 ± 9.7
216	Ph	3,4-OH	NO_2	119 ± 17
217	Ph	3-OMe	NO_2	33.1 ± 5.6
218	Ph	3,4-OMe	NO_2	37.0 ± 5
219	Ph	3-$NHCOCH_3$	NO_2	78.7 ± 13.5
220	Ph	3-F	NO_2	51.5 ± 9.8
221	Ph	3-CF_3	NO_2	49.1 ± 5.8
222	Ph	3-CO_2H	NO_2	904 ± 17
223	4-Pyr	3-CN	NO_2	63.8 ± 13.2
224	3-Pyr	3-OMe	NO_2	47.0 ± 4.0
225	3-Pyr	4-OMe	NO_2	57.7 ± 7.0
226	4-Pyr	4-OMe	NO_2	75.5 ± 14.4
227	3-CF_3-Ph	H	NO_2	59.6 ± 8.00

Table continues on the next page

228	3-CF_3-Ph	3-NO_2-4-OH	NO_2	33.0 ± 4.7
229	3-CF_3-Ph	3-NO_2	NO_2	66.3 ± 13.3
230	3-CF_3-Ph	4-NO_2	NO_2	61.4 ± 5.7
231	3-CF_3-Ph	3-OH	NO_2	27.6 ± 2.4
232	3-CF_3-Ph	3-OMe	NO_2	59.0 ± 5.9
233	3-CF_3-Ph	3,4-OMe	NO_2	30.2 ± 4.3
234	3-CF_3-Ph	3-SMe	NO_2	101 ± 16
235	3-CF_3-Ph	3-F	NO_2	44.8 ± 6.2
236	3-CF_3-Ph	3-$NHCOCH_3$	NO_2	44.8 ± 4.4
237	3-OMe-Ph	4-CN	NO_2	27.8 ± 3.8
238	3-OMe-Ph	3-F	NO_2	23.4 ± 3.4
239	3,4-OMe-Ph	3-CF_3	NO_2	57.2 ± 7.9
240	3-Pyr	3-OMe	NH_2	369 ± 54
241	3-Pyr	4-OMe	NH_2	646 ± 69
242	3-CF_3-Ph	H	NH_2	726 ± 49
243	3-CF_3-Ph	3-OH	NH_2	799 ± 159
244	3-CF_3-Ph	3-OMe	NH_2	835 ± 113
245	3-Pyr	3-OMe	*N*-1-Iminoethyl acetate	5310 ± 240
246	3-Pyr	3-OMe	*N*-3-Nitrobenzamide	1150 ± 190
247	3-Pyr	4-OMe	*N*-3-Nitrobenzamide	1620 ± 70
248	3-Pyr	3-OMe	*N*-Nicotinamide	1040 ± 80
1[b]	Ph	H	H	882 ± 157
3	Ph	3-NO_2-4-OH	H	80.0 ± 9.1
5	Ph	4-CN	H	69.9 ± 10
13[b]	Ph	3,4-OMe	H	152 ± 19
18	Ph	3-F	H	355 ± 53
8	Ph	3-$NHCOCH_3$	H	278 ± 33
Ko143[c]				227 ± 14

[a]: *IC_{50} values are means of three independent experiments.*
[b]: *Compounds synthesized in earlier study.*[198]
[c]: *Used as reference in the assay.*

The significant impact of the 6-nitro function on the inhibitory activity toward ABCG2 becomes evident by comparison of the unsubstituted compounds **211** and **1**. A considerable increase in potency was obtained in the presence of a 6-nitro group resulting in an IC_{50} of 106 nM whereas the unsubstituted scaffold without 6-nitro obtained an IC_{50} of 882 nM.

In the first series of compounds containing a phenyl moiety at R^1 and 6-nitro were investigated with different substituents at R^2. All compounds showed a considerable increase in potency in comparison to the corresponding analogues lacking a 6-nitro group which is illustrated in the compound pairs **211/1**, **212/3**, **214/5**, **218/13**, **219/8** and **220/18**.

Substitution with 3-nitro-4-hydroxy, 3-methoxy and 3,4 methoxy at R^2 led to corresponding compounds **212**, **217** and **218** which all obtained excellent IC_{50} values below 40 nM. The lowest potency among this subset resulted for compound **222** (IC_{50}: 904 nM) containing a carboxylic acid function. This is probably due to a decreased membrane permeability of the anionic species due to deprotonation under physiological conditions.

Replacement of the phenyl residue with 3- and 4-pyridyl functions yielded the highly potent compounds **223**-**226** with IC_{50} values in the range of 47 to 76 nM. Owing to the pyridyl function this modification decreased the logP value considerably in comparison to a phenyl moiety resulting in an enhanced solubility.

Subsequently, a trifluoromethyl substituent was introduced at R^2. Again, increased inhibitory activities were observed in the highly potent compounds **228** (R^2: 3-nitro-4-hydroxy), **231** (R^2: 3-hydroxy) and **233** (R^2: 3,4-dimethoxy) which possessed rather low IC_{50} values of roughly 30 nM.

Since substitution with methoxy and fluoro groups turned out to be beneficial for high potencies, 3-methoxy and 3,4-dimethoxy functions were subsequently introduced at R^1. A substitution with 3-methoxy at R^1 and 3-fluoro at R^2 was found to lead to the highest inhibitory potency among the whole test set. The calculated IC_{50} value of 23 nM for compound **238** is approximately 10-fold lower than that of Ko143. Corresponding concentration-response curves of the two most potent compounds **237** and **238** together with the reference Ko143 are illustrated in Figure 85. Overall, 29 different compounds containing a 6-nitro function were synthesized possessing an extraordinary low average IC_{50} value of roughly 85 nM.

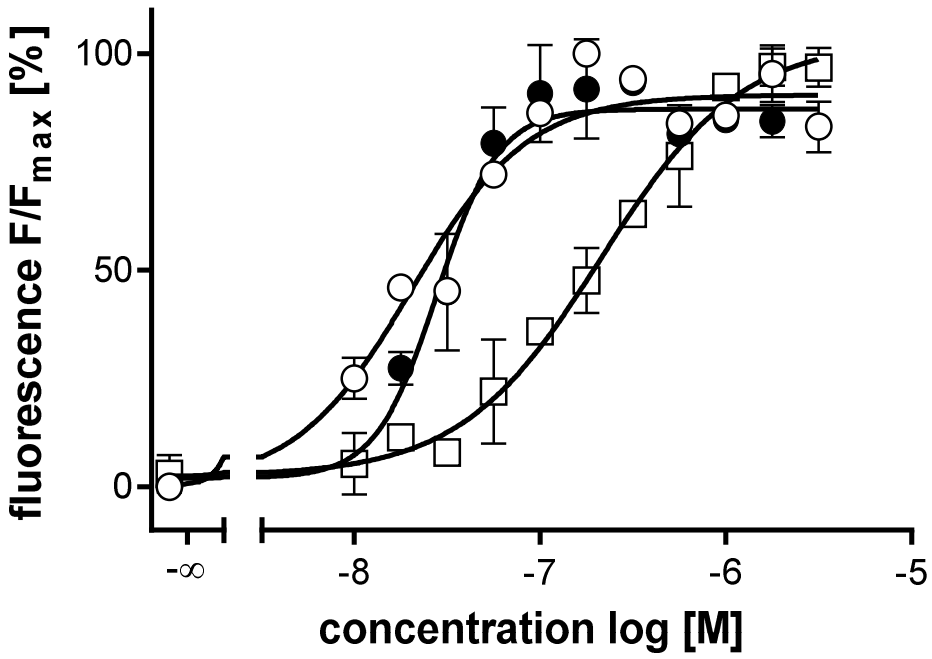

Figure 85: Concentration-response curve of compound ***237*** *(□, IC_{50}: 27.8 nM) and* ***238*** *(▲, IC_{50}: 23.4 nM) in a Hoechst 33342 accumulation assay with Ko143 (■, IC_{50}: 227 nM) as reference, using the ABCG2 overexpressing MDCK II BCRP cell line.*

The reduction of the nitro function at position 6 yielded the corresponding amino derivatives **240**-**244** that led to a considerable decrease in the inhibitory potency of about 10-fold or higher which is illustrated in the compound pairs **240/224**, **241/225**, **242/227**, **243/231** and **244/232**. It is reasonable that HBA functions like nitro are significantly more beneficial than HBD functions like amino. Also, differences in the IC_{50} values were noticeable for the *meta/para* methoxy compound pair **240/241** which is a common phenomenon throughout all projects.

Following, the reaction of the 6-amino functions with substituted acid chlorides yielded an amido function mostly linked to a bulky aromatic residue. Unfortunately, the inhibitory potency decreased further in comparison to their amine analogues.

7.3 Investigation of the inhibitory potency toward ABCB1 and ABCC1 in the calcein AM assay

A calcein AM assay was performed to screen the selectivity of several compounds toward ABCG2. For the assay the ABCB1 overexpressing cell line A2780 adr and the ABCC1 overexpressing cell line H69 AR were used. Further details regarding the assay are described in chapters 3.3 and 10.2.2.4. Screening results regarding the inhibitory activity toward ABCB1 and ABCC1 are depicted as bar charts in Figure 86.

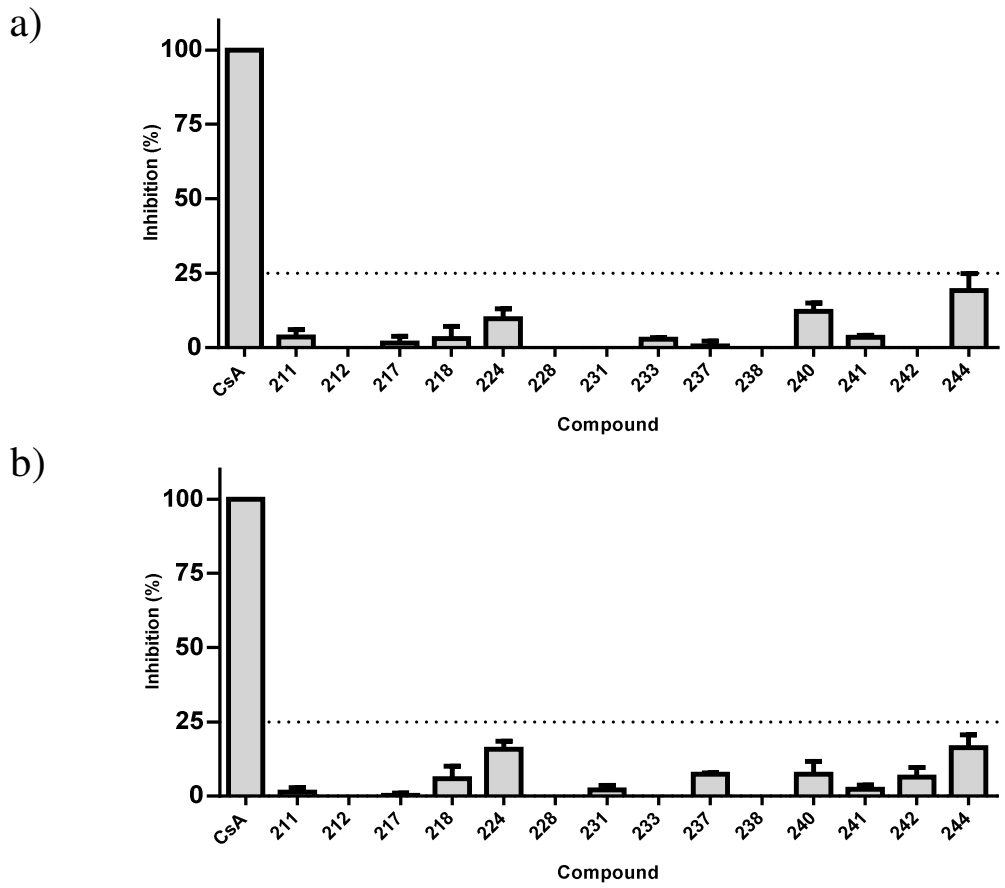

Figure 86 Inhibitory effect of screened compounds toward ABCB1 overexpressing cell line A2780adr (a) and MRP1 overexpressing cell line H69AR (b) in the calcein AM assay at a concentration of 10 µM. Cyclosporine A (CsA) was used as positive control, indicating complete inhibition. The inhibitory effect of each compound is expressed by the length of the bars, representing the inhibition compared to the positive control in percent. For each compound, three independent experiments were performed and the standard deviation is expressed by error bars.

The screening comprises several of the most potent compounds including some 6-amino derivatives and only negligible inhibitory activity less than 25% was found in comparison to CsA. This is surprising since some activity was found for compounds of project I-III containing one or more methoxy groups. Even compound **233** containing a substitution with 3,4-dimethoxy showed no measurable inhibitory activity toward ABCB1 and ABCC1.

7.4 Investigation of the intrinsic cytotoxicity with the MDCK II cell lines in a MTT assay

The intrinsic cytotoxicity of selected compounds was studied in a MTT assay using MDCK II parental and ABCG2 overexpressing cells. Toxic effects were determined after 72 h incubation of the cells in the presence of different compound concentrations and the cell viability was detected using MTT as indicator. Additional details of the procedure are provided in chapters 3.4 and 10.2.2.5 and a summary of the obtained GI_{50} values and the corresponding therapeutic ratios is depicted in Table 24.

In the development of medicinal drugs nitro functions have frequently been found to increase cytotoxicity. The same applies to the 6-nitro derivatives that were investigated in this project. Distinctive differences regarding the toxic effects were observed in compounds bearing a 6-nitro function and the corresponding analogues lacking that function. This is illustrated in the compound pairs **211/1**, **212/3** and **218/13** resulting in GI_{50} values of 18/27, 13/52 and 8/23 µM, respectively. Nevertheless, relatively high TRs were calculated owing to the extraordinarily high inhibitory potency of the majority of compounds. For instance, most potent compound **238** obtained a very poor GI_{50} of 4.38 µM but resulted in a TR of 187 which is still significantly better than Ko143 (TR: 48.9).

Table 24: Intrinsic Toxicity of Selected Compounds on MDCK II ABCG2 Overexpressing and Parental Cells.

Compound	R^1	R^2	R^3	GI_{50} [µM][a] BCRP	GI_{50} [µM][a] Parental	Therapeutic ratio (GI_{50}/IC_{50})[b]
211	Ph	H	NO_2	18	36	170
212	Ph	3-NO_2-4-OH	NO_2	13	9.8	350
217	Ph	3-OMe	NO_2	5.5	6.9	170
218	Ph	3,4-OMe	NO_2	8.1	8.5	220
223	4-Pyr	3-CN	NO_2	77	100	1200
226	4-Pyr	4-OMe	NO_2	85	130	1100
228	3-CF_3-Ph	3-NO_2-4-OH	NO_2	27	24	830
231	3-CF_3-Ph	3-OH	NO_2	3.4	3.0	120
233	3-CF_3-Ph	3,4-OMe	NO_2	3.6	3.2	120
237	3-OMe-Ph	4-CN	NO_2	11	9.1	400
238	3-OMe-Ph	3-F	NO_2	4.4	11	190
241	3-Pyr	4-OMe	NH_2	19	28	31
1	Ph	H	H	27	26	30
3	Ph	3-NO_2-4-OH	H	52	150	660
13	Ph	3,4-OMe	H	23	17	150
Ko143				13	13	49
MeOH/DMSO				96[c]	140[c]	

[a]: *Concentration leading to 50% of cell survival of MDCK II BCRP and parental cells. The data was obtained from at least two independent experiments as mean values.*

[b]: *Therapeutic ratio was calculated from the ratio of the GI_{50} [µM] obtained with BCRP expressing cells and the IC_{50} [µM] obtained from the Hoechst 33342 assay.*

[c]: *Positive control of the cytotoxicity from dilution with DMSO/MeOH without compound.*

Among the 6-nitro derivatives only substitution with 4-pyridyl at R^1 yielded compounds demonstrating a significantly low intrinsic cytotoxicity. Examples are compound **223** (GI_{50}: 77 µM) and **226** (GI_{50}: 85 µM) leading to the highest TR in this project with ratios of 1212 and 1119, respectively. Similar effects were observed in project II where the replacement of phenyl at position 2 with a pyridyl moiety led to a substantial decrease of the intrinsic cytotoxicity (see chapter 3.4 and 4.4).

A concentration-cell viability curve of compound **223**, **226**, **238** and a dilution series without compound is presented in Figure 87.

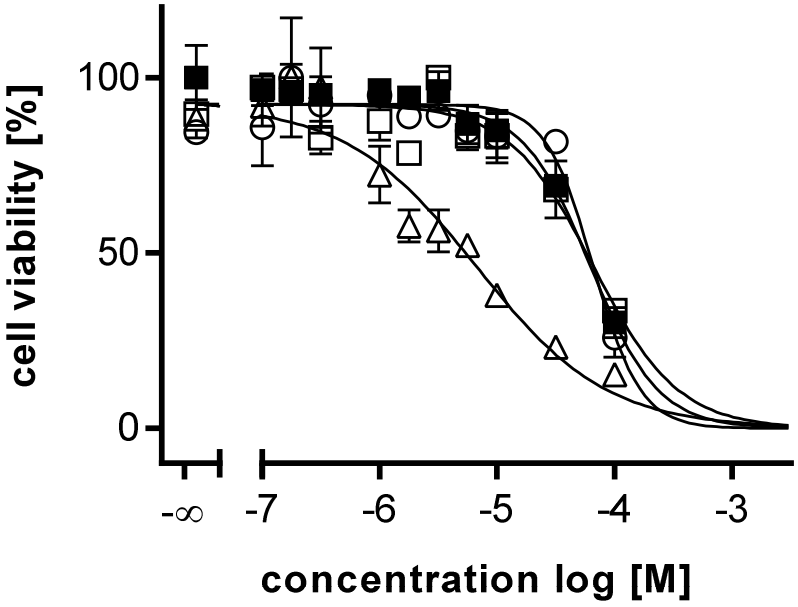

*Figure 87: MTT viability assay of compounds **223** (○), **226** (□), and **238** (Δ) using the ABCG2 overexpressing MDCK II BCRP cell line. The GI_{50} values were determined as 84.5 µM (□), 77.3 µM (○) and 9.46 µM (Δ), respectively. A control with the same concentration of MeOH and DMSO analogues to the dilution of the compounds, was carried out for comparison (■, GI_{50} = 96.1 µM). The amount of MeOH and DMSO used for the dilution was ≤ 1.8% and ≤ 1.0%, respectively.*

An overview of the TRs obtained by selected compounds is given in Figure 88, summarizing that the majority of the investigated compounds yielded values higher than 100. Indeed, this is more than two-fold higher with respect to the standard inhibitor Ko143 which is often labelled as "nontoxic" at effective concentrations in literature. Although the compounds of project V exhibited a relatively high cytotoxicity in comparison to other projects, they still obtain good TRs owing to their high inhibitory potency.

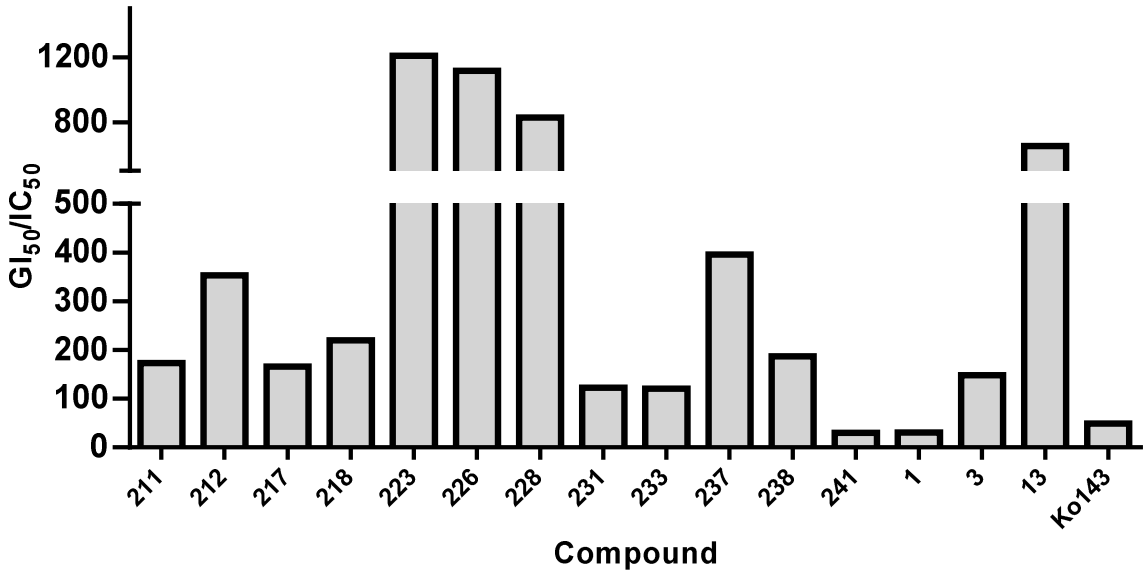

Figure 88: Therapeutic ratio of selected compounds, calculated from the ratio of GI_{50} to IC_{50} derived from MTT viability assay and Hoechst 33342 accumulation assay, respectively. The highest value was calculated for compound ***223*** *(GI_{50}/IC_{50} = 1212), while the reference compound Ko143 yielded GI_{50}/IC_{50} = 48.9.*

Besides **223** and **226**, also compound **228** yielded a good TR containing a disubstitution with 3-nitro-4-hydroxy at R^2 which has proven to be beneficial regarding a high inhibitory potency toward ABCG2 and low cytotoxicity. Similar results have already been detected for compound **3** which contained the same substitution and was one of the most attractive candidates among the compounds of project I.

In particular compounds **223** and **226** that contain a 4-pyridyl residue are promising candidates for *in vivo* investigations due to a low cytotoxicity, enhanced watersolubility and high inhibitory potency toward ABCG2.

7.5 Investigation of the reversal of multidrug resistance

The ability to reverse MDR in ABCG2 overexpressing MDCK II BCRP cell line toward SN-38 by co-administration of the potent compounds **212**, **228** and **238** was investigated in a MDR reversal assay. Further details are provided in chapters 3.5 and 10.2.2.6.

Corresponding concentration-viability curves obtained for parental and ABCG2 expressing MDCK II cell lines are depicted in Figure 89. Full reversal of the resistance of the ABCG2 overexpressing MCDK II BCRP cells toward SN-38 was observed for compounds **212**, **228** and **238** at concentrations less than 1 µM. A full sensitization of the ABCG2 overexpressing cells is indicated by comparable GI_{50} values in the resistant and parental cell line. The increasing sensitization with increasing compound concentrations is marked by the grey arrow in Figure 89 a), c) and d).

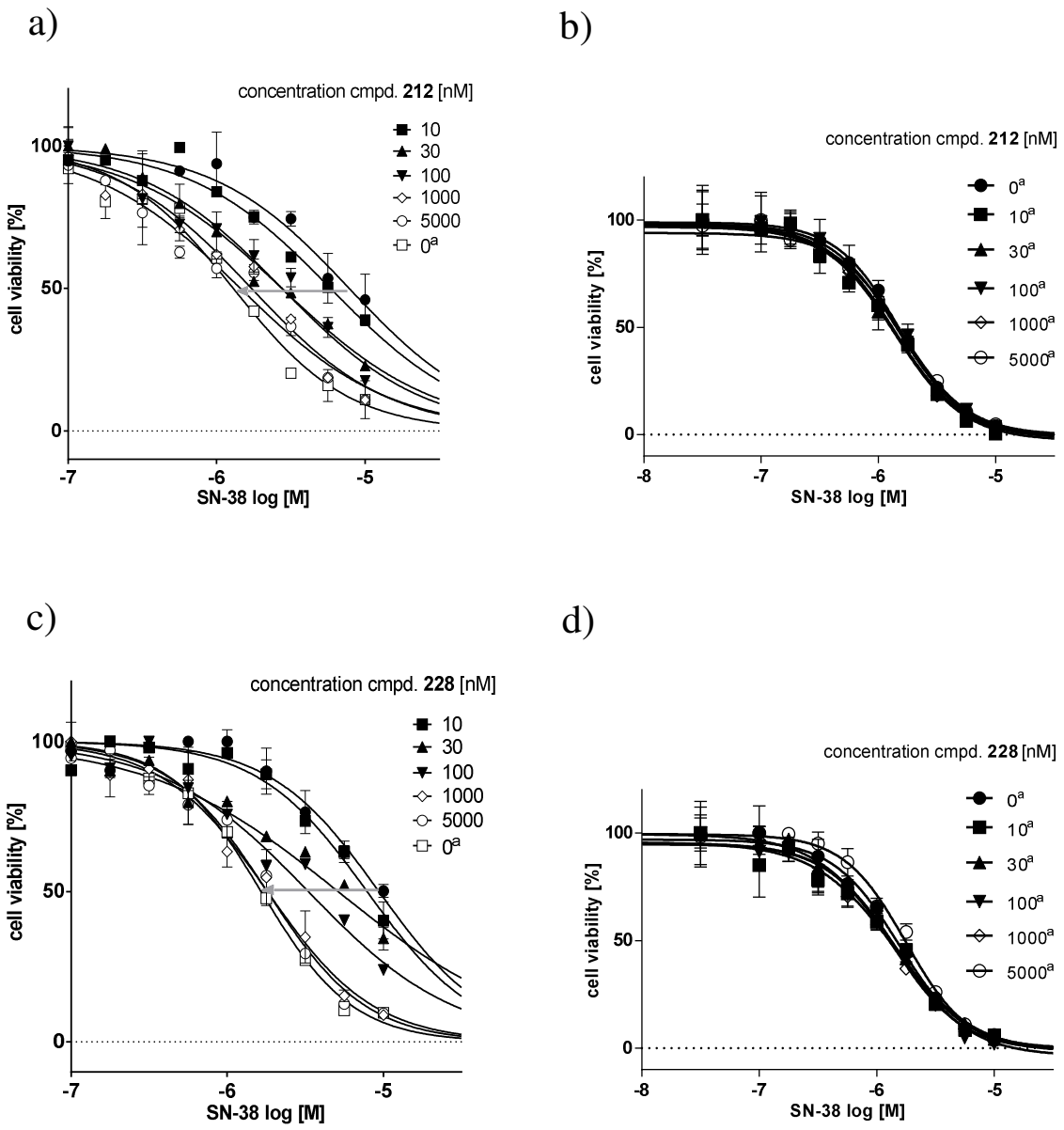

Figure continues on the next page

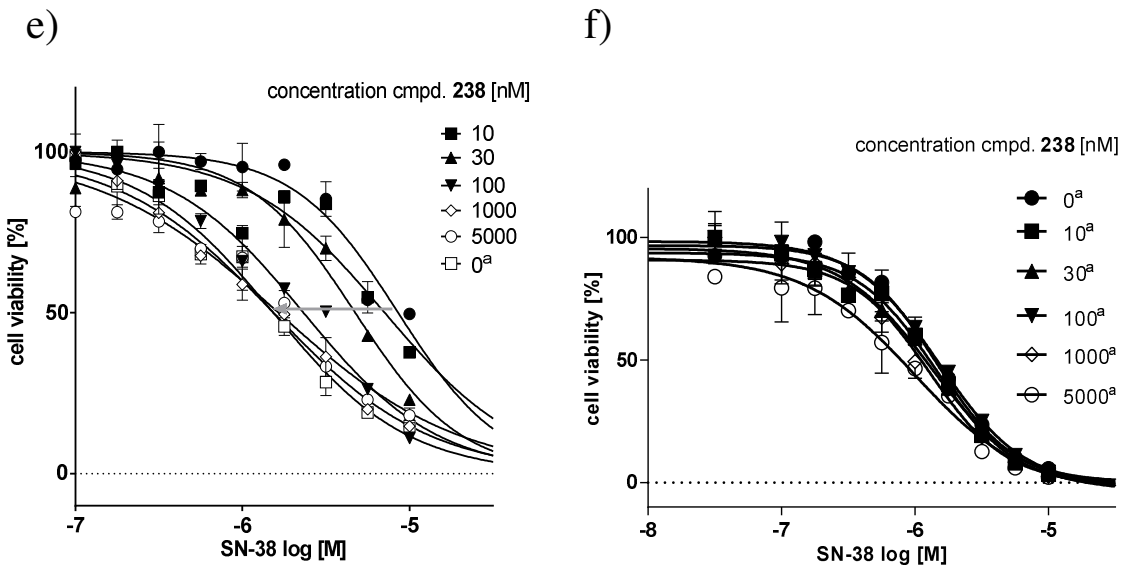

*Figure 89: MDR reversal assay of compound **212**, **228** and **238** demonstrating the ability to reverse the MDR toward the cytostatic drug SN-38, using parental MDCK II and ABCG2 overexpressing cell lines (a, c, e). The dashed arrow indicates the increasing sensitization of the BCRP overexpressing cells with higher compound concentrations (see legend). At a compound concentration of 1 µM, full reversal is achieved, indicated by a similar pGI_{50} as the parental cells. For comparison an analogous assay was performed using only parental MDCK II cells (b, d and f). a: Parental MDCK II cells.*

An analogous assay using only parental cells was carried out to evaluate possible effects between cells, inhibitor and SN-38 that could affect the pGI_{50} value. The obtained concentration-viability curves of the corresponding compounds exhibited no shift in the pGI_{50} values as illustrated in Figure 89 b), d) and f) indicating no side-effects.

For a clear visualization of the obtained results, the pGI_{50} values from the MDR reversal assay were plotted against the logarithm of the corresponding compound concentration. Herby, a sigmoidal concentration-effect curve can be fitted with the logistic equation yielding EC_{50} values characterizing the extent of MDR reversal by a compound as depicted in Figure 90.

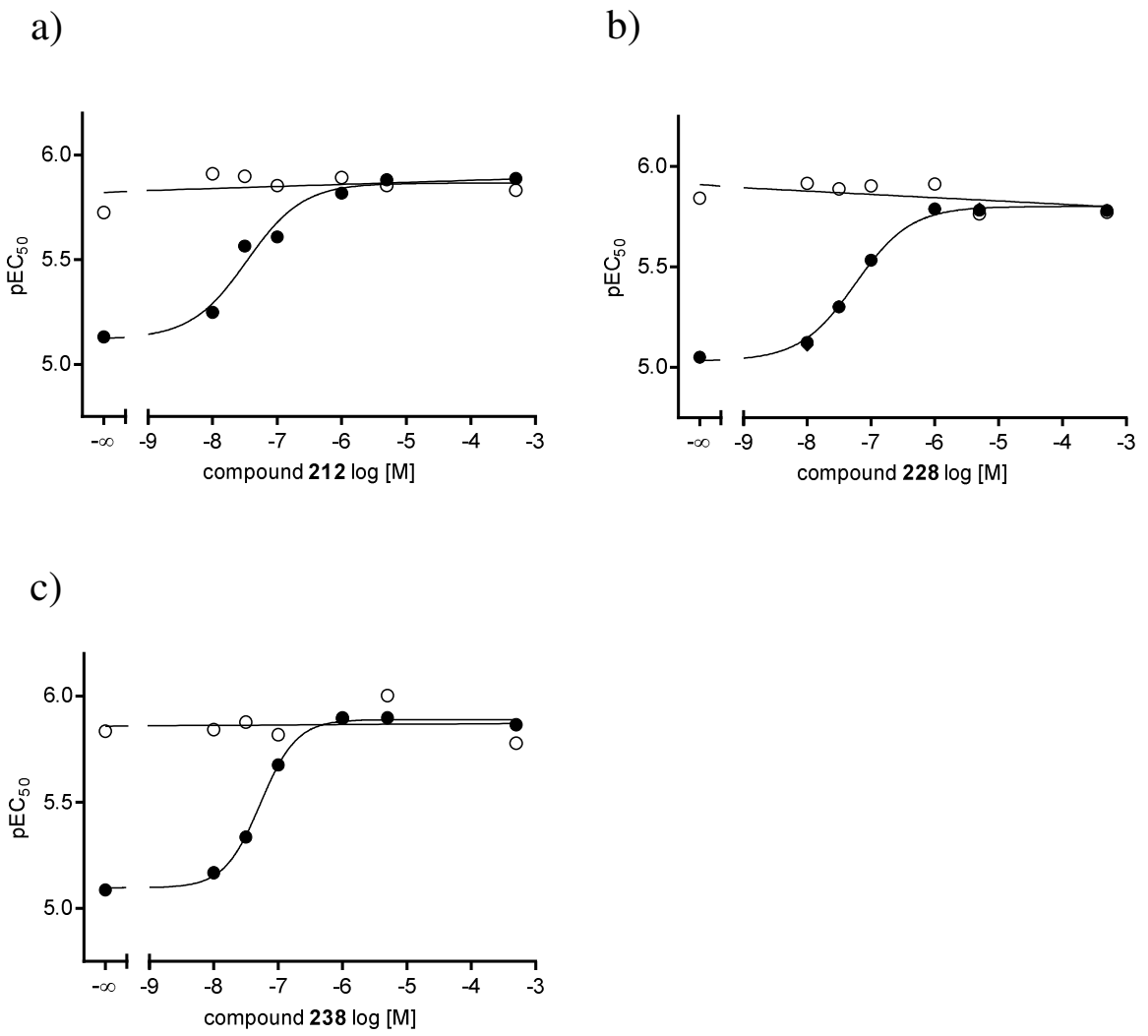

*Figure 90: Nonlinear regression of the pGI_{50} values determined in the viability assay Figure 89 a), c) and e) in presence of different concentrations of compound **212**, **228** and **238**. Correlation of the degree of sensitization toward the corresponding cytostatic drug, indicated by the pEC_{50} value, an EC_{50} of 34.0 nM (**212**) 57.0 nM (**228**) and 51.5 nM (**238**) was determined (●). Compound **212**, **228** and **238** yielded IC_{50} values of 37.4 nM, 33.0 nM and 23.4 nM in the Hoechst 33342 accumulation assay, respectively. A nonlinear regression of the pGI_{50} values determined in an analogous efficacy assay (Figure 89 b), d) and f)), but using only parental MDCK II cells, is depicted with open circles (○).*

From the sigmoidal curves EC_{50} values of 34 nM, 57 nM and 52 nM were calculated for compounds **212**, **228** and **238**, respectively. Those IC_{50} values were slightly higher in compounds **228** and **238** compared to the Hoechst 33342 accumulation assay, whereas **212** exhibited only negligible differences in both assays. A possible reason for the lower potency in the MDR reversal assay could be solubility problems that could lead to precipitation over the long period of time (72 h).

Additionally, the sensitization of the ABCG2 overexpressing MDCK II BCRP cell line toward the cytostatic drug MX was investigated in the presence of compound **231** and **238**. Further details to the assay are provided in chapters 3.5 and 10.2.2.7.

Full reversal of the resistance toward MX was observed for both compounds at a concentration between 0.1 and 1 µM as illustrated in Figure 91.

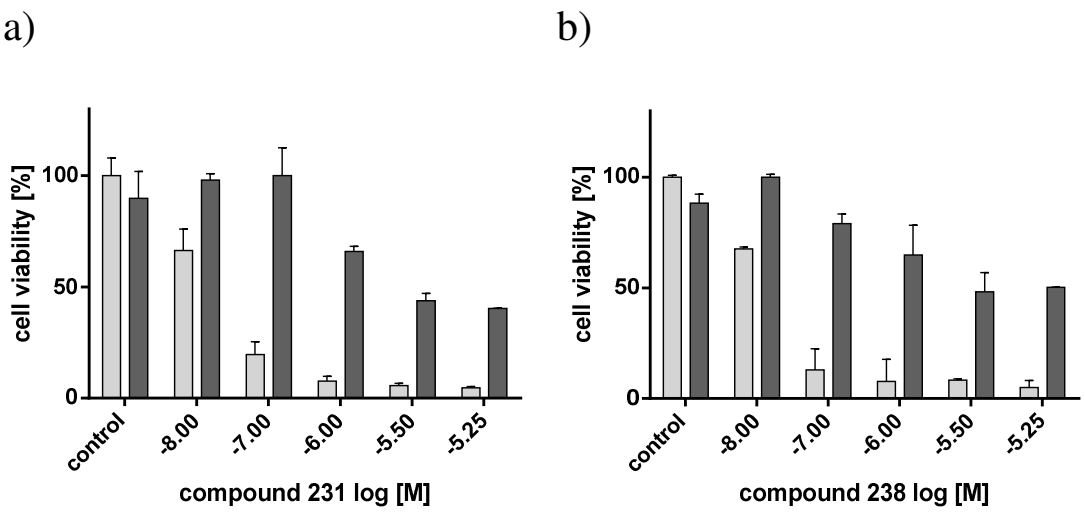

*Figure 91: MDR reversal assay of compounds **231** (a) and **238** (b), demonstrating their ability to reverse MDR toward the cytostatic mitoxantrone, in the ABCG2 overexpressing cell line MDCK II BCRP. The bars represent the cell viability at a given modulator concentration in the presence (light grey) and absence (dark grey) of 0.5 µM mitoxantrone. Control shows viability of cells without modulator. The standard deviation is expressed by error bars.*

Half-maximal growth inhibition was calculated for compound **231** as 21.8 nM and for **238** as 19.5 nM. The calculated IC_{50} values were in excellent accordance to the results of the Hoechst 33342 accumulation assay. Also, the increased cytotoxic effects of both compounds reflect by the decreasing cell viability in the absence of MX (grey bars).

7.6 Investigation of the interaction with Hoechst 33342

Selected compounds were investigated regarding their interaction with Hoechst 33342, using ABCG2 overexpressing MDCK II BCRP cells. Therefore, varying compound concentrations were combined with varying concentrations of Hoechst 33342 and the interaction type could be determined using the Lineweaver-Burk double reciprocal plot, described in chapters 4.6 and 10.2.2.8. The results obtained with the Lineweaver-Burk method are presented in Table 25 listing the intersection of the straight lines together with the corresponding interpretation. Corresponding plots obtained according to the Lineweaver-Burk method are depicted in Figure 92.

Table 25: Interaction with Hoechst 33342 According to the Lineweaver-Burk Double Reciprocal Plot.

Compound	R^1	R^2	R^3	Intersection	type of interaction with Hoechst 33342
217	Ph	3-OMe	NO_2	2. Quadrant	Non-competitive mixed-type
225	3-Pyr	4-OMe	NO_2	2. Quadrant	Non-competitive mixed-type
231	3-CF_3-Ph	3-OH	NO_2	Y-axis	competitive
237	3-OMe-Ph	4-CN	NO_2	2. Quadrant	Non-competitive mixed-type
238	3-OMe-Ph	3-F	NO_2	3. Quadrant	Non-competitive mixed-type
240	3-Pyr	3-OMe	NH_2	2. Quadrant	Non-competitive mixed-type
241	3-Pyr	4-OMe	NH_2	3. Quadrant	Non-competitive mixed-type
244	3-CF_3-Ph	3-OMe	NH_2	2. Quadrant	Non-competitive mixed-type
Ko143				3. Quadrant	Non-competitive mixed-type

In this project non-competitive mixed-type interactions were found to be the predominant interaction type for the selected compounds with the substrate Hoechst 33342. “Mixed-type” inhibitors bind differently from Hoechst 33342 but are able to influence the active site and thus the turnover rate. It is possible that they bind nearby to the Hoechst 33342 binding pocket or could induce substantial conformational change in the protein which

has an impact on the binding of Hoechst 33342. Only compound **231** showed a competitive interaction suggesting the same binding pocket as Hoechst 33342. Indeed, the results are similar to other projects where in the majority of cases a non-competitive interaction was observed.

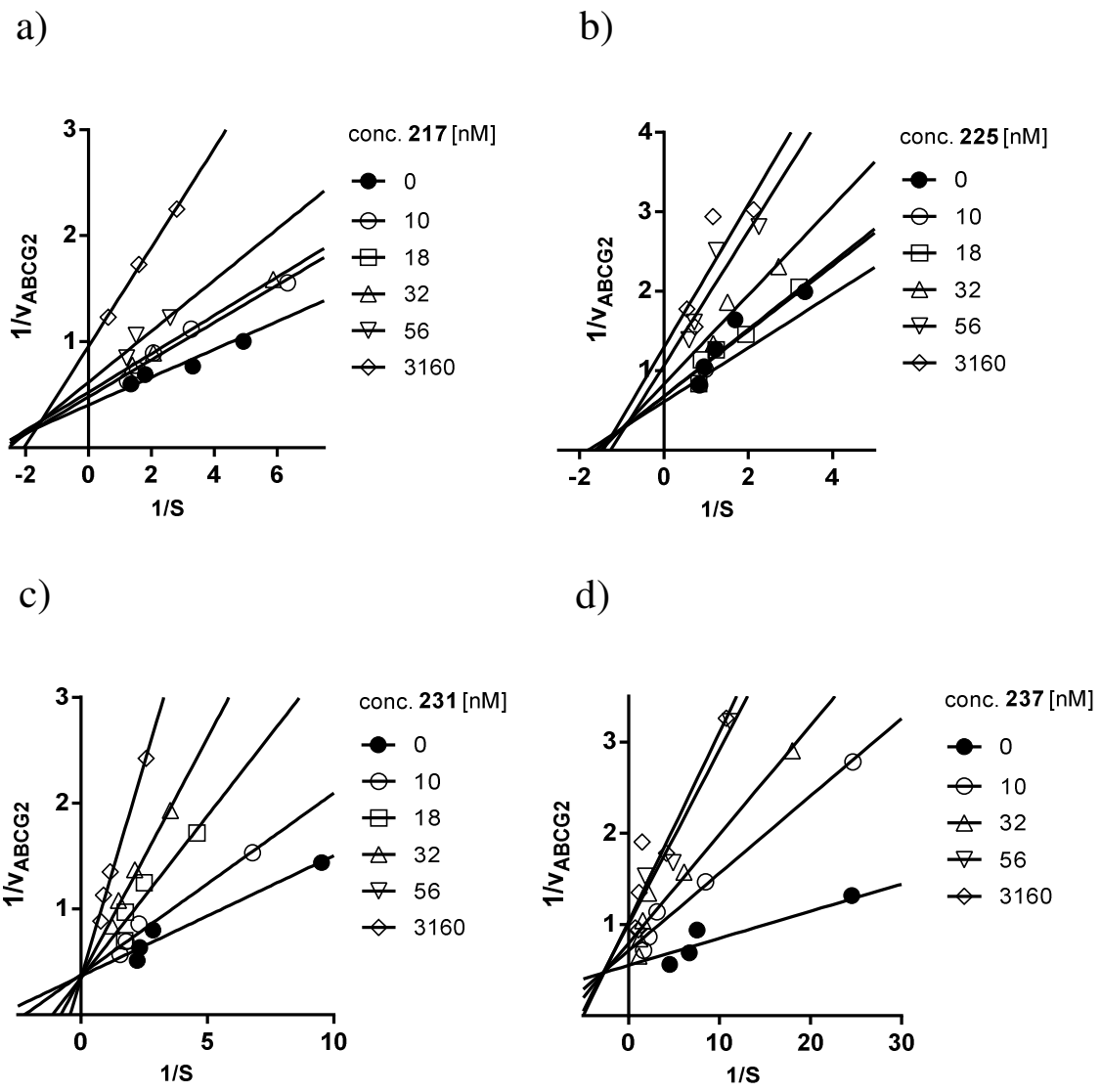

Figure continues on the next page

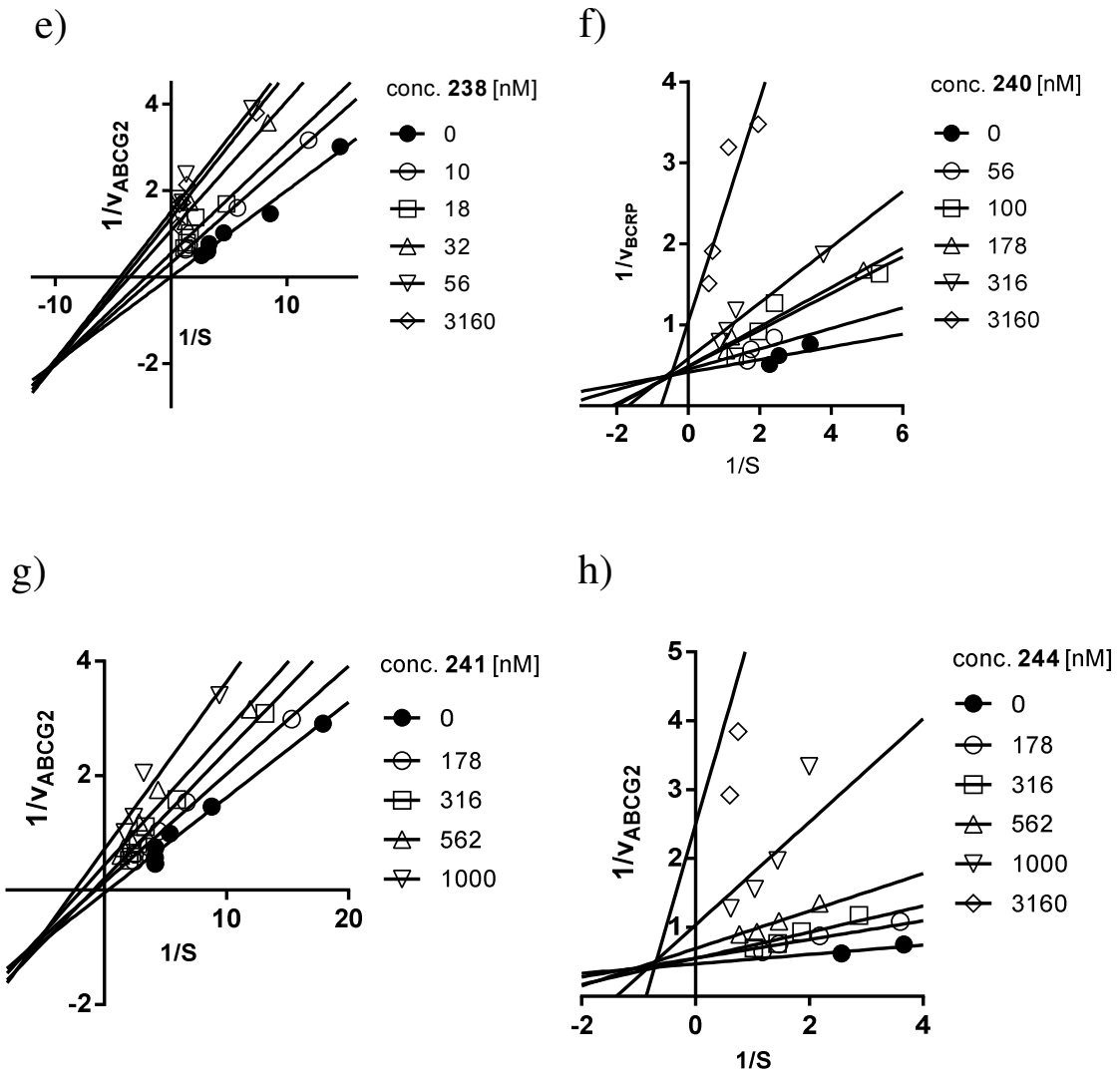

*Figure 92: Lineweaver–Burk plot for compounds **217** (a), **225** (b), **231** (c), **237** (d), **238** (e), **240** (f), **241** (g) and **244** (h) using various concentrations together with the ABCG2 substrate Hoechst 33342. Compound concentrations are specified in the legend.*

In order to validate the results from the Lineweaver-Burk double reciprocal plot, the Cornish-Bowden method was applied which is described in chapters 3.6 and 10.2.2.8. By linear regression of the V_{max} and K_M values slopes were obtained and summarized as a scatter plot in Figure 93. Corresponding linear regression plots are illustrated in Figure 94 (for Ko143 see chapter 3.6).

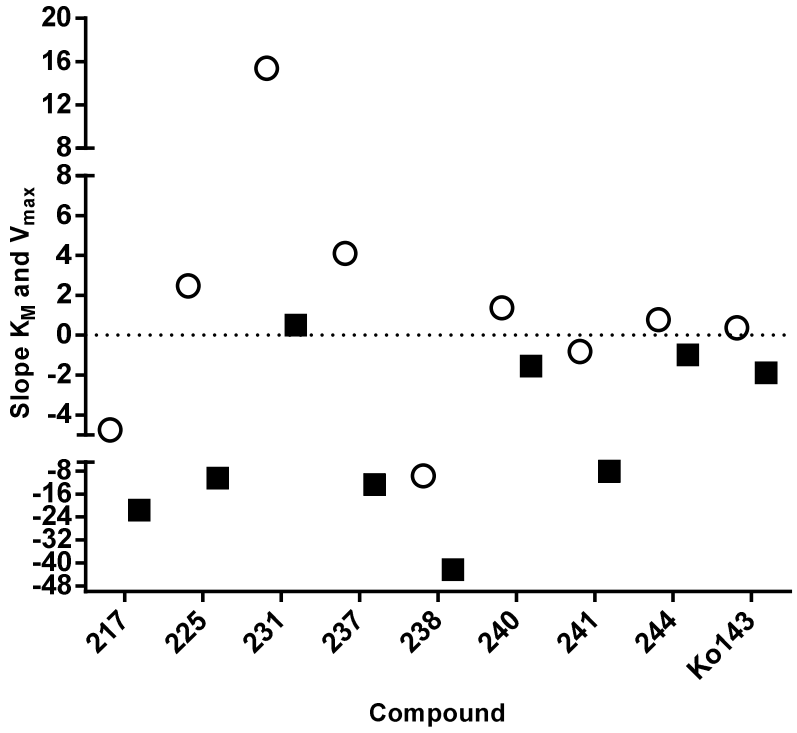

Figure 93: Scatter plot of the slopes obtained from the linear regression of K_M (○) and V_{max} (■) values calculated from the Cornish-Bowden direct linear plot.

Obtained slopes from the linear regression of the K_M and V_{max} values resulting from the Cornish-Bowden plot exhibited a good correlation with the data of the Lineweaver-Burk method. As expected a high positive slope for K_M resulted for compound **231** indicating a competitive interaction with Hoechst 33342. Since the slope of V_{max} was considerably low the data concludes a pure competitive character for **231**, which is in accordance with the result of the Lineweaver-Burk method.

High non-competitive portions were found for compounds **217**, **225**, **237**, **238** and **241**. Compound **240** and **244** showed strong characteristics of both, a non-competitive interaction and a distinct competitive portion, which is typical for a "mixed-type" inhibitor.

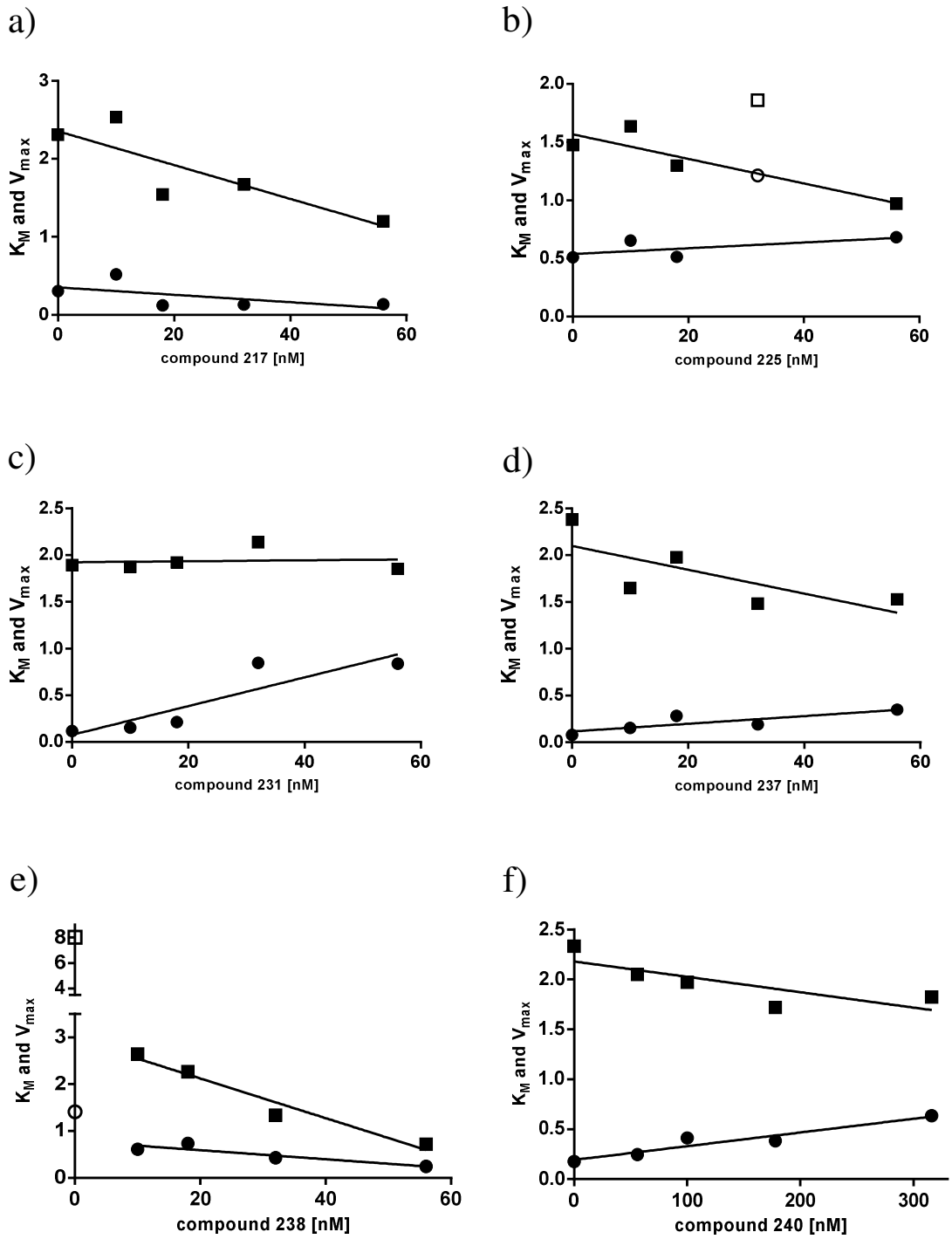

Figure continues on the next page

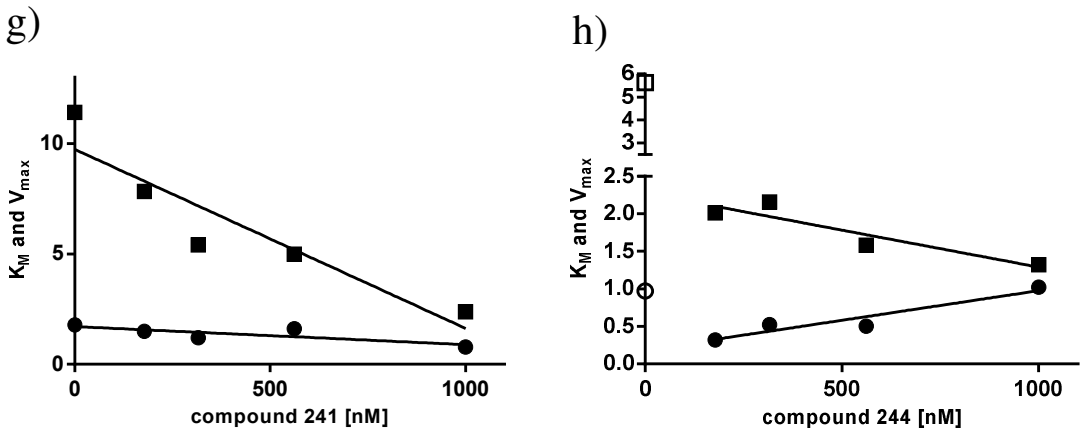

*Figure 94: Direct linear plot of **217** (a), **225** (b), **231** (c), **237** (d), **238** (e), **240** (f), **241** (g), and **244** (h) according to Cornish-Bowden resulting in compound-concentration dependent lines after linear regression of the V_{max} (■) and K_M (●) values. Excluded values are depicted as open symbols of the corresponding shape.*

Again, a significant difference was displayed by the *meta* and *para* analogues **240** and **241** bearing a 3-methoxy or 4-methoxy function at R^2, respectively. According to the Cornish-Bowden method a notable competitive character was determined for **240** and a pronounced non-competitive interaction for **241**.

Also, it is likely that the position of a methoxy group at R^2 has an impact on the interaction with Hoechst 33342. This is illustrated by the 3-methoxy derivatives **217**, **240** and **244** with pronounced competitive characteristics and the 4-methoxy derivatives **241** and **225** that display a rather non-competitive interaction.

7.7 Investigation of the conformation sensitive 5D3 antibody binding to an epitope of ABCG2

The conformation sensitive 5D3 antibody was used to investigate the conformational effect of selected compounds on ABCG2 as it binds specifically to an epitope of the transport protein. The bound antibody emits fluorescence, which was measured with a FACSCalibur flow cytometer using ABCG2 overexpressing PLB-985 cells. Additional

information about the procedure is provided in chapters 3.7 and 10.2.2.9. A summary of the results from this assay is presented as a bar-chart in Figure 95 using Ko143 as positive control representing 100% labelling with the antibody.

Highest conformational sensitive labelling with the antibody was found for compounds **217** and **241** at a concentration of 10 µM. Both compounds resulted in a labelling of 88 and 84% in comparison to Ko143 (10 µM), respectively. Also, the highly potent compound **231** resulted in a high percentage of 66% labelling, even at a concentration of only 1 µM.

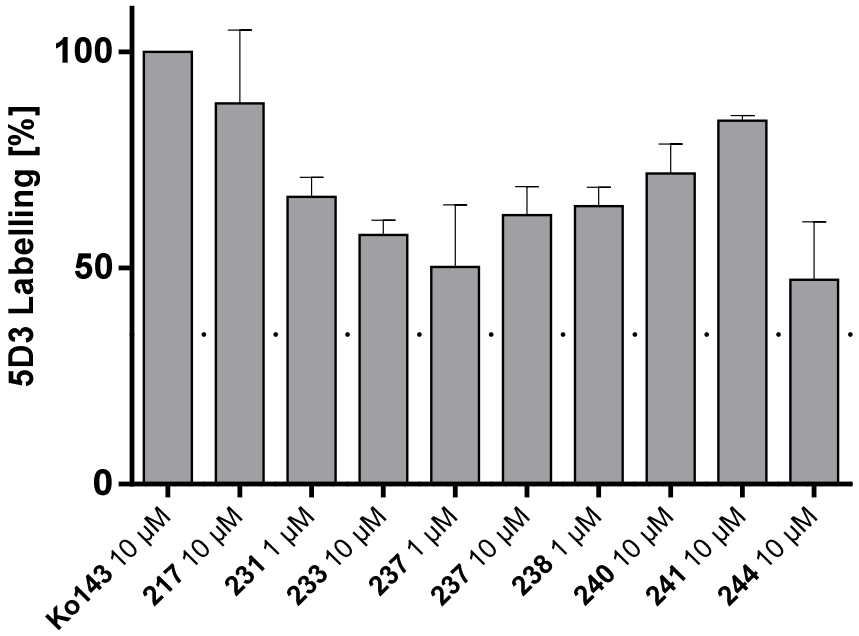

Figure 95: 5D3 immunoreactivity modulation of ABCG2 by various compounds at a concentration of 1 and 10 µM. Fluorescence detected by the 5D3-labeling of ABCG2 in the presence of 10 µM Ko143 was set to 100% and the fluorescence measured in the absence of any compound taken as 0%. The dotted line represents the labelling obtained with Hoechst 33342.

A decreased labelling resulted for compound **244** yielding 47% as compared to Ko143. However, the results obtained in the interaction type investigation are not satisfyingly reflected in the 5D3 shift assay. In previous projects high percentages of conformation dependent labelling were frequently found in compounds displaying a pronounced competitive character. Moreover, marked differences resulted for the majority of the *meta*/*para* compound pairs like **240/241**. Here, the labelling rate was 72 and 84%, respectively, exhibiting a slight but still notable difference.

Furthermore, representative histograms of compounds with the highest and the lowest 5D3 shift in the assay as well as the standard Ko143 are depicted in Figure 96. Histograms of compounds Ko143, **217** and **244** were obtained at a compound concentration of 10 µM, respectively.

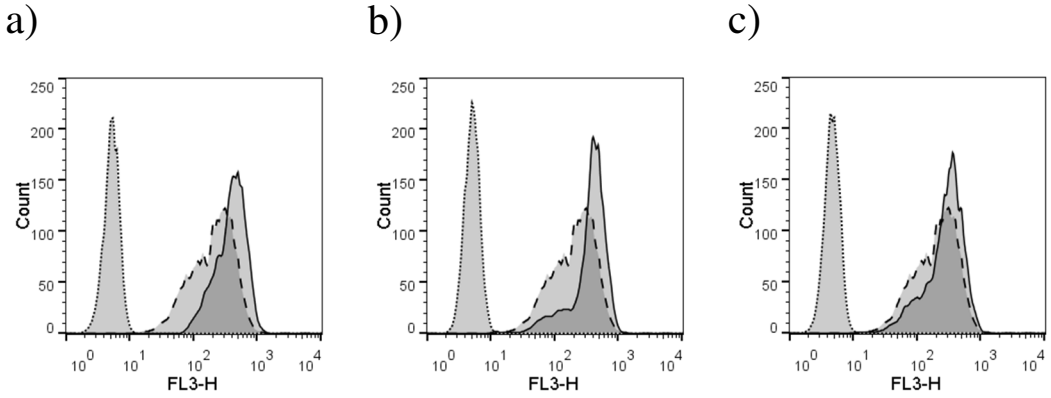

*Figure 96: Histogram of the measured fluorescence at the FL3-H detector (X-axis) and the cell-count gated according to the fluorescence. Depicted is the fluorescence of the isotype-control (dotted curve) as well as of 5D3 antibody in the absence of a compound (dashed curve) and in the presence of a compound (continuous curve).Compounds with the highest and lowest 5D3 shifts: Ko143 (a), **217** (b) and **244** (c) at a concentration of 10 µM.*

7.8 Investigation of the ATPase activity

The investigation was carried out with Ko143 as standard ATPase inhibitor and quercetin as standard stimulator. The ATPase activity assays were performed by Jennifer Gallus. Further details are described in chapters 3.8 and 10.2.2.10.

For the screening the most potent compounds were investigated at three different concentrations (1, 10 and 25 µM) and a summary of the results is provided as bar chart in Figure 97.

Stimulation of the ATPase activity was found in the majority of the selected compounds. Among those, compound **218**, **224**, **227**, **242** and **244** were identified as strong stimulators of ATPase activity. Compound **244** in particular yielded an extraordinarily strong stimulation exceeding the activating effect of the standard Quercetin.

Reduced stimulation was found for compounds **211**, **220** and **240**. Almost no effect on the ATPase activity was detected for compounds **230**, **231** and **232**. This was often

observed in compounds that showed a competitive interaction like compound **231**. A notable deactivation of the ATPase activity was found for compound **233** at high concentrations. According to the screening it showed a bi-phasic trend of ATPase activity changing from activation at a concentration of 1 µM to deactivation at higher concentrations.

Pronounced activation of the ATPase activity was often observed after reduction of the nitro function at position 6 to an amino group. This is illustrated by compounds **232** and **244** where the 6-amino species yielded a significantly higher stimulation of activity than the corresponding 6-nitro species.

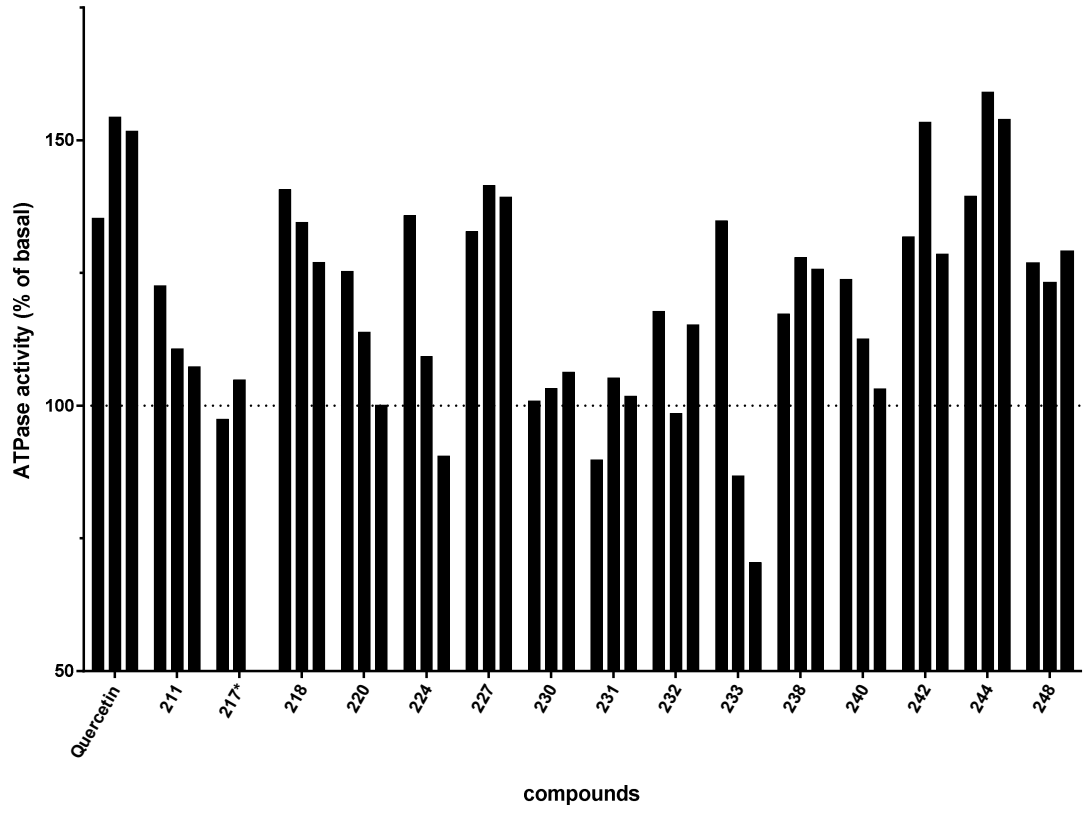

*Figure 97: Screening of ATPase activity of selected compounds at three different concentrations. From left to right the bars correspond to 1, 10 and 25 µM final concentration of compound. Quercetin was used as a standard for activation of ABCG2 ATPase activity. All values are relative vanadate-sensitive ATPase activities in relation to the basal activity, which is set to 100%. *Compound **217** was investigated at a final concentration of 1 and 10 µM.*

A concentration-response curve of the most potent compound **238** is depicted in Figure 98 yielding an EC_{50} of 38 nM which was calculated by using the four-parameter logistic equation. However, the curve reaches a top value of only 126% stimulation in comparison to the basal activity (100 %). Compound **238** resulted roughly in a two-fold lower stimulation of the ATPase activity in comparison to the standard activator quercetin (EC_{50}: 302 nM).

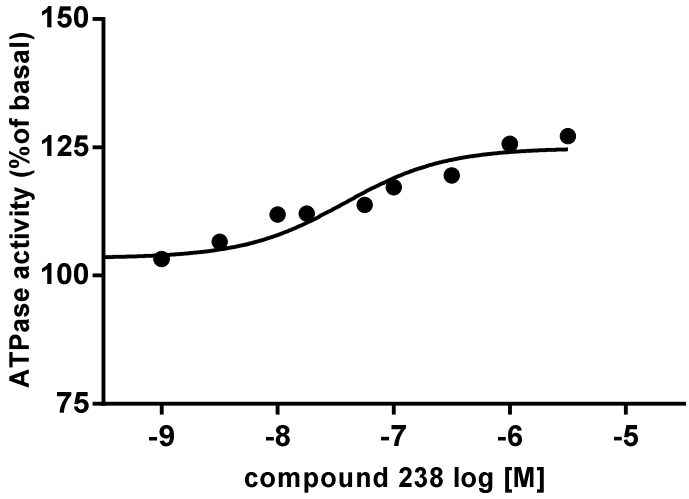

*Figure 98: Concentration-response curve for compound **238** in the ATPase assay. All values are relative vanadate-sensitive ATPase activities in relation to the basal activity, which is set to 100%. High Five insect cell ABCG2 membrane preparations were used for carrying out ATPase activity measurements. An EC_{50} of 38 nM was calculated for this compound.*

8 Project VI: Different modifications at the quinazoline scaffold

In this chapter several modifications at the quinazoline scaffold are described that were investigated. First, 5-membered heteroaromatic functions, namely thiophene and pyrrole, were introduced at position 2 of a substituted 4-anilinoquinazoline derivative. Hereby, similarities and differences in comparison to substitution with a 2-phenyl function were examined. Subsequently, different 4-anilino-2-phenylquinazolines were methylated at the aniline linker to investigate the importance of an H-donor function for the inhibitory activity of a compound. In the next step, a primary amino function was synthesized at position 4 of a 2-phenylquinazoline scaffold. The amine group was then reacted with differently substituted aromatic acid chlorides obtaining amido functions at position 4 and were compared to the corresponding precursors containing an amino linker. Then, substituted 4-anilinoquinazoline derivatives without substitution at position 2 were synthesized to investigate the importance of an aromatic function at this position. Finally, synthesis of two different dimers was carried out reacting a 2-substituted-4-chloroquinazoline derivative with ethylendiamine or 1,3-diaminopropane. Hence, the impact of the different length of the linkers on the inhibition of ABCG2 could be investigated. Further details regarding the reaction mechanisms for the preparation of the compounds are illustrated below.

The calculated logP values correspond to the unsubstituted species, named by scaffold B-D (see chapter 8.1) and are given as 5.01 (scaffold B; R^1 = Ph, R^2 = Me), 3.73 (scaffold C; R^1 = H) and 3.14 (scaffold D; R^1 = H).

8.1 Reaction mechanism

A schematic synthesis route and a detailed reaction mechanism is provided in this chapter.

Scheme 7: General synthesis scheme for the preparation of compounds ***253-280****.*[a]

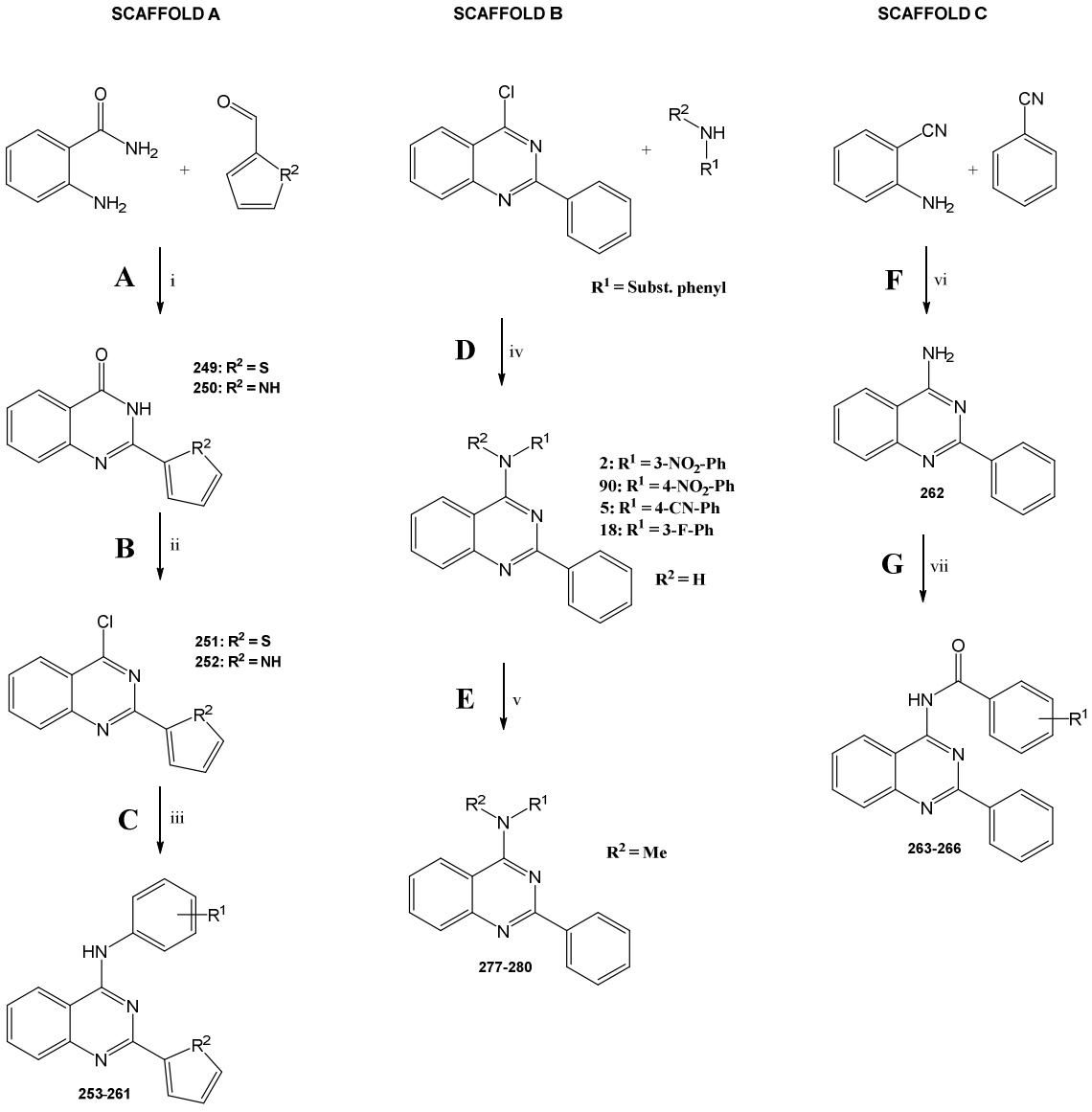

Scheme continues on the next page

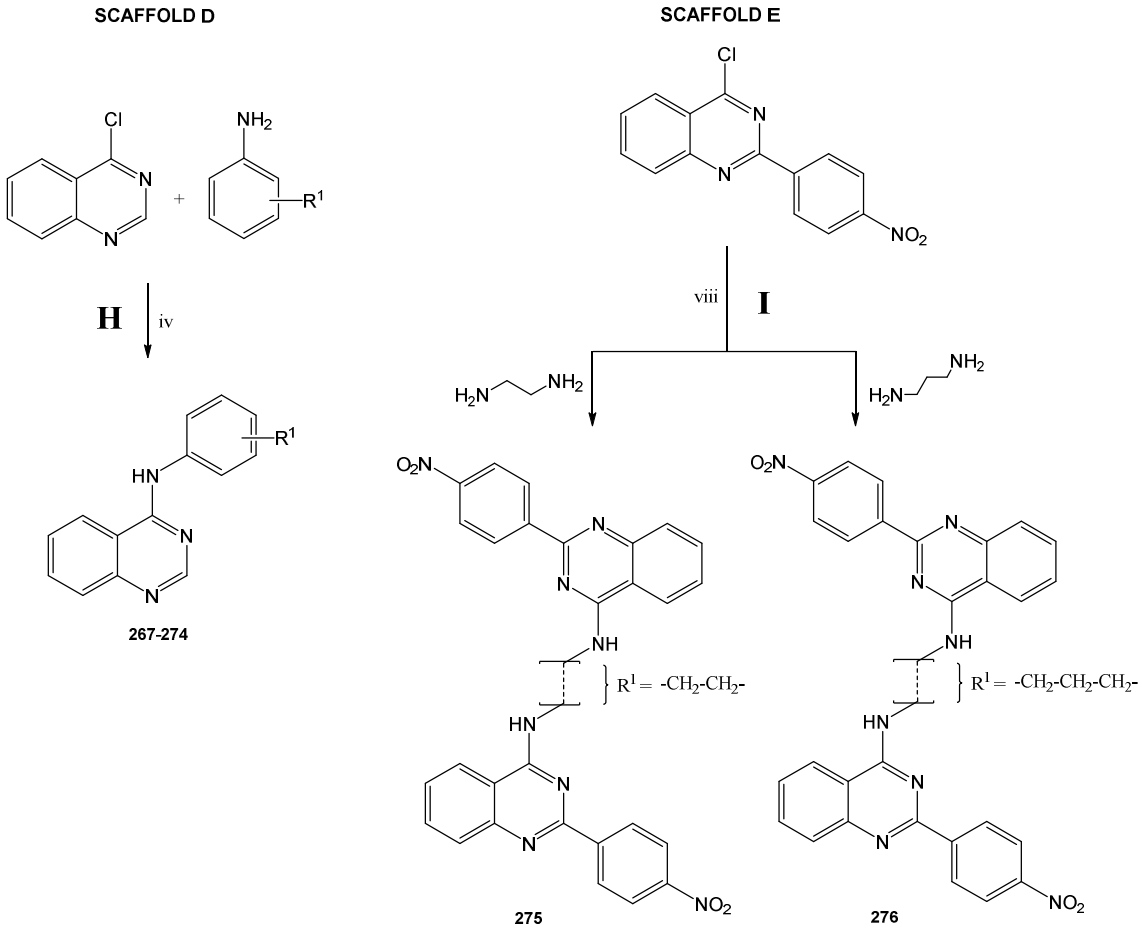

[a]: Reagents and conditions: (i) DMF, I_2, K_2CO_3, 70-90 °C, 4-8 h. (ii) $POCl_3$, reflux, 4-12 h. (iii) Substituted aniline, isopropanol, 100 watt microwave irradiation, 110 °C, 15 - 30 min. (iv) Substituted amine, isopropanol, 100 watt microwave irradiation, 110 °C, 15 - 30 min. (v) 4-Substituted-2-phenylquinazoline, MeI, NaH, DMF, 0 °C 1h, RT 2-6 h. (vi) *t*-BuOK, 150 watt microwave irradiation, 180 °C, 2 min. (vii) substituted benzoyl chloride, THF, TAM, RT, 12 h. (viii) 4-chloro-2-(4-nitrophenyl)quinazoline, TAM, isopropanol, reflux, 4-6 h.

Reaction mechanism **A**:

The reaction mechanism is analogues to that used for the compounds in project II and can be reviewed in chapter 4.1 (reaction mechanism **A**).

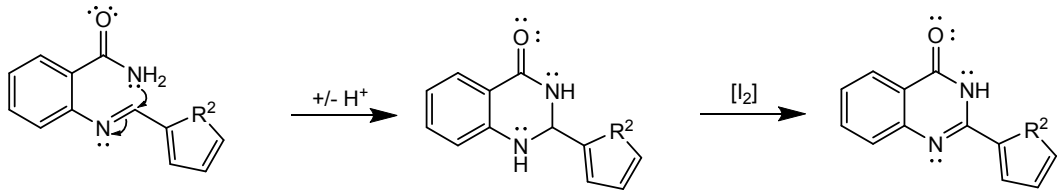

Reaction mechanism **B**:

Substitution of the carbonyl function at position 4 takes place in the presence of $POCl_3$ in a chlorination reaction. The reaction mechanism is described in chapter 4.1 and also illustrated below.

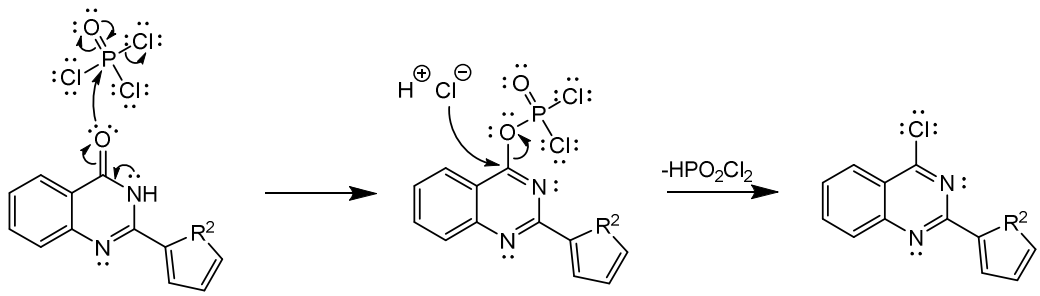

Reaction mechanism **C**:

Final compounds were synthesized by a nucleophilic aromatic substitution of the corresponding 4-chloroquinazoline precursor by reaction with a substituted aniline derivative. The reaction mechanism is analogous to that used for the compounds in project I and can be reviewed in chapter 3.1

Reaction mechanism **D**:

Reaction follows the mechanisms described above for **C**.

Reaction mechanism **E**:

Methylation of the aniline linker is carried out with methyl iodide after deprotonation of the amino function. Therefor, sodium hydride is used as a base which forms hydrogen gas. Subsequently, the deprotonated nitrogen atom performs a nucleophilic substitution reaction at methyl iodide yielding the product and sodium iodide salt.

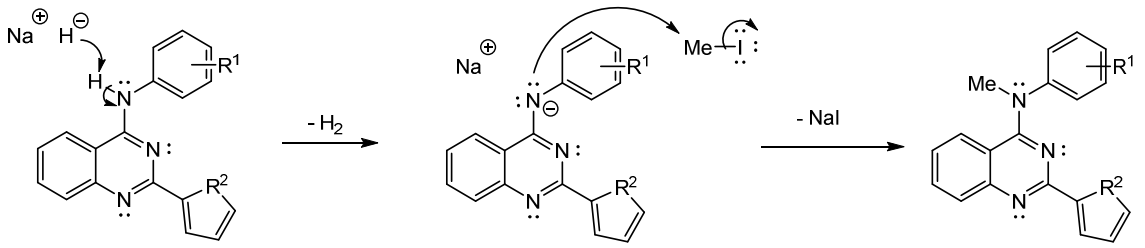

Reaction mechanism **F**:

In the first step the amino function of 2-aminobenzonitrile performs a nucleophilic attack at the carbon of the cyano group. After addition, the imine function achieves intramolecular ring closure by nucleophilic attack at the second cyano group followed by exchange of protons and rearrangement of the electron pairs and doublebonds within the molecule leading to a quinazoline derivative.

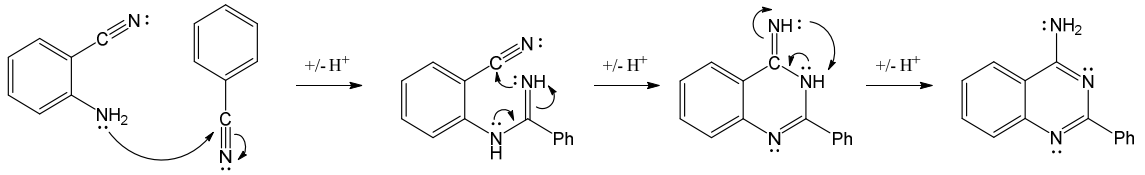

Reaction mechanism **G**:

Formation of the amide is carried out by a nucleophilic attack of the amino function at the carbonyl group of the substituted acid chloride. Nucleophilic addition is followed by elimination of hydrochloric acid to restore the carbonyl function and compensate formal charges at the nitrogen atom leading to an amide function. Hydrochloric acid is precipitated with triethyl amine as a salt.

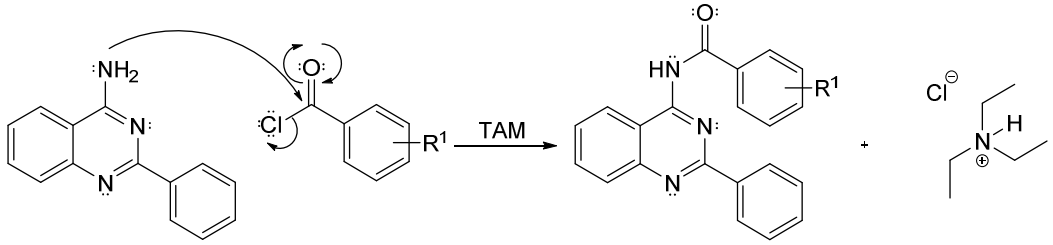

Reaction mechanism **H**:

Reaction follows the mechanisms described above for **C**.

Reaction mechanism **I**:

Reaction follows the mechanism described above for **C**, except that the corresponding diamino species is used as nucleophile. Both amino functions of the corresponding diamine react in a nucleophilic substitution reaction each with one 4-chloroquinazoline derivative forming a dimer.

8.2 Investigation of the inhibitory potency toward ABCG2 in the Hoechst 33342 accumulation assay

A Hoechst 33342 accumulation assay was carried out using the ABCG2 overexpressing MDCK II BCRP and parental cell line to determine the inhibitory potency of the compounds. The Hoechst 33342 accumulation assay as is also described in chapter 3.2 and 10.2.2.2. A summary of the associated activity data is shown in Table 26.

Table 26: Inhibitory Activities Derived from the Hoechst 33342 Accumulations Assay Toward ABCG2 Overexpressing MDCK II BCRP Cell Line. The Corresponding Substitution Pattern is Illustrated Above the Table.

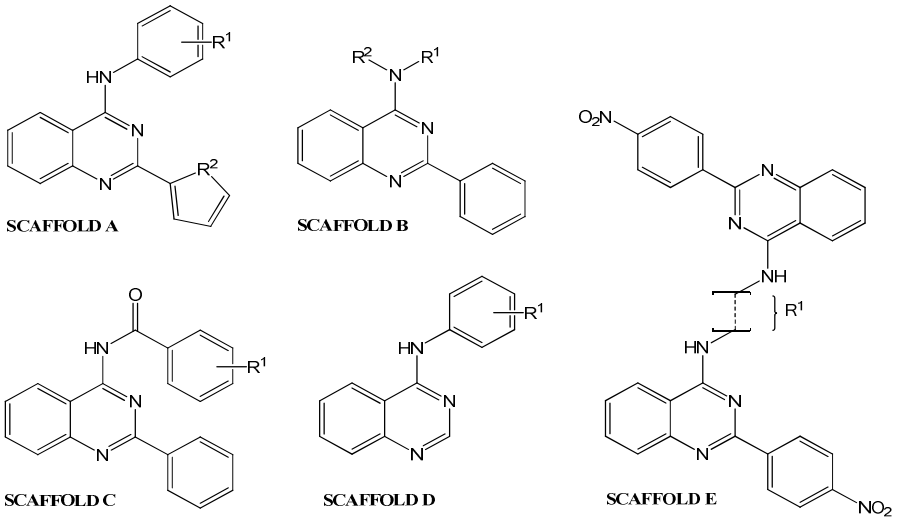

Compound	R^1	R^2	Scaffold	Hoechst 33342 IC_{50} ± SD [µM][a]	Inhibition [%][e]
253	3-NO_2	S	A	300 ± 47	92
254	4-NO_2	S	A	335 ± 42	84
255	3-CN	S	A	178 ± 19	92
256	3,4-OMe	S	A	202 ± 21	102
257	3-F	S	A	953 ± 176	86
258	3-$NHCOCH_3$	S	A	360 ± 20	90
259	3-CN	NH	A	156 ± 10	104
260	4-OMe	NH	A	2570 ± 1560	103
261	3,4-OMe	NH	A	652 ± 137	98
262	H	H	B	n.a.	n.a.
263	H		C	424 ± 32	59
264	2-NO_2		C	994 ± 99	64
265	3-NO_2		C	54.5 ± 9.4	70
266	4-NO_2		C	93.1 ± 8.4	61
267	H		D	10700 ± 2070	[f]
268	3-NO_2-4-OH		D	2900 ± 490	[f]
269	4-OH		D	2630 ± 844	55
270	4-CN		D	1270 ± 460	75
271	3-OMe		D	645 ± 68	67
272	3-SMe		D	1350 ± 320	60
273	3-F		D	8120 ± 2190	[f]
274	3-$NHCOCH_3$		D	28900 ± 4600	[f]
275	-CH_2-CH_2-		E	619 ± 134	90

Table continues on the next page

276	-CH_2-CH_2-CH_2-		E	229 ± 26	95
277	3-NO_2-Ph	Me	B	20305 ± 190	[f]
278	4-NO_2-Ph	Me	B	3670 ± 390	[f]
279	4-CN-Ph	Me	B	10100 ± 2000	[f]
280	3-F-Ph	Me	B	3950 ± 350	[f]
1[b]	Ph	H	B	882 ± 157	96
2[b, c]	3-NO_2-Ph	H	B	130 ± 30	n.d.a.
90[b]	4-NO_2-Ph	H	B	69.6 ± 8.2	84
3	3-NO_2-4-OH-Ph	H	B	81.1 ± 9.1	81
6	4-OH-Ph	H	B	204 ± 37	87
4[c]	3-CN-Ph	H	B	140 ± 40	n.d.a
5	4-CN-Ph	H	B	69.9 ± 10	87
11[c]	3-OMe-Ph	H	B	1320 ± 100	n.d.a.
12[c]	4-OMe-Ph	H	B	1930 ± 110	n.d.a.
13[b]	3,4-OMe-Ph	H	B	152 ± 19	97
10	3-SMe-Ph	H	B	1190 ± 31	86
18	3-F-Ph	H	B	355 ± 53	84
8	3-$NHCOCH_3$-Ph	H	B	278 ± 33	98
Ko143[d]				227 ± 14	100
Gefitinib				1730 ± 270	88
Elacridar				361 ± 48	85

[a]: *IC_{50} values are means of three independent experiments.*
[b]: *Compounds synthesized in earlier study.*[198]
[c]: *IC_{50} value taken from literature. .*[198]
[d]: *Used as reference in the assay.*
[e]: *Percentage of inhibition with regard to Ko143*
[f]: *Top value fixed to top of Ko143*
n.a.: Not active
n.d.a.: No data available

In the first series a thienyl or pyrrolyl moiety was investigated at position 2 of the quinazoline scaffold. High inhibitory potencies toward ABCG2 in the range of 180-360 nM resulted for thiophene in combination with the following substituents at R^2, 3- and 4-nitro, 3-cyano, 3,4-dimethoxy or 3-acetamido. In the case of the pyrrolyl moiety at R^1 a 3-cyano function at R^2 was identified as the best substituent obtaining an excellent IC_{50} of 156 nM. However, both five-membered heteroaromatic residues led to a somewhat lower or at best similar inhibitory potency compared to phenyl at position 2.

The conversion of the anilino-linker into an amido-linker required the synthesis of precursor **262**, containing solely a free amine without aromatic groups at position 4 of the quinazoline scaffold. Interestingly, the precursor exhibited no inhibitory activity leading

to the conclusion that aniline functions at position 4 are crucial for a potent inhibition of ABCG2. Further synthesis was carried out by reacting compound **262** with substituted acid chlorides yielding the 4-amido derivatives **263**-**266** that contain hydrogen or nitro groups as substituents at R^1 of scaffold C. In comparison to the corresponding 4-anilino analogues **1**, **2** and **92**, the amido derivatives showed a significantly increased inhibitory potency. Compound **265** containing a 3-nitro function at R^1 was the most potent one among the compounds of project VI with an excellent IC_{50} value of 55 nM. Unfortunately, the reduced solubility and the lower maximum inhibition in comparison to Ko143 posed a clear disadvantage of this class of compounds. Representative concentration-response curves of the most potent compounds **259** (scaffold A) and **265** (scaffold C) are illustrated in Figure 99.

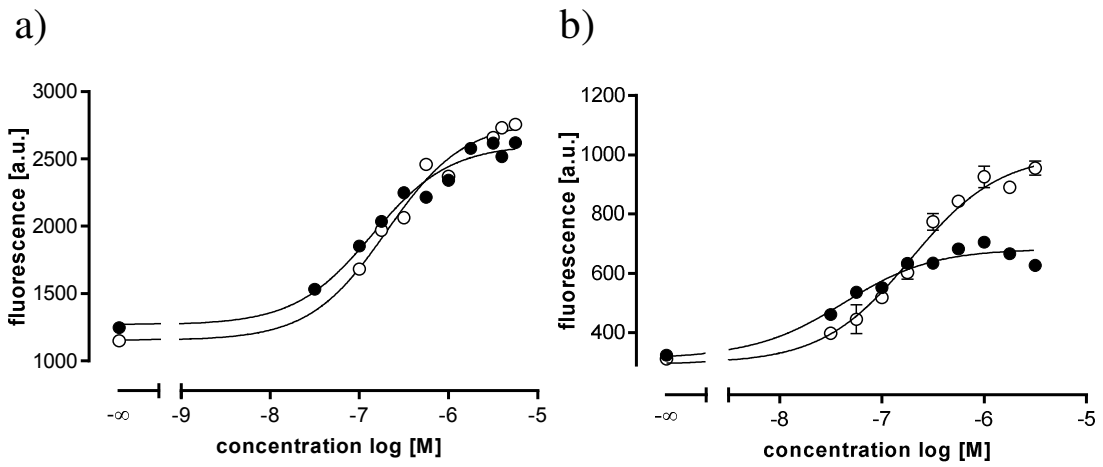

*Figure 99: Concentration-response curve of compound **259** (●; IC_{50}: 156 nM; a)) and **265** (●; IC_{50}: 54.5 nM; b)) in a Hoechst 33342 accumulation assay with Ko143 (○, IC_{50}: 227 nM) as reference, using the ABCG2 overexpressing MDCK II BCRP cell line. Compound **265** reaches an I_{max} of about 70% of the standard Ko143.*

Subsequently, the aromatic moiety at position 2 was replaced by hydrogen and substitution was only carried out on the aniline function at position 4 of the quinazoline scaffold. Apart from the missing modification at position 6 and 7, the resulting compounds **267**-**274** are closely related to the TKI gefitinib. Hereby relatively poor IC_{50} values similar to gefitinib were obtained, and it was concluded that an aromatic residue at position 2 is crucial for high inhibitory potencies toward ABCG2. Only compound **271** with 3-methoxy substitution at R^1 had an IC_{50} value in the high nanomolar range of 645

nM. Also, the percentage of maximal inhibition with regard to Ko143 was reduced in this subset to about 60%.

Following, the dimers **275** and **276** were synthesized by an aromatic nucleophilic substitution between the corresponding diamine derivative and two equivalents of 4-chloro-2-(4-nitrophenyl)quinazoline. A roughly three-fold higher inhibitory potency resulted in the Hoechst 33342 accumulation assay for compound **276** containing a propyl alkyl chain. Its IC_{50} of 229 nM is very similar to the potent inhibitor Ko143 and about three-fold more potent than its analogue **275** that contains a shorter ethyl alkyl chain.

In addition, some substituted 4-anilino-2-phenylquinazolines were synthesized in order to carry out methylation at the anilino-linker. Hence, the H-donor function of the substituted aniline at position 4 was removed and replaced by a methyl group. As a result significant reduction of the inhibitory potency was detected after the methylation, illustrated by the increased IC_{50} values of compound **277**-**280**. These findings substantiate the importance of an HBD function at this position and provide an explanation regarding the findings in the work of A. Spindler. Here, 2-phenylquinazolines were investigated where the amino linker of the substituted aniline at position 4 was replaced by ether or thioether linker.[207] It is not surprising that those groups led to poor inhibitory potencies since both linkers have no HBD functions.

8.3 Investigation of the inhibitory potency toward ABCB1 and ABCC1 in the calcein AM assay

A calcein AM assay was conducted to investigate the selectivity of several compounds toward ABCG2 using the ABCB1 overexpressing cell line A2780 adr and the ABCC1 overexpressing cell line H69 AR. More details regarding the assay are provided in chapters 3.3 and 10.2.2.4. The results of the calculated IC_{50} values of the compounds showing more than 25% of inhibition in the screening is depicted in Table 27. Screening results for the inhibitory activity toward ABCB1 and ABCC1 are illustrated as bar charts given in Figure 100. The screening includes the most potent compounds.

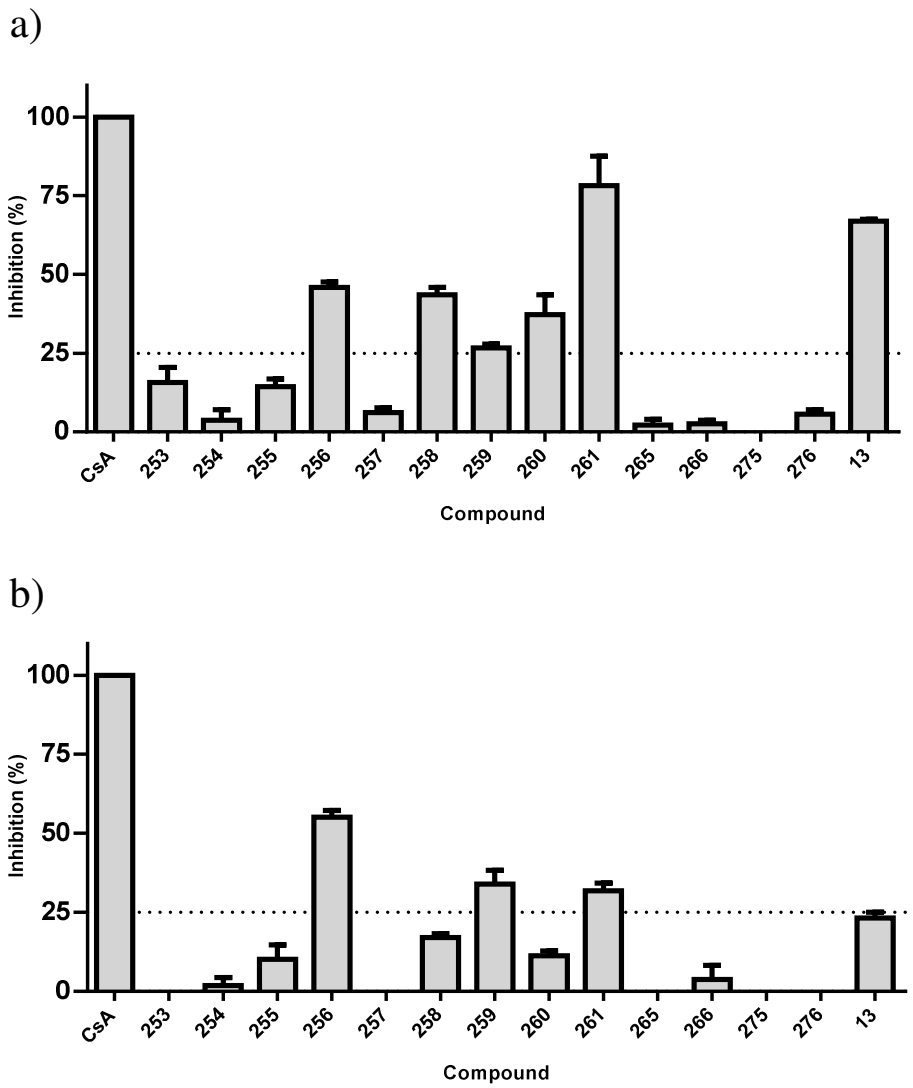

Figure 100: Inhibitory effect of screened compounds toward ABCB1 overexpressing cell line A2780adr (a) and MRP1 overexpressing cell line H69AR (b) in the calcein AM assay at a concentration of 10 µM. Cyclosporine A (CsA) was used as positive control, indicating complete inhibition. The inhibitory effect of each compound is expressed by the length of the bars, representing the inhibition compared to the positive control in percent. For each compound, three independent experiments were performed and the standard deviation is expressed by error bars.

First the inhibitory potencies of compounds **253**-**261** toward ABCB1 were investigated containing substitution with thienyl or pyrrolyl at position 2. The highest potency was found for compounds with 3,4-dimethoxy substitution at R^1. This observation has already been made in previous projects, in which the inhibitory potency toward ABCB1 has been correlated to the presence of methoxy groups. It was not surprising that compounds **256** and **261**, containing a 3,4-dimethoxy function at R^1, reached the highest inhibition in the screening and yielded IC_{50} values of 1.88 and 1.81 µM, respectively.

Table 27: Inhibitory Activity of Compounds Exhibiting an Inhibition of more than 25% in Comparison to the Reference Cyclosporine A (CsA) in the Calcein AM Assay at a Concentration of 10 µM.

Compound	R^1	R^2	Scaffold	Calcein AM (ABCB1) IC_{50} ± SD [µM][a,b]	Calcein AM (ABCC1) IC_{50} ± SD [µM][a,c]
256	3,4-OMe	S	A	1.88 ± 0.71	9.68 ± 0.26
258	3-$NHCOCH_3$	S	A	14.7 ± 4.42	n.d.
259	3-CN	NH	A	18.8 ± 0.87	85.1 ± 7.9
260	4-OMe	NH	A	8.03 ± 0.96	n.d.
261	3,4-OMe	NH	A	1.81 ± 0.21	17.3 ± 1.9
Cyclosporine A[d]				1.17 ± 0.17	3.53 ± 0.61

[a]: *IC_{50} values were determined by at least three independent experiments.*
[b]: *The P-gp overexpressing cell line A2780adr was used.*
[c]: *The MRP1 overexpressing cell line H69AR was used.*
[d]: *Cyclosporine A is used as reference for both assays.*
n.d.: Not determined, due to low effect in the initial screening.

A concentration-response curve of the potent compound **261** using the ABCB1 overexpressing cell line A2780adr is depicted in Figure 101. Low or only negligible potencies resulted for the remainder of substituents at R^1. Indeed, a moderately increased inhibitory potency toward ABCB1 was observed for substitution at R^2 with pyrrolyl in comparison to thienyl, which is illustrated by compound pairs **255/259** and **256/261**. Overall, the compounds exhibited higher potencies toward ABCB1 in comparison to ABCC1. The highest potency toward ABCC1 showed compound **256** that yielded a poor IC_{50} value of 9.68 µM. Interestingly, the 2-pyrrolyl derivative **261** and the 2-phenyl derivative **13** (project I), which both contain a substitution with 3,4-dimethoxy at the anilino moiety, showed a similar trend in potency toward ABCB1 and ABCC1, with higher inhibitory potency toward ABCB1.

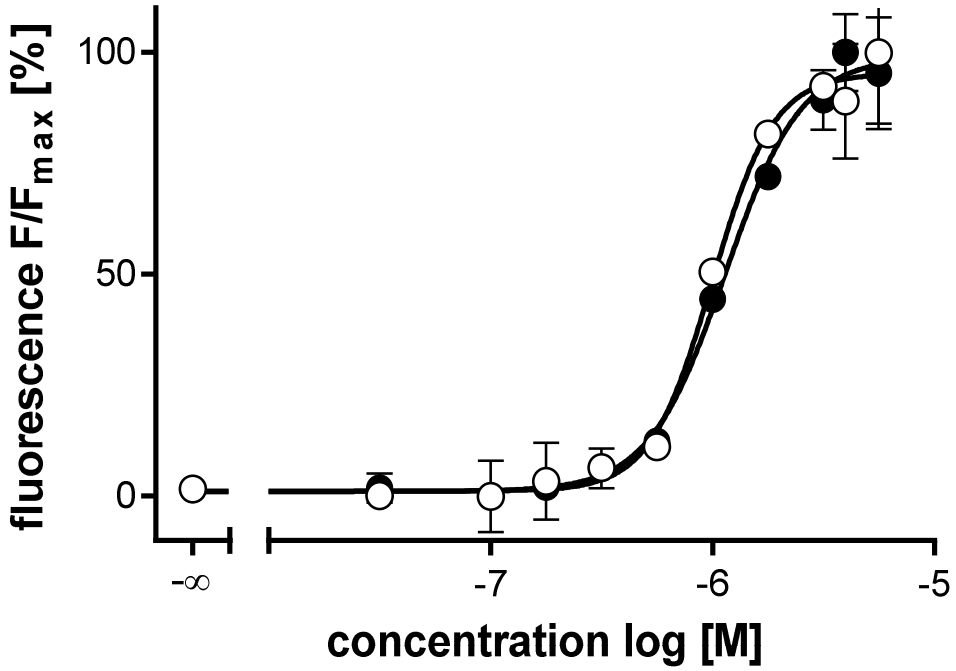

*Figure 101: Concentration-response curve of compound **261** (■, IC_{50}: 1.81 µM) in a calcein AM assay with Cyclosporine A (○, IC_{50}: 1.17 µM) as reference, using the ABCB1 overexpressing cell line A2780adr.*

Moreover, the most potent amide derivatives **265** and **266** as well as the dimers **275** and **276** were investigated but were not active against ABCB1 and ABCC1. It is likely that the presence of a nitro function increases the selectivity toward ABCG2 which was also found in several nitro derivatives of other projects.

8.4 Investigation of the intrinsic cytotoxicity with the MDCK II cell lines in a MTT assay

The intrinsic cytotoxicity of selected compounds was investigated in a MTT assay with MDCK II parental and ABCG2 overexpressing cells. Further details of the assay are provided in chapters 3.4 and 10.2.2.5. A summary of the obtained GI_{50} values and the corresponding therapeutic ratios is given in Table 28.

Table 28: Intrinsic Toxicity of Selected Compounds on MDCK II ABCG2 Overexpressing and Parental Cells.

Compound	R^1	R^2	Scaffold	GI_{50} [µM][a] BCRP	GI_{50} [µM][a] Parental	Therapeutic ratio (GI_{50}/IC_{50})
253	3-NO_2	S	A	14	15	46
254	4-NO_2	S	A	83	110	250
255	3-CN	S	A	59	63	330
259	3-CN	NH	A	39	55	250
263	H		C	72	130	170
265	3-NO_2		C	1.4	4.5	25
266	4-NO_2		C	0.90	1.8	9.7
271	3-OMe		D	14	8.9	6.3
276	-CH_2-CH_2-CH_2-		E	53	132	230
Ko143				13	13	56
Gefitinib				1.4	2.1	0.80
MeOH/DMSO				96[b]	140[b]	

[a]: Concentration leading to 50% of cell survival of MDCK II BCRP and parental cells. The data was obtained from at least two independent experiments as mean values.
[b]: Positive control of the cytotoxicity from dilution with DMSO/MeOH without compound.

First the intrinsic cytotoxicity was investigated for compounds **253**-**259** containing a 2-thienyl or 2-pyrrolyl moiety. Here, quite different GI_{50} values resulted for the *meta*/*para* compound pair. Cytotoxicity of the derivatives with thienyl at position 2 and 3-nitro (compound **253**) or 4-nitro (compound **254**) at R^2 resulted in GI_{50} values of 14 and 83 µM, respectively. In comparison substitution with pyrrolyl a slightly reduced intrinsic cytotoxicity was observed for thienyl, illustrated by compounds **255** and **259**.
Concentration-response curves of both compounds are provided in Figure 102. The highest TR of 331 among the selected compounds was calculated for compound **255** containing a substitution with thienyl at position 2 and 3-cyano at R^2 of scaffold A.
Moreover, marked differences in cytotoxicity of selected amido-derivatives based on scaffold C were found for different substitution patterns. A hydrogen function at R^1 led to an almost nontoxic compound whereas substitution with 3-nitro or 4-nitro yielded considerably decreased GI_{50} values in the range of 1 µM (see compounds **263**, **265** and **266**).

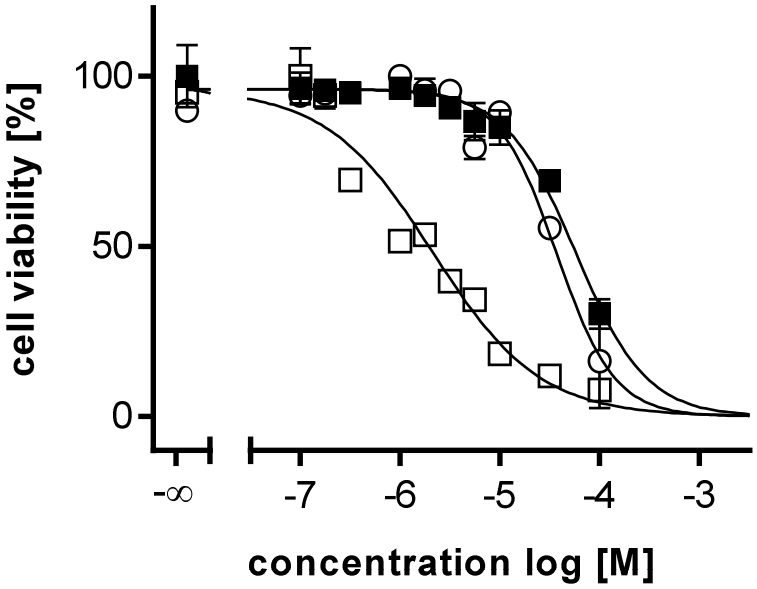

*Figure 102: MTT viability assay of compounds **259** (○) and **265** (□) using the ABCG2 overexpressing MDCK II BCRP cell line. The GI_{50} values were determined as 38.8 µM (○) and 1.35 µM (□), respectively. A control with the same concentration of MeOH and DMSO analogous to the dilution of the compounds, was carried out for comparison (■, GI_{50} = 96.1 µM). The amount of MeOH and DMSO used for the dilution was ≤ 1.8% and ≤ 1.0%, respectively.*

Regarding scaffold D, compound **271**, with a 3-methoxy substituent at R^1, possessed a relatively high cytotoxicity with a GI_{50} value of 14 µM. Due to the lack of substitution at position 2 it shows the highest structural similarity to the TKI gefitinib which was found to be even more cytotoxic resulting in an IC_{50} of 1.36 µM.

Although it was found that the presence of nitro functions may increase the cytotoxic effects, the dimer **276** possessed a high GI_{50} value of 53 µM benefiting its TR. An overview of the TRs of selected compounds is depicted in Figure 103.

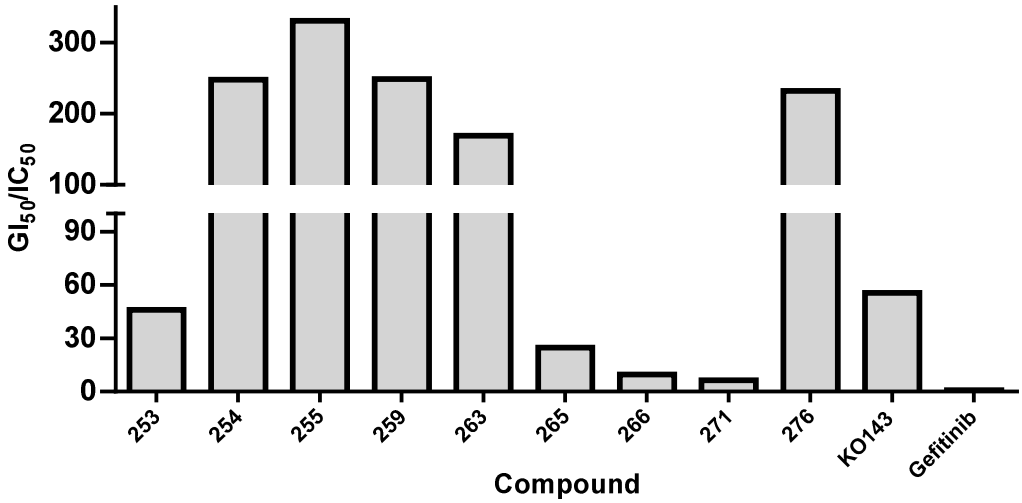

*Figure 103: Therapeutic ratios of selected compounds, calculated from the ratio of GI_{50} to IC_{50} derived from MTT viability assay and Hoechst 33342 accumulation assay, respectively. The highest value was calculated for compound **21** (GI_{50}/IC_{50} = 270), while the reference compound Ko143 yielded GI_{50}/IC_{50} = 55.5.*

Owing to a high inhibitory potency in the Hoechst 33342 accumulation assay, high therapeutic ratios between 250 and 330 resulted for the moderately cytotoxic compounds **254**, **255**, **259** and **276**. The best TR value calculated for compound **255** is about 6-fold higher than for the standard inhibitor Ko143.

8.5 Investigation of the reversal of multidrug resistance

Sensitization of ABCG2 overexpressing MDCK II BCRP cell line toward the cytostatic drug MX was investigated for selected compounds. The assay was carried out at different compound concentrations in the presence and absence of 0.5 µM MX. Further details of the assay are provided in chapters 3.5 and 10.2.2.7.

Here the most potent compounds **255**, **259**, **265** and **266** were investigated in co-administration with MX. Sensitivity of the ABCG2 overexpressing cells was restored by

all four compounds. Full reversal of the resistance toward MX was observed for all compounds at a concentration of about 1 µM, and is illustrated in Figure 104.

Regarding the amido-derivatives **265** and **266** a higher cytotoxic effect was observed in the absence of MX indicated by the decrease in cell viability of MDCK II BCRP cells (dark grey bars) with increasing compound concentrations. No toxic effects were detected for compound **255** and **259** which is in accordance with the results from the MTT cytotoxicity assay described above.

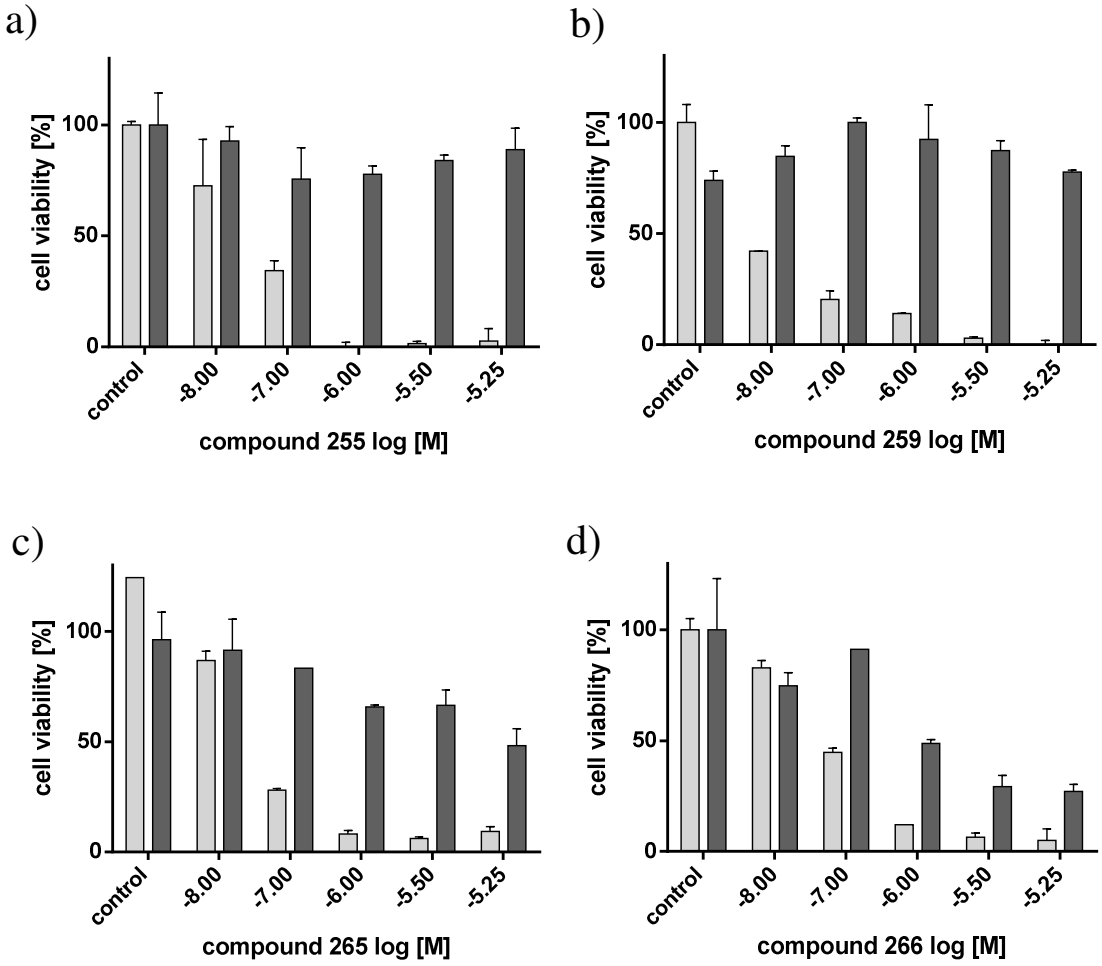

*Figure 104: MDR reversal assay of compounds **255** (a), **259** (b), **265** (c) and **266** (d) demonstrating their ability to reverse MDR toward the cytostatic mitoxantrone, in the ABCG2 overexpressing cell lines MDCK II BCRP. The bars represent the cell viability at a given modulator concentration in the presence (light grey) and absence (dark grey) of 0.5 µM mitoxantrone. Control shows viability of cells without modulator. The standard deviation is expressed by error bars.*

However, a significant decrease of the cell viability was observed in all compounds due to increasing sensitization of the resistant cells toward MX by the corresponding inhibitor (light grey bars). This effect was considerably more pronounced in comparison to the intrinsic cytotoxicity of the compounds.

The half-maximal growth inhibition was calculated from the data using the four-parameter logistic equation. Here, EC_{50} values of 45, 8, 47 and 77 nM were calculated for compounds **255**, **259**, **265** and **266**, respectively. The EC_{50} of compound **255** was about four-fold lower than the IC_{50} determined in the Hoechst 33342 accumulation assay. Although the determined EC_{50} values in the MDR reversal assay with MX are more susceptible to error than with SN-38, due to fewer measuring points, they still provide a good estimation of the efficacy of a compound.

Compounds **265** and **266** yielded EC_{50} values that were in good agreement to those from the Hoechst 33342 accumulation assay. According to the data of the MDR reversal assay, compound **266** could be distinguished as less potent than **265** which agreed with the Hoechst 33342 results. An extraordinarily potent EC_{50} value in the low nanomolar range resulted for compound **259**. This is interesting, since the 3-cyano derivatives **255** and **259** both yielded similar IC_{50} values in the Hoechst 33342 accumulation assay. The exact mechanism that is responsible for this difference is unclear but could be due to the different substituents thienyl and pyrrolyl at position 2 of the quinazoline scaffold.

8.6 Investigation of the interaction with Hoechst 33342

The interaction of selected compounds with Hoechst 33342 was investigated using ABCG2 overexpressing MDCK II BCRP cells. Varying compound concentrations were combined with varying concentrations of Hoechst 33342 and the interaction type could be determined from the Lineweaver-Burk double reciprocal plot, described in chapters 4.6 and 10.2.2.8.

A summary of the results obtained with the Lineweaver-Burk method is presented in Table 29, listing the intersection of the straight lines together with the corresponding interpretation.

Table 29: Interaction with Hoechst 33342 According to the Lineweaver-Burk Double Reciprocal Plot.

Compound	R^1	R^2	Intersection	type of interaction with Hoechst 33342
253	3- NO_2	S	2. Quadrant	Non-competitive mixed-type
254	4- NO_2	S	2. Quadrant	Non-competitive mixed-type
255	3-CN	S	2. Quadrant	Non-competitive mixed-type
259	3-CN	NH	2. Quadrant	Non-competitive mixed-type
265	3- NO_2		2. Quadrant	Non-competitive mixed-type
266	4- NO_2		2. Quadrant	Non-competitive mixed-type
Gefitinib			3. Quadrant	Non-competitive mixed-type
Elacridar			X-axis	Non-competitive
Ko143			3. Quadrant	Non-competitive mixed-type

According to the Lineweaver-Burk plots depicted in Figure 105 a non-competitive interaction with Hoechst 33342 resulted for all compounds. Except for elacridar the remainder of the compounds showed an interaction of the "mixed-type". This was also found for the majority of the compounds of projects I-IV and occurs when the inhibitor binds different from Hoechst 33342 but is still able to influence the turnover rate at the active site.

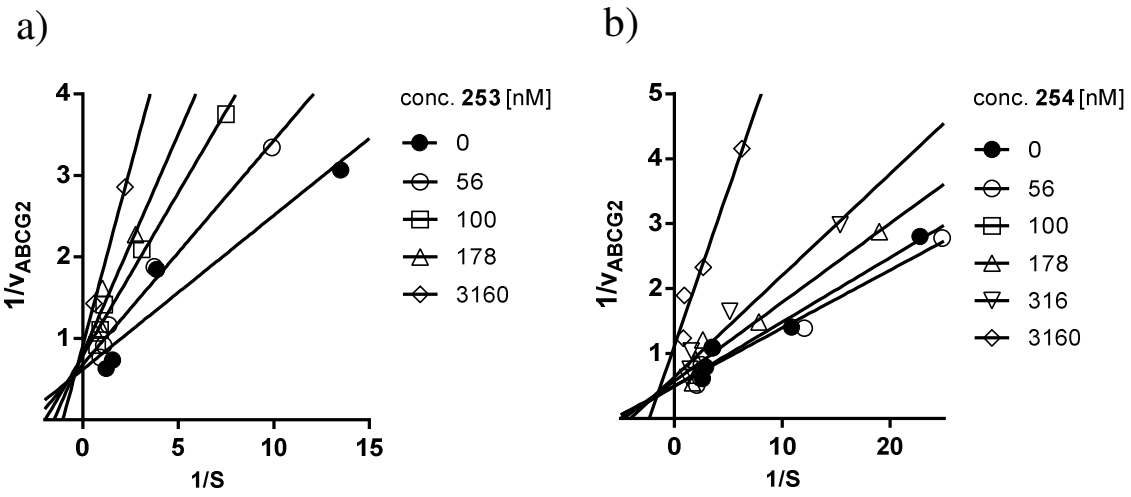

Figure continues on the next page

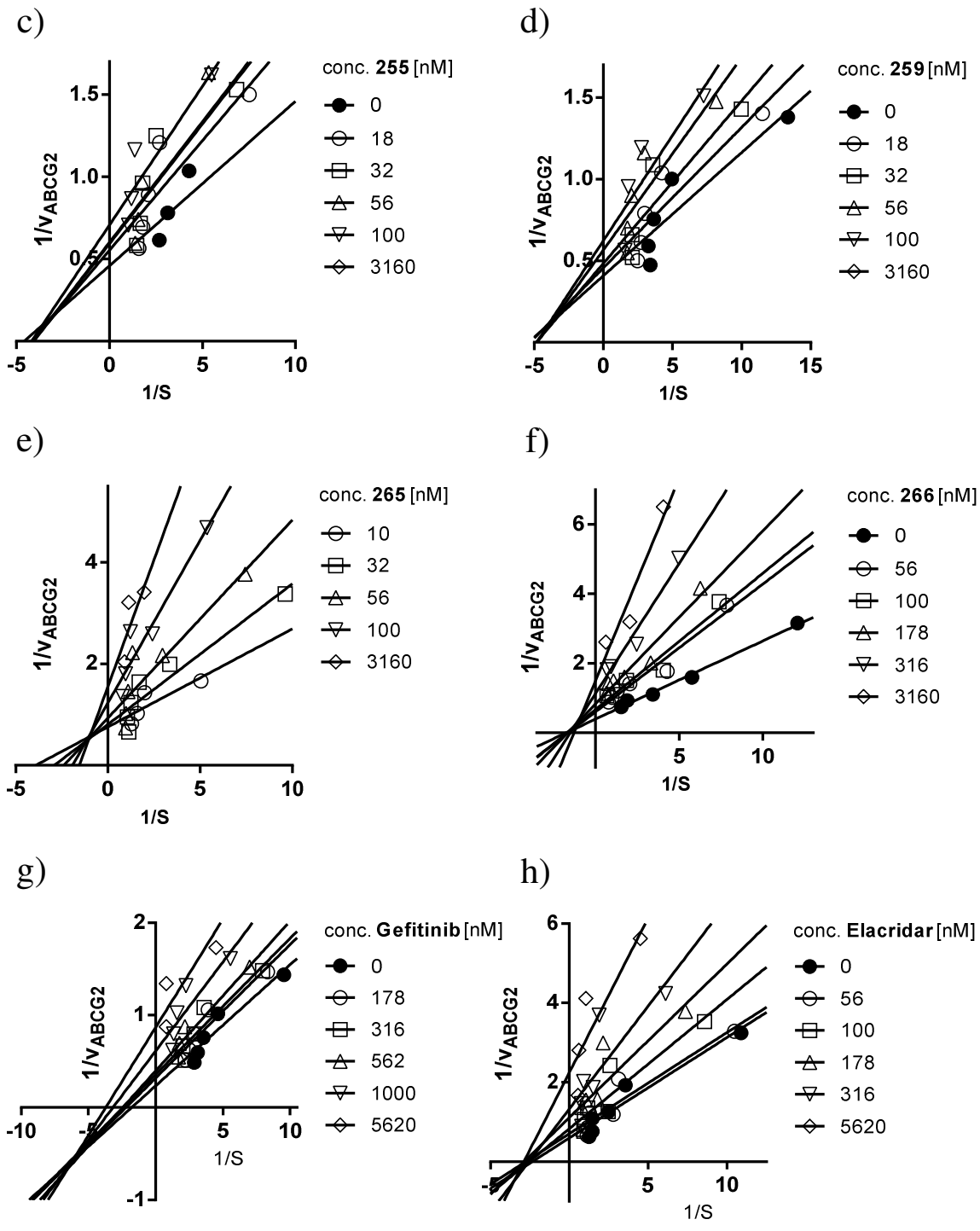

*Figure 105: Lineweaver–Burk plots for compounds **253** (a), **254** (b), **255** (c), **259** (d), **265** (e), **266** (f), gefitinib (g) and elacridar (h) using various concentrations together with the ABCG2 substrate Hoechst 33342. Compound concentrations are specified in the legend.*

Additionally the results from the Lineweaver-Burk double reciprocal plot were reassured using the direct linear method according to Cornish-Bowden. Additional information is provided in chapters 3.6 and 10.2.2.8. A summary of the obtained slopes by linear regression of the results according to the Cornish-Bowden method, is depicted in Figure 106. Corresponding linear regression plots are illustrated in Figure 107.

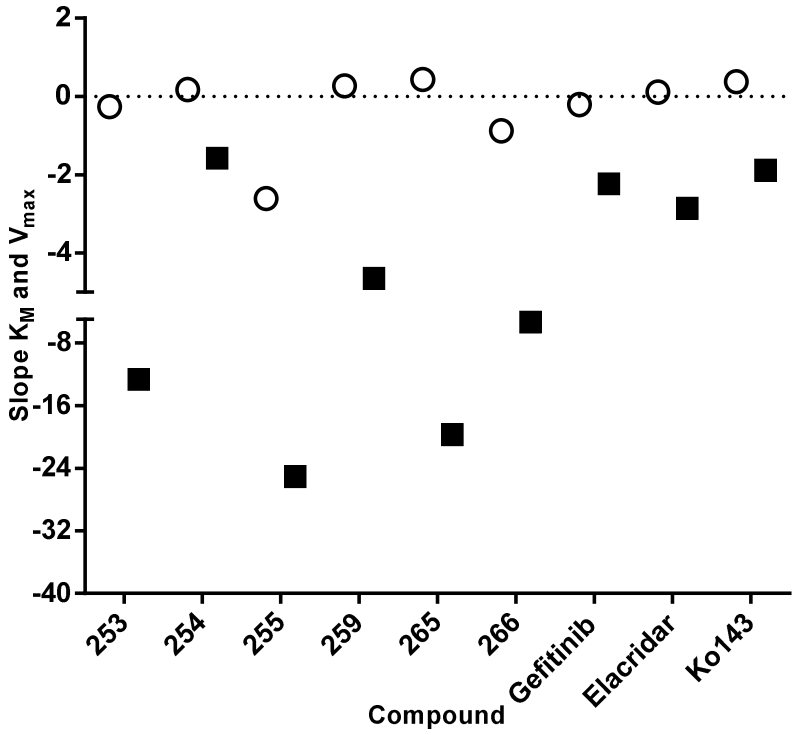

Figure 106: Scatter plot of the slopes obtained from the linear regression of K_M (○) and V_{max} (■) values calculated from the Cornish-Bowden direct linear plot.

The summary of the slopes derived from linear regression of the V_{max} and K_M values of the Cornish-Bowden plot confirmed the results obtained by the Lineweaver-Burk method. All compounds exhibit a significant decrease of the V_{max} values and roughly constant K_M values with increasing compound concentrations, which is characteristic for a non-competitive interaction with Hoechst 33342. The same results were observed for elacridar and the TKI gefitinib.

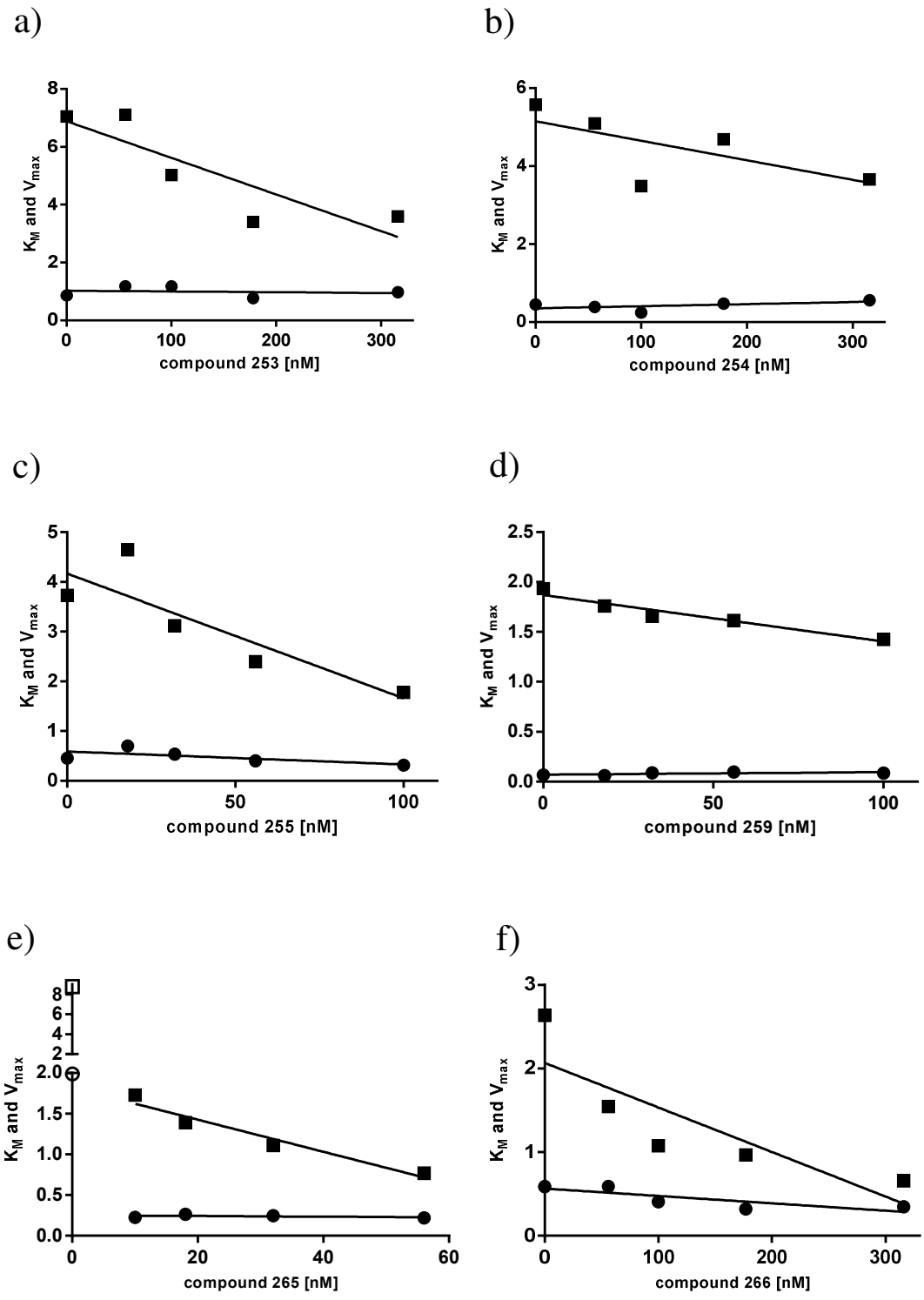

Figure continues on the next page

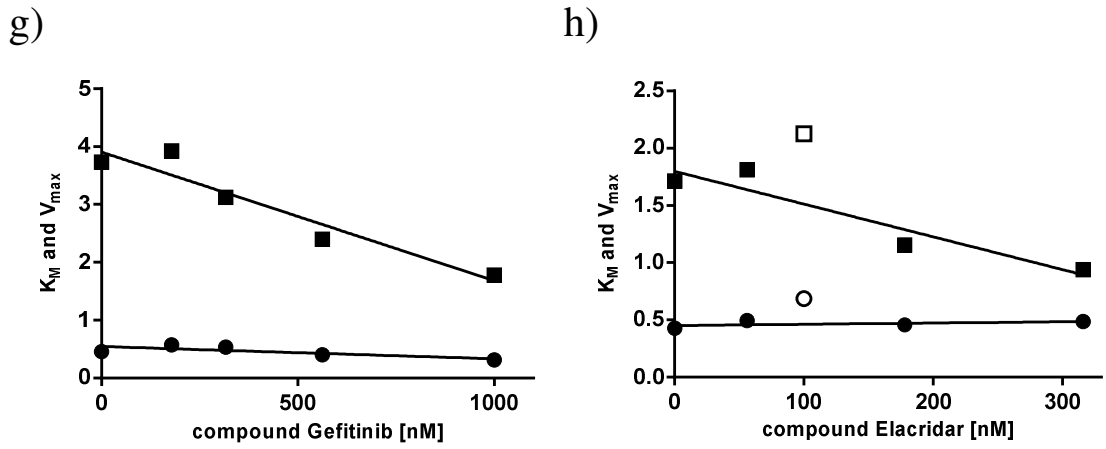

*Figure 107: Direct linear plot of **253** (a), **254** (b), **255** (c), **259** (d), **265** (e), **266** (f), gefitinib (g) and elacridar (h) according to Cornish-Bowden resulting in compound-concentration dependent lines after linear regression of the V_{max} (■) and K_M (●) values. Excluded values are depicted as open symbols of the corresponding shape.*

According to the results, a non-competitive interaction was observed for the selected compounds which included different modifications. Thus, the compounds bind different from the substrate binding site of Hoechst 33342 to ABCG2 but are able to influence the turnover rate at the active site. Moreover, none of the investigated compounds exhibited a significant competitive portion, as indicated by the constant K_M values independent of compound concentrations.

8.7 Investigation of the conformation sensitive 5D3 antibody binding to an epitope of ABCG2

The conformational effect of selected compounds on ABCG2 was studied with the conformation sensitive 5D3 antibody which binds specifically to an epitope of the transport protein. Measurement of the fluorescence emitted by the bound antibody was performed with a FACSCalibur flow cytometer using PLB-985 ABCG2 overexpressing cells. Additional information about the assay is provided in chapters 3.7 and 10.2.2.9. The results from this assay are summarized as a bar-chart in Figure 108 using Ko143 as positive control representing 100% labelling with the antibody.

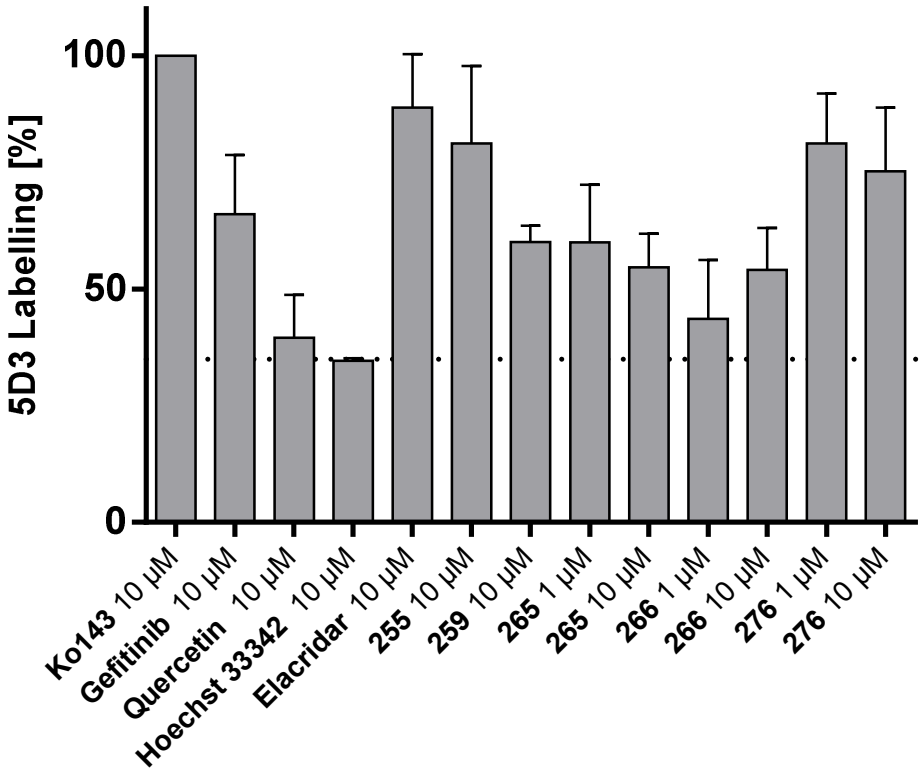

Figure 108: 5D3 immunoreactivity modulation of ABCG2 by various compounds at a concentration of 1 and 10 µM. Fluorescence detected by the 5D3-labeling of ABCG2 in the presence of 10 µM Ko143 was set to 100% and the fluorescence measured in the absence of any compound taken as 0%. The dotted line represents the labelling obtained with Hoechst 33342.

The highest conformational change resulted for compound **255** at a concentration of 10 µM resulting in a labelling by the 5D3 antibody of 81% in comparison to Ko143. The 2-pyrrolyl analog **259**, which also contained a 3-cyano group at R^1, led to a lower labelling of 60% as compared to the thienyl derivative **255**.

Also, the dimer **275** yielded high rates of labelling of around 78% at a concentration of 1 and 10 µM. In many cases a high labelling with the conformation sensitive antibody correlated with a decreased ATPase activity and a high portion of competitive interaction with Hoechst 33342.

Compounds **265** and **266** with an amide linker possessed low IC_{50} values in the Hoechst 33342 accumulation assay but with decreased I_{max} values, and led to a low labelling of

approximately 54% at 10 µM. In comparison, Hoechst 33342, which is a substrate of ABCG2, reached only 35% labelling with the antibody.

Representative histograms of the compounds yielding the highest and the lowest 5D3 shift in the assay as well as the standard Ko143 are depicted in Figure 109. The histograms of compounds Ko143, **255** and **266** were obtained at a compound concentration of 10 µM.

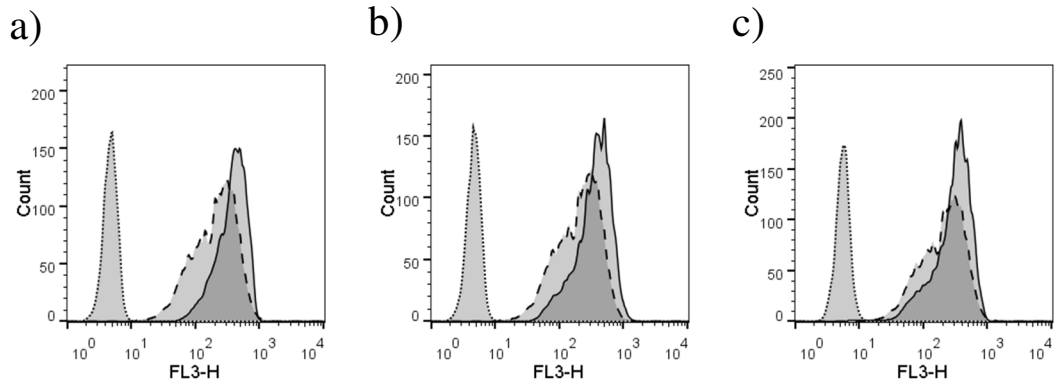

*Figure 109: Histogram of the measured fluorescence at the FL3-H detector (X-axis) and the cell-count gated according to the fluorescence. Depicted is the fluorescence of the isotype-control (dotted curve) as well as of 5D3 antibody in the absence of a compound (dashed curve) and in the presence of a compound (continuous curve). Shown are the compounds with the highest and lowest 5D3 shifts at 10 µM namely Ko143 (a), **255** (b) and **266** (c).*

8.8 Investigation of the ATPase activity

Ko143 was used as standard ATPase inhibitor and quercetin as standard stimulator. The ATPase activity assays were performed by Jennifer Gallus. Further details are provided in chapters 3.8 and 10.2.2.10.

The screening was conducted at three different concentrations (1, 10 and 25 µM) for the most potent compounds in the Hoechst 33342 assay. A summary of the results is provided as bar chart in Figure 110.

A high stimulation of ATPase activity was observed for compounds **254**, **255**, **257** and **259** based on scaffold A containing substitutions with thienyl or pyrrolyl at position 2 as

well as 3-cyano, 3,4-dimethoxy or 3-fluoro at R^1. In contrast, the derivatives **263** and **266** containing an amido-linker (scaffold C), had negligible effect on the ATPase activity as the measured values were in the range of the basal activity.

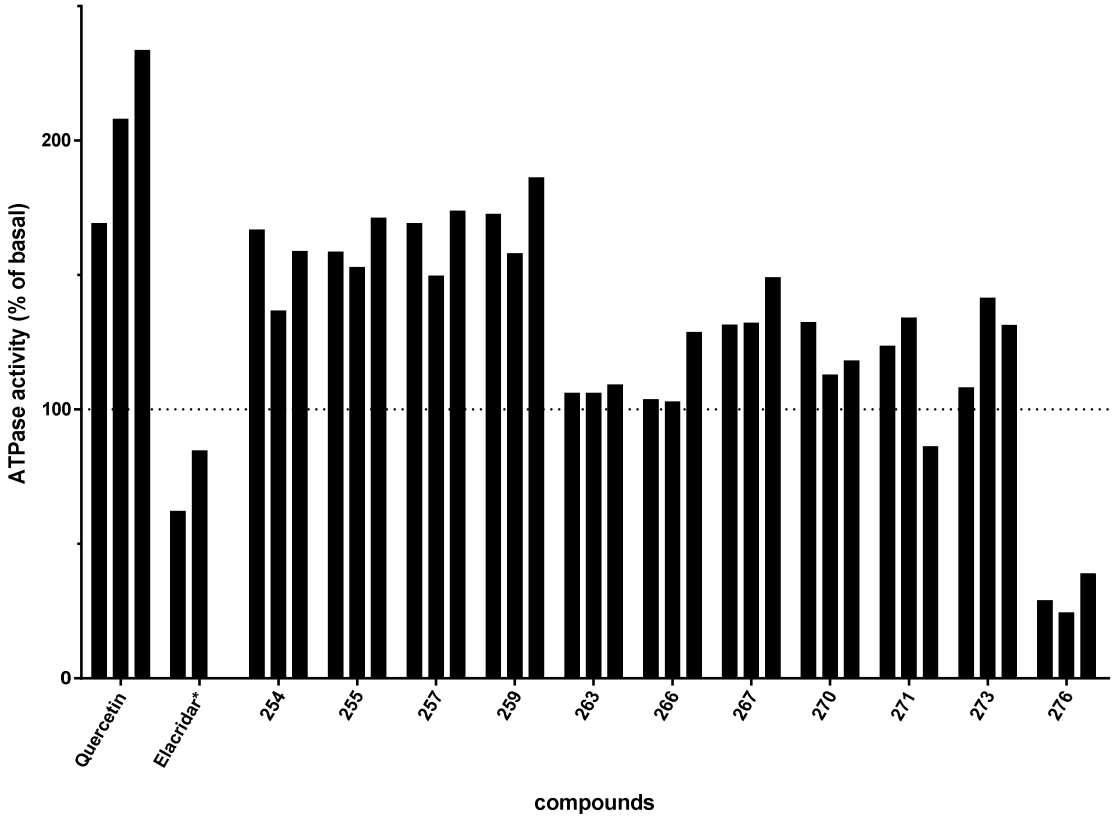

*Figure 110: Screening of ATPase activity of selected compounds at three different concentrations. From left to right the bars correspond to 1, 10 and 25 µM final concentration of compound. Quercetin was used as a standard for activation of ABCG2 ATPase activity. All values are relative vanadate-sensitive ATPase activities in relation to the basal activity, which is set to 100%. *Compound **elacridar** was investigated at a final concentration of 1 and 10 µM.*

Moreover, a slight increase in ATPase activity was detected for the derivatives **267**, **270**, **271** and **273** that lack aromatic substitution at position 2 (scaffold D). The derivatives showed similar stimulation of nearly half of the activation caused by the compounds based on scaffold A. The TKI gefitinib which is related closest to those compounds also yielded negligible stimulation around the basal level (see chapter 3.8). A strong inhibition of the ATPase activity was detected for the dimer **276**. The observed deactivation was even stronger than in case of Ko143, the standard inhibitor of ATPase activity. This led to a more detailed investigation using several concentrations of **276** in co-administration

with quercetin and Ko143 that were kept at 1 µM. Additionally, an analogues assay was carried out with the strongly stimulating compound **259**. The concentration of **259** and **276** was varied between 1 nM and 10 µM and the obtained concentration-response curves are illustrated in Figure 111 a) and b).

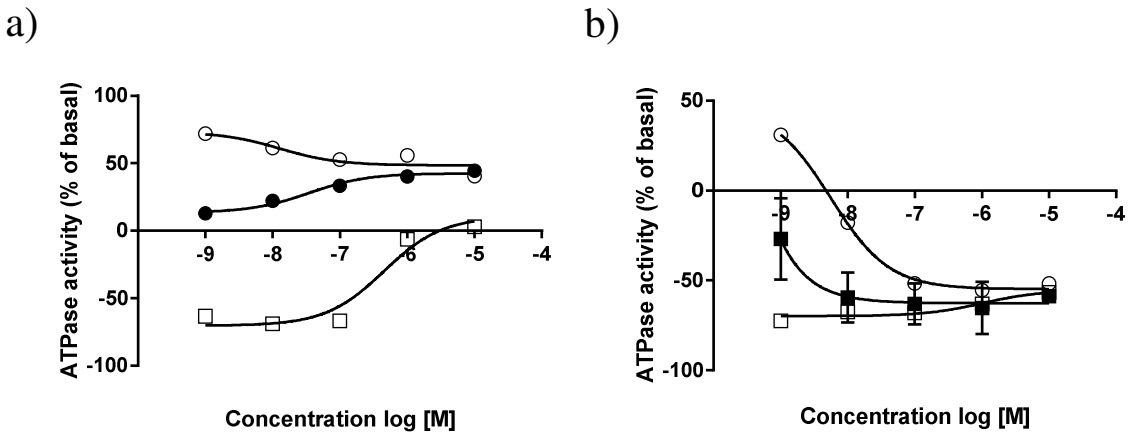

*Figure 111: Concentration-response curves for compounds **259** (a, ■) and **276** (b, ●) in the ATPase assay. Additionally, concentration-response curves of the corresponding compound in the presence of 1 µM Ko143 (□) or 1 µM Quercetin (○) were carried out. All values are relative vanadate-sensitive ATPase activities in relation to the basal activity, which is set to 0%.*

Owing to the strong stimulation effect, compound **259** fully reversed the deactivating effect of 1 µM Ko143 at a concentration of roughly 3 µM. The effect on stimulation by quercetin was rather low, although the compound reduced the stimulation slightly so that both ATPase activities aligned toward higher concentrations.

In contrast, only 4.7 nM of the deactivating compound **276** was needed to reduce the stimulating effect of 1 µM quercetin to basal level. This equals a 213-fold lower dose of compound **276** to produce a full reversal of stimulation by 1 µM Quercetin. In comparison, an equimolar amount of Ko143 was needed to reverse the stimulating effect of quercetin (data not shown). Indeed, the effect on Ko143 was rather low but exhibited a slight increase of the activity values with higher compound concentrations.

8.9 Confocal laser scanning microscopy

Due to the strong fluorescence of compound **244** inside a cell membrane further investigation with ABCG2 expressing MCF-7 MX and parental MCF-7 cells were carried out. Differences in the fluorescence between both cell lines can give further insights if the compound is transported by ABCG2. This cell line was preferred, since the MDCK II ABCG2 expressing cell line is transfected with GFP (green fluorescent protein), which is linked to cDNA of ABCG2 and might interfere with the fluorescence of the compound. Compound **244** exhibits a very strong fluorescence at a maximum emission wavelength of 444 nm after excitation at a wavelength of 405 nm.

a) b)

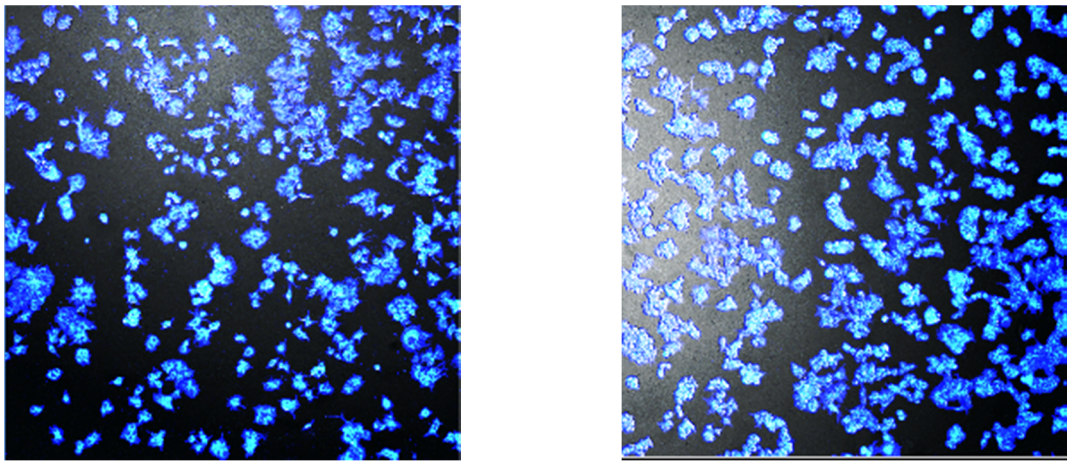

*Figure 112: Fluorescence obtained with Nikon A1 R confocal laser scanning microscope for compound **244** at 1 µM using MCF-7 MX ABCG2 overexpressing (a) and parental MCF-7 (b) cell lines. The cells were incubated fur 20 min and washed with KHB and the washed cells were then measured after 45 minutes. An excitation wavelength of 405 nm was used and the fluorescence emission detected after passing a DAPI bandpass filter.*

The MCF-7 cell lines were incubated at a compound concentration of 1 µM for a period of 20 min. Subsequently, the cells were washed and the cellular fluorescence measured after 45 min using a Nikon A1 R confocal laser scanning microscope. An excitation wavelength of 405 nm was used and the emission detected with a DAPI bandpass filter (478-495 nm). The pictures above show the cellular fluorescence of compound **244**,

recorded 45 min after the washing procedure. According to the similar fluorescence intensity in the MCF-7 MX (a) and parental MCF-7 cells (b), it is unlikely that the compound is a transported substrate of ABCG2. The confocal microscopic pictures were taken by Thomas Ross.

8.10 Investigation of substrate properties of selected compounds by fluorescence measurements

Additionally, the substrate properties of compounds **32** and **33** of project I, containing a phthalimide or coumarin moiety in position 4 of a 2-phenylquinazoline scaffold, were investigated. Due to their interesting properties described in the following text, the compounds could be used in expulsion experiments or functionalized as a fluorescent antibody conjugate.

They exhibited different emission maxima at 10 µM in KHB, illustrated in Figure 113. Further measurements of the fluorescence in ABCG2 expressing and parental cells using a FACSCalibur resulted in a comparable intensity, giving no indication that the compounds are transported substrates (data not shown). Moreover, the fluorescence-spectrum of compound **244** of project V was measured on a Luminescence Spectrometer LS55 using KHB or MDCK II parental and ABCG2 overexpressing cells in KHB. The 6-amino derivative **244** showed almost no fluorescence in KHB whereas the fluorescence increased significantly in the lipophilic environment of cells.

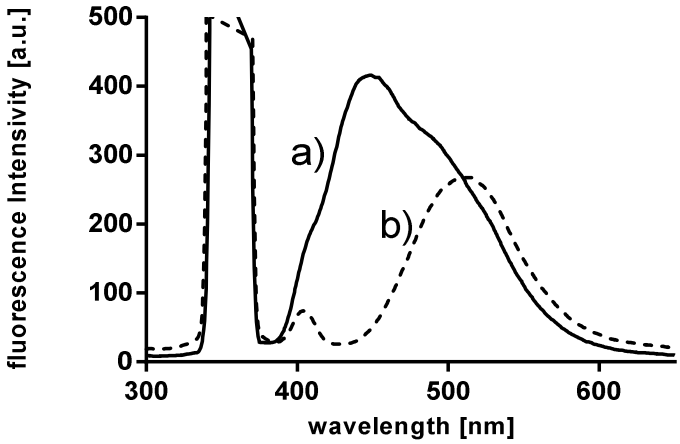

*Figure 113: Fluorescence spectrum obtained with compound **32** (a) and **33** (b) at a concentration of 10 µM using an excitation wavelength of 355 nm. Emission peaks were determined at 443 nm (a) and 508 nm (b).*

A representative fluorescence spectrum of compound **244** in the presence of MDCK II ABCG2 overexpressing, parental cells and KHB at a compound concentration of only 1 µM is depicted in Figure 114.

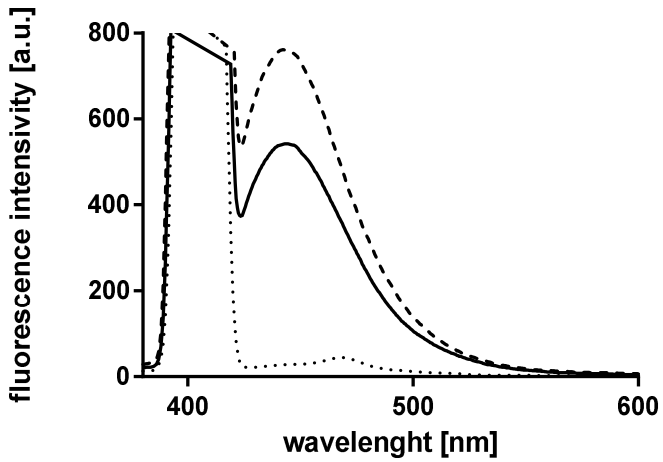

*Figure 114: Fluorescence spectrum obtained with compound **244** at a concentration of 1 µM using an excitation wavelength of 405 nm. Curves show the fluorescence obtained after 1 h of incubation with the compound using MDCK II ABCG2 overexpressing cells (continuous curve), parental cells (dashed curve) and KHB (dotted curve) exhibiting an emission maximum at a wavelength of 444 nm.*

The observed difference in fluorescence between both cell lines is negligibly small, indicating that compound **244** is not a substrate of ABCG2. Additionally, this was

confirmed in a flow cytometric investigation using ABCG2 overexpressing and parental MDCK II cells (data not shown) and also by confocal microscopy (see chapter 8.9).

9 Conclusion

9.1 Summary of the results

The investigation of inhibitors of ABCG2 based on a quinazoline scaffold was divided into 6 projects. Different modifications were synthesized in each project and the compounds examined by several functional assays. Here, the same methodology was applied throughout the investigation in order to provide a meaningful comparison between the different projects. Overall, this work led to a diverse substance library of 219 novel final compounds. A brief summary of the results in each project is provided and discussed in the following chapters.

9.1.1 Project I

The first project focused on 2-phenylquinazolines containing a substituted aniline linker at position 4. Substitution was only carried out in *meta* and *para* position since *ortho* substitution led to low inhibitory potencies toward ABCG2. This served as a starting point, so that the obtained results could easily be compared to other projects. Additionally, 2-phenylquinolines were synthesized analogously to the 2-phenylquinazolines to investigate the importance of the nitrogen atom in position 3 which was replaced by a carbon atom.

Regarding the quinazoline scaffold, considerably high inhibitory potencies resulted in the Hoechst 33342 accumulation assay by monosubstitution with cyano, nitro and hydroxy residues. Moreover, it turned out that disubstitution with 3-nitro,4-hydroxy and 3,4-dimethoxy led to highly potent compounds. The highest activity in this subset was found for compound **5** containing a 4-cyano substituent and yielding an excellent IC_{50} of 70 nM. The standard inhibitor Ko143, which is one of the most potent inhibitors of ABCG2 known in literature, possessed a considerably higher IC_{50} value of 227 nM. In most cases, significant differences between *meta* and *para* substitution were observed which was often also reflected in other assays and is discussed in the following paragraph. For some

compounds the IC_{50} was additionally determined by flow cytometric measurement using pheophorbide A in order to exclude substrate specific effects. A good correlation of the pIC_{50} values ($r^2 = 0.91$) for both assays was found, validating the obtained results with both methods. Regarding the compounds based on a quinoline structure, a significant decrease of the inhibitory potency was observed in comparison to their quinazoline analogues. Hence, the nitrogen atom at position 3 of the quinazoline structure is a vital feature for potent inhibitors of ABCG2. An explanation for this finding could be the decreased planarity of the molecule owing to the sterical hindrance between the hydrogen atom at position 3 and the aromatic core in position 2 leading to a twist. Calculations using the MMFF94x force field showed an torsion angle of roughly 3 degree for the 2-phenylquinazoline and about 33 degree for the 2-phenylquinoline. Several studies concluded that the planarity of an inhibitor of ABCG2 is crucial for its potency.[66,90,112]

The screening against the two other major MDR transport proteins ABCB1 and ABCC1 in a calcein AM assay showed a high selectivity toward ABCG2 for the majority of the compounds. In comparison to a quinazoline scaffold the selectivity toward ABCG2 was considerably lower in the quinoline derivatives. Particularly the presence of methoxy, thiomethyl, ester and carboxylic acid functions increased the potency toward ABCB1 and ABCC1. Here, the non-selective compounds exhibited a slightly higher potency against ABCB1 than ABCC1.

Investigation of the intrinsic cytotoxicity of the compounds yielded moderate GI_{50} values for the quinazoline derivatives that were slightly better than the potent standard inhibitor Ko143 (GI_{50}: 11.1 µM). An excellent GI_{50} of 52 µM was determined for compound **3** containing a disubstitution with 3-nitro,4-hydroxy. Due to its high inhibitory potency the compound had the highest therapeutic ratio (TR: 655) in the subset which is more than 13-fold higher than Ko143. According to the results, a comparable or higher cytotoxicity resulted for ABCG2 overexpressing cells with respect to the parental MDCK II cell line. This is a strong indication that the substances are inhibitors and not substrates of ABCG2. Similar results were observed in the broad majority of compounds from the other projects.

One key point of this work was the investigation of the ability of a compound to reverse the multidrug resistance in ABCG2 overexpressing cells. For that purpose a MDR reversal assay was carried out with co-administration of the cytostatic drugs SN-38 and Hoechst 33342. The most potent compounds, **3** and **5**, led to a full reversal of the MDR

and the derived EC_{50} values from the MTT data of both cytostatic drugs were in a good agreement. In contrast to compound **3**, the 4-cyano derivative **5** was significantly more potent in the MTT assay than in the Hoechst 33342 accumulation assay. A similar MTT assay was carried out with compound **3** and **5** in co-administration with the cytostatic drug MX. Once again, compound **5** demonstrated a significantly higher efficacy than **3** and resulted in a full reversal of the MDR at a concentration of 0.1 µM.

Investigation of the interaction with Hoechst 33342 was carried out utilizing the methods according to Lineweaver-Burk and Cornish-Bowden. Predominantly, a non-competitive interaction with Hoechst 33342 was found for the compounds. Also, the majority of the compounds exhibited a non-competitive interaction of the "mixed type", meaning that they bind distant from the Hoechst 33342 binding pocket but still influence the active site for instance by conformational changes of the protein. Compounds competing with Hoechst 33342 for the active site were found to contain *para* substitutions with lipophilic halogen atoms like chlorine and iodine. On the contrary, the standard inhibitor Ko143 exhibited a non-competitive interaction which has already been found in a previous study.[208] Moreover, it was striking that significant differences between *meta* and *para* substitution were observed in the interaction type investigation. Examples are the *meta*/*para* compound pairs **4/5**, **18/19** and **20/22** where this modification led to an altered binding to ABCG2.

Conformation sensitive binding studies with the monoclonal 5D3 antibody confirmed the before mentioned differences between *meta* and *para* substitution. Compound **4** and **5** containing a 3-cyano and a 4-cynao function, respectively, exhibited a considerable difference regarding the labelling with the 5D3 antibody. Particularly high rates of labelling resulted for compounds that showed a significant competitive interaction with Hoechst 33342 (e.g. **17** and **23**). One of the exceptions to this is the standard inhibitor Ko143 which was used as control for this assay resulting in the highest rate of labelling which was set to 100%.

Further investigations of the modulation of the ABCG2 related ATPase activity by different inhibitors led to interesting results: In this subset different effects on the ATPase activity were observed ranging from deactivation to strong stimulation, including compounds that had no effect on the ATPase activity. Again, strong differences were found for *meta*/*para* derivatives like **4/5**, **18/19**, **20/21**, **22/23**. Activities at or below the

basal level were in particular observed for *para* derivatives. In contrast, the majority of the *meta* derivatives led to increased ATPase activity. A high stimulation of the ATPase activity can for instance be exploited in targeting selective cell death of ABCG2 overexpressing cells by ATP depletion. Based on the results the existence of several binding sites occupied by differently substituted inhibitors is highly likely and will be discussed in more detail in chapter 9.3.

9.1.2 Project II

In this project the phenyl moiety at position 2 of the quinazoline scaffold was exchanged by pyridyl. This led to a lower logP value which can be beneficial in terms of an enhanced bioavailability of a compound. Furthermore, the aromatic quinazoline system was reduced by removing the unsubstituted aromatic core. Due to the convenient preparation a 4-methylpyrimidine scaffold was synthesized and substituted at position 2 by a phenyl or pyridyl moiety. Further substitution was carried out at position 4 bearing substituted anilines. Likewise, the logP value was calculated and proved to be even lower than for the 2-pyridylquinazolines.

Several compounds exhibited high inhibitory potencies in the Hoechst 33342 accumulation assay. The best IC_{50} value of 64 nM was determined for compound **54** containing a 4-nitro function at the aniline linker and 3-pyridyl at position 2. Substitutions with nitro and cyano substituents led to high potencies and the SAR showed similar trends as in project I, but only for *meta* and *para* pyridyl groups at position 2. In general, the substitution in *ortho* position resulted in reduced potencies for all investigated compounds in this work. This could be due to sterical issues leading to unfavorable conformational changes of the residues at position 2 or 4. Also, very similar activities were found for the pyrimidine derivatives in comparison to their quinazoline analogues. Since they consist of only 3 aromatic cores, this class of compounds exhibits an extraordinary high ligand efficiency.

In terms of selectivity toward ABCG2, comparable results as for the compounds in project I were obtained. The presence of methoxy, ester and carboxylic acid functions led to increased inhibitory potencies toward ABCB1 and, to a lesser extent, also toward ABCC1.

A major difference between project I and II was observable in the MTT cytotoxicity assay. Replacement of the phenyl moiety at position 2 of the quinazoline scaffold by pyridyl decreased the cytotoxicity considerably. Some of the pyridyl derivatives exhibited no toxic effect even at concentrations up to 100 µM, including the most potent compound. Since the inhibitory potency was comparable to the analogues of project I, extraordinarily high TRs of more than 1130 were obtained. Hence, the compounds of project II excel as promising candidates for *in vivo* experiments combining low cytotoxicity, high selectivity and potency toward ABCG2 as well as an enhanced watersolubility due to the low logP value.

Moreover, all selected compounds were able to reverse MDR toward SN-38 in the ABCG2 overexpressing MDCK II BCRP cell line at very low doses. According to the MTT data the most potent compound **54** possessed an EC_{50} of 21 nM which was about three-fold lower than determined in the Hoechst 33342 accumulation assay. Also the calculated EC_{50} values of compounds **56** and **87** were slightly lower, but still in good accordance to the IC_{50} value obtained in the Hoechst 33342 accumulation assay. Co-administration of compound **54** and **87** with MX resulted in a high efficacy leading to a full reversal of the MDR at concentrations between 0.1 and 1 µM.

In investigations of the type of interaction according to Lineweaver-Burk essentially all compounds showed non-competitive interactions with Hoechst 33342 that were mostly of the "mixed type". A closer investigation utilizing the Cornish-Bowden method then revealed strong competitive portions for some compounds. A possible reason for this could be an allosteric interaction with the protein influencing the turn-over rate at the active site.

The conformation sensitive labelling with the monoclonal 5D3 antibody yielded a high amount of staining for the most potent compound **54**. Also the competitive inhibitor **61** obtained a high amount of labelling with the antibody which was also observed for compounds with a pronounced competitive interaction in Project I. Most notably, significant differences between *meta* and *para* derivatives resulted as illustrated by compounds **66** and **67**. But, high rates of labelling were not exclusive to inhibitors with a high competitive portion (see compound **54**).

In the study of the ATPase activity solely stimulating effects were observed for the selected compounds. Only a few compounds showed low stimulation near the basal level,

including the competitive compound **61**. Interestingly, a strong competitive interaction often led to low stimulation or even deactivation of the ATPase activity. Although it is still a widespread claim that stimulation of ATPase activity is linked exclusively to substrates, the current work and other studies prove the contrary.[209] High stimulation by the compounds may also be exploited to target ABCG2 expressing cells selectively by depleting the cellular ATP.

9.1.3 Project III

In this project 2,4-substituted quinazoline derivatives were synthesized. Substitution at both aromatic cores resulted in an increased amount of possibilities and enabled the investigation of more complex SAR studies including cumulative effects among the functional groups. In this context the interchangeability of the residues at both aromatic moieties was investigated.

According to the Hoechst 33342 accumulation assay, the presence of an aromatic residue at position 4 of the quinazoline scaffold is crucial for the inhibitory potency. This was confirmed by a cyclohexylamino residue at position 4 leading to a considerably decreased potency in comparison to phenyl. Interestingly, the exchange of the substituents between the aromatic moieties at position 2 and 4 led to comparable IC_{50} values. The highest potency resulted for compound **144** (IC_{50}: 44.2 nM) containing a combination of 3,4-dimethoxy at position 2 and 4-nitro at position 4. In general, excellent potencies were obtained by combination of methoxy groups, particularly 3,4-methoxy, together with nitro functions. This combination led to compounds with IC_{50} values even below 100 nM (e.g. **111**, **127**, **143** and **144**). In many cases, higher inhibitory activities were obtained by *para* substitution with nitro or cyano groups (e.g. **131/132** or **143/144**).

The screening of the selectivity of several compounds toward ABCG2 was carried out in a calcein AM assay, substantiating the results of previous projects: a noticeable decrease of selectivity was observed in most compounds containing two or more methoxy groups. Here, higher inhibitory potencies were detected toward ABCB1 than ABCC1. Since several compounds contained a combination of methoxy and nitro groups, a few potent broadspectrum inhibitors resulted comprising extraordinary high potencies toward ABCG2, ABCB1 and some even toward ABCC1. These compounds could be used to

circumvent the cellular resistance in barrier tissues like the BBB, which contains a high expression of ABCG2 and ABCB1, in order to increase the efficacy of certain drugs. In this regard, broadspectrum inhibitors like elacridar have already been successfully tested.[210]

The intrinsic cytotoxicity of selected compounds was investigated in a MTT assay with MDCK II parental and ABCG2 overexpressing cells. Selected compounds of project III exhibited a similar cytotoxicity in comparison to project I. Although the mean GI_{50} in this subset was in the range of Ko143, most of the TRs were still considerably higher owing to the significantly greater inhibitory potencies toward ABCG2. The highest TR of 270 resulted for compound **111** containing a substitution with 3-nitro at R^1 and 3,4-dimethoxy at R^2. Moreover, it was found that two or more nitro and/or cyano functions led to increased toxic effects in the corresponding compound (e.g. **107** and **109**).

The reversal of the MDR in the ABCG2 overexpressing MDCK II BCRP cell line toward the cytostatic drugs SN-38 and MX was investigated in a MDR reversal assay. Here, the most potent compounds **144** and **150** resulted in a roughly three-fold lower EC_{50} value in co-administration with SN-38 than observed in the Hoechst 33342 accumulation assay. Likewise, considerably increased inhibitory potencies have already been observed in some of the most potent compounds in other projects (e.g. compound **5** and **54**). With regard to SN-38, a very similar potency was observed for compounds **144** and **150** by co-administration of cytostatic drug MX.

Interaction type investigations using the Lineweaver-Burk and Cornish-Bowden method showed that only compound **139** displayed a clear competitive interaction with Hoechst 33342. For the remaining compounds a non-competitive interaction was found, for some with a pronounced competitive portion, which is typical for non-competitive "mixed type" inhibitors. For instance, high competitive portions were found for compounds **130** and **144** that could be due to substitution in *ortho* or *para* position.

The results from this investigation were also reflected in the conformation sensitive 5D3 antibody labelling assay. High shifts were frequently observed for inhibitors with a pronounced competitive portion with regard to the interaction with Hoechst 33342. Hence, the highest shift of 94% with in comparison to Ko143 was found for compound **139**, followed by compound **130** that yielded a labelling of 80%. Besides a few exceptions, certain patterns were noticeable such as the significantly different rate of

labelling between *meta* and *para* derivatives (e.g. **143** and **144**) or the correlation of the interaction with the observed 5D3 shift.

Similar patterns were also found in the screening of the ATPase activity of selected compounds. Compound **130** for instance, that showed a competitive interaction with Hoechst 33342 and also a high 5D3 shift in the immunostaining assay resulted in a strong deactivation of the ATPase activity. In general, inhibitors that had a pronounced competitive interaction and/or a high labelling with the 5D3 antibody were frequently found to deactivate the ATPase activity, mostly at higher concentrations, and often contained a *para* substitution. A more detailed investigation of selected compounds **132**, **144**, **149** and **150** revealed a concentration dependent effect on the ATPase activity with stimulation at low concentrations and inhibition at high concentrations. This is suggested to be due to a concentration dependent activating high affinity and a deactivating low affinity binding site yielding bell-shaped concentration-effect curves.[206] Also, the addition of alkyl groups to amino or ether functions resulted in compounds which inhibited the ATPase activity (compare compounds **113**, **114**, **116**, **118** and **119**). An interpretation of this effect is given in chapter 9.3.

9.1.4 Project IV

In this project the carbon atom at position 8 of the quinazoline scaffold was replaced by nitrogen resulting in a pyrido[2,3-d]pyrimidine scaffold. Substitution was carried out analogously to the quinazoline derivatives of projects I-III on the aniline linker at position 4 and at position 2 by introducing different aromatic moieties. Notably, a very low logP value resulted from this modification probably enhancing the watersolubility in this class of compounds.

The inhibitory potency of all test-compounds toward ABCG2 was determined in a Hoechst 33342 accumulation assay. Surprisingly, all 2-phenyl derivatives exhibited an enantiotopic inhibitory potency toward their quinazoline analogues. Therefore, the lowest IC_{50} value of 149 nM was observed for the unsubstituted compound **162**, whereas the unsubstituted quinazoline analogue **1** led to a poor IC_{50} of only 882 nM. Similarly high inhibitory potencies resulted for compounds with *meta* methoxy and *meta* fluorine substituents at either phenyl ring. Nitro, cyano and hydroxy substituents that previously

led to high inhibitory potencies in the quinazoline derivatives resulted in poor inhibitory potencies in the pyrido[2,3-d]pyrimidine derivatives. Again, significant differences between the *meta* and *para* derivatives were noticeable, for instance illustrated by compounds **166** and **167**.

A great advantage of this class of inhibitors was the selectivity for ABCG2. The screening of selected compounds in the calcein AM assay yielded no noteworthy inhibitory potency toward ABCB1 or ABCC1 emphasizing their benefit for specific investigations involving ABCG2.

The investigation of the intrinsic cytotoxicity of selected compounds in a MTT assay revealed another advantage of the pyrido[2,3-d]pyrimidine scaffold. Most of the compounds possessed intrinsic cytotoxic effects that were either very low or not measurable, similar to the substituted 2-pyridylquinazolines of project II. The cell viability was often restricted by the toxic effects of the solvents (MeOH/DMSO) resulting in a similar GI_{50} as the control. The highest TR of 676 was calculated for compound **175** containing a substitution with 3-trifluoromethyl at the anilino linker at position 4 and a phenyl residue at position 2. Like in other assays, the *meta* and *para* analogues frequently showed considerable toxicity differences, as observed for the *meta*/*para* derivatives **168** and **169** that yielded GI_{50} values differing about two-fold.

A MDR reversal assay was carried out with compounds **162**, **167** and **169** in order to investigate their ability to revert MDR in ABCG2 overexpressing cells toward the cytostatic drug SN-38. According to the MDR reversal data, they all possessed a four-fold higher inhibitory potency than in the Hoechst 33342 assay and the tendencies of the calculated IC_{50} values were very well reflected. The phenomenon of lower IC_{50} values resulting from the MDR reversal assay was also observed for most of the compounds investigated in other projects and is discussed in chapter 9.3. A full reversal of MDR was also obtained in a similar assay using the cytostatic drug MX in co-administration with compound **162** and **169**. Again, the potencies obtained in the MTT assay exhibited similar trends compared to the Hoechst 33342 accumulation assay, but were considerably higher.

The investigation of the type of interaction using the Lineweaver-Burk and Cornish-Bowden methods led to mostly non-competitive or non-competitive interactions of the "mixed type" with Hoechst 33342. Among the selected compounds of project IV the three derivatives **167**, **169** and **188** exhibited strong evidence for a high portion of competitive

interaction. All three of them contain a *para* substitution at the aniline linker in position 4 which was a frequent pattern in inhibitors showing a pronounced competitive interaction with Hoechst 33342. On the contrary, many *meta* derivatives resulted in a more pronounced non-competitive interaction.

The conformation sensitive 5D3 antibody binding study resulted in some familiar patterns: Major differences were found between the *meta* and *para* cyano derivatives **166** and **167**, leading to a labelling of 63 and 93%, respectively. Also the 4-cyano derivative **181** yielded a high staining of 79% with respect to Ko143. This is in accordance to the finding for the 4-cyano derivative **5**, containing a quinazoline scaffold, which has been investigated in project I. In general, compounds showing a pronounced competitive interaction with Hoechst 33342 often yielded a higher amount of labelling by the conformation sensitive 5D3 antibody.

Screening of the ATPase activity resulted solely in stimulating effects. However, increasing concentrations led to a strong decrease of the stimulating effect in some compounds like **167**, **181** and **184.** In A more detailed investigation of compound **178** an even higher stimulation than the standard Quercetin (EC_{50}: 302 nM) was determined with a rather low EC_{50} of 18.0 nM. For compounds **167** and **181** high competitive portions were detected in the interaction type investigation. They also showed the highest amount of labelling with the conformation sensitive 5D3 antibody. This pattern was frequently found in inhibitors with a low stimulating or even deactivating effects on the ATPase activity. Again, a clear distinction between *meta* and *para* derivatives was observed in the ATPase activity assay (e.g. compound **166/167** and **168/169**).

9.1.5 Project V

In this project a nitro function was introduced at position 6 of the 2,4-substituted quinazoline scaffold. Although the calculated logP values was relatively low, a reduced solubility was observed in some of the compounds requiring higher amounts of methanol in the final concentration (MeOH < 5%) for the dilution series. Reduction of the nitro function yielded the corresponding 6-amino derivatives which were further modified by reacting them with different acid chlorides leading to the corresponding amide derivatives.

In most instances, the presence of a 6-nitro function led to extraordinary high inhibitory potencies in the Hoechst 33342 accumulation assay. The clear advantage of this modification is noticeable by comparison of the corresponding quinazoline derivatives **211** and **1**. Here, the 6-nitro derivative **211** was roughly 9-fold more potent than the analogue **1**, which lacks the 6-nitro group. It was discovered that further substitution of the aromatic moieties at position 2 and 4 of the quinazoline scaffold increased the inhibitory potency even more. Beneficial substituents were for instance methoxy and fluorine groups that led to the most potent compound **238** with a superb IC_{50} of 23 nM. Overall 29 different compounds were synthesized containing a 6-nitro function and yielded an average IC_{50} of 85 nM. Reduction of the 6-nitro group yielded 6-amino functions that decreased the inhibitory activity of the corresponding analogues considerably. Even lower potencies resulted for the corresponding amides.

In the investigation of the selectivity toward ABCG2 no noticeable inhibitory potency toward ABCB1 and ABCC1 was observed for the tested compounds. In this regard, a high selectivity has often been observed in the presence of nitro functions, making this class of compounds favorable for further specific investigations of ABCG2.

The study of the intrinsic cytotoxicity in an MTT assay showed increased toxic effects among the investigated compounds. In comparison to their analogues, lacking substitution at position 6, an about three-fold decreased GI_{50} resulted (see compound pairs **211/1**, **212/3** and **218/13)**. However substitution with pyridyl in position 2 of the quinazoline scaffold resulted in a significantly decreased cytotoxicity. Almost no toxic effect was detected for compounds **223** and **226**, **s**imilar to the 2-pyridyl derivatives of project II. Owing to the high inhibitory potency and the low cytotoxicity, extraordinarily high TRs of roughly 1200 and 1100 were calculated for both compounds. Due to the enhanced watersolubility of the 2-pyridyl derivatives, these are promising candidates for *in vivo* studies.

Selected compounds, including the most potent compound **238**, were additionally investigated for their ability to reverse MDR in ABCG2 overexpressing cells toward SN-38 and MX. All compounds led to a full reversal when co-administered with SN-38 with EC_{50} values that were for some compounds negligibly higher compared to the IC_{50} values of the Hoechst 33342 accumulation assay. In general, the derived EC_{50} values were either comparable or even lower than observed for the compounds of other projects. A possible

reason could be some degree of precipitation over the time period of 72 h. However, in the MDR reversal assay in co-administration of MX, the EC_{50} values were in excellent accordance to the IC_{50} values obtained in the Hoechst 33342 accumulation assay.
In the interaction type investigation a pronounced competitive interaction with Hoechst 33342 was found only for compound **231**. For the remaining compounds a non-competitive interaction of the "mixed type" resulted. Among these, many exhibited considerable competitive portions, indicating a binding site nearby Hoechst 33342 or strong allosteric interactions with the active site.
Unfortunately, the results of the interaction type investigation did not agree as well as in other projects with the data determined in the conformation sensitive 5D3 antibody binding assay. Notably, the competitive compound **231** led to a high labelling of 66% using a concentration of only 1 µM. In comparison to other projects the overall labelling was somewhat increased which could be due to the higher competitive portions observed in the corresponding interaction type investigation. In particular, a high percentage of labelling of 84 and 88% was found for compounds **241** and **217** containing a 6-amino or 6-nitro group, respectively.
The investigation of the ATPase activity illustrated that the substituent in position 6 had a strong impact on the modulation of ATPase. This could be seen from the analog compounds **232** and **244** with a 6-nitro or 6-amino substituent, respectively. Overall most of the compounds had a stimulating effect on the ATPase activity, some even in the range of quercetin (e.g. compounds **218**, **227**, **242** and **244**). A deactivation was detected solely for compound **233**. Like in other projects, some compounds had no effect on the ATPase activity yielding values in the basal range (e.g. compounds **230**, **231** and **232**). Among them was compound **231**, which had shown a competitive interaction with Hoechst 33342. In this regard, compounds with high competitive portions were often found to exhibit either none or a deactivating effect on the ATPase activity.

9.1.6 Project VI

In this project, several modifications at position 2 and 4 of the quinazoline scaffold were investigated. These comprised substitution with 5-membered heteroaromatic residues at position 2 (scaffold A), methylation of the aniline linker at position 4 (scaffold B),

exchange of the aniline linker at position 4 by an amide linker (scaffold C), exchange of the aromatic moiety at position 2 by hydrogen (scaffold D), and the formation of two different dimers (scaffold E).

The investigation of the inhibitory potency toward ABCG2 in the Hoechst 33342 accumulation assay resulted in good IC_{50} values for substitution with thienyl and pyrrolyl in position 2 (scaffold A). Both residues led to low IC_{50} values of 178 and 156 nM in combination with a 3-cyano function at the aniline linker in position 4 (see compounds **255** and **259**). Although several potent compounds resulted from both heteroaromatic residues they led to comparable or somewhat higher IC_{50} values in comparison to a substitution with phenyl. A considerable decrease in potency was determined for the compounds based on scaffold B after methylation of the aniline linker. Hence, the H-donor function at position 4 is crucial for a potent inhibition of ABCG2. Also, the inactive compound **262** which contained a free amine in position 4 demonstrated the importance of an aromatic moiety linked to the amine. The exchange of the aniline linker in position 4 by an amido linker (scaffold C) increased the inhibitory potency significantly. Among those, the best derivative **265** led to an excellent IC_{50} value of 55 nM containing a 3-nitro substituent at the aromatic core on position 4. However, this class resulted in lower I_{max} values in the range of about 60% in comparison to Ko143. Removal of the aromatic function at position 2 (scaffold D) led to increased IC_{50} values and also lower I_{max} values in comparison to their 2-phenylquinazoline analogues. Among the synthesized dimers (scaffold E) it was found that a longer alkyl chain enhanced the solubility and also the inhibitory potency. The dimers **275** and **276** containing a 4-nitro substituent at position 2 and the quinazoline scaffold was linked at position 4 by the corresponding diamine to achieve dimerization. Hereby, an IC_{50} of 229 nM which is very similar to Ko143 resulted for **276** containing a propyl chain.

In the calcein AM assay selected compounds including the most potent ones were screened to determine their inhibitory potency toward ABCB1 and ABCC1. Increased potencies resulted only for compounds based on scaffold A that contained methoxy functions. In general, a higher activity was detected toward ABCB1 than ABCC1. Similar results have also been observed for several compounds in other projects.

The investigation of the intrinsic cytotoxicity included several of the most potent compounds and exhibited further interesting SAR. Significant differences were observed

in the GI_{50} values of the nitro *meta*/*para* derivatives **253** and **254** bearing thienyl at position 2. Those differences between *meta* and *para* substituents were also found in other projects and could be an indication of a different interaction with ABCG2. The highest TR of 331 resulted for compound **255** containing a 3-cyano substituent at position 4 and thienyl at position 2. For the most part, the compounds containing scaffold A led to good GI_{50} values and beneficial TRs. Regarding the highly potent compounds **265** and **266** containing an amido linker at position 4 (scaffold B), considerably increased cytotoxic effects were observed for the nitro derivatives and could be a criterion for the exclusion from *in vivo* studies.

The four most potent compounds **255**, **259**, **265** and **266** were additionally investigated in a MDR reversal assay to examine their ability to reverse the MDR toward the cytostatic drug MX. A full reversal was produced by all compounds at a concentration of about 1 µM. Determined EC_{50} values were in very good accordance to the Hoechst 33342 accumulation assay for the derivatives **265** and **266** containing an amido linker at position 4. On the contrary, significantly lower EC_{50} values resulted for the 3-cyano derivatives **255** and **259** which contained a thienyl or pyrrolyl moiety at position 2, respectively. Indeed, the pyrrolyl derivative **259** showed a considerably higher efficacy in comparison to compound **255**.

The interaction type investigation utilizing the Lineweaver-Burk method detected for all of the selected compounds a non-competitive interaction with Hoechst 33342, primarily of the “mixed type”. This interaction-type was also most frequently observed in all projects including the commercial inhibitors Ko143, elacridar and gefitinib. The pronounced non-competitive character of all compounds was supported by an additional analysis using the method of Cornish-Bowden.

In the conformation sensitive 5D3 antibody binding assay a different labelling was determined for the 3-cyano derivatives **255** and **259**: Substitution with thienyl at position 2 led to a high labelling of 81% whereas the corresponding pyrrolyl substitution yielded 60%. Most notably, the dimer **276**, containing a propyl linker, and the dual-inhibitor elacridar showed very high rates of labelling. Interestingly, an increased labelling with the antibody often correlated to high competitive characteristic and a decreased ATPase activity. This relationship is further discussed in the following paragraph.

In the investigation of the ATPase activity the derivatives **254**, **255**, **257** and **259** containing a 5-membered heteroaromatic moiety in position 2 (scaffold A) displayed a strong stimulating effect of around 150% of the basal activity. In contrast, the 4-amide derivatives **263** and **266** (scaffold C) had no effect on the ATPase activity resulting in values near the basal activity. Only low stimulation was found for the derivatives **267**, **270**, **271** and **273** (scaffold D) which lack an aromatic function at position 2. Solely the dimer **276** (scaffold E) inhibited the ATPase activity. A more detailed investigation with several concentrations of the stimulating compound **259** or the deactivating compound **276** in co-administration of 1 µM Ko143 or 1 µM Quercetin illustrated the strong potencies of both compounds: Compound **259** reversed the deactivating effect of 1 µM Ko143 at a concentration of 3 µM whereas compound **276** reversed the stimulating effect of 1 µM Quercetin even at a concentration of only 5 nM.

9.2 SAR of inhibitors of ABCG2

In this paragraph the structural features of a potent inhibitor of ABCG2 based on a quinazoline scaffold are briefly discussed and summarized. First, the SAR of derivatives with 2-phenyl-4-anilinoquinazoline scaffold and substitution at the aromatic moieties at position 2 and 4 will be discussed (Figure 115). These modifications have been performed in compounds discussed in project I and III. The derived patterns were found to be valid to compounds of some other projects as well.

In general, substitution at *ortho* position led to decreased inhibitory potencies throughout this study and confirmed the results of previous research.[196,198] A possible reason for this finding could be the reduced planarity of the molecule caused by an increased sterical hindrance arising from an *ortho* substituent leading to a stronger twist among the corresponding aromatic cores. In this regard, several studies have found that planarity is required for potent inhibitors of ABCG2.[66,112,90] Other studies suggested that $\pi - \pi$ stacking of aromatic cores could increase the binding to ABCG2, which is most effective in a planar molecule.[211]

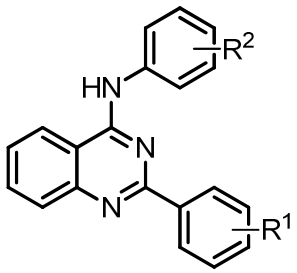

Good: 4-NO_2; 4-CN*; 3-NO_2; 3-CN; 3-OH*; 3-CF_3*; 3-F*; 3-$NHCOCH_3$*; 3-NO_2,4-OH*; 3,4-OMe; 3-OMe,4-Br*;

Poor: 4-F*; 4-OMe; CO_2H*; Me*; *ortho*-Substitution; 3,5-OMe*

} **R^1 or R^2**

(*): Substituents have been tested at R^2 only.

Figure 115: Substitution pattern of a substituted 2-phenyl-4-anilinoquinazoline scaffold. Most substitutions were carried out at R^2 but very similar potencies resulted when swapping substituents between the aromatic cores.

In particular, for the majority of the compounds large differences of IC_{50} values between *meta* and *para* derivatives with the same substituent were found. The substituent position not only had a great impact on the inhibitory potency but also on the interaction/binding of a compound with/to ABCG2. This will be discussed in more detail in chapter 9.3.

Electron withdrawing groups like nitro and cyano have proven to lead to considerably higher potencies in *para* position than in *meta (*e.g. compound **2/89**, **4/5**). This effect was more pronounced on the aniline moiety at R^2 than at R^1 (e.g. compound pairs **126/132** and **127/144**) and led to excellent IC_{50} values below 100 nM for the before mentioned derivatives **2**, **89**, **4** and **5**. In contrary, electron donating groups like methoxy often exhibited a decreased inhibitory potency at *para* position (e.g. compound **11** and **12**). Hence, the potency of a compound is dependent on the position at the corresponding aromatic residue and also the electronic properties of the used substituent. Substituents containing HBA or HBD functions both led to potent compounds, regardless of their positions. Examples are for instance substitutions with nitro and hydroxy (see chapter 3.2). High inhibitory potencies were in particular observed in *meta* or *para* monosubstitution with nitro, cyano, hydroxy, or fluoro groups as well as disubstitution with 3,4-dimethoxy, 3-NO_2,4-OH and 3-OMe,4-Br functions. Regarding the substitution at R^1 and R^2, the collected data indicates an interchangeability of the substituents between the aromatic moieties, leading to mostly comparable inhibitory potencies (see chapter

3.2). Notably, the combination of nitro functions and 3,4-dimethoxy resulted in several highly potent inhibitors (see compound **111**, **127**, **143** and **144**) with IC_{50} values below 100 nM.

An overview of the most important modifications in the projects I-VI is illustrated in Figure 116. Firstly, it was found that the lack of aromatic substitution at R^1 decreased the inhibitory activity significantly. Examples are the compounds **267**-**274** (see chapter 8.2) that exhibited the greatest resemblance to the TKI gefitinib and yielded IC_{50} values that were mostly above 1 µM. Considering substitution at R^1, high inhibitory potencies were found for compounds with phenyl or pyridyl residues. However, the pyridyl group possessed an additional advantage over the phenyl group by leading to low cytotoxic effects and an improved solubility.

Secondly, the presence of a nitrogen atom at R^2 is highly preferable over a carbon atom. The resulting decrease in potency and loss of selectivity that was observed in the quinoline derivatives could be due to the higher basicity of the nitrogen atom at position 1 of the scaffold. Another reason could be the decreased planarity in the 2,4-substituted quinoline caused by the steric hindrance between the hydrogen atom at position 3 and the hydrogen atom on the aromatic moiety at R^1. As discussed above, planarity is one of the characteristics that is frequently found in potent inhibitors of ABCG2.

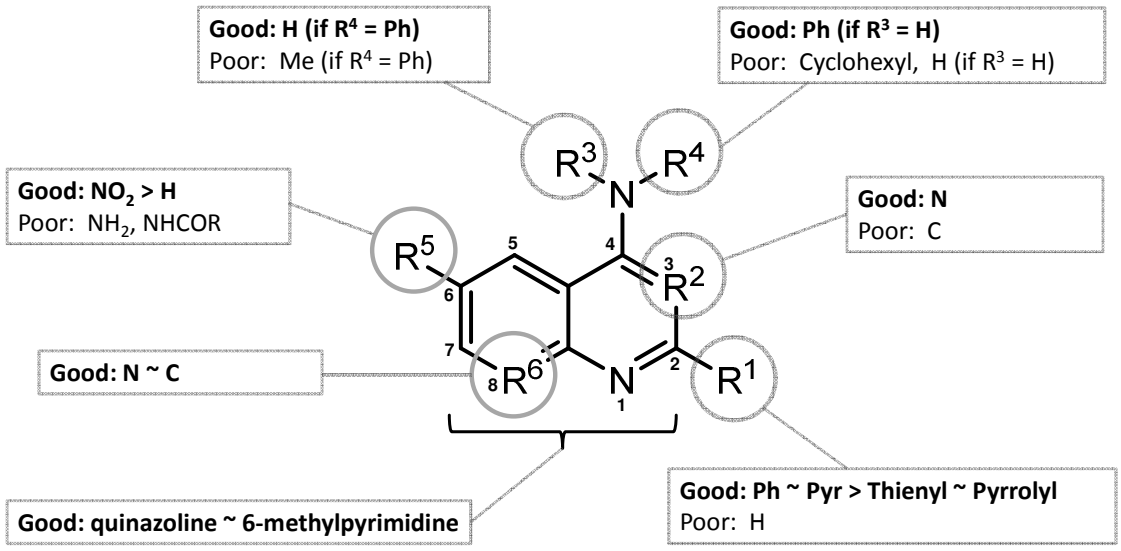

Figure 116: Structural features that are crucial for a potent inhibitor of ABCG2 containing a quinazoline scaffold. Good and poor substituents regarding the inhibitory potency toward ABCG2 are illustrated in the corresponding textbox.

Since most of the compounds contained an aniline linker at position 4 of the quinazoline scaffold (R^3: H; R^4: subst. Ph) the importance of this HBD function was investigated. The replacement of the hydrogen atom at R^3 by a methyl group decreased the inhibitory potency drastically. Hence, it was concluded that the HBD function of the aniline function in position 4 is crucial.

Further modification was carried out at R^5 introducing functions with different electronic and steric properties. Very high inhibitory potencies were determined for 6-nitro derivatives yielding the most active compounds of this work. Here, 29 derivatives were synthesized and almost all of them possessed IC_{50} values well below of 100 nM. On the one hand, the nitro function decreases the electron density at the aromatic core by negative mesomeric effects. On the other hand, it provides HBA functions *via* its oxygen atoms which could play a decisive factor for its high potency. On the contrary, decreased inhibitory potencies resulted from 6-amino functions. This group increases the electron density at the aromatic core and is able to interact *via* HBD functions with its environment. Although, they were significantly less potent than their 6-nitro analogues, the IC_{50} values were still below 1 µM. Structurally related drugs based on a quinazoline scaffold frequently contained ether functions at position 6 and/or 7, like the TKI gefitinib.

It is probable that HBAs at this region are beneficial for potent inhibition which is substantiated by the results of the 6-nitro derivatives in this work.

The introduction of a nitrogen atom at R^6 resulted in some interesting effects regarding the potency of the resulting pyrido[2,3-d]pyrimidine derivatives. In the case of substitution with a 2-phenyl moiety and a substituted aniline linker at position 4 an enantiotopic activity in relation to the corresponding quinazoline analogues was observed. Here, the inhibitory potency in a pyrido[2,3-d]pyrimidine derivative could be altered by exchanging nitrogen at R^6 with a carbon atom, meaning that the inhibitory potency was reversed after the exchange. In this subset several highly potent compounds were found which were superior to Ko143 and exhibited IC_{50} values below 200 nM. Beneficial substituents were methoxy, fluoro, trifluoromethyl and 3-cyano functions. Notably, the highest potency was determined for the unsubstituted derivative **162** (IC_{50}: 149 nM, see chapter 6.2) which previously resulted in a low potency for the quinazoline derivative (compound **1**, IC_{50}: 882 nM). Additionally, a high selectivity toward ABCG2, a low intrinsic cytotoxicity and an enhanced watersolubility compared to a quinazoline scaffold was found for this class of compounds.

Investigations of the importance of the left aromatic condensed core in the quinazoline scaffold highlighted some more interesting SAR regarding its contribution to inhibitory potency toward ABCG2. It was observed that the replacement of the left aromatic ring by a methyl function had only negligible effect on the inhibitory potency. Thus, the resulting 2,4-substituted 6-methylpyrimidine derivatives possessed an extraordinarily high ligand efficiency containing only 3 aromatic cores. This comes with a considerably low calculated logP value and a comparable inhibitory potency toward ABCG2 in comparison to their quinazoline analogues.

9.3 Interaction of inhibitors with ABCG2

Since the discovery of ABCG2 in 1998 some effort has been undertaken to collect information regarding the function of the transport protein. One approach was to utilize homology models based on related X-ray resolution structures, like the recently published ABCG5-ABCG8 heterodimer, which can help to validate experimental data and develop new ideas. [170,178] Here, a possible explanation for the broadened substrate spectrum in the mutant ABCG2 R482G isoform was given by an *in silico* docking study that aimed to identify possible substrate binding pockets in the transport protein. According to several experimental studies, it is known that ABCG2 possesses multiple binding sites for substrates and inhibitors. [66,112,167,209,212] Although the binding of substrates to ABCG2 is comparatively well explored, for instance by mutagenesis, photo-affinity labelling and a few binding studies, little is known about the binding of inhibitors.[93,109,117,120,165,213] Indeed, the need for new studies investigating the polyspecificity and drug binding in ABCG2, in particular in the presence of inhibitors, persists and needs to attract more notice in the future.

This study aimed to find patterns in different cell based assays that will help to draw conclusions regarding the binding and interaction of inhibitors with ABCG2. Also, the collected data can be utilized to develop new inhibitors with the desired properties for further studies.

The investigation of the interaction between selected inhibitors and ABCG2 was carried out in several functional cell based assays including the MDR reversal and cytotoxicity assay, enzyme kinetic studies, conformation sensitive 5D3 antibody binding and an investigation of the ATPase activity. The compounds were picked by criteria like a high inhibitory potency, which was determined in the Hoechst 33342 accumulation assay, or according to the results of previous functional assays.

First and foremost, it is very likely that most of the investigated compounds are inhibitors of ABCG2 and not substrates. This assertion was substantiated by fluorescence spectrometric investigations of some potent fluorophores containing a quinazoline scaffold (see chapter 8.10) and also by means of a flow cytometric analysis on a FACS (data not shown) and confocal microscopy (see chapter 8.9). Moreover, the MTT cytotoxicity data showed for most compounds a very similar half maximal growth

inhibition (GI_{50}) in the ABCG2 overexpressing and parental cells. If the compounds were subject to transport by ABCG2, a considerably lower cytotoxicity would be expected for the ABCG2 overexpressing cells. Also, a large portion of test-compounds reached a maximum inhibition between 80 and 110% in comparison to standard inhibitor Ko143, which suggests that they are no "partial inhibitors".

Regarding the selectivity toward ABCG2 it was found that the presence of methoxy groups led to an increase of the inhibition toward ABCB1 and ABCC1, the other two major MDR transport proteins. Here, the potency toward ABCB1 was more pronounced than toward ABCC1. Moreover, a higher selectivity toward ABCG2 resulted from the presence of nitro functions that were found to lead to potent inhibitors of ABCG2. Notably, some compound classes like the 2,4-substituted pyrido[2,3-d]pyrimidines in project IV and the 2,4-substituted 6-nitroquinazolines of project V were extraordinarily high selective for ABCG2.

One key point in this study was the investigation of several compounds regarding their ability to reverse the MDR in a MDR reversal assay. The assay was carried out by co-administration of the compounds with the cytostatic drugs Hoechst 33342, SN-38 and MX leading to full sensitization of the ABCG2 overexpressing cells toward the corresponding drugs for each compound. Due to several different concentrations that were used for SN-38 as well as for the corresponding compound, an EC_{50} value could be calculated characterizing the potency of a compound. In comparison to the IC_{50} values obtained from the Hoechst 33342 accumulation assay, the calculated EC_{50} values were either similar or frequently even lower, suggesting a higher potency of the compounds. An explanation for the difference in both types of assays could be different affinities of the substrates SN-38 and Hoechst 33342. Indeed, this is probably not the only reason since very similar IC_{50} values have been obtained with both cytostatic drugs as presented in chapter 3.5, which points to other factors like a different passive diffusion coefficient of the substrates. Indeed, the tendencies of the inhibitory potencies in the Hoechst 33342 assay were well reflected in the results of the MDR reversal assay, illustrated for instance by compounds **162**, **167** and **169** (see chapter 6.5). The pEC_{50} values obtained with SN-38 showed a good correlation with those of MX ($r^2 = 0.96$; outliers, namely compound **5** and **162**, were excluded). However, the EC_{50} values resulting with SN-38 were roughly

2.6 times higher, which can be attributed to the previously mentioned factors like a different passive diffusion coefficient.

The enzyme kinetic investigation of the interaction between different compounds and the substrate Hoechst 33342 shed some light on the binding modes at ABCG2. By utilizing the kinetic methods according to Cornish-Bowden and Lineweaver-Burk it was concluded that most compounds exhibited a non-competitive interaction with Hoechst 33342, including the drugs Ko143, gefitinib and elacridar. Hence, the binding sites of the compounds are different from that of the substrate Hoechst 33342. Among these, many compounds showed non-competitive interaction of the "mixed type", meaning that they are able to influence the active site, probably via a conformational allosteric interaction. Also, it is possible that they bind near the Hoechst 33342 binding pocket, which would explain the strong impact of some "mixed-type"-inhibitors on the active site. Another reasonable mechanism could be a concentration depended binding of a compound to different high- and low-affinity binding sites as suggested by Pozza *et al*. who investigated the quenching of the intrinsic fluorescence of purified ABCG2.[110] This theory is substantiated by some compounds giving bell-shaped curves in the ATPase assay which is discussed below. High portions of competitive interaction with Hoechst 33342 were frequently found in compounds bearing *para* substituents, in particular for those containing lipophilic substituents like iodine, bromine and chlorine atoms (see compounds **17**, **21** and **23**, chapter 3.6 and compounds **112** and **150**, chapter 5.6). According to the kinetic data, some of them could bind at the same binding pocket as Hoechst 33342. In large part, the obtained results are in agreement with those of other functional assays described below.

Yet another possibility to distinguish the interactions of different inhibitors with ABCG2 is by studying the conformational change they induce when binding to the protein. For this purpose the conformation sensitive 5D3 antibody was used and Ko143 set as control inhibitor resulting in 100% labelling. A high conformational change is expected for inhibitors of ABCG2 whereas substrates like Hoechst 33342 or Quercetin lead to a lower amount of labelling with the antibody.[201] As expected, a low labelling was found for the substrates Hoechst 33342 (35%) and quercetin (40%) but a high labelling for the inhibitors elacridar (89%) and gefitinib (66%). For most of the investigated compounds of this study a labelling of more than 50% was observed. A high rate of labelling with

5D3 antibody between 70-90% resulted particularly for compounds that exhibited a high competitive portion in the interaction type investigation (e.g. compound **5**, **17**, **23**, **54**, **82** and **139**). Among these, a strong correlation between a high degree of labelling and a *para* substitution with higher halogen atoms or other functions like nitro and cyano was found. Moreover, no apparent relationship between the IC_{50} value of a compound and the degree of labelling was observed at 10 µM. Hence, the 5D3 assay may be utilized to provide information of the interaction of an inhibitor with ABCG2 and possibly to identify binding pockets. The collected data was mostly in accordance to the patterns that were found in the other functional assays that are discussed in this chapter.

Further studies of the vanadate sensitive ATPase activity, which is associated with the transport activity of an ABC transport protein, provided some more insights into the interaction of different inhibitors with ABCG2. For instance, the investigation of the ATPase activity can help to distinguish between substrates and inhibitors of ABCG2. A high stimulation of the ATPase activity is expected for substrates like quercetin whereas inhibitors often led to deactivation, like Ko143. However, this distinction is oversimplified and has been proven not to apply to every inhibitor/substrate. The well-known substrate Hoechst 33342 for instance showed a concentration dependent biphasic trend of the ATPase activity leading to deactivation at higher concentration (see chapter 3.8) and substantiated the results from another research group.[214] Regarding inhibitors of ABCG2 several compounds have been reported to stimulate the ATPase activity, some even to a considerable extent.[209,215] In this study, different effects on ATPase activity could be observed for the investigated compounds. They contained deactivating compounds like Ko143 (e.g. **17**, **23**, **130** and **276**), strongly stimulating compounds (e.g. **4**, **57**, **131**, **170**, **178** and **244**) and compounds that had negligible effect on the ATPase activity (e.g. **5**, **19**, **21**, **58**, **61**, **105**, **162**, **167**, **230**, **263** and **266**). A closer look at the substitution patterns showed that in many cases deactivation or only a low impact on ATPase activity was obtained by *para* substituted and strong stimulation by *meta* substituted derivatives. This phenomenon is for instance clearly seen by the *meta*/*para* compound pairs **130/131** and **143/144** (see chapter 5.8). Compounds containing a 3,4-dimethoxy group like **144**, **149** and **150** (see chapter 5.8) did frequently stimulate the ATPase activity at low concentration and deactivate it at high concentrations which led to bell-shaped concentration-activity curves. As explained previously, it is suggested that

those compounds bind in a concentration dependent matter to an activating high affinity and a deactivating low affinity binding pocket.[110,206] The data also suggests that the lipophilicity of a substituent can influence the ATPase activity. Bulky alkyl substituents were for instance found to result in a sub-basal activity (compared in chapter 5.8 for compounds **113**, **114**, **117**, **118** and **119**). This is in accordance with a study of Egido *et. al.* where lipophilic compounds led to inhibition of ATPase activity and hydrophilic ones stimulated the ATPase activity.[216] Similar observations were made for the less lipophilic compounds of project II and IV, which mostly stimulated the ATPase activity.[217] More lipophilic scaffolds (e.g. project I and III) or functions like iodo and *tert*-butyl esters, as well as substitution in *para* position, frequently resulted in low stimulation or deactivation.

Interestingly, most of the data collected in the kinetic investigation and the 5D3 binding study showed a good correlation with the ATPase activity. In the case of high competitive portions toward Hoechst 33342, an increased labelling by the conformation sensitive 5D3 antibody was frequently observed leading to an ATPase activity at the basal level or lower.

It is surprising, that the interaction of an inhibitor with ABCG2 can be altered considerably by minor modifications of the substitution pattern, as shown by the *meta* and *para* derivatives. Possible reasons for this could be due to the different physicochemical properties (e.g. lipophilicity), a differing sterical demand or changed interactions of the inhibitor with the protein at the binding pocket(s).

In this comprehensive study of inhibitors of ABCG2 that are based on a quinazoline scaffold, a large amount of interesting data was collected about the SAR and also the interaction of the inhibitors with the transport protein. In six different projects several classes of compounds with systematic varied substitution patterns were investigated and the results categorized to find patterns among the functional assays. Hereby, some more light can be shed on the yet unclear function and complex mechanisms of ABCG2. The collected data can also help to develop further highly potent, nontoxic and selective inhibitors of ABCG2 that are promising candidates for clinical trials.

10 Experimental section

10.1 Chemistry

10.1.1 Synthesis procedures and affiliated data

10.1.1.1 Synthesis of 4-Substituted-2-phenylquinazolines and -quinolines

General procedure for the preparation of 4-anilino-2-phenylquinazoline derivatives
4-chloro-2-phenylquinazoline (1 mmol) and a substituted aniline (1 mmol) were added to a 50 mL microwave tube and suspended in 25 mL isopropanol. The tube was sealed and the reaction mixture stirred under 100 watt microwave irradiation at 110 °C for 30 min. Completion of the reaction was monitored by TLC. After cooling, a precipitate was formed and filtered off by suction. If no precipitate was formed, the solvent was removed by rotary evaporation and the obtained solids recrystallized from 75% EtOH. In the case of incomplete reaction, triethylamine (1 mmol) was added to the mixture to react with HCl generated after the nucleophilic substitution.

2-nitro-4-((2-phenylquinazolin-4-yl)amino)phenol (3)

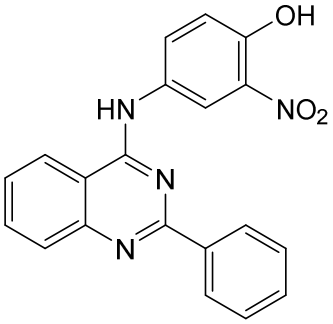

Molecular weight: 358.36 g/mol

The title compound was synthesized from 4-chloro-2-phenylquinazoline (241 mg, 1 mmol) and 4-amino-2-nitrophenol (154 mg, 1 mmol) as described in the general procedure above to yield **3** as yellow solid (229 mg, 60%), mp 283-284 °C (decomp.).

^{1}H NMR (500 MHz, DMSO-d_6) δ 11.63 (s, 1H), 11.30 (s, 1H), 8.89 (d, *J* = 8.3 Hz, 1H), 8.62 (d, *J* = 2.6 Hz, 1H), 8.42 (dt, *J* = 8.2, 1.1 Hz, 2H), 8.31 (d, *J* = 8.4 Hz, 1H), 8.13 – 7.96 (m, 2H), 7.86 – 7.76 (m, 1H), 7.76 – 7.66 (m, 1H), 7.67 – 7.56 (m, 2H), 7.34 (dd, *J* = 9.0, 0.9 Hz, 1H). **^{13}C NMR** (126 MHz, DMSO) δ 158.89, 157.56, 150.36, 141.61, 136.02, 135.84, 133.23, 132.33, 131.32, 129.25, 129.08, 128.71, 128.11, 124.45, 121.52, 120.67, 119.37, 112.95. **Anal. Calcd. for $C_{20}H_{14}N_4O_3$**: C, 67.03; H, 3.94; N, 15.63. Found: C, 66.85; H, 4.30; N, 15.52.

4-((2-phenylquinazolin-4-yl)amino)benzonitrile (5).

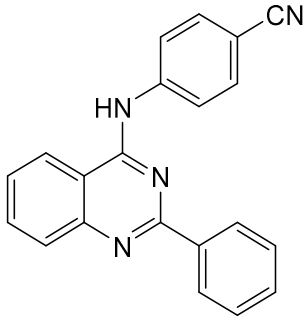

Molecular weight: 322.37 g/mol

The title compound was synthesized from 4-chloro-2-phenylquinazoline (241 mg, 1 mmol) and 4-cyanoaniline (118 mg, 1 mmol) as described in the general procedure above to yield **5** as pale yellow solid (235 mg, 73%), mp 299-302 °C (decomp.).
^{1}H NMR (500 MHz, DMSO-d_6) δ 11.57 (s, 1H), 8.95 (d, *J* = 8.3 Hz, 1H), 8.45 – 8.36 (m, 2H), 8.30 (d, *J* = 8.4 Hz, 1H), 8.21 – 8.12 (m, 2H), 8.12 – 8.03 (m, 1H), 8.02 – 7.92 (m, 2H), 7.86 – 7.76 (m, 1H), 7.72 – 7.65 (m, 1H), 7.65 – 7.57 (m, 2H). **^{13}C NMR** (126 MHz, DMSO) δ 159.08, 157.80, 143.23, 142.14, 135.84, 133.07, 132.94, 129.21, 129.12, 128.06, 124.66, 124.12, 122.56, 118.98, 113.37, 107.45. **Anal. Calcd for $C_{21}H_{14}N_4$**: C, 78.24; H, 4.38; N, 17.38. Found: C, 78.03; H, 4.61; N, 17.56.

4-((2-phenylquinazolin-4-yl)amino)phenol (6).

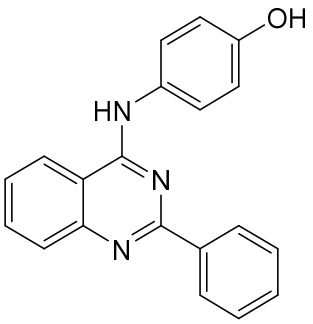

Molecular weight: 313.36 g/mol

The title compound was synthesized from 4-chloro-2-phenylquinazoline (241 mg, 1 mmol) and 3-aminophenol (109 mg, 1 mmol) as described in the general procedure above to yield **6** as bright yellow solid (255 mg, 81%), mp 335-336 °C (decomp.).
^{1}H NMR (500 MHz, DMSO-d_6) δ 11.53 (s, 1H), 9.77 (s, 1H), 8.87 (d, J = 8.3 Hz, 1H), 8.42 – 8.28 (m, 3H), 8.10 – 8.00 (m, 1H), 7.83 – 7.75 (m, 1H), 7.74 – 7.66 (m, 1H), 7.66 – 7.53 (m, 4H), 6.96 – 6.88 (m, 2H). **^{13}C NMR** (126 MHz, DMSO) δ 158.74, 157.21, 156.19, 135.81, 133.41, 131.69, 129.30, 129.10, 128.13, 128.09, 126.17, 124.57, 120.45, 115.35, 112.73. **Anal. Calcd for $C_{20}H_{15}N_3O$**: C, 76.66; H, 4.83; N, 13.41; Found: C, 76.72; H, 4.97; N, 13.34.

4-((2-phenylquinazolin-4-yl)amino)benzenesulfonyl fluoride (7).

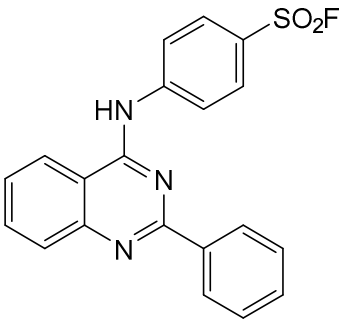

Molecular weight: 379.41 g/mol

The title compound was synthesized from 4-chloro-2-phenylquinazoline (241 mg, 1 mmol) and 4-aminobenzenesulfonyl fluoride (175 mg, 1 mmol) as described in the general procedure above to yield **7** as white solid (245 mg, 76%), mp 278-279 °C (decomp.).

^{1}H NMR (500 MHz, DMSO-d_6) δ 11.68 (s, 1H), 9.02 (t, *J* = 2.0 Hz, 1H), 8.95 (d, *J* = 8.3 Hz, 1H), 8.49 – 8.38 (m, 3H), 8.28 (d, *J* = 8.4 Hz, 1H), 8.14 – 8.04 (m, 1H), 8.05 – 7.98 (m, 1H), 7.92 (t, *J* = 8.1 Hz, 1H), 7.87 – 7.76 (m, 1H), 7.72 – 7.62 (m, 1H), 7.63 – 7.51 (m, 2H). **^{13}C NMR** (126 MHz, DMSO) δ 159.00, 157.86, 139.62, 135.69, 132.80, 131.97, 131.78, 131.09, 130.78, 129.07, 128.98, 127.96, 124.59, 124.43, 123.10, 122.71, 113.34. **Anal. Calcd for $C_{20}H_{14}FN_3O_2S$**: C, 63.31; H, 3.72; N, 11.08. Found: C, 63.68; H, 3.86; N, 10.99.

***N*-(3-((2-phenylquinazolin-4-yl)amino)phenyl)acetamide (8).**

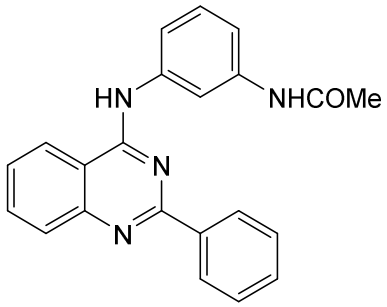

Molecular weight: 354.41 g/mol

The title compound was synthesized from 4-chloro-2-phenylquinazoline (241 mg, 1 mmol) and N-(3-aminophenyl)acetamide (150 mg, 1 mmol) as described in the general procedure above to yield **8** as white solid (135 mg, 38%), mp 291-293 °C. **^{1}H NMR** (500 MHz, DMSO-d_6) δ 11.46 (s, 1H), 10.22 (s, 1H), 8.88 (d, *J* = 8.3 Hz, 1H), 8.42 (dt, *J* = 8.3, 1.2 Hz, 2H), 8.32 (d, *J* = 8.3 Hz, 1H), 8.28 (t, *J* = 2.0 Hz, 1H), 8.13 – 8.02 (m, 1H), 7.87 – 7.76 (m, 1H), 7.75 – 7.65 (m, 1H), 7.61 (dd, *J* = 8.4, 7.0 Hz, 2H), 7.53 (dt, *J* = 7.5, 1.9 Hz, 1H), 7.48 – 7.36 (m, 2H), 2.09 (s, 3H). **^{13}C NMR** (126 MHz, DMSO) δ 168.64, 159.13, 157.46, 140.83, 139.88, 137.30, 135.85, 133.25, 131.89, 129.46, 129.01, 128.82, 128.10, 124.60, 121.01, 119.37, 117.08, 115.22, 112.87, 24.15. **Anal. Calcd. for $C_{22}H_{18}N_4O$**: C, 74.56; H, 5.12; N, 15.81. Found: C, 74.31; H, 5.26; N, 15.48.

***N*-(4-((2-phenylquinazolin-4-yl)amino)phenyl)acetamide (9).**

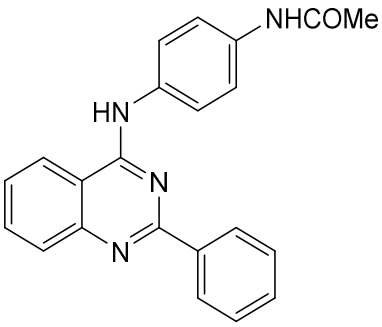

Molecular weight: 354.41 g/mol

The title compound was synthesized from 4-chloro-2-phenylquinazoline (241 mg, 1 mmol) and N-(4-aminophenyl)acetamide (150 mg, 1 mmol) as described in the general procedure above to yield **9** as white solid (163 mg, 46%), mp 238-240 °C. **^{1}H NMR** (500 MHz, DMSO-d_6) δ 11.40 (s, 1H), 10.18 (s, 1H), 8.84 (d, J = 8.3 Hz, 1H), 8.39 – 8.32 (m, 2H), 8.26 (d, J = 8.4 Hz, 1H), 8.06 (ddd, J = 8.4, 7.1, 1.3 Hz, 1H), 7.83 – 7.71 (m, 5H), 7.71 – 7.66 (m, 1H), 7.63 (dd, J = 8.3, 6.7 Hz, 2H), 2.08 (s, 3H). **^{13}C NMR** (126 MHz, DMSO) δ 168.51, 158.80, 157.52, 137.64, 135.73, 133.14, 131.95, 129.15, 129.08, 128.02, 124.85, 124.43, 123.56, 119.96, 119.07, 112.91, 24.14. **Anal. Calcd. for $C_{22}H_{18}N_4O$**: C, 74.56; H, 5.12 N, 15.81. Found: C, 74.69; H, 5.33; N, 15.78.

***N*-(3-(methylthio)phenyl)-2-phenylquinazolin-4-amine (10).**

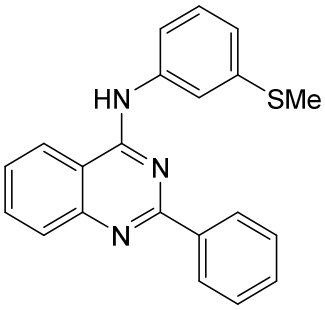

Molecular weight: 343.45 g/mol

The title compound was synthesized from 4-chloro-2-phenylquinazoline (241 mg, 1 mmol) and 3-(methylthio)aniline (139 mg, 1 mmol) as described in the general procedure above to yield **10** as pale yellow solid (243 mg, 71%), mp 138-139 °C. **^{1}H NMR** (600 MHz, DMSO-d_6) δ 10.56 (s, 1H), 8.71 (d, J = 8.1 Hz, 1H), 8.40 (d, J = 7.2 Hz, 2H), 8.04

(d, *J* = 8.1 Hz, 1H), 7.96 (d, *J* = 11.5 Hz, 2H), 7.70 (s, 2H), 7.56 (q, *J* = 6.9, 5.3 Hz, 3H), 7.42 (t, *J* = 7.9 Hz, 1H), 7.12 (d, *J* = 7.6 Hz, 1H), 2.54 (s, 3H). **^{13}C NMR** (151 MHz, DMSO) δ 158.47, 139.13, 138.59, 129.22, 128.81, 128.54, 127.08, 123.80, 122.30, 120.28, 119.57, 113.64, 99.68, 14.91. **Anal. Calcd. for $C_{21}H_{17}N_3S$**: C, 73.44; H, 4.99; N, 12.24. Found: C, 73.56; H, 4.84; N, 11.91

N-(3,4-dimethoxyphenyl)-2-phenylquinazolin-4-amine (13)

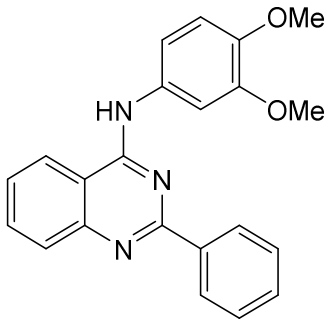

Molecular weight: 357.41 g/mol

The title compound was synthesized from 4-chloro-2-phenylquinazoline (241 mg, 1 mmol) and 3,4-dimethoxyaniline (153 mg, 1 mmol) as described in the general procedure above to yield **13** as bright yellow solid (171 mg, 48%), mp 135-137 °C. ^{1}H NMR (500 MHz, DMSO-d_6) δ 11.46 (s, 1H), 8.90 (d, *J* = 8.3 Hz, 1H), 8.48 – 8.38 (m, 2H), 8.34 (d, *J* = 8.4 Hz, 1H), 8.16 – 7.94 (m, 1H), 7.80 (s, 1H), 7.75 – 7.67 (m, 1H), 7.67 – 7.54 (m, 3H), 7.39 (dd, *J* = 8.7, 2.5 Hz, 1H), 7.09 (d, *J* = 8.7 Hz, 1H), 3.81 (d, *J* = 10.7 Hz, 6H). ^{13}C NMR (126 MHz, DMSO) δ 158.67, 158.14, 148.49, 146.02, 134.00, 132.05, 131.27, 128.66, 128.33, 126.59, 123.46, 114.91, 113.75, 111.89, 108.00, 55.92, 55.67. Anal. Calcd. for $C_{22}H_{19}N_3O_2$: C, 73.93; H, 5.36; N, 11.76. Found: C, 73.63; H, 5.52; N, 11.77.

***N*-(3,5-dimethoxyphenyl)-2-phenylquinazolin-4-amine (14)**

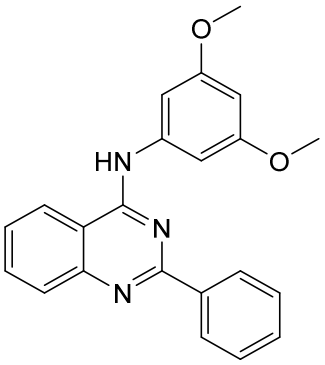

Molecular weight: 357.41 g/mol

The title compound was synthesized from 4-chloro-2-phenylquinazoline (241 mg, 1 mmol) and 3,5-dimethoxyaniline (153 mg, 1 mmol) as described in the general procedure above to yield **14** as yellow solid (279 mg, 78%),.mp 230-231 °C. **^{1}H NMR** (600 MHz, DMSO-d_6) δ 11.25 (s, 1H), 8.90 (d, J = 8.3 Hz, 1H), 8.48 – 8.39 (m, 2H), 8.31 (d, J = 8.4 Hz, 1H), 8.06 (t, J = 7.7 Hz, 1H), 7.80 (t, J = 7.7 Hz, 1H), 7.69 (t, J = 7.3 Hz, 1H), 7.63 (t, J = 7.6 Hz, 2H), 7.21 (d, J = 2.2 Hz, 2H), 6.46 (t, J = 2.2 Hz, 1H), 3.79 (s, 6H). **^{13}C NMR** (151 MHz, DMSO) δ 160.78, 159.29, 157.88, 139.45, 136.04, 133.41, 129.52, 129.39, 128.39, 124.85, 114.98, 113.42, 102.67, 98.90, 55.89. **Anal. Calcd. for $C_{22}H_{19}N_3O_2$**: C, 73.93; H, 5.36 N, 11.76. Found: C, 74.02; H, 5.57; N, 11.51.

***N*-(3-fluoro-4-methoxyphenyl)-2-phenylquinazolin-4-amine (15).**

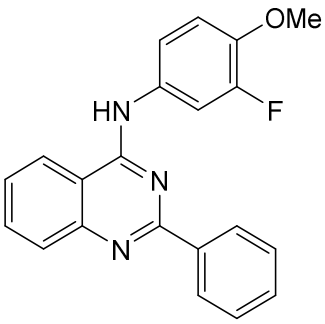

Molecular weight: 345.38 g/mol

The title compound was synthesized from 4-chloro-2-phenylquinazoline (241 mg, 1 mmol) and 3-fluoro-4-methoxyaniline (141 mg, 1 mmol) as described in the general

procedure above to yield **15** as light yellow solid (192 mg, 56%), mp 262-263 °C (decomp.). **^{1}H NMR** (500 MHz, DMSO-d_6) δ 11.65 (s, 1H), 8.95 (d, J = 8.3 Hz, 1H), 8.43 – 8.29 (m, 3H), 8.11 – 8.02 (m, 1H), 7.83 (dd, J = 13.1, 2.5 Hz, 1H), 7.82 – 7.77 (m, 1H), 7.73 – 7.67 (m, 1H), 7.67 – 7.60 (m, 3H), 7.31 (t, J = 9.3 Hz, 1H), 3.90 (s, 3H). **^{13}C NMR** (126 MHz, DMSO) δ 158.93, 157.59, 151.75, 149.81, 145.45 (d, J = 10.4 Hz), 141.44, 135.86, 133.23, 132.40, 130.17 (d, J = 9.5 Hz), 129.15, 128.13, 124.52, 121.38, 120.65, 113.77 – 113.76 (d), 112.91, 112.75 (d, J = 21.9 Hz), 56.41. **Anal. Calcd. for $C_{21}H_{16}FN_3O$**: C, 73.03; H, 4.67; N, 12.17. Found: C, 72.70; H, 4.84; N, 12.38.

***N*-(4-bromo-3-methoxyphenyl)-2-phenylquinazolin-4-amine (16).**

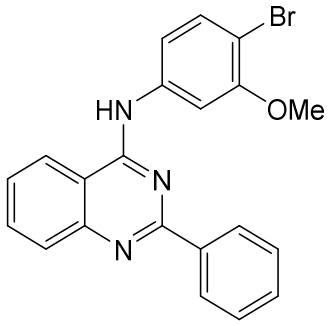

Molecular weight: 406.28 g/mol

The title compound was synthesized from 4-chloro-2-phenylquinazoline (241 mg, 1 mmol) and 4-bromo-3-methoxyaniline (202 mg, 1 mmol) as described in the general procedure above to yield **16** as yellow solid (280 mg, 69%), mp 276-278 °C (decomp.). **^{1}H NMR** (500 MHz, DMSO-d_6) δ 11.20 (s, 1H), 8.85 (d, J = 8.3 Hz, 1H), 8.52 – 8.31 (m, 2H), 8.22 (d, J = 8.4 Hz, 1H), 8.06 (t, J = 7.8 Hz, 1H), 7.89 – 7.75 (m, 2H), 7.74 – 7.54 (m, 4H), 3.90 (s, 3H). **^{13}C NMR** (151 MHz, DMSO) δ 158.90, 157.69, 155.42, 138.56, 135.72, 132.78, 129.16, 129.09, 128.06, 124.47, 117.43, 114.66, 113.16, 108.65, 56.44. **Anal. Calcd. for $C_{21}H_{16}BrN_3O$**: C, 62.08; H, 3.97; N, 10.34. Found: C, 61.81; H, 4.23; N, 10.29.

***N*-(4-iodo-3-methylphenyl)-2-phenylquinazolin-4-amine (17).**

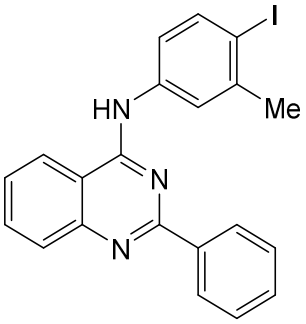

Molecular weight: 437.28 g/mol

The title compound was synthesized from 4-chloro-2-phenylquinazoline (241 mg, 1 mmol) and 4-iodo-3-methylaniline (233 mg, 1 mmol) as described in the general procedure above to yield **17** as beige solid (224 mg, 51%), mp 274-276 °C (decomp.). **^{1}H NMR** (500 MHz, DMSO-d_6) δ 11.48 (s, 1H), 8.91 (d, J = 8.4 Hz, 1H), 8.43 – 8.36 (m, 2H), 8.33 (d, J = 8.5 Hz, 1H), 8.12 – 8.01 (m, 1H), 7.94 (d, J = 8.5 Hz, 1H), 7.88 (d, J = 2.5 Hz, 1H), 7.83 – 7.75 (m, 1H), 7.74 – 7.66 (m, 1H), 7.66 – 7.58 (m, 2H), 7.52 (dd, J = 8.5, 2.6 Hz, 1H), 2.44 (s, 3H). **^{13}C NMR** (126 MHz, DMSO) δ 158.85, 157.54, 141.24, 138.74, 137.69, 135.78, 133.12, 129.19, 129.11, 128.06, 125.38, 124.49, 123.57, 121.67, 113.07, 97.31, 27.76. **Anal. Calcd. for $C_{21}H_{16}IN_3$**: C, 57.68; H, 3.69; N, 9.61. Found: C, 57.96; H, 3.82; N, 9.51.

***N*-(3-fluorophenyl)-2-phenylquinazolin-4-amine (18).**

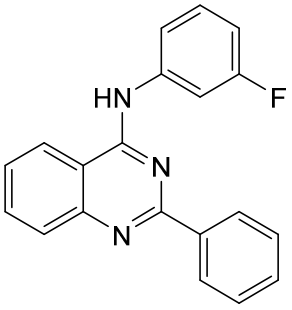

Molecular weight: 315.35 g/mol

The title compound was synthesized from 4-chloro-2-phenylquinazoline (241 mg, 1 mmol) and 3-fluoroaniline (111 mg, 1 mmol) as described in the general procedure above to yield **18** as pale yellow solid (269 mg, 85%), mp 298-299 °C (decomp.). **^{1}H NMR** (500

MHz, DMSO-d_6) δ 11.59 (s, 1H), 8.96 (d, *J* = 8.6 Hz, 1H), 8.39 (dq, *J* = 7.1, 1.5 Hz, 2H), 8.35 (d, *J* = 8.9 Hz, 1H), 8.12 – 8.01 (m, 1H), 7.90 – 7.77 (m, 2H), 7.77 – 7.72 (m, 1H), 7.72 – 7.66 (m, 1H), 7.63 (t, *J* = 7.5 Hz, 2H), 7.56 (td, *J* = 8.2, 6.7 Hz, 1H), 7.16 (td, *J* = 8.5, 2.6 Hz, 1H). **^{13}C NMR** (126 MHz, DMSO) δ 162.92, 160.99, 159.15, 157.59, 139.08 (d, *J* = 6.3 Hz), 135.87, 133.14, 130.38 (d, *J* = 9.2 Hz), 129.19, 129.08, 128.10, 124.65, 120.17, 113.03, 112.74 (d, *J* = 16.3 Hz), 111.29 (d, *J* = 24.3 Hz).**Anal. Calcd. for $C_{20}H_{14}FN_3$**: C, 76.18; H, 4.48; N, 13.33. Found: C, 76.54; H, 4.60; N, 13.08.

***N*-(4-fluorophenyl)-2-phenylquinazolin-4-amine (19).**

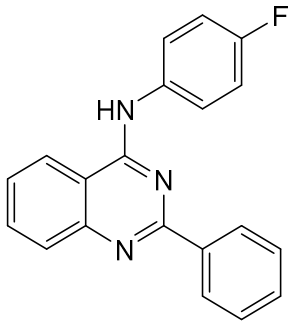

Molecular weight: 315.35 g/mol

The title compound was synthesized from 4-chloro-2-phenylquinazoline (241 mg, 1 mmol) and 4-fluoroaniline (111 mg, 1 mmol) as described in the general procedure above to yield **19** as beige solid (213 mg, 68%), mp 271-272 °C (decomp.). **^{1}H NMR** (500 MHz, DMSO-d_6) δ 11.52 (s, 1H), 8.89 (d, *J* = 8.3 Hz, 1H), 8.43 – 8.34 (m, 2H), 8.30 (d, *J* = 8.7 Hz, 1H), 8.13 – 7.99 (m, 1H), 7.97 – 7.84 (m, 2H), 7.85 – 7.75 (m, 1H), 7.74 – 7.65 (m, 1H), 7.64 – 7.54 (m, 2H), 7.44 – 7.32 (m, 2H). **^{13}C NMR** (126 MHz, DMSO) δ 161.01 – 159.08 (J = 233 Hz) , 159.15, 157.51, 141.64, 135.80, 133.53, 133.16, 132.26, 129.24 – 129.06 (J = 21,7 Hz), 128.04, 126.68 – 126.62 (J = 7,9 Hz), 124.62, 121.35, 115.66 – 115.48 (22,6 Hz), 112.90. **Anal. Calcd. for $C_{20}H_{14}FN_3$**: C, 76.18; H, 4.48; N, 13.33. Found: C, 76.32; H, 4.87; N, 13.12.

***N*-(4-chlorophenyl)-2-phenylquinazolin-4-amine (21)**

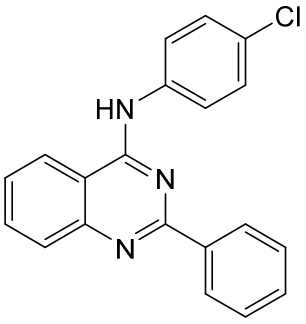

Molecular weight: 331.80 g/mol

The title compound was synthesized from 4-chloro-2-phenylquinazoline (241 mg, 1 mmol) and 4-chloroaniline (128 mg, 1 mmol) as described in the general procedure above to yield **21** as pale yellow solid (227 mg, 69%), mp 288-289 °C (decomp.). **^{1}H NMR** (500 MHz, DMSO-d_6) δ 11.54 (s, 1H), 8.91 (d, J = 8.4 Hz, 1H), 8.45 – 8.34 (m, 2H), 8.31 (d, J = 8.5 Hz, 1H), 8.15 – 8.01 (m, 1H), 7.99 – 7.86 (m, 2H), 7.87 – 7.75 (m, 1H), 7.77 – 7.66 (m, 1H), 7.66 – 7.47 (m, 4H). **^{13}C NMR** (126 MHz, DMSO) δ 159.08, 157.93, 150.63, 138.44, 138.32, 133.47, 130.45, 128.59, 128.52, 128.29, 128.04, 127.32, 126.17, 123.84, 123.14, 114.10. **Anal. Calcd. for $C_{20}H_{14}ClN_3$**: C, 72.40; H, 4.25; N, 12.66. Found: C, 72.17; H, 4.39; N, 12.58.

***N*-(3-iodophenyl)-2-phenylquinazolin-4-amine (22).**

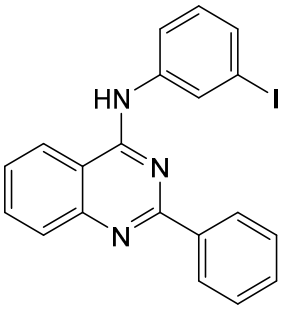

Molecular weight: 423.26 g/mol

The title compound was synthesized from 4-chloro-2-phenylquinazoline (241 mg, 1 mmol) and 3-iodoaniline (219 mg, 1 mmol) as described in the general procedure above to yield **22** as pale yellow solid (145 mg, 34%), mp 226-227 °C. **^{1}H NMR** (500 MHz,

DMSO-d_6) δ 11.51 (s, 1H), 8.91 (d, J = 8.3 Hz, 1H), 8.49 – 8.38 (m, 3H), 8.32 (d, J = 8.4 Hz, 1H), 8.12 – 8.02 (m, 1H), 7.93 – 7.84 (m, 1H), 7.84 – 7.76 (m, 1H), 7.73 – 7.65 (m, 2H), 7.65 – 7.57 (m, 2H), 7.32 (t, J = 8.0 Hz, 1H). **^{13}C NMR** (126 MHz, DMSO) δ 158.96, 157.42, 142.00, 138.74, 135.81, 134.41, 133.16, 132.70, 130.71, 129.20, 129.03, 128.06, 124.55, 123.36, 121.70, 113.02, 94.03. **Anal. Calcd. for $C_{20}H_{14}IN_3$**: C, 56.76; H, 3.33; N, 9.93. Found: C, 56.38; H, 3.68; N, 10.04.

***N*-(4-iodophenyl)-2-phenylquinazolin-4-amine (23).**

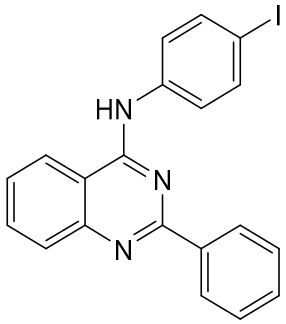

Molecular weight: 423.26 g/mol

The title compound was synthesized from 4-chloro-2-phenylquinazoline (241 mg, 1 mmol) and 4-iodoaniline (219 mg, 1 mmol) as described in the general procedure above to yield **23** as pale yellow solid (166 mg, 39%), mp 271-272 °C (decomp.). **^{1}H NMR** (500 MHz, DMSO-d_6) δ 11.50 (s, 1H), 8.91 (d, J = 8.4 Hz, 1H), 8.47 – 8.35 (m, 2H), 8.31 (d, J = 8.4 Hz, 1H), 8.11 – 8.00 (m, 1H), 7.94 – 7.83 (m, 2H), 7.83 – 7.75 (m, 1H), 7.76 – 7.66 (m, 3H), 7.66 – 7.56 (m, 2H). **^{13}C NMR** (126 MHz, DMSO) δ 159.17, 158.03, 142.34, 137.83, 137.43, 136.14, 133.33, 132.90, 129.43, 129.29, 128.41, 126.57, 124.50, 122.06, 113.26, 91.09. **Anal. Calcd. for $C_{20}H_{14}IN_3$**: C, 56.76; H, 3.33; N, 9.93. Found: C, 56.65; H, 3.62; N, 9.91.

methyl 4-((2-phenylquinazolin-4-yl)amino)benzoate (24).

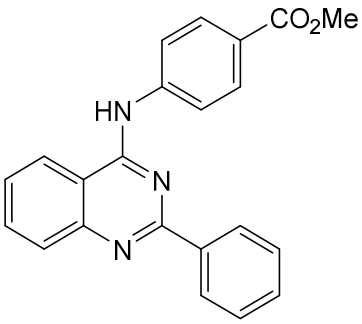

Molecular weight: 355.40 g/mol

The title compound was synthesized from 4-chloro-2-phenylquinazoline (241 mg, 1 mmol) and methyl 3-aminobenzoate (193 mg, 1 mmol) as described in the general procedure above to yield **24** as white solid (195 mg, 55%), mp 273-275 °C (decomp.). **^{1}H NMR** (500 MHz, DMSO-d_6) δ 10.11 (s, 1H), 8.61 (d, J = 8.4 Hz, 1H), 8.47 (d, J = 7.3 Hz, 2H), 8.20 (d, J = 8.4 Hz, 2H), 8.07 (d, J = 8.3 Hz, 2H), 7.90 (d, J = 4.1 Hz, 2H), 7.65 (t, J = 5.8 Hz, 1H), 7.54 (q, J = 8.9, 7.9 Hz, 3H), 3.86 (s, 3H). **^{13}C NMR** (126 MHz, DMSO) δ 166.06, 159.04, 157.86, 150.78, 144.26, 138.21, 133.63, 130.53, 130.08, 128.66, 128.35, 128.08, 126.34, 123.95, 123.27, 121.12, 114.29, 52.01, 40.20. **Anal. Calcd. for $C_{22}H_{17}N_3O_2$**: C, 74.35; H, 4.82; N, 11.82. Found: C, 74.29; H, 5.13 N, 11.43.

***tert*-butyl 4-((2-phenylquinazolin-4-yl)amino)benzoate (25).**

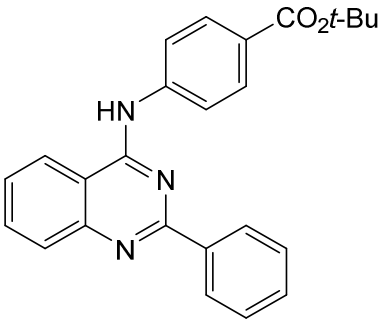

Molecular weight: 397.48 g/mol

The title compound was synthesized from 4-chloro-2-phenylquinazoline (241 mg, 1 mmol) and tert-butyl 3-aminobenzoate (193 mg, 1 mmol) as described in the general procedure above to yield **25** as pale yellow solid (302 mg,76%), mp 328- 330 °C (decomp.). **^{1}H NMR** (600 MHz, DMSO-d_6) δ 11.44 (s, 1H), 8.91 (t, J = 7.8 Hz, 1H), 8.47

– 8.35 (m, 2H), 8.28 (d, *J* = 7.9 Hz, 1H), 8.12 – 7.98 (m, 5H), 7.81 (dd, *J* = 9.2, 6.2 Hz, 1H), 7.68 (t, *J* = 7.2 Hz, 1H), 7.64 (dd, *J* = 8.2, 6.5 Hz, 2H), 1.57 (s, 9H). **^{13}C NMR** (126 MHz, DMSO) δ 166.91, 164.61, 158.99, 157.78, 141.68, 135.74, 132.92, 130.08, 129.81, 129.18, 129.10, 128.13, 127.99, 124.52, 123.43, 122.20, 113.25, 80.86, 27.98. **Anal. Calcd. for $C_{25}H_{23}N_3O_2$**: C, 75.55; H, 5.83; N, 10.57. Found: C, 75.43; H, 5.89 N, 10.87.

4-((2-phenylquinazolin-4-yl)amino)benzoic acid (26).

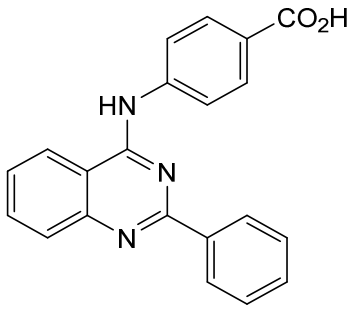

Molecular weight: 341.37 g/mol

The title compound was synthesized from 4-chloro-2-phenylquinazoline (241 mg, 1 mmol) and 4-aminobenzoic acid (137 mg, 1 mmol) as described in the general procedure above to yield **26** as light yellow solid (254 mg, 74%), mp 336-337 °C (decomp.). **^{1}H NMR** (600 MHz, DMSO-d_6) δ 11.98 (s, 1H), 11.79 (s, 1H), 9.03 (d, *J* = 8.3 Hz, 1H), 8.43 (d, *J* = 7.6 Hz, 3H), 8.25 – 7.93 (m, 5H), 7.81 (t, *J* = 7.7 Hz, 1H), 7.66 (dt, *J* = 36.7, 7.5 Hz, 3H). **^{13}C NMR** (151 MHz, DMSO) δ 166.92, 159.17, 157.47, 141.35, 136.03, 133.33, 130.05, 129.45, 129.14, 128.22, 128.04, 124.89, 123.95, 113.11. **Anal. Calcd. for $C_{21}H_{15}N_3O_2$**: C, 73.89; H, 4.43; N, 12.31. Found: C, 74.26; H, 4.64 N, 12.10.

***N*-(3-ethynylphenyl)-2-phenylquinazolin-4-amine (27).**

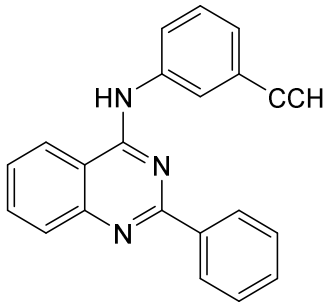

Molecular weight: 321.38 g/mol

The title compound was synthesized from 4-chloro-2-phenylquinazoline (241 mg, 1 mmol) and 3-ethynylaniline (117 mg, 1 mmol) as described in the general procedure above to yield **27** as pale yellow solid (213 mg, 66%), mp 222-224 °C. **^{1}H NMR** (500 MHz, DMSO-d_6) δ 11.77 (s, 1H), 9.01 (d, J = 8.3 Hz, 1H), 8.49 – 8.31 (m, 3H), 8.14 – 8.00 (m, 2H), 7.98 – 7.87 (m, 1H), 7.86 – 7.75 (m, 1H), 7.74 – 7.65 (m, 1H), 7.61 (t, J = 7.6 Hz, 2H), 7.54 (t, J = 7.9 Hz, 1H), 7.43 (dt, J = 7.6, 1.2 Hz, 1H), 4.27 (s, 1H). **^{13}C NMR** (126 MHz, DMSO) δ 157.23, 141.16, 137.44, 135.91, 133.31, 131.87, 129.33, 129.27, 129.18, 128.99, 128.12, 127.57, 125.09, 124.78, 122.07, 121.00, 112.88, 82.95, 81.23. **Anal. Calcd. for $C_{22}H_{15}N_3$**: C, 82.22; H, 4.70; N, 13.08. Found: C, 82.14; H, 5.05 N, 12.83.

2-phenyl-*N*-(m-tolyl)quinazolin-4-amine (28).

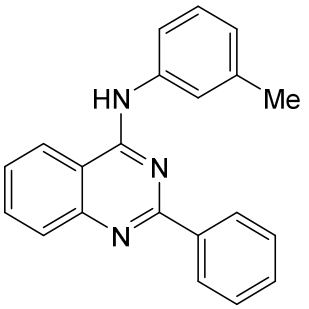

Molecular weight: 311.39 g/mol

The title compound was synthesized from 4-chloro-2-phenylquinazoline (241 mg, 1 mmol) and 3-methylaniline (107 mg, 1 mmol) as described in the general procedure above to yield **28** as pale yellow solid (247 mg, 79%), mp >300 °C. **^{1}H NMR** (500 MHz, DMSO-d_6) δ 11.58 (s, 1H), 8.95 (d, J = 8.3 Hz, 1H), 8.51 – 8.28 (m, 3H), 8.15 – 7.97 (m, 1H), 7.87 – 7.76 (m, 1H), 7.75 – 7.55 (m, 5H), 7.41 (t, J = 7.8 Hz, 1H), 7.22 – 7.10 (m, 1H), 2.40 (s, 3H). **^{13}C NMR** (126 MHz, DMSO) δ 159.01, 157.35, 141.16, 138.12, 137.07, 135.82, 133.26, 132.18, 129.25, 129.07, 128.63, 128.09, 127.05, 124.96, 124.59, 121.62, 121.19, 112.91, 21.20. **Anal. Calcd. for $C_{21}H_{17}N_3$**: C, 81.00; H, 5.50; N, 13.49. Found: C, 80.84; H, 5.79; N, 13.55.

2-phenyl-N-(p-tolyl)quinazolin-4-amine. (29)

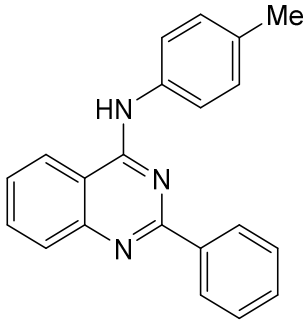

Molecular weight: 311.39 g/mol

The title compound was synthesized from 4-chloro-2-phenylquinazoline (241 mg, 1 mmol) and 4-methylaniline (107 mg, 1 mmol) as described in the general procedure above to yield **29** as pale yellow solid (256 mg, 82%), mp 254-256 °C (decomp.). ^{1}H NMR (500 MHz, DMSO-d_6) δ 11.56 (s, 1H), 8.92 (d, J = 8.3 Hz, 1H), 8.45 – 8.28 (m, 3H), 8.14 – 8.00 (m, 1H), 7.87 – 7.76 (m, 1H), 7.76 – 7.66 (m, 3H), 7.65 – 7.55 (m, 2H), 7.39 – 7.26 (m, 2H), 2.37 (s, 3H). ^{13}C NMR (126 MHz, DMSO) δ 158.98, 157.39, 140.84, 135.90, 134.49, 133.36, 131.93, 129.31, 129.29, 129.12, 128.17, 124.65, 124.46, 120.85, 112.87, 20.86. Anal. Calcd. for $C_{21}H_{17}N_3$: C, 81.00; H, 5.50; N, 13.49. Found: C, 81.37; H, 5.58; N, 13.23.

N-(3-(*tert*-butyl)phenyl)-2-phenylquinazolin-4-amine (30).

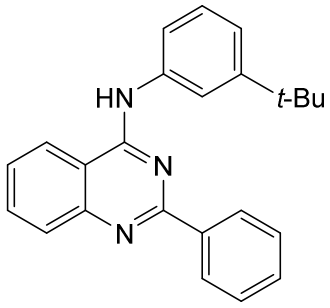

Molecular weight: 353.47 g/mol

The title compound was synthesized from 4-chloro-2-phenylquinazoline (241 mg, 1 mmol) and 3-(*tert*-butyl)aniline (149 mg, 1 mmol) as described in the general procedure above to yield **30** as pale yellow solid (263 mg, 74%), mp 223-224 °C. **^{1}H NMR** (500 MHz, DMSO-d_6) δ 11.63 (s, 1H), 8.98 (d, J = 8.3 Hz, 1H), 8.52 – 8.33 (m, 3H), 8.13 –

8.02 (m, 1H), 7.94 (t, *J* = 2.0 Hz, 1H), 7.81 (td, *J* = 7.7, 7.2, 1.2 Hz, 1H), 7.69 (td, *J* = 7.3, 1.2 Hz, 1H), 7.66 – 7.62 (m, 1H), 7.62 – 7.55 (m, 2H), 7.45 (t, *J* = 7.9 Hz, 1H), 7.40 – 7.35 (m, 1H), 1.34 (d, *J* = 0.9 Hz, 9H). **^{13}C NMR** (126 MHz, DMSO) δ 158.99, 157.24, 151.37, 140.98, 136.81, 135.83, 133.34, 131.86, 129.31, 128.91, 128.45, 128.08, 124.65, 123.37, 121.69, 121.62, 120.89, 112.89, 34.72, 31.22. **Anal. Calcd. for $C_{24}H_{23}N_3$**: C, 81.55; H, 6.56; N, 11.89. Found: C, 81.47; H, 6.89; N, 11.70.

N-(4-(tert-butyl)phenyl)-2-phenylquinazolin-4-amine (31).

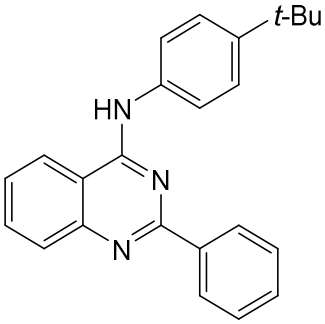

Molecular weight: 353.47 g/mol

The title compound was synthesized from 4-chloro-2-phenylquinazoline (241 mg, 1 mmol) and 4-(*tert*-butyl)aniline (149 mg, 1 mmol) as described in the general procedure above to yield **31** as pale yellow solid (233 mg, 66%), mp 287-289 °C (decomp.). **^{1}H NMR** (500 MHz, DMSO-d_6) δ 11.66 (s, 1H), 9.02 (d, *J* = 8.3 Hz, 1H), 8.53 – 8.29 (m, 3H), 8.11 – 7.99 (m, 1H), 7.89 – 7.73 (m, 3H), 7.70 (td, *J* = 7.1, 6.7, 1.4 Hz, 1H), 7.62 (td, *J* = 7.2, 6.6, 1.3 Hz, 2H), 7.57 – 7.45 (m, 2H), 1.33 (d, *J* = 1.1 Hz, 9H). **^{13}C NMR** (126 MHz, DMSO) δ 158.82, 157.46, 148.93, 140.82, 135.83, 134.56, 133.25, 131.92, 129.32, 129.07, 128.08, 125.45, 124.70, 123.87, 120.84, 112.86, 34.48, 31.27. **Anal. Calcd. for $C_{24}H_{23}N_3$**: C, 81.55; H, 6.56; N, 11.89. Found: C, 81.68; H, 6.62; N, 11.89.

5-((2-phenylquinazolin-4-yl)amino)isoindoline-1,3-dione (32).

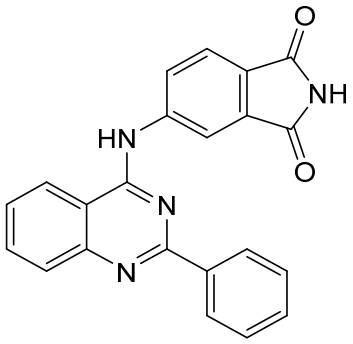

Molecular weight: 366.38 g/mol

The title compound was synthesized from 4-chloro-2-phenylquinazoline (241 mg, 1 mmol) and 5-aminoisoindoline-1,3-dione (162 mg, 1 mmol) as described in the general procedure above to yield **32** as slightly yellow solid (227 mg, 62%), mp >300 °C. **^{1}H NMR** (500 MHz, DMSO-d_6) δ 11.44 (s, 1H), 11.33 (s, 1H), 8.90 (d, J = 8.4 Hz, 1H), 8.52 (d, J = 1.8 Hz, 1H), 8.46 – 8.39 (m, 2H), 8.35 (dd, J = 8.2, 1.9 Hz, 1H), 8.22 (d, J = 8.4 Hz, 1H), 8.05 (ddd, J = 8.3, 6.9, 1.2 Hz, 1H), 7.95 (d, J = 8.2 Hz, 1H), 7.79 (ddd, J = 8.3, 7.0, 1.2 Hz, 1H), 7.69 – 7.63 (m, 1H), 7.60 (dd, J = 8.2, 6.6 Hz, 2H). **^{13}C NMR** (126 MHz, DMSO) δ 168.98, 168.89, 158.93, 157.90, 143.48, 135.59, 133.79, 132.66, 129.03, 128.41, 128.08, 127.87, 124.47, 123.81, 117.37, 113.47. **Anal. Calcd. for $C_{22}H_{14}N_4O_2$**: C, 72.12; H, 3.85 N, 15.29. Found: C, 72.31; H, 4.06; N, 15.21.

4-methyl-7-((2-phenylquinazolin-4-yl)amino)-2H-chromen-2-one (33).

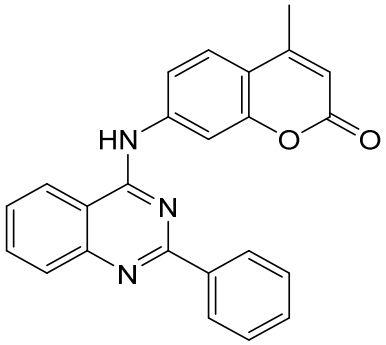

Molecular weight: 379.42 g/mol

The title compound was synthesized from 4-chloro-2-phenylquinazoline (241 mg, 1 mmol) and 7-amino-4-methyl-2H-chromen-2-one (175 mg, 1 mmol) as described in the general procedure above to yield **33** as a yellow solid (292 mg, 77%), mp >300 °C. **^{1}H NMR** (500 MHz, DMSO-d_6) δ 11.37 (s, 1H), 8.91 (d, *J* = 8.3 Hz, 1H), 8.44 – 8.36 (m, 2H), 8.24 (d, *J* = 8.3 Hz, 1H), 8.11 – 8.03 (m, 2H), 8.00 (dd, *J* = 8.6, 2.1 Hz, 1H), 7.88 (d, *J* = 8.6 Hz, 1H), 7.79 (t, *J* = 7.6 Hz, 1H), 7.67 (dd, *J* = 8.2, 6.1 Hz, 1H), 7.62 (dd, *J* = 8.2, 6.4 Hz, 2H), 6.36 (d, *J* = 1.4 Hz, 1H), 2.47 (d, *J* = 1.2 Hz, 3H). **^{13}C NMR** (126 MHz, DMSO) δ 160.00, 158.88, 157.93, 153.34, 153.11, 141.17, 135.61, 132.72, 129.05, 127.89, 125.71, 124.42, 119.30, 116.82, 113.47, 113.40, 110.34, 18.19. **Anal. Calcd. for $C_{24}H_{17}N_3O_2$**: C, 75.98; H, 4.52 N, 11.08. Found: C, 75.94; H, 4.78; N, 11.06.

General Procedure for the preparation of 4-anilino-2-phenylquinoline derivatives

4-chloro-2-phenylquinoline (1 mmol) and a substituted aniline (1 mmol) were added to a 50 mL microwave tube and suspended in 25 mL isopropanol. The tube was sealed and the reaction mixture stirred under 100 watt microwave irradiation at 110 °C for 15 min. Reaction control was performed by TLC. Workup of the compounds was analogous to 4-anilino-quinazoline compounds. For some quinoline derivatives it was necessary to recrystallize from acetone. In the case of incomplete reaction, triethylamine (1 mmol) was added to the mixture to react with HCl generated by the nucleophilic substitution.

2-nitro-4-((2-phenylquinolin-4-yl)amino)phenol (34).

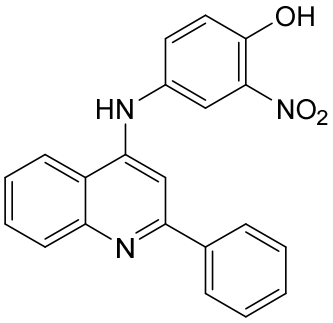

Molecular weight: 357.37 g/mol

The title compound was synthesized from 4-chloro-2-phenylquinoline (240 mg, 1 mmol) and 4-amino-2-nitrophenol (154 mg, 1 mmol) as described in the general procedure above to yield **34** as a yellow solid (218 mg, 61%), mp 238-239 °C. **^{1}H NMR** (500 MHz,

DMSO-d_6) δ 11.50 (s, 1H), 11.05 (s, 1H), 8.82 (dd, *J* = 8.7, 1.3 Hz, 1H), 8.34 (dd, *J* = 8.5, 1.1 Hz, 1H), 8.11 – 7.98 (m, 2H), 7.97 – 7.86 (m, 2H), 7.80 (ddd, *J* = 8.3, 7.0, 1.2 Hz, 1H), 7.75 (dd, *J* = 8.8, 2.7 Hz, 1H), 7.70 – 7.57 (m, 3H), 7.39 (d, *J* = 8.9 Hz, 1H), 6.95 (s, 1H). **^{13}C NMR** (126 MHz, DMSO) δ 155.10, 153.13, 151.34, 139.26, 137.21, 134.13, 132.67, 132.32, 132.02, 129.33, 128.74, 128.32, 127.14, 123.59, 122.61, 120.90, 120.60, 116.63, 99.01. **Anal. Calcd. for $C_{21}H_{15}N_3O_3$**: C, 70.58; H, 4.23 N, 11.76. Found: C, 70.93; H, 4.49; N, 11.71.

3-((2-phenylquinolin-4-yl)amino)benzonitrile (35).

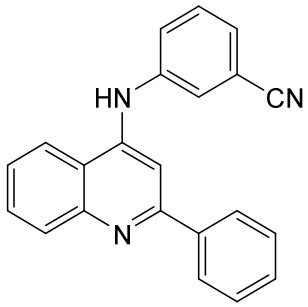

Molecular weight: 321.38 g/mol

The title compound was synthesized from 4-chloro-2-phenylquinoline (240 mg, 1 mmol) and 3-aminobenzonitrile (118 mg, 1 mmol) as described in the general procedure above to yield **35** as a yellow solid (273 mg, 85%), mp 267-269 °C. **^{1}H NMR** (500 MHz, DMSO-d_6) δ 11.33 (s, 1H), 8.98 – 8.90 (m, 1H), 8.45 – 8.37 (m, 1H), 8.09 (t, *J* = 1.8 Hz, 1H), 8.05 (ddd, *J* = 8.3, 6.9, 1.2 Hz, 1H), 7.99 – 7.93 (m, 3H), 7.87 – 7.78 (m, 2H), 7.75 (t, *J* = 7.9 Hz, 1H), 7.69 – 7.58 (m, 3H), 7.09 (s, 1H). **^{13}C NMR** (126 MHz, DMSO) δ 154.38, 153.40, 139.46, 138.75, 134.16, 132.30, 132.04, 131.33, 130.74, 130.11, 129.30, 128.85, 128.63, 127.24, 123.93, 121.06, 118.33, 117.02, 112.89, 99.65. **Anal. Calcd. for $C_{22}H_{15}N_3$**: C, 82.22; H, 4.70 N, 13.08. Found: C, 82.34; H, 5.02; N, 12.70.

4-((2-phenylquinolin-4-yl)amino)benzonitrile (36).

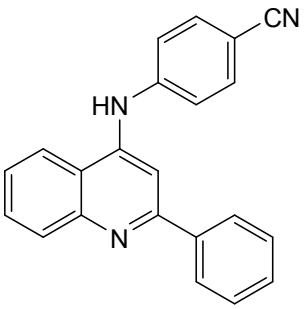

Molecular weight: 321.38 g/mol

The title compound was synthesized from 4-chloro-2-phenylquinoline (240 mg, 1 mmol) and 4-aminobenzonitrile (118 mg, 1 mmol) to yield **36** as pale yellow solid (170 mg, 53%), mp 290 °C (decomp.). **^{1}H NMR** (500 MHz, DMSO-d_6) δ 14.53 (s, 1H), 11.21 (s, 1H), 8.87 (d, J = 8.6 Hz, 1H), 8.38 (d, J = 8.5 Hz, 1H), 8.06 (t, J = 7.7 Hz, 1H), 8.02 – 7.93 (m, 4H), 7.82 (t, J = 9.0 Hz, 3H), 7.74 – 7.58 (m, 3H), 7.33 (s, 1H). **^{13}C NMR** (126 MHz, DMSO) δ 156.48, 148.43, 142.42, 137.61, 131.24, 130.26, 129.83, 129.02, 128.05, 127.50, 124.69, 123.66, 118.99. ^{13}C NMR (126 MHz, DMSO) δ 153.65, 142.62, 134.14, 132.05, 129.33, 128.85, 127.34, 124.58, 123.89, 118.78, 117.58, 100.74. **Anal. Calcd. for $C_{22}H_{16}N_3$**: C, 81.96; H, 5.00; N, 13.03. Found: C, 81.73; H, 5.39; N, 12.82.

N-(3-((2-phenylquinolin-4-yl)amino)phenyl)acetamide (37).

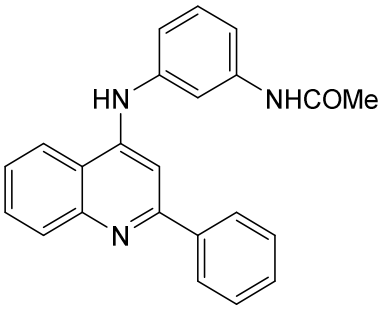

Molecular weight: 353.43 g/mol

The title compound was synthesized from 4-chloro-2-phenylquinoline (240 mg, 1 mmol) and N-(3-aminophenyl)acetamide (150 mg, 1 mmol) to yield **37** as pale yellow solid (136 mg, 38%), mp 281 °C (decomp.). **^{1}H NMR** (500 MHz, DMSO-d_6) δ 14.25 (s, 1H), 11.05 (s, 1H), 10.38 (s, 1H), 8.85 (dd, J = 8.6, 1.3 Hz, 1H), 8.35 (dd, J = 8.6, 1.1 Hz, 1H), 8.08

– 8.01 (m, 1H), 7.98 (d, *J* = 2.1 Hz, 1H), 7.96 – 7.91 (m, 2H), 7.82 – 7.76 (m, 1H), 7.68 – 7.58 (m, 3H), 7.52 – 7.43 (m, 2H), 7.23 (dt, *J* = 7.2, 1.9 Hz, 1H), 7.05 (s, 1H), 2.08 (s, 3H). **^{13}C NMR** (126 MHz, DMSO) δ 168.89, 154.61, 153.04, 140.80, 139.35, 137.52, 134.10, 132.39, 132.00, 130.23, 129.38, 128.67, 127.09, 123.66, 120.89, 119.61, 117.85, 116.73, 115.58, 99.01, 24.17. **Anal. Calcd. for $C_{23}H_{20}N_3O$**: C, 77.94; H, 5.69; N, 11.86. Found: C, 78.20; H, 5.65; N, 11.97.

N-(3-methoxyphenyl)-2-phenylquinolin-4-amine (38).

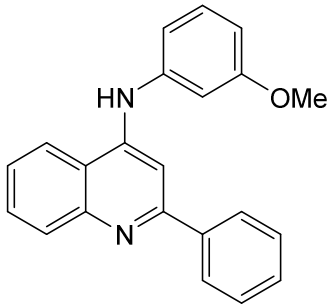

Molecular weight: 326.40 g/mol

The title compound was synthesized from 4-chloro-2-phenylquinoline (240 mg, 1 mmol) and 3-methoxyaniline (123 mg, 1 mmol) to yield **38** as yellow solid (76 mg, 23%), mp 279 °C (decomp.). **^{1}H NMR** (500 MHz, DMSO-d_6) δ 14.41 (s, 1H), 11.17 (s, 1H), 8.93 (dd, *J* = 8.6, 1.2 Hz, 1H), 8.44 (dd, *J* = 8.6, 1.2 Hz, 1H), 8.07 – 7.97 (m, 1H), 7.95 – 7.83 (m, 2H), 7.82 – 7.71 (m, 1H), 7.69 – 7.52 (m, 3H), 7.51 – 7.38 (m, 1H), 7.22 – 7.07 (m, 2H), 7.05 – 6.90 (m, 2H), 3.80 (d, *J* = 0.9 Hz, 3H). **^{13}C NMR** (126 MHz, DMSO) δ 160.51, 154.74, 152.96, 139.40, 138.61, 134.02, 132.37, 131.94, 130.84, 129.35, 128.63, 127.00, 123.83, 120.90, 117.30, 116.74, 113.15, 111.14, 99.23, 55.58. **Anal. Calcd. for $C_{22}H_{19}N_2O$**: C, 80.71; H, 5.85; N, 8.56. Found: C, 80.74; H, 5.81; N, 8.86.

N-(3-(methylthio)phenyl)-2-phenylquinolin-4-amine (39).

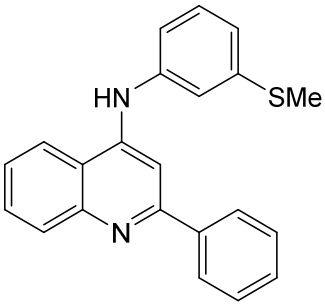

Molecular weight: 342.46 g/mol

The title compound was synthesized from 4-chloro-2-phenylquinoline (240 mg, 1 mmol) and 3-(methylthio)aniline (139 mg, 1 mmol) to yield **39** as pale yellow solid (243 mg, 71%), mp 238-240 °C. **^{1}H NMR** (600 MHz, DMSO-d_6) δ 14.42 (s, 1H), 11.22 (s, 1H), 8.93 (dd, *J* = 8.5, 3.1 Hz, 1H), 8.43 (dd, *J* = 8.6, 3.1 Hz, 1H), 8.03 (td, *J* = 7.9, 3.1 Hz, 1H), 7.90 (dd, *J* = 7.8, 3.0 Hz, 2H), 7.78 (td, *J* = 7.9, 3.1 Hz, 1H), 7.72 – 7.54 (m, 3H), 7.54 – 7.42 (m, 2H), 7.42 – 7.32 (m, 1H), 7.27 (t, *J* = 5.4 Hz, 1H), 6.98 (d, *J* = 3.2 Hz, 1H). **^{13}C NMR** (151 MHz, DMSO) δ 154.68, 152.99, 140.47, 139.37, 138.15, 134.10, 132.35, 132.01, 130.36, 129.38, 128.68, 127.08, 124.58, 123.89, 122.29, 121.45, 120.89, 116.80, 99.27, 14.71. **Anal. Calcd. for $C_{22}H_{19}N_2S$**: C, 76.93; H, 5.58; N, 8.16. Found: C, 77.31; H, 5.48; N, 7.99.

N-(3-fluorophenyl)-2-phenylquinolin-4-amine (40).

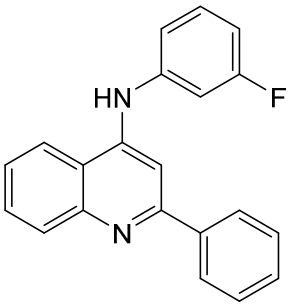

Molecular weight: 342.46 g/mol

The title compound was synthesized from 4-chloro-2-phenylquinoline (240 mg, 1mmol) and 3-fluoroaniline (111 mg, 1 mmol) to yield **40** as yellow solid (188 mg, 60%), mp 283 °C (decomp.). **^{1}H NMR** (500 MHz, DMSO-d_6) δ 14.44 (s, 1H), 11.22 (s, 1H), 8.92 (dd, *J* = 8.5, 1.4 Hz, 1H), 8.41 (dd, *J* = 8.5, 1.1 Hz, 1H), 8.13 – 8.00 (m, 1H), 8.00 – 7.89 (m,

2H), 7.85 – 7.75 (m, 1H), 7.72 – 7.55 (m, 4H), 7.56 – 7.43 (m, 2H), 7.31 – 7.19 (m, 1H), 7.08 (s, 1H). **^{13}C NMR** (126 MHz, DMSO) δ 163.72, 161.78, 154.50, 153.24, 139.34 (d, *J* = 10.4 Hz), 134.15, 132.32, 132.02, 131.68 (d, *J* = 9.3 Hz), 129.35, 128.75, 127.18, 123.85, 121.25, 120.96, 116.89, 114.10 (d, *J* = 20.7 Hz), 112.48 (d, *J* = 23.7 Hz), 99.52. **Anal. Calcd. for $C_{22}H_{16}N_2O$**: C, 79.98; H, 5.11; N, 8.88. Found: C, 80.24; H, 4.81; N, 8.91.

10.1.1.2 Synthesis of 4-Substituted-2-pyridylquinazolines and –pyrimidines

General Procedure for the Preparation of the 2-pyridylquinazolin-4(3*H*)-one derivatives 41-43. A mixture of anthranilamide (2.72 g, 20 mmol), the corresponding pyridinecarboxaldehyde (20 mmol), iodine (3.17 g, 25 mmol), anhydrous potassium carbonate (2.76 g, 20 mmol) and 20 ml DMF was stirred at 70-90 °C for 4-8 h. The end of the reaction was monitored by TLC and the mixture poured on crushed ice to form a precipitate. Incomplete precipitation was prevented by adjusting the pH with concentrated HCl solution to about 7. After filtering off the precipitate, it was thoroughly washed with 100 mL of a 20% sodium thiosulfate solution followed by 100 mL of hot distilled water. Purification was performed by recrystallization from ethanol.

2-(pyridin-2-yl)quinazolin-4(3H)-one (41).

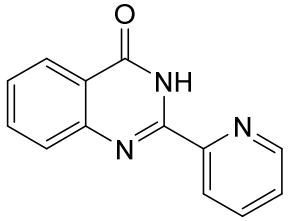

Molecular weight: 223.24 g/mol

The compound was synthesized from picolinaldehyde (2.14 g, 20 mmol) as described in the general procedure for **41-43** to yield **41** as a white solid (3,84 g, 86%). **^{1}H NMR** (500 MHz, DMSO-d_6) δ 11.77 (s, 1H), 8.76 (ddd, *J* = 4.7, 1.7, 0.9 Hz, 1H), 8.46 (dt, *J* = 7.9, 1.1 Hz, 1H), 8.18 (dd, *J* = 7.9, 1.5 Hz, 1H), 8.07 (td, *J* = 7.7, 1.7 Hz, 1H), 7.87 (ddd, *J* = 8.5, 7.0, 1.6 Hz, 1H), 7.80 (d, *J* = 8.0 Hz, 1H), 7.66 (ddd, *J* = 7.6, 4.8, 1.2 Hz, 1H), 7.57

(ddd, *J* = 8.1, 7.0, 1.2 Hz, 1H). **^{13}C NMR** (126 MHz, DMSO) δ 149.10, 148.82, 138.11, 134.80, 127.82, 127.37, 126.70, 126.23, 122.29, 122.13.

2-(pyridin-3-yl)quinazolin-4(3H)-one (42).

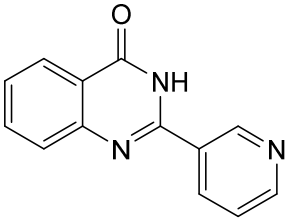

Molecular weight: 223.24 g/mol

The compound was synthesized from nicotinaldehyde (2.14 g, 20 mmol) as described in the general procedure for **41-43** to yield **42** as a white solid (3,34 g, 75%). **^{1}H NMR** (500 MHz, DMSO-d_6) δ 12.70 (s, 1H), 9.30 (d, *J* = 2.3 Hz, 1H), 8.76 (dd, *J* = 4.8, 1.6 Hz, 1H), 8.51 (dt, *J* = 8.1, 1.9 Hz, 1H), 8.17 (dd, *J* = 7.9, 1.5 Hz, 1H), 7.85 (ddd, *J* = 8.5, 7.0, 1.6 Hz, 1H), 7.76 (dd, *J* = 8.2, 1.1 Hz, 1H), 7.60 (ddd, *J* = 8.0, 4.9, 0.8 Hz, 1H), 7.55 (ddd, *J* = 8.1, 7.1, 1.2 Hz, 1H). **^{13}C NMR** (126 MHz, DMSO) δ 162.22, 151.71, 150.84, 148.68, 148.57, 135.75, 134.82, 128.95, 127.64, 127.09, 126.01, 123.74, 121.27.

2-(pyridin-4-yl)quinazolin-4(3H)-one (43).

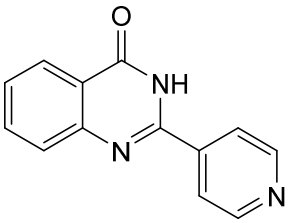

Molecular weight: 223.24 g/mol

The compound was synthesized from isonicotinaldehyde (2.14 g, 20 mmol) as described in the general procedure for **41-43** to yield **43** as a white solid (3,04 g, 68%). **^{1}H NMR** (500 MHz, DMSO-d_6) δ 12.73 (s, 1H), 8.83 – 8.74 (m, 2H), 8.18 (dd, *J* = 7.9, 1.5 Hz, 1H), 8.14 – 8.08 (m, 2H), 7.87 (ddd, *J* = 8.5, 7.1, 1.6 Hz, 1H), 7.79 (dd, *J* = 8.2, 1.1 Hz, 1H), 7.58 (ddd, *J* = 8.1, 7.1, 1.2 Hz, 1H). **^{13}C NMR** (126 MHz, DMSO) δ 162.13, 150.65, 150.30, 148.36, 140.14, 134.88, 127.88, 127.52, 126.05, 121.73, 121.61.

General Procedure for the Preparation of the 4-chloro-2-pyridylquinazoline derivatives 44-46.

The corresponding 2-pyridylquinazolin-4(3*H*)-one derivative (10 mmol) was added to phosphorus oxychloride (30 mL, 0.32 mol) and stirred for 10 min at room temperature. The mixture was then refluxed for 4-8 h and the reaction monitored by TLC. After completion of the reaction, excess $POCl_3$ was removed under reduced pressure and the residue poured into 50 mL ice water. Subsequently, 50 mL DCM was added while stirring and the pH of the mixture slowly adjusted to 7 with 25% ammonium solution. With a separatory funnel, the organic phase was collected, washed with 50 mL brine and dried over $MgSO_4$. The solvent was removed under reduced pressure and the obtained solid recrystallized from isopropanol.

4-chloro-2-(pyridin-2-yl)quinazoline (44).

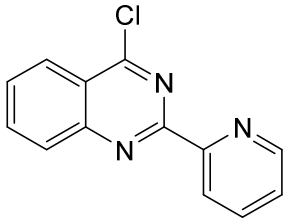

Molecular weight: 241.68 g/mol

The compound was synthesized from **41** (2.23 g, 10 mmol) as described in the general procedure for **44-46** to yield **44** as a white solid (2.15 g, 89%). **^{1}H NMR** (500 MHz, DMSO-d_6) δ 8.77 (ddd, *J* = 4.8, 1.8, 1.0 Hz, 1H), 8.47 (dt, *J* = 7.9, 1.1 Hz, 1H), 8.21 – 8.14 (m, 1H), 8.09 (td, *J* = 7.8, 1.7 Hz, 1H), 7.87 (ddd, *J* = 8.5, 7.0, 1.6 Hz, 1H), 7.82 (dd, *J* = 7.9, 1.5 Hz, 1H), 7.67 (ddd, *J* = 7.6, 4.8, 1.2 Hz, 1H), 7.57 (ddd, *J* = 8.2, 7.0, 1.3 Hz, 1H). **^{13}C NMR** (126 MHz, DMSO) δ 160.88, 150.11, 148.95, 148.38, 147.83, 138.13, 134.73, 127.32, 127.24, 126.71, 126.12, 122.33, 121.88.

4-chloro-2-(pyridin-3-yl)quinazoline (45).

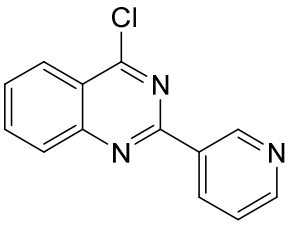

Molecular weight: 241.68 g/mol

The compound was synthesized from **42** (2.23 g, 10 mmol) as described in the general procedure for **44-46** to yield **45** as a white solid (2.27 g, 94%). **^{1}H NMR** (500 MHz, DMSO-d_6) δ 9.29 (d, *J* = 2.2 Hz, 1H), 8.74 (dd, *J* = 4.8, 1.6 Hz, 1H), 8.49 (dt, *J* = 8.0, 2.0 Hz, 1H), 8.16 (dd, *J* = 7.9, 1.5 Hz, 1H), 7.84 (ddd, *J* = 8.5, 7.0, 1.6 Hz, 1H), 7.78 – 7.72 (m, 1H), 7.61 – 7.49 (m, 2H). **^{13}C NMR** (126 MHz, DMSO) δ 162.22, 151.93, 150.91, 148.88, 148.60, 135.50, 134.79, 128.85, 127.66, 127.05, 126.00, 123.62, 121.26.

4-chloro-2-(pyridin-4-yl)quinazoline (46).

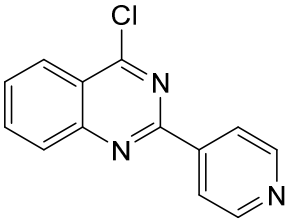

Molecular weight: 241.68 g/mol

The compound was synthesized from **3** (2.23 g, 10 mmol) as described in the general procedure for **44-46** to yield **46** as a white solid (2.18 g, 90%). **^{1}H NMR** (500 MHz, DMSO-d_6) δ 9.05 – 8.96 (m, 2H), 8.54 – 8.46 (m, 2H), 8.20 (dd, *J* = 8.0, 1.4 Hz, 1H), 7.90 (ddd, *J* = 8.5, 7.1, 1.6 Hz, 1H), 7.83 (dd, *J* = 8.3, 1.2 Hz, 1H), 7.62 (ddd, *J* = 8.1, 7.1, 1.2 Hz, 1H). **^{13}C NMR** (126 MHz, DMSO) δ 161.98, 149.36, 147.97, 145.50, 144.99, 135.06, 128.19, 128.08, 126.12, 123.99, 121.78.

6-methyl-2-(pyridin-4-yl)pyrimidin-4(3H)-one (47).

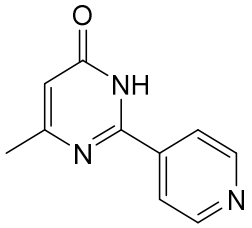

Molecular weight: 187.20 g/mol

To a solution of isonicotinimidamide hydrochloride (158 mg, 1 mmol) in methanol (5 mL) was added sodium methoxide (54.0 mg, 1 mmol) and stirred for 10 min at room temperature. After adding methyl acetoacetate (116 mg, 1 mmol) the mixture was transferred into a microwave tube, sealed and heated to 70 °C at 60 watt microwave irradiation for 4 h. After cooling to room temperature, the pH of the mixture was adjusted with 1 M hydrochloric acid to 7 and the formed precipitate filtered off with suction. The solid was washed with water and dried *in vacuo* to give **47** as a white solid (76.8 mg, 41%). **^{1}H NMR** (500 MHz, DMSO-d_6) δ 12.59 (s, 1H), 8.80 – 8.66 (m, 2H), 8.09 – 7.99 (m, 2H), 6.37 (s, 1H), 2.39 – 2.24 (m, 3H). **^{13}C NMR** (126 MHz, DMSO) δ 150.39, 121.62, 23.48.

6-methyl-2-phenylpyrimidin-4(3H)-one (48).

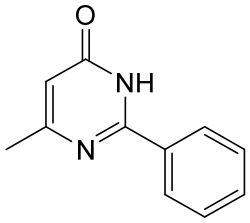

Molecular weight: 186.21 g/mol

This compound was synthesized according to the procedure described for **47**. Instead of isonicotinimidamide hydrochloride, benzimidamide hydrochloride (157 mg, 1 mmol) was used in the first step to yield **48** as a white solid (89.4 mg, 48%). **^{1}H NMR** (500 MHz, DMSO-d_6) δ 12.47 (s, 1H), 8.22 – 7.99 (m, 2H), 7.60 – 7.42 (m, 3H), 6.19 (s, 1H), 2.26 (s, 3H). **^{13}C NMR** (126 MHz, DMSO) δ 164.72, 163.86, 157.15, 132.92, 131.61, 128.70, 127.88, 110.03, 23.63.

General Procedure for the Preparation of the 2-substituted 4-chloro-6-methylpyrimidine derivatives 49-50.

The compounds were synthesized according to the method described in the general methods for compounds **44**-**46** from the corresponding 2-substituted 6-methyl-pyrimidin-4(3H)-ones **47** and **48**. Complete chlorination was achieved within 4 h.

4-chloro-6-methyl-2-(pyridin-4-yl)pyrimidine (49).

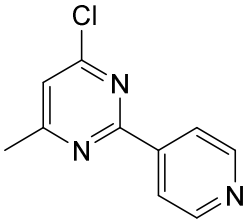

Molecular weight: 205.65 g/mol

The compound was synthesized from **47** (1.87 g, 10 mmol) as described in the general procedure for **49-50** to yield **49** as a white solid (1.79 g, 87%). **^{1}H NMR** (600 MHz, DMSO-d_6) δ 8.81 – 8.74 (m, 2H), 8.21 – 8.16 (m, 2H), 7.69 (d, J = 0.7 Hz, 1H), 2.58 (s, 3H). **^{13}C NMR** (151 MHz, DMSO) δ 170.58, 162.06, 160.86, 150.79, 143.04, 121.75, 120.74, 23.73.

4-chloro-6-methyl-2-phenylpyrimidine (50).

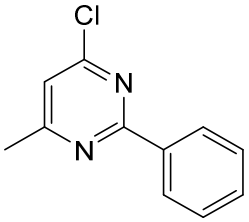

Molecular weight: 204.66 g/mol

The compound was synthesized from **48** (1.86 g, 10 mmol) as described in the general procedure for **49-50** to yield **50** as a white solid (1.90 g, 93%). **^{1}H NMR** (500 MHz, DMSO-d_6) δ 8.39 – 8.27 (m, 2H), 7.60 – 7.45 (m, 4H), 2.55 (d, J = 0.6 Hz, 3H). **^{13}C NMR** (126 MHz, DMSO) δ 170.05, 163.83, 160.56, 135.88, 131.62, 128.91, 128.08, 119.01, 23.75.

General Procedure for the Preparation of the substituted 4-anilinoquinazolines 51-81.

The corresponding 4-chloroquinazoline derivative **44-46** (1 mmol) was added to isopropanol (5 mL) with the corresponding substituted aniline derivative (1 mmol) and sealed in a microwave tube. The mixture was heated by 100 watt microwave irradiation to 110 °C for a period of 15 – 30 min until completion of the reaction as indicated by TLC. The formed precipitate was filtered off, washed with 10 mL isopropanol and dried in vacuo. If no precipitate is formed, the solvent was removed under reduced pressure and the remaining solid recrystallized from ethanol.

N-(3-nitrophenyl)-2-(pyridin-2-yl)quinazolin-4-amine (51).

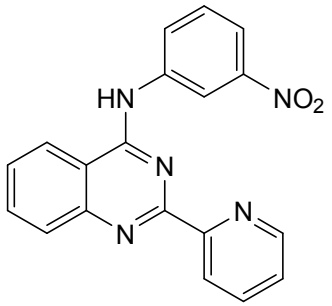

Molecular weight: 343.35 g/mol

The compound was synthesized from **44** (242 mg, 1 mmol) and 3-nitroaniline (138 mg, 1 mmol) as described in the general procedure for compounds **51-81** to yield **51** as a yellow solid (292 mg, 85%), mp 274-275 °C. **^{1}H NMR** (500 MHz, DMSO-d_6) δ 12.09 (s, 1H), 9.09 (dd, *J* = 8.4, 1.3 Hz, 1H), 9.02 (t, *J* = 2.2 Hz, 1H), 8.93 (ddd, *J* = 4.8, 1.7, 0.9 Hz, 1H), 8.43 (dt, *J* = 7.9, 1.1 Hz, 1H), 8.39 (ddd, *J* = 8.1, 2.1, 0.9 Hz, 1H), 8.33 (dd, *J* = 8.5, 1.1 Hz, 1H), 8.24 – 8.17 (m, 2H), 8.14 (ddd, *J* = 8.5, 7.1, 1.2 Hz, 1H), 7.89 (ddd, *J* = 8.3, 7.1, 1.2 Hz, 1H), 7.86 – 7.78 (m, 2H). **^{13}C NMR** (126 MHz, DMSO) δ 159.82, 154.93, 149.40, 148.32, 147.96, 141.44, 139.41, 138.53, 136.44, 130.22, 128.80, 128.20, 124.95, 124.66, 122.07, 120.62, 118.80, 113.81. **Anal. Calcd. for $C_{19}H_{13}N_5O_2$**: C, 66.47; H, 3.82; N, 20.40. Found: C, 66.38 ; H, 4.19; N, 20.16.

N-(3-nitrophenyl)-2-(pyridin-3-yl)quinazolin-4-amine (52).

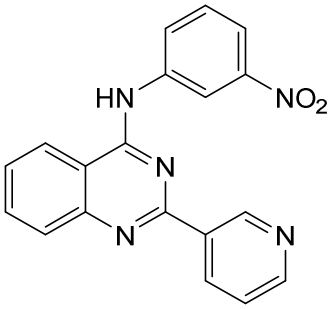

Molecular weight: 343.35 g/mol

The compound was synthesized from **45** (242 mg, 1 mmol) and 3-nitroaniline (138 mg, 1 mmol) as described in the general procedure for compounds **51-81** to yield **52** as a yellow-beige solid (278 mg, 81%), mp >300 °C. **^{1}H NMR** (500 MHz, DMSO-d_6) δ 10.51 (s, 1H), 9.61 (s, 1H), 9.17 (t, *J* = 2.2 Hz, 1H), 8.99 (dt, *J* = 8.1, 1.9 Hz, 1H), 8.84 (d, *J* = 4.9 Hz, 1H), 8.68 (dt, *J* = 8.4, 1.0 Hz, 1H), 8.36 (ddd, *J* = 8.2, 2.2, 0.9 Hz, 1H), 8.04 (ddd, *J* = 8.2, 2.3, 0.9 Hz, 1H), 8.01 – 7.95 (m, 2H), 7.81 (dd, *J* = 8.0, 5.0 Hz, 1H), 7.79 – 7.72 (m, 2H). **^{13}C NMR** (126 MHz, DMSO) δ 158.22, 156.37, 149.89, 148.03, 140.38, 134.86, 134.27, 130.07, 128.16, 128.10, 127.34, 125.06, 123.45, 118.37, 116.52, 114.33. **Anal. Calcd. for $C_{19}H_{13}N_5O_2$**: C, 66.47; H, 3.82; N, 0.40. Found: C, 66.73; H, 4.10; N, 20.14.

***N*-(3-nitrophenyl)-2-(pyridin-4-yl)quinazolin-4-amine (53).**

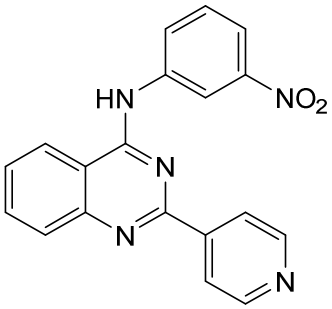

Molecular weight: 343.35 g/mol

The compound was synthesized from **46** (242 mg, 1 mmol) and 3-nitroaniline (138 mg, 1 mmol) as described in the general procedure for compounds **51-81** to yield **53** as a yellow solid (264 mg, 77%), mp >300 °C. **^{1}H NMR** (500 MHz, DMSO-d_6) δ 10.59 (s, 1H), 9.16 (t, *J* = 2.2 Hz, 1H), 8.97 (d, *J* = 5.6 Hz, 2H), 8.73 (dt, *J* = 8.3, 1.0 Hz, 1H), 8.71

– 8.64 (m, 2H), 8.37 (ddd, *J* = 8.2, 2.2, 0.9 Hz, 1H), 8.07 – 7.97 (m, 3H), 7.83 – 7.73 (m, 2H). **^{13}C NMR** (126 MHz, DMSO) δ 158.39, 155.47, 150.50, 150.01, 148.02, 145.51, 140.31, 134.39, 128.71, 128.23, 123.83, 123.59, 118.44, 116.61, 114.72. **Anal. Calcd. for $C_{19}H_{13}N_5O_2$**: C, 66.47; H, 3.82; N, 20.40. Found: C, 66.33; H, 4.20; N, 20.20.

N-(4-nitrophenyl)-2-(pyridin-4-yl)quinazolin-4-amine (54).

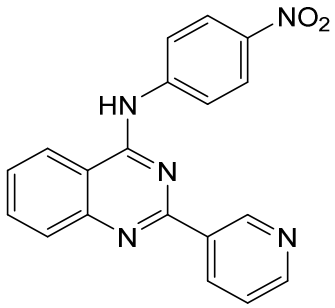

Molecular weight: 343.35 g/mol

The compound was synthesized from **45** (242 mg, 1 mmol) and 4-nitroaniline (138 mg, 1 mmol) as described in the general procedure for compounds **51-81** to yield **54** as a yellow solid (247 mg, 72%), mp >300 °C. **^{1}H NMR** (500 MHz, DMSO-d_6) δ 10.72 (s, 1H), 9.64 – 9.55 (m, 1H), 9.13 (dt, *J* = 8.1, 1.8 Hz, 1H), 8.98 – 8.87 (m, 1H), 8.76 (dd, *J* = 8.3, 1.0 Hz, 1H), 8.39 – 8.33 (m, 2H), 8.33 – 8.27 (m, 2H), 8.04 – 7.94 (m, 3H), 7.76 (ddd, *J* = 8.3, 5.5, 2.7 Hz, 1H). **^{13}C NMR** (126 MHz, DMSO) δ 158.21, 155.55, 149.84, 146.35, 145.56, 144.68, 142.58, 140.77, 135.17, 134.55, 128.02, 127.71, 126.16, 124.74, 123.82, 121.89, 114.63. **Anal. Calcd. for $C_{19}H_{13}N_5O_2$**: C, 66.47; H, 3.82; N, 20.40. Found: C, 66.52; H, 3.66; N, 20.15.

3-((2-(pyridin-2-yl)quinazolin-4-yl)amino)benzonitrile (55).

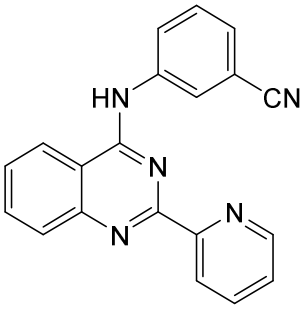

Molecular weight: 323.36 g/mol

The compound was synthesized from **44** (242 mg, 1 mmol) and 3-aminobenzonitrile (118 mg, 1 mmol) as described in the general procedure for compounds **51-81** to yield **55** as a light yellow solid (242 mg, 75%), mp 261-263 °C (decomp.). **^{1}H NMR** (500 MHz, DMSO-d_6) δ 12.27 (s, 1H), 9.15 (dd, *J* = 8.3, 1.3 Hz, 1H), 8.92 (ddd, *J* = 4.8, 1.8, 0.9 Hz, 1H), 8.39 (t, *J* = 1.9 Hz, 1H), 8.33 (dd, *J* = 8.5, 1.1 Hz, 1H), 8.31 – 8.24 (m, 2H), 8.20 (td, *J* = 7.7, 1.7 Hz, 1H), 8.13 (ddd, *J* = 8.3, 7.0, 1.2 Hz, 1H), 7.87 (ddd, *J* = 8.3, 7.1, 1.2 Hz, 1H), 7.84 – 7.79 (m, 2H), 7.77 (t, *J* = 7.9 Hz, 1H). **^{13}C NMR** (126 MHz, DMSO) δ 159.95, 154.85, 149.49, 148.15, 140.91, 139.27, 138.10, 136.52, 130.28, 129.88, 129.39, 128.78, 128.23, 127.91, 125.17, 124.47, 121.62, 118.51, 113.66, 111.70. **Anal. Calcd. for $C_{20}H_{13}N_5$**: C, 74.29; H, 4.05; N, 21.66. Found: C, 74.05; H, 4.34; N, 21.50.

3-((2-(pyridin-3-yl)quinazolin-4-yl)amino)benzonitrile (56).

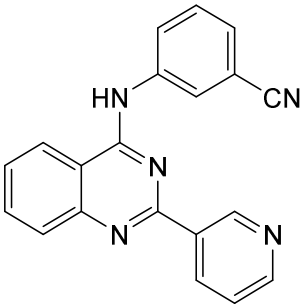

Molecular weight: 323.36 g/mol

The compound was synthesized from **45** (242 mg, 1 mmol) and 3-aminobenzonitrile (118 mg, 1 mmol) as described in the general procedure for compounds **51-81** to yield **56** as a yellow solid (252 mg, 78%), mp >300 °C. **^{1}H NMR** (500 MHz, DMSO-d_6) δ 10.17 (s,

1H), 9.52 (s, 1H), 8.68 (ddd, *J* = 9.9, 4.9, 3.0 Hz, 2H), 8.57 (dt, *J* = 8.4, 1.1 Hz, 1H), 8.45 (t, *J* = 1.8 Hz, 1H), 8.27 (ddd, *J* = 8.3, 2.2, 1.1 Hz, 1H), 7.96 – 7.90 (m, 2H), 7.73 – 7.65 (m, 2H), 7.62 (dt, *J* = 7.7, 1.3 Hz, 1H), 7.55 (ddd, *J* = 7.9, 4.7, 0.9 Hz, 1H). **^{13}C NMR** (126 MHz, DMSO) δ 158.07, 157.46, 151.20, 150.50, 149.29, 140.20, 135.21, 133.90, 133.61, 130.14, 128.41, 127.25, 126.96, 126.84, 125.33, 123.79, 123.22, 118.92, 114.23, 111.52. **Anal. Calcd. for $C_{20}H_{13}N_5$**: C, 74.29; H, 4.05; N, 21.66. Found: C, 74.27; H, 4.22; N, 21.46.

3-((2-(pyridin-4-yl)quinazolin-4-yl)amino)benzonitrile (57).

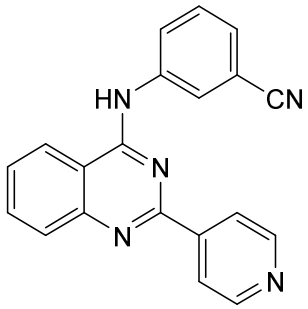

Molecular weight: 323.36 g/mol

The compound was synthesized from **46** (242 mg, 1 mmol) and 3-aminobenzonitrile (118 mg, 1 mmol) as described in the general procedure for compounds **51-81** to yield **57** as a yellow solid (252 mg, 78%), mp >300 °C. **^{1}H NMR** (500 MHz, DMSO-d_6) δ 10.62 (s, 1H), 9.04 – 8.94 (m, 2H), 8.81 – 8.72 (m, 1H), 8.68 – 8.60 (m, 2H), 8.36 (t, *J* = 1.8 Hz, 1H), 8.31 (dt, *J* = 7.8, 1.9 Hz, 1H), 8.03 – 7.95 (m, 2H), 7.77 (ddd, *J* = 8.3, 5.7, 2.5 Hz, 1H), 7.71 – 7.63 (m, 2H). **^{13}C NMR** (126 MHz, DMSO) δ 158.53, 155.14, 151.52, 149.76, 144.32, 139.81, 134.40, 130.14, 128.50, 128.27, 127.73, 127.50, 125.84, 124.17, 123.78, 118.81, 114.68, 111.57. **Anal. Calcd. for $C_{20}H_{13}N_5$**: C, 74.29; H, 4.05; N, 21.66. Found: C, 74.66; H, 4.32; N, 21.40.

4-((2-(pyridin-3-yl)quinazolin-4-yl)amino)benzonitrile (58).

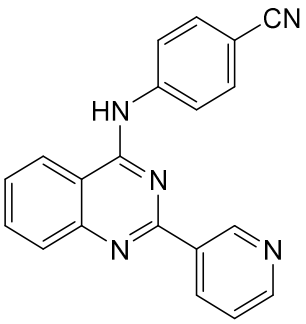

Molecular weight: 323.36 g/mol

The compound was synthesized from **45** (242 mg, 1 mmol) and 4-aminobenzonitrile (118 mg, 1 mmol) as described in the general procedure for compounds **51-81** to yield **58** as a light yellow solid (278 mg, 86%), mp 285-287 °C (decomp.). **^{1}H NMR** (500 MHz, DMSO-d_6) δ 10.75 (s, 1H), 9.54 (d, J = 2.0 Hz, 1H), 9.12 (dt, J = 8.1, 1.8 Hz, 1H), 8.95 (dd, J = 5.4, 1.5 Hz, 1H), 8.83 – 8.74 (m, 1H), 8.24 – 8.16 (m, 2H), 8.05 – 7.94 (m, 3H), 7.93 – 7.85 (m, 2H), 7.73 (ddd, J = 8.3, 6.6, 1.6 Hz, 1H). **^{13}C NMR** (126 MHz, DMSO) δ 158.33, 155.20, 149.10, 145.78, 144.00, 143.32, 141.35, 135.13, 134.58, 133.01, 127.72, 127.46, 126.38, 124.01, 122.68, 119.22, 114.50, 105.79. **Anal. Calcd. for $C_{20}H_{13}N_5$**: C, 74.29; H, 4.05; N, 21.66. Found: C, 74.42; H, 4.33; N, 21.33.

N-(3-methoxyphenyl)-2-(pyridin-2-yl)quinazolin-4-amine (59).

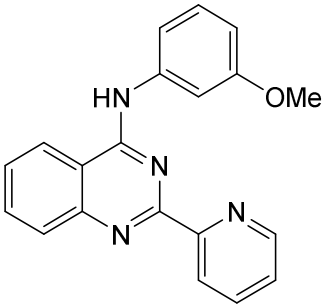

Molecular weight: 328.38 g/mol

The compound was synthesized from **44** (242 mg, 1 mmol) and 3-methoxyaniline (123 mg, 1 mmol) as described in the general procedure for compounds **51-81** to yield **59** as a yellow solid (207 mg, 63%), mp 115-117 °C. **^{1}H NMR** (500 MHz, DMSO-d_6) δ 9.83 (s, 1H), 8.78 – 8.68 (m, 1H), 8.64 (d, J = 8.2 Hz, 1H), 8.44 (dt, J = 8.0, 1.1 Hz, 1H), 8.27 (t,

J = 2.2 Hz, 1H), 8.00 – 7.86 (m, 3H), 7.66 (ddd, *J* = 8.3, 6.6, 1.5 Hz, 1H), 7.56 (ddd, *J* = 8.2, 2.0, 0.9 Hz, 1H), 7.50 (ddd, *J* = 7.6, 4.7, 1.2 Hz, 1H), 7.30 (t, *J* = 8.1 Hz, 1H), 6.69 (ddd, *J* = 8.2, 2.5, 0.9 Hz, 1H), 3.88 (s, 3H). **^{13}C NMR** (126 MHz, DMSO) δ 159.64, 159.04, 158.13, 155.79, 150.57, 149.63, 141.08, 136.93, 133.43, 129.24, 128.63, 126.73, 124.81, 123.53, 123.14, 114.46, 113.67, 109.90, 107.03, 55.28. **Anal. Calcd. for $C_{20}H_{16}N_4O$**: C, 73.15; H, 4.91; N, 17.06. Found: C, 73.43; H, 5.27; N, 16.99.

N-(3-methoxyphenyl)-2-(pyridin-3-yl)quinazolin-4-amine (60).

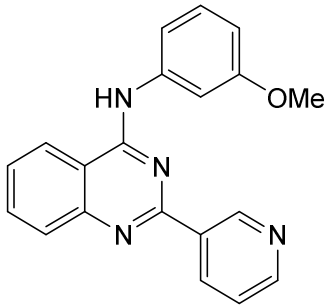

Molecular weight: 328.38 g/mol

The compound was synthesized from **45** (242 mg, 1 mmol) and 3-methoxyaniline (123 mg, 1 mmol) as described in the general procedure for compounds **51-81** to yield **60** as a light yellow solid (213 mg, 65%), mp 182-184 °C. **^{1}H NMR** (500 MHz, DMSO-d_6) δ 9.88 (s, 1H), 9.56 (d, *J* = 2.0 Hz, 1H), 8.72 – 8.65 (m, 2H), 8.60 (dt, *J* = 8.4, 1.1 Hz, 1H), 7.92 – 7.85 (m, 2H), 7.70 (t, *J* = 2.3 Hz, 1H), 7.67 – 7.61 (m, 1H), 7.58 – 7.50 (m, 2H), 7.36 (t, *J* = 8.1 Hz, 1H), 6.76 (ddd, *J* = 8.2, 2.6, 0.8 Hz, 1H), 3.82 (s, 3H). **^{13}C NMR** (126 MHz, DMSO) δ 159.55, 158.11, 157.59, 151.06, 150.39, 149.33, 140.48, 135.16, 133.80, 133.55, 129.37, 128.30, 126.50, 123.71, 123.22, 114.59, 114.34, 109.75, 107.91, 55.25. **Anal. Calcd. for $C_{20}H_{16}N_4O$**: C, 73.15; H, 4.91; N, 17.06. Found: C, 73.20; H, 4.82; N, 17.11.

N-(3-methoxyphenyl)-2-(pyridin-4-yl)quinazolin-4-amine (61).

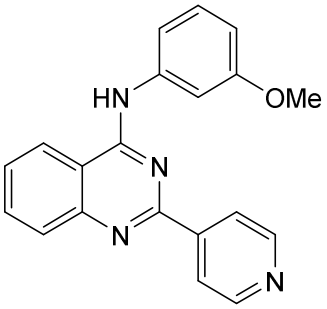

Molecular weight: 328.38 g/mol

The compound was synthesized from **46** (242 mg, 1 mmol) and 3-methoxyaniline (123 mg, 1 mmol) as described in the general procedure for compounds **51-81** to yield **61** as a light beige solid (230 mg, 70%), mp 202-203 °C. **^{1}H NMR** (500 MHz, DMSO-d_6) δ 9.92 (s, 1H), 8.79 – 8.69 (m, 2H), 8.61 (dt, *J* = 8.4, 1.0 Hz, 1H), 8.32 – 8.24 (m, 2H), 7.97 – 7.86 (m, 2H), 7.72 – 7.64 (m, 2H), 7.56 (ddd, *J* = 8.0, 2.0, 0.9 Hz, 1H), 7.37 (t, *J* = 8.1 Hz, 1H), 6.76 (ddd, *J* = 8.2, 2.5, 0.9 Hz, 1H), 3.83 (s, 3H). **^{13}C NMR** (126 MHz, DMSO) δ 159.57, 158.27, 157.38, 150.36, 150.28, 145.68, 140.41, 133.64, 129.40, 128.51, 126.99, 123.25, 121.85, 114.60, 109.93, 107.82, 55.28. **Anal. Calcd. for $C_{20}H_{16}N_4O$**: C, 73.15; H, 4.91; N, 17.06. Found: C, 73.42; H, 4.69; N,17.00.

N-(4-methoxyphenyl)-2-(pyridin-4-yl)quinazolin-4-amine (62).

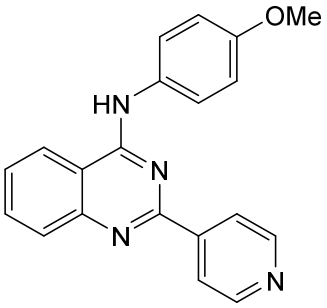

Molecular weight: 328.38 g/mol

The compound was synthesized from **46** (242 mg, 1 mmol) and 4-methoxyaniline (123 mg, 1 mmol) as described in the general procedure for compounds **51-81** to yield **62** as a light yellow solid (233 mg, 71%), mp 233-235 °C (decomp.). **^{1}H NMR** (500 MHz, DMSO-d_6) δ 9.89 (s, 1H), 8.76 – 8.68 (m, 2H), 8.56 (dt, *J* = 8.2, 1.0 Hz, 1H), 8.28 – 8.20

(m, 2H), 7.93 – 7.85 (m, 2H), 7.85 – 7.76 (m, 2H), 7.65 (ddd, *J* = 8.3, 4.7, 3.4 Hz, 1H), 7.09 – 7.00 (m, 2H), 3.81 (s, 3H). **^{13}C NMR** (126 MHz, DMSO) δ 158.35, 157.47, 156.07, 150.31, 150.18, 145.74, 133.44, 131.95, 128.39, 126.78, 124.35, 123.16, 121.85, 114.51, 113.88, 55.40. **Anal. Calcd. for $C_{20}H_{16}N_4O$**: C, 73.15; H, 4.91; N, 17.06. Found: C, 73.43; H, 5.01; N, 16.75.

N-(3,4-dimethoxyphenyl)-2-(pyridin-2-yl)quinazolin-4-amine (63).

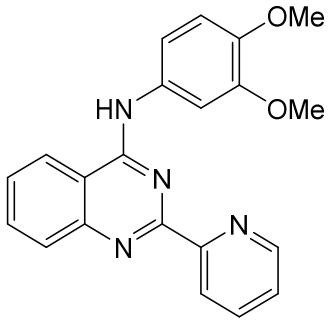

Molecular weight: 358.40 g/mol

The compound was synthesized from **44** (242 mg, 1 mmol) and 3,4-dimethoxyaniline (153 mg, 1 mmol) as described in the general procedure for compounds **51-81** to yield **63** as a yellow solid (204 mg, 57%), mp 191-193 °C. **^{1}H NMR** (500 MHz, DMSO-d_6) δ 9.82 (s, 1H), 8.72 (ddd, *J* = 4.7, 1.9, 0.9 Hz, 1H), 8.65 – 8.57 (m, 1H), 8.45 (dt, *J* = 7.9, 1.1 Hz, 1H), 8.37 (d, *J* = 2.5 Hz, 1H), 7.96 (td, *J* = 7.7, 1.8 Hz, 1H), 7.94 – 7.85 (m, 2H), 7.65 (ddd, *J* = 8.3, 6.6, 1.6 Hz, 1H), 7.50 (ddd, *J* = 7.5, 4.7, 1.2 Hz, 1H), 7.43 (dd, *J* = 8.7, 2.5 Hz, 1H), 7.00 (d, *J* = 8.7 Hz, 1H), 3.91 (s, 3H), 3.78 (s, 3H). **^{13}C NMR** (126 MHz, DMSO) δ 158.96, 157.89, 155.67, 149.50, 148.49, 145.07, 136.87, 133.31, 128.33, 126.55, 124.80, 123.47, 123.03, 114.34, 113.28, 112.00, 107.24, 55.92, 55.58. **Anal. Calcd. for $C_{21}H_{18}N_4O_2$**: C, 70.38; H, 5.06; N, 15.63. Found: C, 70.01; H, 5.31; N, 15.95.

N-(3,4-dimethoxyphenyl)-2-(pyridin-3-yl)quinazolin-4-amine (64).

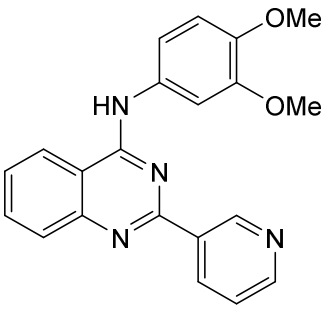

Molecular weight: 358.40 g/mol

The compound was synthesized from **45** (242 mg, 1 mmol) and 3,4-dimethoxyaniline (153 mg, 1 mmol) as described in the general procedure for compounds **51-81** to yield **64** as a yellow solid (240 mg, 67%), mp 201-202 °C. **^{1}H NMR** (500 MHz, DMSO-d_6) δ 10.76 (s, 1H), 9.51 (d, *J* = 2.2 Hz, 1H), 8.97 (dt, *J* = 8.1, 1.8 Hz, 1H), 8.89 (dd, *J* = 5.1, 1.6 Hz, 1H), 8.77 (d, *J* = 8.2 Hz, 1H), 8.11 (d, *J* = 8.3 Hz, 1H), 7.99 (ddd, *J* = 8.4, 7.0, 1.3 Hz, 1H), 7.87 (dd, *J* = 8.1, 5.1 Hz, 1H), 7.75 (ddd, *J* = 8.3, 7.0, 1.2 Hz, 1H), 7.59 (d, *J* = 2.4 Hz, 1H), 7.40 (dd, *J* = 8.6, 2.5 Hz, 1H), 7.07 (d, *J* = 8.7 Hz, 1H), 3.81 (s, 3H), 3.81 (s, 3H). **^{13}C NMR** (126 MHz, DMSO) δ 158.48, 155.72, 148.55, 146.65, 134.80, 131.12, 127.69, 125.22, 123.96, 115.80, 113.78, 111.79, 108.56, 55.89, 55.80. **Anal. Calcd. for $C_{21}H_{18}N_4O_2$**: C, 70.38; H, 5.06; N, 15.63. Found: C, 70.41; H, 4.93; N, 15.34.

N-(3,4-dimethoxyphenyl)-2-(pyridin-4-yl)quinazolin-4-amine (65).

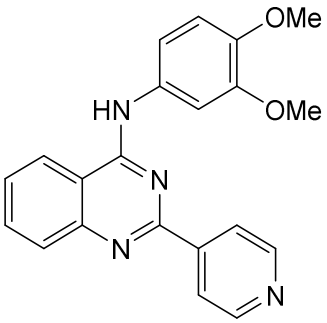

Molecular weight: 358.40 g/mol

The compound was synthesized from **46** (242 mg, 1 mmol) and 3,4-dimethoxyaniline (153 mg, 1 mmol) as described in the general procedure for compounds **51-81** to yield **65** as a yellow solid (219 mg, 61%), mp 134-135 °C. **^{1}H NMR** (500 MHz, DMSO-d_6) δ 9.86

(s, 1H), 8.78 – 8.69 (m, 2H), 8.58 (dt, *J* = 8.5, 1.0 Hz, 1H), 8.31 – 8.24 (m, 2H), 7.93 – 7.86 (m, 2H), 7.72 – 7.61 (m, 2H), 7.46 (dd, *J* = 8.6, 2.5 Hz, 1H), 7.06 (d, *J* = 8.7 Hz, 1H), 3.83 (s, 3H), 3.80 (s, 3H). **^{13}C NMR** (126 MHz, DMSO) δ 158.22, 157.47, 150.33, 148.52, 145.80, 133.50, 132.46, 128.44, 126.85, 123.14, 121.86, 114.58, 111.96, 107.75, 55.92, 55.69. **Anal. Calcd. for $C_{21}H_{18}N_4O_2$**: C, 70.38; H, 5.06; N, 15.63. Found: C, 70.70; H, 5.05; N, 15.28.

2-(pyridin-4-yl)-N-(3-(trifluoromethyl)phenyl)quinazolin-4-amine (66).

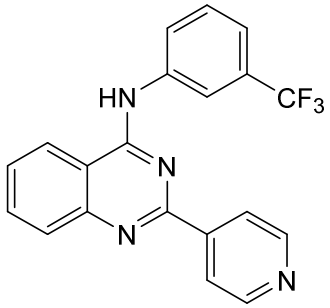

Molecular weight: 366.35 g/mol

The compound was synthesized from **46** (242 mg, 1 mmol) and 3-(trifluoromethyl)aniline (161 mg, 1 mmol) as described in the general procedure for compounds **51-81** to yield **66** as a white solid (322 mg, 88%), mp 249-250 °C (decomp.). **^{1}H NMR** (500 MHz, DMSO-d_6) δ 10.21 (s, 1H), 8.74 (d, *J* = 5.0 Hz, 2H), 8.62 (dt, *J* = 8.3, 1.0 Hz, 1H), 8.57 (d, *J* = 2.0 Hz, 1H), 8.32 – 8.24 (m, 2H), 8.21 (dd, *J* = 8.3, 2.0 Hz, 1H), 7.99 – 7.88 (m, 2H), 7.76 – 7.65 (m, 2H), 7.52 (ddd, *J* = 7.8, 1.9, 0.9 Hz, 1H). **^{13}C NMR** (126 MHz, DMSO) δ 158.20, 157.16, 150.36, 150.33, 145.45, 140.10, 133.89, 129.87, 129.37 (d, *J* = 31.6 Hz), 128.60, 127.25, 125.65, 123.24, 121.81, 120.01 (d, *J* = 3.9 Hz), 118.54 (d, *J* = 4.1 Hz), 114.54. **Anal. Calcd. for $C_{20}H_{13}F_3N_4$**: C, 65.57; H, 3.58; N, 15.29. Found: C, 65.53; H, 3.93; N, 14.90.

2-(pyridin-4-yl)-N-(4-(trifluoromethyl)phenyl)quinazolin-4-amine (67).

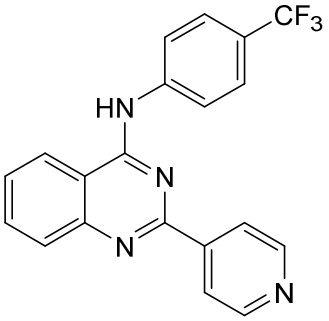

Molecular weight: 366.35 g/mol

The compound was synthesized from **46** (242 mg, 1 mmol) and 4-(trifluoromethyl)aniline (161 mg, 1 mmol) as described in the general procedure for compounds **51-81** to yield **67** as a white solid (308 mg, 84%), mp 264-265 °C (decomp.). **^{1}H NMR** (500 MHz, DMSO-d_6) δ 10.22 (s, 1H), 8.83 – 8.68 (m, 2H), 8.64 (dt, *J* = 8.4, 1.1 Hz, 1H), 8.34 – 8.27 (m, 2H), 8.28 – 8.19 (m, 2H), 7.98 – 7.91 (m, 2H), 7.87 – 7.80 (m, 2H), 7.72 (ddd, *J* = 8.3, 5.4, 2.8 Hz, 1H). **^{13}C NMR** (126 MHz, DMSO) δ 158.19, 157.24, 150.40, 150.36, 145.47, 143.03, 133.95, 128.60, 127.29, 125.93 (d, *J* = 3.6 Hz), 123.59 (d, *J* = 32.1 Hz), 123.36, 121.99, 121.89, 114.63. **Anal. Calcd. for $C_{20}H_{13}F_3N_4$**: C, 65.57; H, 3.58; N, 15.29. Found: C, 65.29; H, 3.86; N, 15.20.

N-(4-methoxy-3-(trifluoromethyl)phenyl)-2-(pyridin-4-yl)quinazolin-4-amine (68).

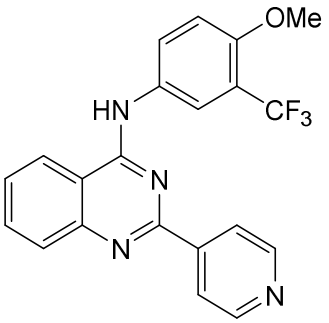

Molecular weight: 396.37 g/mol

The compound was synthesized from **46** (242 mg, 1 mmol) and 4-methoxy-3-(trifluoromethyl)aniline (191 mg, 1 mmol) as described in the general procedure for compounds **51-81** to yield **68** as a light beige solid (226 mg, 57%), mp 256-257 °C (decomp.). **^{1}H NMR** (500 MHz, DMSO-d_6) δ 10.06 (s, 1H), 8.76 – 8.68 (m, 2H), 8.57

(dt, *J* = 8.4, 1.1 Hz, 1H), 8.39 (d, *J* = 2.7 Hz, 1H), 8.28 – 8.22 (m, 2H), 8.17 (dd, *J* = 9.0, 2.7 Hz, 1H), 7.95 – 7.88 (m, 2H), 7.69 (ddd, *J* = 8.3, 5.0, 3.2 Hz, 1H), 7.40 (d, *J* = 9.1 Hz, 1H), 3.94 (s, 3H). **^{13}C NMR** (126 MHz, DMSO) δ 158.16, 157.26, 153.33, 150.25, 150.20, 145.62, 133.68, 131.98, 128.51, 127.73, 127.05, 124.95, 123.13, 122.79, 121.80, 120.94 (d, *J* = 5.8 Hz), 116.59 (d, *J* = 30.2 Hz), 114.46, 113.36, 56.49. **Anal. Calcd. for $C_{21}H_{15}F_3N_4O$**: C, 63.63; H, 3.81; N, 14.14. Found: C, 63.87; H, 3.87; N, 13.76.

N-(3-fluorophenyl)-2-(pyridin-3-yl)quinazolin-4-amine (69).

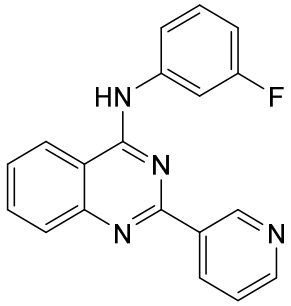

Molecular weight: 316.34 g/mol

The compound was synthesized from **45** (242 mg, 1 mmol) and 3-fluoroaniline (111 mg, 1 mmol) as described in the general procedure for compounds **51-81** to yield **69** as a yellow solid (253 mg, 80%), mp 272-274 °C (decomp.) . **^{1}H NMR** (500 MHz, DMSO-d_6) δ 10.60 (s, 1H), 9.52 (d, *J* = 2.0 Hz, 1H), 9.04 (dt, *J* = 8.1, 1.9 Hz, 1H), 8.91 (dd, *J* = 5.3, 1.5 Hz, 1H), 8.76 (d, *J* = 8.2 Hz, 1H), 8.10 – 8.01 (m, 1H), 8.01 – 7.98 (m, 1H), 7.98 – 7.92 (m, 1H), 7.89 (dt, *J* = 11.6, 2.4 Hz, 1H), 7.82 – 7.76 (m, 1H), 7.74 (ddd, *J* = 8.1, 6.6, 1.3 Hz, 1H), 7.51 (td, *J* = 8.2, 6.8 Hz, 1H), 7.06 (td, *J* = 8.5, 2.6 Hz, 1H). **^{13}C NMR** (126 MHz, DMSO) δ 163.07, 161.15, 158.49, 155.66, 145.18, 140.38 (d, *J* = 10.9 Hz), 134.51, 130.28 (d, *J* = 9.4 Hz), 127.57, 126.83, 125.76, 123.82, 118.79, 111.16 (d, *J* = 21.2 Hz), 109.82 (d, *J* = 25.7 Hz). **Anal. Calcd. for $C_{19}H_{13}FN_4$**: C, 72.14; H, 4.14; N, 17.71. Found: C, 72.13; H, 4.38; N, 17.69.

3-((2-(pyridin-4-yl)quinazolin-4-yl)amino)benzenesulfonyl fluoride (70).

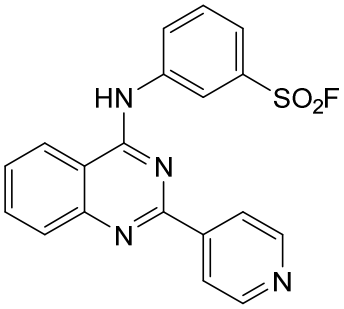

Molecular weight: 380.40 g/mol

The compound was synthesized from **46** (242 mg, 1 mmol) and 3-aminobenzenesulfonyl fluoride (175 mg, 1 mmol) as described in the general procedure for compounds **51-81** to yield **70** as a yellow solid (293 mg, 77%), mp 291-292 °C (decomp.). **^{1}H NMR** (600 MHz, DMSO-d_6) δ 10.40 (s, 1H), 9.14 (t, J = 1.9 Hz, 1H), 8.73 (d, J = 5.1 Hz, 2H), 8.62 (d, J = 8.4 Hz, 1H), 8.42 (dt, J = 7.2, 2.1 Hz, 1H), 8.35 – 8.26 (m, 2H), 8.01 – 7.92 (m, 2H), 7.92 – 7.83 (m, 2H), 7.74 (ddd, J = 8.2, 5.5, 2.7 Hz, 1H). **^{13}C NMR** (151 MHz, DMSO) δ 158.10, 157.08, 150.40, 150.39, 145.24, 141.04, 134.10, 131.85 (d, J = 23.1 Hz), 131.00, 128.96, 128.69, 127.46, 123.27, 122.78, 121.91, 120.60, 114.54. **Anal. Calcd. for $C_{19}H_{13}FN_4O_2S$**: C, 59.99; H, 3.44; N, 14.73. Found: C, 60.36; H, 3.68; N, 14.48.

***N*^{1},*N*^{1}-dimethyl-*N*^{3}-(2-(pyridin-3-yl)quinazolin-4-yl)benzene-1,3-diamine (71).**

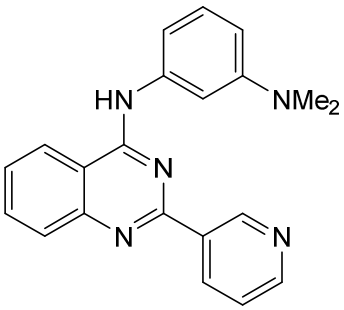

Molecular weight: 341.42 g/mol

The compound was synthesized from **5** (242 mg, 1 mmol) and *N*^{1},*N*^{1}-dimethylbenzene-1,3-diamine (136 mg, 1 mmol) as described in the general procedure for compounds **51-81** to yield **71** as a light brown solid (201 mg, 59%), mp 202-203 °C. **^{1}H NMR** (500 MHz,

DMSO-d_6) δ 10.87 (s, 1H), 9.62 – 9.48 (m, 1H), 9.18 (d, *J* = 8.1 Hz, 1H), 9.02 – 8.90 (m, 1H), 8.83 (dd, *J* = 8.5, 1.4 Hz, 1H), 8.11 (d, *J* = 8.3 Hz, 1H), 8.01 (ddd, *J* = 8.4, 5.9, 1.3 Hz, 3H), 7.76 (ddd, *J* = 8.3, 7.0, 1.2 Hz, 1H), 7.62 (s, 1H), 7.51 (t, *J* = 8.1 Hz, 1H), 7.25 (s, 1H), 3.09 (s, 6H). **^{13}C NMR** (126 MHz, DMSO) δ 158.64, 155.19, 141.28, 139.26, 134.84, 129.86, 127.86, 126.07, 124.09, 114.05, 43.50. **Anal. Calcd. for $C_{21}H_{19}N_5$:** C, 73.88; H, 5.61; N, 20.51. Found: C, 73.97; H, 5.37; N, 20.25.

3-((2-(pyridin-4-yl)quinazolin-4-yl)amino)phenol (72).

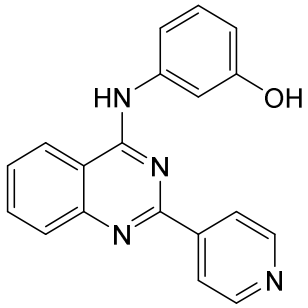

Molecular weight: 314.35 g/mol

The compound was synthesized from **46** (242 mg, 1 mmol) and 3-aminophenol (109 mg, 1 mmol) as described in the general procedure for compounds **51-81** to yield **72** as a yellow solid (148 mg, 47%), mp >300 °C. **^{1}H NMR** (500 MHz, DMSO-d_6) δ 10.13 (s, 1H), 9.60 (s, 1H), 8.97 – 8.91 (m, 2H), 8.70 (dt, *J* = 8.4, 0.9 Hz, 1H), 8.65 – 8.58 (m, 2H), 8.01 – 7.90 (m, 2H), 7.73 (ddd, *J* = 8.3, 6.5, 1.7 Hz, 1H), 7.44 (t, *J* = 2.2 Hz, 1H), 7.36 (ddd, *J* = 8.0, 2.0, 1.0 Hz, 1H), 7.25 (t, *J* = 8.0 Hz, 1H), 6.64 (ddd, *J* = 8.1, 2.4, 1.0 Hz, 1H). **^{13}C NMR** (126 MHz, DMSO) δ 158.52, 157.73, 155.80, 149.34, 145.76, 139.73, 134.05, 129.32, 128.07, 127.80, 123.76, 123.64, 114.66, 113.64, 111.75, 109.97. **Anal. Calcd. for $C_{19}H_{14}N_4O$**: C, 72.60; H, 4.49; N, 17.82. Found: C, 72.86; H, 4.63; N, 17.44.

4-((2-(pyridin-4-yl)quinazolin-4-yl)amino)phenol (73).

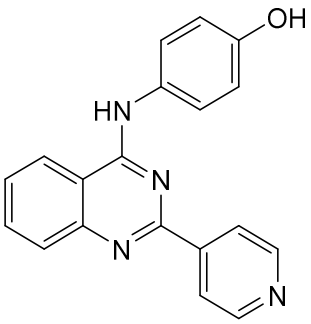

Molecular weight: 314.35 g/mol

The compound was synthesized from **46** (242 mg, 1 mmol) and 4-aminophenol (109 mg, 1 mmol) as described in the general procedure for compounds **51-81** to yield **73** as a yellow solid (182 mg, 58%), mp 293-295 °C (decomp). **^{1}H NMR** (500 MHz, DMSO-d_6) δ 10.34 (s, 1H), 9.52 (s, 1H), 8.96 (d, *J* = 5.7 Hz, 2H), 8.73 – 8.63 (m, 1H), 8.63 – 8.50 (m, 2H), 8.00 (dd, *J* = 8.4, 1.3 Hz, 1H), 7.95 (ddd, *J* = 8.2, 6.8, 1.2 Hz, 1H), 7.72 (ddd, *J* = 8.2, 6.9, 1.4 Hz, 1H), 7.67 – 7.56 (m, 2H), 6.94 – 6.84 (m, 2H). **^{13}C NMR** (126 MHz, DMSO) δ 158.67, 155.44, 154.95, 134.17, 129.56, 127.91, 125.22, 123.92, 123.64, 115.27, 114.43. **Anal. Calcd. for $C_{19}H_{14}N_4O$**: C, 72.60; H, 4.49; N, 17.82. Found: C, 72.69; H, 4.67; N, 17.54.

(4-((2-(pyridin-3-yl)quinazolin-4-yl)amino)phenyl)methanol (74).

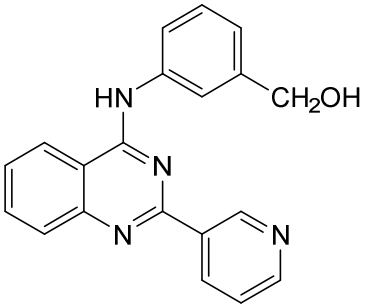

Molecular weight: 328.38 g/mol

The compound was synthesized from **45** (242 mg, 1 mmol) and (3-aminophenyl)methanol (123 mg, 1 mmol) as described in the general procedure for compounds **51-81** to yield **74** as a yellow solid (210 mg, 64%), mp >300 °C. **^{1}H NMR** (500 MHz, DMSO-d_6) δ 10.65 (s, 1H), 9.56 (d, *J* = 2.1 Hz, 1H), 9.07 (dt, *J* = 8.1, 1.9 Hz, 1H), 8.92 (dd, *J* = 5.2, 1.6 Hz,

1H), 8.83 – 8.73 (m, 1H), 8.08 (d, *J* = 8.3 Hz, 1H), 8.05 – 7.97 (m, 2H), 7.91 (dd, *J* = 8.1, 5.2 Hz, 1H), 7.82 – 7.73 (m, 2H), 7.45 (t, *J* = 7.8 Hz, 1H), 7.20 (d, *J* = 7.5 Hz, 1H), 4.63 (s, 2H). **^{13}C NMR** (126 MHz, DMSO) δ 158.57, 155.67, 143.33, 138.17, 134.59, 128.37, 127.59, 125.53, 123.86, 122.98, 121.58, 121.35, 114.05, 62.87. **Anal. Calcd. for $C_{20}H_{16}N_4O$**: C, 73.15; H, 4.91; N, 17.06. Found: C, 73.17; H, 5.07; N, 16.83.

(4-((2-(pyridin-4-yl)quinazolin-4-yl)amino)phenyl)methanol (75).

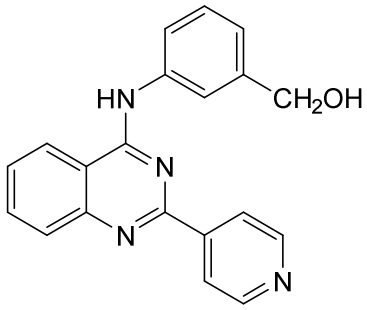

Molecular weight: 328.38 g/mol

The compound was synthesized from **46** (242 mg, 1 mmol) and (3-aminophenyl)methanol (123 mg, 1 mmol) as described in the general procedure for compounds **51-81** to yield **75** as a yellow solid (200 mg, 61%), mp >300 °C. **^{1}H NMR** (500 MHz, DMSO-d_6) δ 10.36 (s, 1H), 8.97 (d, *J* = 5.7 Hz, 2H), 8.80 – 8.60 (m, 3H), 8.06 (t, *J* = 1.9 Hz, 1H), 8.03 – 7.90 (m, 2H), 7.81 – 7.68 (m, 2H), 7.42 (t, *J* = 7.8 Hz, 1H), 7.19 – 7.12 (m, 1H), 4.62 (s, 2H). **^{13}C NMR** (126 MHz, DMSO) δ 158.52, 155.29, 149.20, 144.54, 143.25, 138.58, 134.15, 128.31, 128.03, 124.18, 123.66, 122.49, 121.13, 121.01, 114.64, 62.91. **Anal. Calcd. for $C_{20}H_{16}N_4O$**: C, 73.15; H, 4.91; N, 17.06. Found: C, 73.06; H, 5.27; N, 16.69.

2-nitro-4-((2-(pyridin-3-yl)quinazolin-4-yl)amino)phenol (76).

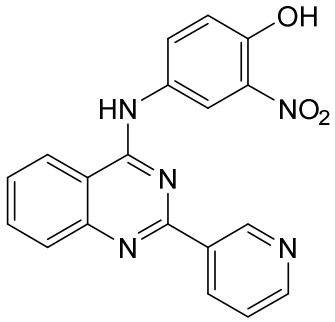

Molecular weight: 359.35 g/mol

The compound was synthesized from **45** (242 mg, 1 mmol) and 4-amino-2-nitrophenol (154 mg, 1 mmol) as described in the general procedure for compounds **51-81** to yield **76** as a yellow-orange solid (223 mg, 62%), mp 284-286 °C (decomp.). **^{1}H NMR** (500 MHz, DMSO-d_6) δ 10.83 (s, 1H), 10.06 (s, 1H), 9.56 (dd, *J* = 2.2, 0.9 Hz, 1H), 8.78 (d, *J* = 2.7 Hz, 1H), 8.74 – 8.70 (m, 1H), 8.68 (dd, *J* = 4.7, 1.7 Hz, 1H), 8.54 (dt, *J* = 8.4, 1.1 Hz, 1H), 8.04 (dd, *J* = 9.0, 2.7 Hz, 1H), 7.92 – 7.86 (m, 2H), 7.68 – 7.61 (m, 1H), 7.56 – 7.50 (m, 1H), 7.24 (d, *J* = 9.0 Hz, 1H). **^{13}C NMR** (126 MHz, DMSO) δ 158.02, 157.53, 151.12, 150.34, 149.39, 148.98, 135.68, 135.27, 133.66, 133.64, 131.04, 130.26, 128.35, 126.63, 123.71, 123.12, 119.39, 118.37, 114.18. **Anal. Calcd. for $C_{19}H_{13}N_5O_3$**: C, 63.51; H, 3.65; N, 19.49. Found: C, 63.90; H, 3.81; N, 19.21.

methyl 3-((2-(pyridin-3-yl)quinazolin-4-yl)amino)benzoate (77).

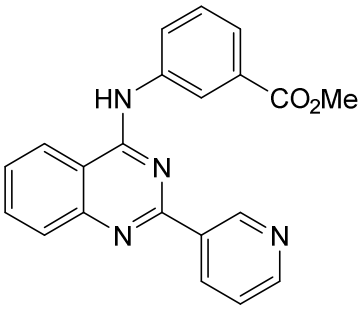

Molecular weight: 356.39 g/mol

The compound was synthesized from **45** (242 mg, 1 mmol) and methyl 3-aminobenzoate (151 mg, 1 mmol) as described in the general procedure for compounds **51-81** to yield **77** as a light yellow solid (282 mg, 79%), mp 233-234 °C. **^{1}H NMR** (600 MHz, DMSO-d_6) δ 10.73 (s, 1H), 9.55 (d, *J* = 2.1 Hz, 1H), 9.09 (dt, *J* = 8.2, 1.8 Hz, 1H), 8.92 (dd, *J* = 5.4, 1.5 Hz, 1H), 8.84 – 8.70 (m, 2H), 8.20 (ddd, *J* = 8.1, 2.3, 1.1 Hz, 1H), 8.08 – 8.01 (m, 1H), 8.01 – 7.90 (m, 2H), 7.80 (dt, *J* = 7.8, 1.3 Hz, 1H), 7.74 (ddd, *J* = 8.3, 6.9, 1.3 Hz, 1H), 7.62 (t, *J* = 7.9 Hz, 1H), 3.92 (s, 3H). **^{13}C NMR** (151 MHz, DMSO) δ 166.27, 158.50, 155.45, 145.09, 140.34, 139.04, 134.64, 130.15, 129.24, 127.71, 127.32, 126.54, 125.87, 125.16, 123.91, 123.36, 114.20, 52.56. **Anal. Calcd. for $C_{21}H_{16}N_4O_2$**: C, 70.77; H, 4.53; N, 15.72. Found: C, 71.08; H, 4.62; N, 15.49.

methyl 3-((2-(pyridin-4-yl)quinazolin-4-yl)amino)benzoate (78).

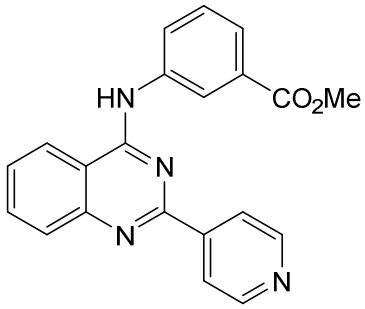

Molecular weight: 356.39 g/mol

The compound was synthesized from **46** (242 mg, 1 mmol) and methyl 3-aminobenzoate (151 mg, 1 mmol) as described in the general procedure for compounds **51-81** to yield **78** as a yellow solid (256 mg, 76%), mp 251-252 °C (decomp.). **^{1}H NMR** (600 MHz, DMSO-d_6) δ 10.46 (s, 1H), 9.01 – 8.94 (m, 2H), 8.81 (t, J = 2.0 Hz, 1H), 8.75 (d, J = 8.3 Hz, 1H), 8.71 – 8.65 (m, 2H), 8.22 (ddd, J = 8.1, 2.3, 1.1 Hz, 1H), 8.04 – 7.95 (m, 2H), 7.83 – 7.74 (m, 2H), 7.63 (t, J = 7.9 Hz, 1H), 3.93 (s, 3H). **^{13}C NMR** (151 MHz, DMSO) δ 166.32, 158.44, 155.33, 151.08, 149.69, 144.88, 139.39, 134.28, 130.13, 129.24, 128.49, 128.17, 126.90, 124.77, 124.01, 123.66, 123.00, 114.72, 52.50. **Anal. Calcd. for $C_{21}H_{16}N_4O_2$**: C, 70.77; H, 4.53; N, 15.72. Found: C, 70.92; H, 4.63; N, 15.72.

***tert*-butyl 3-((2-(pyridin-4-yl)quinazolin-4-yl)amino)benzoate (79).**

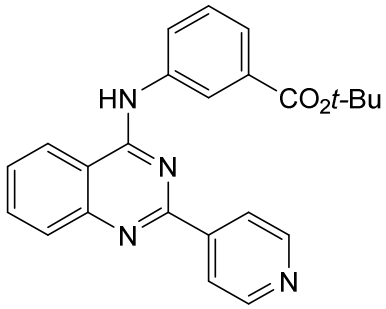

Molecular weight: 398.47 g/mol

The compound was synthesized from **46** (242 mg, 1 mmol) and methyl tert-butyl 3-aminobenzoate (193 mg, 1 mmol) as described in the general procedure for compounds **51-81** to yield **79** as a yellow solid (255 mg, 64%), mp >300 °C. **^{1}H NMR** (600 MHz, DMSO-d_6) δ 10.20 (s, 1H), 8.81 – 8.74 (m, 2H), 8.68 – 8.61 (m, 1H), 8.34 – 8.26 (m, 2H),

8.18 – 8.09 (m, 2H), 8.05 – 7.99 (m, 2H), 7.99 – 7.91 (m, 2H), 7.72 (ddd, *J* = 8.2, 5.8, 2.4 Hz, 1H), 1.57 (s, 9H). **^{13}C NMR** (151 MHz, DMSO) δ 164.83, 158.14, 157.32, 150.51, 150.42, 145.40, 143.50, 133.93, 129.97, 128.59, 127.26, 126.08, 123.39, 121.92, 121.29, 114.69, 80.52, 28.05. **Anal. Calcd. for $C_{24}H_{22}N_4O_2$**: C, 72.34; H, 5.57; N, 14.06. Found: C, 72.50; H, 5.88; N, 13.99.

3-((2-(pyridin-3-yl)quinazolin-4-yl)amino)benzoic acid (80).

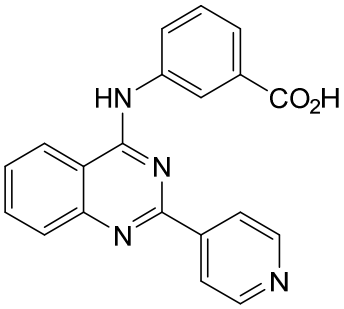

Molecular weight: 342.36 g/mol

The compound was synthesized from **46** (242 mg, 1 mmol) and methyl 3-aminobenzoic acid (137 mg, 1 mmol) as described in the general procedure for compounds **51-81** to yield **80** as a yellow-beige solid (147 mg, 43%), mp >300 °C. **^{1}H NMR** (500 MHz, DMSO-d_6) δ 13.07 (s, 1H), 10.48 (s, 1H), 9.11 – 8.88 (m, 2H), 8.84 (t, *J* = 1.9 Hz, 1H), 8.81 – 8.61 (m, 3H), 8.20 (ddd, *J* = 8.2, 2.3, 1.1 Hz, 1H), 8.11 – 7.90 (m, 2H), 7.90 – 7.68 (m, 2H), 7.62 (t, *J* = 7.9 Hz, 1H). **^{13}C NMR** (126 MHz, DMSO) δ 167.30, 158.45, 155.43, 150.75, 149.63, 145.07, 139.22, 134.20, 131.32, 128.97, 128.40, 128.06, 126.52, 124.93, 123.96, 123.60, 123.35, 114.69. **Anal. Calcd. for $C_{20}H_{14}N_4O_2$**: C, 70.17; H, 4.12; N, 16.37. Found: C, 70.27; H, 4.44; N, 16.45.

4-((2-(pyridin-3-yl)quinazolin-4-yl)amino)benzoic acid (81).

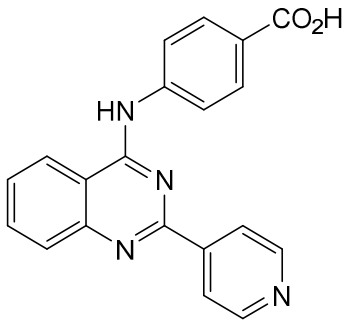

Molecular weight: 342.36 g/mol

The compound was synthesized from **46** (242 mg, 1 mmol) and methyl 4-aminobenzoic acid (137 mg, 1 mmol) as described in the general procedure for compounds **51-81** to yield **81** as a brown-beiges solid (188 mg, 55%), mp >300 °C. **^{1}H NMR** (500 MHz, DMSO-d_6) δ 12.51 (s, 1H), 10.52 (s, 1H), 9.03 – 8.95 (m, 2H), 8.78 (dd, J = 8.3, 1.1 Hz, 1H), 8.74 – 8.68 (m, 2H), 8.16 – 8.09 (m, 2H), 8.08 – 8.03 (m, 2H), 8.03 – 7.95 (m, 2H), 7.77 (ddd, J = 8.2, 6.1, 2.1 Hz, 1H).**^{13}C NMR** (126 MHz, DMSO) δ 167.06, 158.39, 155.19, 151.54, 149.82, 144.33, 143.10, 134.32, 130.22, 128.52, 128.23, 125.94, 124.29, 123.79, 121.79, 114.84. **Anal. Calcd. for $C_{20}H_{14}N_4O_2$**: C, 70.17; H, 4.12; N, 16.37. Found: C, 70.49; H, 4.38; N, 16.25.

General Procedure for the Preparation of the 2-substituted 6-methyl-4-anilinopyrimidines 82-88.

To the corresponding 2-substituted 6-methyl-4-chloropyrimidine derivatives **49** and **50** (1 mmol) isopropanol (5 mL) was added together with the corresponding substituted aniline (1 mmol) and sealed in a microwave tube. The mixture was heated by 100 watt microwave irradiation to 110 °C for a period of 15 – 30 min until completion of the reaction as indicated by TLC. The formed precipitate was filtered off, washed with 10 mL isopropanol and dried in vacuo. If no precipitate was formed, the solvent was removed under reduced pressure and the remaining solid recrystallized from acetone.

3-((6-methyl-2-(pyridin-4-yl)pyrimidin-4-yl)amino)benzonitrile (82).

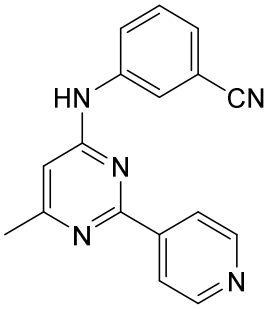

Molecular weight: 287.33 g/mol

The compound was synthesized from **49** (206 mg, 1 mmol) and methyl 3-aminobenzonitrile (118 mg, 1 mmol) as described in the general procedure for compounds **82-88** to yield **82** as a white solid (135 mg, 47%), mp >300 °C. **^{1}H NMR** (600 MHz, DMSO-d_6) δ 9.97 (s, 1H), 8.73 (d, J = 4.8 Hz, 2H), 8.21 (t, J = 1.9 Hz, 1H), 8.18 – 8.10 (m, 2H), 8.07 – 7.95 (m, 1H), 7.58 (t, J = 8.0 Hz, 1H), 7.47 (dt, J = 7.7, 1.2 Hz, 1H), 6.69 (s, 1H), 2.43 (s, 3H). **^{13}C NMR** (151 MHz, DMSO) δ 165.92, 160.79, 160.63, 150.37, 145.11, 140.84, 130.41, 125.74, 124.33, 122.48, 121.70, 119.00, 111.78, 105.53, 23.89. **Anal. Calcd. for $C_{17}H_{13}N_5$**: C, 71.06; H, 4.56; N, 24.37. Found: C, 71.17; H, 4.37; N, 24.07.

***N*-(3-methoxyphenyl)-6-methyl-2-(pyridin-4-yl)pyrimidin-4-amine (83).**

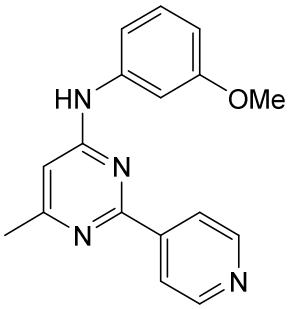

Molecular weight: 292.34 g/mol

The compound was synthesized from **49** (206 mg, 1 mmol) and methyl 3-methoxyaniline (123 mg, 1 mmol) as described in the general procedure for compounds **82-88** to yield **83** as a light beige solid (140 mg, 48%), mp 227-229 (decomp.). **^{1}H NMR** (500 MHz, DMSO-d_6) δ 10.23 (s, 1H), 9.04 – 8.95 (m, 2H), 8.63 – 8.53 (m, 2H), 7.43 (t, J = 2.2 Hz,

1H), 7.34 – 7.23 (m, 2H), 6.85 (s, 1H), 6.66 (ddd, *J* = 7.6, 2.4, 1.3 Hz, 1H), 3.78 (s, 3H), 2.45 (s, 3H). **^{13}C NMR** (126 MHz, DMSO) δ 164.56, 161.03, 159.77, 158.51, 144.39, 140.62, 129.77, 124.02, 112.63, 108.92, 106.14, 105.87, 55.22, 23.33. **Anal. Calcd. for $C_{17}H_{16}N_4O$**: C, 69.85; H, 5.52; N, 19.17. Found: C, 69.53; H, 5.71; N, 19.52.

***N*-(4-methoxyphenyl)-6-methyl-2-(pyridin-4-yl)pyrimidin-4-amine (84).**

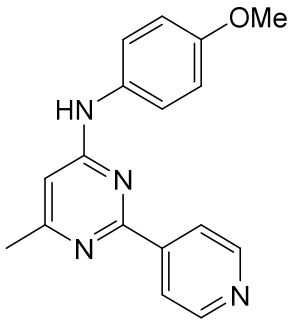

Molecular weight: 292.34 g/mol

The compound was synthesized from **49** (206 mg, 1 mmol) and methyl 4-methoxyaniline (123 mg, 1 mmol) as described in the general procedure for compounds **82-88** to yield **84** as a light beige solid (114 mg, 39%), mp >300 °C. **^{1}H NMR** (500 MHz, DMSO-d_6) δ 9.59 (s, 1H), 8.81 – 8.76 (m, 2H), 8.29 – 8.24 (m, 2H), 7.58 (d, *J* = 8.4 Hz, 2H), 7.00 – 6.94 (m, 2H), 6.59 (d, *J* = 0.8 Hz, 1H), 3.76 (s, 3H), 2.39 (d, *J* = 0.7 Hz, 3H). **^{13}C NMR** (126 MHz, DMSO) δ 148.81, 122.31, 114.30, 55.39, 23.61. **Anal. Calcd. for $C_{17}H_{16}N_4O$**: C, 69.85; H, 5.52; N, 19.17. Found: C, 69.53; H, 5.71; N, 19.52.

3-((6-methyl-2-phenylpyrimidin-4-yl)amino)benzonitrile (85).

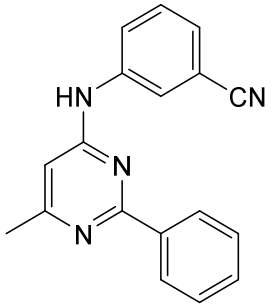

Molecular weight: 286.34 g/mol

The compound was synthesized from **50** (205 mg, 1 mmol) and methyl 3-aminobenzonitrile (118 mg, 1 mmol) as described in the general procedure for compounds **82-88** to yield **85** as a white solid (157 mg, 55%), mp 290-291 °C (decomp.). **^{1}H NMR** (500 MHz, DMSO-d_6) δ 10.87 (s, 1H), 8.33 – 8.17 (m, 3H), 8.02 (d, J = 8.1 Hz, 1H), 7.69 – 7.47 (m, 5H), 6.83 (s, 1H), 2.52 (s, 3H). **^{13}C NMR** (126 MHz, DMSO) δ 160.90, 132.20, 130.53, 128.92, 128.41, 118.76, 111.89, 104.43. **Anal. Calcd. for $C_{18}H_{14}N_4$**: C, 75.50.85; H, 4.93; N, 19.57. Found: C, 75.82; H, 5.24; N, 19.38.

4-((6-methyl-2-phenylpyrimidin-4-yl)amino)benzonitrile (86).

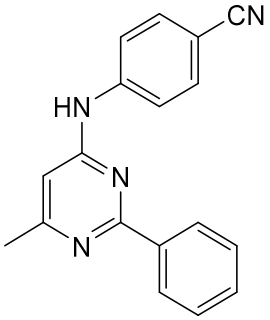

Molecular weight: 286.34 g/mol

The compound was synthesized from **50** (205 mg, 1 mmol) and methyl 4-aminobenzonitrile (118 mg, 1 mmol) as described in the general procedure for compounds **82-88** to yield **86** as a white solid (180 mg, 63%), mp 262-264 °C (decomp.). **^{1}H NMR** (600 MHz, DMSO-d_6) δ 11.41 (s, 1H), 8.36 – 8.22 (m, 2H), 8.02 (d, J = 8.4 Hz, 2H), 7.94 – 7.82 (m, 2H), 6.98 (s, 1H), 2.55 (s, 3H). **^{13}C NMR** (151 MHz, DMSO) δ 161.20, 160.87, 133.80, 132.83, 129.36, 129.07, 121.26, 119.47, 25.96. **Anal. Calcd. for $C_{18}H_{14}N_4$**: C, 75.50; H, 4.93; N, 19.57. Found: C, 75.74; H, 5.22; N, 19.22.

4-((6-methyl-2-phenylpyrimidin-4-yl)amino)-2-nitrophenol (87).

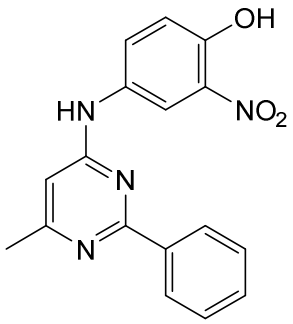

Molecular weight: 322.32 g/mol

The compound was synthesized from **50** (205 mg, 1 mmol) and methyl 4-amino-2-nitrophenol (154 mg, 1 mmol) as described in the general procedure for compounds **82-88** to yield **87** as a yellow solid (168 mg, 52%), mp 276-278 °C (decomp.). **^{1}H NMR** (600 MHz, DMSO-d_6) δ 11.07 (s, 1H), 8.61 (s, 1H), 8.35 – 8.25 (m, 2H), 7.76 (d, *J* = 8.9 Hz, 1H), 7.68 (t, *J* = 7.3 Hz, 1H), 7.61 (t, *J* = 7.6 Hz, 2H), 7.26 (d, *J* = 9.0 Hz, 1H), 6.82 (s, 1H), 2.53 (s, 3H). **^{13}C NMR** (151 MHz, DMSO) δ 129.02, 128.77, 119.90. **Anal. Calcd. for $C_{17}H_{14}N_4O_3$**: C, 63.35; H, 4.38; N, 17.38. Found: C, 63.63; H, 4.73; N, 17.26.

6-methyl-*N*,2-diphenylpyrimidin-4-amine (88).

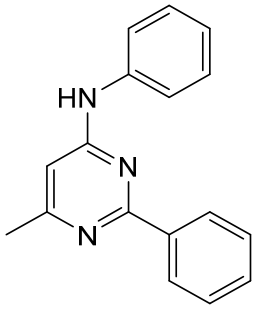

Molecular weight: 261.33 g/mol

The compound was synthesized from **50** (205 mg, 1 mmol) and methyl aniline (93 mg, 1 mmol) as described in the general procedure for compounds **82-88** to yield **88** as a white solid (165 mg, 63%), mp 250-251 °C (decomp.). **^{1}H NMR** (500 MHz, DMSO-d_6) δ 11.09 (s, 1H), 8.32 – 8.19 (m, 2H), 7.86 – 7.64 (m, 3H), 7.62 (dd, *J* = 8.3, 6.6 Hz, 2H), 7.50 – 7.39 (m, 2H), 7.21 (t, *J* = 7.4 Hz, 1H), 6.86 (s, 1H), 2.54 (s, 3H). ^{13}C NMR (126 MHz, DMSO) δ 161.03, 159.79, 137.90, 132.75, 129.21, 129.02, 128.74, 125.00, 121.88,

104.02, 20.08. Anal. Calcd. for $C_{17}H_{15}N_3$; C, 78.13; H, 5.79; N, 16.08. Found: C, 78.05; H, 5.63; N, 16.00.

10.1.1.3 Synthesis of 2,4-Substituted quinazolines

General Procedure for the Preparation of the 2-phenylquinazolin-4(3*H*)-one derivatives 91-97. A mixture of anthranilamide (2.72 g, 20 mmol), the corresponding pyridinecarboxaldehyde (20 mmol), iodine (3.17 g, 25 mmol), anhydrous potassium carbonate (2.76 g, 20 mmol) and 20 mL DMF was stirred at 70-90 °C for 4-8 h. The end of the reaction was monitored by TLC and the mixture poured on crushed ice to form a precipitate. Incomplete precipitation can be prevented by adjusting the pH with concentrated HCl solution to about 7. After filtration of the precipitate, it was thoroughly washed with 100 mL of a 20% sodium thiosulfate solution followed by 100 mL of hot distilled water. Purification was performed by recrystallization from ethanol.

2-(3-nitrophenyl)quinazolin-4(3H)-one (91).

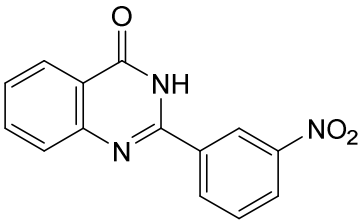

Molecular weight: 267.24 g/mol

The title compound was synthesized from 3-nitrobenzaldehyde (3.02 g, 20 mmol) as described in the general procedure for **91-97** to yield **91** as a white solid (5,18 g, 97%). **^{1}H NMR** (500 MHz, DMSO-d_6) δ 12.63 (s, 1H), 9.02 (t, *J* = 2.1 Hz, 1H), 8.61 (ddd, *J* = 7.9, 1.8, 1.0 Hz, 1H), 8.40 (ddd, *J* = 8.2, 2.3, 1.0 Hz, 1H), 8.18 (ddd, *J* = 7.8, 1.5, 0.5 Hz, 1H), 7.88 – 7.81 (m, 2H), 7.79 (dd, *J* = 8.0, 1.7 Hz, 1H), 7.55 (ddd, *J* = 8.2, 7.0, 1.3 Hz, 1H). **^{13}C NMR** (126 MHz, DMSO) δ 161.90, 150.46, 148.18, 148.03, 134.42, 134.38, 133.72, 130.00, 127.35, 126.83, 125.70, 125.41, 122.45, 121.15.

2-(4-nitrophenyl)quinazolin-4(3H)-one (92).

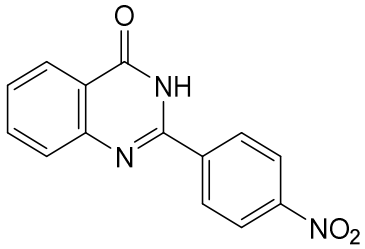

Molecular weight: 267.24 g/mol

The title compound was synthesized from 4-nitrobenzaldehyde (3.02 g, 20 mmol) as described in the general procedure for **91-97** to yield **92** as a white solid (4,92 g, 92%). **^{1}H NMR** (500 MHz, DMSO-d_6) δ 12.79 (s, 1H), 8.44 – 8.34 (m, 4H), 8.18 (dd, J = 8.1, 1.3 Hz, 1H), 7.87 (ddd, J = 8.5, 7.1, 1.6 Hz, 1H), 7.79 (dd, J = 7.9, 1.0 Hz, 1H), 7.57 (ddd, J = 8.2, 7.1, 1.2 Hz, 1H). **^{13}C NMR** (126 MHz, DMSO) δ 162.21, 150.91, 149.11, 148.42, 138.71, 134.88, 129.42, 127.83, 127.45, 126.03, 123.73, 121.36.

3-(4-oxo-3,4-dihydroquinazolin-2-yl)benzonitrile (93).

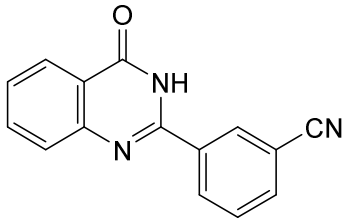

Molecular weight: 247.26 g/mol

The title compound was synthesized from 3-formylbenzonitrile (2.62 g, 20 mmol) as described in the general procedure for **91-97** to yield **93** as a white solid (4,25 g, 86%). **^{1}H NMR** (500 MHz, DMSO-d_6) δ 12.66 (s, 1H), 8.58 (m, 1H), 8.48 (m, 1H), 8.16 (m, 1H), 8.04 (m, 1H), 7.85 (m, 1H), 7.76 (m, 2H), 7.54 (m, 1H). **^{13}C NMR** (126 MHz, DMSO) δ 162.21, 150.91, 149.11, 148.42, 138.71, 134.88, 129.42, 127.83, 127.45, 126.03, 123.73, 121.36. ^{13}C NMR (126 MHz, DMSO) δ 148.54, 134.74, 132.54, 131.58, 130.04, 127.67, 127.11, 126.01, 118.40, 111.90, 99.64.

2-(2-methoxyphenyl)quinazolin-4(3H)-one (94).

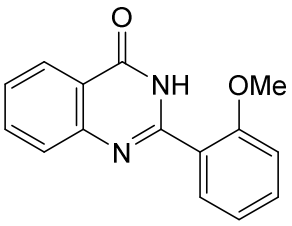

Molecular weight: 252.27 g/mol

The title compound was synthesized from 2-methoxybenzaldehyde (2.72 g, 20 mmol) as described in the general procedure for **91-97** to yield **94** as a white solid (4,14 g, 82%). **^{1}H NMR** (500 MHz, DMSO-d_6) δ 12.05 (s, 1H), 8.14 (dd, J = 8.0, 1.6 Hz, 1H), 7.82 (ddd, J = 8.6, 7.1, 1.6 Hz, 1H), 7.70 (ddd, J = 10.3, 7.8, 1.5 Hz, 2H), 7.57 – 7.47 (m, 2H), 7.19 (dd, J = 8.5, 1.0 Hz, 1H), 7.09 (td, J = 7.5, 1.0 Hz, 1H), 3.86 (s, 3H). **^{13}C NMR** (126 MHz, DMSO) δ 161.31, 157.29, 152.44, 149.16, 134.51, 132.33, 130.56, 127.50, 126.65, 125.89, 122.76, 121.14, 120.56, 112.04, 55.93.

2-(3-methoxyphenyl)quinazolin-4(3H)-one (95).

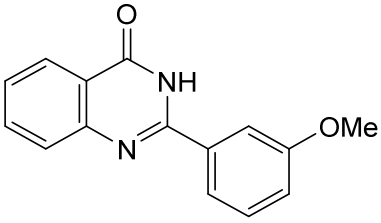

Molecular weight: 252.27 g/mol

The title compound was synthesized from 3-methoxybenzaldehyde (2.72 g, 20 mmol) as described in the general procedure for **91-97** to yield **95** as a white solid (4,24 g, 82%). **^{1}H NMR** (500 MHz, Chloroform-d) δ 11.01 (s, 1H), 8.34 – 8.24 (m, 1H), 7.86 – 7.76 (m, 2H), 7.76 – 7.67 (m, 2H), 7.52 – 7.41 (m, 2H), 7.11 (ddd, J = 8.2, 2.5, 0.9 Hz, 1H), 3.94 (s, 3H). **^{13}C NMR** (126 MHz, $CDCl_3$) δ 163.36, 160.19, 151.42, 149.38, 134.86, 134.14, 130.14, 128.03, 126.85, 126.35, 120.95, 119.35, 118.20, 112.07, 55.58.

2-(4-methoxyphenyl)quinazolin-4(3H)-one (96).

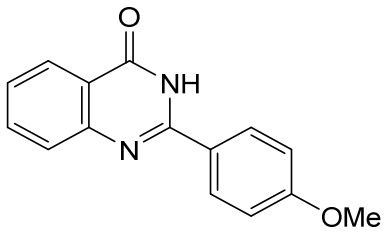

Molecular weight: 252.27 g/mol

The title compound was synthesized from 4-methoxybenzaldehyde (2.72 g, 20 mmol) as described in the general procedure for **91-97** to yield **96** as a white solid (3,73 g, 82%). **^{1}H NMR** (500 MHz, DMSO-d_6) δ 12.36 (s, 1H), 8.24 – 8.15 (m, 2H), 8.12 (ddd, *J* = 7.9, 1.6, 0.7 Hz, 1H), 7.80 (ddd, *J* = 8.2, 7.1, 1.6 Hz, 1H), 7.69 (ddd, *J* = 8.2, 1.2, 0.6 Hz, 1H), 7.47 (ddd, *J* = 8.1, 7.1, 1.2 Hz, 1H), 7.12 – 7.03 (m, 2H), 3.84 (s, 3H). **^{13}C NMR** (126 MHz, DMSO) δ 162.44, 161.99, 152.03, 134.61, 129.56, 127.31, 126.20, 125.93, 124.95, 120.79, 114.11, 55.58.

2-(3,4-dimethoxyphenyl)quinazolin-4(3H)-one (97).

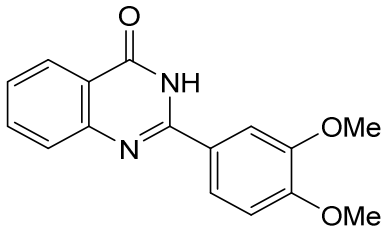

Molecular weight: 282.30 g/mol

The title compound was synthesized from 3,4-dimethoxybenzaldehyde (3.32 g, 20 mmol) as described in the general procedure for **91-97** to yield **97** as a white solid (4,07 g, 72%). **^{1}H NMR** (500 MHz, DMSO-d_6) δ 12.39 (s, 1H), 8.12 (dd, *J* = 8.0, 1.6 Hz, 1H), 7.86 (dd, *J* = 8.5, 2.2 Hz, 1H), 7.83 – 7.75 (m, 2H), 7.70 (dd, *J* = 8.3, 1.2 Hz, 1H), 7.47 (ddd, *J* = 8.1, 7.2, 1.2 Hz, 1H), 7.10 (d, *J* = 8.5 Hz, 1H), 3.88 (s, 3H), 3.84 (s, 3H). **^{13}C NMR** (126 MHz, DMSO) δ 151.75, 148.71, 134.63, 127.42, 126.23, 125.96, 124.91, 121.29, 120.82, 111.55, 110.91, 55.85, 55.83.

General Procedure for the Preparation of the 4-chloro-2-phenylquinazoline derivatives 98-104. The corresponding 2-phenylquinazolin-4(3*H*)-one derivative **91-97** (10 mmol) was added to phosphorous trichloride (30 mL, 0.32 mol) and stirred for 10 min at room temperature. The mixture was then refluxed for 4-8 h and the reaction monitored by TLC. After completion of the reaction, excess $POCl_3$ was removed under reduced pressure and 50 mL ice water added. Subsequently, 50 mL DCM was added while stirring and the pH of the mixture slowly adjusted to 7 with 25% ammonium solution. The organic phase was collected, with a separatory funnel, washed with 50 mL brine and dried under $MgSO_4$. The solvent was removed under reduced pressure and the obtained solid recrystallized from isopropanol.

4-chloro-2-(3-nitrophenyl)quinazoline (98).

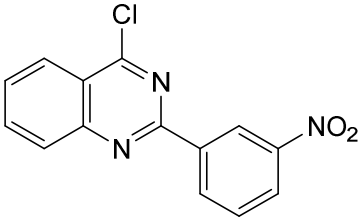

Molecular weight: 285.69 g/mol

The title compound was synthesized from **1** (2.67 g, 10 mmol) as described in the general procedure for **98-104** to yield **98** as white solid (2.31 g, 81%). **^{1}H NMR** (500 MHz, DMSO-d_6) δ 9.19 (t, J = 2.0 Hz, 1H), 8.92 – 8.84 (m, 1H), 8.51 – 8.38 (m, 1H), 8.33 (d, J = 8.3 Hz, 1H), 8.28 – 8.11 (m, 2H), 7.90 (q, J = 7.8 Hz, 2H). **^{13}C NMR** (126 MHz, DMSO) δ 162.54, 156.94, 151.14, 148.55, 137.79, 136.44, 134.26, 130.87, 130.19, 128.84, 125.95, 125.89, 122.54, 122.32.

4-chloro-2-(4-nitrophenyl)quinazoline (99).

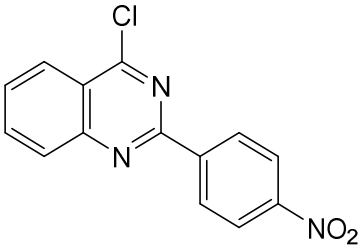

Molecular weight: 285.69 g/mol

The title compound was synthesized from **2** (2.67 g, 10 mmol) as described in the general procedure for **98-104** to yield **99** as light yellow solid (2.19 g, 77%). **^{1}H NMR** (500 MHz, DMSO-d_6) δ 8.69 (d, *J* = 8.4 Hz, 2H), 8.40 (d, *J* = 7.9 Hz, 2H), 8.31 (d, *J* = 8.6 Hz, 1H), 8.24 – 8.08 (m, 2H), 7.91 (d, *J* = 8.8 Hz, 1H). **^{13}C NMR** (126 MHz, DMSO) δ 162.47, 157.08, 151.13, 149.25, 141.89, 136.43, 130.40, 129.49, 128.94, 125.88, 124.20, 122.27.

3-(4-chloroquinazolin-2-yl)benzonitrile (100).

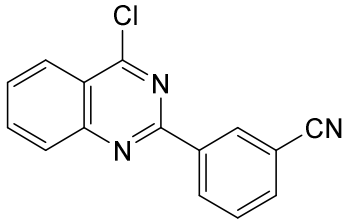

Molecular weight: 265.70 g/mol

The title compound was synthesized from **93** (2.47 g, 10 mmol) as described in the general procedure for **98-104** to yield **100** as white solid (2.39 g, 90%). **^{1}H NMR** (500 MHz, DMSO-d_6) δ 8.59 – 8.56 (m, 1H), 8.48 (ddd, *J* = 8.0, 1.9, 1.1 Hz, 1H), 8.18 – 8.14 (m, 1H), 8.06 – 8.03 (m, 1H), 7.88 – 7.83 (m, 1H), 7.79 – 7.74 (m, 2H), 7.58 – 7.53 (m, 1H). **^{13}C NMR** (126 MHz, DMSO) δ 162.48, 157.13, 151.17, 137.34, 136.40, 134.81, 132.70, 131.58, 130.54, 130.11, 128.82, 125.88, 122.28, 118.51, 112.35.

4-chloro-2-(2-methoxyphenyl)quinazoline (101).

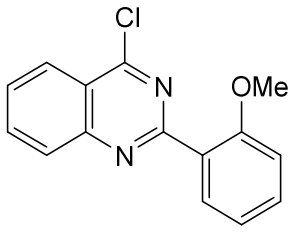

Molecular weight: 270.72 g/mol

The title compound was synthesized from **94** (2.52 g, 10 mmol) as described in the general procedure for **98-104** to yield **101** as light yellow solid (2.38 g, 88%). **^{1}H NMR** (500 MHz, DMSO-d_6) δ 8.15 (dd, *J* = 8.0, 1.5 Hz, 1H), 7.84 (ddd, *J* = 8.5, 7.1, 1.6 Hz, 1H), 7.74 – 7.67 (m, 2H), 7.59 – 7.51 (m, 2H), 7.20 (dd, *J* = 8.5, 0.9 Hz, 1H), 7.10 (td, *J* = 7.5,

1.0 Hz, 1H), 3.86 (s, 3H). **^{13}C NMR** (126 MHz, DMSO) δ 161.25, 157.31, 152.76, 148.31, 134.67, 132.59, 130.64, 126.85, 125.99, 122.21, 121.02, 120.58, 112.09, 55.98.

4-chloro-2-(3-methoxyphenyl)quinazoline (102).

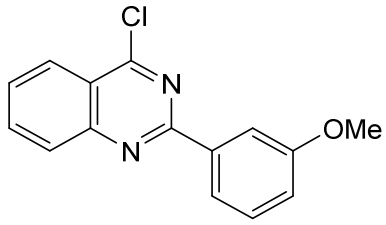

Molecular weight: 270.72 g/mol

The title compound was synthesized from **95** (2.52 g, 10 mmol) as described in the general procedure for **98-104** to yield **102** as light yellow solid (2.51 g, 93%). **^{1}H NMR** (500 MHz, DMSO-d_6) δ 8.31 – 8.25 (m, 1H), 8.15 – 8.10 (m, 2H), 8.10 – 8.06 (m, 1H), 8.00 (dd, J = 2.7, 1.5 Hz, 1H), 7.84 (ddd, J = 8.2, 6.2, 1.9 Hz, 1H), 7.49 (t, J = 8.0 Hz, 1H), 7.16 (ddd, J = 8.2, 2.7, 1.0 Hz, 1H), 3.87 (s, 3H). **^{13}C NMR** (126 MHz, DMSO) δ 162.02, 159.84, 158.80, 151.29, 137.55, 136.06, 130.16, 129.51, 128.69, 125.76, 121.98, 120.80, 117.51, 113.12, 55.44.

4-chloro-2-(4-methoxyphenyl)quinazoline (103).

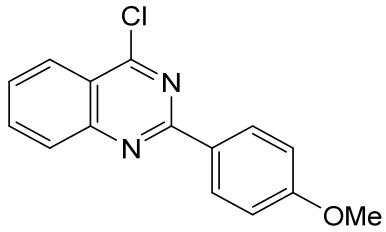

Molecular weight: 270.72 g/mol

The title compound was synthesized from **96** (2.52 g, 10 mmol) as described in the general procedure for **98-104** to yield **103** as light yellow solid (2.46 g, 91%). **^{1}H NMR** (500 MHz, DMSO-d_6) δ 8.21 – 8.09 (m, 3H), 7.94 – 7.83 (m, 2H), 7.56 (ddd, J = 8.1, 6.4, 2.0 Hz, 1H), 7.17 – 7.11 (m, 2H), 3.87 (s, 3H). **^{13}C NMR** (126 MHz, DMSO) δ 162.91, 161.60, 153.92, 135.23, 130.62, 127.10, 126.25, 124.68, 120.26, 114.28, 55.78.

4-chloro-2-(3,4-dimethoxyphenyl)quinazoline (104).

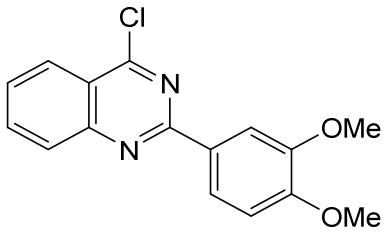

Molecular weight: 300.74 g/mol

The title compound was synthesized from **7** (2.82 g, 10 mmol) as described in the general procedure for **98-104** to yield **104** as light yellow solid (2.13 g, 71%). **^{1}H NMR** (500 MHz, DMSO-d_6) δ 8.16 (ddd, *J* = 7.9, 1.6, 0.6 Hz, 1H), 7.98 (d, *J* = 8.2 Hz, 1H), 7.91 – 7.85 (m, 2H), 7.83 (d, *J* = 2.3 Hz, 1H), 7.56 (ddd, *J* = 8.2, 7.2, 1.1 Hz, 1H), 7.17 (d, *J* = 8.6 Hz, 1H), 3.91 (s, 3H), 3.87 (s, 3H). **^{13}C NMR** (126 MHz, DMSO) δ 161.52, 153.90, 152.79, 148.65, 135.26, 127.16, 126.27, 124.54, 122.61, 120.20, 111.75, 111.58, 55.99, 55.98.

General Procedure for the Preparation of the 4-anilino-2-phenylquinazoline derivatives 105-152.

The corresponding 4-chloroquinazoline derivative **98-104** (1 mmol) was added to isopropanol (5 mL) with the corresponding substituted aniline derivative (1 mmol) and sealed in a microwave tube. The mixture was heated by 100 watt microwave irradiation to 110 °C for a period of 15 – 30 min to completion of the reaction, indicated by TLC. The formed precipitate was filtered, washed with 10 mL isopropanol and dried in vacuo. If no precipitate is formed, the solvent was removed under reduced pressure and the remaining solid recrystallized from ethanol.

2-(3-nitrophenyl)-*N*-phenylquinazolin-4-amine (105).

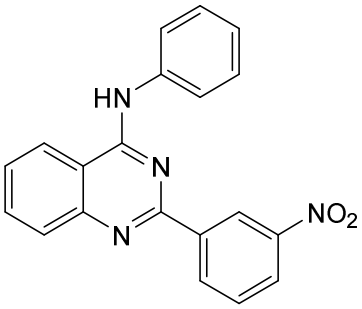

Molecular weight: 342.36 g/mol

The title compound was synthesized from **98** (2.85 g, 10 mmol) and aniline (931 mg, 10 mmol) as described in the general procedure for **105-152** to yield **105** as beige-yellow solid (2.16 g, 63%), mp >300 °C. **^{1}H NMR** (500 MHz, DMSO-d_6) δ 9.98 (s, 1H), 9.19 (dd, J = 2.4, 1.6 Hz, 1H), 8.81 – 8.75 (m, 1H), 8.59 (dt, J = 8.3, 0.9 Hz, 1H), 8.31 (ddd, J = 8.2, 2.5, 1.1 Hz, 1H), 7.96 – 7.88 (m, 4H), 7.79 (t, J = 8.0 Hz, 1H), 7.65 (ddd, J = 8.2, 6.2, 2.0 Hz, 1H), 7.51 – 7.43 (m, 2H), 7.21 (tt, J = 7.4, 1.2 Hz, 1H). **^{13}C NMR** (126 MHz, DMSO) δ 158.26, 157.05, 150.36, 148.32, 140.15, 139.10, 133.87, 133.63, 130.26, 128.61, 128.37, 126.71, 124.85, 124.19, 123.28, 122.75, 122.44, 114.38. **Anal. Calcd. for $C_{20}H_{14}N_4O_2$**: C, 70.17; H, 4.12; N, 16.37. Found: C, 70.52; H, 4.37; N, 16.07.

***N*-cyclohexyl-2-(3-nitrophenyl)quinazolin-4-amine (106).**

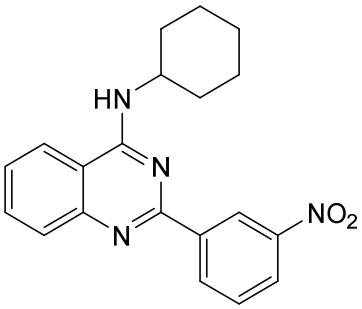

Molecular weight: 348.41 g/mol

The title compound was synthesized from **98** (2.85 g, 10 mmol) and cyclohexanamine (992 mg, 10 mmol) as described in the general procedure for **105-152** to yield **106** as light yellow solid (1.88 g, 54%), mp 186-187 °C. **^{1}H NMR** (500 MHz, DMSO-d_6) δ 9.23 (dd, J = 2.5, 1.6 Hz, 1H), 8.85 (dt, J = 7.8, 1.3 Hz, 1H), 8.37 (dd, J = 8.1, 1.1 Hz, 1H), 8.32

(ddd, *J* = 8.2, 2.5, 1.1 Hz, 1H), 8.09 (d, *J* = 7.4 Hz, 1H), 7.83 – 7.77 (m, 3H), 7.51 (ddd, *J* = 8.2, 6.1, 2.1 Hz, 1H), 4.38 – 4.25 (m, 1H), 2.12 – 1.78 (m, 4H), 1.71 (d, *J* = 13.1 Hz, 1H), 1.54 – 1.37 (m, 4H), 1.30 – 1.15 (m, 1H). **^{13}C NMR** (126 MHz, DMSO) δ 159.16, 157.23, 149.86, 148.26, 140.61, 133.89, 133.01, 130.14, 128.00, 125.82, 124.62, 123.20, 122.24, 114.19, 50.28, 32.05, 25.55, 25.25. **Anal. Calcd. for $C_{20}H_{20}N_4O_2$**: C, 68.95; H, 5.79; N, 16.08. Found: C, 69.22; H, 6.03; N, 15.87.

***N*,2-bis(3-nitrophenyl)quinazolin-4-amine (107).**

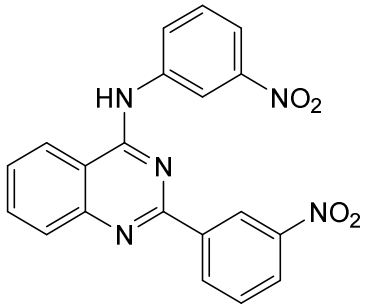

Molecular weight: 387.36 g/mol

The title compound was synthesized from **98** (2.85 g, 10 mmol) and 3-nitroaniline (1.38 g, 10 mmol) as described in the general procedure for **105-152** to yield **107** as light yellow solid (3.33 g, 86%), mp >300 °C. **^{1}H NMR** (500 MHz, DMSO-d_6) δ 10.66 (s, 1H), 9.17 (dd, *J* = 2.4, 1.7 Hz, 1H), 9.10 (t, *J* = 2.2 Hz, 1H), 8.88 – 8.81 (m, 1H), 8.69 (dd, *J* = 8.4, 1.5 Hz, 1H), 8.36 (dddd, *J* = 8.1, 4.6, 2.3, 1.0 Hz, 2H), 8.05 (ddd, *J* = 8.2, 2.3, 0.9 Hz, 1H), 8.01 (dd, *J* = 8.4, 1.3 Hz, 1H), 7.97 (ddd, *J* = 8.2, 6.8, 1.2 Hz, 1H), 7.82 (t, *J* = 8.0 Hz, 1H), 7.77 – 7.70 (m, 2H). **^{13}C NMR** (126 MHz, DMSO) δ 158.30, 156.59, 148.36, 147.97, 140.19, 134.41, 134.15, 130.43, 129.96, 128.40, 127.38, 125.46, 123.59, 122.64, 118.59, 116.82, 114.14. **Anal. Calcd. for $C_{20}H_{13}N_5O_4$**: C, 62.02; H, 3.38; N, 18.08. Found: C, 62.33; H, 3.51; N, 17.73.

2-nitro-4-((2-(3-nitrophenyl)quinazolin-4-yl)amino)phenol (108).

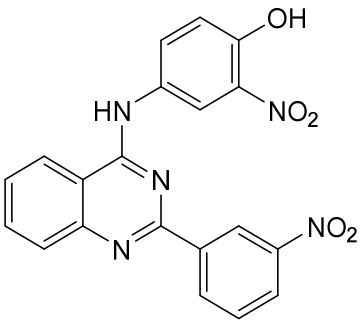

Molecular weight: 403.35 g/mol

The title compound was synthesized from **98** (2.85 g, 10 mmol) and 4-amino-2-nitrophenol (1.54, 10 mmol) as described in the general procedure for **105-152** to yield **108** as orange solid (2.46 g, 61%), mp 299-300 °C (decomp.). **^{1}H NMR** (500 MHz, DMSO-d_6) δ 10.91 (s, 1H), 10.26 (s, 1H), 9.13 (dd, *J* = 2.4, 1.6 Hz, 1H), 8.79 (dt, *J* = 7.8, 1.3 Hz, 1H), 8.67 (d, *J* = 2.7 Hz, 1H), 8.55 (dd, *J* = 8.2, 1.1 Hz, 1H), 8.33 (ddd, *J* = 8.1, 2.5, 1.1 Hz, 1H), 8.05 (dd, *J* = 9.0, 2.7 Hz, 1H), 7.95 – 7.86 (m, 2H), 7.78 (t, *J* = 8.0 Hz, 1H), 7.66 (ddd, *J* = 8.2, 6.2, 2.0 Hz, 1H), 7.25 (d, *J* = 9.0 Hz, 1H). **^{13}C NMR** (126 MHz, DMSO) δ 158.13, 156.72, 149.19, 148.30, 135.67, 134.05, 133.98, 130.60, 130.43, 130.26, 127.01, 125.19, 123.27, 122.50, 119.26, 118.72, 114.06. **Anal. Calcd. for $C_{20}H_{13}N_5O_5$**: C, 59.56; H, 3.25; N, 17.36. Found: C, 59.73; H, 3.47; N, 17.14.

3-((2-(3-nitrophenyl)quinazolin-4-yl)amino)benzonitrile (109).

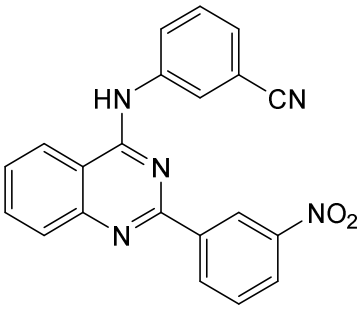

Molecular weight: 367.37 g/mol

The title compound was synthesized from **98** (2.85 g, 10 mmol) and 3-aminobenzonitrile (1.18, 10 mmol) as described in the general procedure for **105-152** to yield **109** as light beige solid (3.09 g, 84%), mp 272-274 °C (decomp.). **^{1}H NMR** (500 MHz, DMSO-d_6) δ

10.24 (s, 1H), 9.14 (dd, *J* = 2.4, 1.6 Hz, 1H), 8.77 (dt, *J* = 7.7, 1.4 Hz, 1H), 8.57 (dd, *J* = 8.3, 1.1 Hz, 1H), 8.41 (t, *J* = 1.9 Hz, 1H), 8.34 (ddd, *J* = 8.2, 2.5, 1.1 Hz, 1H), 8.30 – 8.21 (m, 1H), 7.98 – 7.88 (m, 2H), 7.80 (t, *J* = 8.0 Hz, 1H), 7.73 – 7.60 (m, 3H). **^{13}C NMR** (126 MHz, DMSO) δ 158.11, 156.80, 150.29, 148.31, 140.05, 139.78, 133.96, 133.79, 130.29, 130.01, 128.35, 127.38, 127.06, 127.02, 125.43, 125.01, 123.26, 122.35, 118.74, 114.24, 111.57. **Anal. Calcd. for $C_{21}H_{13}N_5O_2$**: C, 68.66; H, 3.57; N, 19.06. Found: C, 69.00; H, 3.90; N, 18.94.

***N*-(3-methoxyphenyl)-2-(3-nitrophenyl)quinazolin-4-amine (110).**

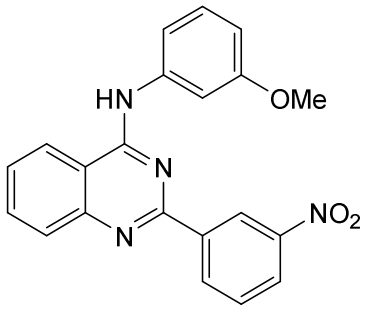

Molecular weight: 372.38 g/mol

The title compound was synthesized from **98** (2.85 g, 10 mmol) and 3-methoxyaniline (1.23 g, 10 mmol) as described in the general procedure for **105-152** to yield **110** as yellow solid (3.09 g, 84%), mp 189-191 °C. **^{1}H NMR** (500 MHz, DMSO-d_6) δ 9.94 (s, 1H), 9.20 (t, *J* = 2.0 Hz, 1H), 8.83 (dt, *J* = 7.9, 1.4 Hz, 1H), 8.60 (d, *J* = 8.2 Hz, 1H), 8.34 (ddd, *J* = 8.2, 2.5, 1.1 Hz, 1H), 7.97 – 7.85 (m, 2H), 7.82 (t, *J* = 8.0 Hz, 1H), 7.70 – 7.61 (m, 2H), 7.53 (dd, *J* = 8.0, 2.0 Hz, 1H), 7.36 (t, *J* = 8.1 Hz, 1H), 6.78 (dd, *J* = 7.8, 2.5 Hz, 1H), 3.83 (s, 3H). **^{13}C NMR** (126 MHz, DMSO) δ 159.62, 158.24, 157.08, 150.33, 148.36, 140.20, 133.91, 133.68, 130.27, 129.32, 128.39, 126.76, 124.94, 123.27, 122.35, 114.72, 114.42, 110.17, 107.88, 55.25. **Anal. Calcd. for $C_{21}H_{16}N_4O_3$**: C, 67.73; H, 4.33; N, 15.05. Found: C, 67.64; H, 4.69; N, 14.80.

***N*-(3,4-dimethoxyphenyl)-2-(3-nitrophenyl)quinazolin-4-amine (111).**

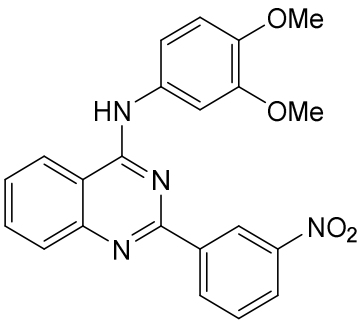

Molecular weight: 402.41 g/mol

The title compound was synthesized from **98** (2.85 g, 10 mmol) and 3,4-dimethoxyaniline (1.53 g, 10 mmol) as described in the general procedure for **105-152** to yield **111** as yellow solid (3.18 g, 75%), mp 184-185 °C. **^{1}H NMR** (500 MHz, DMSO-d_6) δ 9.88 (s, 1H), 9.18 (dd, *J* = 2.4, 1.6 Hz, 1H), 8.83 (dt, *J* = 7.8, 1.3 Hz, 1H), 8.61 – 8.53 (m, 1H), 8.33 (ddd, *J* = 8.2, 2.4, 1.1 Hz, 1H), 7.94 – 7.85 (m, 2H), 7.81 (t, *J* = 8.0 Hz, 1H), 7.70 – 7.60 (m, 2H), 7.38 (dd, *J* = 8.6, 2.4 Hz, 1H), 7.04 (d, *J* = 8.7 Hz, 1H), 3.83 (s, 3H), 3.81 (s, 3H). **^{13}C NMR** (126 MHz, DMSO) δ 158.19, 157.15, 150.21, 148.58, 148.31, 145.75, 140.33, 133.94, 133.50, 132.37, 130.21, 128.30, 126.59, 124.87, 123.15, 122.27, 114.69, 114.36, 111.89, 107.80, 55.92, 55.60. **Anal. Calcd. for $C_{22}H_{18}N_4O_4$**: C, 65.66; H, 4.51; N, 13.92. Found: C, 65.53; H, 4.88; N, 14.11.

N-(4-bromo-3-methoxyphenyl)-2-(3-nitrophenyl)quinazolin-4-amine (112).

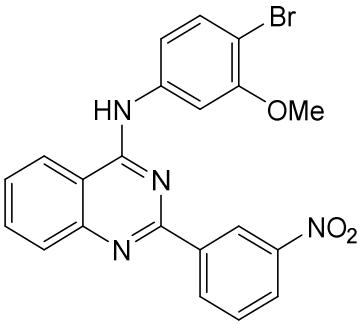

Molecular weight: 451.28 g/mol

The title compound was synthesized from **98** (2.85 g, 10 mmol) and 4-bromo-3-methoxyaniline (2.02 g, 10 mmol) as described in the general procedure for **105-152** to yield **112** as yellow solid (3.25 g, 72%), mp 190-191 °C (decomp.). **^{1}H NMR** (600 MHz,

DMSO-d_6) δ 10.59 (s, 1H), 9.16 (t, *J* = 2.0 Hz, 1H), 8.82 (dd, *J* = 7.7, 1.6 Hz, 1H), 8.72 (d, *J* = 8.4 Hz, 1H), 8.40 (dd, *J* = 8.2, 2.3 Hz, 1H), 8.05 (d, *J* = 8.4 Hz, 1H), 7.99 (t, *J* = 7.7 Hz, 1H), 7.89 – 7.80 (m, 2H), 7.74 (t, *J* = 7.6 Hz, 1H), 7.65 (d, *J* = 8.5 Hz, 1H), 7.47 (dd, *J* = 8.5, 2.3 Hz, 1H), 3.90 (s, 3H). **^{13}C NMR** (151 MHz, DMSO) δ 158.77, 156.92, 155.77, 148.64, 139.66, 135.01, 134.77, 132.95, 130.87, 127.86, 126.18, 124.09, 123.16, 116.71, 114.34, 107.96, 106.19, 56.64. **Anal. Calcd. for $C_{21}H_{15}BrN_4O_3$**: C, 55.89; H, 3.35; N, 12.42. Found: C, 55.74; H, 3.59; N, 12.23.

***N*-(3,4-diethoxyphenyl)-2-(3-nitrophenyl)quinazolin-4-amine (113).**

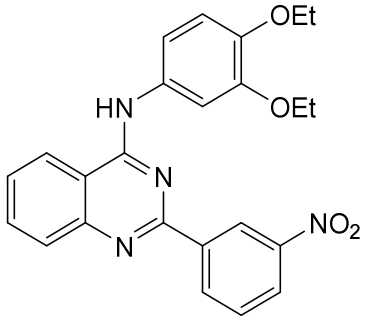

Molecular weight: 430.46 g/mol

The title compound was synthesized from **98** (2.85 g, 10 mmol) and 3,4-diethoxyaniline (1.81 g, 10 mmol) as described in the general procedure for **105-152** to yield **113** as orange solid (1.85 g, 43%), mp 272-273 °C (decomp.). **^{1}H NMR** (500 MHz, DMSO-d_6) δ 11.10 (s, 1H), 9.12 (t, *J* = 2.0 Hz, 1H), 8.91 – 8.73 (m, 2H), 8.45 (ddd, *J* = 8.2, 2.3, 1.0 Hz, 1H), 8.20 (d, *J* = 8.4 Hz, 1H), 8.02 (ddd, *J* = 8.3, 7.0, 1.2 Hz, 1H), 7.88 (t, *J* = 8.0 Hz, 1H), 7.76 (ddd, *J* = 8.3, 7.0, 1.2 Hz, 1H), 7.57 (d, *J* = 2.5 Hz, 1H), 7.34 (dd, *J* = 8.7, 2.5 Hz, 1H), 7.05 (d, *J* = 8.7 Hz, 1H), 4.15 – 4.02 (m, 4H), 1.35 (dt, *J* = 9.5, 7.0 Hz, 6H). **^{13}C NMR** (126 MHz, DMSO) δ 158.53, 155.95, 148.22, 148.13, 146.34, 135.25, 134.85, 130.69, 130.57, 127.94, 126.67, 124.24, 123.49, 116.23, 113.43, 113.31, 110.06, 64.24, 64.12, 14.93. **Anal. Calcd. for $C_{24}H_{22}N_4O_4$**: C, 66.97; H, 5.15; N, 13.02. Found: C, 66.89; H, 5.36; N, 13.05.

***N*-(2,3-dihydrobenzo[*b*][1,4]dioxin-6-yl)-2-(3-nitrophenyl)quinazolin-4-amine (114).**

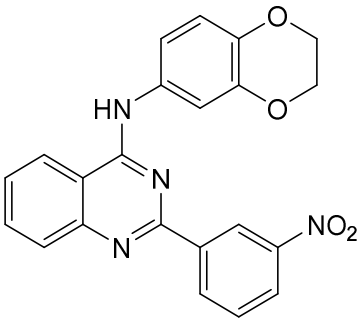

Molecular weight: 400.39 g/mol

The title compound was synthesized from **98** (2.85 g, 10 mmol) and 2,3-dihydrobenzo[b][1,4]dioxin-6-amine (1.51 g, 10 mmol) as described in the general procedure for **105-152** to yield **114** as yellow solid (2.04 g, 51%), mp 267-270 °C (decomp.). **^{1}H NMR** (500 MHz, DMSO-d_6) δ 10.58 (s, 1H), 9.21 – 9.08 (m, 1H), 8.78 (dt, *J* = 7.8, 1.3 Hz, 1H), 8.68 (d, *J* = 8.3 Hz, 1H), 8.40 (ddd, *J* = 8.2, 2.4, 1.0 Hz, 1H), 8.05 (d, *J* = 8.3 Hz, 1H), 7.96 (ddd, *J* = 8.3, 6.9, 1.3 Hz, 1H), 7.85 (t, *J* = 8.0 Hz, 1H), 7.71 (ddd, *J* = 8.2, 6.9, 1.2 Hz, 1H), 7.42 (d, *J* = 2.5 Hz, 1H), 7.36 (dd, *J* = 8.7, 2.5 Hz, 1H), 6.96 (d, *J* = 8.7 Hz, 1H), 4.33 – 4.26 (m, 4H). **^{13}C NMR** (126 MHz, DMSO) δ 158.47, 156.32, 148.28, 143.17, 141.05, 134.65, 134.37, 131.46, 130.49, 127.44, 125.97, 123.82, 123.12, 116.83, 116.71, 113.74, 112.64, 64.37, 64.29. **Anal. Calcd. for $C_{22}H_{16}N_4O_4$**: C, 66.00; H, 4.03; N, 13.99. Found: C, 65.93; H, 4.24; N, 13.81.

***N*-(3-(methylthio)phenyl)-2-(3-nitrophenyl)quinazolin-4-amine (115).**

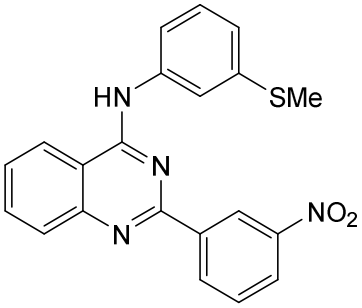

Molecular weight: 388.45 g/mol

The title compound was synthesized from **98** (2.85 g, 10 mmol) and 3-(methylthio)aniline (1.39 g, 10 mmol) as described in the general procedure for **105-152** to yield **115** as yellow solid (3.42 g, 88%), mp 184-185 °C. **^{1}H NMR** (500 MHz, DMSO-d_6) δ 9.95 (s, 1H), 9.19 – 9.15 (m, 1H), 8.80 (ddd, *J* = 7.8, 1.7, 1.1 Hz, 1H), 8.60 – 8.55 (m, 1H), 8.33 (ddd, *J* = 8.2, 2.4, 1.1 Hz, 1H), 7.94 – 7.87 (m, 3H), 7.79 (ddd, *J* = 8.2, 7.7, 0.4 Hz, 1H), 7.76 (ddd, *J* = 8.2, 2.1, 0.9 Hz, 1H), 7.66 (ddd, *J* = 8.2, 6.3, 1.9 Hz, 1H), 7.40 (t, *J* = 8.0 Hz, 1H), 7.09 (ddd, *J* = 7.9, 1.9, 0.9 Hz, 1H), 2.52 (s, 3H). **^{13}C NMR** (126 MHz, DMSO) δ 158.20, 157.00, 150.33, 148.33, 140.13, 139.72, 138.56, 133.89, 133.70, 130.22, 129.06, 128.39, 126.78, 124.93, 123.23, 122.32, 121.62, 119.64, 119.05, 114.38, 14.92. **Anal. Calcd. for $C_{21}H_{16}N_4O_2S$**: C, 64.93; H, 4.15; N, 14.42. Found: C, 65.25; H, 4.42; N, 14.21.

***N*-(4-(methylthio)phenyl)-2-(3-nitrophenyl)quinazolin-4-amine (116).**

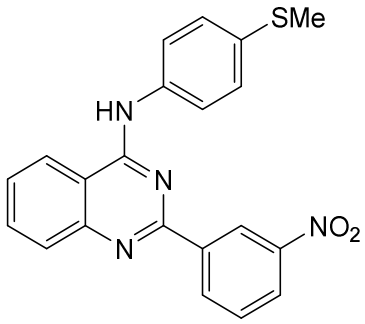

Molecular weight: 388.45 g/mol

The title compound was synthesized from **98** (2.85 g, 10 mmol) and 4-(methylthio)aniline (1.39 g, 10 mmol) as described in the general procedure for **105-152** to yield **116** as yellow solid (3.22 g, 83%), mp 234-235 °C (decomp.). **^{1}H NMR** (600 MHz, DMSO-d_6) δ 9.95 (s, 1H), 9.14 (t, *J* = 2.0 Hz, 1H), 8.74 (dt, *J* = 7.8, 1.3 Hz, 1H), 8.53 (d, *J* = 8.2 Hz, 1H), 8.28 (ddd, *J* = 8.1, 2.5, 1.1 Hz, 1H), 7.90 – 7.82 (m, 4H), 7.76 (t, *J* = 7.9 Hz, 1H), 7.61 (ddd, *J* = 8.2, 6.3, 1.9 Hz, 1H), 7.38 – 7.31 (m, 2H), 2.49 (s, 3H). **^{13}C NMR** (151 MHz, DMSO) δ 158.12, 157.02, 150.28, 148.29, 140.08, 136.48, 133.89, 133.62, 132.96, 130.63, 130.29, 128.32, 126.78, 124.84, 123.31, 122.44, 115.51, 114.37, 40.11, 39.97, 15.63. **Anal. Calcd. for $C_{21}H_{16}N_4O_2S$**: C, 64.93; H, 4.15; N, 14.42. Found: C, 64.90; H, 4.42; N, 14.08.

***N*^{1}-(2-(3-nitrophenyl)quinazolin-4-yl)benzene-1,3-diamine (117).**

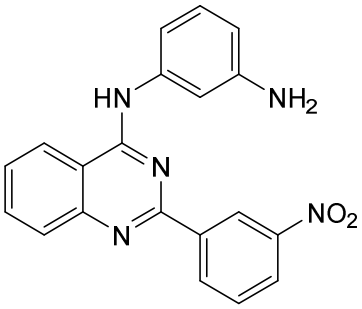

Molecular weight: 357.37 g/mol

The title compound was synthesized from **98** (2.85 g, 10 mmol) and benzene-1,3-diamine (1.08 g, 10 mmol) as described in the general procedure for **105-152** to yield **117** as yellow solid (1.57 g, 44%), mp 229-230 °C (decomp.). **^{1}H NMR** (500 MHz, DMSO-d_6) δ 9.74 (s, 1H), 9.23 (dd, *J* = 2.4, 1.6 Hz, 1H), 8.82 (ddd, *J* = 7.8, 1.6, 1.1 Hz, 1H), 8.65 – 8.53 (m, 1H), 8.33 (ddd, *J* = 8.1, 2.5, 1.1 Hz, 1H), 7.94 – 7.84 (m, 2H), 7.81 (t, *J* = 8.0 Hz, 1H), 7.62 (ddd, *J* = 8.3, 6.5, 1.7 Hz, 1H), 7.23 – 7.18 (m, 1H), 7.15 – 7.01 (m, 2H), 6.47 – 6.32 (m, 1H), 5.13 (s, 2H). **^{13}C NMR** (126 MHz, DMSO) δ 158.27, 157.16, 150.31, 149.10, 148.35, 140.25, 139.65, 134.01, 133.46, 130.25, 128.83, 128.30, 126.55, 124.78, 123.30, 122.56, 114.44, 110.62, 110.27, 108.30. **Anal. Calcd. for $C_{20}H_{15}N_5O_2$**: C, 67.22; H, 4.23; N, 19.60. Found: C, 67.51; H, 4.33; N, 19.33.

***N*^{1},*N*^{1}-dimethyl-*N*^{3}-(2-(3-nitrophenyl)quinazolin-4-yl)benzene-1,3-diamine (118).**

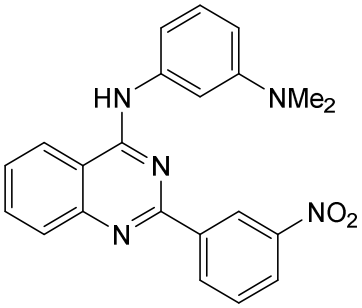

Molecular weight: 385.43 g/mol

The title compound was synthesized from **98** (2.85 g, 10 mmol) and *N*^{1},*N*^{1}-dimethylbenzene-1,3-diamine (1.36 g, 10 mmol) as described in the general procedure for **105**-**152** to yield **118** as light yellow solid (2.78 g, 72%), mp 243-245 °C (decomp.).

^{1}H NMR (500 MHz, DMSO-d_6) δ 11.02 (s, 1H), 9.15 (s, 1H), 8.88 (dt, *J* = 7.9, 1.4 Hz, 1H), 8.83 (d, *J* = 8.2 Hz, 1H), 8.45 – 8.41 (m, 1H), 8.17 (d, *J* = 8.4 Hz, 1H), 8.03 (t, *J* = 7.7 Hz, 1H), 7.87 (t, *J* = 8.0 Hz, 2H), 7.80 – 7.74 (m, 1H), 7.60 (s, 1H), 7.51 (d, *J* = 8.1 Hz, 1H), 7.23 (s, 1H), 3.08 (s, 6H). **^{13}C NMR** (126 MHz, DMSO) δ 158.74, 156.18, 148.24, 138.96, 135.14, 134.84, 130.52, 129.79, 127.84, 126.34, 124.18, 123.35, 113.65, 25.59. **Anal. Calcd. for $C_{22}H_{19}N_5O_2$**: C, 68.56; H, 4.97; N, 18.17. Found: C, 68.61; H, 5.21; N, 18.43.

***N*^{1},*N*^{1}-diethyl-*N*^{3}-(2-(3-nitrophenyl)quinazolin-4-yl)benzene-1,3-diamine (119).**

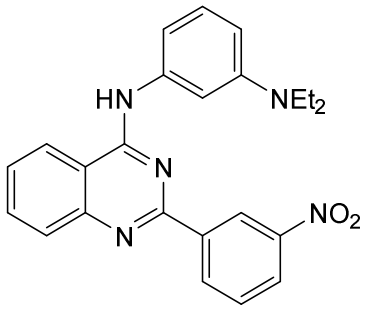

Molecular weight: 413.48 g/mol

The title compound was synthesized from **98** (2.85 g, 10 mmol) and *N*^{1},*N*^{1}-diethylbenzene-1,3-diamine (1.64 g, 10 mmol) as described in the general procedure for **105-152** to yield **119** as dark-yellow solid (2.23 g, 54%), mp 168-170 °C (decomp.). **^{1}H NMR** (500 MHz, DMSO-d_6) δ 9.80 (s, 1H), 9.19 (dd, *J* = 2.4, 1.6 Hz, 1H), 8.79 (dt, *J* = 7.8, 1.3 Hz, 1H), 8.53 (dd, *J* = 8.2, 1.1 Hz, 1H), 8.31 (ddd, *J* = 8.2, 2.5, 1.1 Hz, 1H), 7.89 – 7.80 (m, 2H), 7.78 (t, *J* = 7.9 Hz, 1H), 7.66 (d, *J* = 8.5 Hz, 2H), 7.60 (ddd, *J* = 10.5, 6.0, 2.9 Hz, 1H), 6.77 (d, *J* = 8.4 Hz, 2H), 3.38 (q, *J* = 6.9 Hz, 4H), 1.14 (t, *J* = 7.0 Hz, 6H). **^{13}C NMR** (126 MHz, DMSO) δ 158.14, 157.21, 150.20, 148.28, 144.83, 140.39, 133.84, 133.27, 130.16, 128.19, 127.16, 126.36, 124.72, 124.56, 123.13, 122.50, 114.42, 111.56, 44.01, 12.58. **Anal. Calcd. for $C_{24}H_{23}N_5O_2$**: C, 69.72; H, 5.61; N, 16.94. Found: C, 69.42; H, 5.85; N, 16.65.

***N*-(3-((2-(3-nitrophenyl)quinazolin-4-yl)amino)phenyl)acetamide (120).**

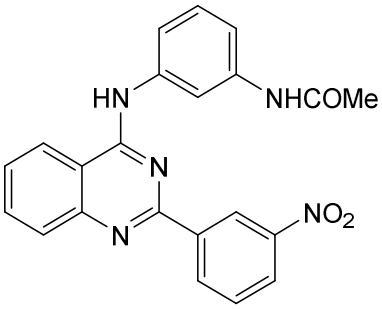

Molecular weight: 399.41 g/mol

The title compound was synthesized from **98** (2.85 g, 10 mmol) and N-(3-aminophenyl)acetamide (1.50 g, 10 mmol) as described in the general procedure for **105-152** to yield **120** as light yellow (3.04 g, 76%), mp 251-252 °C. **^{1}H NMR** (600 MHz, DMSO-d_6) δ 10.01 (s, 1H), 9.99 (s, 1H), 9.24 – 9.19 (m, 1H), 8.89 (dt, *J* = 7.8, 1.3 Hz, 1H), 8.62 (dd, *J* = 8.1, 1.2 Hz, 1H), 8.49 (t, *J* = 2.1 Hz, 1H), 8.33 (ddd, *J* = 8.1, 2.4, 1.1 Hz, 1H), 7.96 – 7.87 (m, 2H), 7.79 (t, *J* = 7.9 Hz, 1H), 7.65 (ddd, *J* = 8.2, 6.5, 1.7 Hz, 1H), 7.55 (ddd, *J* = 8.1, 2.1, 1.0 Hz, 1H), 7.36 (t, *J* = 8.0 Hz, 1H), 7.29 (ddd, *J* = 8.1, 2.1, 1.0 Hz, 1H), 2.07 (s, 3H). **^{13}C NMR** (151 MHz, DMSO) δ 168.82, 158.56, 157.44, 150.73, 148.73, 140.36, 140.08, 139.71, 134.50, 133.98, 130.52, 128.93, 128.70, 127.04, 125.20, 123.71, 123.13, 117.74, 115.22, 114.74, 113.93, 24.52. **Anal. Calcd. for $C_{22}H_{17}N_5O_3$**: C, 66.16; H, 4.29; N, 17.53. Found: C, 65.95; H, 4.43; N, 17.24.

2-(3-nitrophenyl)-N-(3-(trifluoromethyl)phenyl)quinazolin-4-amine (121).

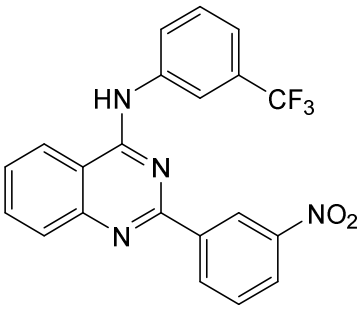

Molecular weight: 410.36 g/mol

The title compound was synthesized from **98** (2.85 g, 10 mmol) and 3-(trifluoromethyl)aniline (1.61 g, 10 mmol) as described in the general procedure for **105-**

152 to yield **121** as white-yellow solid (3.45 g, 84%), mp 148-151 °C. **^{1}H NMR** (600 MHz, DMSO-d_6) δ 9.17 (t, *J* = 5.8 Hz, 1H), 9.15 (dd, *J* = 2.4, 1.6 Hz, 1H), 8.79 (dt, *J* = 7.8, 1.3 Hz, 1H), 8.36 – 8.28 (m, 2H), 7.89 – 7.77 (m, 4H), 7.75 (t, *J* = 7.9 Hz, 1H), 7.61 – 7.53 (m, 3H). **^{13}C NMR** (151 MHz, DMSO) δ 159.87, 157.17, 149.77, 148.27, 141.30, 140.30, 133.98, 133.37, 131.72, 130.08, 129.59, 129.20 (q, *J* = 31.5 Hz), 128.18, 126.42, 124.78, 124.40 (q, *J* = 272.3 Hz), 124.29 (q, *J* = 3.8 Hz), 123.76 (q, *J* = 3.7 Hz), 122.92, 122.22, 114.16. **Anal. Calcd. for $C_{21}H_{13}F_3N_4O_2$**: C, 61.47; H, 3.19; N, 13.89. Found: C, 61.86; H, 3.37; N, 13.60.

***N*-(4-methoxy-3-(trifluoromethyl)phenyl)-2-(3-nitrophenyl)quinazolin-4-amine (122).**

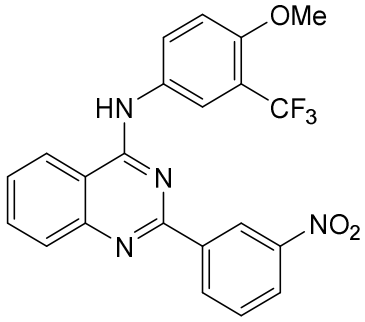

Molecular weight: 440.38 g/mol

The title compound was synthesized from **98** (2.85 g, 10 mmol) and 4-methoxy-3-(trifluoromethyl)aniline (1.91 g, 10 mmol) as described in the general procedure for **105-152** to yield **122** as light yellow solid (2.00 g, 66%), mp 272-275 °C (decomp.). **^{1}H NMR** (500 MHz, DMSO-d_6) δ 10.99 (s, 1H), 9.11 (t, *J* = 2.0 Hz, 1H), 8.81 – 8.71 (m, 2H), 8.42 (ddd, *J* = 8.2, 2.4, 1.1 Hz, 1H), 8.29 (d, *J* = 2.6 Hz, 1H), 8.15 – 8.05 (m, 2H), 8.00 (ddd, *J* = 8.4, 6.9, 1.2 Hz, 1H), 7.84 (t, *J* = 8.0 Hz, 1H), 7.75 (ddd, *J* = 8.2, 7.0, 1.2 Hz, 1H), 7.39 (d, *J* = 9.0 Hz, 1H), 3.95 (s, 3H). **^{13}C NMR** (126 MHz, DMSO) δ 158.61, 156.22, 154.35, 148.29, 134.98, 134.46, 130.70, 130.47, 129.07, 127.74, 126.23, 124.77, 124.00, 123.07, 122.60, 122.21 (d, *J* = 3.9 Hz), 116.80 (d, *J* = 30.4 Hz), 113.66, 113.30, 56.58. **Anal. Calcd. for $C_{22}H_{15}F_3N_4O_3$**: C, 60.00; H, 3.43; N, 12.72. Found: C, 59.88; H, 3.81; N, 12.52.

***N*-(4-iodophenyl)-2-(3-nitrophenyl)quinazolin-4-amine (123).**

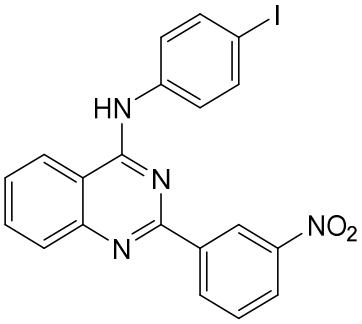

Molecular weight: 468.25 g/mol

The title compound was synthesized from **98** (2.85 g, 10 mmol) and 4-iodoaniline (2.19 g, 10 mmol) as described in the general procedure for **105-152** to yield **123** as light yellow solid (2.58 g, 55%), mp 245-247 °C (decomp.). **^{1}H NMR** (500 MHz, DMSO-d_6) δ 10.03 (s, 1H), 9.18 (t, *J* = 2.0 Hz, 1H), 8.78 (dd, *J* = 7.8, 1.3 Hz, 1H), 8.56 (d, *J* = 8.3 Hz, 1H), 8.33 (dd, *J* = 8.1, 2.4 Hz, 1H), 7.95 – 7.87 (m, 2H), 7.83 – 7.76 (m, 5H), 7.66 (ddd, *J* = 8.3, 6.2, 2.1 Hz, 1H). **^{13}C NMR** (126 MHz, DMSO) δ 158.04, 156.96, 150.31, 148.33, 139.95, 139.06, 137.26, 133.95, 133.79, 130.39, 128.38, 126.86, 124.92, 124.71, 123.26, 122.44, 114.39, 87.78. **Anal. Calcd. for $C_{20}H_{13}IN_4O_2$**: C, 51.30; H, 2.80; N, 11.97. Found: C, 51.55; H, 2.92; N, 11.79.

***N*-(3-nitrophenyl)-2-(4-nitrophenyl)quinazolin-4-amine (124).**

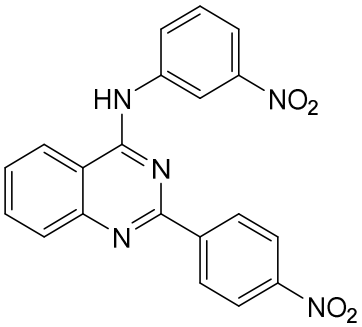

Molecular weight: 387.36 g/mol

The title compound was synthesized from **99** (2.85 g, 10 mmol) and 3-nitroaniline (1.38 g, 10 mmol) as described in the general procedure for **105-152** to yield **124** as bright yellow solid (3.45 g, 89%), mp >300 °C. **^{1}H NMR** (500 MHz, DMSO-d_6) δ 10.37 (s, 1H), 9.21 (d, *J* = 2.4 Hz, 1H), 8.75 – 8.68 (m, 2H), 8.64 (d, *J* = 8.3 Hz, 1H), 8.39 – 8.34 (m,

3H), 8.03 (d, *J* = 8.1 Hz, 1H), 7.97 (d, *J* = 5.7 Hz, 2H), 7.80 – 7.71 (m, 2H). **^{13}C NMR** (126 MHz, DMSO) δ 157.08, 152.37, 134.10, 130.07, 129.15, 128.66, 127.85, 127.42, 123.84, 123.27, 118.13, 116.25, 114.28. **Anal. Calcd. for $C_{20}H_{13}N_5O_4$**: C, 62.01; H, 3.67; N, 18.08. Found: C, 62.04; H, 3.67; N, 17.78.

3-((2-(4-nitrophenyl)quinazolin-4-yl)amino)benzonitrile (125).

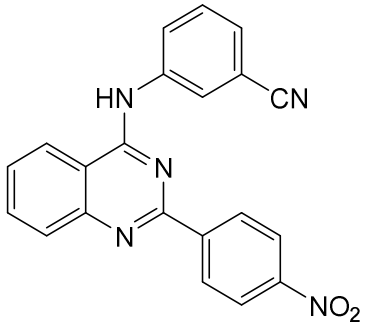

Molecular weight: 367.37 g/mol

The title compound was synthesized from **99** (2.85 g, 10 mmol) and 3-aminobenzonitrile (1.18 g, 10 mmol) as described in the general procedure for **105-152** to yield **125** as bright yellow solid (2.68 g, 73%), mp >300 °C. **^{1}H NMR** (500 MHz, DMSO-d_6) δ 10.37 (s, 1H), 8.68 (ddd, *J* = 8.3, 1.4, 0.6 Hz, 1H), 8.65 – 8.58 (m, 2H), 8.40 (dd, *J* = 2.2, 1.6 Hz, 1H), 8.37 – 8.28 (m, 3H), 8.03 – 7.92 (m, 2H), 7.76 – 7.65 (m, 2H), 7.62 (dt, *J* = 7.6, 1.3 Hz, 1H). **^{13}C NMR** (126 MHz, DMSO) δ 158.14, 156.82, 149.24, 148.75, 143.34, 139.78, 133.83, 129.76, 128.92, 127.47, 127.15, 127.04, 126.88, 125.37, 123.37, 123.21, 118.38, 113.89, 111.40. **Anal. Calcd. for $C_{21}H_{13}N_5O_4$**: C, 68.66; H, 3.57; N, 19.06. Found: C, 68.59; H, 3.71; N, 18.70.

***N*-(3-methoxyphenyl)-2-(4-nitrophenyl)quinazolin-4-amine (126).**

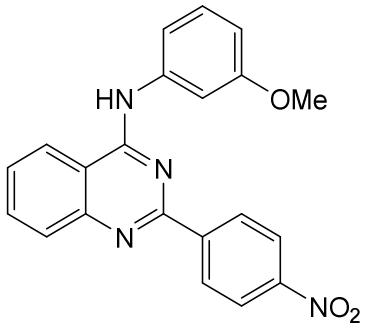

Molecular weight: 372.38 g/mol

The title compound was synthesized from **99** (2.85 g, 10 mmol) and 3-methoxyaniline (1.23 g, 10 mmol) as described in the general procedure for **105-152** to yield **126** as yellow solid (2.57 g, 69%), mp 201-203 °C. **^{1}H NMR** (500 MHz, DMSO-d_6) δ 9.93 (s, 1H), 8.69 – 8.64 (m, 2H), 8.64 – 8.59 (m, 1H), 8.41 – 8.35 (m, 2H), 7.97 – 7.90 (m, 2H), 7.72 – 7.65 (m, 2H), 7.55 (ddd, *J* = 8.0, 2.0, 0.9 Hz, 1H), 7.37 (t, *J* = 8.1 Hz, 1H), 6.77 (ddd, *J* = 8.3, 2.6, 0.8 Hz, 1H), 3.83 (s, 3H). **^{13}C NMR** (126 MHz, DMSO) δ 159.58, 157.32, 150.33, 148.69, 144.50, 140.39, 133.71, 129.43, 129.01, 128.50, 127.02, 123.83, 123.27, 114.58, 114.35, 110.08, 107.70, 55.29. **Anal. Calcd. for $C_{21}H_{16}N_4O_3$**: C, 67.73; H, 4.33; N, 15.05. Found: C, 67.47; H, 4.49; N, 14.83.

***N*-(3,4-dimethoxyphenyl)-2-(4-nitrophenyl)quinazolin-4-amine (127).**

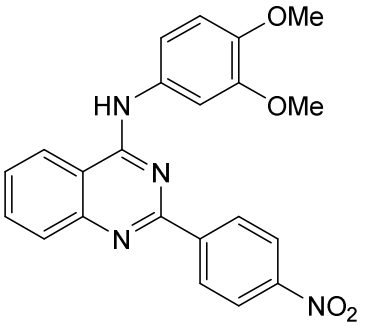

Molecular weight: 402.41 g/mol

The title compound was synthesized from **99** (2.85 g, 10 mmol) and 3,4-dimethoxyaniline (1.53 g, 10 mmol) as described in the general procedure for **105-152** to yield **127** as light orange solid (3.26 g, 81%), mp 250-251 °C (decomp.). **^{1}H NMR** (600 MHz, DMSO-d_6) δ 10.47 (s, 1H), 8.69 (d, *J* = 8.3 Hz, 1H), 8.64 – 8.53 (m, 2H), 8.45 – 8.34 (m, 2H), 8.02 (d, *J* = 8.4 Hz, 1H), 7.96 (t, *J* = 7.6 Hz, 1H), 7.72 (t, *J* = 7.5 Hz, 1H), 7.63 (d, *J* = 2.5 Hz, 1H), 7.41 (dd, *J* = 8.6, 2.5 Hz, 1H), 7.06 (d, *J* = 8.7 Hz, 1H), 3.81 (d, *J* = 3.1 Hz, 6H). **^{13}C NMR** (151 MHz, DMSO) δ 158.30, 156.78, 149.14, 148.53, 146.31, 134.45, 131.58, 129.56, 127.52, 123.90, 123.68, 115.29, 113.83, 111.82, 108.08, 55.87, 55.75. **Anal. Calcd. for $C_{22}H_{18}N_4O_4$**: C, 65.66; H, 4.51; N, 13.92. Found: C, 65.51; H, 4.71; N, 13.77.

3-(4-((3-hydroxy-4-methoxyphenyl)amino)quinazolin-2-yl)benzonitrile (128).

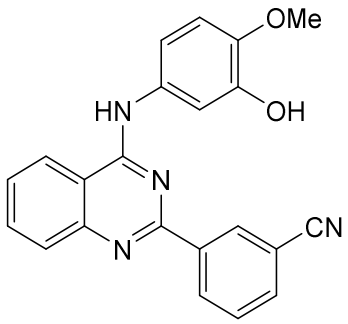

Molecular weight: 368.40 g/mol

The title compound was synthesized from **100** (2.67 g, 10 mmol) and 5-amino-2-methoxyphenol (1.39 g, 10 mmol) as described in the general procedure for **105-152** to yield **128** as dark-red solid (2.73 g, 74%), mp 222-223 °C. **^{1}H NMR** (500 MHz, DMSO-d_6) δ 9.76 (s, 1H), 9.13 (s, 1H), 8.70 (dt, *J* = 5.7, 1.7 Hz, 2H), 8.56 – 8.52 (m, 1H), 7.95 (dt, *J* = 7.7, 1.5 Hz, 1H), 7.89 – 7.84 (m, 2H), 7.75 – 7.70 (m, 1H), 7.64 – 7.58 (m, 1H), 7.43 (d, *J* = 2.6 Hz, 1H), 7.25 (dd, *J* = 8.6, 2.5 Hz, 1H), 6.99 (d, *J* = 8.7 Hz, 1H), 3.81 (s, 3H). **^{13}C NMR** (126 MHz, DMSO) δ 158.20, 157.35, 150.23, 146.48, 144.71, 139.73, 133.67, 133.41, 132.43, 132.37, 131.38, 129.97, 128.25, 126.45, 123.19, 118.90, 114.32, 113.60, 112.30, 111.77, 111.21, 56.09. **Anal. Calcd. for $C_{22}H_{16}N_4O_2$**: C, 71.73; H, 4.38; N, 15.21. Found: C, 71.95; H, 4.74; N, 14.87.

***N*-(3-((2-(3-cyanophenyl)quinazolin-4-yl)amino)phenyl)acetamide (129).**

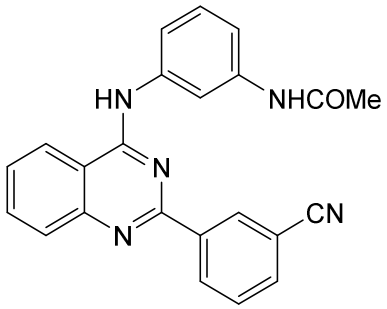

Molecular weight: 379.42 g/mol

The title compound was synthesized from **100** (2.67 g, 10 mmol) and *N*-(3-aminophenyl)acetamide (1.50 g, 10 mmol) as described in the general procedure for **105-152** to yield **129** as light yellow solid (2.62 g, 69%), mp 256-258 °C (decomp.). **^{1}H NMR**

(500 MHz, DMSO-d_6) δ 10.02 (s, 1H), 9.96 (s, 1H), 8.81 (td, *J* = 1.7, 0.6 Hz, 1H), 8.80 – 8.74 (m, 1H), 8.67 (t, *J* = 2.1 Hz, 1H), 8.61 (dt, *J* = 8.4, 1.0 Hz, 1H), 7.94 (ddd, *J* = 7.6, 1.7, 1.2 Hz, 1H), 7.92 – 7.86 (m, 2H), 7.71 (td, *J* = 7.8, 0.6 Hz, 1H), 7.64 (ddd, *J* = 8.3, 4.7, 3.5 Hz, 1H), 7.45 (ddd, *J* = 8.1, 2.2, 1.1 Hz, 1H), 7.35 (t, *J* = 8.0 Hz, 1H), 7.22 (ddd, *J* = 8.0, 2.0, 1.0 Hz, 1H), 2.11 (s, 3H). **^{13}C NMR** (126 MHz, DMSO) δ 168.53, 158.17, 157.33, 150.39, 139.71, 139.46, 139.41, 133.75, 133.59, 132.51, 131.90, 129.85, 128.59, 128.34, 126.61, 123.33, 118.91, 117.19, 114.70, 114.35, 113.53, 111.88, 24.16. **Anal. Calcd. for $C_{23}H_{17}N_5O$**: C, 72.81; H, 4.52; N, 18.46. Found: C, 73.13; H, 4.14; N, 18.21.

2-(2-methoxyphenyl)-*N*-(3-nitrophenyl)quinazolin-4-amine (130).

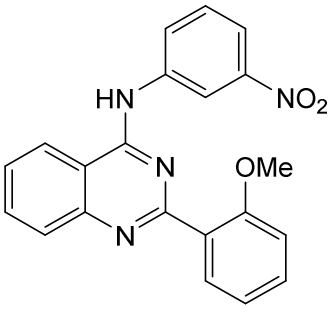

Molecular weight: 372.38 g/mol

The title compound was synthesized from **101** (2.71 g, 10 mmol) and 3-nitroaniline (1.38 g, 10 mmol) as described in the general procedure for **105-152** to yield **130** as light yellow solid (3.20 g, 86%), mp 203-204 °C. **^{1}H NMR** (500 MHz, DMSO-d_6) δ 11.97 (s, 1H), 9.05 (d, *J* = 8.4 Hz, 1H), 8.96 (t, *J* = 2.2 Hz, 1H), 8.38 (ddd, *J* = 8.1, 2.1, 1.0 Hz, 1H), 8.17 – 8.09 (m, 3H), 7.96 – 7.85 (m, 2H), 7.78 (t, *J* = 8.2 Hz, 1H), 7.67 (ddd, *J* = 8.4, 7.4, 1.8 Hz, 1H), 7.33 (dd, *J* = 8.5, 0.9 Hz, 1H), 7.17 (td, *J* = 7.6, 1.0 Hz, 1H), 3.95 (s, 3H). **^{13}C NMR** (126 MHz, DMSO) δ 159.34, 158.04, 156.96, 147.92, 138.52, 136.41, 134.51, 131.91, 130.26, 130.14, 128.66, 124.93, 120.98, 120.61, 118.77, 112.76, 112.60, 56.38. **Anal. Calcd. for $C_{21}H_{16}N_4O_3$**: C, 67.73; H, 4.33; N, 15.05. Found: C, 67.81; H, 4.67; N, 14.74.

2-(3-methoxyphenyl)-*N*-(3-nitrophenyl)quinazolin-4-amine (131).

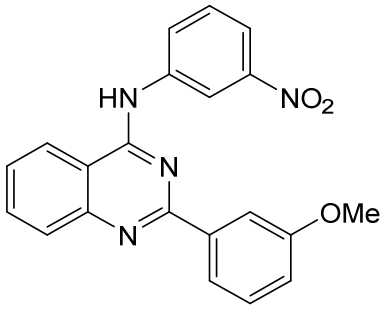

Molecular weight: 372.38 g/mol

The title compound was synthesized from **102** (2.71 g, 10 mmol) and 3-nitroaniline (1.38 g, 10 mmol) as described in the general procedure for **105-152** to yield **131** as yellow solid (3.35 g, 90%), mp 276-278 °C (decomp.). **^{1}H NMR** (500 MHz, DMSO-d_6) δ 11.36 (s, 1H), 9.02 (s, 1H), 8.85 (d, J = 8.3 Hz, 1H), 8.41 – 8.32 (m, 1H), 8.23 (d, J = 8.4 Hz, 1H), 8.12 (dd, J = 8.3, 2.2 Hz, 1H), 8.09 – 8.01 (m, 2H), 7.99 (t, J = 2.1 Hz, 1H), 7.80 (td, J = 7.9, 5.2 Hz, 2H), 7.51 (t, J = 8.0 Hz, 1H), 7.22 (dd, J = 8.3, 2.6 Hz, 1H), 3.85 (s, 3H). **^{13}C NMR** (126 MHz, DMSO) δ 159.70, 158.89, 157.73, 147.97, 139.23, 135.53, 130.16, 130.11, 129.62, 127.90, 124.25, 121.40, 119.85, 118.80, 117.96, 113.73, 113.40, 55.53. **Anal. Calcd. for $C_{21}H_{16}N_4O_3$**: C, 67.73; H, 4.33; N, 15.05. Found: C, 68.04; H, 4.53; N, 14.99.

2-(3-methoxyphenyl)-N-(4-nitrophenyl)quinazolin-4-amine (132).

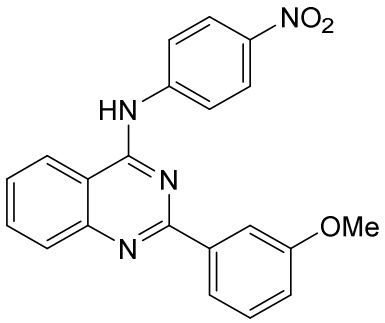

Molecular weight: 372.38 g/mol

The title compound was synthesized from **102** (2.71 g, 10 mmol) and 4-nitroaniline (1.38 g, 10 mmol) as described in the general procedure for **105-152** to yield **132** as light yellow (2.87 g, 77%), mp 285-287 °C (decomp.). **^{1}H NMR** (500 MHz, DMSO-d_6) δ 11.58 (s,

1H), 8.93 (d, *J* = 8.3 Hz, 1H), 8.41 – 8.30 (m, 3H), 8.30 – 8.20 (m, 2H), 8.11 – 7.99 (m, 3H), 7.80 (ddd, *J* = 8.3, 7.1, 1.2 Hz, 1H), 7.52 (t, *J* = 8.2 Hz, 1H), 7.22 (ddd, *J* = 8.2, 2.5, 1.1 Hz, 1H), 3.88 (s, 3H). **^{13}C NMR** (126 MHz, DMSO) δ 159.61, 158.86, 157.52, 144.20, 143.80, 135.68, 130.23, 127.98, 124.53, 124.45, 123.59, 121.53, 118.98, 113.80, 113.50, 55.57. **Anal. Calcd. for $C_{21}H_{16}N_4O_3$**: C, 67.73; H, 4.33; N, 15.05. Found: C, 67.63; H, 4.70; N, 15.14.

***N*-(3,5-dinitrophenyl)-2-(3-methoxyphenyl)quinazolin-4-amine (133).**

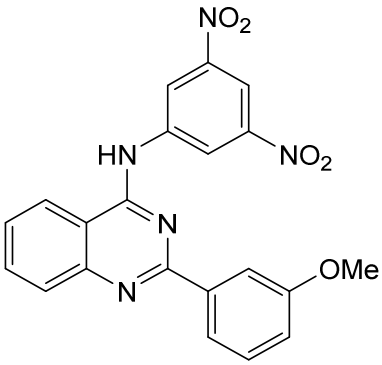

Molecular weight: 417.38 g/mol

The title compound was synthesized from **102** (2.71 g, 10 mmol) and 3,5-dimethoxyaniline (1.53 g, 10 mmol) as described in the general procedure for **105-152** to yield **133** as yellow solid (3.84 g, 92%), mp >300 °C. **^{1}H NMR** (500 MHz, DMSO-d_6) δ 11.21 (s, 1H), 9.47 (d, *J* = 2.1 Hz, 2H), 8.78 (d, *J* = 8.3 Hz, 1H), 8.59 (t, *J* = 2.1 Hz, 1H), 8.16 – 8.06 (m, 2H), 8.06 – 7.98 (m, 2H), 7.77 (ddd, *J* = 8.2, 6.9, 1.2 Hz, 1H), 7.48 (t, *J* = 8.0 Hz, 1H), 7.18 (ddd, *J* = 8.1, 2.7, 0.9 Hz, 1H), 3.85 (s, 3H). **^{13}C NMR** (126 MHz, DMSO) δ 159.75, 158.35, 158.10, 148.13, 141.08, 135.03, 129.95, 127.59, 123.75, 121.63, 121.21, 117.95, 113.69, 113.50, 113.02, 55.48. **Anal. Calcd. for $C_{21}H_{15}N_5O_5$**: C, 60.43; H, 3.62; N, 16.78. Found: C, 60.73; H, 3.98; N, 16.40.

***N*-(4-fluoro-3-nitrophenyl)-2-(3-methoxyphenyl)quinazolin-4-amine (134).**

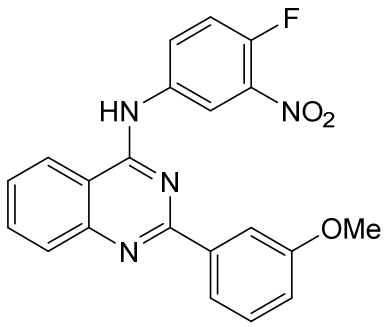

Molecular weight: 390.37 g/mol

The title compound was synthesized from **102** (2.71 g, 10 mmol) and 4-fluoro-3-nitroaniline (1.56 g, 10 mmol) as described in the general procedure for **105-152** to yield **134** as white solid (3.40 g, 87%), mp 269-271 °C (decomp.). **^{1}H NMR** (500 MHz, DMSO-d_6) δ 11.48 (s, 1H), 8.91 (dd, *J* = 6.9, 2.7 Hz, 1H), 8.86 (d, *J* = 8.3 Hz, 1H), 8.32 (ddd, *J* = 9.1, 3.9, 2.7 Hz, 1H), 8.26 (d, *J* = 8.3 Hz, 1H), 8.06 (ddd, *J* = 8.4, 7.0, 1.3 Hz, 1H), 8.02 (ddd, *J* = 7.7, 1.7, 0.9 Hz, 1H), 7.99 (dd, *J* = 2.6, 1.6 Hz, 1H), 7.80 (ddd, *J* = 8.3, 7.0, 1.2 Hz, 1H), 7.75 (dd, *J* = 11.1, 9.0 Hz, 1H), 7.51 (t, *J* = 8.0 Hz, 1H), 7.22 (ddd, *J* = 8.4, 2.7, 1.0 Hz, 1H), 3.86 (s, 3H). **^{13}C NMR** (126 MHz, DMSO) δ 159.69, 158.87, 157.65, 151.87 (d, *J* = 261.1 Hz), 136.45 (d, *J* = 8.1 Hz), 135.63, 134.61, 131.28, 130.16, 127.97, 124.31, 121.51, 120.72, 120.68, 118.80 (d, *J* = 22.0 Hz), 113.77, 113.24, 55.59. **Anal. Calcd. for $C_{21}H_{15}FN_4O_3$**: C, 64.61; H, 3.87; N, 14.35. Found: C, 64.93; H, 4.08; N, 14.15.

3-((2-(3-methoxyphenyl)quinazolin-4-yl)amino)benzonitrile (135).

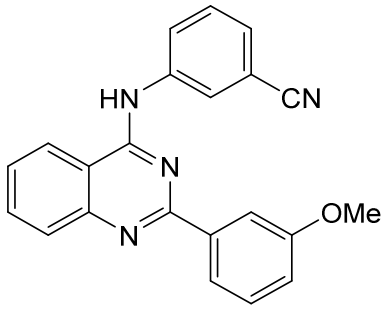

Molecular weight: 352.40 g/mol

The title compound was synthesized from **102** (2.71 g, 10 mmol) and 3-aminobenzonitrile (1.18 g, 10 mmol) as described in the general procedure for **105-152** to yield **135** as light yellow solid (2.61 g, 74%), mp 257-259 °C (decomp.). **^{1}H NMR** (500 MHz, DMSO-d_6) δ 11.38 (s, 1H), 8.82 (dd, *J* = 8.4, 1.2 Hz, 1H), 8.43 (s, 1H), 8.22 (d, *J* = 8.3 Hz, 1H), 8.19 (ddd, *J* = 7.7, 2.2, 1.5 Hz, 1H), 8.06 (ddd, *J* = 8.4, 7.0, 1.2 Hz, 1H), 7.96 (ddd, *J* = 7.7, 1.7, 0.9 Hz, 1H), 7.92 (dd, *J* = 2.6, 1.6 Hz, 1H), 7.80 (ddd, *J* = 8.4, 7.0, 1.2 Hz, 1H), 7.77 – 7.70 (m, 2H), 7.51 (t, *J* = 8.0 Hz, 1H), 7.22 (ddd, *J* = 8.2, 2.7, 0.9 Hz, 1H), 3.87 (s, 3H). **^{13}C NMR** (126 MHz, DMSO) δ 159.68, 158.99, 157.56, 138.67, 135.69, 130.22, 130.17, 129.23, 128.72, 127.99, 127.18, 124.35, 121.30, 119.21, 118.63, 113.52, 113.22, 111.60, 55.58. **Anal. Calcd. for $C_{22}H_{16}N_4O$**: C, 74.98; H, 4.58; N, 15.90. Found: C, 75.16; H, 4.86; N, 15.99.

***N*-(3-fluorophenyl)-2-(3-methoxyphenyl)quinazolin-4-amine (136).**

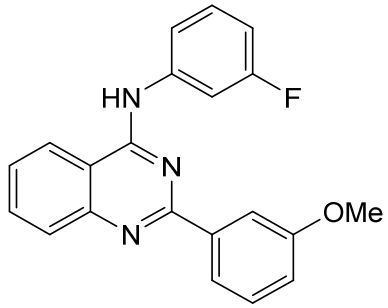

Molecular weight: 345.38 g/mol

The title compound was synthesized from **102** (2.71 g, 10 mmol) and 3-fluoroaniline (1.11 g, 10 mmol) as described in the general procedure for **105-152** to yield **136** as light yellow solid (2.07 g, 60%), mp 232-235 °C (decomp.). **^{1}H NMR** (600 MHz, DMSO-d_6) δ 11.49 (s, 1H), 8.90 (d, *J* = 8.4 Hz, 1H), 8.39 – 8.30 (m, 1H), 8.07 (t, *J* = 7.7 Hz, 1H), 8.03 – 7.97 (m, 2H), 7.89 (dt, *J* = 11.2, 2.3 Hz, 1H), 7.81 (t, *J* = 7.7 Hz, 1H), 7.75 – 7.69 (m, 1H), 7.59 – 7.50 (m, 2H), 7.24 (dd, *J* = 8.4, 2.6 Hz, 1H), 7.16 (td, *J* = 8.5, 2.6 Hz, 1H), 3.87 (s, 3H). **^{13}C NMR** (151 MHz, DMSO) δ 161.97 (d, *J* = 242.4 Hz), 159.64, 159.00, 157.31, 139.19, 135.77, 130.35 (d, *J* = 9.2 Hz), 130.23, 128.08, 124.51, 121.41, 120.07, 119.36, 113.83, 113.12, 112.59, 111.32, 55.53. **Anal. Calcd. for $C_{21}H_{16}FN_3O$**: C, 73.03; H, 4.67; N, 12.17. Found: C, 73.27; H, 4.94; N, 11.95.

***N*,2-bis(3-methoxyphenyl)quinazolin-4-amine (137).**

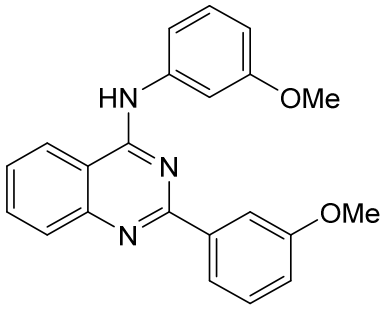

Molecular weight: 357.41 g/mol

The title compound was synthesized from **102** (2.71 g, 10 mmol) and 3-methoxyaniline (1.23 g, 10 mmol) as described in the general procedure for **105-152** to yield **137** as light yellow solid (1.93 g, 54%), mp 133-135 °C. **^{1}H NMR** (500 MHz, DMSO-d_6) δ 9.94 (s, 1H), 8.60 (d, J = 8.3 Hz, 1H), 8.07 – 8.01 (m, 2H), 7.93 – 7.86 (m, 2H), 7.75 (t, J = 2.2 Hz, 1H), 7.63 (ddd, J = 8.3, 5.5, 2.7 Hz, 1H), 7.54 (ddd, J = 8.1, 2.1, 0.9 Hz, 1H), 7.43 (t, J = 7.9 Hz, 1H), 7.35 (t, J = 8.1 Hz, 1H), 7.08 (ddd, J = 8.1, 2.7, 1.0 Hz, 1H), 6.78 – 6.73 (m, 1H), 3.85 (s, 3H), 3.82 (s, 3H). **^{13}C NMR** (126 MHz, DMSO) δ 159.57, 159.54, 158.70, 158.01, 140.46, 133.60, 129.63, 129.29, 126.32, 123.25, 120.45, 116.74, 114.61, 114.08, 113.04, 109.53, 108.18, 55.26, 55.20. **Anal. Calcd. for $C_{22}H_{19}N_3O_2$**: C, 73.93; H, 5.36; N, 11.76. Found: C, 74.11; H, 5.29; N, 11.61.

***N*-(3,4-dimethoxyphenyl)-2-(3-methoxyphenyl)quinazolin-4-amine (138).**

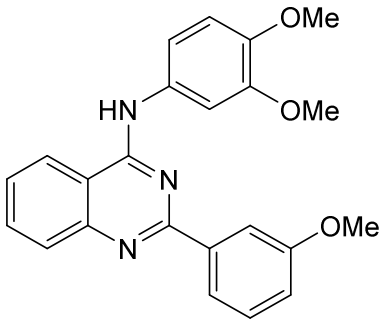

Molecular weight: 387.44 g/mol

The title compound was synthesized from **102** (2.71 g, 10 mmol) and 3,4-dimethoxyaniline (1.53 g, 10 mmol) as described in the general procedure for **105-152** to yield **138** as light beige solid (2.44 g, 63%), mp 139-141 °C. **^{1}H NMR** (500 MHz, DMSO-

d_6) δ 9.74 (s, 1H), 8.54 (dt, *J* = 8.4, 1.0 Hz, 1H), 8.05 (dt, *J* = 7.8, 1.1 Hz, 1H), 8.02 (dd, *J* = 2.7, 1.5 Hz, 1H), 7.88 – 7.81 (m, 2H), 7.70 (d, *J* = 2.5 Hz, 1H), 7.59 (ddd, *J* = 8.3, 4.9, 3.3 Hz, 1H), 7.45 (dd, *J* = 8.7, 2.5 Hz, 1H), 7.41 (t, *J* = 7.9 Hz, 1H), 7.06 (ddd, *J* = 8.1, 2.8, 1.0 Hz, 1H), 7.03 (d, *J* = 8.7 Hz, 1H), 3.83 (s, 3H), 3.83 (s, 3H), 3.79 (s, 3H). **^{13}C NMR** (126 MHz, DMSO) δ 159.53, 158.93, 157.88, 150.46, 148.50, 145.51, 140.10, 133.17, 132.79, 129.49, 128.24, 125.96, 123.01, 120.38, 115.97, 114.44, 114.15, 113.35, 111.94, 107.77, 55.95, 55.68, 55.24. **Anal. Calcd. for $C_{23}H_{21}N_3O_3$**: C, 71.30; H, 5.46; N, 10.85. Found: C, 71.27; H, 5.49; N, 10.93.

2-(4-methoxyphenyl)-N-(3-nitrophenyl)quinazolin-4-amine (139).

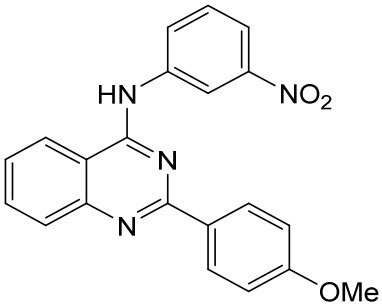

Molecular weight: 372.38 g/mol

The title compound was synthesized from **103** (2.71 g, 10 mmol) and 3-nitroaniline (1.38 g, 10 mmol) as described in the general procedure for **105-152** to yield **139** as light yellow (2.49 g, 67%), mp 282-283 °C (decomp.). **^{1}H NMR** (500 MHz, DMSO-d_6) δ 11.55 (s, 1H), 9.06 (s, 1H), 8.89 (d, *J* = 8.1 Hz, 1H), 8.53 – 8.39 (m, 2H), 8.39 – 8.02 (m, 4H), 7.82 (dt, *J* = 14.1, 6.2 Hz, 2H), 7.23 – 7.11 (m, 2H), 3.90 (s, 3H). **^{13}C NMR** (126 MHz, DMSO) δ 163.44, 158.91, 157.23, 147.95, 138.91, 135.83, 131.30, 130.19, 129.81, 127.74, 124.44, 120.15, 118.30, 114.62, 112.94, 55.87. **Anal. Calcd. for $C_{21}H_{16}N_4O_3$**: C, 67.73; H, 4.33; N, 15.05. Found: C, 67.87; H, 4.67; N, 14.84.

3-((2-(4-methoxyphenyl)quinazolin-4-yl)amino)benzonitrile (140).

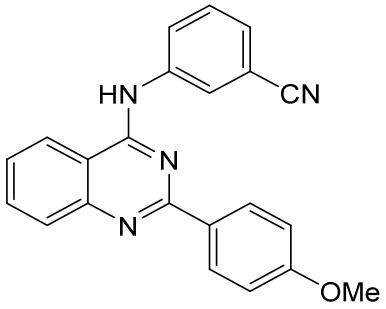

Molecular weight: 352.40 g/mol

The title compound was synthesized from **103** (2.71 g, 10 mmol) and 3-aminobenzonitrile (1.18 g, 10 mmol) as described in the general procedure for **105-152** to yield **140** as light yellow solid (2.57 g, 73%), mp 279-281 °C (decomp.). **^{1}H NMR** (500 MHz, DMSO-d_6) δ 11.75 (s, 1H), 8.92 (d, J = 8.3 Hz, 1H), 8.42 – 8.35 (m, 2H), 8.35 – 8.27 (m, 2H), 8.20 (ddd, J = 8.1, 2.1, 1.2 Hz, 1H), 8.06 (ddd, J = 8.4, 7.1, 1.3 Hz, 1H), 7.83 – 7.67 (m, 3H), 7.21 – 7.12 (m, 2H), 3.88 (s, 3H). **^{13}C NMR** (126 MHz, DMSO) δ 163.64, 159.10, 156.94, 138.29, 136.03, 131.37, 130.23, 129.59, 129.22, 127.87, 127.72, 124.69, 118.53, 114.64, 112.70, 111.63, 55.89. **Anal. Calcd. for $C_{22}H_{16}N_4O$**: C, 74.98; H, 4.58; N, 15.90. Found: C, 74.99; H, 4.81; N, 15.75.

***N*-(3-methoxyphenyl)-2-(4-methoxyphenyl)quinazolin-4-amine (141).**

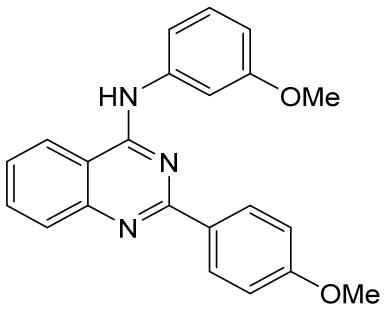

Molecular weight: 357.41 g/mol

The title compound was synthesized from **103** (2.71 g, 10 mmol) and 3-methoxyaniline (1.23 g, 10 mmol) as described in the general procedure for **105-152** to yield **141** as yellow solid (1.60 g, 45%), mp 211-213 °C. **^{1}H NMR** (500 MHz, DMSO-d_6) δ 10.19 (s, 1H), 8.62 (d, J = 8.4 Hz, 1H), 8.38 (dd, J = 8.8, 2.0 Hz, 2H), 7.91 (d, J = 6.7 Hz, 2H), 7.70 – 7.60 (m, 2H), 7.56 – 7.49 (m, 1H), 7.37 (dd, J = 9.5, 6.8 Hz, 1H), 7.10 (dd, J = 9.4,

2.5 Hz, 2H), 6.79 (dd, *J* = 8.3, 2.5 Hz, 1H), 3.85 (s, 3H), 3.82 (s, 3H). **^{13}C NMR** (126 MHz, DMSO) δ 159.55, 158.37, 158.16, 130.10, 129.41, 126.27, 123.51, 114.98, 114.15, 113.55, 110.45, 108.22, 55.58, 55.32. **Anal. Calcd. for $C_{22}H_{19}N_3O_2$**: C, 73.93; H, 5.36; N, 11.76. Found: C, 74.06; H, 5.43; N, 11.53.

***N*-(3,4-dimethoxyphenyl)-2-(4-methoxyphenyl)quinazolin-4-amine (142).**

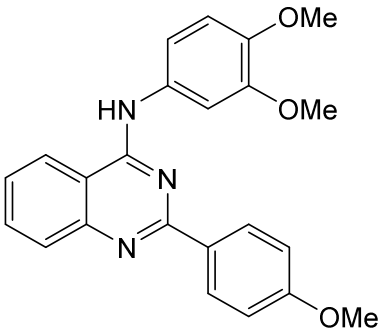

Molecular weight: 387.44 g/mol

The title compound was synthesized from **103** (2.71 g, 10 mmol) and 3,4-dimethoxyaniline (1.53 g, 10 mmol) as described in the general procedure for **105-152** to yield **142** as orange-yellow solid (2.60 g, 67%), mp 238-239 °C (decomp.). **^{1}H NMR** (500 MHz, DMSO-d_6) δ 11.28 (s, 1H), 8.78 (d, *J* = 8.3 Hz, 1H), 8.43 – 8.30 (m, 2H), 8.23 (d, *J* = 8.3 Hz, 1H), 8.04 (t, *J* = 7.8 Hz, 1H), 7.77 (t, *J* = 7.7 Hz, 1H), 7.56 (d, *J* = 2.4 Hz, 1H), 7.35 (dd, *J* = 8.6, 2.4 Hz, 1H), 7.24 – 7.15 (m, 2H), 7.10 (d, *J* = 8.7 Hz, 1H), 3.88 (s, 3H), 3.82 (s, 3H), 3.80 (s, 3H). **^{13}C NMR** (126 MHz, DMSO) δ 163.59, 158.45, 156.80, 148.50, 135.67, 131.24, 127.71, 124.32, 116.48, 114.63, 112.59, 111.64, 109.05, 55.87, 55.85, 55.79. **Anal. Calcd. for $C_{23}H_{21}N_3O_3$**: C, 73.30; H, 5.46; N, 10.85. Found: C, 71.60; H, 5.58; N, 10.55.

2-(3,4-dimethoxyphenyl)-N-(3-nitrophenyl)quinazolin-4-amine (143).

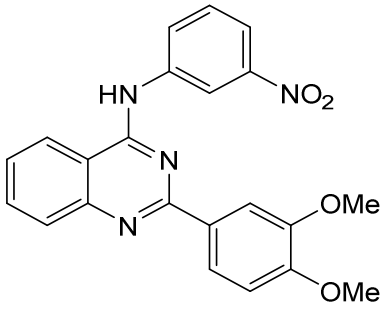

Molecular weight: 402.41 g/mol

The title compound was synthesized from **104** (3.01 g, 10 mmol) and 3-nitroaniline (1.38 g, 10 mmol) as described in the general procedure for **105-152** to yield **143** as light yellow solid (3.14 g, 78%), mp 274-275 °C (decomp.). **^{1}H NMR** (500 MHz, DMSO-d_6) δ 11.60 (s, 1H), 8.93 (t, J = 2.2 Hz, 1H), 8.86 (d, J = 8.5 Hz, 1H), 8.38 (d, J = 7.8 Hz, 1H), 8.36 – 8.32 (m, 1H), 8.14 (ddd, J = 14.6, 8.6, 2.2 Hz, 2H), 8.10 – 8.01 (m, 2H), 7.80 (q, J = 7.7 Hz, 2H), 7.17 (d, J = 8.8 Hz, 1H), 3.88 (s, 3H), 3.85 (s, 3H). **^{13}C NMR** (126 MHz, DMSO) δ 158.85, 157.04, 148.92, 147.90, 138.79, 135.87, 130.11, 127.79, 124.46, 123.62, 120.25, 118.50, 112.84, 112.02, 111.75, 56.04, 55.87. **Anal. Calcd. for $C_{22}H_{18}N_4O_4$**: C, 65.66; H, 4.51; N, 13.92. Found: C, 65.85; H, 4.78; N, 13.59.

2-(3,4-dimethoxyphenyl)-N-(4-nitrophenyl)quinazolin-4-amine (144).

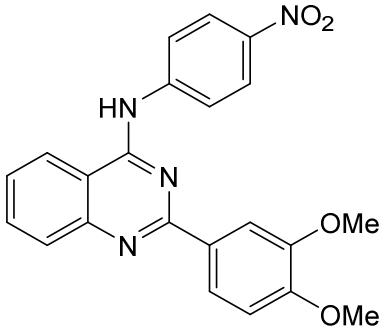

Molecular weight: 402.41 g/mol

The title compound was synthesized from **104** (3.01 g, 10 mmol) and 4-nitroaniline (1.38 g, 10 mmol) as described in the general procedure for **105-152** to yield **144** as light yellow solid (3.30 g, 82%), mp >300 °C. **^{1}H NMR** (500 MHz, DMSO-d_6) δ 11.53 (s, 1H), 8.86 (d, J = 8.3 Hz, 1H), 8.38 (dd, J = 9.6, 2.4 Hz, 3H), 8.27 – 8.16 (m, 2H), 8.12 (dd, J = 6.9,

2.1 Hz, 2H), 8.05 (t, *J* = 7.8 Hz, 1H), 7.78 (t, *J* = 7.7 Hz, 1H), 7.25 – 7.15 (m, 1H), 3.90 (s, 3H), 3.87 (s, 3H). **^{13}C NMR** (126 MHz, DMSO) δ 158.66, 157.05, 153.26, 148.87, 144.04, 135.82, 127.71, 124.49, 124.43, 123.87, 123.53, 113.07, 111.97, 111.85, 55.98, 55.89. **Anal. Calcd. for $C_{22}H_{18}N_4O_4$**: C, 65.66; H, 4.51; N, 13.92. Found: C, 65.86; H, 4.43; N, 13.74.

2-(3,4-dimethoxyphenyl)-*N*-(3,5-dinitrophenyl)quinazolin-4-amine (145).

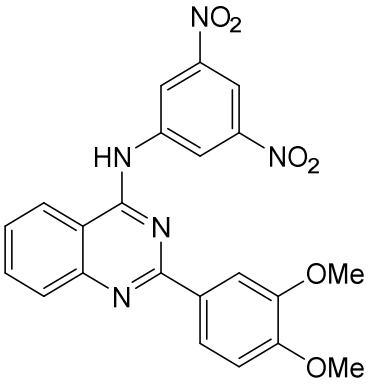

Molecular weight: 447.41 g/mol

The title compound was synthesized from **104** (3.01 g, 10 mmol) and 3,5-dinitroaniline (1.83 g, 10 mmol) as described in the general procedure for **105-152** to yield **145** as light yellow solid (2.82 g, 63%), mp 283-284 °C (decomp.). **^{1}H NMR** (500 MHz, DMSO-d_6) δ 11.12 (s, 1H), 9.45 (dd, *J* = 2.1, 1.0 Hz, 2H), 8.76 (d, *J* = 8.1 Hz, 1H), 8.63 (t, *J* = 2.1 Hz, 1H), 8.16 (dd, *J* = 8.6, 6.6 Hz, 2H), 8.11 (d, *J* = 2.2 Hz, 1H), 8.00 (ddd, *J* = 8.4, 7.0, 1.3 Hz, 1H), 7.74 (ddd, *J* = 8.2, 6.9, 1.3 Hz, 1H), 7.13 (d, *J* = 8.5 Hz, 1H), 3.89 (s, 3H), 3.87 (s, 3H). **^{13}C NMR** (126 MHz, DMSO) δ 162.05, 157.97, 157.83, 148.96, 148.02, 141.03, 134.54, 126.72, 123.41, 122.63, 121.43, 113.17, 112.68, 112.28, 111.79, 55.86, 55.78. **Anal. Calcd. for $C_{22}H_{17}N_5O_6$**: C, 59.06; H, 3.38; N, 15.65. Found: C, 59.20; H, 3.55; N, 15.29.

4-((2-(3,4-dimethoxyphenyl)quinazolin-4-yl)amino)-2-nitrophenol (146).

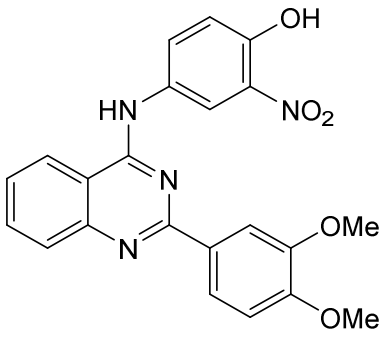

Molecular weight: 418.41 g/mol

The title compound was synthesized from **104** (3.01 g, 10 mmol) and 4-amino-2-nitrophenol (1.54 g, 10 mmol) as described in the general procedure for **105-152** to yield **146** as yellow solid (1.92 g, 46%), mp 258-259 °C (decomp.). **^{1}H NMR** (600 MHz, DMSO-d_6) δ 11.53 (s, 1H), 11.30 (s, 1H), 8.79 (d, J = 8.3 Hz, 1H), 8.49 (d, J = 2.6 Hz, 1H), 8.45 – 8.29 (m, 1H), 8.10 (dd, J = 8.6, 2.2 Hz, 1H), 8.05 – 8.00 (m, 3H), 7.76 (ddd, J = 8.3, 7.1, 1.1 Hz, 1H), 7.33 (d, J = 9.0 Hz, 1H), 7.16 (d, J = 8.6 Hz, 1H), 3.87 (s, 3H), 3.85 (s, 3H). **^{13}C NMR** (151 MHz, DMSO) δ 158.65, 156.71, 153.56, 150.54, 148.89, 136.00, 135.85, 131.71, 128.53, 127.83, 124.43, 123.70, 120.87, 119.28, 112.54, 112.07, 111.70, 56.05, 55.90. **Anal. Calcd. for $C_{22}H_{18}N_4O_5$**: C, 63.15; H, 4.34; N, 13.39. Found: C, 63.38; H, 4.66; N, 13.08.

3-((2-(3,4-dimethoxyphenyl)quinazolin-4-yl)amino)benzonitrile (147).

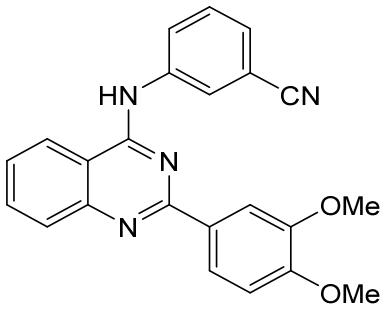

Molecular weight: 382.42 g/mol

The title compound was synthesized from **104** (3.01 g, 10 mmol) and 3-aminobenzonitrile (1.18 g, 10 mmol) as described in the general procedure for **105-152** to yield **147** as white solid (3.08 g, 80%), mp 289-292 °C (decomp.). **^{1}H NMR** (500 MHz, DMSO-d_6) δ 11.30

(s, 1H), 8.76 (d, *J* = 8.3 Hz, 1H), 8.43 (s, 1H), 8.22 (s, 1H), 8.17 (dt, *J* = 7.9, 1.8 Hz, 1H), 8.06 (dd, *J* = 8.5, 2.2 Hz, 2H), 7.96 (d, *J* = 2.1 Hz, 1H), 7.82 – 7.69 (m, 3H), 7.20 (d, *J* = 8.6 Hz, 1H), 3.88 (s, 6H). **^{13}C NMR** (126 MHz, DMSO) δ 158.77, 148.90, 130.24, 127.61, 124.22, 118.63, 112.85, 111.77, 111.71, 56.03, 55.76. **Anal. Calcd. for $C_{23}H_{18}N_4O_2$**: C, 72.24; H, 4.74; N, 14.65. Found: C, 72.40; H, 5.00; N, 14.33.

2-(3,4-dimethoxyphenyl)-*N*-(4-methoxy-3-(trifluoromethyl)phenyl)quinazolin-4-amine (148).

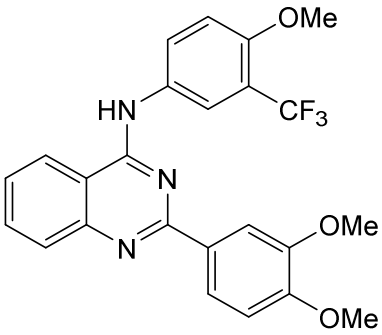

Molecular weight: 455.44 g/mol

The title compound was synthesized from **104** (3.01 g, 10 mmol) and 4-methoxy-3-(trifluoromethyl)aniline (1.91 g, 10 mmol) as described in the general procedure for **105-152** to yield **148** as light yellow solid (2.91 g, 64%), mp 272-273 °C. **^{1}H NMR** (500 MHz, DMSO-d_6) δ 11.64 (s, 1H), 8.86 (d, *J* = 8.2 Hz, 1H), 8.45 (d, *J* = 8.4 Hz, 1H), 8.16 (d, *J* = 2.6 Hz, 1H), 8.11 – 8.01 (m, 4H), 7.77 (ddd, *J* = 8.3, 7.1, 1.2 Hz, 1H), 7.43 (d, *J* = 9.0 Hz, 1H), 7.15 (d, *J* = 8.6 Hz, 1H), 3.95 (s, 3H), 3.87 (s, 3H), 3.85 (s, 3H). **^{13}C NMR** (126 MHz, DMSO) δ 158.73, 156.61, 155.14, 153.61, 148.89, 135.86, 130.32, 129.66, 127.84, 126.84, 124.67, 124.56, 123.63, 123.25 (d, *J* = 3.7 Hz), 122.51, 116.74 (d, *J* = 30.6 Hz), 113.26, 112.53, 112.13, 111.63, 56.64, 56.04, 55.92. **Anal. Calcd. for $C_{24}H_{20}F_3N_3O_3$**: C, 63.29; H, 4.43; N, 9.23. Found: C, 63.44; H, 4.49; N, 8.87.

2-(3,4-dimethoxyphenyl)-*N*-(3-methoxyphenyl)quinazolin-4-amine (149).

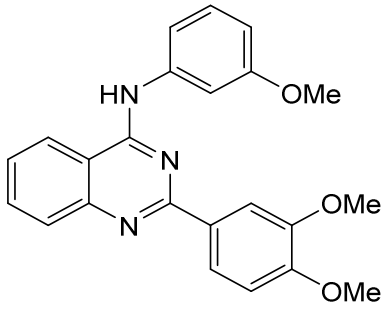

Molecular weight: 387.44 g/mol

The title compound was synthesized from **104** (3.01 g, 10 mmol) and 3-methoxyaniline (1.23 g, 10 mmol) as described in the general procedure for **105-152** to yield **149** as yellow solid (2.13 g, 55%), mp 144-145 °C. **^{1}H NMR** (500 MHz, DMSO-d_6) δ 9.86 (s, 1H), 8.56 (dt, J = 8.3, 1.0 Hz, 1H), 8.10 – 8.05 (m, 2H), 7.89 – 7.81 (m, 2H), 7.75 (t, J = 2.3 Hz, 1H), 7.61 – 7.53 (m, 2H), 7.35 (t, J = 8.1 Hz, 1H), 7.13 – 7.06 (m, 1H), 6.75 (ddd, J = 8.2, 2.5, 0.8 Hz, 1H), 3.87 (s, 3H), 3.84 (s, 3H), 3.81 (s, 3H). **^{13}C NMR** (126 MHz, DMSO) δ 159.54, 158.74, 157.81, 151.23, 148.66, 140.56, 133.44, 129.25, 125.76, 123.20, 121.30, 114.60, 113.82, 111.54, 111.28, 108.99, 108.43, 55.76, 55.39, 55.28. Anal. Calcd. for $C_{23}H_{21}N_3O_3$: C, 71.30; H, 5.46; N, 10.85. Found: C, 71.58; H, 5.31; N, 10.58.

***N*-(4-bromo-3-methoxyphenyl)-2-(3,4-dimethoxyphenyl)quinazolin-4-amine (150).**

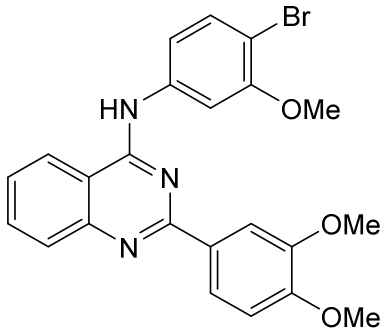

Molecular weight: 466.34 g/mol

The title compound was synthesized from **104** (3.01 g, 10 mmol) and 4-bromo-3-methoxyaniline (2.02 g, 10 mmol) as described in the general procedure for **105-152** to yield **150** as yellow solid (3.68 g, 79%), mp 254-256 °C. **^{1}H NMR** (500 MHz, DMSO-

d_6) δ 11.37 (s, 1H), 8.80 (d, *J* = 8.2 Hz, 1H), 8.37 (d, *J* = 8.3 Hz, 1H), 8.13 – 8.01 (m, 3H), 7.78 (t, *J* = 7.7 Hz, 1H), 7.71 (d, *J* = 8.5 Hz, 1H), 7.66 (d, *J* = 2.3 Hz, 1H), 7.47 (dd, *J* = 8.5, 2.3 Hz, 1H), 7.22 (d, *J* = 8.4 Hz, 1H), 3.89 (s, 3H), 3.87 (s, 3H), 3.87 (s, 3H). **^{13}C NMR** (126 MHz, DMSO) δ 158.69, 156.80, 155.46, 153.47, 148.88, 138.13, 135.82, 132.67, 127.76, 124.35, 123.60, 117.85, 112.72, 112.15, 111.85, 109.13, 107.48, 56.51, 56.04, 55.97. **Anal. Calcd. for $C_{23}H_{20}BrN_3O_3$**: C, 59.24; H, 4.32; N, 9.01. Found: C, 59.03; H, 4.54; N, 8.98.

2-(3,4-dimethoxyphenyl)-*N*-(3-fluorophenyl)quinazolin-4-amine (151).

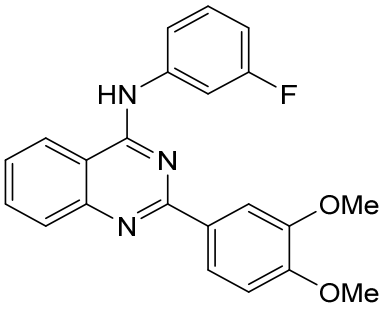

Molecular weight: 375.40 g/mol

The title compound was synthesized from **104** (3.01 g, 10 mmol) and 3-fluoroaniline (1.11 g, 10 mmol) as described in the general procedure for **105-152** to yield **151** as light yellow solid (2.89 g, 77%), 266-268 °C (decomp.). **^{1}H NMR** (600 MHz, DMSO-d_6) δ 11.39 (s, 1H), 8.81 (d, *J* = 8.4 Hz, 1H), 8.33 (s, 1H), 8.11 (dd, *J* = 8.5, 2.2 Hz, 1H), 8.05 (dd, *J* = 13.3, 5.0 Hz, 2H), 7.89 (dt, *J* = 11.1, 2.3 Hz, 1H), 7.78 (t, *J* = 7.7 Hz, 1H), 7.69 (dd, *J* = 8.1, 1.9 Hz, 1H), 7.56 (td, *J* = 8.2, 6.7 Hz, 1H), 7.22 (d, *J* = 8.6 Hz, 1H), 7.17 (td, *J* = 8.5, 2.6 Hz, 1H), 3.88 (s, 3H), 3.87 (s, 3H). **^{13}C NMR** (151 MHz, DMSO) δ 162.79, 161.19, 158.78, 156.91, 148.91, 135.88, 130.41 (d, *J* = 9.3 Hz), 127.81, 124.44, 123.28, 120.21, 112.75, 111.92 (d, *J* = 22.2 Hz), 56.09, 55.72. **Anal. Calcd. for $C_{22}H_{18}FN_3O_2$**: C, 70.39; H, 4.83; N, 11.19. Found: C, 70.14; H, 4.53; N, 11.39.

3-((2-(3,4-dimethoxyphenyl)quinazolin-4-yl)amino)benzenesulfonyl fluoride (152).

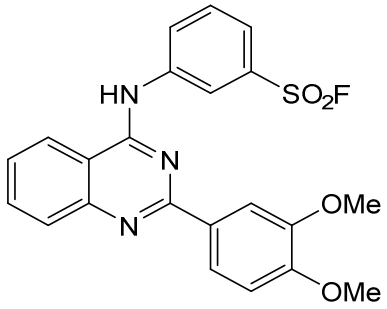

Molecular weight: 439.46 g/mol

The title compound was synthesized from **104** (3.01 g, 10 mmol) and 3-aminobenzenesulfonyl fluoride (1.75 g, 10 mmol) as described in the general procedure for **105-152** to yield **152** as bright yellow solid (3.25 g, 74%), mp 225-227 °C. **^{1}H NMR** (500 MHz, DMSO-d_6) δ 11.74 (s, 1H), 8.89 (d, J = 8.4 Hz, 1H), 8.79 (t, J = 2.0 Hz, 1H), 8.48 – 8.39 (m, 2H), 8.11 (d, J = 2.2 Hz, 1H), 8.09 – 8.01 (m, 3H), 7.94 (t, J = 8.1 Hz, 1H), 7.79 (ddd, J = 8.3, 7.1, 1.1 Hz, 1H), 7.13 (d, J = 8.6 Hz, 1H), 3.88 (s, 6H). **^{13}C NMR** (126 MHz, DMSO) δ 158.93, 156.99, 153.50, 148.93, 139.22, 135.99, 131.91 (d, J = 23.7 Hz), 131.57, 131.04, 127.87, 125.18, 124.55, 123.77, 123.18, 112.83, 112.15, 111.62, 56.04, 56.02. **Anal. Calcd. for $C_{22}H_{18}FN_3O_4S$**: C, 60.13; H, 4.13; N, 9.56. Found: C, 60.02; H, 4.43; N, 9.20.

10.1.1.4 Synthesis of 2,4-Substituted Pyrido[2,3-d]pyrimidines

General Procedure for the Preparation of compounds 153-155. To mixture of methyl 2-aminonicotinate (4.90 g, 32 mmol) and Et_3N (5.5 mL, 38 mmol) in $CHCl_3$ (40 mL) was slowly added the corresponding acyl chloride (32 mmol) at 0 °C and subsequently stirred for 12 h at room temperature. The mixture was diluted with $CHCl_3$ and extracted in a separatory funnel using saturated $NaHCO_3$ followed by brine. The organic phase was then dried over $MgSO_4$ and evaporated under reduced pressure. The resulting residue was recrystallized from a mixture of AcOEt and petroleum ether.

methyl 2-benzamidonicotinate (153).

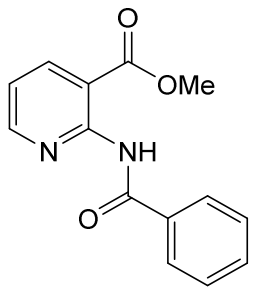

Molecular weight: 256.26 g/mol

The compound was synthesized according to the general procedure for compounds **153-155** using benzoyl chloride (4.50 g, 32 mmol) to yield **153** as a white solid (5.66 g, 69%). **^{1}H NMR** (500 MHz, DMSO-d_6) δ 11.08 (s, 1H), 8.60 (dd, J = 4.8, 1.9 Hz, 1H), 8.16 (dd, J = 7.7, 1.9 Hz, 1H), 8.03 – 7.93 (m, 2H), 7.80 – 7.72 (m, 1H), 7.64 – 7.57 (m, 1H), 7.45 (dd, J = 7.5, 0.9 Hz, 1H), 7.35 (dd, J = 7.7, 4.8 Hz, 1H), 3.70 (s, 3H). **^{13}C NMR** (126 MHz, DMSO) δ 166.45, 165.91, 151.31, 149.64, 138.98, 133.86, 132.26, 128.63, 127.97, 120.49, 120.45, 52.29, 40.04.

methyl 2-(3-methoxybenzamido)nicotinate (154).

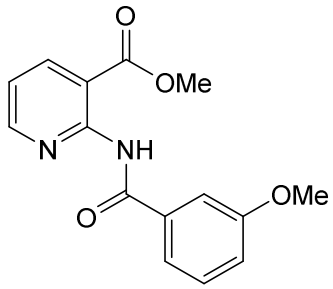

Molecular weight: 286.29 g/mol

The compound was synthesized according to the general procedure for compounds **153-155** using 3-methoxybenzoyl chloride (5.46 g, 32 mmol) to yield **154** as a white solid (7.24 g, 79%). **^{1}H NMR** (500 MHz, DMSO-d_6) δ 11.07 (s, 1H), 8.60 (ddd, J = 4.7, 1.9, 0.7 Hz, 1H), 8.15 (ddd, J = 7.7, 1.9, 0.7 Hz, 1H), 7.64 – 7.52 (m, 2H), 7.44 (t, J = 7.9 Hz, 1H), 7.35 (ddd, J = 7.7, 4.8, 0.7 Hz, 1H), 7.17 (ddt, J = 8.1, 2.4, 0.8 Hz, 1H), 3.84 (s, 3H), 3.71 (s, 3H). **^{13}C NMR** (126 MHz, DMSO) δ 166.44, 165.61, 159.39, 151.28, 149.55, 138.98, 135.20, 129.79, 120.58, 120.53, 120.24, 118.34, 112.91, 55.49, 52.29.

methyl 2-(nicotinamido)nicotinate (155).

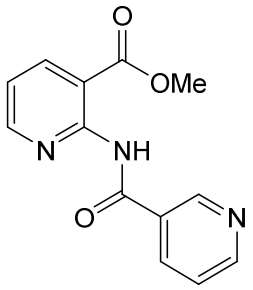

Molecular weight: 257.25 g/mol

The compound was synthesized according to the general procedure for compounds **153-155** using nicotinoyl chloride (4.53 g, 32 mmol) to yield **155** as a white solid (5.60 g, 68%). **^{1}H NMR** (500 MHz, DMSO-d_6) δ 11.27 (s, 1H), 9.11 (dd, *J* = 2.4, 0.9 Hz, 1H), 8.78 (dd, *J* = 4.8, 1.6 Hz, 1H), 8.62 (dd, *J* = 4.8, 1.9 Hz, 1H), 8.31 (ddd, *J* = 8.0, 2.4, 1.7 Hz, 1H), 8.17 (dd, *J* = 7.7, 1.9 Hz, 1H), 7.57 (ddd, *J* = 7.9, 4.9, 0.9 Hz, 1H), 7.39 (dd, *J* = 7.7, 4.9 Hz, 1H), 3.70 (s, 3H). **^{13}C NMR** (126 MHz, DMSO) δ 166.26, 164.86, 152.75, 151.31, 149.07, 149.01, 139.07, 135.72, 129.50, 123.72, 121.04, 120.90, 52.31.

General Procedure for the Preparation of compounds 156-158. To a solution of the corresponding compound **153-155** (10 mmol) in MeOH (200 mL) was added 28% aqueous NH_3 (250 mL). The mixture was stirred for 24 h, concentrated to about half the initial volume and the formed precipitate filtered with suction.

2-phenylpyrido[2,3-d]pyrimidin-4(3H)-one (156).

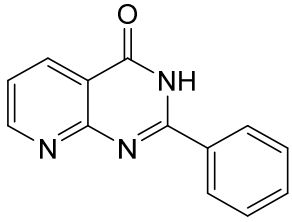

Molecular weight: 223.24 g/mol

The compound was synthesized according to the general procedure for compounds **156-158** from **153** (2.56 g, 10 mmol) to yield **156** as a white solid (1.43 g, 64%). **^{1}H NMR**

(500 MHz, DMSO-d_6) δ 12.79 (s, 1H), 8.96 (dd, J = 4.5, 2.0 Hz, 1H), 8.52 (dd, J = 7.8, 2.0 Hz, 1H), 8.25 – 8.13 (m, 2H), 7.65 – 7.60 (m, 1H), 7.60 – 7.55 (m, 2H), 7.53 (dd, J = 7.9, 4.5 Hz, 1H). **^{13}C NMR** (126 MHz, DMSO) δ 163.12, 156.20, 155.56, 135.60, 132.60, 132.04, 128.79, 128.20, 122.34, 116.28.

2-(3-methoxyphenyl)pyrido[2,3-d]pyrimidin-4(3H)-one (157).

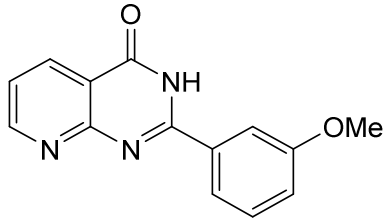

Molecular weight: 253.26 g/mol

The compound was synthesized according to the general procedure for compounds **156-158** from **154** (2.86 g, 10 mmol) to yield **157** as a white solid (1.90 g, 75%). **^{1}H NMR** (500 MHz, DMSO-d_6) δ 12.77 (s, 1H), 8.96 (dd, J = 4.6, 2.0 Hz, 1H), 8.52 (dd, J = 7.8, 2.1 Hz, 1H), 7.82 (ddt, J = 7.8, 1.9, 0.9 Hz, 1H), 7.78 (t, J = 2.1 Hz, 1H), 7.53 (ddd, J = 7.8, 4.5, 0.8 Hz, 1H), 7.51 – 7.43 (m, 1H), 7.18 (ddd, J = 8.3, 2.6, 1.0 Hz, 1H), 3.87 (s, 3H). **^{13}C NMR** (126 MHz, DMSO) δ 163.01, 159.51, 158.80, 156.26, 155.22, 135.60, 133.88, 129.95, 122.39, 120.55, 118.38, 116.38, 112.86, 55.56.

2-(pyridin-3-yl)pyrido[2,3-d]pyrimidin-4(3H)-one (158).

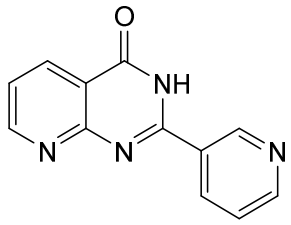

Molecular weight: 224.22 g/mol

The compound was synthesized according to the general procedure for compounds **156-158** from **155** (2.57 g, 10 mmol) to yield **158** as a white solid (1.28 g, 57%). **^{1}H NMR** (600 MHz, DMSO-d_6) δ 13.14 – 12.84 (m, 1H), 9.31 (d, J = 2.4 Hz, 1H), 8.97 (dd, J = 4.6, 2.0 Hz, 1H), 8.78 (dd, J = 4.8, 1.6 Hz, 1H), 8.60 – 8.48 (m, 2H), 7.60 (ddd, J = 8.0,

4.8, 0.9 Hz, 1H), 7.55 (dd, *J* = 7.8, 4.5 Hz, 1H). **^{13}C NMR** (151 MHz, DMSO) δ 156.26, 154.13, 152.41, 149.11, 135.85, 135.68, 128.68, 123.72, 122.69, 116.55.

General Procedure for the Preparation of compounds 159-161. The corresponding compound **156**-**158** (10 mmol) was added to phosphorous trichloride (30 mL, 0.32 mol) and stirred for 10 min at room temperature. The mixture was then refluxed for 4-8 h and the reaction monitored by TLC. After completion of the reaction, excess $POCl_3$ was removed under reduced pressure and 50 mL ice water added. Subsequently, 50 mL DCM was added while stirring and the pH of the mixture slowly adjusted to 7 with 25% ammonium solution. The organic phase was collected with a separatory funnel, washed with 50 mL brine and dried under $MgSO_4$. The solvent was removed under reduced pressure and the obtained solid recrystallized from isopropanol.

4-chloro-2-phenylpyrido[2,3-d]pyrimidine (159).

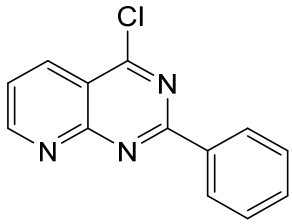

Molecular weight: 241.68 g/mol

The compound was synthesized according to the general procedure for compounds **159-161** from **156** (2.23 g, 10 mmol) to yield **7** as a white solid (2.30 g, 95%). **^{1}H NMR** (600 MHz, DMSO-d_6) δ 9.03 (dd, *J* = 5.1, 1.9 Hz, 1H), 8.77 (dd, *J* = 7.8, 1.9 Hz, 1H), 8.31 – 8.19 (m, 2H), 7.71 (dd, *J* = 7.8, 5.0 Hz, 1H), 7.69 – 7.64 (m, 1H), 7.60 (dd, *J* = 8.4, 7.0 Hz, 2H). **^{13}C NMR** (151 MHz, DMSO) δ 162.02, 157.87, 156.14, 152.61, 139.63, 132.89, 131.76, 128.99, 128.60, 122.63, 117.69.

4-chloro-2-(3-methoxyphenyl)pyrido[2,3-d]pyrimidine (160).

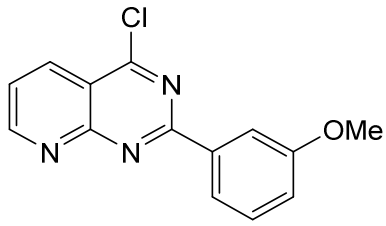

Molecular weight: 271.70 g/mol

The compound was synthesized according to the general procedure for compounds **159-161** from **157** (2.35 g, 10 mmol) to yield **160** as a white solid (2.28 g, 84%). **^{1}H NMR** (500 MHz, DMSO-d_6) δ 9.01 (dd, *J* = 4.9, 2.0 Hz, 1H), 8.70 (ddd, *J* = 7.9, 3.3, 1.9 Hz, 1H), 7.84 (ddd, *J* = 7.8, 1.7, 0.9 Hz, 1H), 7.79 (dd, *J* = 2.6, 1.7 Hz, 1H), 7.69 – 7.62 (m, 1H), 7.50 (t, *J* = 8.0 Hz, 1H), 7.22 (ddd, *J* = 8.3, 2.6, 0.9 Hz, 1H), 3.87 (s, 3H). **^{13}C NMR** (126 MHz, DMSO) δ 162.32, 159.55, 156.86, 153.74, 138.38, 133.26, 130.10, 122.56, 120.83, 118.91, 117.29, 113.14, 55.63.

4-chloro-2-(pyridin-3-yl)pyrido[2,3-d]pyrimidine (161).

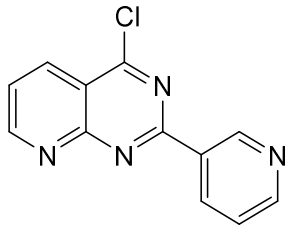

Molecular weight: 242.67 g/mol

The compound was synthesized according to the general procedure for compounds **159-161** from **158** (2.24 g, 10 mmol) to yield **161** as a white solid (2.14 g, 88%). **^{1}H NMR** (600 MHz, DMSO-d_6) δ 9.42 (d, *J* = 2.3 Hz, 1H), 9.02 (dd, *J* = 4.7, 2.0 Hz, 1H), 8.93 (dd, *J* = 5.2, 1.6 Hz, 1H), 8.80 (dt, *J* = 8.2, 1.9 Hz, 1H), 8.64 (dd, *J* = 7.9, 2.0 Hz, 1H), 7.88 (dd, *J* = 8.1, 5.1 Hz, 1H), 7.65 (dd, *J* = 7.9, 4.7 Hz, 1H). **^{13}C NMR** (151 MHz, DMSO) δ 162.47, 157.35, 154.96, 153.98, 149.22, 146.25, 139.64, 137.32, 129.77, 125.24, 123.10, 117.25.

General Procedure for the Preparation of compounds 162-197.

The corresponding 4-chloro derivative **159-161** (1 mmol) was added to isopropanol (5 mL) with the corresponding substituted aniline derivative (1 mmol) and sealed in a microwave tube. The mixture was heated by 100 watt microwave irradiation to 110 °C for a period of 2 – 10 min to completion of the reaction, indicated by TLC. The formed precipitate was filtered, washed with 10 mL isopropanol and dried in vacuo. If no precipitate is formed, the solvent was removed under reduced pressure and the remaining solid recrystallized from ethanol.

***N*,2-diphenylpyrido[2,3-d]pyrimidin-4-amine (162).**

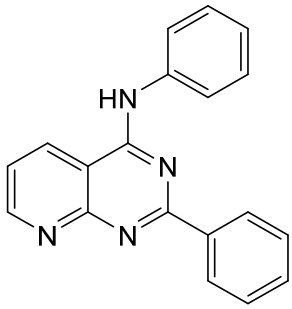

Molecular weight: 298.35 g/mol

The compound was synthesized according to the general procedure for compounds **162-197** from **159** (242 mg, 1 mmol) and aniline (93.1 mg, 1 mmol) to yield **162** as a bright yellow solid (283 mg, 95%), mp >300 °C. **^{1}H NMR** (600 MHz, DMSO-d_6) δ 10.98 (s, 1H), 9.36 (dd, J = 8.2, 1.7 Hz, 1H), 9.12 (dd, J = 4.6, 1.7 Hz, 1H), 8.43 – 8.35 (m, 2H), 7.98 – 7.88 (m, 2H), 7.77 (dd, J = 8.2, 4.6 Hz, 1H), 7.63 – 7.54 (m, 3H), 7.54 – 7.47 (m, 2H), 7.27 (tt, J = 7.4, 1.2 Hz, 1H). **^{13}C NMR** (151 MHz, DMSO) δ 162.33, 159.33, 155.81, 155.28, 138.19, 135.81, 135.53, 132.13, 128.79, 125.28, 123.26, 122.20, 109.65. **Anal. Calcd. for $C_{19}H_{14}N_4$**: C, 76.49; H, 4.73; N, 18.78. Found: C, 76.22; H, 4.94; N, 18.62.

***N*-(3-nitrophenyl)-2-phenylpyrido[2,3-d]pyrimidin-4-amine (163).**

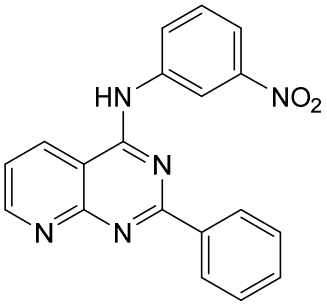

Molecular weight: 343.35 g/mol

The compound was synthesized according to the general procedure for compounds **162-197** from **159** (242 mg, 1 mmol) and 3-nitroaniline (138 mg, 1 mmol) to yield **163** as a bright yellow solid (278 mg, 81%), mp >300 °C. **^{1}H NMR** (500 MHz, DMSO-d_6) δ 11.21 (s, 1H), 9.48 (d, J = 8.3 Hz, 1H), 9.21 (t, J = 2.2 Hz, 1H), 9.16 (dd, J = 4.6, 1.8 Hz, 1H), 8.54 – 8.44 (m, 2H), 8.41 (ddd, J = 8.1, 2.2, 0.9 Hz, 1H), 8.06 (ddd, J = 8.3, 2.3, 0.9 Hz, 1H), 7.83 – 7.69 (m, 2H), 7.65 – 7.51 (m, 3H). **^{13}C NMR** (126 MHz, DMSO) δ 162.55, 159.03, 156.08, 154.74, 147.91, 136.04, 135.77, 131.70, 129.68, 128.59, 128.48, 128.14, 121.79, 118.67, 116.69, 109.60. **Anal. Calcd. for $C_{19}H_{13}N_5O_2$**: C, 66.47; H, 3.82; N, 20.40. Found: C, 66.74; H, 4.13; N, 20.39.

2-nitro-4-((2-phenylpyrido[2,3-d]pyrimidin-4-yl)amino)phenol (164).

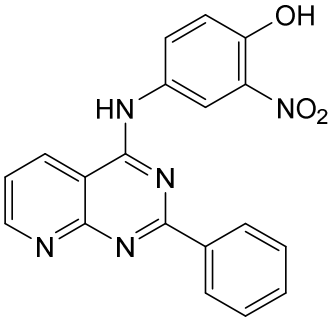

Molecular weight: 359.35 g/mol

The compound was synthesized according to the general procedure for compounds **162-197** from **159** (242 mg, 1 mmol) and 4-amino-2-nitrophenol (154 mg, 1 mmol) to yield **164** as a yellow solid (313 mg, 87%), mp >300 °C. **^{1}H NMR** (600 MHz, DMSO-d_6) δ 11.08 (s, 1H), 11.01 (s, 1H), 9.29 (dd, J = 8.3, 1.8 Hz, 1H), 9.12 (dd, J = 4.6, 1.7 Hz, 1H),

8.79 (d, *J* = 2.7 Hz, 1H), 8.49 – 8.40 (m, 2H), 8.04 (dd, *J* = 9.0, 2.7 Hz, 1H), 7.77 (dd, *J* = 8.2, 4.6 Hz, 1H), 7.64 – 7.59 (m, 1H), 7.56 (dd, *J* = 8.2, 6.5 Hz, 2H), 7.30 (d, *J* = 8.9 Hz, 1H). **^{13}C NMR** (151 MHz, DMSO) δ 162.39, 159.05, 155.26, 149.67, 135.90, 135.81, 135.39, 132.17, 130.36, 129.94, 128.89, 122.22, 119.46, 119.18, 109.61. **Anal. Calcd. for $C_{19}H_{13}N_5O_3$**: C, 63.51; H, 3.65; N, 19.49. Found: C, 63.38; H, 3.77; N, 19.26.

***N*-(4-nitrophenyl)-2-phenylpyrido[2,3-d]pyrimidin-4-amine (165).**

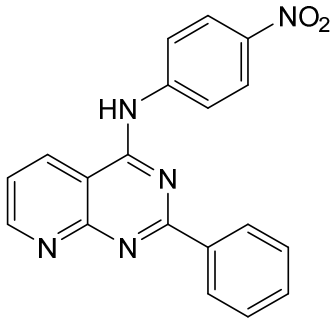

Molecular weight: 343.35 g/mol

The compound was synthesized according to the general procedure for compounds **162-197** from **159** (242 mg, 1 mmol) and 4-nitroaniline (138 mg, 1 mmol) to yield **165** as a yellow solid (313 mg, 87%), mp >300 °C. **^{1}H NMR** (600 MHz, DMSO-d_6) δ 10.76 (s, 1H), 9.17 (d, *J* = 6.4 Hz, 2H), 8.53 – 8.47 (m, 2H), 8.43 – 8.37 (m, 2H), 8.34 – 8.27 (m, 2H), 7.78 – 7.73 (m, 1H), 7.61 – 7.57 (m, 3H). **^{13}C NMR** (126 MHz, DMSO) δ 162.29, 158.83, 158.08, 155.95, 145.21, 142.62, 137.03, 133.90, 131.08, 128.45, 128.34, 124.32, 121.60, 121.37, 109.35. **Anal. Calcd. for $C_{19}H_{13}N_5O_2$**: C, 66.47; H, 3.82; N, 20.40. Found: C, 66.69; H, 4.12; N, 20.03.

3-((2-phenylpyrido[2,3-d]pyrimidin-4-yl)amino)benzonitrile (166).

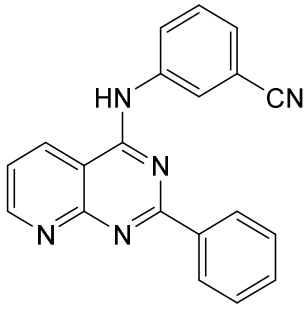

Molecular weight: 323.36 g/mol

The compound was synthesized according to the general procedure for compounds **162-197** from **159** (242 mg, 1 mmol) and 3-aminobenzonitrile (118 mg, 1 mmol) to yield **166** as a light yellow solid (304 mg, 94%), mp 299-300 °C (decomp.). **^{1}H NMR** (500 MHz, DMSO-d_6) δ 10.69 (s, 1H), 9.19 – 9.08 (m, 2H), 8.47 (t, J = 1.9 Hz, 1H), 8.45 – 8.36 (m, 2H), 8.25 (dt, J = 8.1, 1.9 Hz, 1H), 7.78 – 7.63 (m, 3H), 7.62 – 7.51 (m, 3H). **^{13}C NMR** (126 MHz, DMSO) δ 162.35, 159.20, 157.72, 156.01, 139.61, 136.93, 134.29, 131.66, 130.21, 128.78, 128.49, 127.83, 127.11, 125.62, 122.05, 118.73, 111.55, 109.39. **Anal. Calcd. for $C_{20}H_{13}N_5$**: C, 74.29; H, 4.05; N, 21.66. Found: C, 74.46; H, 4.16; N, 21.56.

4-((2-phenylpyrido[2,3-d]pyrimidin-4-yl)amino)benzonitrile (167).

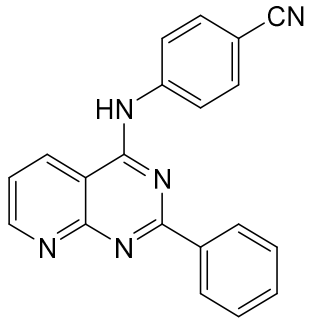

Molecular weight: 323.36 g/mol

The compound was synthesized according to the general procedure for compounds **162-197** from **159** (242 mg, 1 mmol) and 4-aminobenzonitrile (118 mg, 1 mmol) to yield **167** as a bright yellow solid (288 mg, 89%), mp >300 °C. **^{1}H NMR** (600 MHz, DMSO-d_6) δ 10.83 (s, 1H), 9.25 (d, J = 8.3 Hz, 1H), 9.17 (d, J = 4.4 Hz, 1H), 8.49 – 8.41 (m, 2H), 8.21 (d, J = 8.5 Hz, 2H), 7.99 – 7.91 (m, 2H), 7.78 (dd, J = 8.2, 4.5 Hz, 1H), 7.63 – 7.54 (m, 3H). **^{13}C NMR** (151 MHz, DMSO) δ 164.64, 162.57, 159.14, 143.18, 136.73, 133.18, 131.84, 128.94, 128.72, 122.41, 122.16, 119.16, 109.84, 106.02. **Anal. Calcd. for $C_{20}H_{13}N_5$**: C, 74.29; H, 4.05; N, 21.66. Found: C, 74.17; H, 4.21; N, 21.47.

***N*-(3-methoxyphenyl)-2-phenylpyrido[2,3-d]pyrimidin-4-amine (168).**

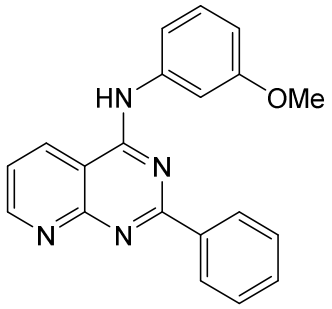

Molecular weight: 328.38 g/mol

The compound was synthesized according to the general procedure for compounds **162-197** from **159** (242 mg, 1 mmol) and 3-methoxyaniline (123 mg, 1 mmol) to yield **168** as a yellow solid (286 mg, 87%), mp 261-262 °C (decomp.). **^{1}H NMR** (600 MHz, DMSO-d_6) δ 10.80 (s, 1H), 9.31 (dd, J = 8.3, 1.8 Hz, 1H), 9.13 (dd, J = 4.6, 1.7 Hz, 1H), 8.47 – 8.39 (m, 2H), 7.77 (dd, J = 8.2, 4.6 Hz, 1H), 7.67 (s, 1H), 7.65 – 7.54 (m, 3H), 7.52 (ddd, J = 8.0, 1.9, 0.9 Hz, 1H), 7.40 (t, J = 8.1 Hz, 1H), 6.83 (dd, J = 8.2, 2.5 Hz, 1H), 3.82 (d, J = 0.7 Hz, 3H). **^{13}C NMR** (151 MHz, DMSO) δ 162.40, 159.58, 159.24, 155.31, 139.50, 136.04, 135.40, 132.13, 129.58, 128.87, 128.80, 122.19, 115.19, 111.07, 109.69, 108.48, 55.37. **Anal. Calcd. for $C_{20}H_{16}N_4O$**: C, 73.15; H, 4.91; N, 17.06. Found: C, 73.09; H, 5.11; N, 16.87.

***N*-(4-methoxyphenyl)-2-phenylpyrido[2,3-d]pyrimidin-4-amine (169).**

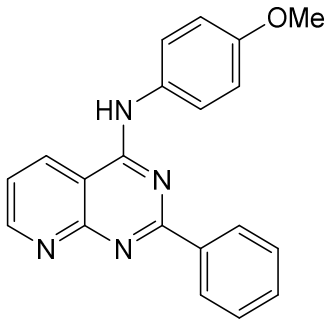

Molecular weight: 328.38 g/mol

The compound was synthesized according to the general procedure for compounds **162-197** from **159** (242 mg, 1 mmol) and 4-methoxyaniline (123 mg, 1 mmol) to yield **169** as an orange solid (246 mg, 75%), mp 300-302 °C (decomp.). **^{1}H NMR** (600 MHz, DMSO-

d_6) δ 10.88 (s, 1H), 9.25 (dd, *J* = 8.3, 1.8 Hz, 1H), 9.10 (dd, *J* = 4.6, 1.7 Hz, 1H), 8.45 – 8.31 (m, 2H), 7.86 – 7.78 (m, 2H), 7.75 (dd, *J* = 8.2, 4.6 Hz, 1H), 7.64 – 7.50 (m, 3H), 7.13 – 7.03 (m, 2H), 3.81 (s, 3H). **^{13}C NMR** (151 MHz, DMSO) δ 162.48, 159.51, 157.21, 155.72, 136.02, 135.35, 132.46, 131.28, 129.17, 125.18, 122.52, 114.34, 109.80, 55.82. **Anal. Calcd. for $C_{20}H_{16}N_4O$**: C, 73.15; H, 4.91; N, 17.06. Found: C, 73.09; H, 5.11; N, 16.87.

***N*-(3,4-dimethoxyphenyl)-2-phenylpyrido[2,3-d]pyrimidin-4-amine (170).**

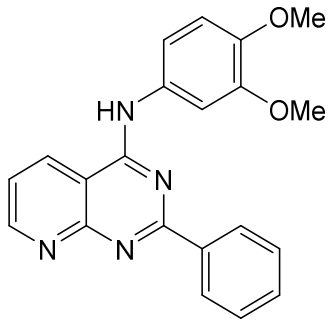

Molecular weight: 358.40 g/mol

The compound was synthesized according to the general procedure for compounds **162-197** from **159** (242 mg, 1 mmol) and 3,4-dimethoxyaniline (153 mg, 1 mmol) to yield **170** as a red solid (262 mg, 73%), mp 275-276 °C (decomp.). **^{1}H NMR** (500 MHz, DMSO-d_6) δ 10.78 (s, 1H), 9.33 – 9.17 (m, 1H), 9.16 – 9.01 (m, 1H), 8.50 – 8.32 (m, 2H), 7.75 (dd, *J* = 8.2, 4.5 Hz, 1H), 7.68 (d, *J* = 2.5 Hz, 1H), 7.65 – 7.49 (m, 3H), 7.43 (dd, *J* = 8.7, 2.5 Hz, 1H), 7.08 (d, *J* = 8.7 Hz, 1H), 3.82 (s, 3H), 3.81 (s, 3H). **^{13}C NMR** (126 MHz, DMSO) δ 162.18, 158.98, 155.36, 148.51, 146.51, 135.82, 135.66, 134.96, 132.15, 131.41, 128.82, 122.18, 115.20, 111.84, 109.52, 108.04, 55.90, 55.71. **Anal. Calcd. for $C_{21}H_{18}N_4O_2$**: C, 70.38; H, 5.06; N, 15.63. Found: C, 70.34; H, 5.17; N, 15.37.

***N*-(3-(methylthio)phenyl)-2-phenylpyrido[2,3-d]pyrimidin-4-amine (171).**

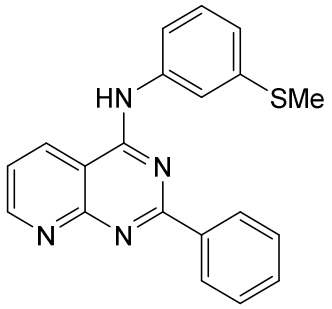

Molecular weight: 344.44 g/mol

The compound was synthesized according to the general procedure for compounds **162-197** from **159** (242 mg, 1 mmol) and 3-(methylthio)aniline (139 mg, 1 mmol) to yield **171** as a yellow solid (317 mg, 92%), mp 275-276 °C (decomp.). **^{1}H NMR** (600 MHz, DMSO-d_6) δ 10.93 (s, 1H), 9.36 (dd, *J* = 8.3, 1.7 Hz, 1H), 9.21 – 9.06 (m, 1H), 8.50 – 8.33 (m, 2H), 7.96 (s, 1H), 7.77 (dd, *J* = 8.2, 4.6 Hz, 1H), 7.76 – 7.68 (m, 1H), 7.65 – 7.51 (m, 3H), 7.43 (t, *J* = 7.9 Hz, 1H), 7.18 – 7.08 (m, 1H), 2.53 (s, 3H). **^{13}C NMR** (151 MHz, DMSO) δ 162.37, 159.25, 155.92, 155.23, 138.89, 138.69, 135.95, 135.62, 132.17, 129.27, 128.82, 122.55, 122.20, 120.21, 119.48, 109.73, 14.92. **Anal. Calcd. for $C_{20}H_{16}N_4S$**: C, 69.74; H, 4.68; N, 16.27. Found: C, 70.02; H, 4.81; N, 16.10.

3-((2-phenylpyrido[2,3-d]pyrimidin-4-yl)amino)phenol (172).

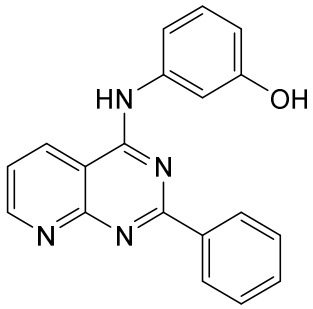

Molecular weight: 314.35 g/mol

The compound was synthesized according to the general procedure for compounds **162-197** from **159** (242 mg, 1 mmol) and 3-aminophenol (109 mg, 1 mmol) to yield **172** as an orange solid (207 mg, 66%), mp 248-249 °C. **^{1}H NMR** (600 MHz, DMSO-d_6) δ 10.84 (s, 1H), 9.68 (s, 1H), 9.35 (dd, *J* = 8.2, 1.7 Hz, 1H), 9.11 (dd, *J* = 4.6, 1.7 Hz, 1H), 8.51 –

8.34 (m, 2H), 7.76 (dd, *J* = 8.2, 4.6 Hz, 1H), 7.65 – 7.50 (m, 3H), 7.42 (t, *J* = 2.2 Hz, 1H), 7.37 (dd, *J* = 7.9, 1.9 Hz, 1H), 7.27 (t, *J* = 8.0 Hz, 1H), 6.68 (dd, *J* = 8.1, 2.3 Hz, 1H). **^{13}C NMR** (151 MHz, DMSO) δ 162.34, 159.25, 157.76, 155.62, 155.16, 139.11, 135.73, 135.62, 132.17, 129.39, 128.95, 128.85, 122.17, 113.92, 112.50, 110.31, 109.69. **Anal. Calcd. for $C_{19}H_{14}N_4O$**: C, 72.60; H, 4.49; N, 17.82. Found: C, 72.70; H, 4.20; N, 17.46.

4-((2-phenylpyrido[2,3-d]pyrimidin-4-yl)amino)phenol (173).

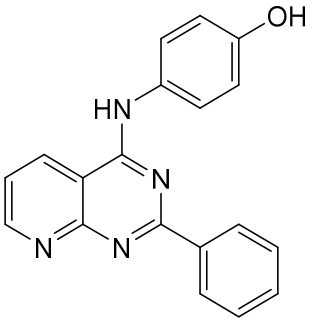

Molecular weight: 314.35 g/mol

The compound was synthesized according to the general procedure for compounds **162-197** from **159** (242 mg, 1 mmol) and 4-aminophenol (109 mg, 1 mmol) to yield **173** as a yellow-orange solid (245 mg, 78%), mp >300 °C. **^{1}H NMR** (600 MHz, DMSO-d_6) δ 11.71 (s, 1H), 9.56 (dd, *J* = 8.3, 1.7 Hz, 1H), 9.12 (dd, *J* = 4.8, 1.6 Hz, 1H), 8.31 (dd, *J* = 8.1, 1.3 Hz, 2H), 7.85 (dd, *J* = 8.2, 4.8 Hz, 1H), 7.70 – 7.62 (m, 3H), 7.60 (dd, *J* = 8.3, 7.0 Hz, 2H), 6.92 (d, *J* = 8.8 Hz, 2H). **^{13}C NMR** (151 MHz, DMSO) δ 161.63, 158.99, 155.99, 154.66, 152.29, 136.88, 133.35, 133.18, 129.27, 129.05, 128.47, 125.62, 122.89, 115.34, 109.81. **Anal. Calcd. for $C_{19}H_{14}N_4O$**: C, 72.60; H, 4.49; N, 17.82. Found: C, 72.51; H, 4.71; N, 17.63.

***N*-(3-((2-phenylpyrido[2,3-d]pyrimidin-4-yl)amino)phenyl)acetamide (174).**

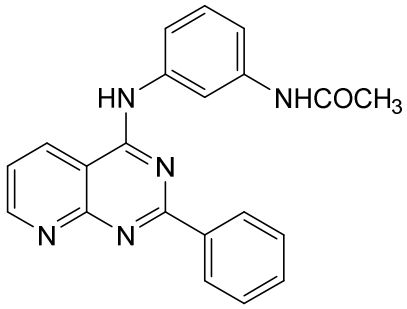

Molecular weight: 355.40 g/mol

The compound was synthesized according to the general procedure for compounds **162-197** from **159** (242 mg, 1 mmol) and *N*-(3-aminophenyl)acetamide (150 mg, 1 mmol) to yield **174** as a yellow solid (316 mg, 89%), mp >300 °C. **^{1}H NMR** (600 MHz, DMSO-d_6) δ 10.95 (s, 1H), 10.16 (s, 1H), 9.35 (dd, J = 8.2, 1.8 Hz, 1H), 9.11 (dd, J = 4.6, 1.7 Hz, 1H), 8.52 – 8.39 (m, 2H), 8.34 (t, J = 2.1 Hz, 1H), 7.76 (dd, J = 8.2, 4.6 Hz, 1H), 7.68 – 7.57 (m, 2H), 7.55 (dd, J = 8.3, 6.6 Hz, 2H), 7.40 (t, J = 8.0 Hz, 1H), 7.37 – 7.29 (m, 1H), 2.09 (s, 3H). **^{13}C NMR** (151 MHz, DMSO) δ 168.57, 162.41, 159.35, 155.68, 155.16, 139.83, 138.39, 135.70, 135.67, 132.13, 129.08, 128.80, 128.77, 122.16, 118.16, 116.08, 114.14, 109.68, 24.19. **Anal. Calcd. for $C_{21}H_{17}N_5O$**: C, 70.97; H, 4.82; N, 19.71. Found: C, 70.85; H, 4.91; N, 19.41.

2-phenyl-*N*-(3-(trifluoromethyl)phenyl)pyrido[2,3-d]pyrimidin-4-amine (175).

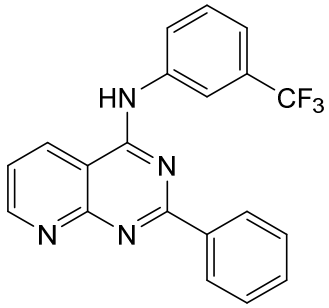

Molecular weight: 366.35 g/mol

The compound was synthesized according to the general procedure for compounds **162-197** from **159** (242 mg, 1 mmol) and 3-(trifluoromethyl)aniline (161 mg, 1 mmol) to yield **175** as a bright yellow solid (333 mg, 91%), mp >300 °C. **^{1}H NMR** (500 MHz, DMSO-

d_6) δ 10.92 (s, 1H), 9.35 (ddd, *J* = 8.3, 1.8, 0.8 Hz, 1H), 9.13 (dd, *J* = 4.6, 1.8 Hz, 1H), 8.59 (d, *J* = 2.0 Hz, 1H), 8.49 – 8.37 (m, 2H), 8.28 – 8.15 (m, 1H), 7.78 – 7.68 (m, 2H), 7.63 – 7.47 (m, 4H). **^{13}C NMR** (126 MHz, DMSO) δ 162.31, 159.05, 156.71, 155.13, 139.30, 136.39, 134.88, 131.46, 129.28 (d, *J* = 31.6 Hz), 128.35, 125.83, 124.06 (d, *J* = 272.4 Hz), 121.65, 120.49 (d, *J* = 3.8 Hz), 118.90 (d, *J* = 4.0 Hz), 109.35. **Anal. Calcd. for $C_{20}H_{13}F_3N_4$**: C, 65.57; H, 3.58; N, 15.29. Found: C, 65.66; H, 3.80; N, 15.20.

***N*-(3-fluorophenyl)-2-phenylpyrido[2,3-d]pyrimidin-4-amine (176).**

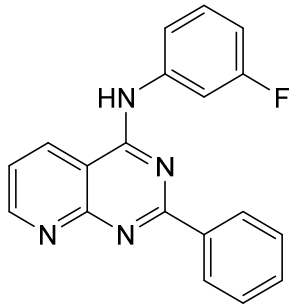

Molecular weight: 316.34 g/mol

The compound was synthesized according to the general procedure for compounds **162-197** from **159** (242 mg, 1 mmol) and 3-fluoroaniline (111 mg, 1 mmol) to yield **176** as a bright yellow solid (269 mg, 85%), mp >300 °C. **^{1}H NMR** (500 MHz, DMSO-d_6) δ 10.92 (s, 1H), 9.34 (dd, *J* = 8.3, 1.8 Hz, 1H), 9.14 (dd, *J* = 4.6, 1.7 Hz, 1H), 8.48 – 8.33 (m, 2H), 7.95 (dt, *J* = 11.5, 2.3 Hz, 1H), 7.82 – 7.72 (m, 2H), 7.64 – 7.49 (m, 4H), 7.08 (tdd, *J* = 8.5, 2.7, 0.9 Hz, 1H). **^{13}C NMR** (126 MHz, DMSO) δ 162.08 (d, *J* = 241.8 Hz), 161.12, 159.25, 156.34, 155.32, 140.20 (d, *J* = 10.9 Hz), 136.27, 135.55, 132.04, 130.38 (d, *J* = 9.4 Hz), 128.81 (d, *J* = 23.9 Hz), 122.17, 118.62, 111.42 (d, *J* = 21.0 Hz), 109.71 (d, *J* = 25.9 Hz). **Anal. Calcd. for $C_{19}H_{13}FN_4$**: C, 72.14; H, 4.14; N, 17.71. Found: C, 72.41; H, 4.28; N, 17.53.

***N*-(3-chlorophenyl)-2-phenylpyrido[2,3-d]pyrimidin-4-amine (177).**

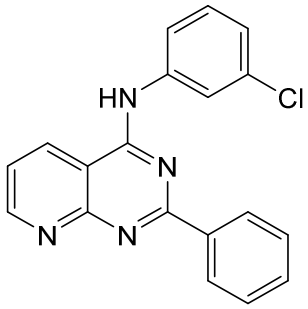

Molecular weight: 332.79 g/mol

The compound was synthesized according to the general procedure for compounds **162-197** from **159** (242 mg, 1 mmol) and 3-chloroaniline (128 mg, 1 mmol) to yield **177** as a bright yellow solid (280 mg, 84%), mp >300 °C. **^{1}H NMR** (600 MHz, DMSO-d_6) δ 10.79 (s, 1H), 9.25 (dd, *J* = 8.3, 1.7 Hz, 1H), 9.19 – 9.09 (m, 1H), 8.48 – 8.38 (m, 2H), 8.19 (t, *J* = 2.1 Hz, 1H), 7.90 (dd, *J* = 8.2, 2.0 Hz, 1H), 7.77 (dd, *J* = 8.2, 4.5 Hz, 1H), 7.65 – 7.55 (m, 3H), 7.53 (t, *J* = 8.1 Hz, 1H), 7.30 (dd, *J* = 7.9, 2.0 Hz, 1H). **^{13}C NMR** (151 MHz, DMSO) δ 162.78, 159.55, 155.87, 140.35, 136.78, 135.45, 133.33, 132.31, 130.79, 129.22, 129.01, 124.78, 122.77, 122.49, 121.45, 109.98. **Anal. Calcd. for $C_{19}H_{13}ClN_4$**: C, 68.57; H, 3.94; N, 16.84. Found: C, 68.52; H, 4.03; N, 16.66.

2-(3-methoxyphenyl)-*N*-(3-nitrophenyl)pyrido[2,3-d]pyrimidin-4-amine (178).

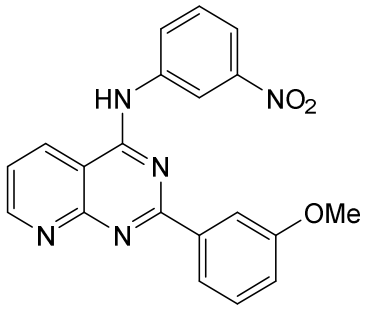

Molecular weight: 373.37 g/mol

The compound was synthesized according to the general procedure for compounds **162-197** from **160** (272 mg, 1 mmol) and 3-nitroaniline (138 mg, 1 mmol) to yield **178** as a light yellow solid (310 mg, 83%), mp >300 °C. **^{1}H NMR** (500 MHz, DMSO-d_6) δ 11.14 (s, 1H), 9.36 (d, *J* = 8.1 Hz, 1H), 9.18 (d, *J* = 4.6 Hz, 1H), 9.11 (t, *J* = 2.3 Hz, 1H), 8.38

(d, *J* = 7.7 Hz, 1H), 8.09 (t, *J* = 7.4 Hz, 2H), 8.00 (t, *J* = 2.0 Hz, 1H), 7.88 – 7.73 (m, 2H), 7.49 (t, *J* = 8.0 Hz, 1H), 7.18 (dd, *J* = 8.3, 2.6 Hz, 1H), 3.84 (s, 3H). **^{13}C NMR** (126 MHz, DMSO) δ 162.37, 159.69, 159.19, 155.33, 148.00, 139.77, 137.66, 135.77, 130.11, 130.00, 128.60, 122.30, 121.31, 119.16, 118.38, 116.91, 113.31, 109.87, 55.33. **Anal. Calcd. for $C_{20}H_{15}N_5O_3$**: C, 64.34; H, 4.05; N, 18.76. Found: C, 64.26; H, 4.31; N, 18.52.

4-((2-(3-methoxyphenyl)pyrido[2,3-d]pyrimidin-4-yl)amino)-2-nitrophenol (179).

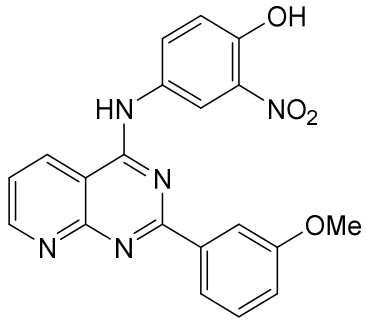

Molecular weight: 389.37 g/mol

The compound was synthesized according to the general procedure for compounds **162-197** from **160** (272 mg, 1 mmol) and 4-amino-2-nitrophenol (154 mg, 1 mmol) to yield **179** as a light orange solid (296 mg, 76%), mp 295-297 °C (decomp.). **^{1}H NMR** (600 MHz, DMSO-d_6) δ 11.08 (s, 1H), 11.01 (s, 1H), 9.27 (d, *J* = 8.2 Hz, 1H), 9.12 (d, *J* = 4.5 Hz, 1H), 8.67 (dd, *J* = 2.8, 1.5 Hz, 1H), 8.14 – 7.99 (m, 2H), 7.99 – 7.87 (m, 1H), 7.76 (dd, *J* = 8.3, 4.7 Hz, 1H), 7.46 (t, *J* = 8.0 Hz, 1H), 7.29 (d, *J* = 8.9 Hz, 1H), 7.23 – 7.07 (m, 1H), 3.83 (s, 3H). **^{13}C NMR** (151 MHz, DMSO) δ 162.05, 159.60, 159.05, 155.33, 149.68, 137.29, 135.84, 135.26, 130.53, 129.91, 129.85, 122.23, 121.32, 119.35, 119.20, 118.42, 113.29, 109.57, 55.30. **Anal. Calcd. for $C_{20}H_{15}N_5O_4$**: C, 61.69; H, 3.88; N, 17.99. Found: C, 61.83; H, 4.04; N, 17.72.

3-((2-(3-methoxyphenyl)pyrido[2,3-d]pyrimidin-4-yl)amino)benzonitrile (180).

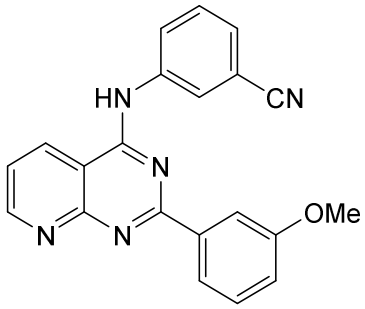

Molecular weight: 353.39 g/mol

The compound was synthesized according to the general procedure for compounds **162-197** from **160** (272 mg, 1 mmol) and 3-aminobenzonitrile (118 mg, 1 mmol) to yield **180** as a yellow solid (286 mg, 81%), mp >300 °C. **^{1}H NMR** (500 MHz, DMSO-d_6) δ 10.99 (s, 1H), 9.28 (d, *J* = 8.2 Hz, 1H), 9.17 (s, 1H), 8.50 (s, 1H), 8.22 (d, *J* = 7.1 Hz, 1H), 8.03 (d, *J* = 7.8 Hz, 1H), 7.97 (s, 1H), 7.81 (s, 1H), 7.71 (d, *J* = 6.6 Hz, 2H), 7.48 (t, *J* = 8.1 Hz, 1H), 7.17 (d, *J* = 8.4 Hz, 1H), 3.87 (s, 3H). **^{13}C NMR** (126 MHz, DMSO) δ 162.23, 159.63, 137.70, 130.22, 129.96, 127.51, 125.89, 122.28, 121.11, 118.73, 118.55, 112.95, 111.57, 55.34. **Anal. Calcd. for $C_{21}H_{15}N_5O$**: C, 71.38; H, 4.28; N, 19.82. Found: C, 71.65; H, 4.60; N, 19.57.

4-((2-(3-methoxyphenyl)pyrido[2,3-d]pyrimidin-4-yl)amino)benzonitrile (181).

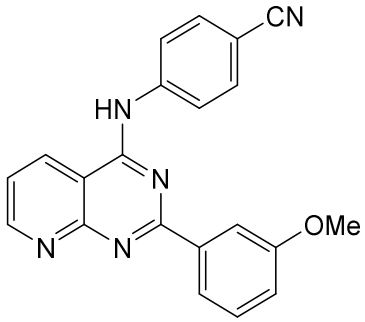

Molecular weight: 353.39 g/mol

The compound was synthesized according to the general procedure for compounds **162-197** from **160** (272 mg, 1 mmol) and 4-aminobenzonitrile (118 mg, 1 mmol) to yield **181** as a yellow solid (304 mg, 86%), mp >300 °C. **^{1}H NMR** (500 MHz, DMSO-d_6) δ 11.35 (s, 1H), 9.52 (dd, *J* = 8.3, 1.8 Hz, 1H), 9.18 (dd, *J* = 4.7, 1.7 Hz, 1H), 8.29 – 8.16 (m, 2H),

8.02 (dt, *J* = 7.8, 1.3 Hz, 1H), 8.00 – 7.89 (m, 3H), 7.85 (dd, *J* = 8.3, 4.7 Hz, 1H), 7.50 (t, *J* = 8.0 Hz, 1H), 7.19 (ddd, *J* = 8.3, 2.8, 0.9 Hz, 1H), 3.87 (s, 3H). **^{13}C NMR** (126 MHz, DMSO) δ 162.51, 159.64, 159.10, 155.55, 154.73, 142.76, 137.20, 136.99, 133.05, 130.13, 122.95, 122.36, 121.34, 119.06, 118.64, 113.33, 110.26, 106.60, 55.38. **Anal. Calcd. for $C_{21}H_{15}N_5O$**: C, 71.38; H, 4.28; N, 19.82. Found: C, 71.29; H, 4.58; N, 19.59.

3-((2-(3-methoxyphenyl)pyrido[2,3-d]pyrimidin-4-yl)amino)phenol (182).

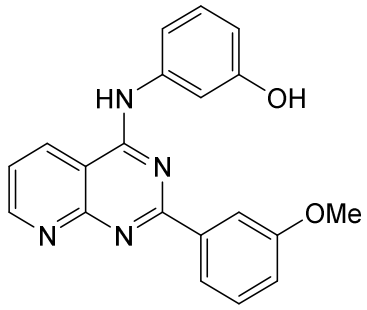

Molecular weight: 344.37 g/mol

The compound was synthesized according to the general procedure for compounds **162-197** from **160** (272 mg, 1 mmol) and 3-aminophenol (109 mg, 1 mmol) to yield **182** as a yellow-orange solid (276 mg, 80%), mp 250-251 °C. **^{1}H NMR** (500 MHz, DMSO-d_6) δ 10.79 (s, 1H), 9.63 (s, 1H), 9.30 (dd, *J* = 8.3, 1.8 Hz, 1H), 9.11 (dd, *J* = 4.6, 1.7 Hz, 1H), 8.10 – 7.93 (m, 2H), 7.76 (dd, *J* = 8.2, 4.6 Hz, 1H), 7.47 (t, *J* = 7.9 Hz, 1H), 7.43 (t, *J* = 2.2 Hz, 1H), 7.35 (ddd, *J* = 8.1, 2.1, 1.0 Hz, 1H), 7.26 (t, *J* = 8.0 Hz, 1H), 7.16 (ddd, *J* = 8.2, 2.7, 0.9 Hz, 1H), 6.68 (ddd, *J* = 8.0, 2.4, 0.9 Hz, 1H), 3.85 (s, 3H). **^{13}C NMR** (126 MHz, DMSO) δ 161.93, 159.57, 159.15, 157.75, 155.76, 155.27, 139.13, 137.18, 135.38, 129.94, 129.31, 122.18, 121.27, 118.56, 113.91, 113.32, 112.44, 110.37, 109.66, 55.30. **Anal. Calcd. for $C_{20}H_{16}N_4O_2$**: C, 69.76; H, 4.68; N, 16.27. Found: C, 69.95; H, 5.00; N, 16.35.

4-((2-(3-methoxyphenyl)pyrido[2,3-d]pyrimidin-4-yl)amino)phenol (183).

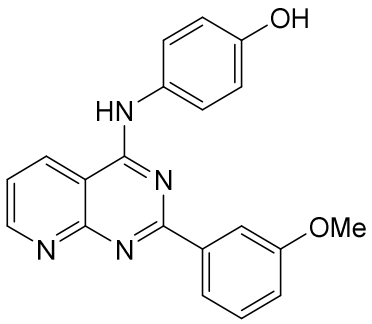

Molecular weight: 344.37 g/mol

The compound was synthesized according to the general procedure for compounds **162-197** from **160** (272 mg, 1 mmol) and 4-aminophenol (109 mg, 1 mmol) to yield **183** as an orange solid (265 mg, 77%), mp 270-272 °C (decomp.). **^{1}H NMR** (500 MHz, DMSO-d_6) δ 10.57 (s, 1H), 9.11 (dd, J = 8.3, 1.8 Hz, 1H), 9.06 (dd, J = 4.5, 1.8 Hz, 1H), 8.01 – 7.92 (m, 2H), 7.68 (dd, J = 8.2, 4.5 Hz, 1H), 7.67 – 7.60 (m, 2H), 7.45 (t, J = 7.9 Hz, 1H), 7.13 (ddd, J = 8.2, 2.7, 1.0 Hz, 1H), 6.93 – 6.84 (m, 2H), 3.84 (s, 3H). **^{13}C NMR** (126 MHz, DMSO) δ 161.77, 159.49, 159.11, 156.65, 155.66, 155.04, 137.75, 134.13, 129.83, 129.56, 125.00, 121.94, 121.04, 117.94, 115.16, 113.37, 109.27, 55.27. **Anal. Calcd. for $C_{20}H_{16}N_4O_2$**: C, 69.76; H, 4.68; N, 16.27. Found: C, 69.69; H, 4.93; N, 16.17.

***N*-(3,4-dimethoxyphenyl)-2-(3-methoxyphenyl)pyrido[2,3-d]pyrimidin-4-amine (184).**

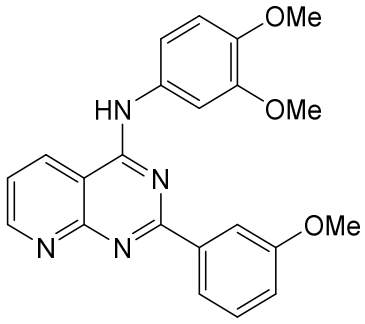

Molecular weight: 388.43 g/mol

The compound was synthesized according to the general procedure for compounds **162-197** from **160** (272 mg, 1 mmol) and 3,4-dimethoxyaniline (153 mg, 1 mmol) to yield **184** as an orange solid (346 mg, 89%), mp 251-252 °C. **^{1}H NMR** (600 MHz, DMSO-d_6)

δ 10.88 (s, 1H), 9.28 (dd, *J* = 8.3, 1.8 Hz, 1H), 9.09 (dd, *J* = 4.6, 1.7 Hz, 1H), 8.01 (dt, *J* = 7.8, 1.2 Hz, 1H), 7.97 (dd, *J* = 2.7, 1.5 Hz, 1H), 7.75 (dd, *J* = 8.2, 4.6 Hz, 1H), 7.65 (d, *J* = 2.4 Hz, 1H), 7.48 (t, *J* = 8.0 Hz, 1H), 7.43 (dd, *J* = 8.6, 2.4 Hz, 1H), 7.17 (ddd, *J* = 8.2, 2.7, 1.0 Hz, 1H), 7.06 (d, *J* = 8.7 Hz, 1H), 3.84 (s, 3H), 3.81 (s, 3H), 3.80 (s, 3H). **^{13}C NMR** (151 MHz, DMSO) δ 161.78, 159.59, 158.94, 155.59, 155.36, 148.50, 146.56, 137.11, 135.04, 131.35, 129.93, 122.22, 121.19, 118.04, 115.39, 113.82, 111.77, 109.54, 108.22, 55.92, 55.75, 55.41. **Anal. Calcd. for $C_{22}H_{20}N_4O_3$**: C, 68.03; H, 5.19; N, 14.42. Found: C, 68.26; H, 5.34; N, 14.08.

2-(3-methoxyphenyl)-*N*-(3-(methylthio)phenyl)pyrido[2,3-d]pyrimidin-4-amine (185).

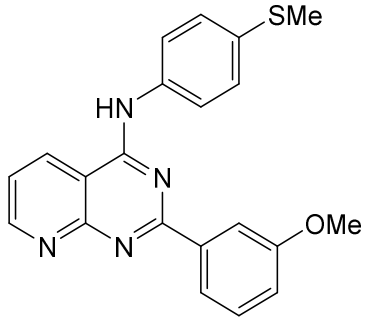

Molecular weight: 374.46 g/mol

The compound was synthesized according to the general procedure for compounds **162-197** from **160** (272 mg, 1 mmol) and 3-(methylthio)aniline (139 mg, 1 mmol) to yield **185** as a red solid (345 mg, 92%), mp 275-276 °C (decomp.). **^{1}H NMR** (600 MHz, DMSO-d_6) δ 11.07 (s, 1H), 9.37 (dd, *J* = 8.2, 1.7 Hz, 1H), 9.10 (dd, *J* = 4.6, 1.7 Hz, 1H), 7.98 (ddd, *J* = 7.7, 1.6, 1.0 Hz, 1H), 7.95 (dd, *J* = 2.7, 1.6 Hz, 1H), 7.92 – 7.86 (m, 2H), 7.76 (dd, *J* = 8.2, 4.6 Hz, 1H), 7.47 (t, *J* = 7.9 Hz, 1H), 7.43 – 7.35 (m, 2H), 7.16 (ddd, *J* = 8.2, 2.7, 1.0 Hz, 1H), 3.84 (s, 3H), 2.52 (s, 3H). **^{13}C NMR** (151 MHz, DMSO) δ 161.87, 159.53, 159.01, 155.53, 155.19, 137.00, 135.55, 135.35, 134.61, 129.98, 126.45, 123.83, 122.22, 121.24, 118.45, 113.37, 109.69, 55.32, 15.32. **Anal. Calcd. for $C_{21}H_{18}N_4OS$**: C, 67.36; H, 4.85; N, 14.96. Found: C, 67.27; H, 4.96; N, 14.60.

***N*-(3-((2-(3-methoxyphenyl)pyrido[2,3-d]pyrimidin-4-yl)amino)phenyl)acetamide (186).**

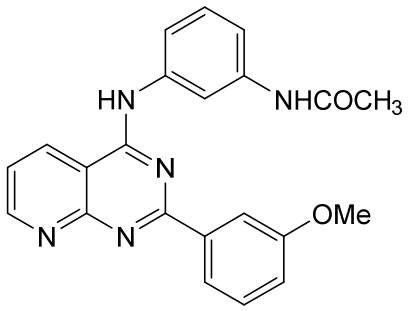

Molecular weight: 385.43 g/mol

The compound was synthesized according to the general procedure for compounds **162-197** from **160** (272 mg, 1 mmol) and N-(3-aminophenyl)acetamide (150 mg, 1 mmol) to yield **186** as a yellow (304 mg, 79%), mp 278-280 °C (decomp.). **^{1}H NMR** (600 MHz, DMSO-d_6) δ 11.46 (s, 1H), 10.22 (s, 1H), 9.51 (dd, *J* = 8.2, 1.7 Hz, 1H), 9.15 (dd, *J* = 4.8, 1.6 Hz, 1H), 8.28 (d, *J* = 2.2 Hz, 1H), 8.02 (dt, *J* = 7.8, 1.2 Hz, 1H), 7.94 (dd, *J* = 2.7, 1.6 Hz, 1H), 7.86 (dd, *J* = 8.2, 4.8 Hz, 1H), 7.58 (dq, *J* = 7.8, 3.4, 2.3 Hz, 1H), 7.48 (t, *J* = 8.0 Hz, 1H), 7.44 – 7.34 (m, 2H), 7.20 (ddd, *J* = 8.2, 2.7, 1.0 Hz, 1H), 3.83 (s, 3H), 2.08 (s, 3H). **^{13}C NMR** (151 MHz, DMSO) δ 168.64, 161.92, 159.56, 159.33, 154.53, 153.55, 139.86, 137.77, 137.11, 135.63, 130.08, 128.77, 122.65, 121.75, 119.31, 118.70, 116.67, 114.62, 113.65, 110.01, 55.32, 24.14. **Anal. Calcd. for $C_{22}H_{19}N_5O_2$**: C, 68.56; H, 4.97; N, 18.17. Found: C, 68.66; H, 5.30; N, 17.97.

***N*-(3-fluorophenyl)-2-(3-methoxyphenyl)pyrido[2,3-d]pyrimidin-4-amine (187).**

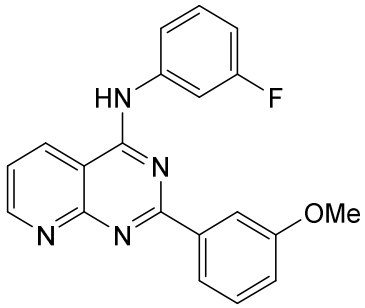

Molecular weight: 346.37 g/mol

The compound was synthesized according to the general procedure for compounds **162-197** from **160** (272 mg, 1 mmol) and 3-fluoroaniline (111 mg, 1 mmol) to yield **187** as a yellow solid (312 mg, 90%), mp 282-284 °C (decomp.). **^{1}H NMR** (500 MHz, DMSO-d_6) δ 11.43 (s, 1H), 9.58 (dd, *J* = 8.2, 1.7 Hz, 1H), 9.16 (dd, *J* = 4.8, 1.7 Hz, 1H), 8.06 – 7.92 (m, 3H), 7.85 (dd, *J* = 8.2, 4.8 Hz, 1H), 7.78 (ddd, *J* = 8.2, 2.0, 0.9 Hz, 1H), 7.59 – 7.45 (m, 2H), 7.19 (ddd, *J* = 8.2, 2.7, 0.9 Hz, 1H), 7.11 (tdd, *J* = 8.5, 2.7, 0.9 Hz, 1H), 3.85 (s, 3H). **^{13}C NMR** (126 MHz, DMSO) δ 162.96, 162.30, 161.04, 159.62, 159.17, 154.60, 154.49, 139.77 (d, *J* = 11.0 Hz), 137.14, 136.61, 130.32 (d, *J* = 9.4 Hz), 130.11, 122.44, 121.31, 119.08 (d, *J* = 2.5 Hz), 118.95, 113.39, 111.93 (d, *J* = 20.9 Hz), 110.22 (d, *J* = 25.4 Hz), 110.10, 55.30. **Anal. Calcd. for $C_{20}H_{15}FN_4O$**: C, 69.35; H, 4.37; N, 16.18. Found: C, 69.60; H, 4.63; N, 15.82.

***N*-(4-fluorophenyl)-2-(3-methoxyphenyl)pyrido[2,3-d]pyrimidin-4-amine (188).**

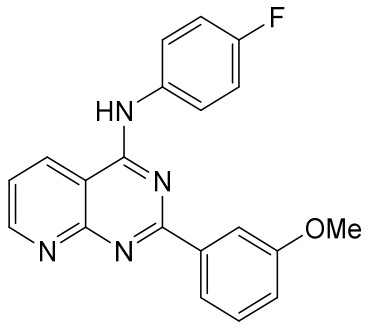

Molecular weight: 346.37 g/mol

The compound was synthesized according to the general procedure for compounds **162-197** from **160** (272 mg, 1 mmol) and 4-fluoroaniline (111 mg, 1 mmol) to yield **188** as a yellow (291 mg, 84%), mp 283-284 °C (decomp.). **^{1}H NMR** (500 MHz, DMSO-d_6) δ 11.43 (s, 1H), 9.48 (dd, *J* = 8.1, 1.7 Hz, 1H), 9.15 (dd, *J* = 4.7, 1.7 Hz, 1H), 8.00 – 7.88 (m, 4H), 7.84 (dd, *J* = 8.2, 4.7 Hz, 1H), 7.49 (t, *J* = 8.0 Hz, 1H), 7.41 – 7.29 (m, 2H), 7.19 (ddd, *J* = 8.4, 2.6, 1.0 Hz, 1H), 3.84 (s, 3H). **^{13}C NMR** (126 MHz, DMSO) δ 161.90, 159.56 (d, *J* = 243.0 Hz), 159.57, 159.33, 154.85, 154.25, 136.54, 136.11, 134.08 (d, *J* = 2.3 Hz), 130.10, 125.79 (d, *J* = 8.2 Hz), 122.55, 121.42, 118.95, 115.49 (d, *J* = 22.6 Hz), 113.52, 109.81, 55.39. **Anal. Calcd. for $C_{20}H_{15}FN_4O$**: C, 69.35; H, 4.37; N, 16.18. Found: C, 69.67; H, 4.67; N, 15.83.

***N*-(3,4-difluorophenyl)-2-(3-methoxyphenyl)pyrido[2,3-d]pyrimidin-4-amine (189).**

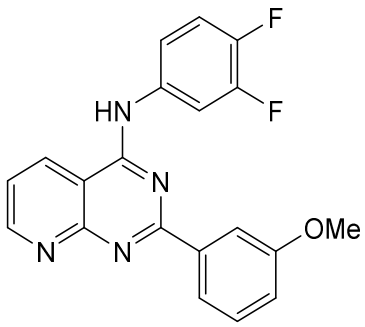

Molecular weight: 364.36 g/mol

The compound was synthesized according to the general procedure for compounds **162-197** from **160** (272 mg, 1 mmol) and 3,4-difluoroaniline (129 mg, 1 mmol) to yield **189** as a yellow solid (317 mg, 87%), mp 283-285 °C (decomp.). **^{1}H NMR** (600 MHz, DMSO-d_6) δ 10.98 (s, 1H), 9.29 (d, *J* = 8.2 Hz, 1H), 9.15 (d, *J* = 4.6 Hz, 1H), 8.17 (dd, *J* = 13.1, 7.5 Hz, 1H), 8.01 (d, *J* = 7.8 Hz, 1H), 7.97 (s, 1H), 7.80 (dd, *J* = 8.2, 4.6 Hz, 1H), 7.71 (d, *J* = 8.9 Hz, 1H), 7.57 (q, *J* = 9.6 Hz, 1H), 7.49 (t, *J* = 8.0 Hz, 1H), 7.17 (d, *J* = 8.2 Hz, 1H), 3.86 (s, 3H). **^{13}C NMR** (151 MHz, DMSO) δ 162.22, 159.63, 159.16, 155.33, 137.42, 135.61, 135.60, 130.06, 122.32, 121.16, 119.66 (d, *J* = 2.1 Hz), 118.53, 117.48 (d, *J* = 17.7 Hz), 113.23, 112.38 (d, *J* = 21.3 Hz), 109.69, 55.28. **Anal. Calcd. for $C_{20}H_{14}F_2N_4O$**: C, 65.93; H, 3.87; N, 15.38. Found: C, 65.96; H, 4.13; N, 15.05.

2-(3-methoxyphenyl)-N-(3-(trifluoromethyl)phenyl)pyrido[2,3-d]pyrimidin-4-amine (190).

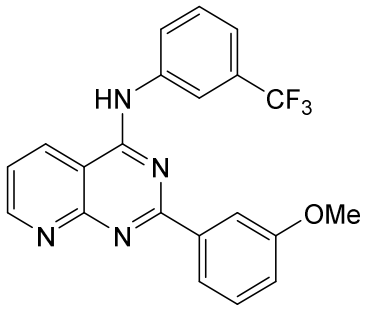

Molecular weight: 396.37 g/mol

The compound was synthesized according to the general procedure for compounds **162-197** from **160** (272 mg, 1 mmol) and 3-(trifluoromethyl)aniline (161 mg, 1 mmol) to yield

190 as a bright yellow solid (381 mg, 96%), mp 283-285 °C (decomp.). **^{1}H NMR** (500 MHz, DMSO-d_6) δ 11.67 (s, 1H), 9.65 (dd, *J* = 8.3, 1.7 Hz, 1H), 9.18 (dd, *J* = 4.7, 1.7 Hz, 1H), 8.49 (d, *J* = 2.1 Hz, 1H), 8.24 (dt, *J* = 8.0, 1.4 Hz, 1H), 7.98 (dt, *J* = 7.7, 1.0 Hz, 1H), 7.94 (t, *J* = 2.1 Hz, 1H), 7.88 (dd, *J* = 8.3, 4.7 Hz, 1H), 7.74 (t, *J* = 8.0 Hz, 1H), 7.65 – 7.59 (m, 1H), 7.47 (t, *J* = 7.9 Hz, 1H), 7.20 (dd, *J* = 8.2, 2.6 Hz, 1H), 3.84 (s, 3H). **^{13}C NMR** (126 MHz, DMSO) δ 162.38, 159.70, 159.31, 154.39, 154.36, 138.85, 137.50, 136.46, 130.00 (d, *J* = 6.6 Hz), 129.45 (d, *J* = 32.0 Hz), 127.50, 126.96, 124.25 (d, *J* = 272.1 Hz), 122.53, 121.70 (d, *J* = 4.2 Hz), 121.00, 119.79 (d, *J* = 3.7 Hz), 118.78, 113.72, 110.22, 55.41. **Anal. Calcd. for $C_{21}H_{15}F_3N_4O$**: C, 63.63; H, 3.81; N, 14.14. Found: C, 63.80; H, 4.04; N, 13.86.

2-(3-methoxyphenyl)-N-(4-(trifluoromethyl)phenyl)pyrido[2,3-d]pyrimidin-4-amine (191).

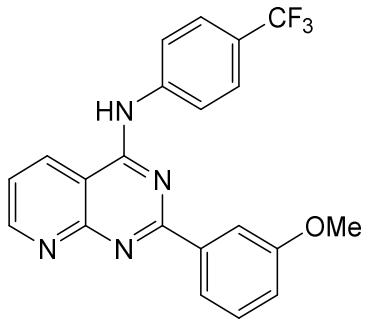

Molecular weight: 396.37 g/mol

The compound was synthesized according to the general procedure for compounds **162-197** from **160** (272 mg, 1 mmol) and 4-(trifluoromethyl)aniline (161 mg, 1 mmol) to yield **191** as a bright yellow solid (333 mg, 84%), mp 286-288 °C (decomp.). **^{1}H NMR** (500 MHz, DMSO-d_6) δ 11.55 (s, 1H), 9.62 (dd, *J* = 8.2, 1.7 Hz, 1H), 9.18 (dd, *J* = 4.7, 1.7 Hz, 1H), 8.22 (d, *J* = 8.5 Hz, 2H), 8.01 (dt, *J* = 7.6, 1.3 Hz, 1H), 7.95 (dd, *J* = 2.7, 1.6 Hz, 1H), 7.92 – 7.81 (m, 3H), 7.50 (t, *J* = 8.0 Hz, 1H), 7.19 (ddd, *J* = 8.3, 2.7, 0.9 Hz, 1H), 3.85 (s, 3H). **^{13}C NMR** (126 MHz, DMSO) δ 162.47, 159.60, 159.27, 154.70, 154.39, 141.82, 137.50, 136.64, 130.16, 127.66, 125.91 (q, *J* = 3.8 Hz), 125.89, 125.86, 125.50, 125.15 (d, *J* = 32.0 Hz), 123.36, 122.44, 121.44, 118.87, 113.44, 110.26, 55.31. **Anal. Calcd. for $C_{21}H_{15}F_3N_4O$**: C, 63.63; H, 3.81; N, 14.14. Found: C, 63.95; H, 4.02; N, 13.91.

***N*-(3-chlorophenyl)-2-(3-methoxyphenyl)pyrido[2,3-d]pyrimidin-4-amine (192).**

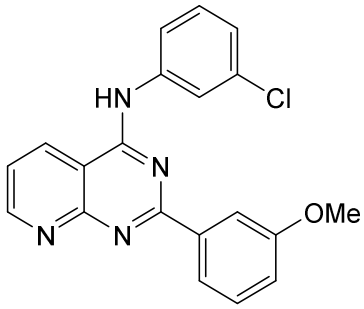

Molecular weight: 362.82 g/mol

The compound was synthesized according to the general procedure for compounds **162-197** from **160** (272 mg, 1 mmol) and 3-chloroaniline (128 mg, 1 mmol) to yield **192** as a yellow solid (305 mg, 84%), mp 279-282 °C (decomp.). **^{1}H NMR** (500 MHz, DMSO-d_6) δ 10.99 (s, 1H), 9.33 (d, *J* = 8.1 Hz, 1H), 9.16 (d, *J* = 4.5 Hz, 1H), 8.19 (s, 1H), 8.03 (d, *J* = 7.7 Hz, 1H), 7.98 (s, 1H), 7.88 (d, *J* = 8.2 Hz, 1H), 7.81 (dd, *J* = 8.3, 4.7 Hz, 1H), 7.51 (dt, *J* = 16.5, 8.1 Hz, 2H), 7.31 (d, *J* = 8.1 Hz, 1H), 7.18 (d, *J* = 8.2 Hz, 1H), 3.87 (s, 3H). **^{13}C NMR** (126 MHz, DMSO) δ 162.21, 159.66, 159.18, 155.20, 139.78, 135.82, 132.99, 130.42, 130.02, 124.77, 122.63, 122.33, 121.41, 121.21, 118.64, 113.21, 109.82, 55.38. **Anal. Calcd. for $C_{20}H_{15}ClN_4O$**: C, 66.21; H, 4.17; N, 15.44. Found: C, 66.02; H, 4.51; N, 15.17.

***N*-(3-bromophenyl)-2-(3-methoxyphenyl)pyrido[2,3-d]pyrimidin-4-amine (193).**

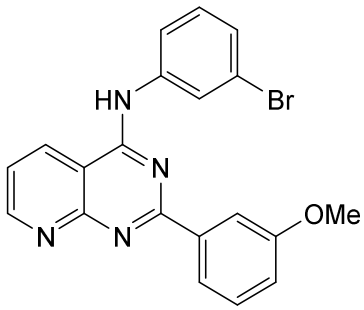

Molecular weight: 407.27 g/mol

The compound was synthesized according to the general procedure for compounds **162-197** from **160** (272 mg, 1 mmol) and 3-bromoaniline (172 mg, 1 mmol) to yield **193** as a yellow solid (289 mg, 71%), mp 283-284 °C (decomp.). **^{1}H NMR** (500 MHz, DMSO-d_6)

δ 11.44 (s, 1H), 9.53 (s, 1H), 9.19 (s, 1H), 8.31 (s, 1H), 8.01 (d, *J* = 7.6 Hz, 1H), 7.98 – 7.84 (m, 3H), 7.58 – 7.43 (m, 3H), 7.22 (d, *J* = 8.1 Hz, 1H), 3.87 (s, 3H). **^{13}C NMR** (126 MHz, DMSO) δ 162.27, 159.67, 159.21, 139.46, 136.27, 130.71, 130.12, 128.14, 125.93, 122.59, 122.22, 121.44, 121.29, 119.14, 113.44, 110.14, 55.49. **Anal. Calcd. for $C_{20}H_{15}BrN_4O$**: C, 58.98; H, 3.71; N, 13.76. Found: C, 58.82; H, 3.95; N, 13.51.

***N*-(3-nitrophenyl)-2-(pyridin-3-yl)pyrido[2,3-d]pyrimidin-4-amine (194).**

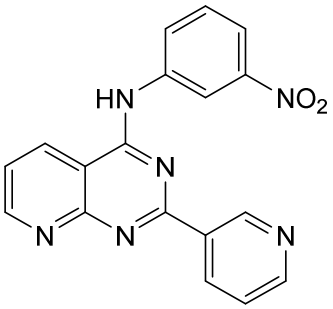

Molecular weight: 344.33 g/mol

The compound was synthesized according to the general procedure for compounds **162-197** from **161** (272 mg, 1 mmol) and 3-nitroaniline (138 mg, 1 mmol) to yield **194** as a light yellow solid (227 mg, 66%), mp 283-284 °C (decomp.). **^{1}H NMR** (500 MHz, DMSO-d_6) δ 11.06 (s, 1H), 9.62 (s, 1H), 9.38 – 9.29 (m, 1H), 9.20 (s, 1H), 9.12 (s, 2H), 8.93 (s, 1H), 8.39 (d, *J* = 7.5 Hz, 1H), 8.08 (d, *J* = 7.5 Hz, 1H), 7.96 (s, 1H), 7.85 – 7.73 (m, 2H). **^{13}C NMR** (126 MHz, DMSO) δ 160.93, 160.31, 159.23, 157.23, 150.13, 149.00, 148.18, 140.96, 138.92, 134.80, 130.76, 129.01, 125.57, 123.10, 119.41, 117.49, 110.58. **Anal. Calcd. for $C_{18}H_{12}N_6O_2$**: C, 62.79; H, 3.51; N, 24.41. Found: C, 63.03; H, 3.85; N, 24.17.

***N*-(4-nitrophenyl)-2-(pyridin-3-yl)pyrido[2,3-d]pyrimidin-4-amine (195).**

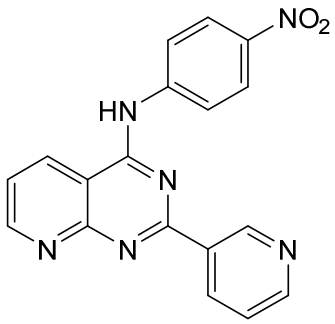

Molecular weight: 344.33 g/mol

The compound was synthesized according to the general procedure for compounds **162-197** from **161** (272 mg, 1 mmol) and 4-nitroaniline (138 mg, 1 mmol) to yield **195** as a yellow solid (241 mg, 70%), mp >300 °C. **^{1}H NMR** (500 MHz, DMSO-d_6) δ 11.01 (s, 1H), 9.62 (d, *J* = 2.0 Hz, 1H), 9.29 (dd, *J* = 8.3, 1.8 Hz, 1H), 9.19 (dd, *J* = 4.4, 1.8 Hz, 1H), 9.08 (dt, *J* = 8.1, 1.9 Hz, 1H), 8.92 (dd, *J* = 5.2, 1.6 Hz, 1H), 8.40 – 8.34 (m, 2H), 8.32 – 8.27 (m, 2H), 7.94 (dd, *J* = 8.2, 5.2 Hz, 1H), 7.78 (dd, *J* = 8.3, 4.4 Hz, 1H). **^{13}C NMR** (126 MHz, DMSO) δ 159.42, 159.39, 158.38, 156.82, 147.65, 145.78, 145.20, 142.83, 140.27, 134.68, 134.42, 125.88, 124.77, 122.74, 122.00, 110.18. **Anal. Calcd. for $C_{18}H_{12}N_6O_2$**: C, 62.79; H, 3.51; N, 24.41. Found: C, 62.70; H, 3.80; N, 24.17.

***N*-(3-fluorophenyl)-2-(pyridin-3-yl)pyrido[2,3-d]pyrimidin-4-amine (196).**

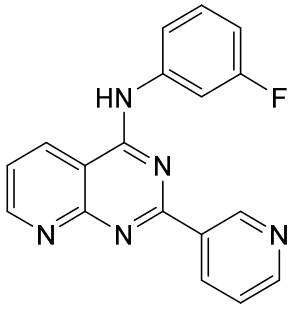

Molecular weight: 317.33 g/mol

The compound was synthesized according to the general procedure for compounds **162-197** from **161** (272 mg, 1 mmol) and 4-fluoroaniline (111 mg, 1 mmol) to yield **196** as a yellow solid (209 mg, 66%), mp 293-294 °C (decomp.). **^{1}H NMR** (500 MHz, DMSO-d_6) δ 10.75 (s, 1H), 9.55 (d, *J* = 2.1 Hz, 1H), 9.27 (dd, *J* = 8.3, 1.8 Hz, 1H), 9.16 (dd, *J* = 4.5,

1.8 Hz, 1H), 8.98 (dt, *J* = 8.1, 1.8 Hz, 1H), 8.90 (dd, *J* = 5.4, 1.6 Hz, 1H), 7.95 – 7.85 (m, 2H), 7.83 – 7.74 (m, 2H), 7.53 (td, *J* = 8.2, 6.8 Hz, 1H), 7.07 (tdd, *J* = 8.5, 2.6, 0.9 Hz, 1H). **^{13}C NMR** (126 MHz, DMSO) δ 162.13 (d, *J* = 241.7 Hz), 159.83, 159.48, 157.86, 156.15, 148.23, 146.18, 140.32 (d, *J* = 11.0 Hz), 139.52, 134.66, 130.40 (d, *J* = 9.4 Hz), 125.58, 122.52, 118.61, 111.31 (d, *J* = 21.0 Hz), 109.98, 109.65 (d, *J* = 25.8 Hz). **Anal. Calcd. for $C_{18}H_{12}FN_5$**: C, 68.13; H, 3.81; N, 22.07. Found: C, 68.00; H, 4.18; N, 21.86.

3-((2-(pyridin-3-yl)pyrido[2,3-d]pyrimidin-4-yl)amino)phenol (197).

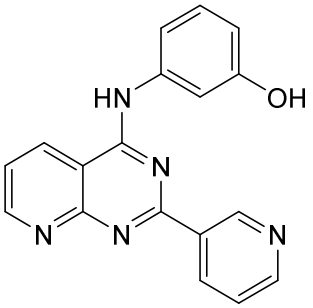

Molecular weight: 315.34 g/mol

The compound was synthesized according to the general procedure for compounds **162-197** from **161** (272 mg, 1 mmol) and 3-aminophenol (109 mg, 1 mmol) to yield **197** as a yellow solid (249 mg, 79%), mp 253-255 °C. **^{1}H NMR** (500 MHz, DMSO-d_6) δ 10.43 (s, 1H), 9.56 (dd, *J* = 2.2, 0.8 Hz, 2H), 9.19 (dd, *J* = 8.3, 1.8 Hz, 1H), 9.13 (dd, *J* = 4.5, 1.8 Hz, 1H), 8.92 (dt, *J* = 8.1, 1.8 Hz, 1H), 8.85 (dd, *J* = 5.1, 1.6 Hz, 1H), 7.81 (dd, *J* = 8.1, 5.0 Hz, 1H), 7.74 (dd, *J* = 8.2, 4.5 Hz, 1H), 7.44 (t, *J* = 2.1 Hz, 1H), 7.34 (ddd, *J* = 8.0, 2.0, 1.0 Hz, 1H), 7.27 (t, *J* = 8.0 Hz, 1H), 6.66 (ddd, *J* = 8.0, 2.4, 1.0 Hz, 1H). **^{13}C NMR** (126 MHz, DMSO) δ 160.29, 159.47, 158.55, 157.83, 155.93, 147.38, 139.47, 138.64, 134.59, 134.04, 130.74, 129.50, 125.10, 122.34, 113.66, 112.18, 110.02, 109.95. **Anal. Calcd. for $C_{18}H_{13}N_5O$**: C, 68.75; H, 4.35; N, 21.85. Found: C, 68.56; H, 4.16; N, 22.21.

10.1.1.5 Synthesis of 2,4-Substituted 6-nitroquinazolines

2-amino-5-nitrobenzamide (198).

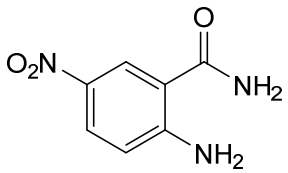

Molecular weight: 181.15 g/mol

To a solution of 2-amino-5-nitrobenzoic acid (1.80 g, 10 mmol) in 100 mL dry tetrahydrofurane (THF) was slowly added triphosgene (1.19 g, 4 mmol) while stirring at room temperature. The mixture was then refluxed under moisture exclusion for 3 h. Under stirring, a constant stream of ammonia gas was bubbled through the mixture for 30 min at 50 °C. Then, 50 mL of water was added and the precipitate filtered off. Additional product was obtained by concentrating the mixture under reduced pressure to one half of the initial volume to yield **198** as bright yellow crystals (1.58 g, 87%). **^{1}H NMR** (500 MHz, DMSO-d_6) δ 12.97 (s, 1H), 8.84 (d, J = 2.7 Hz, 1H), 8.56 (dd, J = 9.0, 2.7 Hz, 1H), 8.27 – 8.19 (m, 2H), 7.92 (d, J = 9.0 Hz, 1H), 7.68 – 7.62 (m, 1H), 7.58 (dd, J = 8.3, 6.7 Hz, 2H). **^{13}C NMR** (126 MHz, DMSO) δ 160.74, 155.16, 152.43, 144.86, 132.40, 128.86, 128.65, 128.24, 127.99, 126.66, 122.18, 121.22.

General Procedure for the Preparation of compounds 199-204. A mixture of 2-amino-5-nitrobenzamide **198** (3.62 g, 20 mmol), the corresponding aldehyde derivative (20 mmol), iodine (3.17 g, 25 mmol), anhydrous potassium carbonate (2.76 g, 20 mmol) and 20 ml DMF was stirred at 90 - 110 °C for 8-24 h. The end of the reaction was monitored by TLC and the mixture poured on crushed ice to form a precipitate. Incomplete precipitation can be prevented by adjusting the pH with concentrated HCl solution to 7. After filtration of the precipitate, it was thoroughly washed with 100 mL of a 20% sodium thiosulfate solution followed by 100 mL of hot distilled water. Purification was performed by recrystallization from ethanol.

6-nitro-2-phenylquinazolin-4(3H)-one (199).

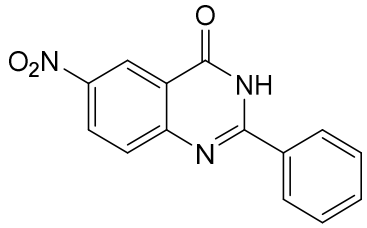

Molecular weight: 267.24 g/mol

The compound was synthesized from **198** (3.62 g, 20 mmol) and benzaldehyde (2.12 g, 20 mmol) as described in the general procedure for compounds **199-204** to yield **199** as a yellow solid (3.85 g, 72%). **^{1}H NMR** (500 MHz, DMSO-d_6) δ 12.97 (s, 1H), 8.84 (d, J = 2.7 Hz, 1H), 8.56 (dd, J = 9.0, 2.7 Hz, 1H), 8.27 – 8.19 (m, 2H), 7.92 (d, J = 9.0 Hz, 1H), 7.68 – 7.62 (m, 1H), 7.58 (dd, J = 8.3, 6.7 Hz, 2H). **^{13}C NMR** (126 MHz, DMSO) δ 144.86, 132.40, 132.24, 128.86, 128.65, 128.39, 122.18.

6-nitro-2-(pyridin-3-yl)quinazolin-4(3H)-one (200).

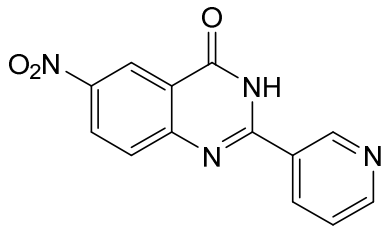

Molecular weight: 268.23 g/mol

The compound was synthesized from **198** (3.62 g, 20 mmol) and nicotinaldehyde (2.14 g, 20 mmol) as described in the general procedure for compounds **199-204** to yield **200** as a yellow-orange solid (3.70 g, 69%). **^{1}H NMR** (500 MHz, DMSO-d_6) δ 9.58 – 9.44 (m, 1H), 8.82 (d, J = 2.8 Hz, 1H), 8.67 (dt, J = 7.9, 2.0 Hz, 1H), 8.61 (dd, J = 4.9, 1.7 Hz, 1H), 8.24 (dd, J = 9.0, 2.8 Hz, 1H), 7.94 (s, 1H), 7.58 (d, J = 9.0 Hz, 1H), 7.45 (ddd, J = 7.9, 4.7, 0.8 Hz, 1H). **^{13}C NMR** (126 MHz, DMSO) δ 171.52, 163.89, 162.42, 156.83, 150.48, 149.70, 141.89, 135.45, 135.21, 127.35, 125.06, 123.24, 120.82.

6-nitro-2-(pyridin-4-yl)quinazolin-4(3H)-one (201).

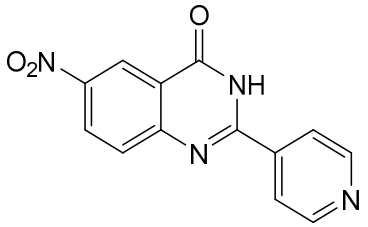

Molecular weight: 268.23 g/mol

The compound was synthesized from **198** (3.62 g, 20 mmol) and isonicotinaldehyde (2.14 g, 20 mmol) as described in the general procedure for compounds **199-204** to yield **201** as a yellow solid (2.74 g, 51%). **^{1}H NMR** (500 MHz, DMSO-d_6) δ 13.18 (s, 1H), 8.82 (dd, J = 8.1, 4.1 Hz, 3H), 8.57 (dd, J = 9.2, 2.7 Hz, 1H), 8.16 – 8.07 (m, 2H), 7.95 (d, J = 9.3 Hz, 1H). **^{13}C NMR** (126 MHz, DMSO) δ 161.62, 154.18, 152.54, 150.51, 145.35, 139.58, 129.56, 128.73, 122.09, 121.96, 121.77.

6-nitro-2-(3-(trifluoromethyl)phenyl)quinazolin-4(3H)-one (202).

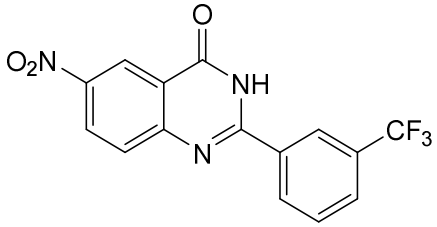

Molecular weight: 335.24 g/mol

The compound was synthesized from **198** (3.62 g, 20 mmol) and 3-(trifluoromethyl)benzaldehyde (3.48 g, 20 mmol) as described in the general procedure for compounds **199-204** to yield **202** as a yellow solid (5.16 g, 77%). **^{1}H NMR** (500 MHz, DMSO-d_6) δ 13.18 (s, 1H), 8.82 (d, J = 2.7 Hz, 1H), 8.59 – 8.53 (m, 2H), 8.50 (ddd, J = 8.2, 2.0, 1.1 Hz, 1H), 8.00 (ddt, J = 7.9, 1.9, 1.0 Hz, 1H), 7.97 – 7.91 (m, 1H), 7.87 – 7.77 (m, 1H). **^{13}C NMR** (126 MHz, DMSO) δ 161.67, 154.51, 152.69, 145.07, 133.26, 132.33, 130.07, 129.61 (d, J = 32.3 Hz), 129.37, 128.71 (d, J = 3.5 Hz), 128.65, 127.25, 125.04 (d, J = 3.8 Hz), 122.92, 122.07, 121.36.

2-(3-methoxyphenyl)-6-nitroquinazolin-4(3H)-one (203).

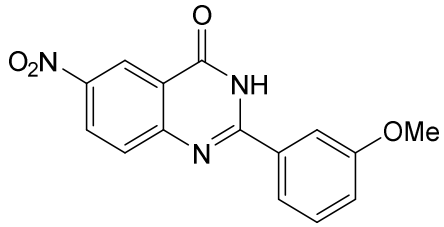

Molecular weight: 297.27 g/mol

The compound was synthesized from **198** (3.62 g, 20 mmol) and 3-methoxybenzaldehyde (2.72 g, 20 mmol) as described in the general procedure for compounds **199-204** to yield **203** as a yellow solid (4.88 g, 82%). **^{1}H NMR** (500 MHz, DMSO-d_6) δ 12.94 (s, 1H), 8.83 (d, J = 2.7 Hz, 1H), 8.52 (dd, J = 9.0, 2.8 Hz, 1H), 7.88 (d, J = 8.9 Hz, 1H), 7.85 (ddd, J = 7.8, 1.7, 0.9 Hz, 1H), 7.80 (t, J = 2.2 Hz, 1H), 7.47 (t, J = 8.0 Hz, 1H), 7.18 (ddd, J = 8.2, 2.6, 0.9 Hz, 1H), 3.86 (s, 3H). **^{13}C NMR** (126 MHz, DMSO) δ 161.65, 161.42, 159.51, 153.03, 144.84, 142.84, 133.43, 130.00, 128.61, 122.13, 120.75, 118.60, 113.11, 55.59.

2-(3,4-dimethoxyphenyl)-6-nitroquinazolin-4(3H)-one (204).

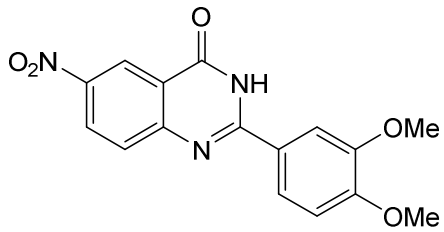

Molecular weight: 327.30 g/mol

The compound was synthesized from **198** (3.62 g, 20 mmol) and 3,4-dimethoxybenzaldehyde (3.32 g, 20 mmol) as described in the general procedure for compounds **199-204** to yield **204** as a yellow solid (4.19 g, 64%). **^{1}H NMR** (500 MHz, DMSO-d_6) δ 12.81 (s, 1H), 8.80 (d, J = 2.7 Hz, 1H), 8.50 (dd, J = 9.0, 2.8 Hz, 1H), 7.94 (dd, J = 8.5, 2.2 Hz, 1H), 7.88 – 7.82 (m, 2H), 7.13 (d, J = 8.7 Hz, 1H), 3.88 (s, 3H), 3.85 (s, 3H). **^{13}C NMR** (126 MHz, DMSO) δ 162.24, 155.65, 153.41, 152.49, 148.72, 144.28, 128.86, 128.42, 124.35, 122.24, 122.18, 120.68, 111.58, 111.20, 55.89, 55.87.

General Procedure for the Preparation of compounds 205-210.

The corresponding 2-substituted 6-nitroquinazolin-4(3*H*)-one derivative **199-204** (10 mmol) was added to phosphorous trichloride (30 mL, 0.32 mol) and stirred for 10 min at room temperature. The mixture was then refluxed for 4-12 h and the reaction monitored by TLC. After completion of the reaction, excess $POCl_3$ was removed under reduced pressure and 50 mL ice water added. Subsequently, 50 mL DCM was added while stirring and the pH of the mixture slowly adjusted to 7 with 25% ammonium solution. With a separatory funnel, the organic phase was collected, washed with 50 mL brine and dried under $MgSO_4$. The solvent was removed under reduced pressure and the obtained solid recrystallized from isopropanol.

3-(6-nitro-4-oxo-3,4-dihydroquinazolin-2-yl)benzonitrile (205).

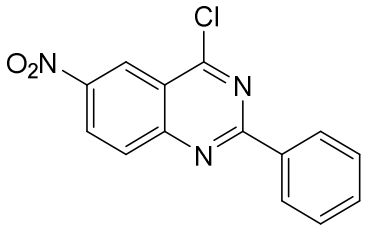

Molecular weight: 285.69 g/mol

The compound was synthesized from **199** (2.67 g, 10 mmol) as described in the general procedure for compounds **205-210** to yield **205** as a yellow solid (2.46 g, 86%). **^{1}H NMR** (500 MHz, DMSO-d_6) δ 8.83 (d, J = 2.7 Hz, 1H), 8.55 (dd, J = 9.0, 2.8 Hz, 1H), 8.24 – 8.19 (m, 2H), 7.91 (d, J = 9.0 Hz, 1H), 7.67 – 7.62 (m, 1H), 7.60 – 7.55 (m, 2H). **^{13}C NMR** (126 MHz, DMSO) δ 161.74, 155.85, 152.97, 144.85, 132.41, 132.16, 129.19, 128.85, 128.64, 128.39, 122.16, 121.14.

4-chloro-6-nitro-2-(pyridin-3-yl)quinazoline (206).

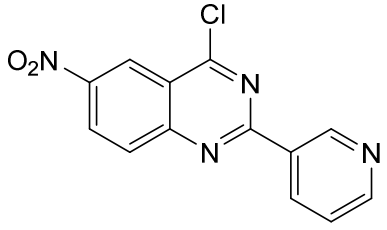

Molecular weight: 286.68 g/mol

The compound was synthesized from **200** (2.68 g, 10 mmol) as described in the general procedure for compounds **205-210** to yield **206** as an orange solid (2.38 g, 83%). **^{1}H NMR** (500 MHz, DMSO-d_6) δ 9.38 (dd, J = 2.3, 0.8 Hz, 1H), 8.88 (dd, J = 5.0, 1.6 Hz, 1H), 8.82 (d, J = 2.7 Hz, 1H), 8.72 (ddd, J = 8.1, 2.3, 1.6 Hz, 1H), 8.60 – 8.54 (m, 1H), 7.94 (d, J = 8.8 Hz, 1H), 7.79 (ddd, J = 8.1, 5.1, 0.8 Hz, 1H). **^{13}C NMR** (126 MHz, DMSO) δ 161.49, 153.56, 152.52, 150.29, 147.22, 145.21, 138.43, 129.36, 129.20, 128.77, 124.70, 122.09, 121.42.

4-chloro-6-nitro-2-(pyridin-4-yl)quinazoline (207).

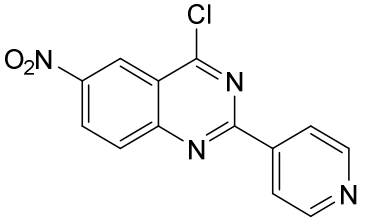

Molecular weight: 286.68 g/mol

The compound was synthesized from **201** (2.68 g, 10 mmol) as described in the general procedure for compounds **205-210** to yield **207** as an orange solid (2.12 g, 74%). **^{1}H NMR** (500 MHz, DMSO-d_6) δ 13.21 (s, 1H), 8.85 – 8.81 (m, 2H), 8.57 (dd, J = 9.0, 2.7 Hz, 1H), 8.18 – 8.10 (m, 2H), 7.95 (d, J = 9.0 Hz, 1H). **^{13}C NMR** (126 MHz, DMSO) δ 161.55, 153.98, 152.46, 150.07, 145.44, 140.03, 129.63, 128.80, 122.10, 121.81.

4-chloro-6-nitro-2-(3-(trifluoromethyl)phenyl)quinazoline (208).

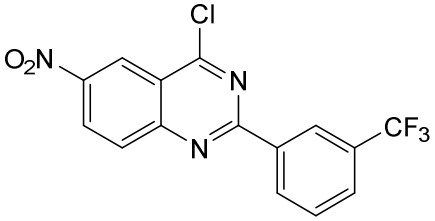

Molecular weight: 353.69 g/mol

The compound was synthesized from **202** (3.35 g, 10 mmol) as described in the general procedure for compounds **205-210** to yield **208** as a yellow solid (3.18 g, 90%). **^{1}H NMR** (600 MHz, DMSO-d_6) δ 8.81 (d, J = 2.7 Hz, 1H), 8.59 – 8.52 (m, 2H), 8.52 – 8.46 (m,

1H), 8.03 – 7.97 (m, 1H), 7.94 (d, *J* = 8.9 Hz, 1H), 7.82 (t, *J* = 7.9 Hz, 1H). **^{13}C NMR** (151 MHz, DMSO) δ 161.68, 154.53, 152.67, 145.14, 133.24, 132.40, 130.14, 129.66 (d, *J* = 32.5 Hz), 129.42, 128.80 (d, *J* = 3.8 Hz), 128.74, 125.09 (t, *J* = 3.9 Hz), 123.16, 122.13, 121.40.

4-chloro-2-(3-methoxyphenyl)-6-nitroquinazoline (209).

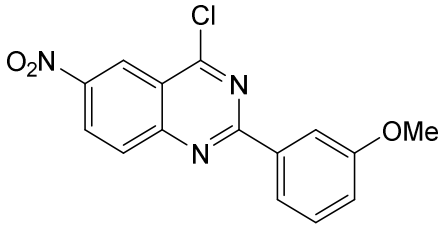

Molecular weight: 315.71 g/mol

The compound was synthesized from **203** (2.97 g, 10 mmol) as described in the general procedure for compounds **205-210** to yield **209** as a yellow solid (2.81 g, 89%). **^{1}H NMR** (500 MHz, DMSO-d_6) δ 8.83 (d, *J* = 2.7 Hz, 1H), 8.55 (dd, *J* = 9.0, 2.8 Hz, 1H), 7.92 (d, *J* = 9.0 Hz, 1H), 7.83 (ddd, *J* = 7.7, 1.7, 0.9 Hz, 1H), 7.78 (dd, *J* = 2.6, 1.7 Hz, 1H), 7.49 (t, *J* = 8.0 Hz, 1H), 7.20 (ddd, *J* = 8.2, 2.6, 0.9 Hz, 1H), 3.87 (s, 3H). **^{13}C NMR** (126 MHz, DMSO) δ 161.74, 159.51, 155.56, 152.89, 144.87, 133.42, 130.02, 129.23, 128.65, 122.15, 121.18, 120.77, 118.63, 113.14, 55.61.

4-chloro-2-(3,4-dimethoxyphenyl)-6-nitroquinazoline (210).

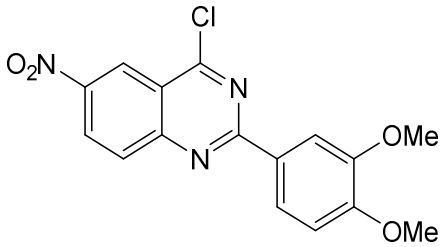

Molecular weight: 345.74 g/mol

The compound was synthesized from **7** (3.27 g, 10 mmol) as described in the general procedure for compounds **205-210** to yield **210** as a yellow solid (2.75 g, 71%). ^{1}H NMR (500 MHz, DMSO-d_6) δ 8.79 (d, *J* = 2.7 Hz, 1H), 8.50 (dd, *J* = 9.0, 2.7 Hz, 1H), 7.92 (dd, *J* = 8.5, 2.2 Hz, 1H), 7.89 – 7.77 (m, 2H), 7.13 (d, *J* = 8.6 Hz, 1H), 3.88 (s, 3H), 3.85 (s,

3H). ^{13}C NMR (126 MHz, DMSO) δ 161.80, 155.29, 153.05, 152.61, 148.73, 144.43, 128.80, 128.59, 123.85, 122.26, 122.19, 120.66, 111.60, 111.20, 55.91, 55.89.

General Procedure for the Preparation of compounds 211-239. The corresponding 2 substituted 4-chloroquinazoline **205-210** (1 mmol) and a substituted aniline (1 mmol) were added to a 50 mL microwave tube and suspended in 25 mL isopropanol. The tube was sealed and the reaction mixture stirred under 100 watt microwave irradiation at 110 °C for 20-40 min. Completion of the reaction was monitored by TLC. After cooling, a precipitate was formed and filtered off by suction. Recrystallization was carried out with ethanol.

6-nitro-N,2-diphenylquinazolin-4-amine (211).

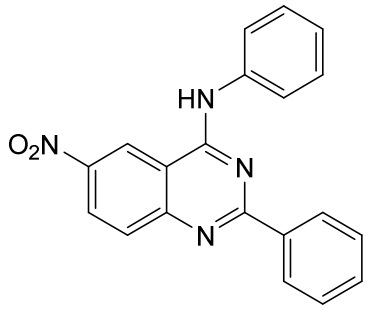

Molecular weight: 342.36 g/mol

The compound was synthesized according to the general procedure for compounds **211-239** from **205** (2.86 g, 10 mmol) and aniline (0.93 g, 10 mmol) to yield **211** as an orange solid (2.40 g, 70%), mp 264-265 °C. **^{1}H NMR** (500 MHz, DMSO-d_6) δ 10.47 (s, 1H), 9.65 (d, J = 2.5 Hz, 1H), 8.53 (dd, J = 9.2, 2.5 Hz, 1H), 8.46 – 8.36 (m, 2H), 7.96 (d, J = 9.2 Hz, 1H), 7.94 – 7.89 (m, 2H), 7.58 – 7.44 (m, 5H), 7.23 (tt, J = 7.4, 1.1 Hz, 1H). **^{13}C NMR** (126 MHz, DMSO) δ 162.32, 159.06, 154.21, 144.24, 138.67, 137.59, 131.33, 129.68, 128.69, 128.49, 126.90, 124.59, 122.90, 121.05, 113.35. **Anal. Calcd. for $C_{20}H_{14}N_4O_2$**: C, 70.17; H, 4.12; N, 16.37. Found: C, 70.32; H, 4.26; N, 16.17.

2-nitro-4-((6-nitro-2-phenylquinazolin-4-yl)amino)phenol (212).

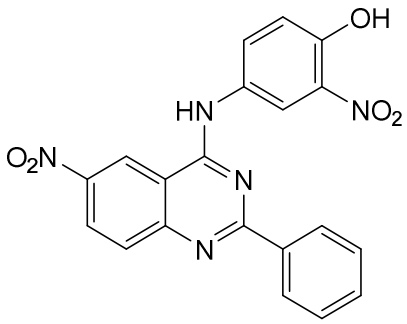

Molecular weight: 403.35 g/mol

The compound was synthesized according to the general procedure for compounds **211-239** from **205** (2.86 g, 10 mmol) and 4-amino-2-nitrophenol (1.54 g, 10 mmol) to yield **212** as an orange-red solid (2.58 g, 64%), mp >300 °C. **^{1}H NMR** (500 MHz, DMSO-d_6) δ 10.90 (s, 1H), 10.56 (s, 1H), 9.61 (d, J = 2.5 Hz, 1H), 8.80 (d, J = 2.7 Hz, 1H), 8.54 (dd, J = 9.2, 2.4 Hz, 1H), 8.51 – 8.44 (m, 2H), 8.04 (dd, J = 9.0, 2.7 Hz, 1H), 7.98 (d, J = 9.2 Hz, 1H), 7.60 – 7.46 (m, 3H), 7.26 (d, J = 9.0 Hz, 1H). **^{13}C NMR** (126 MHz, DMSO) δ 162.19, 158.80, 154.07, 149.22, 144.31, 137.40, 135.70, 131.45, 130.49, 130.16, 129.76, 128.67, 128.57, 127.00, 120.86, 119.39, 118.70, 113.25. **Anal. Calcd. for $C_{20}H_{13}N_5O_5$**: C, 59.56; H, 3.25; N, 17.36. Found: C, 59.69; H, 3.01; N, 17.22.

3-((6-nitro-2-phenylquinazolin-4-yl)amino)benzonitrile (213).

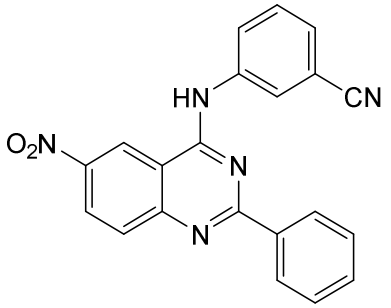

Molecular weight: 367.37 g/mol

The compound was synthesized according to the general procedure for compounds **211-239** from **205** (2.86 g, 10 mmol) and 3-aminobenzonitrile (1.18 g, 10 mmol) to yield **213** as a yellow solid (2.98 g, 81%), mp >300 °C. **^{1}H NMR** (500 MHz, DMSO-d_6) δ 11.03 (s, 1H), 9.69 (d, J = 2.4 Hz, 1H), 8.59 (dd, J = 9.2, 2.4 Hz, 1H), 8.48 – 8.31 (m, 3H), 8.24

(dt, *J* = 7.5, 2.1 Hz, 1H), 8.11 (d, *J* = 9.1 Hz, 1H), 7.78 – 7.65 (m, 2H), 7.64 – 7.47 (m, 3H). **^{13}C NMR** (126 MHz, DMSO) δ 161.54, 159.13, 152.28, 144.68, 139.27, 136.16, 132.05, 130.19, 128.83, 128.70, 128.48, 128.22, 127.67, 127.57, 126.17, 121.14, 118.71, 113.20, 111.57. **Anal. Calcd. for $C_{21}H_{13}N_5O_2$**: C, 68.66; H, 3.57; N, 19.06. Found: C, 68.70; H, 3.90; N, 18.75.

4-((6-nitro-2-phenylquinazolin-4-yl)amino)benzonitrile (214).

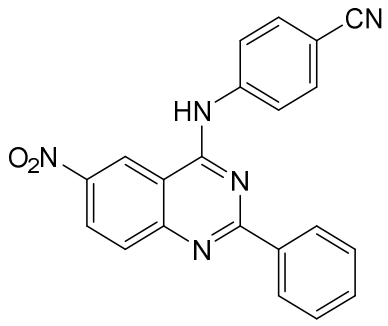

Molecular weight: 367.37 g/mol

The compound was synthesized according to the general procedure for compounds **211-239** from **205** (2.86 g, 10 mmol) and 4-aminobenzonitrile (1.18 g, 10 mmol) to yield **214** as a yellow solid (2.53 g, 69%), mp >300 °C. **^{1}H NMR** (600 MHz, DMSO-d_6) δ 10.93 (s, 1H), 9.71 (d, *J* = 2.4 Hz, 1H), 8.60 (dd, *J* = 9.2, 2.4 Hz, 1H), 8.47 – 8.41 (m, 2H), 8.22 – 8.14 (m, 2H), 8.08 (d, *J* = 9.1 Hz, 1H), 7.99 – 7.92 (m, 2H), 7.61 – 7.52 (m, 3H). **^{13}C NMR** (151 MHz, DMSO) δ 161.79, 159.03, 153.14, 144.64, 143.02, 136.60, 133.08, 131.84, 129.13, 128.88, 128.70, 127.53, 122.69, 121.20, 119.12, 113.45, 106.12. **Anal. Calcd. for $C_{21}H_{13}N_5O_2$**: C, 68.66; H, 3.57; N, 19.06. Found: C, 68.59; H, 3.80; N, 18.79.

3-((6-nitro-2-phenylquinazolin-4-yl)amino)phenol (215).

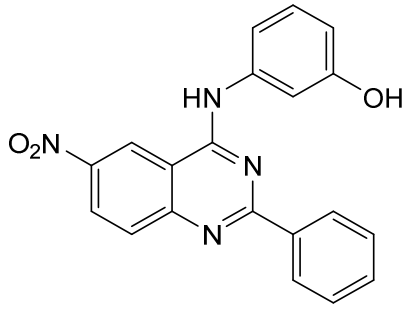

Molecular weight: 358.36 g/mol

The compound was synthesized according to the general procedure for compounds **211-239** from **205** (2.86 g, 10 mmol) and 3-aminophenol (1.09 g, 10 mmol) to yield **215** as a yellow solid (2.39 g, 66%), mp 277-278 °C (decomp.). **^{1}H NMR** (500 MHz, DMSO-d_6) δ 10.35 (s, 1H), 9.67 (d, *J* = 2.4 Hz, 1H), 9.53 (s, 1H), 8.53 (dd, *J* = 9.2, 2.5 Hz, 1H), 8.49 – 8.41 (m, 2H), 7.96 (d, *J* = 9.1 Hz, 1H), 7.57 – 7.48 (m, 3H), 7.43 (t, *J* = 2.2 Hz, 1H), 7.38 (ddd, *J* = 8.1, 2.1, 1.0 Hz, 1H), 7.26 (t, *J* = 8.0 Hz, 1H), 6.64 (ddd, *J* = 8.1, 2.4, 1.0 Hz, 1H). **^{13}C NMR** (126 MHz, DMSO) δ 162.38, 159.03, 157.67, 154.22, 144.25, 139.70, 137.63, 131.33, 129.67, 129.29, 128.67, 128.60, 126.89, 121.11, 113.59, 113.41, 111.76, 109.95. **Anal. Calcd. for $C_{20}H_{14}N_4O_3$**: C, 67.03; H, 3.94; N, 15.63. Found: C, 67.24; H, 4.17; N, 15.41.

4-((6-nitro-2-phenylquinazolin-4-yl)amino)benzene-1,2-diol (216).

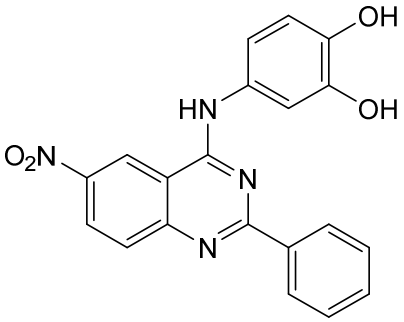

Molecular weight: 374.36 g/mol

The compound was synthesized from a solution of **218** (4.02 g, 10 mmol) in dry DCM kept at – 60 °C under moisture exclusion. Boron tribromide was slowly added under stirring via a dropping funnel within 30 min and the cooling bath removed. After another 12 h stirring at room temperature, the solvent was evaporated under reduced pressure and the obtained solid recrystallized from 75% ethanol to yield **216** as red solid (3.14 g, 84%), mp >300 °C. **^{1}H NMR** (500 MHz, DMSO-d_6) δ 10.27 (s, 1H), 9.62 (d, *J* = 2.5 Hz, 1H), 9.07 (s, 1H), 8.86 (s, 1H), 8.52 (dd, *J* = 9.2, 2.5 Hz, 1H), 8.47 – 8.39 (m, 2H), 7.93 (d, *J* = 9.2 Hz, 1H), 7.56 – 7.48 (m, 3H), 7.34 (d, *J* = 2.5 Hz, 1H), 7.14 (dd, *J* = 8.5, 2.5 Hz, 1H), 6.82 (d, *J* = 8.5 Hz, 1H). **^{13}C NMR** (126 MHz, DMSO) δ 162.48, 158.90, 154.19, 145.08, 144.09, 142.75, 137.70, 131.25, 130.22, 129.42, 128.61, 128.59, 126.77, 121.02, 115.24, 114.44, 113.35, 111.57. **Anal. Calcd. for $C_{20}H_{14}N_4O_4$**: C, 64.17; H, 3.77; N, 14.97. Found: C, 64.15; H, 3.67; N, 14.67.

N-(3-methoxyphenyl)-6-nitro-2-phenylquinazolin-4-amine (217).

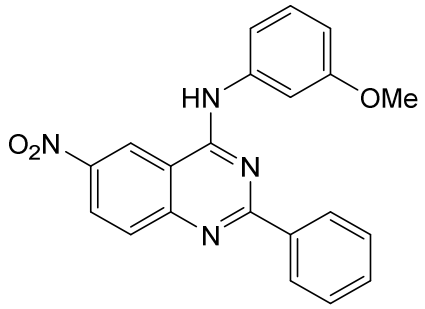

Molecular weight: 372.38 g/mol

The compound was synthesized according to the general procedure for compounds **211-239** from **205** (2.86 g, 10 mmol) and 3-methoxyaniline (1.23 g, 10 mmol) to yield **217** as an orange solid (2.20 g, 59%), mp 242-243 °C. **^{1}H NMR** (600 MHz, DMSO-d_6) δ 10.42 (s, 1H), 9.66 (d, J = 2.4 Hz, 1H), 8.53 (dd, J = 9.1, 2.4 Hz, 1H), 8.49 – 8.39 (m, 2H), 7.97 (d, J = 9.1 Hz, 1H), 7.67 (s, 1H), 7.62 – 7.48 (m, 4H), 7.38 (t, J = 8.1 Hz, 1H), 6.80 (dd, J = 8.1, 2.4 Hz, 1H), 3.83 (s, 3H). **^{13}C NMR** (151 MHz, DMSO) δ 162.27, 159.53, 158.98, 154.18, 144.28, 139.95, 137.61, 131.39, 129.73, 129.41, 128.67, 128.47, 126.93, 121.02, 114.87, 113.40, 110.49, 108.09, 55.30. **Anal. Calcd. for $C_{21}H_{16}N_4O_3$**: C, 67.73; H, 4.33; N, 15.05. Found: C, 67.48; H, 4.25; N, 14.85.

N-(3,4-dimethoxyphenyl)-6-nitro-2-phenylquinazolin-4-amine (218).

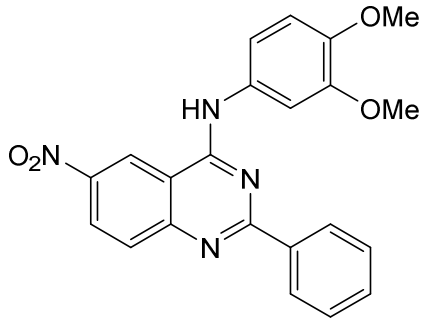

Molecular weight: 402.41 g/mol

The compound was synthesized according to the general procedure for compounds **211-239** from **205** (2.86 g, 10 mmol) and 3,4-dimethoxyaniline (1.53 g, 10 mmol) to yield **218** as a red-orange solid (3.10 g, 77%), mp 238-240 °C. **^{1}H NMR** (500 MHz, DMSO-d_6) δ 10.35 (s, 1H), 9.63 (d, J = 2.5 Hz, 1H), 8.51 (dd, J = 9.2, 2.4 Hz, 1H), 8.49 – 8.42 (m,

2H), 7.94 (d, *J* = 9.2 Hz, 1H), 7.68 (d, *J* = 2.5 Hz, 1H), 7.57 – 7.47 (m, 3H), 7.43 (dd, *J* = 8.7, 2.4 Hz, 1H), 7.06 (d, *J* = 8.7 Hz, 1H), 3.83 (s, 3H), 3.81 (s, 3H). **^{13}C NMR** (126 MHz, DMSO) δ 162.36, 158.78, 154.19, 148.45, 145.98, 144.16, 137.71, 131.99, 131.31, 129.60, 128.60, 128.46, 126.81, 120.91, 114.76, 113.35, 111.85, 107.81, 55.89, 55.66. **Anal. Calcd. for $C_{22}H_{18}N_4O_4$**: C, 65.66; H, 4.51; N, 13.92. Found: C, 65.74; H, 4.88; N, 13.55.

N-(3-((6-nitro-2-phenylquinazolin-4-yl)amino)phenyl)acetamide (219).

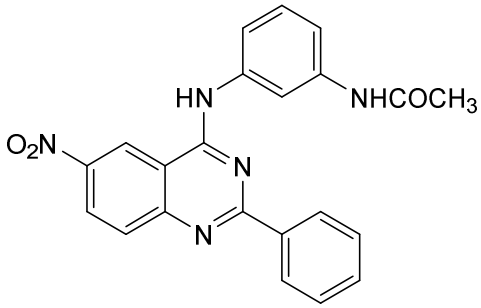

Molecular weight: 399.41 g/mol

The compound was synthesized according to the general procedure for compounds **211-239** from **205** (2.86 g, 10 mmol) and N-(3-aminophenyl)acetamide (1.50 g, 10 mmol) to yield **219** as a yellow solid (2.80 g, 70%), mp >300 °C. **^{1}H NMR** (500 MHz, DMSO-d_6) δ 10.83 (s, 1H), 10.09 (s, 1H), 9.73 (d, *J* = 2.4 Hz, 1H), 8.60 (dd, *J* = 9.2, 2.5 Hz, 1H), 8.54 – 8.39 (m, 2H), 8.33 (t, *J* = 2.1 Hz, 1H), 8.08 (d, *J* = 9.2 Hz, 1H), 7.67 – 7.47 (m, 4H), 7.41 (t, *J* = 8.1 Hz, 1H), 7.31 (ddd, *J* = 8.0, 2.1, 1.0 Hz, 1H), 2.09 (s, 3H). **^{13}C NMR** (126 MHz, DMSO) δ 168.54, 161.74, 159.20, 152.19, 144.58, 139.80, 138.46, 136.12, 131.93, 128.97, 128.76, 128.09, 127.54, 121.33, 118.20, 115.93, 114.17, 113.29, 24.18. **Anal. Calcd. for $C_{22}H_{17}N_5O_3$**: C, 66.16; H, 4.29; N, 17.53. Found: C, 66.26; H, 4.53; N, 17.25.

N-(3-fluorophenyl)-6-nitro-2-phenylquinazolin-4-amine (220).

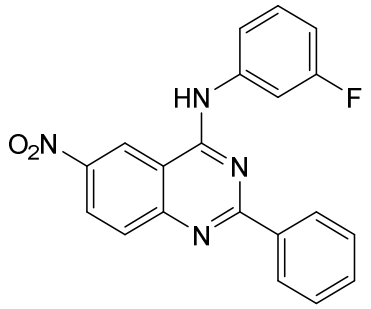

Molecular weight: 360.35 g/mol

The compound was synthesized according to the general procedure for compounds **211-239** from **205** (2.86 g, 10 mmol) and 3-fluoroaniline (1.11 g, 10 mmol) to yield **220** as a yellow solid (3.17 g, 88%), mp 288-289 °C (decomp.). **^{1}H NMR** (500 MHz, DMSO-d_6) δ 11.10 (s, 1H), 9.73 (d, *J* = 2.5 Hz, 1H), 8.61 (dd, *J* = 9.2, 2.4 Hz, 1H), 8.51 – 8.36 (m, 2H), 8.18 (d, *J* = 9.2 Hz, 1H), 7.89 (dt, *J* = 11.4, 2.3 Hz, 1H), 7.75 (ddd, *J* = 8.2, 2.0, 0.9 Hz, 1H), 7.67 – 7.42 (m, 4H), 7.10 (tdd, *J* = 8.4, 2.5, 0.9 Hz, 1H). **^{13}C NMR** (126 MHz, DMSO) δ 162.01 (d, *J* = 241.9 Hz), 161.25, 159.12, 144.76, 139.82 (d, *J* = 11.1 Hz), 135.45, 132.28, 130.31 (d, *J* = 9.4 Hz), 128.86, 127.86, 127.48, 121.23, 118.97, 113.18, 111.73 (d, *J* = 20.9 Hz), 110.12 (d, *J* = 26.0 Hz). **Anal. Calcd. for $C_{20}H_{13}FN_4O_2$**: C, 66.66; H, 3.64; N, 15.55. Found: C, 66.30; H, 3.92; N, 15.30.

6-nitro-2-phenyl-N-(3-(trifluoromethyl)phenyl)quinazolin-4-amine (221).

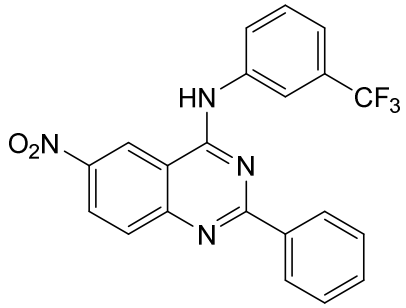

Molecular weight: 410.36 g/mol

The compound was synthesized according to the general procedure for compounds **211-239** from **205** (2.86 g, 10 mmol) and 3-(trifluoromethyl)aniline (1.61 g, 10 mmol) to yield **221** as a yellow solid (3.08 g, 75%), mp 278-279 °C (decomp.). **^{1}H NMR** (600 MHz,

DMSO-d_6) δ 10.65 (s, 1H), 9.65 (d, *J* = 2.4 Hz, 1H), 8.57 (d, *J* = 2.0 Hz, 1H), 8.54 (dd, *J* = 9.1, 2.4 Hz, 1H), 8.43 (dt, *J* = 7.1, 1.4 Hz, 2H), 8.20 – 8.13 (m, 1H), 7.98 (dd, *J* = 9.1, 1.8 Hz, 1H), 7.71 (t, *J* = 8.0 Hz, 1H), 7.59 – 7.53 (m, 2H), 7.53 – 7.47 (m, 2H). **^{13}C NMR** (151 MHz, DMSO) δ 162.10, 158.99, 154.15, 144.44, 139.67, 137.40, 131.57, 129.91 (d, *J* = 5.2 Hz), 129.40 (d, *J* = 31.6 Hz), 128.71, 128.47, 127.13, 125.94, 124.44 (d, *J* = 272.5 Hz), 120.98, 120.55 (d, *J* = 3.7 Hz), 118.99 (d, *J* = 4.0 Hz), 113.37. **Anal. Calcd. for $C_{21}H_{13}F_3N_4O_2$**: C, 61.47; H, 3.19; N, 13.65. Found: C, 61.77; H, 3.35; N, 13.44.

3-((6-nitro-2-phenylquinazolin-4-yl)amino)benzoic acid (222).

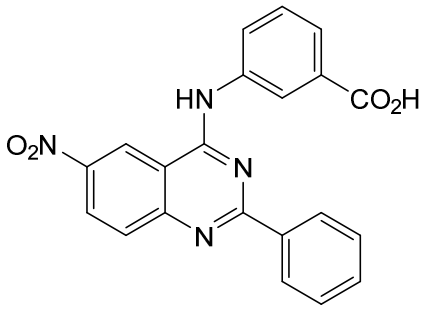

Molecular weight: 386.37 g/mol

The compound was synthesized according to the general procedure for compounds **211-239** from **205** (2.86 g, 10 mmol) and 3-aminobenzoic acid (1.37 g, 10 mmol) to yield **222** as a yellow solid (2.43 g, 63%), mp >300 °C. **^{1}H NMR** (500 MHz, DMSO-d_6) δ 10.97 (s, 1H), 9.71 (d, *J* = 2.5 Hz, 1H), 8.58 (dd, *J* = 9.2, 2.4 Hz, 1H), 8.47 – 8.35 (m, 2H), 8.14 – 7.99 (m, 5H), 7.67 – 7.44 (m, 3H). **^{13}C NMR** (126 MHz, DMSO) δ 167.01, 161.57, 159.04, 152.15, 144.67, 142.47, 136.04, 132.03, 130.16, 128.88, 128.83, 128.30, 127.63, 126.64, 122.28, 121.25, 113.35. **Anal. Calcd. for $C_{21}H_{14}N_4O_4$**: C, 65.28; H, 3.65; N, 14.50. Found: C, 65.58; H, 3.88; N, 14.29.

3-((6-nitro-2-(pyridin-4-yl)quinazolin-4-yl)amino)benzonitrile (223).

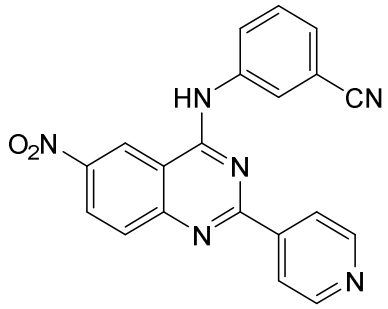

Molecular weight: 368.36 g/mol

The compound was synthesized according to the general procedure for compounds **211-239** from **10** (2.87 g, 10 mmol) and 3-aminobenzonitrile (1.18 g, 10 mmol) to yield **223** as a yellow solid (2.65 g, 72%), mp >300 °C. **^{1}H NMR** (500 MHz, DMSO-d_6) δ 10.97 (s, 1H), 9.67 (d, J = 2.4 Hz, 1H), 8.98 – 8.92 (m, 2H), 8.59 (dd, J = 9.2, 2.4 Hz, 1H), 8.55 – 8.49 (m, 2H), 8.28 (q, J = 1.4 Hz, 1H), 8.27 – 8.20 (m, 1H), 8.05 (d, J = 9.1 Hz, 1H), 7.72 – 7.67 (m, 2H). **^{13}C NMR** (126 MHz, DMSO) δ 159.40, 158.49, 153.32, 149.88, 145.51, 145.40, 139.14, 130.33, 130.25, 128.34, 127.66, 126.09, 124.07, 121.03, 118.67, 114.02, 111.67. **Anal. Calcd. for $C_{22}H_{14}N_6O_2$**: C, 65.21; H, 3.28; N, 22.82. Found: C, 65.43; H, 3.49; N, 22.44.

N-(3-methoxyphenyl)-6-nitro-2-(pyridin-3-yl)quinazolin-4-amine (224).

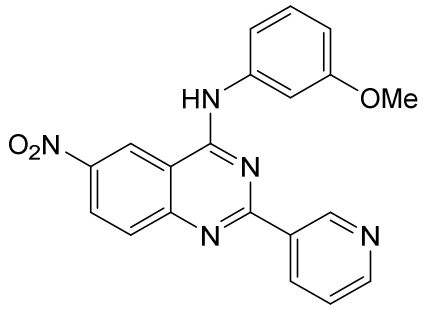

Molecular weight: 373.37 g/mol

The compound was synthesized according to the general procedure for compounds **211-239** from **206** (2.87 g, 10 mmol) and 3-methoxyaniline (1.23 g, 10 mmol) to yield **224** as a yellow solid (2.17 g, 58%), mp 268-269 °C (decomp.). **^{1}H NMR** (500 MHz, DMSO-d_6) δ 10.38 (s, 1H), 9.56 (d, J = 2.5 Hz, 1H), 9.48 – 9.44 (m, 1H), 8.67 (dd, J = 4.7, 1.8

Hz, 1H), 8.59 (dt, *J* = 7.8, 2.0 Hz, 1H), 8.46 (dd, *J* = 9.0, 2.5 Hz, 1H), 7.88 (d, *J* = 9.1 Hz, 1H), 7.58 (t, *J* = 2.2 Hz, 1H), 7.52 – 7.42 (m, 2H), 7.35 (t, *J* = 8.1 Hz, 1H), 6.78 (ddd, *J* = 8.2, 2.5, 0.9 Hz, 1H), 3.81 (s, 3H). **^{13}C NMR** (126 MHz, DMSO) δ 160.63, 159.49, 158.85, 153.77, 151.66, 149.59, 144.39, 139.70, 135.54, 132.91, 129.66, 129.34, 126.89, 123.69, 120.89, 114.95, 113.47, 110.43, 108.29, 55.29. **Anal. Calcd. for $C_{20}H_{15}N_5O_3$**: C, 64.34; H, 4.05; N, 18.76. Found: C, 64.26; H, 4.16; N, 19.10.

N-(4-methoxyphenyl)-6-nitro-2-(pyridin-3-yl)quinazolin-4-amine (225).

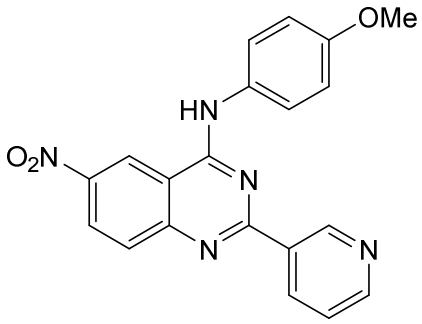

Molecular weight: 373.37 g/mol

The compound was synthesized according to the general procedure for compounds **211-239** from **206** (2.87 g, 10 mmol) and 4-methoxyaniline (1.23 g, 10 mmol) to yield **225** as a yellow solid (2.24 g, 60%), mp 269-270 °C (decomp.). **^{1}H NMR** (500 MHz, DMSO-d_6) δ 10.54 (s, 1H), 9.50 (d, *J* = 2.6 Hz, 1H), 9.47 (dd, *J* = 2.1, 0.9 Hz, 1H), 8.66 (dd, *J* = 4.7, 1.7 Hz, 1H), 8.62 (dt, *J* = 7.9, 1.9 Hz, 1H), 8.42 (dd, *J* = 9.1, 2.5 Hz, 1H), 7.79 (d, *J* = 9.1 Hz, 1H), 7.75 – 7.68 (m, 2H), 7.50 (ddd, *J* = 7.9, 4.7, 0.9 Hz, 1H), 7.08 – 6.94 (m, 2H), 3.79 (s, 3H). **^{13}C NMR** (126 MHz, DMSO) δ 161.04, 158.51, 155.77, 154.68, 151.32, 149.68, 143.63, 135.52, 133.70, 128.69, 126.37, 124.72, 123.61, 121.23, 115.36, 113.72, 55.38. **Anal. Calcd. for $C_{20}H_{15}N_5O_3$**: C, 64.34; H, 4.05; N, 18.76. Found: C, 64.48; H, 4.00; N, 18.39.

N-(4-methoxyphenyl)-6-nitro-2-(pyridin-4-yl)quinazolin-4-amine (226).

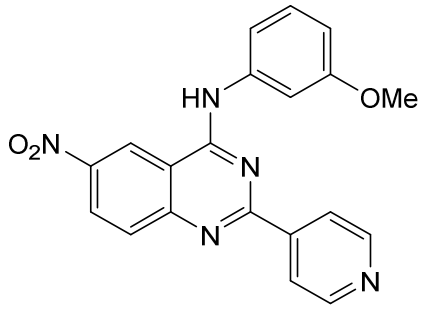

Molecular weight: 373.37 g/mol

The compound was synthesized according to the general procedure for compounds **211-239** from **207** (2.87 g, 10 mmol) and 4-methoxyaniline (1.23 g, 10 mmol) to yield **226** as an orange-red solid (2.31 g, 62%), mp 297-299 °C (decomp.). **^{1}H NMR** (500 MHz, DMSO-d_6) δ 10.71 (s, 1H), 9.67 (d, J = 2.4 Hz, 1H), 9.02 – 8.84 (m, 2H), 8.61 – 8.48 (m, 3H), 8.03 (dd, J = 9.1, 1.2 Hz, 1H), 7.83 – 7.69 (m, 2H), 7.06 (dq, J = 9.4, 2.6, 1.8 Hz, 2H), 3.82 (s, 3H). **^{13}C NMR** (126 MHz, DMSO) δ 159.30, 158.77, 156.69, 153.35, 150.11, 145.36, 145.24, 130.91, 129.98, 127.32, 124.79, 124.06, 121.01, 114.05, 113.97, 55.42. **Anal. Calcd. for $C_{20}H_{15}N_5O_3$**: C, 64.34; H, 4.05; N, 18.76. Found: C, 64.56; H, 4.27; N, 18.49.

6-nitro-N-phenyl-2-(3-(trifluoromethyl)phenyl)quinazolin-4-amine (227).

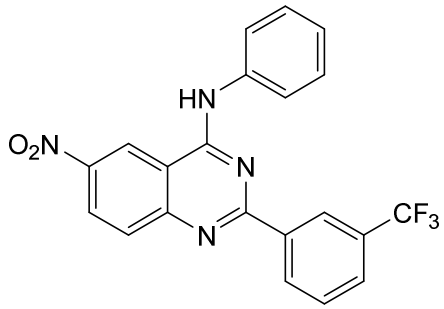

Molecular weight: 410.36 g/mol

The compound was synthesized according to the general procedure for compounds **211-239** from **208** (3.54 g, 10 mmol) and aniline (0.93 g, 10 mmol) to yield **227** as a yellow solid (3.08 g, 75%), mp 238-240 °C. **^{1}H NMR** (500 MHz, DMSO-d_6) δ 10.56 (s, 1H), 9.63 (d, J = 2.5 Hz, 1H), 8.68 (dq, J = 1.4, 0.8 Hz, 1H), 8.64 (dd, J = 7.8, 1.6 Hz, 1H),

8.53 (dd, *J* = 9.2, 2.5 Hz, 1H), 7.98 (d, *J* = 9.2 Hz, 1H), 7.92 – 7.84 (m, 3H), 7.80 – 7.68 (m, 1H), 7.53 – 7.40 (m, 2H), 7.31 – 7.20 (m, 1H). **^{13}C NMR** (126 MHz, DMSO) δ 160.63, 159.11, 153.96, 144.53, 138.52, 138.42, 132.01, 129.97, 129.79, 129.51 (d, *J* = 31.7 Hz), 129.13, 128.56, 127.66 (d, *J* = 3.3 Hz), 127.52, 127.03, 125.35, 124.86, 124.71 (d, *J* = 3.9 Hz), 123.13, 120.99, 113.55. **Anal. Calcd. for $C_{21}H_{13}F_3N_4O_2$**: C, 61.71; H, 3.29; N, 13.31. Found: C, 61.47; H, 3.19; N, 13.65.

2-nitro-4-((6-nitro-2-(3-(trifluoromethyl)phenyl)quinazolin-4-yl)amino)phenol (228).

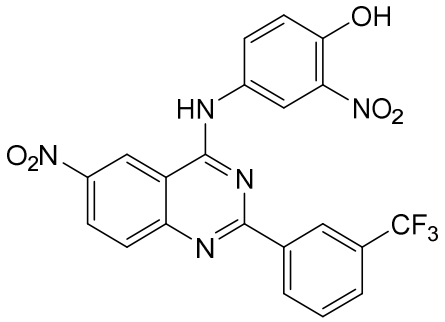

Molecular weight: 471.35 g/mol

The compound was synthesized according to the general procedure for compounds **211-239** from **208** (3.54 g, 10 mmol) and 4-amino-2-nitrophenol (1.54 g, 10 mmol) to yield **228** as a yellow solid (3.25 g, 69%), mp 280-281 °C (decomp.). **^{1}H NMR** (500 MHz, DMSO-d_6) δ 10.89 (s, 1H), 10.50 (s, 1H), 9.49 (d, *J* = 2.5 Hz, 1H), 8.66 – 8.57 (m, 3H), 8.46 (dd, *J* = 9.1, 2.4 Hz, 1H), 7.97 (dd, *J* = 9.0, 2.7 Hz, 1H), 7.91 (d, *J* = 9.1 Hz, 1H), 7.85 (ddt, *J* = 7.7, 1.9, 1.0 Hz, 1H), 7.73 – 7.66 (m, 1H), 7.20 (d, *J* = 9.0 Hz, 1H). **^{13}C NMR** (126 MHz, DMSO) δ 160.45, 158.71, 153.68, 149.33, 144.48, 138.27, 135.57, 132.08, 130.15, 130.12, 129.81 (d, *J* = 3.5 Hz), 129.67, 129.41, 127.71, 127.69, 126.98, 124.61, 124.58, 124.21 (d, *J* = 272.4 Hz), 120.69, 119.19, 118.72, 113.34. **Anal. Calcd. for $C_{21}H_{12}F_3N_5O_5$**: C, 53.51; H, 2.57; N, 14.86. Found: C, 53.75; H, 2.61; N, 14.59.

6-nitro-N-(3-nitrophenyl)-2-(3-(trifluoromethyl)phenyl)quinazolin-4-amine (229).

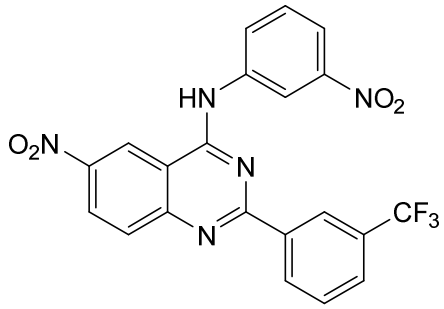

Molecular weight: 455.35 g/mol

The compound was synthesized according to the general procedure for compounds **211-239** from **208** (3.54 g, 10 mmol) and 3-nitroaniline (1.38 g, 10 mmol) to yield **229** as a yellow solid (3.92 g, 86%), mp 278-279 °C. **^{1}H NMR** (500 MHz, DMSO-d_6) δ 10.87 (s, 1H), 9.69 (s, 1H), 9.10 (d, J = 2.6 Hz, 1H), 8.74 (d, J = 16.3 Hz, 2H), 8.63 – 8.56 (m, 1H), 8.30 (d, J = 8.2 Hz, 1H), 8.08 (t, J = 8.1 Hz, 2H), 7.93 (d, J = 8.0 Hz, 1H), 7.77 (q, J = 8.2 Hz, 2H). **^{13}C NMR** (126 MHz, DMSO) δ 160.46, 159.11, 153.84, 147.92, 144.79, 138.27, 132.17, 130.07, 129.98, 128.39, 127.89, 127.35, 124.65, 120.93, 118.85, 116.87. **Anal. Calcd. for $C_{21}H_{12}F_3N_5O_4$**: C, 55.39; H, 2.66; N, 15.38. Found: C, 55.35; H, 2.61; N, 15.08.

6-nitro-N-(4-nitrophenyl)-2-(3-(trifluoromethyl)phenyl)quinazolin-4-amine (230).

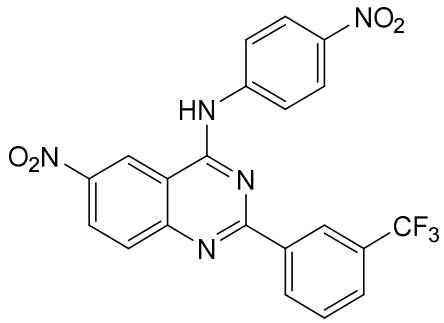

Molecular weight: 455.35 g/mol

The compound was synthesized according to the general procedure for compounds **211-239** from **208** (3.54 g, 10 mmol) and 4-nitroaniline (1.38 g, 10 mmol) to yield **230** as a bright yellow solid (3.23 g, 71%), mp >300 °C. **^{1}H NMR** (500 MHz, DMSO-d_6) δ 10.86

(s, 1H), 9.63 (d, *J* = 2.4 Hz, 1H), 8.68 (s, 1H), 8.66 (d, *J* = 7.9 Hz, 1H), 8.57 (dd, *J* = 9.1, 2.5 Hz, 1H), 8.36 – 8.30 (m, 2H), 8.25 – 8.19 (m, 2H), 8.05 (d, *J* = 9.2 Hz, 1H), 7.91 (d, *J* = 7.7 Hz, 1H), 7.80 (q, *J* = 8.3, 7.8 Hz, 1H). **^{13}C NMR** (126 MHz, DMSO) δ 160.41, 158.98, 153.87, 145.14, 144.84, 142.85, 138.11, 132.24, 130.25, 130.09, 129.73, 129.48, 127.92, 127.89, 127.41, 124.69, 124.66, 124.54, 123.17, 122.09, 121.00, 120.32, 120.27, 113.76. **Anal. Calcd. for $C_{21}H_{12}F_3N_5O_4$**: C, 55.39; H, 2.66; N, 15.38. Found: C, 55.42; H, 2.67; N, 15.12.

3-((6-nitro-2-(3-(trifluoromethyl)phenyl)quinazolin-4-yl)amino)phenol (231).

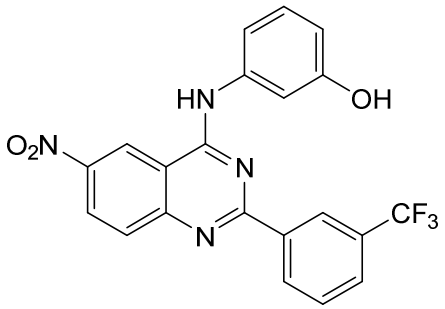

Molecular weight: 426.36 g/mol

The compound was synthesized according to the general procedure for compounds **211-239** from **208** (3.54 g, 10 mmol) and 3-aminophenol (1.09 g, 10 mmol) to yield **231** as a yellow solid (3.54 g, 83%), mp 275-278 °C (decomp.). **^{1}H NMR** (500 MHz, DMSO-*d*6) δ 10.64 (s, 1H), 9.68 (d, *J* = 2.6 Hz, 1H), 8.55 (dd, *J* = 9.2, 2.4 Hz, 1H), 8.46 (ddd, *J* = 6.4, 3.1, 1.4 Hz, 2H), 8.20 – 8.09 (m, 2H), 8.11 – 8.03 (m, 2H), 8.00 (d, *J* = 9.2 Hz, 1H), 7.65 – 7.48 (m, 3H). **^{13}C NMR** (126 MHz, DMSO) δ 165.49, 162.17, 158.92, 154.15, 144.43, 143.31, 137.35, 131.46, 130.01, 129.85, 128.80, 128.57, 127.10, 125.07, 121.73, 121.08, 113.46. **Anal. Calcd. for $C_{21}H_{13}F_3N_4O_3$**: C, 59.16; H, 3.07; N, 13.14. Found: C, 59.29; H

N-(3-methoxyphenyl)-6-nitro-2-(3-(trifluoromethyl)phenyl)quinazolin-4-amine (232).

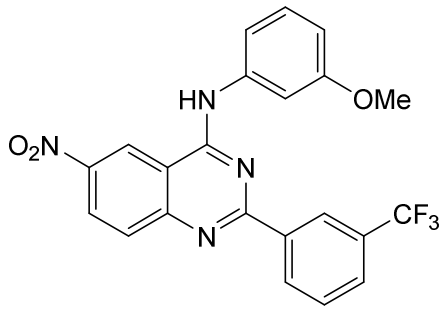

Molecular weight: 440.38 g/mol

The compound was synthesized according to the general procedure for compounds **211-239** from **208** (3.54 g, 10 mmol) and 3-methoxyaniline (1.23 g, 10 mmol) to yield **232** as a yellow solid (3.21 g, 73%), mp 207-209 °C. **^{1}H NMR** (500 MHz, DMSO-d_6) δ 10.48 (s, 1H), 9.62 (d, J = 2.5 Hz, 1H), 8.71 – 8.63 (m, 2H), 8.52 (dd, J = 9.1, 2.5 Hz, 1H), 7.98 (d, J = 9.2 Hz, 1H), 7.92 – 7.85 (m, 1H), 7.75 (tt, J = 7.5, 0.8 Hz, 1H), 7.60 (t, J = 2.2 Hz, 1H), 7.47 (ddd, J = 8.0, 2.0, 0.9 Hz, 1H), 7.36 (t, J = 8.1 Hz, 1H), 6.81 (ddd, J = 8.2, 2.5, 0.9 Hz, 1H), 3.81 (s, 3H). **^{13}C NMR** (126 MHz, DMSO) δ 160.63, 159.56, 159.06, 153.91, 144.56, 139.65, 138.57, 132.04, 129.94, 129.82, 129.55 (d, J = 31.8 Hz), 129.29, 129.17, 127.72, 127.69, 127.04, 125.35, 124.69, 124.66, 123.19, 120.96, 115.09, 113.59, 110.62, 108.51, 55.27. **Anal. Calcd. for $C_{22}H_{15}F_3N_4O_3$**: C, 60.00; H, 3.43; N, 12.72. Found: C, 59.99; H, 3.34; N, 12.34.

N-(3,4-dimethoxyphenyl)-6-nitro-2-(3-(trifluoromethyl)phenyl)quinazolin-4-amine (233).

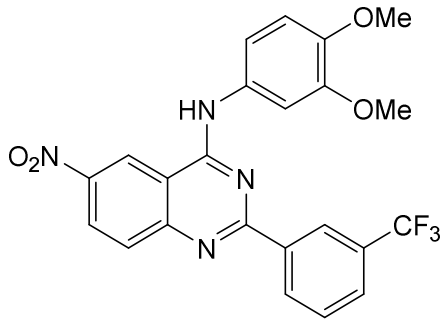

Molecular weight: 470.41 g/mol

The compound was synthesized according to the general procedure for compounds **211-239** from **208** (3.54 g, 10 mmol) and 3,4-dimethoxyaniline (1.53 g, 10 mmol) to yield **233** as a red solid (2.78 g, 59%), mp 217-218 °C. **^{1}H NMR** (500 MHz, DMSO-d_6) δ 10.45 (s, 1H), 9.59 (d, *J* = 2.4 Hz, 1H), 8.69 – 8.59 (m, 2H), 8.50 (dd, *J* = 9.2, 2.5 Hz, 1H), 7.95 (d, *J* = 9.2 Hz, 1H), 7.92 – 7.83 (m, 1H), 7.78 – 7.70 (m, 1H), 7.60 (d, *J* = 2.4 Hz, 1H), 7.35 (dd, *J* = 8.6, 2.5 Hz, 1H), 7.02 (d, *J* = 8.7 Hz, 1H), 3.81 (s, 3H), 3.80 (s, 3H). **^{13}C NMR** (126 MHz, DMSO) δ 160.66, 158.88, 153.68, 148.51, 146.22, 144.45, 138.56, 132.09, 131.62, 129.89, 129.53, 129.47 (d, *J* = 31.8 Hz), 127.69, 127.66, 127.52, 126.96, 124.59 (d, *J* = 3.7 Hz), 124.28 (d, *J* = 272.4 Hz), 120.87, 115.10, 113.52, 111.70, 107.98, 55.88, 55.60. **Anal. Calcd. for $C_{23}H_{17}F_3N_4O_4$**: C, 58.73; H, 3.64; N, 11.91. Found: C, 58.53; H, 3.63; N, 11.58.

N-(3-(methylthio)phenyl)-6-nitro-2-(3-(trifluoromethyl)phenyl)quinazolin-4-amine (234).

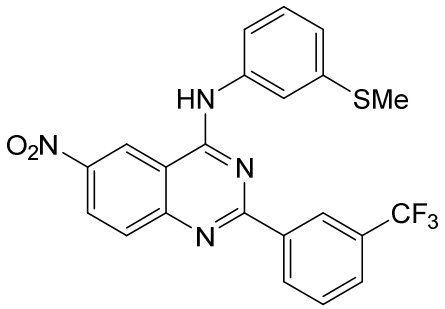

Molecular weight: 456.44 g/mol

The compound was synthesized according to the general procedure for compounds **211-239** from **208** (3.54 g, 10 mmol) and 3-(methylthio)aniline (1.39 g, 10 mmol) to yield **234** as an orange solid (3.56 g, 78%), mp 209-211 °C. **^{1}H NMR** (600 MHz, DMSO-d_6) δ 10.48 (s, 1H), 9.58 (d, *J* = 2.5 Hz, 1H), 8.68 – 8.61 (m, 2H), 8.50 (dd, *J* = 9.1, 2.4 Hz, 1H), 7.96 (d, *J* = 9.1 Hz, 1H), 7.90 – 7.83 (m, 2H), 7.76 – 7.70 (m, 1H), 7.66 (ddd, *J* = 8.1, 2.1, 0.9 Hz, 1H), 7.39 (t, *J* = 7.9 Hz, 1H), 7.12 (ddd, *J* = 7.9, 1.9, 0.9 Hz, 1H), 2.51 (s, 3H). **^{13}C NMR** (151 MHz, DMSO) δ 160.55, 159.03, 153.87, 144.53, 139.01, 138.64, 138.49, 132.06, 129.89, 129.82, 129.56 (d, *J* = 31.8 Hz), 129.03, 127.76, 127.05, 125.16, 124.61 (d, *J* = 4.0 Hz), 123.35, 122.17, 120.91, 120.12, 119.36, 113.54, 14.94. **Anal.**

Calcd. for $C_{22}H_{15}F_3N_4O_2S$: C, 57.89; H, 3.31; N, 12.27. Found: C, 57.99; H, 3.25; N, 12.03.

N-(3-fluorophenyl)-6-nitro-2-(3-(trifluoromethyl)phenyl)quinazolin-4-amine (235).

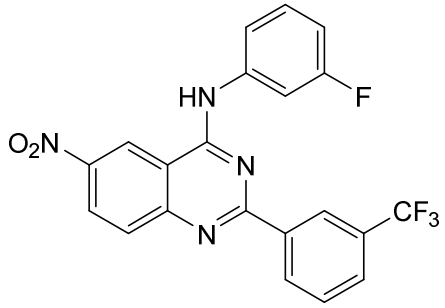

Molecular weight: 428.35 g/mol

The compound was synthesized according to the general procedure for compounds **211-239** from **208** (3.54 g, 10 mmol) and 3-fluoroaniline (1.11 g, 10 mmol) to yield **235** as a yellow solid (3.47 g, 81%), mp 238-239 °C. **^{1}H NMR** (500 MHz, DMSO-d_6) δ 10.52 (s, 1H), 9.54 (d, *J* = 2.5 Hz, 1H), 8.61 (td, *J* = 1.7, 0.8 Hz, 1H), 8.59 (dd, *J* = 7.8, 1.5 Hz, 1H), 8.48 (dd, *J* = 9.1, 2.5 Hz, 1H), 7.98 – 7.82 (m, 3H), 7.77 – 7.68 (m, 1H), 7.65 (ddd, *J* = 8.1, 2.0, 0.9 Hz, 1H), 7.46 (td, *J* = 8.2, 6.8 Hz, 1H), 7.04 (tdd, *J* = 8.4, 2.6, 0.8 Hz, 1H). **^{13}C NMR** (126 MHz, DMSO) δ 163.02, 161.10, 160.41, 158.86, 153.76, 144.55, 140.25 (d, *J* = 11.0 Hz), 138.30, 131.89, 130.08, 130.01, 129.92, 129.84, 129.67, 129.42, 129.16, 127.72, 127.69, 127.47, 127.04, 125.30, 124.65 (d, *J* = 3.9 Hz), 123.14, 120.81, 118.32 (d, *J* = 2.3 Hz), 113.43, 111.05 (d, *J* = 21.0 Hz), 109.62 (d, *J* = 26.2 Hz). **Anal. Calcd. for $C_{21}H_{12}F_4N_4O_2$**: C, 58.88; H, 2.82; N, 13.08. Found: C, 58.91; H, 2.73; N, 12.81.

N-(3-((6-nitro-2-(3-(trifluoromethyl)phenyl)quinazolin-4-yl)amino)phenyl)acetamide (236).

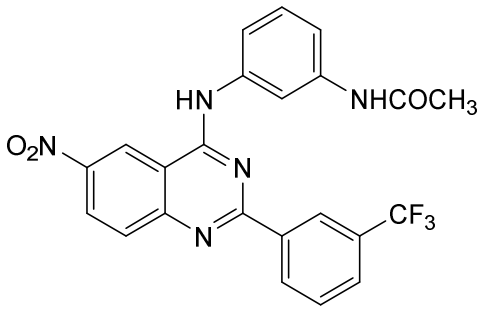

Molecular weight: 467.41 g/mol

The compound was synthesized according to the general procedure for compounds **211-239** from **208** (3.54 g, 10 mmol) and N-(3-aminophenyl)acetamide (1.50 g, 10 mmol) to yield **236** as a yellow solid (2.85 g, 61%), mp >300 °C. **^{1}H NMR** (500 MHz, DMSO-d_6) δ 10.63 (s, 1H), 10.04 (s, 1H), 9.68 (d, *J* = 2.5 Hz, 1H), 8.80 – 8.63 (m, 2H), 8.55 (dd, *J* = 9.2, 2.5 Hz, 1H), 8.43 (t, *J* = 2.1 Hz, 1H), 8.01 (d, *J* = 9.1 Hz, 1H), 7.89 (dd, *J* = 7.9, 1.5 Hz, 1H), 7.75 (t, *J* = 7.8 Hz, 1H), 7.53 (ddd, *J* = 8.0, 2.2, 1.1 Hz, 1H), 7.37 (t, *J* = 8.0 Hz, 1H), 7.29 (ddd, *J* = 8.0, 2.1, 1.1 Hz, 1H), 2.07 (s, 3H). **^{13}C NMR** (126 MHz, DMSO) δ 168.46, 160.66, 159.16, 153.79, 144.58, 139.76, 138.62, 138.32, 132.32, 129.91, 129.62, 129.39, 129.14, 128.55, 127.75, 127.73, 127.12, 125.02, 124.99, 124.28 (d, *J* = 272.3 Hz), 121.14, 117.85, 115.55, 114.05, 113.58, 24.10. **Anal. Calcd. for $C_{23}H_{16}F_3N_5O_3$**: C, 59.10; H, 3.45; N, 14.98. Found: C, 59.42; H, 3.59; N, 14.73.

4-((2-(3-methoxyphenyl)-6-nitroquinazolin-4-yl)amino)benzonitrile (237).

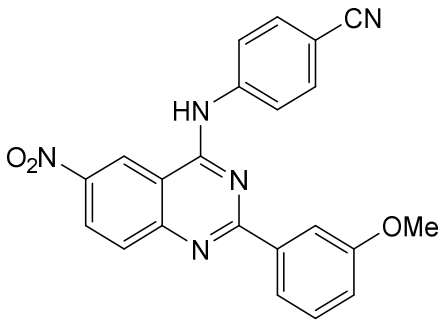

Molecular weight: 397.39 g/mol

The compound was synthesized according to the general procedure for compounds **211-239** from **209** (3.16 g, 10 mmol) and 4-aminobenzonitrile (1.18 g, 10 mmol) to yield **237** as a yellow solid (2.34 g, 59%), mp 184-186 °C. **^{1}H NMR** (500 MHz, DMSO-d_6) δ 10.63 (s, 1H), 9.56 (d, *J* = 2.4 Hz, 1H), 8.50 (dt, *J* = 9.0, 2.8 Hz, 1H), 8.20 – 8.11 (m, 2H), 7.99 – 7.92 (m, 2H), 7.91 – 7.87 (m, 3H), 7.40 (t, *J* = 7.9 Hz, 1H), 7.09 (ddd, *J* = 8.2, 2.7, 0.9 Hz, 1H), 3.83 (s, 3H). **^{13}C NMR** (126 MHz, DMSO) δ 161.71, 159.53, 158.73, 154.03, 144.44, 143.21, 138.64, 132.93, 129.90, 129.81, 127.11, 122.36, 120.96, 120.91, 119.15, 117.66, 113.42, 113.05, 105.82, 55.20. **Anal. Calcd. for $C_{22}H_{15}N_5O_3$**: C, 66.49; H, 3.80; N, 17.62. Found: C, 66.24; H, 4.00; N, 17.33.

N-(3-fluorophenyl)-2-(3-methoxyphenyl)-6-nitroquinazolin-4-amine (238).

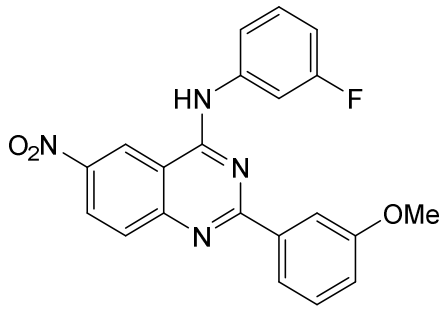

Molecular weight: 390.37 g/mol

The compound was synthesized according to the general procedure for compounds **211-239** from **209** (3.16 g, 10 mmol) and 3-fluoroaniline (1.11 g, 10 mmol) to yield **238** as a yellow-orange solid (3.44 g, 88%), mp 276-277 °C (decomp.). **^{1}H NMR** (500 MHz, DMSO-d_6) δ 10.51 (s, 1H), 9.61 (d, *J* = 2.5 Hz, 1H), 8.51 (dd, *J* = 9.2, 2.5 Hz, 1H), 8.05 – 7.91 (m, 4H), 7.71 (ddd, *J* = 8.3, 2.0, 0.9 Hz, 1H), 7.49 (td, *J* = 8.3, 6.9 Hz, 1H), 7.42 (t, *J* = 7.9 Hz, 1H), 7.10 (ddd, *J* = 8.2, 2.8, 1.0 Hz, 1H), 7.03 (tdd, *J* = 8.4, 2.6, 0.9 Hz, 1H), 3.83 (s, 3H). **^{13}C NMR** (126 MHz, DMSO) δ 162.07 (d, *J* = 241.3 Hz), 161.84, 159.53, 158.80, 154.04, 144.34, 140.53 (d, *J* = 11.1 Hz), 138.88, 130.13 (d, *J* = 9.4 Hz), 129.81, 129.74, 126.96, 120.91, 120.82, 118.26, 118.24, 117.70, 113.32, 112.96, 110.83 (d, *J* = 21.1 Hz), 109.47 (d, *J* = 26.2 Hz), 55.08. **Anal. Calcd. for $C_{21}H_{15}FN_4O_3$**: C, 64.61; H, 3.87; N, 14.35. Found: C, 64.84; H, 3.93; N, 14.23.

2-(3,4-dimethoxyphenyl)-6-nitro-N-(3-(trifluoromethyl)phenyl)quinazolin-4-amine (239).

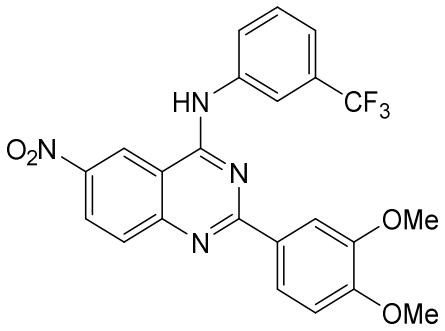

Molecular weight: 470.41 g/mol

The compound was synthesized according to the general procedure for compounds **211-239** from **210** (3.46 g, 10 mmol) and 3-(trifluoromethyl)aniline (1.61 g, 10 mmol) to yield **239** as an orange solid (3.39 g, 72%), mp >300 °C. **^{1}H NMR** (600 MHz, DMSO-d_6) δ 10.63 (s, 1H), 9.64 (d, *J* = 2.4 Hz, 1H), 8.54 (dd, *J* = 9.2, 2.4 Hz, 1H), 8.41 (d, *J* = 2.0 Hz, 1H), 8.31 – 8.23 (m, 1H), 8.07 (dd, *J* = 8.4, 2.0 Hz, 1H), 8.01 (d, *J* = 2.0 Hz, 1H), 7.97 (d, *J* = 9.1 Hz, 1H), 7.72 (t, *J* = 8.0 Hz, 1H), 7.55 (d, *J* = 7.9 Hz, 1H), 7.08 (d, *J* = 8.5 Hz, 1H), 3.85 (s, 3H), 3.84 (s, 3H). **^{13}C NMR** (126 MHz, DMSO) δ 161.85, 158.65, 154.21, 152.00, 148.67, 143.93, 139.69, 129.79, 129.74, 129.51, 126.94, 126.09, 125.46, 123.29, 122.15, 120.91, 120.49 (d, *J* = 3.5 Hz), 118.73 (d, *J* = 3.8 Hz), 112.94, 111.36, 55.74, 55.38. **Anal. Calcd. for $C_{23}H_{17}F_3N_4O_4$**: C, 58.73; H, 3.64; N, 11.91. Found: C, 58.79; H, 3.92; N, 11.65.

General Procedure for the Preparation of compounds 240-244. The corresponding 2- and 4-substituted 6-nitroquinazoline derivative (1 mmol) was dissolved in dry THF (200 mL) and added to a pressure vessel together with 1% (by weight of the educt) of palladium on activated charcoal. After evacuating and flushing the vessel with N_2 three times, it was pressurized with hydrogen gas (4 bar) and sealed. The mixture was stirred for 24 h at room temperature until completion of the reaction indicated by TLC. Charcoal was removed by several filtration cycles and the remaining solvent evaporated under reduced pressure to obtain the corresponding compound as a solid product. Purification was carried out by column chromatography using DCM and methanol as eluent.

N4-(3-methoxyphenyl)-2-(pyridin-3-yl)quinazoline-4,6-diamine (240).

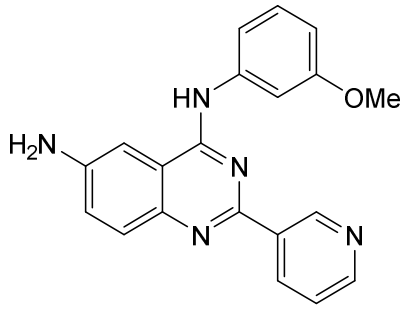

Molecular weight: 343.39 g/mol

The compound was synthesized according to the general procedure for compounds **240-244** from **224** (3.73 g, 10 mmol) to yield **240** as a yellow solid (1.65 g, 45%), mp 209-211 °C. **^{1}H NMR** (500 MHz, DMSO-d_6) δ 9.50 (dd, *J* = 2.1, 0.9 Hz, 1H), 9.44 (s, 1H), 8.68 – 8.57 (m, 2H), 7.72 (t, *J* = 2.3 Hz, 1H), 7.64 (d, *J* = 8.8 Hz, 1H), 7.56 – 7.52 (m, 1H), 7.49 (ddd, *J* = 7.9, 4.8, 0.9 Hz, 1H), 7.41 (d, *J* = 2.4 Hz, 1H), 7.33 (d, *J* = 8.2 Hz, 1H), 7.31 – 7.25 (m, 1H), 6.69 (ddd, *J* = 8.2, 2.5, 0.9 Hz, 1H), 5.65 (s, 2H), 3.81 (s, 3H). **^{13}C NMR** (126 MHz, DMSO) δ 159.53, 156.25, 152.87, 150.10, 148.73, 147.73, 143.12, 141.26, 134.36, 134.31, 129.28, 125.01, 124.04, 123.60, 115.91, 113.89, 108.86, 107.15, 101.49, 55.17. **Anal. Calcd. for $C_{20}H_{17}N_5O$**: C, 69.96; H, 4.99; N, 20.40. Found: C, 69.83; H, 5.21; N, 20.47.

N4-(4-methoxyphenyl)-2-(pyridin-3-yl)quinazoline-4,6-diamine (241).

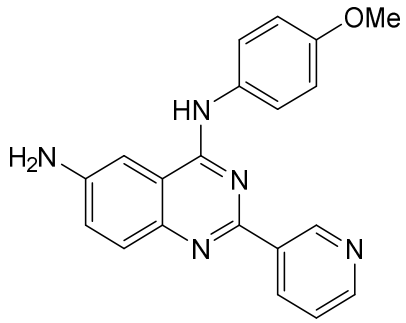

Molecular weight: 343.39 g/mol

The compound was synthesized according to the general procedure for compounds **240-244** from **225** (3.73 g, 10 mmol) to yield **241** as a yellow solid (2.13 g, 62%), mp 202-203 °C. **^{1}H NMR** (500 MHz, DMSO-d_6) δ 9.45 (d, *J* = 2.1 Hz, 1H), 9.39 (s, 1H), 8.63 –

8.54 (m, 2H), 7.86 – 7.75 (m, 2H), 7.60 (d, *J* = 8.8 Hz, 1H), 7.47 (dd, *J* = 7.8, 4.8 Hz, 1H), 7.40 (d, *J* = 2.4 Hz, 1H), 7.25 (dd, *J* = 8.9, 2.2 Hz, 1H), 7.07 – 6.95 (m, 2H), 5.60 (s, 2H), 3.79 (s, 3H). **^{13}C NMR** (126 MHz, DMSO) δ 156.46, 155.47, 153.04, 149.97, 148.75, 147.55, 142.90, 139.28, 134.36, 132.88, 129.15, 125.01, 123.69, 123.54, 115.72, 113.74, 101.63, 55.36. **Anal. Calcd. for $C_{20}H_{17}N_5O$**: C, 69.96; H, 4.99; N, 20.40. Found: C, 70.16; H, 5.32; N, 20.56.

N4-phenyl-2-(3-(trifluoromethyl)phenyl)quinazoline-4,6-diamine (242).

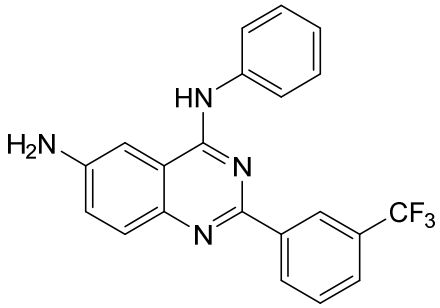

Molecular weight: 380.37 g/mol

The compound was synthesized according to the general procedure for compounds **240-244** from **227** (4.10 g, 10 mmol) to yield **242** as a beige solid (2.40 g, 63%), mp 191-192 °C. **^{1}H NMR** (500 MHz, DMSO-d_6) δ 9.50 (s, 1H), 8.67 (d, *J* = 1.7 Hz, 1H), 8.62 (dd, *J* = 7.8, 1.5 Hz, 1H), 7.96 – 7.90 (m, 2H), 7.80 – 7.74 (m, 1H), 7.75 – 7.68 (m, 1H), 7.66 (d, *J* = 8.8 Hz, 1H), 7.45 – 7.37 (m, 3H), 7.28 (dd, *J* = 8.9, 2.3 Hz, 1H), 7.12 (tt, *J* = 7.4, 1.2 Hz, 1H), 5.66 (s, 2H). **^{13}C NMR** (126 MHz, DMSO) δ 156.36, 153.02, 147.79, 143.11, 140.02, 139.96, 130.84, 129.71, 129.35 (d, *J* = 31.5 Hz), 129.35, 128.42, 125.77 (d, *J* = 3.5 Hz), 125.58, 124.05, 123.57 (d, *J* = 3.8 Hz), 123.25, 122.00, 115.90, 101.52. **Anal. Calcd. for $C_{21}H_{15}F_3N_4$**: C, 66.31; H, 3.98; N, 14.73. Found: C, 66.42; H, 4.07; N, 14.45.

3-((6-amino-2-(3-(trifluoromethyl)phenyl)quinazolin-4-yl)amino)phenol (243).

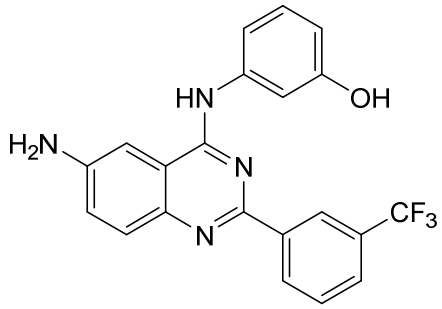

Molecular weight: 396.37 g/mol

The compound was synthesized according to the general procedure for compounds **240-244** from **231** (4.26 g, 10 mmol) to yield **243** as a yellow solid (2.89 g, 73%), mp 190-192 °C. **^{1}H NMR** (500 MHz, DMSO-d_6) δ 9.72 (s, 1H), 8.42 – 8.36 (m, 2H), 8.21 – 8.13 (m, 2H), 8.04 – 7.99 (m, 2H), 7.65 (d, *J* = 8.9 Hz, 1H), 7.54 – 7.47 (m, 2H), 7.47 – 7.38 (m, 2H), 7.30 (dd, *J* = 8.9, 2.4 Hz, 1H), 5.66 (s, 2H). **^{13}C NMR** (126 MHz, DMSO) δ 165.65, 155.88, 154.46, 147.57, 144.96, 143.68, 138.77, 130.03, 129.50, 129.30, 128.53, 127.34, 124.37, 123.37, 120.23, 115.87, 101.34. **Anal. Calcd. for $C_{21}H_{15}F_3N_4O$**: C, 63.63; H, 3.81; N, 14.14. Found: C, 63.49; H, 4.14; N, 14.08.

N4-(3-methoxyphenyl)-2-(3-(trifluoromethyl)phenyl)quinazoline-4,6-diamine (244).

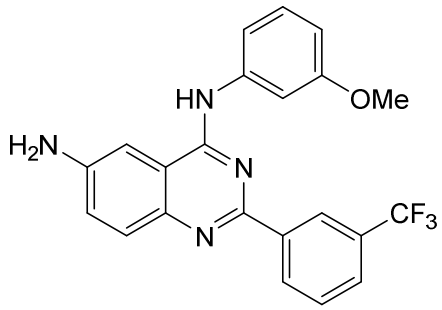

Molecular weight: 410.40 g/mol

The compound was synthesized according to the general procedure for compounds **240-244** from **232** (4.40 g, 10 mmol) to yield **244** as a beige solid (2.42 g, 59%), mp 203-205 °C. **^{1}H NMR** (500 MHz, DMSO-d_6) δ 9.46 (s, 1H), 8.71 – 8.61 (m, 2H), 7.81 – 7.75 (m, 1H), 7.74 – 7.68 (m, 2H), 7.66 (d, *J* = 8.9 Hz, 1H), 7.50 (ddd, *J* = 8.1, 2.0, 0.9 Hz, 1H), 7.41 (d, *J* = 2.4 Hz, 1H), 7.33 – 7.26 (m, 2H), 6.69 (ddd, *J* = 8.2, 2.5, 0.9 Hz, 1H), 5.67

(s, 2H), 3.80 (s, 3H). **^{13}C NMR** (126 MHz, DMSO) δ 159.54, 156.27, 152.97, 147.80, 143.08, 141.20, 140.04, 130.86, 129.65, 129.50, 129.35, 129.24, 129.10, 127.71, 125.80, 125.55, 124.07, 123.50, 123.38, 115.95, 113.95, 108.99, 107.22, 101.46, 55.11. Anal. Calcd. for $C_{22}H_{17}F_3N_4O$: C, 64.39; H, 4.18; N, 13.65. Found: C, 64.32; H, 4.29; N, 13.40.

General Procedure for the Preparation of compounds 245-248.

The corresponding 6-amino-derivative **240** or **241** (10 mmol) was dissolved in a solution of 20 mL TAM in 80 mL THF under nitrogen in a Schlenk flask. The temperature was adjusted with a cooling bath to 0 °C and a solution of two (20 mmol, for **245**) or one equivalent (10 mmol, for **246**-**248**) of the corresponding acid chloride in THF added drop wise, respectively. After 30 min the cooling bath was removed and the solution was stirred for further 6-12 h. Completion of the reaction was monitored by TLC and the excess THF removed under reduced pressure. Water was added to the mixture until precipitation of the product was visible. The formed precipitate was then filtered with suction and washed thoroughly with water. Recrystallization of the product was carried out with MeOH/H_2O to yield compounds **245**-**248**.

(E)-acetic (E)-N-(4-((3-methoxyphenyl)amino)-2-(pyridin-3-yl)quinazolin-6-yl)acetimidic anhydride (245).

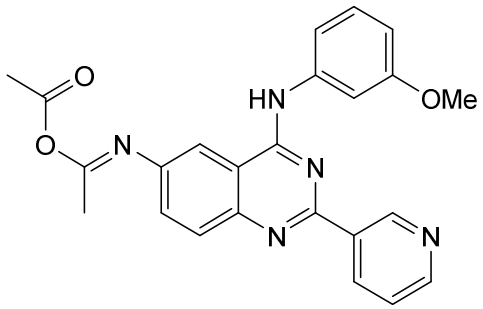

Molecular weight: 427.46 g/mol

The compound was synthesized according to the general procedure for compounds **245-248** from **240** (4.28 g, 10 mmol) and acetyl chloride (0.78 g, 20 mmol) to yield **245** as a beige-white solid (3.16 g, 74%), mp 242-244 °C. **^{1}H NMR** (500 MHz, DMSO-d_6) δ 10.50 (s, 1H), 9.56 (s, 1H), 8.77 – 8.67 (m, 2H), 8.60 (d, J = 2.3 Hz, 1H), 8.17 – 8.08 (m, 2H), 7.58 (dd, J = 7.7, 5.0 Hz, 1H), 7.52 – 7.46 (m, 2H), 7.04 – 6.96 (m, 2H), 3.74 (s, 3H),

2.15 (s, 3H), 2.10 (s, 3H). **^{13}C NMR** (126 MHz, DMSO) δ 170.67, 169.36, 162.31, 158.82, 156.77, 151.46, 149.33, 149.09, 139.44, 135.17, 133.36, 132.55, 129.45, 128.62, 124.03, 120.74, 114.87, 111.37, 55.49, 24.32, 22.98. **Anal. Calcd. for $C_{24}H_{21}N_5O_3$**: C, 67.44; H, 4.95; N; 16.38. Found: C, 67.72; H, 5.20; N; 16.07.

N-(4-((3-methoxyphenyl)amino)-2-(pyridin-3-yl)quinazolin-6-yl)-3-nitrobenzamide (246).

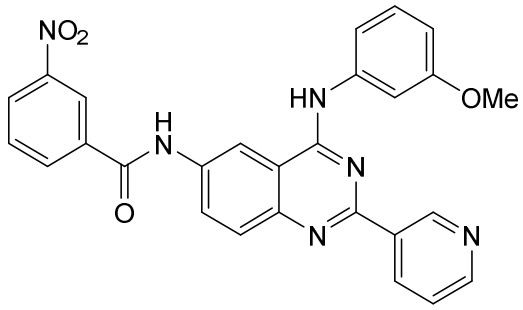

Molecular weight: 492.50 g/mol

The compound was synthesized according to the general procedure for compounds **245-248** from **240** (4.28 g, 10 mmol) and 3-nitrobenzoyl chloride (1.86 g, 10 mmol) to yield **246** as a beige-white solid (3.99 g, 81%), mp >300 °C. **^{1}H NMR** (500 MHz, DMSO-d_6) δ 10.97 (s, 1H), 9.97 (s, 1H), 9.55 (d, J = 1.9 Hz, 1H), 8.98 – 8.84 (m, 2H), 8.68 (td, J = 6.9, 5.8, 1.9 Hz, 2H), 8.56 – 8.42 (m, 2H), 8.10 (dd, J = 8.9, 2.2 Hz, 1H), 7.94 (d, J = 8.8 Hz, 1H), 7.89 (t, J = 8.0 Hz, 1H), 7.67 (t, J = 2.3 Hz, 1H), 7.59 – 7.50 (m, 2H), 7.36 (t, J = 8.1 Hz, 1H), 6.75 (dd, J = 8.3, 2.5 Hz, 1H), 3.82 (s, 3H). **^{13}C NMR** (126 MHz, DMSO) δ 163.56, 159.52, 157.89, 156.81, 150.94, 149.21, 148.00, 147.77, 140.64, 136.43, 135.92, 135.00, 134.30, 133.77, 130.53, 129.31, 128.78, 128.76, 126.57, 123.71, 122.51, 114.55, 114.51, 109.63, 107.84, 55.22. **Anal. Calcd. for $C_{27}H_{20}N_6O_4$**: C, 65.85; H, 4.09; N; 17.06. Found: C, 65.73; H, 4.37 N; 17.03.

N-(4-((4-methoxyphenyl)amino)-2-(pyridin-3-yl)quinazolin-6-yl)-3-nitrobenzamide (247).

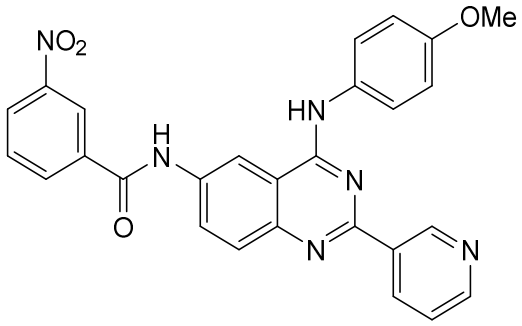

Molecular weight: 492.50 g/mol

The compound was synthesized according to the general procedure for compounds **245-248** from **241** (4.28 g, 10 mmol) and 3-nitrobenzoyl chloride (1.86 g, 10 mmol) to yield **247** as a yellow solid (3.35 g, 68%), mp >300 °C. **^{1}H NMR** (500 MHz, DMSO-d_6) δ 11.03 (s, 1H), 9.96 (s, 1H), 9.50 (d, J = 2.1 Hz, 1H), 8.93 (s, 1H), 8.90 (s, 1H), 8.67 – 8.62 (m, 2H), 8.51 (s, 1H), 8.48 (d, J = 8.2 Hz, 1H), 8.09 (d, J = 8.9 Hz, 1H), 7.90 (d, J = 8.7 Hz, 2H), 7.81 (d, J = 8.4 Hz, 2H), 7.55 – 7.48 (m, 1H), 7.04 (d, J = 8.5 Hz, 2H), 3.80 (s, 3H). **^{13}C NMR** (126 MHz, DMSO) δ 163.51, 158.01, 156.92, 155.93, 150.81, 149.22, 148.00, 147.62, 136.30, 135.96, 135.01, 134.31, 133.85, 132.24, 130.49, 128.63, 128.50, 126.53, 124.30, 123.66, 122.55, 114.57, 114.37, 113.79, 55.38. **Anal. Calcd. for $C_{27}H_{20}N_6O_4$**: C, 65.85; H, 4.09; N, 17.06. Found: C, 65.61; H, 4.44; N, 16.77.

N-(4-((3-methoxyphenyl)amino)-2-(pyridin-3-yl)quinazolin-6-yl)-3-nitrobenzamide (248).

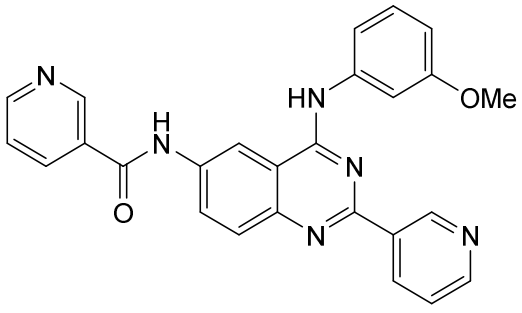

Molecular weight: 448.49 g/mol

The compound was synthesized according to the general procedure for compounds **245-248** from **240** (4.28 g, 10 mmol) and nicotinoyl chloride (1.42 g, 10 mmol) to yield **248** as a yellow solid (2.56 g, 57%), mp 204-206 °C. ^{1}H NMR (500 MHz, DMSO-d_6) δ 9.96 (s, 1H), 9.55 (d, *J* = 2.0 Hz, 1H), 9.21 (d, *J* = 2.3 Hz, 1H), 8.94 (d, *J* = 2.2 Hz, 1H), 8.80 (dd, *J* = 4.8, 1.5 Hz, 1H), 8.75 – 8.65 (m, 2H), 8.39 (dt, *J* = 7.8, 2.1 Hz, 1H), 8.05 (dd, *J* = 8.9, 2.2 Hz, 1H), 7.93 (d, *J* = 8.9 Hz, 1H), 7.67 (t, *J* = 2.3 Hz, 1H), 7.62 (ddd, *J* = 7.9, 4.8, 0.9 Hz, 1H), 7.58 – 7.51 (m, 2H), 7.36 (t, *J* = 8.1 Hz, 1H), 6.80 – 6.70 (m, 1H), 3.82 (d, *J* = 0.8 Hz, 3H). ^{13}C NMR (126 MHz, DMSO) δ 164.29, 159.54, 157.90, 156.75, 152.53, 150.94, 149.22, 148.86, 147.70, 140.69, 136.59, 135.59, 135.00, 133.80, 130.26, 129.31, 128.79, 128.64, 123.78, 123.73, 114.58, 114.55, 114.25, 109.63, 107.86, 55.24. Anal. Calcd. for $C_{26}H_{20}N_6O_2$: C, 69.63; H, 4.50; N, 18.74. Found: C, 69.91; H, 4.77; N, 18.36.

10.1.1.6 Synthesis of differently modified 2,4-substituted quinazolines

General Procedure for the Preparation Compounds 249-250. A mixture of anthranilamide (2.72 g, 20 mmol), the corresponding five-membered heterocycle bearing a 2-carbaldehyd residue (20 mmol), iodine (3.17 g, 25 mmol), anhydrous potassium carbonate (2.76 g, 20 mmol) and 20 ml DMF was stirred at 70-90 °C for 4-8 h. The end of the reaction was monitored by TLC and the mixture poured on crushed ice to form a precipitate. Incomplete precipitation can be prevented by adjusting the pH with concentrated HCl solution to about 7. After filtration of the precipitate, it was thoroughly washed with 100 mL of a 20% sodium thiosulfate solution followed by 100 mL of hot distilled water. Purification was performed by recrystallization from ethanol.

2-(thiophen-2-yl)quinazolin-4(3H)-one (249).

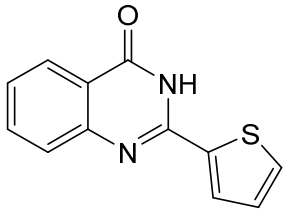

Molecular weight: 228.27 g/mol

The compound was synthesized from anthranilamide (136 mg, 1 mmol) and thiophene-2-carbaldehyde (112 mg, 1 mmol) as described in the general procedure for compounds **249-250** to yield **249** as a white solid (199 mg, 87%). **^{1}H NMR** (500 MHz, DMSO-d_6) δ 12.61 (s, 1H), 8.22 (dd, *J* = 3.8, 1.1 Hz, 1H), 8.11 (ddd, *J* = 7.9, 1.6, 0.6 Hz, 1H), 7.85 (dd, *J* = 5.0, 1.1 Hz, 1H), 7.79 (ddd, *J* = 8.2, 7.1, 1.6 Hz, 1H), 7.68 – 7.60 (m, 1H), 7.48 (ddd, *J* = 8.1, 7.1, 1.1 Hz, 1H), 7.23 (dd, *J* = 5.0, 3.8 Hz, 1H). **^{13}C NMR** (126 MHz, DMSO) δ 161.93, 148.01, 142.56, 137.52, 134.79, 132.26, 129.51, 128.61, 127.04, 126.44, 126.11, 121.01.

2-(1H-pyrrol-2-yl)quinazolin-4(3H)-one (250).

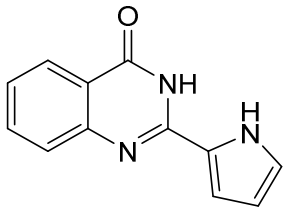

Molecular weight: 211.22 g/mol

The compound was synthesized from anthranilamide (136 mg, 1 mmol) and 1*H*-pyrrole-2-carbaldehyde (95.1 mg, 1 mmol) as described in the general procedure for compounds **249-250** to yield **250** as a white solid (118 mg, 56%). **^{1}H NMR** (500 MHz, DMSO-d_6) δ 12.17 (s, 1H), 11.70 (s, 1H), 8.08 (dd, *J* = 7.9, 1.5 Hz, 1H), 7.75 (ddd, *J* = 8.5, 7.1, 1.6 Hz, 1H), 7.60 (dt, *J* = 8.2, 0.8 Hz, 1H), 7.39 (ddd, *J* = 8.1, 7.1, 1.2 Hz, 1H), 7.30 (ddd, *J* = 3.9, 2.5, 1.5 Hz, 1H), 7.03 (td, *J* = 2.7, 1.4 Hz, 1H), 6.20 (dt, *J* = 3.8, 2.4 Hz, 1H). **^{13}C NMR** (126 MHz, DMSO) δ 161.98, 149.40, 146.50, 134.57, 126.54, 126.06, 125.30, 124.39, 123.95, 120.60, 112.59, 109.84.

General Procedure for the Preparation of compounds derivatives 251-252.

The corresponding 2-substituted quinazolinon derivative **249-250** (10 mmol) was added to phosphorous trichloride (30 mL, 0.32 mol) and stirred for 10 min at room temperature. The mixture was then refluxed for 4-8 h and the reaction monitored by TLC. After completion of the reaction, excess $POCl_3$ was removed under reduced pressure and 50 mL ice water added. Subsequently, 50 mL DCM was added while stirring and the pH of the mixture slowly adjusted to 7 with 25% ammonium solution. With a separatory funnel, the organic phase was collected, washed with 50 mL brine and dried under $MgSO_4$. The solvent was removed under reduced pressure and the obtained solid recrystallized from isopropanol.

4-chloro-2-(thiophen-2-yl)quinazoline (251).

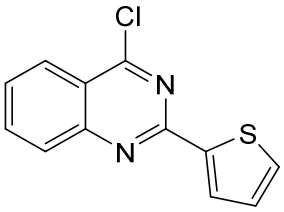

Molecular weight: 246.71 g/mol

The compound was synthesized from **249** (228 mg, 1 mmol) as described in the general procedure for compounds **251-252** to yield **251** as a white solid (175 mg, 71%). **^{1}H NMR** (500 MHz, DMSO-d_6) δ 8.23 (dd, *J* = 3.8, 1.1 Hz, 1H), 8.11 (dd, *J* = 7.9, 1.4 Hz, 1H), 7.86 (dd, *J* = 5.0, 1.1 Hz, 1H), 7.79 (ddd, *J* = 8.5, 7.1, 1.6 Hz, 1H), 7.65 (dt, *J* = 8.0, 0.7 Hz, 1H), 7.48 (ddd, *J* = 8.1, 7.1, 1.1 Hz, 1H), 7.22 (dd, *J* = 5.1, 3.8 Hz, 1H). **^{13}C NMR** (126 MHz, DMSO) δ 161.93, 148.55, 148.07, 137.35, 134.82, 132.36, 129.66, 128.62, 126.89, 126.47, 126.12, 120.98.

4-chloro-2-(1H-pyrrol-2-yl)quinazoline (252).

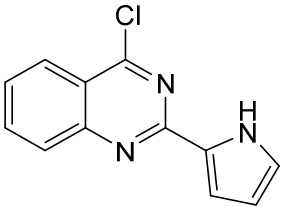

Molecular weight: 229.67 g/mol

The compound was synthesized from **250** (211 mg, 1 mmol) as described in the general procedure for compounds **251**-**252** to yield **252** as a white solid (106 mg, 46%). **^{1}H NMR** (500 MHz, DMSO-d_6) δ 9.58 (dd, *J* = 2.2, 0.9 Hz, 1H), 8.79 – 8.71 (m, 2H), 8.33 – 8.27 (m, 1H), 8.18 – 8.12 (m, 2H), 7.88 (ddd, *J* = 8.2, 5.8, 2.3 Hz, 1H), 7.65 – 7.57 (m, 1H). **^{13}C NMR** (126 MHz, DMSO) δ 162.34, 157.51, 151.18, 149.38, 136.29, 135.65, 131.77, 129.90, 128.72, 125.85, 124.11, 122.19.

General Procedure for the Preparation of compounds 253-261.

The corresponding 4-chloroquinazoline derivative **251-252** (1 mmol) was added to isopropanol (5 mL) with the corresponding substituted aniline derivative (1 mmol) and sealed in a microwave tube. The mixture was heated by 100 watt microwave irradiation to 110 °C for a period of 15 – 30 min to completion of the reaction, indicated by TLC. The formed precipitate was filtered, washed with 10 mL isopropanol and dried in vacuo. If no precipitate is formed, the solvent was removed under reduced pressure and the remaining solid recrystallized from ethanol.

N-(3-nitrophenyl)-2-(thiophen-2-yl)quinazolin-4-amine (253).

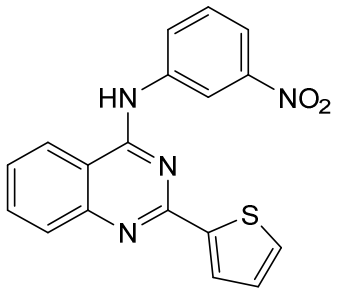

Molecular weight: 348.38 g/mol

The compound was synthesized from **251** (246 mg, 1 mmol) and 3-nitroaniline (138 mg, 1 mmol) as described in the general procedure for compounds **253-261** to yield **253** as a white-yellowish solid (275 mg, 79%), mp >300 °C. **^{1}H NMR** (500 MHz, DMSO-d_6) δ 11.02 (s, 1H), 9.10 (s, 1H), 8.74 (d, *J* = 8.1 Hz, 1H), 8.40 (s, 1H), 8.34 (ddd, *J* = 8.1, 2.1, 0.9 Hz, 1H), 8.13 – 8.04 (m, 2H), 8.00 (ddd, *J* = 8.3, 7.0, 1.3 Hz, 1H), 7.95 (d, *J* = 5.0 Hz, 1H), 7.78 (t, *J* = 8.2 Hz, 1H), 7.73 (ddd, *J* = 8.2, 6.9, 1.2 Hz, 1H), 7.32 (dd, *J* = 4.9, 3.8 Hz, 1H). **^{13}C NMR** (126 MHz, DMSO) δ 158.38, 147.95, 135.23, 130.05, 129.20, 128.93,

127.15, 124.06, 119.33, 117.39, 113.39. **Anal. Calcd. for $C_{18}H_{12}N_4O_2S$**: C, 62.40; H, 3.85; N, 15.69. Found: C, 62.06; H, 3.47; N, 16.08.

N-(4-nitrophenyl)-2-(thiophen-2-yl)quinazolin-4-amine (254).

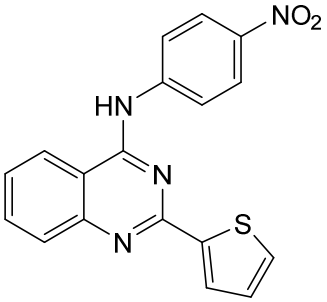

Molecular weight: 348.38 g/mol

The compound was synthesized from **251** (246 mg, 1 mmol) and 4-nitroaniline (138 mg, 1 mmol) as described in the general procedure for compounds **253-261** to yield **254** as a light-yellow solid (244 mg, 70%), mp >300 °C. **^{1}H NMR** (500 MHz, DMSO-d_6) δ 10.75 (s, 1H), 8.69 (d, J = 7.9 Hz, 1H), 8.37 (d, J = 7.1 Hz, 2H), 8.31 (d, J = 7.7 Hz, 2H), 8.21 (s, 1H), 7.97 (s, 2H), 7.86 (d, J = 4.0 Hz, 1H), 7.70 (s, 1H), 7.31 – 7.24 (m, 1H). ^{13}C NMR (126 MHz, DMSO) δ 134.79, 128.99, 126.83, 124.65, 123.86, 122.00, 113.84. Anal. Calcd. for $C_{18}H_{12}N_4O_2S$: C, 62.06; H, 3.47; N, 16.08. Found: C, 62.01; H, 3.81; N, 15.71.

3-((2-(thiophen-2-yl)quinazolin-4-yl)amino)benzonitrile (255).

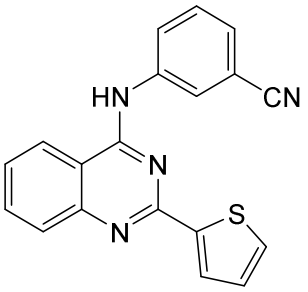

Molecular weight: 328.39 g/mol

The compound was synthesized from **251** (246 mg, 1 mmol) and 3-aminobenzonitrile (118 mg, 1 mmol) as described in the general procedure for compounds **253-261** to yield **255** as a light-yellow solid (210 mg, 64%), mp 296-297 °C (decomp.). **^{1}H NMR** (500 MHz, DMSO-d_6) δ 11.34 (s, 1H), 8.81 (d, J = 8.3 Hz, 1H), 8.58 (s, 1H), 8.46 (t, J = 1.8

Hz, 1H), 8.29 – 8.13 (m, 2H), 8.10 – 7.95 (m, 2H), 7.79 – 7.65 (m, 3H), 7.34 (dd, *J* = 5.0, 3.8 Hz, 1H). **^{13}C NMR** (126 MHz, DMSO) δ 165.60, 158.68, 153.34, 138.62, 135.72, 130.15, 129.53, 128.95, 128.28, 127.49, 126.99, 124.42, 118.63, 113.07, 111.56. **Anal. Calcd. for $C_{19}H_{12}N_4S$**: C, 69.49; H, 3.68; N, 17.06. Found: C, 69.30; H, 4.06; N, 16.99.

N-(3,4-dimethoxyphenyl)-2-(thiophen-2-yl)quinazolin-4-amine (256).

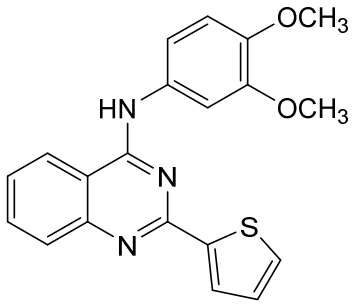

Molecular weight: 363.44 g/mol

The compound was synthesized from **251** (246 mg, 1 mmol) and 3,4-dimethoxyanilin (153 mg, 1 mmol) as described in the general procedure for compounds **253-261** to yield **256** as a yellow solid (244 mg, 67%), mp 250-251 °C (decomp.). **^{1}H NMR** (500 MHz, DMSO-d_6) δ 10.97 (s, 1H), 8.70 (d, *J* = 8.3 Hz, 1H), 8.51 (s, 1H), 8.10 (s, 1H), 8.00 (t, *J* = 7.4 Hz, 2H), 7.73 (t, *J* = 7.7 Hz, 1H), 7.55 (d, *J* = 2.5 Hz, 1H), 7.38 (dd, *J* = 8.6, 2.4 Hz, 1H), 7.34 (t, *J* = 4.5 Hz, 1H), 7.08 (d, *J* = 8.7 Hz, 1H), 3.83 (s, 3H), 3.82 (s, 3H). **^{13}C NMR** (126 MHz, DMSO) δ 158.18, 148.48, 129.42, 124.19, 112.97, 111.60, 108.68, 55.88, 55.86. **Anal. Calcd. for $C_{20}H_{17}N_3O_2S$**: C, 66.10; H, 4.72; N, 11.56. Found: C, 66.31; H, 4.99; N, 11.64.

N-(3-fluorophenyl)-2-(thiophen-2-yl)quinazolin-4-amine (257).

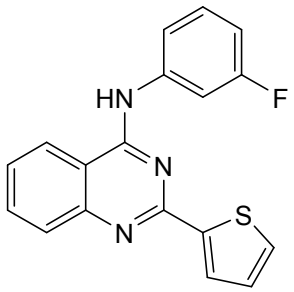

Molecular weight: 321.37 g/mol

The compound was synthesized from **251** (246 mg, 1 mmol) and 3-fluoroaniline (111 mg, 1 mmol) as described in the general procedure for compounds **253-261** to yield **257** as a light-yellow solid (247 mg, 77%), mp 292-293 °C (decomp.). **^{1}H NMR** (500 MHz, DMSO-d_6) δ 11.29 (s, 1H), 8.84 (d, *J* = 8.2 Hz, 1H), 8.69 (s, 1H), 8.27 (d, *J* = 8.3 Hz, 1H), 8.10 – 7.98 (m, 2H), 7.92 (dt, *J* = 11.5, 2.4 Hz, 1H), 7.81 – 7.66 (m, 2H), 7.54 (td, *J* = 8.2, 6.7 Hz, 1H), 7.35 (dd, *J* = 5.0, 3.8 Hz, 1H), 7.14 (td, *J* = 8.4, 2.6 Hz, 1H). **^{13}C NMR** (126 MHz, DMSO) δ 161.96 (d, *J* = 242.2 Hz), 158.65, 153.07, 139.25, 139.18, 135.79, 130.27 (d, *J* = 9.3 Hz), 129.58, 127.55, 124.53, 119.62, 113.00, 112.40 (d, *J* = 22.4 Hz), 110.92 (d, *J* = 27.8 Hz). **Anal. Calcd. for $C_{18}H_{12}FN_3S$**: C, 67.27; H, 3.76; N, 13.08. Found: C, 67.22; H, 3.98; N, 12.76.

N-(3-((2-(thiophen-2-yl)quinazolin-4-yl)amino)phenyl)acetamide (258).

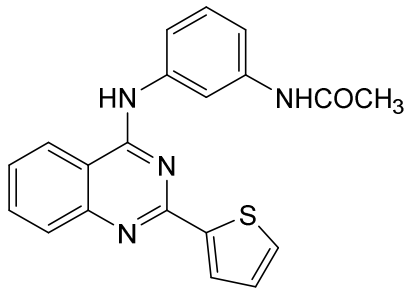

Molecular weight: 360.44 g/mol

The compound was synthesized from **251** (246 mg, 1 mmol) and N-(3-aminophenyl)acetamide (150 mg, 1 mmol) as described in the general procedure for compounds **253-261** to yield **258** as a light-yellow solid (288 mg, 80%), mp >300 °C. **^{1}H NMR** (500 MHz, DMSO-d_6) δ 11.33 (s, 1H), 10.18 (s, 1H), 8.94 – 8.62 (m, 2H), 8.30 (d, *J* = 8.4 Hz, 1H), 8.11 (t, *J* = 1.9 Hz, 1H), 8.03 (dd, *J* = 8.9, 7.0 Hz, 2H), 7.74 (t, *J* = 7.5 Hz, 1H), 7.59 (dt, *J* = 6.8, 2.1 Hz, 1H), 7.52 – 7.38 (m, 2H), 7.34 (dd, *J* = 5.0, 3.9 Hz, 1H), 2.08 (s, 3H). **^{13}C NMR** (126 MHz, DMSO) δ 168.58, 158.75, 152.74, 139.80, 137.30, 135.78, 133.14, 129.49, 128.66, 127.56, 124.55, 119.28, 116.93, 115.00, 112.79, 24.15. **Anal. Calcd. for $C_{20}H_{16}N_4OS$**: C, 66.65; H, 4.47; N, 15.54. Found: C, 66.72; H, 4.65; N, 15.30.

3-((2-(1H-pyrrol-2-yl)quinazolin-4-yl)amino)benzonitrile (259).

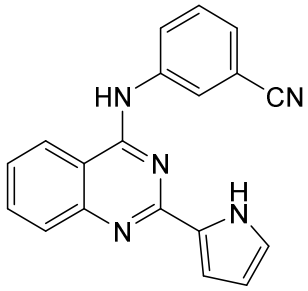

Molecular weight: 311.35 g/mol

The compound was synthesized from **252** (230 mg, 1 mmol) and 3-aminobenzonitrile (118 mg, 1 mmol) as described in the general procedure for compounds **253-261** to yield **259** as a light-yellow solid (177 mg, 57%), mp 172-173 °C. **^{1}H NMR** (500 MHz, DMSO-d_6) δ 10.80 (s, 1H), 9.49 (d, *J* = 2.0 Hz, 1H), 9.04 (dt, *J* = 8.1, 1.8 Hz, 1H), 8.92 (dd, *J* = 5.3, 1.6 Hz, 1H), 8.78 (dd, *J* = 8.5, 1.3 Hz, 1H), 8.37 (q, *J* = 1.3, 0.9 Hz, 1H), 8.30 (dt, *J* = 7.4, 2.1 Hz, 1H), 8.03 (dd, *J* = 8.5, 1.4 Hz, 1H), 7.99 – 7.91 (m, 2H), 7.78 – 7.63 (m, 3H). **^{13}C NMR** (126 MHz, DMSO) δ 158.50, 155.42, 144.76, 140.44, 139.57, 134.58, 130.12, 127.99, 127.75, 127.65, 126.97, 126.05, 125.92, 123.92, 118.77, 114.19, 111.56. **Anal. Calcd. for $C_{19}H_{13}N_5$**: C, 73.30; H, 4.21; N, 22.49. Found: C, 73.02; H, 4.32; N, 22.25.

N-(4-methoxyphenyl)-2-(1H-pyrrol-2-yl)quinazolin-4-amine (260).

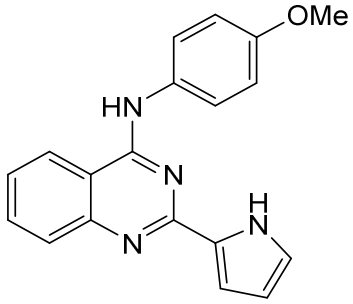

Molecular weight: 316.36 g/mol

The compound was synthesized from **252** (230 mg, 1 mmol) and 4-methoxyaniline (123 mg, 1 mmol) as described in the general procedure for compounds **253-261** to yield **260** as a light-beige solid (155 mg, 49%), mp 268-269 °C (decomp.). **^{1}H NMR** (500 MHz, DMSO-d_6) δ 9.85 (s, 1H), 9.51 (dd, *J* = 2.1, 0.9 Hz, 1H), 8.73 – 8.59 (m, 2H), 8.54 (dt, *J*

= 8.5, 1.1 Hz, 1H), 7.90 – 7.84 (m, 2H), 7.84 – 7.76 (m, 2H), 7.65 – 7.57 (m, 1H), 7.56 – 7.47 (m, 1H), 7.10 – 6.98 (m, 2H), 3.80 (s, 3H). **^{13}C NMR** (126 MHz, DMSO) δ 158.21, 157.69, 156.06, 150.29, 149.33, 135.15, 133.85, 133.34, 132.01, 128.18, 126.28, 124.40, 123.65, 123.13, 114.24, 113.85, 55.40. **Anal. Calcd. for $C_{19}H_{16}N_4O$**: C, 72.13; H, 5.10; N, 17.71. Found: C, 72.36; H, 4.94; N, 17.45.

N-(3,4-dimethoxyphenyl)-2-(1H-pyrrol-2-yl)quinazolin-4-amine (261).

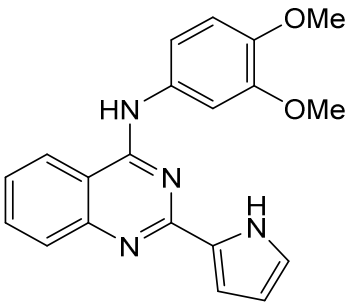

Molecular weight: 346.39 g/mol

The compound was synthesized from **252** (230 mg, 1 mmol) and 3,4-dimethoxyaniline (153 mg, 1 mmol) as described in the general procedure for compounds **253-261** to yield **261** as a light-yellow solid (184 mg, 53%), mp 161-163 °C. **^{1}H NMR** (500 MHz, DMSO-d_6) δ 9.82 (s, 1H), 9.56 (s, 1H), 8.69 (dt, *J* = 8.0, 1.9 Hz, 2H), 8.56 (dt, *J* = 8.5, 1.1 Hz, 1H), 7.89 – 7.84 (m, 2H), 7.66 (d, *J* = 2.5 Hz, 1H), 7.65 – 7.60 (m, 1H), 7.54 (dd, *J* = 7.8, 4.8 Hz, 1H), 7.44 (dd, *J* = 8.7, 2.5 Hz, 1H), 7.06 (d, *J* = 8.7 Hz, 1H), 3.82 (s, 3H), 3.80 (s, 3H). **^{13}C NMR** (126 MHz, DMSO) δ 158.06, 157.68, 150.99, 150.28, 149.32, 148.49, 145.64, 135.12, 133.38, 132.52, 128.22, 126.34, 123.10, 114.60, 114.28, 111.95, 107.80, 55.92, 55.65. Anal. Calcd. for $C_{20}H_{18}N_4O_2$: C, 69.35; H, 5.24; N, 16.17. Found: C, 69.16; H, 5.24; N, 16.17.

General Procedure for the Preparation of 2-phenylquinazolin-4-amine (262).

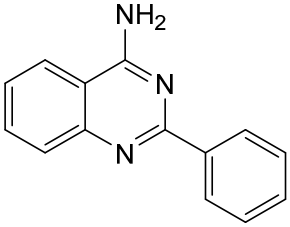

Molecular weight: 221.26 g/mol

2-aminobenzonitrile (1.03 g, 10 mmol), benzonitrile (1.03 g, 10 mmol) and *t*-BuOK (112 mg, 1 mmol) were transferred to a microwave tube and sealed. The mixture was heated at 150 watt microwave irradiation to 180 °C, held for 2 min at this temperature and then poured into ice water. The formed precipitate was filtered off under suction and the solid recrystallized from methanol to yield **262** as a slightly yellow solid (951 mg, 43%), mp 149-151 °C. **^{1}H NMR** (500 MHz, DMSO-d_6) δ 8.48 – 8.42 (m, 2H), 8.23 (dt, J = 8.2, 1.2 Hz, 1H), 7.90 – 7.72 (m, 4H), 7.50 – 7.42 (m, 4H). **^{13}C NMR** (126 MHz, DMSO) δ 162.20, 159.84, 150.50, 138.70, 133.04, 130.00, 128.23, 127.93, 127.77, 125.21, 123.69, 113.38. **Anal. Calcd. for $C_{14}H_{11}N_3$**: C, 76.00; H, 5.01; N, 18.99. Found: C, 76.35; H, 5.10; N, 18.66.

General Procedure for the Preparation of compound 263-266.

Compound **262** (2.21 g, 10 mmol) was dissolved in a mixture of triethylamine (10.1 g, 0.1 mol) and THF (50 mL) and chilled to 0 °C. A dilution of the corresponding substituted benzoyl chloride (10 mmol) in THF was slowly added while stirring with a dropping funnel under exclusion of moisture and the mixture then allowed to warm up to room temperature. After 12 h excess solvent was evaporated under reduced pressure and 50 mL water added. The formed precipitate was filtered under suction and the product purified by column chromatography with DCM/MeOH as eluent.

N-(2-phenylquinazolin-4-yl)benzamide (263).

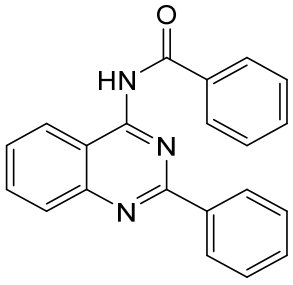

Molecular weight: 325.37 g/mol

The compound was synthesized from **262** (221 mg, 1 mmol) and benzoyl chloride (141 mg, 1 mmol) as described in the general procedure for compounds **263-266** to yield **263** as a light-yellow solid (153 mg, 47%), 157-159 °C. **^{1}H NMR** (500 MHz, DMSO-d_6) δ

11.31 (s, 1H), 8.43 – 8.33 (m, 2H), 8.22 (d, *J* = 8.3 Hz, 1H), 8.06 – 7.96 (m, 4H), 7.70 – 7.63 (m, 2H), 7.59 – 7.54 (m, 2H), 7.51 (d, *J* = 5.7 Hz, 3H). **^{13}C NMR** (126 MHz, DMSO) δ 168.05, 159.20, 159.09, 151.88, 137.34, 134.60, 134.19, 132.39, 130.91, 128.68, 128.62, 128.53, 128.25, 128.16, 127.15, 125.72, 117.41. **Anal. Calcd. for $C_{21}H_{15}N_3O$**: C, 77.52; H, 4.65; N, 12.91. Found: C, 77.71; H, 4.94; N, 12.71.

2-nitro-N-(2-phenylquinazolin-4-yl)benzamide (264).

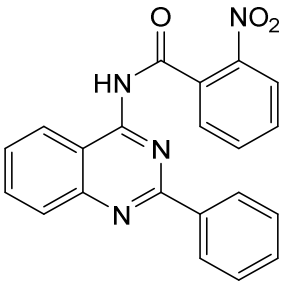

Molecular weight: 370.37 g/mol

The compound was synthesized from **262** (221 mg, 1 mmol) and 2-nitrobenzoyl chloride (186 mg, 1 mmol) as described in the general procedure for compounds **263-266** to yield **264** as a light-yellow solid (181 mg, 49%), mp 205-206 °C. **^{1}H NMR** (600 MHz, DMSO-d_6) δ 11.81 (s, 1H), 8.56 (dt, *J* = 8.4, 1.0 Hz, 1H), 8.28 (dd, *J* = 8.6, 1.2 Hz, 1H), 8.02 – 7.94 (m, 2H), 7.88 (td, *J* = 7.5, 1.2 Hz, 1H), 7.85 – 7.74 (m, 4H), 7.70 (ddd, *J* = 8.3, 5.5, 2.6 Hz, 1H), 7.48 – 7.41 (m, 1H), 7.36 (t, *J* = 7.6 Hz, 2H). **^{13}C NMR** (151 MHz, DMSO) δ 167.70, 158.87, 156.97, 151.78, 145.83, 137.41, 135.38, 135.05, 134.41, 131.16, 130.82, 128.75, 128.71, 128.66, 128.17, 127.69, 124.95, 124.72, 115.22. **Anal. Calcd. for $C_{21}H_{14}N_4O_3$:** C, 68.10; H, 3.81; N, 15.13. Found: C, 68.39; H, 3.90; N, 14.86.

3-nitro-N-(2-phenylquinazolin-4-yl)benzamide (265).

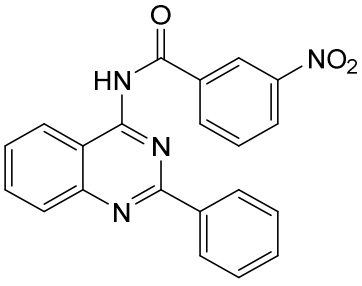

Molecular weight: 370.37 g/mol

The compound was synthesized from **262** (221 mg, 1 mmol) and 3-nitrobenzoyl chloride (186 mg, 1 mmol) as described in the general procedure for compounds **263-266** to yield **265** as a light-yellow solid (303 mg, 82%), mp 230-233 °C. **^{1}H NMR** (500 MHz, DMSO-d_6) δ 11.68 (s, 1H), 8.86 (s, 1H), 8.49 (ddd, *J* = 8.2, 2.4, 1.0 Hz, 2H), 8.38 (s, 2H), 8.27 (s, 1H), 8.03 (dt, *J* = 14.9, 8.2 Hz, 2H), 7.86 (t, *J* = 8.0 Hz, 1H), 7.69 (t, *J* = 7.6 Hz, 1H), 7.53 (s, 3H). **^{13}C NMR** (126 MHz, DMSO) δ 166.04, 159.15, 158.66, 151.98, 147.95, 137.22, 135.76, 134.87, 134.81, 131.02, 130.45, 128.74, 128.32, 128.13, 127.30, 126.80, 125.76, 123.31, 117.34. **Anal. Calcd. for $C_{21}H_{14}N_4O_3$**: C, 68.10; H, 3.81; N, 15.13. Found: C, 68.05; H, 4.18; N, 14.97.

4-nitro-N-(2-phenylquinazolin-4-yl)benzamide (266).

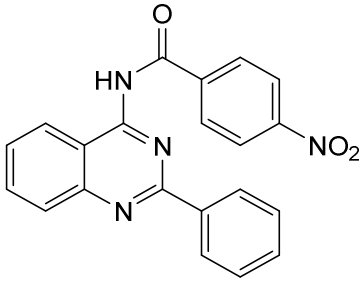

Molecular weight: 370.37 g/mol

The compound was synthesized from **262** (221 mg, 1 mmol) and 4-nitrobenzoyl chloride (186 mg, 1 mmol) as described in the general procedure for compounds **263-266** to yield **266** as a light-yellow solid (285 mg, 77%), mp 233-235 °C. **^{1}H NMR** (500 MHz, DMSO-d_6) δ 11.68 (s, 1H), 8.43 – 8.29 (m, 3H), 8.28 – 8.15 (m, 4H), 8.09 – 7.95 (m, 2H), 7.75 – 7.65 (m, 1H), 7.48 (d, *J* = 10.6 Hz, 3H). **^{13}C NMR** (126 MHz, DMSO) δ 167.13, 158.97, 158.38, 151.88, 149.45, 140.44, 137.16, 134.80, 131.00, 129.87, 128.63, 128.31, 128.04, 127.32, 125.45, 123.75, 116.87. **Anal. Calcd. for $C_{21}H_{14}N_4O_3$**: C, 68.10; H, 3.81; N, 15.13. Found: C, 68.27; H, 3.90; N, 14.80.

General Procedure for the Preparation of compounds 267-274.

4-chloroquinazoline (164 mg, 1 mmol) was added to isopropanol (5 mL) with the corresponding substituted aniline derivative (1 mmol) and sealed in a microwave tube. The mixture was heated by 100 watt microwave irradiation to 110 °C for a period of 15 – 30 min to completion of the reaction, indicated by TLC. The formed precipitate was

filtered, washed with 10 mL isopropanol and dried in vacuo. If no precipitate is formed, the solvent was removed under reduced pressure and the remaining solid recrystallized from ethanol.

N-phenylquinazolin-4-amine (267).

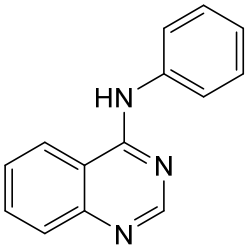

Molecular weight: 221.26 g/mol

The compound was synthesized from 4-chloroquinazoline (165 mg, 1 mmol) and aniline (93.1 mg, 1 mmol) as described in the general procedure for compounds **267-274** to yield **267** as a white solid (184 mg, 83%), mp 226-227 °C. **^{1}H NMR** (500 MHz, DMSO-d_6) δ 9.76 (s, 1H), 8.61 – 8.49 (m, 2H), 7.94 – 7.81 (m, 3H), 7.78 (dd, *J* = 8.3, 1.3 Hz, 1H), 7.63 (ddd, *J* = 8.3, 6.9, 1.4 Hz, 1H), 7.44 – 7.33 (m, 2H), 7.13 (tt, *J* = 7.4, 1.2 Hz, 1H). **^{13}C NMR** (126 MHz, DMSO) δ 157.91, 154.61, 149.82, 139.28, 133.09, 128.56, 127.92, 126.33, 123.86, 123.10, 122.60, 115.30. **Anal. Calcd. for $C_{14}H_{11}N_3$**: C, 76.00; H, 5.01; N, 18.99. Found: C, 76.15; H, 5.05; N, 18.65.

2-nitro-4-(quinazolin-4-ylamino)phenol (268).

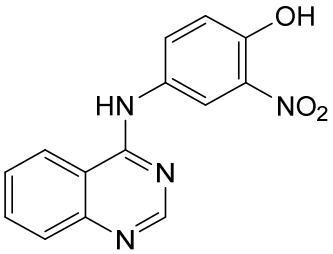

Molecular weight: 282.26 g/mol

The compound was synthesized from 4-chloroquinazoline (165 mg, 1 mmol) and 4-amino-2-nitrophenol (109 mg, 1 mmol) as described in the general procedure for

compounds **267-274** to yield **268** as a yellow solid (208 mg, 74%), mp 288-289 °C (decomp.). **^{1}H NMR** (500 MHz, DMSO-d_6) δ 11.97 (s, 1H), 11.39 (s, 1H), 9.04 – 8.96 (m, 1H), 8.95 (s, 1H), 8.33 (d, *J* = 2.7 Hz, 1H), 8.09 (ddd, *J* = 8.4, 7.1, 1.2 Hz, 1H), 8.00 (dd, *J* = 8.5, 1.2 Hz, 1H), 7.93 (dd, *J* = 9.0, 2.7 Hz, 1H), 7.84 (ddd, *J* = 8.3, 7.1, 1.2 Hz, 1H), 7.32 (d, *J* = 8.9 Hz, 1H). **^{13}C NMR** (126 MHz, DMSO) δ 159.99, 151.05, 150.85, 138.50, 136.42, 136.18, 131.97, 128.80, 128.00, 125.14, 121.40, 119.67, 119.33, 113.58. **Anal. Calcd. for $C_{14}H_{10}N_4O_3$**: C, 59.57; H, 3.57; N, 19.85. Found: C, 59.43; H, 3.80; N, 19.68.

4-(quinazolin-4-ylamino)phenol (269).

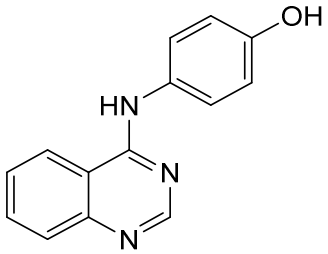

Molecular weight: 237.26 g/mol

The compound was synthesized from 4-chloroquinazoline (165 mg, 1 mmol) and 4-aminophenol (109 mg, 1 mmol) as described in the general procedure for compounds **267-274** to yield **269** as a bright yellow solid (157 mg, 66%), mp >300 °C. **^{1}H NMR** (500 MHz, DMSO-d_6) δ 11.61 (s, 1H), 9.75 (s, 1H), 8.99 – 8.72 (m, 2H), 8.07 (t, *J* = 7.8 Hz, 1H), 7.96 (d, *J* = 8.3 Hz, 1H), 7.82 (t, *J* = 7.7 Hz, 1H), 7.59 – 7.38 (m, 2H), 6.96 – 6.77 (m, 2H). **^{13}C NMR** (126 MHz, DMSO) δ 159.57, 156.45, 150.92, 138.31, 136.14, 128.61, 127.76, 126.45, 124.88, 119.55, 115.38, 113.46. **Anal. Calcd. for $C_{14}H_{11}N_3O$**: C, 70.87; H, 4.67; N, 17.71. Found: C, 71.24; H, 5.00; N, 17.37.

4-(quinazolin-4-ylamino)benzonitrile (270).

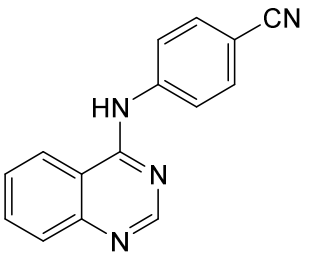

Molecular weight: 246.27 g/mol

The compound was synthesized from 4-chloroquinazoline (165 mg, 1 mmol) and 4-aminobenzonitrile (118 mg, 1 mmol) as described in the general procedure for compounds **267-274** to yield **270** as a light yellow solid (185 mg, 75%), mp >300 °C. **^{1}H NMR** (500 MHz, DMSO-d_6) δ 12.04 (s, 1H), 9.34 – 8.80 (m, 2H), 8.09 (td, J = 17.4, 15.8, 7.9 Hz, 4H), 8.02 – 7.68 (m, 3H). **^{13}C NMR** (126 MHz, DMSO) δ 160.08, 151.17, 141.46, 139.49, 136.54, 132.98, 128.86, 125.33, 124.91, 120.27, 118.80, 114.02, 108.29. **Anal. Calcd. for $C_{15}H_{10}N_4$**: C, 73.16; H, 4.09; N, 22.75. Found: C, 73.00; H, 4.32; N, 22.50.

N-(3-methoxyphenyl)quinazolin-4-amine (271).

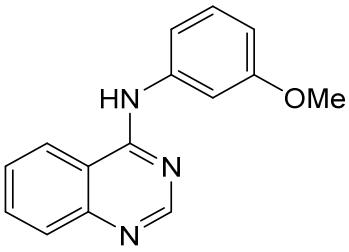

Molecular weight: 251.29 g/mol

The compound was synthesized from 4-chloroquinazoline (165 mg, 1 mmol) and 3-methoxyaniline (123 mg, 1 mmol) as described in the general procedure for compounds **267-274** to yield **271** as a yellow solid (204 mg, 81%), mp 235-237 °C. **^{1}H NMR** (500 MHz, DMSO-d_6) δ 11.86 (s, 1H), 9.07 (dd, J = 8.5, 1.2 Hz, 1H), 8.92 (s, 1H), 8.09 (ddd, J = 8.3, 7.0, 1.2 Hz, 1H), 8.06 – 7.98 (m, 1H), 7.84 (ddd, J = 8.3, 7.0, 1.3 Hz, 1H), 7.45 – 7.32 (m, 3H), 6.94 – 6.84 (m, 1H), 3.78 (s, 3H). **^{13}C NMR** (126 MHz, DMSO) δ 160.00, 159.49, 150.89, 138.60, 137.85, 136.30, 129.58, 128.67, 125.25, 119.64, 117.19, 113.60, 112.20, 111.09, 55.44. **Anal. Calcd. for $C_{15}H_{13}N_3O$**: C, 71.70; H, 5.21; N, 16.72. Found: C, 72.01; H, 5.56; N, 16.44.

N-(3-(methylthio)phenyl)quinazolin-4-amine (272).

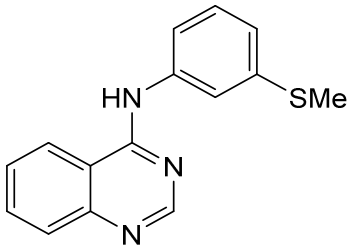

Molecular weight: 267.35 g/mol

The compound was synthesized from 4-chloroquinazoline (165 mg, 1 mmol) and 3-(methylthio)aniline (139 mg, 1 mmol) as described in the general procedure for compounds **267-274** to yield **272** as a bright yellow solid (230 mg, 89%), mp 233-234 °C. **^{1}H NMR** (500 MHz, DMSO-d_6) δ 11.82 (s, 1H), 9.08 – 9.00 (m, 1H), 8.92 (s, 1H), 8.09 (ddd, J = 8.3, 7.0, 1.2 Hz, 1H), 8.05 – 7.97 (m, 1H), 7.84 (ddd, J = 8.4, 7.1, 1.3 Hz, 1H), 7.69 (t, J = 1.9 Hz, 1H), 7.55 (ddd, J = 8.0, 2.0, 1.0 Hz, 1H), 7.41 (t, J = 7.9 Hz, 1H), 7.20 (ddd, J = 7.9, 1.9, 1.0 Hz, 1H), 2.50 (s, 3H). **^{13}C NMR** (126 MHz, DMSO) δ 159.95, 151.07, 139.05, 138.87, 137.46, 136.20, 129.22, 128.59, 125.13, 123.97, 122.03, 121.30, 119.97, 113.67, 14.84. **Anal. Calcd. for $C_{15}H_{13}N_3S$**: C, 67.39; H, 4.90; N, 15.72. Found: C, 67.36; H, 5.10; N, 15.35.

N-(3-fluorophenyl)quinazolin-4-amine (273).

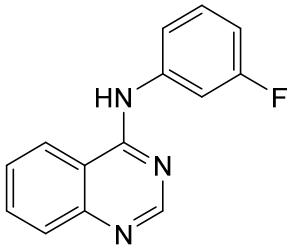

Molecular weight: 239.25 g/mol

The compound was synthesized from 4-chloroquinazoline (165 mg, 1 mmol) and 3-fluoroaniline (111 mg, 1 mmol) as described in the general procedure for compounds **267-274** to yield **273** as a light yellow solid (199 mg, 83%), mp 266-267 °C (decomp.). **^{1}H NMR** (500 MHz, DMSO-d_6) δ 11.95 (s, 1H), 9.08 (dt, *J* = 8.4, 0.9 Hz, 1H), 8.98 (s, 1H), 8.11 (ddd, *J* = 8.3, 7.1, 1.2 Hz, 1H), 8.04 (dd, *J* = 8.4, 1.3 Hz, 1H), 7.86 (ddd, *J* = 8.3, 7.1, 1.2 Hz, 1H), 7.76 (ddd, *J* = 10.9, 2.5, 1.9 Hz, 1H), 7.65 (ddd, *J* = 8.1, 2.0, 0.9 Hz, 1H), 7.52 (td, *J* = 8.2, 6.6 Hz, 1H), 7.16 (tdd, *J* = 8.6, 2.6, 0.9 Hz, 1H). **^{13}C NMR** (126 MHz, DMSO) δ 161.87 (d, *J* = 242.7 Hz), 160.08, 151.09, 138.94, 138.57 (d, *J* = 10.8 Hz), 136.44, 130.41 (d, *J* = 9.2 Hz), 128.79, 125.26, 120.77, 119.93, 113.73, 113.34 (d, *J* = 21.0 Hz), 111.99 (d, *J* = 25.3 Hz). **Anal. Calcd. for $C_{14}H_{10}FN_3$**: C, 70.28; H, 4.21; N, 17.56. Found: C, 70.39; H, 4.59; N, 17.31.

N-(3-(quinazolin-4-ylamino)phenyl)acetamide (274).

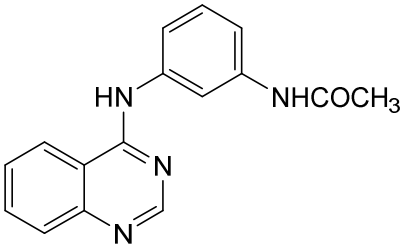

Molecular weight: 278.32 g/mol

The compound was synthesized from 4-chloroquinazoline (165 mg, 1 mmol) and N-(3-aminophenyl)acetamide (150 mg, 1 mmol) as described in the general procedure for compounds **267-274** to yield **274** as a yellow solid (256 mg, 92%), mp >300 °C. **^{1}H NMR** (500 MHz, DMSO-d_6) δ 11.94 – 11.75 (m, 1H), 10.30 (s, 1H), 8.98 (dd, *J* = 8.5, 1.3 Hz, 1H), 8.90 (s, 1H), 8.09 (ddd, *J* = 8.4, 7.1, 1.2 Hz, 1H), 8.05 – 7.98 (m, 2H), 7.84 (ddd, *J* = 8.4, 7.0, 1.2 Hz, 1H), 7.50 (pd, *J* = 4.3, 2.0 Hz, 1H), 7.42 – 7.30 (m, 2H), 2.07 (s, 3H). **^{13}C NMR** (126 MHz, DMSO) δ 168.67, 160.14, 150.87, 139.97, 138.49, 136.80, 136.34, 128.91, 128.73, 125.14, 120.02, 119.57, 117.62, 115.83, 113.52, 24.14. **Anal. Calcd. for $C_{16}H_{14}N_4O$**: C, 69.05; H, 5.07 N, 20.13. Found: C, 69.21; H, 5.37; N, 19.87.

General procedure for the preparation of the dimers 275-276 based on a 2-(4-nitrophenyl)quinazoline scaffold.

Precursor **99** (2 mmol) was dissolved in isopropanol and a triethylamine (2 mmol) added to the mixture. Following ethane-1,2-diamine (1 mmol, for **275**) or propane-1,3-diamine (1 mmol, for **276**) in 100 mL isopropanol were slowly added under stirring via dropping funnel over 2 h to the refluxing mixture, which was kept under moisture exclusion. After 4-6 h refluxing the mixture was allowed to cool yielding crystals of the corresponding product. If necessary, purification is carried out by re-crystallization from ethanol.

***N*1,*N*2-bis(2-(4-nitrophenyl)quinazolin-4-yl)ethane-1,2-diamine (275).**

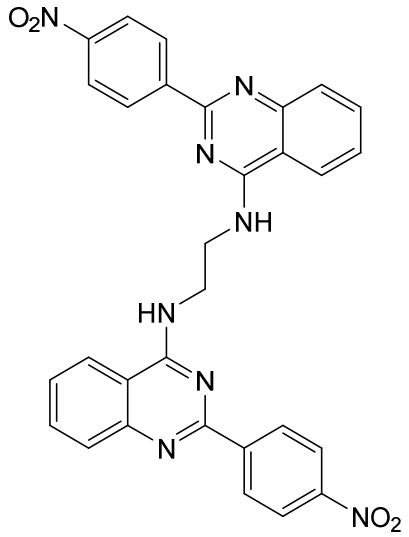

Molecular weight: 558.56 g/mol

The compound was synthesized from **99** (571.38 mg, 2 mmol) and ethane-1,2-diamine (120.20 mg, 2 mmol) as described in the general procedure for compounds **275-276** to yield **275** as a yellow solid (430 mg, 77%), mp >300 °C. **^{1}H NMR** (500 MHz, DMSO-d_6) δ 8.62 – 8.55 (m, 4H), 8.47 (s, 2H), 8.19 – 8.12 (m, 6H), 7.77 – 7.72 (m, 4H), 7.44 (ddd, J = 8.2, 5.9, 2.2 Hz, 2H), 4.19 – 4.13 (m, 4H). **^{13}C NMR** (126 MHz, DMSO) δ 160.17, 157.26, 149.55, 148.21, 144.59, 132.55, 128.57, 127.77, 125.69, 122.90, 122.52, 114.00, 40.02. **Anal. Calcd. for $C_{30}H_{22}N_8O_4$**: C, 64.51; H, 3.97 N, 20.06. Found: C, 64.81; H, 4.18; N, 20.02.

***N*1,*N*3-bis(2-(4-nitrophenyl)quinazolin-4-yl)propane-1,3-diamine (276).**

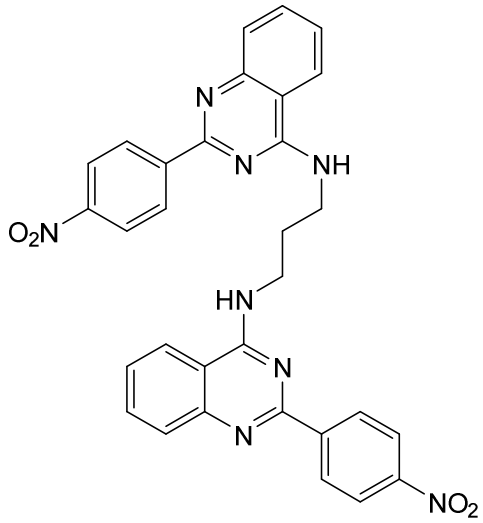

Molecular weight: 572.59 g/mol

The compound was synthesized from **99** (571.38 mg, 2 mmol) and propane-1,3-diamine (148.26 mg, 2 mmol) as described in the general procedure for compounds **275-276** to yield **275** as a yellow solid (395 mg, 69%), mp >300 °C. **^{1}H NMR** (500 MHz, DMSO-d_6) δ 8.49 (t, *J* = 5.6 Hz, 2H), 8.47 – 8.40 (m, 4H), 8.26 (dd, *J* = 8.4, 1.3 Hz, 2H), 8.08 – 8.01 (m, 4H), 7.73 (ddd, *J* = 8.2, 6.8, 1.3 Hz, 2H), 7.68 (dd, *J* = 8.3, 1.4 Hz, 2H), 7.50 (ddd, *J* = 8.3, 6.8, 1.4 Hz, 2H), 3.90 (q, *J* = 6.5 Hz, 4H), 2.23 (p, *J* = 6.7 Hz, 2H). **^{13}C NMR** (126 MHz, DMSO) δ 159.95, 157.24, 149.66, 148.25, 144.66, 132.85, 128.64, 128.09, 126.10, 123.22, 122.77, 114.09, 38.41, 28.66. **Anal. Calcd. for $C_{31}H_{24}N_8O_4$**: C, 65.03; H, 4.23 N, 19.57. Found: C, 65.22; H, 4.21; N, 19.28.

General procedure for the preparation of 4-N-methylanilino-2-phenylquinazoline derivatives 277-280. Preparation of the precursors was carried out according to the general method described below. Compounds were not further characterized as they are already described in literature.[197, 198] Second step was carried out with some modifications

according to literature.[218] Therefore, 4-chloro-2-phenylquinazoline (1 mmol) and the corresponding substituted aniline (1 mmol) were added to a 50 mL microwave tube and suspended in 25 mL isopropanol. The tube was sealed and the reaction mixture stirred under 100 watt microwave irradiation at 110 °C for 30 min. Completion of the reaction was monitored by TLC. After cooling, a precipitate was formed and filtered off by suction. If no precipitate was formed, the solvent was removed by rotary evaporation and the obtained solids recrystallized from 75% EtOH.

The corresponding synthesized 4-Substituted-2-phenylquinazoline derivative **30**, **31**, **35** or **40** (1 mmol) was subsequently dissolved in the necessary amount of dried DMF using a round bottom flask equipped with a drying tube and an ultrasonic bath at 50 °C. The solution was then cooled with an ice bath to 0 °C and sodium hydride (1.5 mmol) followed by methyl iodide (1.5 mmol) were added under stirring. After 1h the mixture was allowed to warm up to room temperature and stirred for another 2-6 h. After completion of the reaction, excess DMF was evaporated and ice-water added to induce precipitation. Solids were collected by suction and either re-crystallized from ethanol or purified by column chromatography using DCM as eluent.

N-methyl-N-(3-nitrophenyl)-2-phenylquinazolin-4-amine (277).

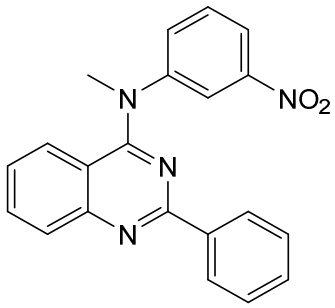

Molecular weight: 356.39 g/mol

The compound was synthesized from **30** (342.36 mg, 1 mmol), sodium hydride (36.0 mg, 1.5 mmol) and methyl iodide (212.91 mg, 1.5 mmol) as described in the general procedure for compounds **277-280** to yield **277** as a yellow solid (281 mg, 79%), mp 132-133 °C. **^{1}H NMR** (600 MHz, Chloroform-*d*) δ 8.71 – 8.55 (m, 2H), 8.16 – 7.99 (m, 3H), 7.65 (dt, *J* = 8.3, 4.1 Hz, 1H), 7.56 – 7.49 (m, 3H), 7.46 (t, *J* = 8.1 Hz, 1H), 7.37 (dd, *J* = 8.0, 2.2 Hz, 1H), 7.11 (d, *J* = 4.1 Hz, 2H), 3.83 (s, 3H). **^{13}C NMR** (151 MHz, $CDCl_3$) δ 162.15,

159.62, 152.27, 149.62, 149.26, 137.54, 132.81, 130.75, 130.41, 130.39, 128.91, 128.54, 128.50, 125.55, 125.52, 120.04, 119.15, 115.26, 42.07. **Anal. Calcd. for $C_{21}H_{16}N_4O_2$**: C, 70.77; H, 4.53 N, 15.72. Found: C, 70.63; H, 4.38; N, 15.90.

N-methyl-N-(4-nitrophenyl)-2-phenylquinazolin-4-amine (278).

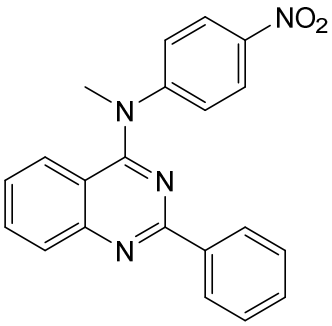

Molecular weight: 356.39 g/mol

The compound was synthesized from **31** (342.36 mg, 1 mmol), sodium hydride (36.0 mg, 1.5 mmol) and methyl iodide (212.91 mg, 1.5 mmol) as described in the general procedure for compounds **277-280** to yield **278** as a yellow solid (299 mg, 84%), mp 173-174 °C. **^{1}H NMR** (600 MHz, Chloroform-*d*) δ 8.70 – 8.55 (m, 2H), 8.17 (d, *J* = 8.6 Hz, 3H), 7.76 – 7.68 (m, 1H), 7.52 (h, *J* = 3.8 Hz, 3H), 7.22 (p, *J* = 9.0, 8.1 Hz, 2H), 7.16 (d, *J* = 8.6 Hz, 2H), 3.86 (d, *J* = 2.3 Hz, 3H). **^{13}C NMR** (151 MHz, $CDCl_3$) δ 162.56, 159.87, 159.81, 153.58, 152.02, 143.44, 137.25, 133.38, 131.02, 128.59, 126.13, 125.43, 122.23, 116.01, 41.31. **Anal. Calcd. for $C_{21}H_{16}N_4O_2$**: C, 70.77; H, 4.53 N, 15.72. Found: C, 70.91; H, 4.46; N, 15.87.

4-(methyl(2-phenylquinazolin-4-yl)amino)benzonitrile (279).

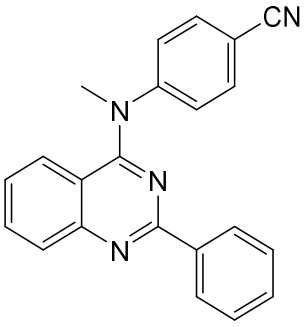

Molecular weight: 336.40 g/mol

The compound was synthesized from **35** (322.37 mg, 1 mmol), sodium hydride (36.0 mg, 1.5 mmol) and methyl iodide (212.91 mg, 1.5 mmol) as described in the general procedure for compounds **277-280** to yield **279** as a yellow solid (313 mg, 93%), mp 201-203 °C. **^{1}H NMR** (500 MHz, DMSO-d_6) δ 8.61 – 8.46 (m, 2H), 7.95 (dd, *J* = 8.5, 1.3 Hz, 1H), 7.82 – 7.72 (m, 3H), 7.55 (dtd, *J* = 10.6, 4.9, 4.4, 1.6 Hz, 3H), 7.41 – 7.33 (m, 2H), 7.30 (ddd, *J* = 8.2, 6.8, 1.3 Hz, 1H), 7.21 (dd, *J* = 8.4, 1.3 Hz, 1H), 3.76 (s, 3H). **^{13}C NMR** (126 MHz, DMSO) δ 162.37, 158.91, 152.35, 151.98, 137.77, 133.87, 133.29, 130.71, 128.90, 128.63, 128.11, 126.02, 125.65, 123.90, 118.85, 115.84, 106.47, 41.00. **Anal. Calcd. for $C_{22}H_{16}N_4$**: C, 78.55; H, 4.79 N, 16.66. Found: C, 78.69; H, 4.59; N, 16.76.

N-(3-fluorophenyl)-N-methyl-2-phenylquinazolin-4-amine (280).

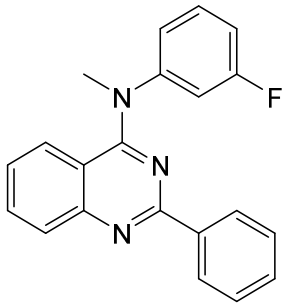

Molecular weight: 329.38 g/mol

The compound was synthesized from **40** (315.35 mg, 1 mmol), sodium hydride (36.0 mg, 1.5 mmol) and methyl iodide (212.91 mg, 1.5 mmol) as described in the general procedure for compounds **277-280** to yield **279** as a yellow solid (260 mg, 79%), mp 109-111 °C. **^{1}H NMR** (500 MHz, DMSO-d_6) δ 8.61 – 8.46 (m, 2H), 7.95 (dd, *J* = 8.5, 1.3 Hz, 1H), 7.82 – 7.72 (m, 3H), 7.55 (dtd, *J* = 10.6, 4.9, 4.4, 1.6 Hz, 3H), 7.41 – 7.33 (m, 2H), 7.30 (ddd, *J* = 8.2, 6.8, 1.3 Hz, 1H), 7.21 (dd, *J* = 8.4, 1.3 Hz, 1H), 3.76 (s, 3H). **^{13}C NMR** (500 MHz, DMSO-d_6) δ 8.60 – 8.49 (m, 2H), 7.87 (dd, *J* = 8.5, 1.2 Hz, 1H), 7.70 (ddd, *J* = 8.4, 6.9, 1.4 Hz, 1H), 7.57 – 7.49 (m, 3H), 7.42 (td, *J* = 8.2, 6.7 Hz, 1H), 7.26 (dt, *J* = 10.5, 2.3 Hz, 1H), 7.19 (ddd, *J* = 8.2, 6.8, 1.3 Hz, 1H), 7.13 (tdd, *J* = 8.5, 2.5, 0.9 Hz, 1H), 7.10 – 7.04 (m, 2H), 3.71 (s, 3H). **^{13}C NMR** (126 MHz, DMSO) δ 162.90 (d, *J* = 245.2 Hz), 161.73, 158.63, 152.15, 149.85 (d, *J* = 10.0 Hz), 138.08, 132.71, 131.53 (d, *J* = 9.5 Hz), 130.54, 128.71, 128.55, 128.09, 125.74, 125.25, 121.55, 115.19, 113.04 (d, *J* = 21.0

Hz), 112.68 (d, *J* = 23.0 Hz), 41.91. **Anal. Calcd. for $C_{21}H_{16}FN_3$**: C, 76.58; H, 4.90 N, 12.76. Found: C, 76.44; H, 4.78; N, 12.50.

10.1.2 Materials and Methods

Chemicals employed for the synthesis of all precursors and final compounds were purchased from Acros Organics (Geel, Belgium), Alfa Aesar (Karlsruhe, Germany), Sigma-Aldrich (Steinheim, Germany), Merck (Darmstadt, Germany) or TCI (Zwijndrecht, Belgium).

Reaction progress was monitored by thin layer chromatography (TLC) using an aluminum plate coated with silica gel 60 F_{254} (Merck Millipore, Billerica, MA, USA). As eluent a mixture of dichloromethane and methanol (9:1) was used for most of the compounds. The fluorescent indicator in the silica gel shows a bright background in UV light which enables the detection of compounds as black spots upon absorption. For this purpose, a UV cabinet with an excitation wavelength of 254 nm was used.

Column chromatography was utilized for purification of some compounds. Therefore, chromatography columns of different lengths depending on the experimental parameters (eluent, yield…) were filled with silica gel 60 (40-63 µm, Merck) as stationary phase with the desired amount. Embedments of air were removed by gentle shaking followed by carefully adding the chosen mobile phase. The silica gel was homogenously coated with the mobile phase and slightly compressed by adding pressure via a hand pump. On top of the stationary phase a layer of see sand was added to preserve the surface of the column material and enable readily addition of the compound, which was initially solved in a small amount of mobile phase. The purification was performed under slight pressure and the obtained fractions sorted by monitoring the process by TLC. Fractions containing the target compound were collected and the solvent evaporated under reduced pressure to yield the corresponding solid compound.

NMR-Spectroscopy was applied to confirm the identity of all compounds. For this purpose ^{1}H and ^{13}C spectra were either obtained on a Bruker Advance 500 MHZ (500/126 MHz) or a Bruker Advance 600 MHZ (600/151 MHz). Compounds were either dissolved in DMSO-*d*6 or chloroform-*d*1, which were also used as internal standards, and the chemical shifts (δ) given in ppm. Assignment of the ^{13}C signals was performed by distortionless enhancement by polarization transfer (DEPT) and attached proton test (APT). Signal multiplicity is indicated as singlet (s), doublet (d), doublet of doublets (dd), triplet of doublets (td), triplet (t), doublet of triplets (dt), quartet (q) and multiplet (m) and the coupling constants J are given in Hz.

Elemental analysis was utilized to determine the purity of the test measuring with a Vario EL V24 CHN Elemental Analyzer (Elementar Analysesysteme GmbH, Hanau, Germany). All values found were in the range of ±0.4% of the theoretical values, unless indicated.

10.2 Biological investigation

10.2.1 Cell culture

Cell culture in general was performed under sterile conditions using a laminar flow cabinet. All supplements employed for culturing were either bought sterile or prepared under sterile conditions to avoid bacterial growth and other contamination.

10.2.1.1 MDCK II wild-type and ABCG2/BCRP overexpressing cell line

The MDCK II cell lines (Madin-Darby canine kidney) with overexpression of ABCG2 and the parental cell line were received as a kind gift of Dr. A. Schinkel (The Netherlands Cancer Institute, Amsterdam, The Netherlands). MDCK II ABCG2/BCRP cells were generated by transfection of the canine kidney epithelial cell line MDCK II with human wild-type cDNA C-terminally linked to the cDNA of the green fluorescent protein (GFP).

Cell culture was performed with Dulbecco's modified Eagle's medium (DMEM) containing 10% fetal bovine serum (FBS), 50 µg/mL streptomycin, 50 U/mL penicillin G and 2 mM *L*-glutamine. Cells were incubated in T75 or T175 tissue culture flasks in a humidified atmosphere at 37 °C and 5% CO_2 containing 20 or 30 mL of culture medium, respectively. At a confluence of about 80-90%, the cells were harvested as described below in the section "subculturing". Acidification of the medium by cellular processes was additionally controlled visually by inspecting its color. The supplemented phenyl red indicator changes from a pink color to yellow. To sustain the resistance of the cells, they were cultured for less than 25 passages.

Subculturing of the cells was performed at a confluence of 80-90% by removing the culture medium in a sterile laminar flow cabinet using suction. The remaining medium was washed by adding 5 mL PBS with gentle shaking. After removing the liquids by suction, 3-5 mL Trypsin solution was added according to the size of the flask followed by a 10 minute incubation period in the incubator to detach the cells from the bottom. After about half of the cells were detached, they were collected by washing them off with 7-10 mL culture medium and transferring the cell suspension to a 50 mL centrifugation tube for centrifugation at 1200 x g for 4 minutes at 4 °C. Subsequently, the supernatants were removed from the formed cell pellet by suction and the pellet resuspended in 5 mL fresh medium. The so prepared cells can be used for further culturing or for cell based assays. Counting of the cells was performed with a CASY1 model TT. Therefor, 20 µL of a cell suspension was thoroughly mixed with 10 mL sterile filtered Casy ton solution and measured with a 150 µm capillary. In order to exclude cell debris and agglomerates the cells were counted according to their size between 8 and 40 µm. Subsequently, the desired amount of cells was centrifuged in a 1.5 mL Eppendorf reaction vessel and the supernatants discarded. KHP was used to resuspend the cell pellet and the procedure repeated with KHB two more times to yield a cell suspension of washed cells in KHB.

Cryoconservation was performed by resuspending the cells after centrifugation (see "subculturing" above) in a mixture of 90% culture medium and 10% DMSO. For each cryovial 1 mL of the prepared cell suspension containing a cell density of about 5-10 million cells was used. The cryovials were then quickly transferred to a -80 °C freezer to reduce the toxic effect of the DMSO. After 48 h the cryovials were transferred to a liquid nitrogen tank to allow preservative storage for longer time periods.

Defrosting of the cells was performed by allowing the cryovials which were taken from the liquid nitrogen tank to warm up in a 37 °C water bath. As soon as the containments liquidate, the obtained cell suspension was immediately transferred to a T75 tissue culture flask, together with 20 mL of cell culture medium. After 24 h, the old medium was replaced with fresh medium and the cells were cultured for 1-2 more passages before using them in cell based assays.

10.2.1.2 PLB-985 (ABCG2 overexpressing)

PLB-985 cells were established from the peripheral blood of a 38-year-old woman with acute myeloid leukemia (AML FAB M4) in relapse in the year 1985 and were a kind gift of Csilla Özvegy-Laczka (National Medical Center, Institute of Haematology and Immunology, Membrane Research Group, Hungarian Academy of Sciences, 1113 Budapest, Hungary). According to the DNA fingerprint, PLB-985 is a subclone of cell line HL-60.

Cell culture was carried out in RPMI 1640 medium with 10% FBS, 50 mg/mL streptomycin, 50 U/mL penicillin G and 2 mM *L*-glutamine under a 5% CO_2 humidified atmosphere at 37 °C. Cells were cultured in T25, T75 and T175 tissue culture flasks and do not attach to the bottom. Cell density was maintained at 0.3 million cells to 1.5 million cells per mL. Doubling of the suspension cells was achieved within 24 h and the cell density needed to be monitored after two days whether it was necessary to replace the medium of the suspension cells. Acidification of the medium by cellular processes was additionally controlled visually by inspecting its color. The supplemented phenyl red indicator changes from a pink color to yellow. To sustain the resistance of the cells, they were cultured for less than 20 passages.

Subculturing of the cells was performed by centrifugation of the cell suspension in a 50 mL centrifugation tube (266 x g, 4 °C, 4 min) obtaining a cell pellet. The supernatants were removed from the formed cell pellet by suction and the pellet re-suspended in 5 mL fresh medium. The so prepared cells can be used for further culturing or for cell based assays. Counting of the cells was performed as described in chapter 10.2.1.1.

Cryoconservation of the cells was performed by resuspending the cells after centrifugation (see “subculturing” above) in a mixture of 70% culture medium, 20% FBS

and 10% DMSO. The prepared cell suspension was added in 1 mL aliquots to cryovials at a cell density of 5-10 million cells/mL and immediately stored at -80 °C for 48 h. Subsequently, the cryovials were stored in a liquid nitrogen tank at -190 °C as backups. The so prepared cryovials can later be defrosted by placing them into a 37 °C water bath. After liquidation of the mixture it was quickly transferred to a 50 mL centrifugal tube containing 10 mL culture medium. After centrifugation (266 x g, 4 °C, 4 min) the supernatants were removed and the cell pellet resuspended in 5 mL culture medium. Cells were then counted with a CASY1 model TT as described above, transferred to a tissue culture flask and the cell density adjusted to 750,000 cells/mL. After 3 passages cells were used for cell based assays.

10.2.1.3 A2780 Adr (ABCB1/P-gp overexpressing)

Human ovarian carcinoma cell line A2780adr was purchased from European Collection of Animal Cell Culture (ECACC, No 93112520). The cell line shows an overexpression of ABCB1 and resistance against doxorubicin.

Cell culture was performed with RPMI-1640 medium supplemented with 20% FBS, 50 µg/mL streptomycin, 50 U/mL penicillin G and 2 mM *L*-glutamine under a 5% CO_2 humidified atmosphere at 37 °C. Acidification of the medium by cellular processes was additionally controlled visually by inspecting its color. The supplemented phenyl red indicator changes from a pink color to yellow.

Subculturing was performed as described in chapter 10.2.1.1 in the section "subculturing". To ensure the overexpression of ABCB1, treatment with 100 nmol/L doxorubicin was carried out every 10 passages but for less than a total of 40 passages. Acidification of the medium by cellular processes was additionally controlled visually by inspecting its color. The supplemented phenyl red indicator changes from a pink color to yellow.

Cryoconservation was carried out as described in chapter 10.2.1.1 in the section "cryoconservation".

10.2.1.4 H69AR (ABCC1/MRP1 overexpressing)

The small cell lung cancer cell line H69 AR with overexpression of ABCC1 was purchased from American Type Culture Collection (ATCC, CRL-11351). Resistant cell line H69AR was established from NCI-H69 cells which were grown in the presence of increasing concentrations of doxorubicin over 14 month.

Cell culture was carried out in RPMI-1640 medium with 20% FBS, 50 mg/mL streptomycin, 50 U/mL penicillin G and 2 mM *L*-glutamine and kept under a 5% CO_2 humidified atmosphere at 37 °C. Acidification of the medium by cellular processes was additionally controlled visually by inspecting its color. The supplemented phenyl red indicator changes from a pink color to yellow.

Subculturing of the cells was performed according to chapter 10.2.1.1 in the section "subculturing".

Cryoconservation was carried out as described in chapter 10.2.1.1 (section "cryoconservation") using a mixture of 95% culture medium and 5% DMSO to re-suspend the cells before storing the cells at -80 °C followed by final storage at -190 °C, respectively.

10.2.2 Cell based assays

For all cell based assays, stock solutions were prepared from the test compounds using DMSO and obtaining a final compound concentration of 10 mM. The preparation of the compound dilutions was carried out with sterile filtered KHB. For compounds with low solubility in aqueous media methanol was added to yield a final concentration of less than 5% MeOH in the highest concentration of the corresponding dilution series. Likewise, the highest concentration of DMSO in the final concentrations was less than 0.1%.

10.2.2.1 Buffers used for cell based assays

Krebs-HEPES buffer (KHB) was used for most of the call based assays to prepare the compound dilutions or maintain the cell viability during the assays. KHB contains no supplements of dyes or enzymes which may influence the corresponding assay.

Preparation of KHB was carried out with a mixture of chemicals listed in Table 30 to yield a 5X concentrated solution which can be stored at -20 °C for later application.

Table 30: Chemicals for the Preparation of Krebs-HEPES Buffer.

Chemical (molecular formula)	**Molecular weight [g/mol]**	**Conc. 5X solution [mM]**	**Weigh in for 5X solution (500 mL) [g]**
Sodium chloride (NaCl)	58.44	593	17.33
Potassium chloride (KCl)	74.55	5.64	0.876
Monopotassium phosphate (KH_2PO_4)	136.09	6.00	0.408
Sodium bicarbonate ($NaHCO_3$)	84.01	21	0.882
D-glucose-monohydrate ($C_6H_{12}O_6*H_2O$)	198.17	58.5	5.796
HEPES, free acid ($C_8H_{18}N_2O_4S$)	238.31	50	5.958

Preparation of the buffer was carried out by adding the weighted chemicals to a 500 mL volumetric flask together with a magnetic stirrer and 450 mL distilled water. The mixture was stirred until complete solution of the solid components and the pH adjusted with 0.1 N NaOH (aq) to 7.4. Subsequently, the volume was added up under stirring with distilled water to a final volume of 500 mL and the obtained 5X KHB solution stored as 50 mL aliquots at -20 °C.

Preparation of the 1X KHB solution was carried out by adding 100 mL of the 5X KHB to a 500 mL volumetric flask and adding 650 µL of 1M calcium chloride (final conc. 2.50 mmol) followed by 350 mL distilled water. The mixture was stirred and 600 µL of a 1M magnesium sulfate heptahydrate (final conc. 1.20 mM) was added, followed by further addition of distilled water to a final volume of 500 mL. The resulting solution was filtered sterile using a 0.2 µm membrane filter, obtaining 50 mL aliquots which were sealed and frozen at -20 °C for later use.

Phosphate buffered saline (PBS) was prepared according to the following procedure using the chemicals listed in Table 31. Due to its isotonic and nontoxic properties with most cells it was applied for the preparation of dilutions and work with cells.

Table 31: Chemicals for the Preparation of Phosphate-buffered Saline (PBS) Solution.

Chemical (molecular formula)	**Molecular weight [g/mol]**	**Conc. 1X solution [mM]**	**Weigh in for 1X solution (100 mL) [g]**
Sodium chloride (NaCl)	58.44	137	8.01
Potassium chloride (KCl)	74.55	2.7	0.20
Monopotassium phosphate (KH_2PO_4)	136.09	2.0	0.27
Disodium phosphate (Na_2HPO_4)	141.9	10	1.44

Preparation of the buffer was carried out by weighing the listed chemicals in a 1000 mL volumetric flask together with a magnetic stirrer and 800 mL distilled water. After complete dissolution of the chemicals, the pH was adjusted to 7.4 using 0.1 M NaOH (aq) and filled with distilled water to a final volume of 1000 mL. Sterilization of the mixture was carried out in an autoclave heating to 121 °C at a pressure of 2 bar over 20 minutes. The sterilized KHB was stored at -4 °C and used under sterile conditions.

10.2.2.2 Hoechst 33342 accumulation assay

The Bisbenzimidazole derivative Hoechst 33342 (2'-(4-Ethoxyphenyl)-6-(4-methyl-1-piperazinyl)-1*H*,3'*H*-2,5'-bibenzimidazole) is a fluorescent dye with an excitation maximum at 340 nm and an emission maximum at 450 nm.[219] Due to the fact that it is also a substrate of ABCB1 and ABCG2 it is broadly used in functional efflux assays of the mentioned transport proteins.[45, 189] By binding of Hoechst to DNA or a lipophilic environment like a cell membrane the fluorescence intensity increases drastically by a factor of 750 to 1500 compared to an aqueous environment.[182,183,184,187, 188] Owing to its relatively high lipophilicity, Hoechst 33342 is able to permeate cell membranes. The corresponding fluorescence can then be correlated to the concentration of Hoechst 33342 in a cell. Since its accumulation is restricted by the expression of transport proteins, such as ABCG2 and ABCB1, addition of an inhibitor of the corresponding transport protein can reduce the efflux rate by inhibiting the transport of Hoechst 33342. Thereby, the potency of an inhibitor can be determined by correlation of the compound concentration with the obtained fluorescence. A general scheme of a Hoechst 33342 accumulation assay

is presented in Figure 117. Overall fluorescence is measured for 120 minutes to ensure the steady-state of Hoechst 33342 in the cell is reached, since the increase of the fluorescence follows a first order kinetic (hyperbolic).[190]

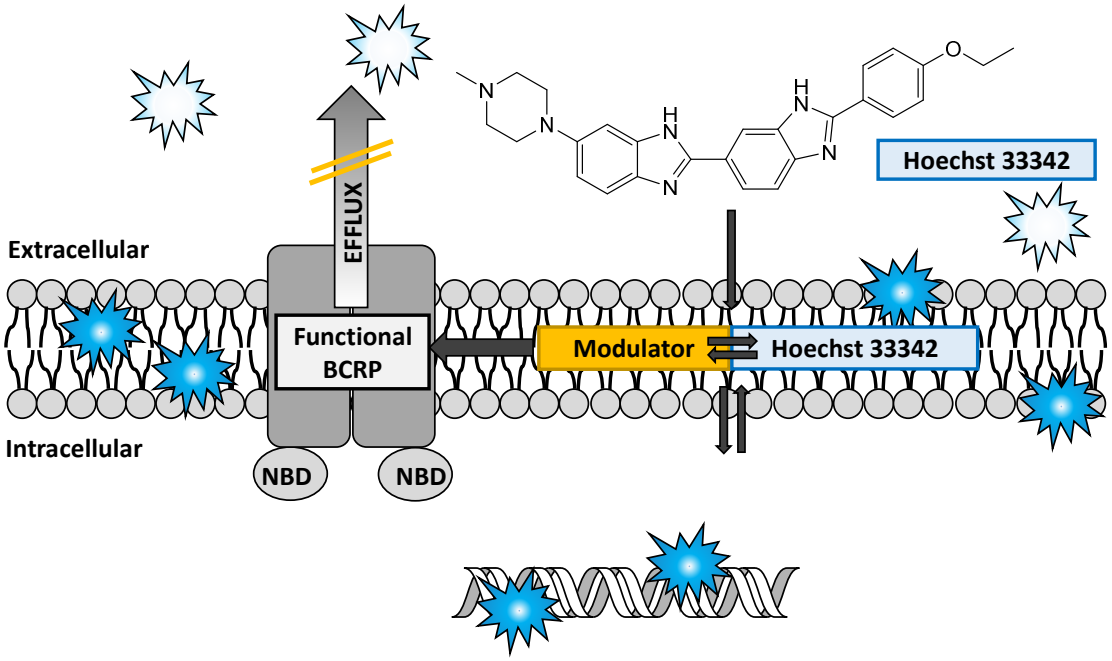

Figure 117: Principle of the Hoechst 33342 accumulation assay.

Procedure: The Hoechst 33342 accumulation assay was carried out with MDCK II wild-type and ABCG2 overexpressing cells to investigate the inhibitory effect of the test-compounds on ABCG2. The procedure is described in earlier studies and was performed with small modifications.[220,221,222,223,224,225,226,227,228,229,230,231] Cells were cultivated, prepared, counted and washed as described in chapter 10.2.1. Approximately 3 million washed cells, suspended in KHB, were used for one 96 well microplate. A typical pipetting scheme for this assay with two different compounds and a standard inhibitor is illustrated in Figure 118. A volume of 160 µL of KHB was added to the rows A, D and G. Then the same volume of a cell suspension containing resistant cells or sensitive cells (each approx. 30,000 cells/well) was added to B, E, H and C, F, respectively. Subsequently, 20 µL of different dilutions of the corresponding compound was added to the wells giving a total volume of 180 µL and the plate stored for a preincubation period of 30 min at 37 °C and 5% CO_2. Then, 20 µL of a 10 µM Hoechst 33342 solution (protected from light) was quickly added to each well yielding a final concentration of

1 µM Hoechst 33342. The amount of methanol and DMSO in the final concentration was chosen not to exceed 5% and 0.1%, respectively. Compound concentrations were varied between 10 µM and 1 nM, depending on the potency of a compound, and added from column 2 (lowest concentration) to column 12 (highest concentration). Ko143 or WK-X24 was used as standard to check the reliability of the assay.

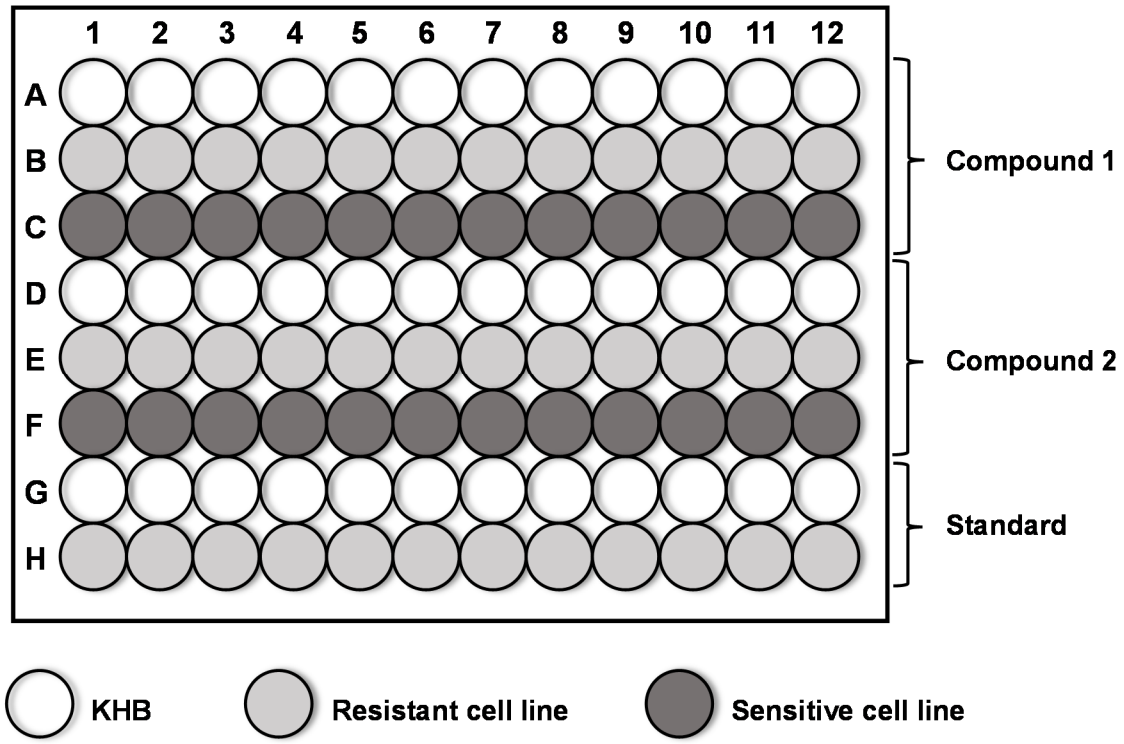

Figure 118: Layout of the 96 microwell plate employed in the Hoechst 33342 accumulation assay. Ko143 or WK-X24 was used as standard.

Measurement of the fluorescence was performed immediately in constant time intervals (60 s) up to 120 min with an excitation wavelength of 355 nm and an emission wavelength of 460 nm, using a BMG POLARstar or FLUOstar microplate reader. Further parameters are given in Table 32.

Table 32: Parameters Used for the Measurement of the Fluorescence with a FLUOstar and a POLARstar Microplate Reader.

Parameter	Value
Incubation temperature	37 °C
Excitation wavelength	355 nm
Emission wavelength	460 nm
Gain (for FLUOstar)	1700-1800
Gain (for POLARstar)	45-50
Required value	20%
Number of cycles	120
Cycle time	60 sec
Number of light flashes	10/sec

For the analysis of the data, the fluorescence of the wells containing only compound in KHB was subtracted from the fluorescence reading obtained from the MDCK II cells to correct for potential fluorescence of the compound. Average of the fluorescence measured between 100 and 109 min (steady state) was calculated for each concentration and plotted against the logarithm of the compound concentration. Concentration-response curves were fitted by nonlinear regression using the four-parameter logistic equation with variable Hill slope, or the three-parameter logistic equation with a fixed Hill slope of one, whatever equation was statistically preferred (GraphPad Prism, version 5.0, San Diego, CA, USA). From the pIC_{50} values and their standard deviation the IC_{50} values and standard deviations were calculated according to the equation for log-normal distributed values.[232,233]

10.2.2.3 Pheophorbide A accumulation assay

Pheophorbide A (PhA) is a chlorophyll catabolite and proven to be a selective substrate of ABCG2, based on ABCG2(-/-) knockout mice studies.[234] In contrast to Hoechst 33342 it is no substrate of ABCB1 and can be excited at a wavelength of 488 nm (e.g. blue argon laser) showing a maximum emission at a wavelength of 670 nm.[129] PhA is able to pass

lipophilic cell membranes leading to an accumulation of the fluorescent dye in the cell. This process can be used for flow cytometric assays using ABCG2 overexpressing cells.[235] The transport protein performs an active efflux of PhA out of the cell, limiting the intracellular concentration. The addition of an inhibitor of ABCG2 leads to a higher intracellular concentration due to inhibition of the active efflux which is illustrated in Figure 119. Hence, the potency of the inhibitor correlates with the observed fluorescence in the cell. For the measurement of the fluorescence, a FACSCalibur cell analyzer was used. Hereby, the fluorescence of individual cells was measured after sorting and gating the cells accordingly.

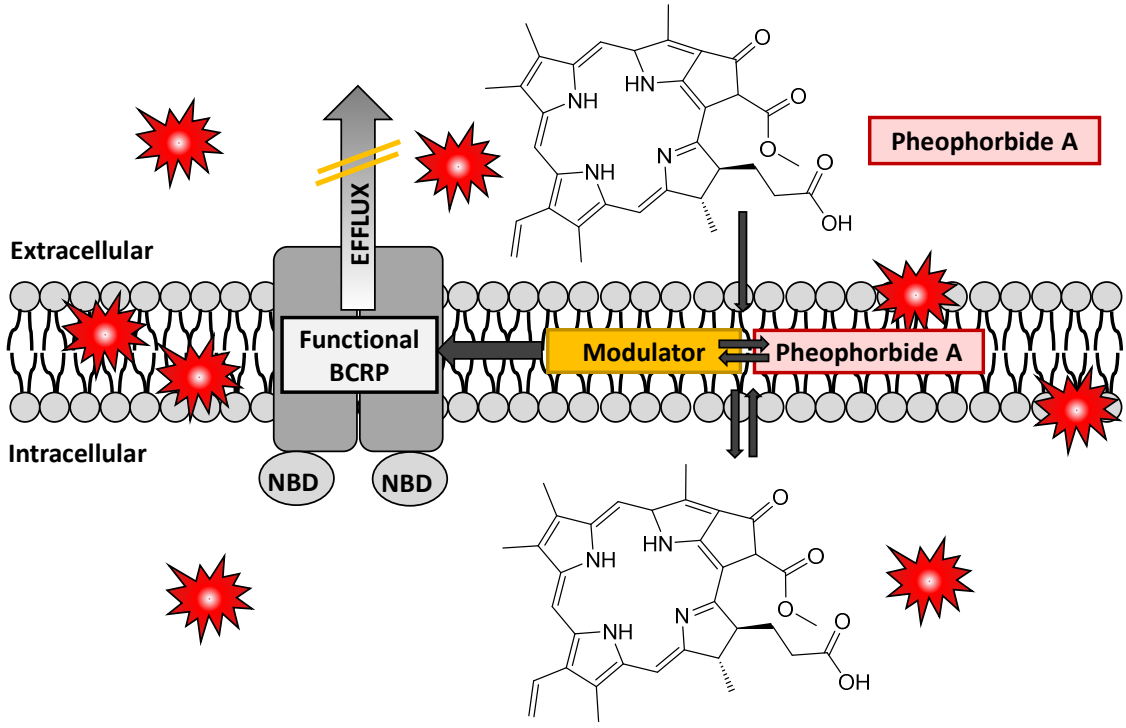

Figure 119: Principle of the Pheophorbide A accumulation assay.

Procedure: Preparation of the assay was similar to the Hoechst 33342 accumulation assay but with some modifications. The MDCK II ABCG2 expressing and sensitive cell lines were prepared as described in chapter 10.2.1.1 and suspended in KHB. Subsequently, 160 µL of the corresponding cell suspension, containing approximately 45,000 cells, was added to a clear U-shaped 96 well microplate according to the layout illustrated in Figure 120.

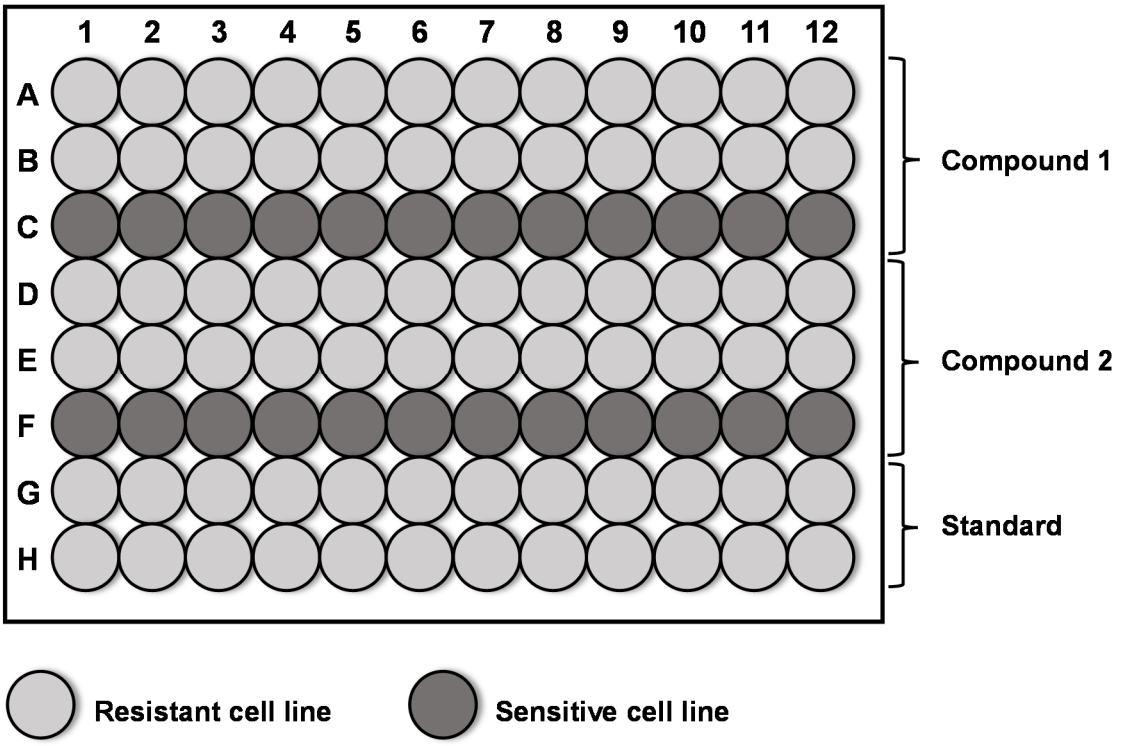

Figure 120: Layout of the 96 microwell plate employed in the Pheophorbide A accumulation assay. Ko143 or WK-X24 were used as standard.

Additionally, 20 µl of different compound dilutions were added to the wells as described for the Hoechst 33342 accumulation assay above (concentration was adapted to the potency of the compounds) and the microplate preincubated for 30 min at 5% CO_2 and 37 °C. Then, 20 µl of a 5 µM pheophorbide A solution (protected from light) was added to each well, followed by a 120 min period of incubation to reach steady state. After incubation, the cells were resuspended in the wells with a multichannel pipette and the fluorescence measured on a FACSCalibur cell analyzer by flow cytometry. Pheophorbide A was excited at a wavelength of 488 nm and emission was detected in the FL3 channel (≥ 670 nm). Prior to the evaluation of the measured fluorescence of PhA inside the cells, a gate was set to exclude agglomerates and cell debris. The IC_{50} values were then calculated by creating concentration-response curves *via* nonlinear regression, using the four-parameter logistic equation with variable Hill-slope.

Principles of flow cytometry: The advantage of a flow cytometric measurement of the fluorescence is based on the sorting of different cells or particles according to size, granularity as well as the emitted fluorescence at very high rates (FACSCalibur: analyzing up to 4000 cells/sec). In general, the cell suspensions are gathered from each well by a cytometer unit. The sample is then accelerated by a laminar flow of a carrier liquid focussing the cells into a consecutive string (hydrodynamic focussing) so that the cells pass a laser beam one by one. Detectors collect the scattered light from the laser beam as forward scatter (FSC), generated by light diffraction, and side scatter (SSC), which is induced by light refraction and light reflection and is detected in a 90° angle to the laser beam. The FSC provides information about the relative size of the particle whereas the SSC gives information about the relative granularity of a particle. Optical filter split the emitted fluorescence of a sample into three specific fluorescence regions after which the corresponding relative fluorescence intensity is measured by three detectors (FL1, FL2 and FL3). A schematic structure and function of the flow cytometric cell analyzer FACSCalibur is depicted in Figure 121.

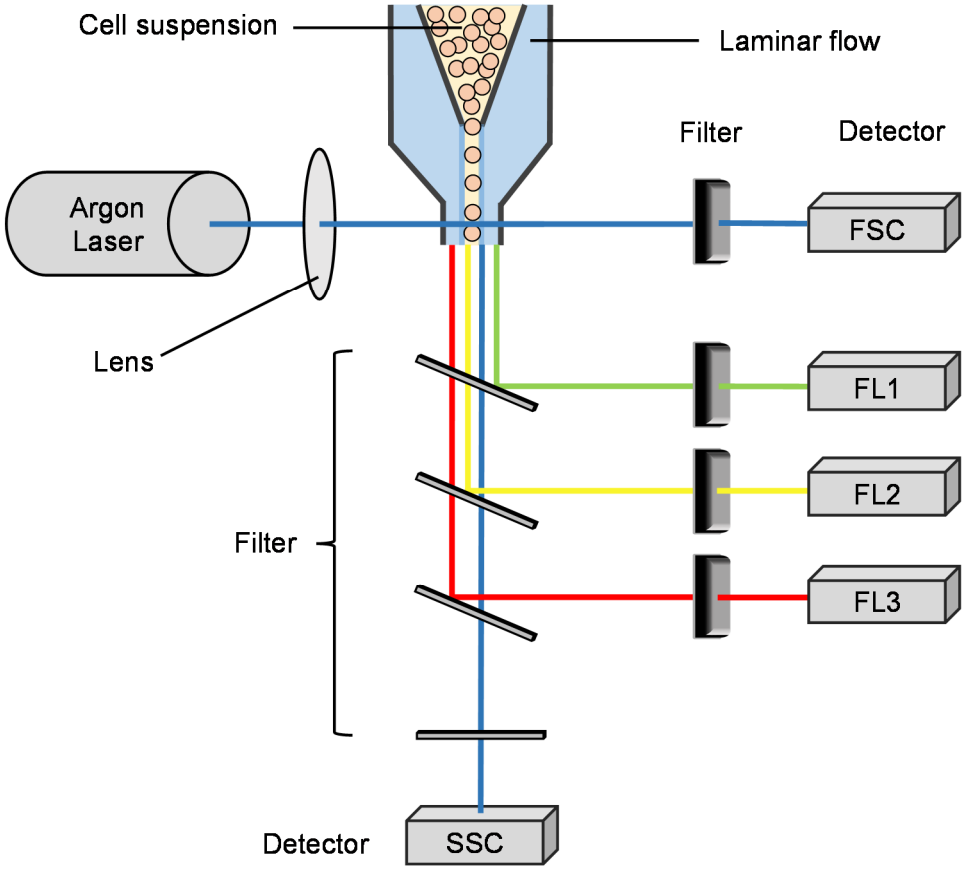

Figure 121: Schematic structure and function of a flow cytometric cell analyzer.

10.2.2.4 Calcein AM assay

Calcein AM is a non-fluorescent, hydrophobic probe containing four acetoxymethyl esters (AM) and one lactone function connected as a spiro species. Due to its high lipophilicity calcein AM is able to enter cell membranes where the ester functions undergo cleavage by unspecific intracellular esterases. Hereby, five carboxylate functions are formed under physiological conditions and the conjugated pi-system of the fluorescein scaffold is restored. Due to the high hydrophilicity of the resulting calcein anion, it is no more able to permeate the cell membrane. Calcein AM is a substrate for two of the three major types of mammalian ABC transport proteins, namely ABCB1 and ABCC1, but not ABCG2.[236, 237,238,239] With regard to ABCC1 it is known that it is able to transport a variety of anionic substrates.[50] However, the anionic calcein molecule is only a poor substrate of ABCC1 and not a substrate of ABCB1 and ABCG2.[240]

By inhibition of ABCB1 or ABCC1 calcein AM accumulates in the cell and forms the fluorescent calcein anion which can be measured fluorometrically. The intracellular concentration of calcein is mostly dependent on the velocity of the diffusion of calcein AM into the cell membrane, the turnover-rate to calcein by esterases, the efflux of calcein AM by a transport protein and the concentration of calcein AM. Addition of an inhibitor restricts the efflux of calcein AM according to its inhibitory potency. Hence, the increase of the intracellular fluorescence correlates directly with the inhibitory potency of a compound which is exploited to calculate IC_{50} values. A schematic view of the underlying principle of the calcein AM assay is illustrated in Figure 122.

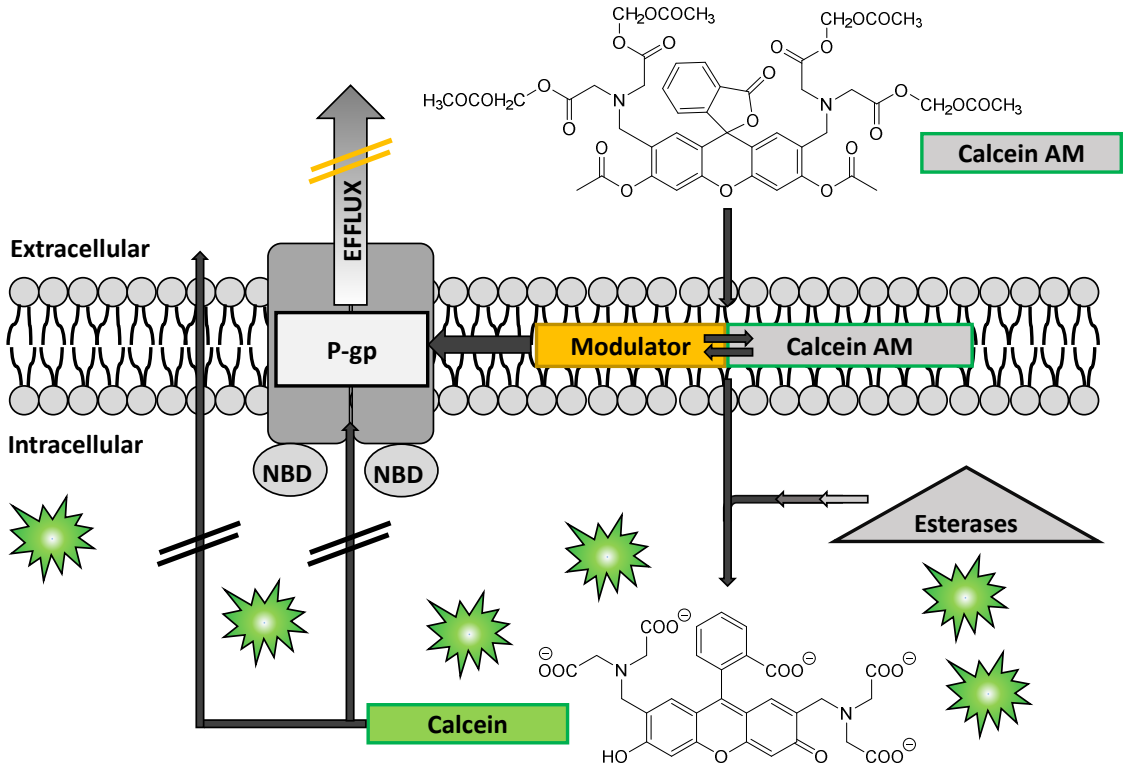

Figure 122: Principle of the calcein AM assay with ABCB1 overexpressing cells.

Procedure: The selectivity of the test compounds toward ABCG2 was investigated by determining the inhibitory activity against ABCB1 and ABCC1 in the calcein AM assay. The ABCB1 overexpressing cell line A2780adr and the ABCC1 overexpressing cell line H69AR were used for the assay. Both cell lines were prepared and washed as described in chapter 10.2.1.3 and 10.2.1.4. After washing the cells three times with KHB, 90 µL of

a suspension containing approximately 30,000 cells was seeded in each well of a colorless flat bottom 96 well microplate. Then 10 µL of different compound dilutions was added according to the microplate layout in Figure 123 giving a final volume of 100 µL.

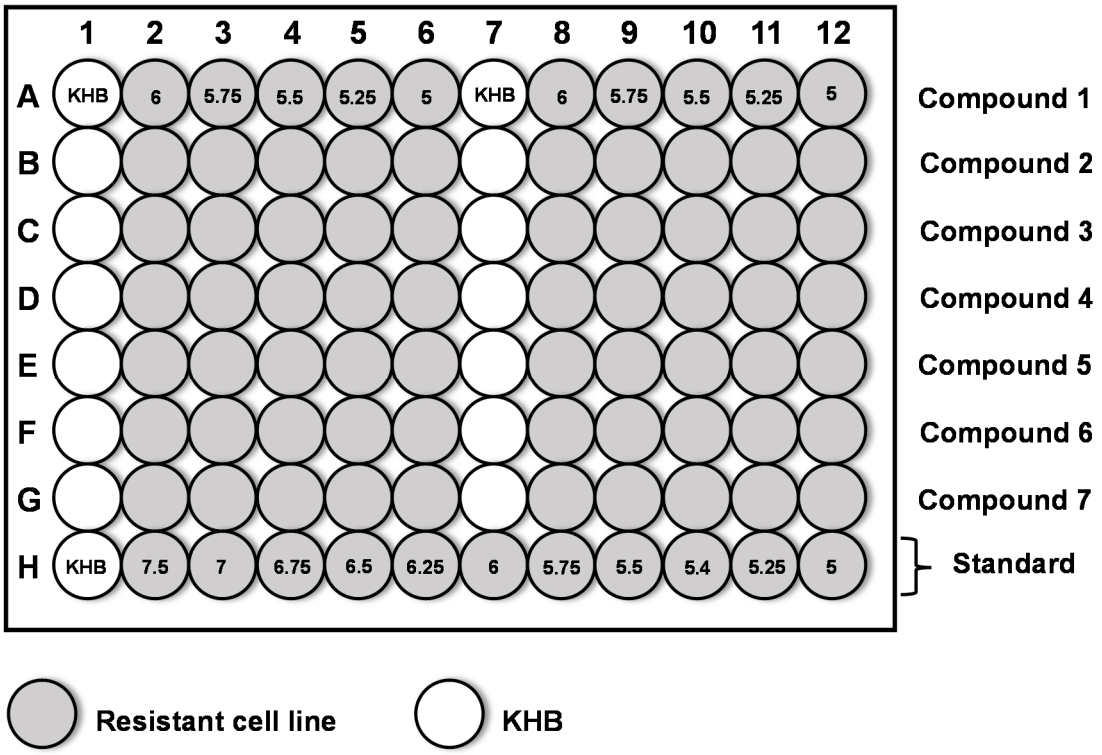

Figure 123: Layout of the microplate used for the calcein AM assay. Each compound was added to a row (A-G) as duplicates (2-6 and 8-12), whereas the depicted final concentrations (in µM) are exemplarily for compound 1 and the standard. Cyclosporine A was used as standard inhibitor with eleven different concentrations.

The prepared plates were kept at 5% CO_2 and 37 °C for a period of 30 min. After this preincubation, 33 µL of a 1.25 µM calcein AM solution (protected from light) was quickly added to each well and the fluorescence measured immediately in a 37 °C tempered BMG POLARstar OPTIMA or FLUOstar OPTIMA microplate reader. The measurement of the fluorescence was carried out for 60 min in constant time intervals (60 s) using an excitation wavelength of 485 nm and an emission wavelength of 520 nm. Further parameters are given in Table 33.

Table 33: Parameters used for the Measurement of the Fluorescence with a FLUOstar and a POLARstar Microplate Reader.

Parameter	Value
Incubation temperature	37 °C
Excitation wavelength	485 nm
Emission wavelength	520 nm
Gain (for FLUOstar)	1700-1800
Gain (for POLARstar)	45-50
Required value	20%
Number of cycles	90
Cycle time	60 sec
Number of light flashes	10/sec

The increase of the fluorescence follows a kinetic of pseudo-zero-order (linear) for as long as the concentration of calcein AM is nearly unchanged. The slope for each concentration was calculated from the initial linear part of the obtained fluorescence time curve. Thereby a slope concentration response curve was obtained which could be fitted by nonlinear regression, using the four-parameter logistic equation with variable Hill slope, or the three-parameter logistic equation with a Hill slope of one, whatever equation was statistically preferred. From the pIC_{50} values and their standard deviation the IC_{50} values and standard deviations were calculated according to the equation for log-normal distributed values.[232,233]

10.2.2.5 MTT assay determining the intrinsic cytotoxicity

The MTT (3-(4,5-dimethylthiazol-2-yl)-2,5-diphenyltetrazolium bromide) reagent is a water soluble tetrazolium salt which is used to determine the viability of cells. Since the molecule is able to permeate cell membranes the yellow dye is reduced by intracellular oxidoreductase enzymes by oxidation of NADH, forming its hydrophobic formazan species. This process takes mostly place in active mitochondria and thus, the formation of the purple formazan species is correlated with the cell viability.[241,242] The concentration

of the purple dye can be measured colorimetrically giving information about the cell viability. A schematic view of the reduction of MTT by living cells to the formazan species is illustrated in Figure 124.

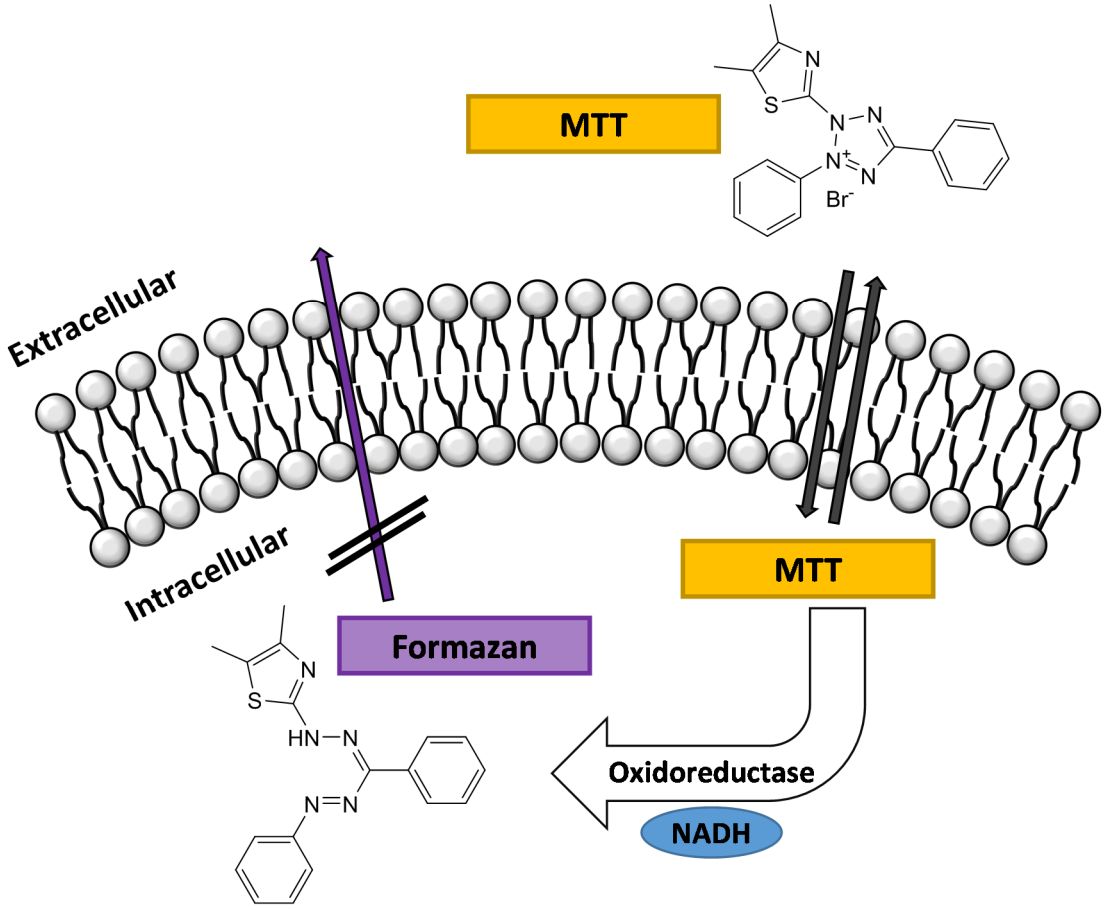

Figure 124: Principle of the MTT reduction in living cells to a formazan species.

Procedure: The intrinsic cytotoxicity of selected compounds was investigated using the MTT cytotoxicity assay as described earlier with slight modifications.[222,225,226,227,228,231,243] In order to avoid contamination of the medium and the cells, the preparation of the assay was carried out under aseptic conditions, using a bench with laminar airflow. MDCK II BCRP and sensitive cells were seeded in 96 well tissue culture microplates at a density of approximately 2,000 cells per well, suspended in a volume of 180 µL culture medium, and kept under 5% CO_2 at 37 °C for 12 h. The old medium in

the microplates was replaced by 180 µL of fresh medium and 20 µL of different compound dilutions was added to each well to a final volume of 200 µL. For the dilution of the compounds the culture medium was supplemented with small amounts of methanol and DMSO, attaining less than 1.8% (MeOH) and 1% (DMSO) volume percent in the final volume. Toxic effects caused by the DMSO and methanol content, was determined by an additional analogue dilution without compound. Moreover, a positive control with medium and 10% (v/v) DMSO as well as a negative control of only medium were carried out. The layout of the microplate is illustrated in Figure 125.

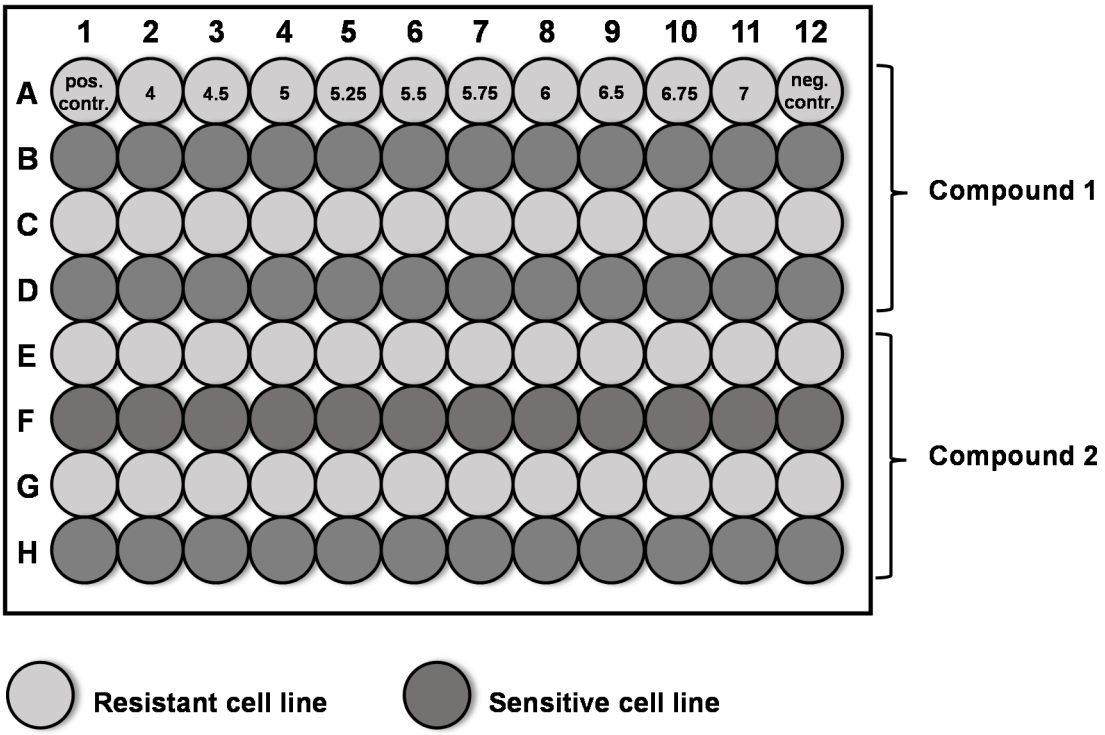

Figure 125: Layout of the microplate used for the MTT cytotoxicity assay. The final compound concentrations (in µM) and positive and negative controls are depicted exemplarily in row A. PBS was added to the interspace between the wells to reduce evaporation of the medium.

The interspace between the wells was carefully filled with 10 mL of PBS in order to reduce evaporation of the medium and the so prepared microplates, were stored at 5% CO_2 and 37 °C for 72 h. After the incubation period, 40 µL of MTT reagent was added to each well and the plate incubated for one hour. After removing the supernatants, 100 µL of DMSO was added to each well resulting in lysis of the cells and solubilisation of

the formed formazan. The absorbance was determined spectrophotometrically at 544 nm and a background correction at 710 nm using a BMG POLARstar microplate reader. Calculation was carried out with the values of the absorbance, setting the negative control as 100% cell viability. Concentration-response curves were fitted by nonlinear regression using the four-parameter logistic equation with variable Hill slope, or the three-parameter logistic equation with a fixed Hill slope of one, whatever equation was statistically preferred (GraphPad Prism, version 5.0, San Diego, CA, USA). From the pIC_{50} values and their standard deviation IC_{50} values and standard deviations were calculated according to the equation for log-normal distributed values.[232,233]

10.2.2.6 MDR reversal assay with Hoechst 33342 and SN-38

A MDR reversal assay was carried out to determine a compounds ability to reverse resistance of ABCG2 expressing MDCK II BCRP cells toward cytotoxic substrates like SN-38 and Hoechst 33342. Addition of an inhibitor of ABCG2 to ABCG2 overexpressing cells leads to a decreased efflux activity of the transport protein dependent on the potency of the compound. In the presence of cytostatic drugs like Hoechst 33342 and SN-38, the reduced efflux of those substrates leads to an intracellular accumulation inducing cell death. Gradual sensitization of the cells with increasing compound concentrations can be derived by measuring the cell viability and enabling the deduction of EC_{50} values by correlation of the cell viability with the corresponding compound concentration.

Procedure: A clear 96 well tissue culture plate was prepared and preincubated for 12 h, as described in chapter 10.2.2.5. The old medium was replaced with 160 µL fresh medium and 20 µL of a compound dilution in culture medium was added to each row as a duplicate. Then, 20 µL of a dilution series of Hoechst 33342 or SN-38 were added column wise, adding to a final volume of 200 µL.

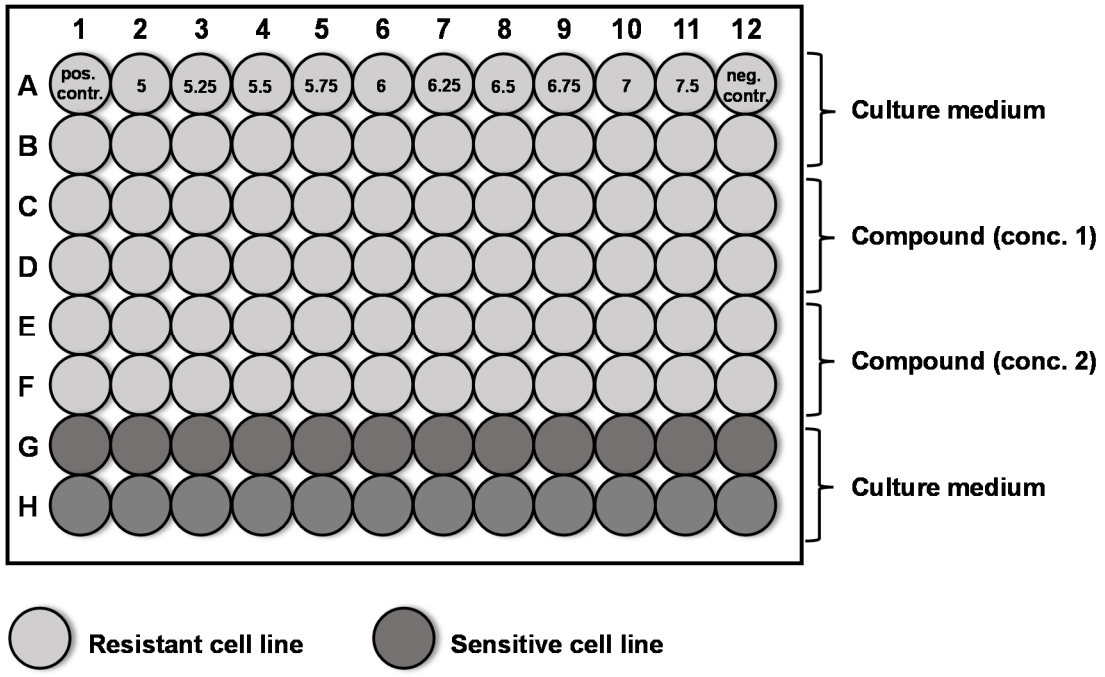

Figure 126: Layout of the microplate used for the MDR reversal assay with Hoechst 33342 and SN-38. The compound concentrations were chosen between 0.01 and 5 µM. The final concentration (in µM) of the cytostatic drug is given exemplarily for row A. PBS was added to the interspace between the wells to reduce evaporation of the medium.

A positive control was established using 10% (v/v) of DMSO as well as a negative control by adding MDCK II BCRP cells and medium without modulator. Further details of the plate layout are illustrated in Figure 126. After 72 h of incubation the plates were prepared and measured as described in chapter 10.2.2.5.

10.2.2.7 MDR reversal assay with mitoxantrone

Mitoxantrone (MX) is an anthraquinone derivative which is applied among others in chemotherapeutic treatment of leukemia, lymphoma, breast and ovarian cancer, acute no lymphocytic leukemia, acute myeloid leukemia, and Hodgkin's lymphoma.[244] The MDR reversal assay with MX as cytostatic drug and substrate of ABCG2 was carried out similar to the Hoechst 33342 and SN-38 efficacy assay described in chapter 10.2.2.6 above. The aim of the assay was to investigate the ability of selected compounds to restore sensitivity of MDCK II ABCG2 overexpressing cells toward MX. Since MX is a substrate of

ABCG2, inhibition of the transport protein leads to a reduced efflux of MX. Owing to the increased intracellular accumulation of the cytotoxic drug the cell death is induced. Subsequently, the viability of the cells can be measured and correlated to the efficacy of an inhibitor.

Procedure: The microplates were prepared only with MDCK II ABCG2 overexpressing cells, similar to the procedure described in chapter 10.2.2.6. Here, the cell density was set to 3000 cells per well and the used microplate layout is depicted in Figure 127.

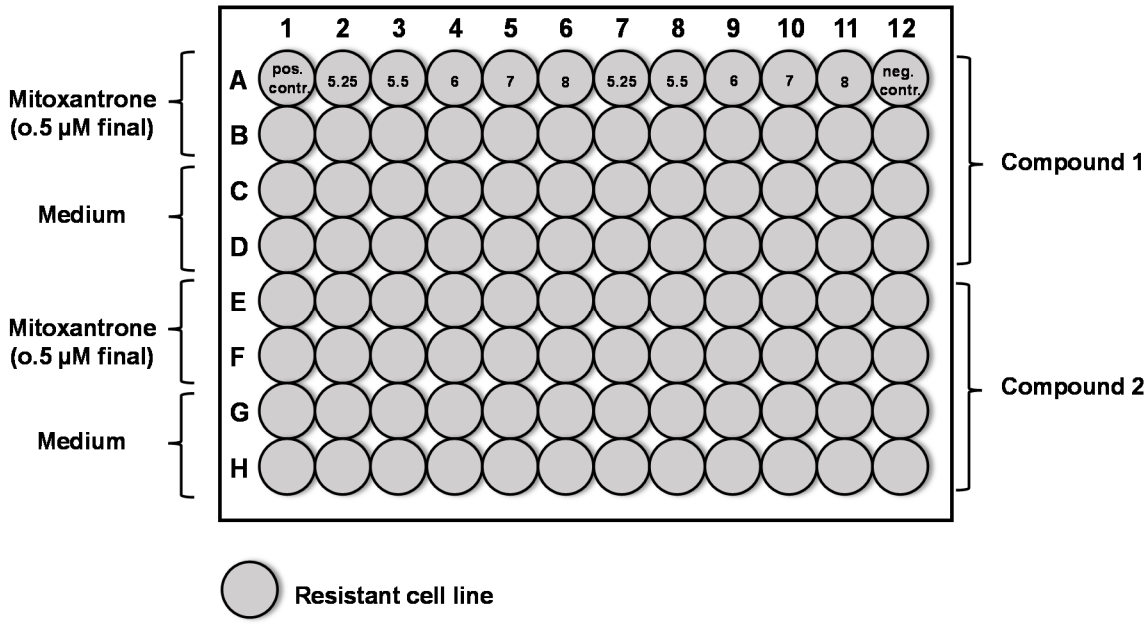

Figure 127: Layout of the microplate used for the MDR reversal assay using mitoxantrone. Final compound concentrations (in µM) are given exemplarily in row A. The final concentration of MX was 0.5 mM. PBS was added to the interspace between the wells to reduce evaporation of the medium.

After replacement of the old medium with fresh culture medium, 20 µL of different compound dilutions were added to the rows. Then, 20 µL of either 5 µM MX or culture medium were added as duplicates in an alternating order to the rows yielding a final volume of 200 µL and a final concentration of 0.5 µM MX. This concentration was chosen after a GI_{50} value slightly higher than 0.5 µM resulted in a MTT viability assay with the ABCG2 overexpressing MDCK II BCRP cell line. For comparison, complete cell death was induced by adding 10% (v/v) of DMSO (positive control) to some wells

and the negative control was established by using medium without compound. This scheme can also be modified using more concentrations of each compound to create concentration-response curves. The preparation of the plate, the subsequent measurement and the data analysis was carried out as described in chapter 10.2.2.6.

10.2.2.8 Enzyme kinetic investigation

Extended enzyme kinetic experiments were performed with selected compounds to study the interaction with the ABCG2 substrate Hoechst 33342. The enzyme kinetic theory describes enzymatically catalyzed chemical reactions and can be transferred to the transport of substrates by the transport protein ABCG2 in the presence of inhibitors. Therefore, the Michaelis-Menten equation, which is used for calculating the rate of enzymatic reactions, can be applied to this problem. The equation describes the reaction rate v in relation to a substrate concentration [S]. Usually, increasing substrate concentrations result in an increasing reaction rate v, following a hyperbolic fashion, until the maximum velocity V_{max} is reached. The Michaelis-Menten constant K_M is defined as the substrate concentration giving $\frac{1}{2} V_{max}$.

$$v = \frac{d[P]}{dt} = \frac{V_{max} \cdot [S]}{K_M + [S]}$$

Equation 1: Michaelis-Menten equation.

Due to the limited concentration range of the substrate, important kinetic parameters like the maximum velocity are difficult to deduce from the Michaelis-Menten curve. In 1934 Lineweaver and Burk invented a method to transform the Michaelis-Menten equation into straight lines by using the reciprocal of the equation (Equation 2).[245]

$$\frac{1}{v} = \frac{K_M + [S]}{V_{max} \cdot [S]} = \frac{K_M}{V_{max}} \cdot \frac{1}{[S]} + \frac{1}{V_{max}}$$

Equation 2: Reciprocal of the Michaelis-Menten equation.

This representation allows the double reciprocal plot of $\frac{1}{v}$ versus $\frac{1}{[S]}$ yielding a straight line that follows the function $f(x) = mx + b$. Hence, $\frac{K_M}{V_{max}}$ can be derived from the slope of the function, $\frac{1}{[S]}$ as the intersection with the Y-axis and $-\frac{1}{K_M}$ as the intersection with the X-axis (compare Figure 128).

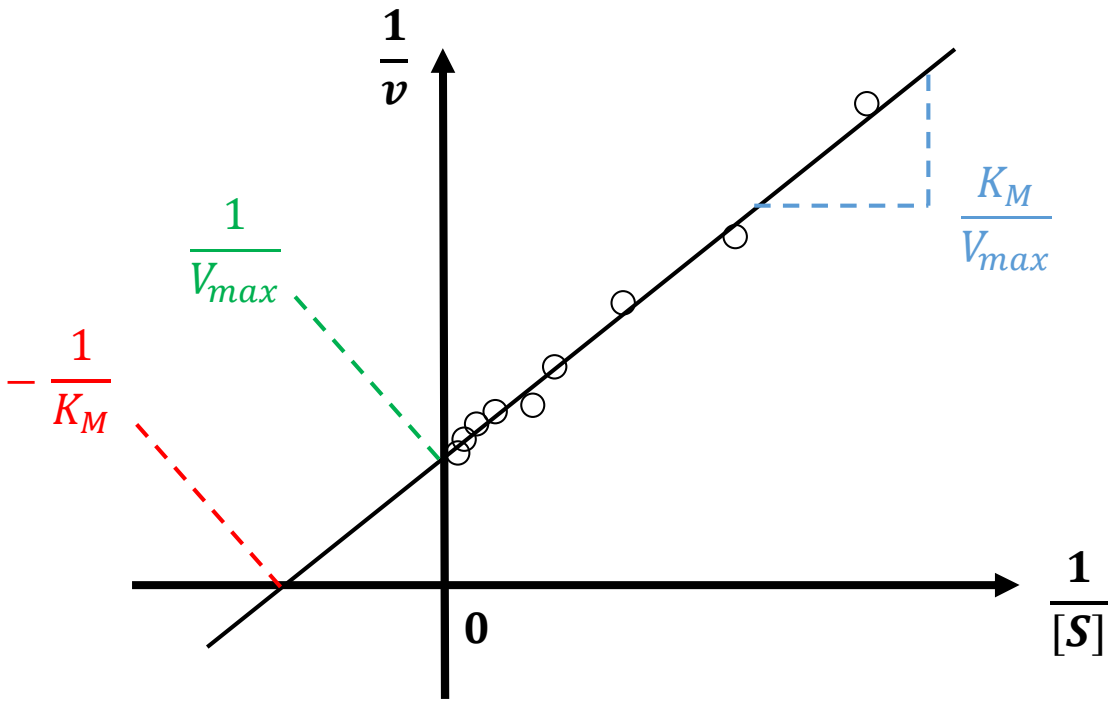

Figure 128: Double reciprocal plot according to Lineweaver-Burk.

The inhibition of the enzyme activity can follow three mechanisms: In the case of a **competitive inhibition**, the substrate S and the inhibitor I bind to the same site of the enzyme. Although I competes with S for the same binding site, sufficiently high substrate concentrations are capable to displace I from the active site of the enzyme, resulting in constant V_{max} values. Here, the K_M values increase with higher inhibitor concentrations and an intersection on the Y-axis in the Lineweaver-Burk plot is obtained. A **non-competitive inhibition** is observed when I binds apart from the active site to the enzyme or the enzyme-substrate-complex [ES]. Due to inactivation of [ES] by the inhibitor even high substrate concentrations are not able to overcome the inhibition, resulting in different V_{max} values for different inhibitor concentrations. This results in an intersection of the lines in the Lineweaver-Burk plot at the X-axis. A special form of the non-competitive

inhibition is a “mixed-type” inhibition. Here, the inhibitor binds apart from the substrate but still affects the active site, for instance by conformational changes after binding of the inhibitor. In this case V_{max} and K_M vary with different [S] and the obtained lines in the Lineweaver-Burk diagram give an intersection in the second or third quadrant of the coordinate system. An **uncompetitive inhibition** is observed, when I only binds to [ES]. Higher [S] lead to an increase of [ES] and thus more binding of I to [ES]. V_{max} and K_M values both increase for this type with increasing inhibitor concentrations. The Lineweaver-Burk diagrams of a double reciprocal plot with the characteristic straight lines to each kinetic type of inhibition are illustrated in Figure 129.

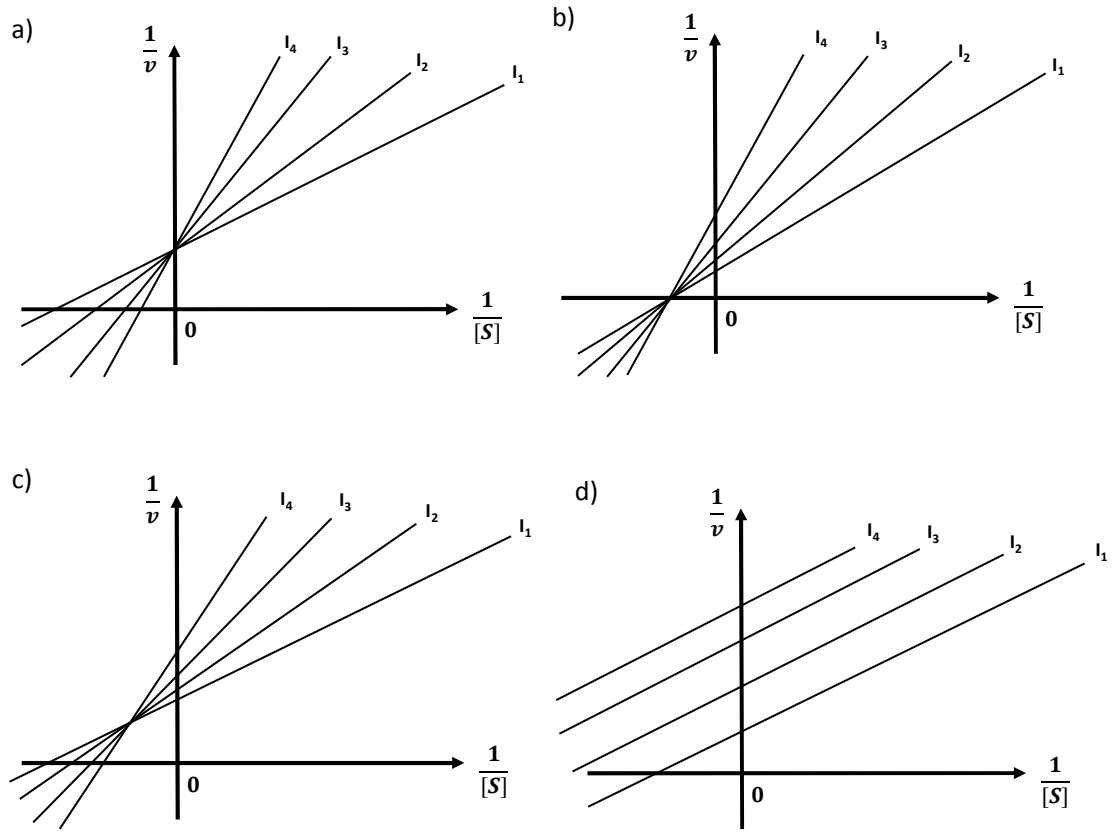

Figure 129: Double reciprocal plot according to Lineweaver-Burk with increasing inhibitor concentrations I_1 to I_4. Type of interaction with substrate: a) competitive; b) non-competitive; c) non-competitive mixed-type; d) uncompetitive.

Although, linearization according to Lineweaver-Burk gives direct information on the type of interaction, this method has been criticized as being notoriously susceptible to

experimental errors, due to the double reciprocal plot. Hence, the results were additionally analyzed by using the data for a direct linear plot according to Cornish-Bowden, since this method has been claimed to be insensitive to outliers.[246] As mentioned before, enzyme kinetic reactions obtain in most cases a hyperbolic curve when the reaction velocity v is plotted against the substrate concentration [S] due to saturation of the enzyme's active site. The Cornish-Bowden linearization plots the reaction velocity v against the negative of the substrate concentration [S]. Transformation of the Michaelis-Menten equation (see Equation 1) results in Equation 3:

$$V_{max} = v + v \cdot \frac{K_M}{[S]}$$

Equation 3: Transformation of the Michaelis-Menten equation used for the Cornish-Bowden plot.

Since substrate concentration [S] and reaction velocity v can be directly derived from the experimental data, the above equation is solved for K_M and V_{max} by inserting at least two corresponding [S] and v value pairs. Graphic representation of the problem illustrates that each straight line consists of one corresponding pair of values, whereas -[S] is plotted on the X-axis and v on the Y-axis.

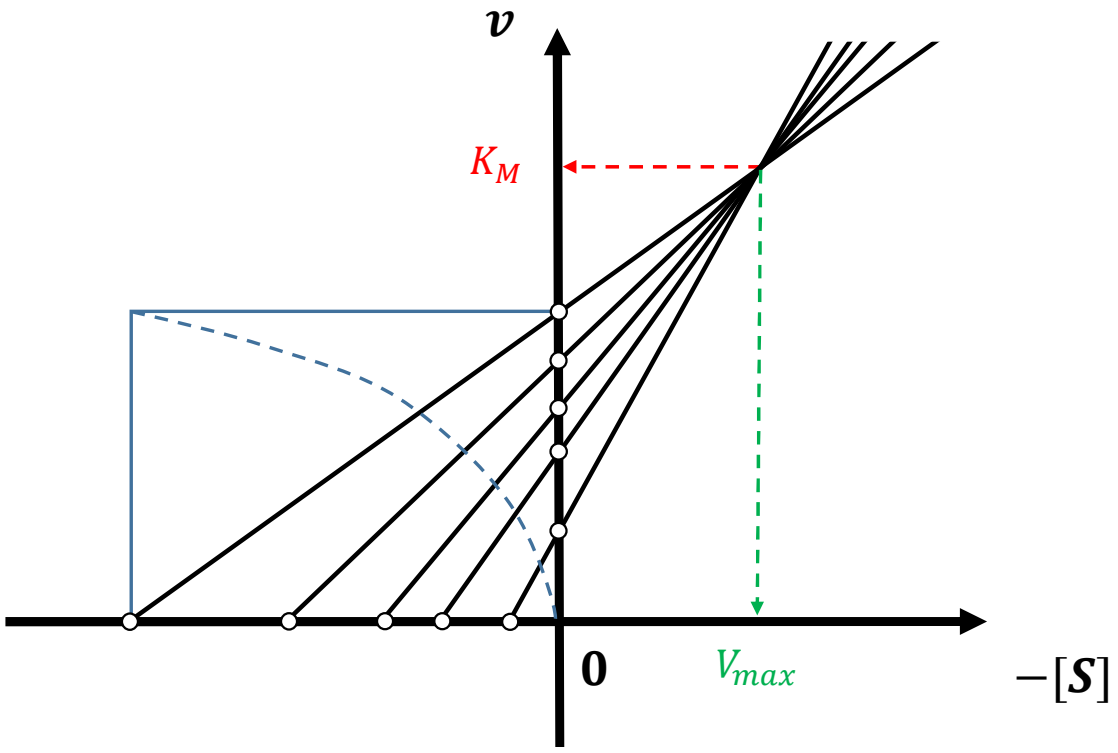

Figure 130: Cornish-Bowden plot including a rectangular hyperbolic curve of an Michaelis-Menten enzyme kinetic (dashed blue curve) from which the corresponding [S] and v values were plotted on the X- and Y-axis, respectively. Connection of those corresponding points forms a family of lines, which yield an intersection giving information about K_M (red arrow) and V_{max} (green arrow).

From the intersection of at least two straight lines the values of V_{max} and K_M are given on the corresponding axes (compare Figure 130). In the case of a rectangular hyperbolic Michaelis-Menten curve, all generated lines for an inhibitor concentration intersect in the same point. Due to experimental error, several intersections for each [S] pair will be obtained. For the calculation the median of the intersections is taken to reduce the experimental error. In case of negative values, they were replaced by large positive values. By the obtained V_{max} and K_M values for every inhibitor concentration, the kinetic interaction between the inhibitor and the substrate can be derived (compare Table 34).

Table 34: Effect of the Type of Inhibitory Enzyme Kinetic on the Values V_{max} and K_M with Increasing Substrate Concentrations.

Type of inhibitory enzyme kinetic	**V_{max} [a]**	**K_M [a]**
Competitive	constant	increases
Non-competitive	decreases	constant
Non-competitive-mixed	decreases	increases
Uncompetitive	decreases	decreases

[a]: effects on the values are given with increasing substrate concentrations.

Procedure: The experiments were carried out with various concentrations of a selected compound as well as of Hoechst 33342. Preparation and measurement of the assay was performed analogously to the Hoechst 33342 assay described in chapter 10.2.2.2, except that the concentration of Hoechst 33342 varied in the range of 0.4 µM to 2.4 µM and the different concentrations of the test-compound were adjusted to the corresponding IC_{50} value. For this purpose several inhibitor concentrations below the IC_{50} value were chosen together with one higher concentration which reached the top fluorescence value in a previous Hoechst 33342 accumulation assay. Each concentration was added row wise to the wells (C-H). The response in absence of the investigated compound was used as control, carried out in row A and B, whereas row A does not contain cells but only KHB. The layout of the microplate is illustrated in Figure 131.

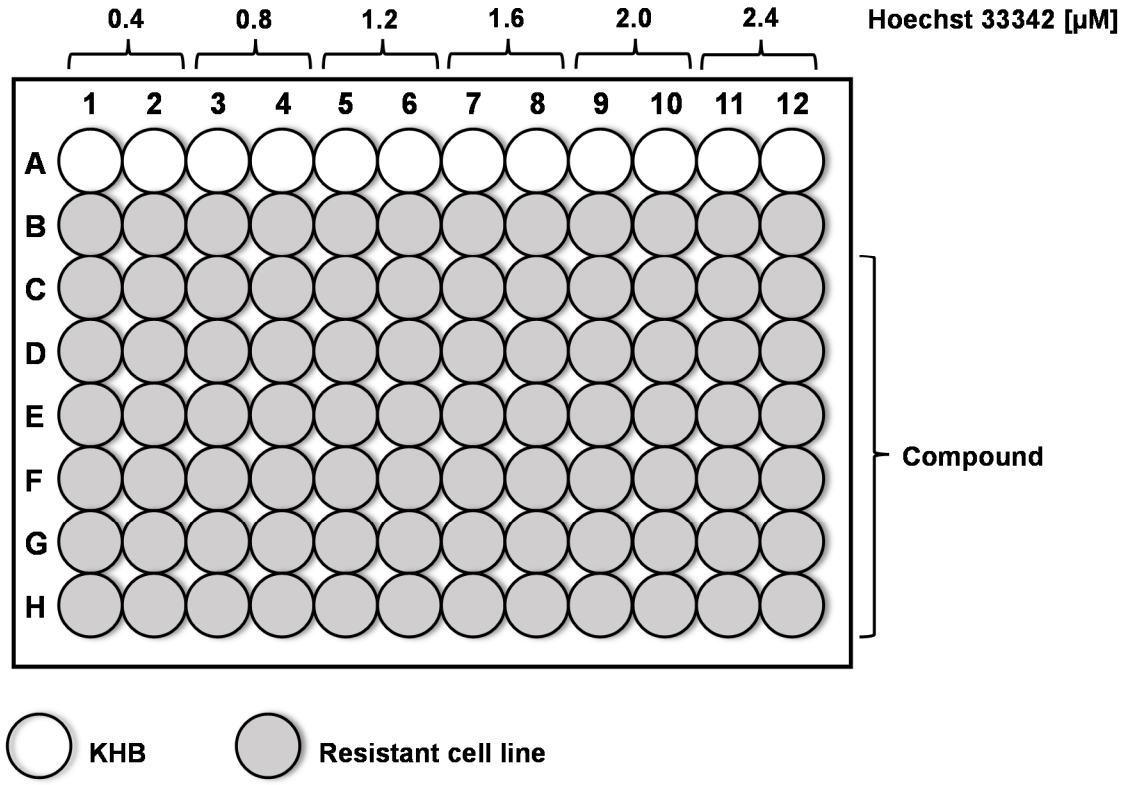

Figure 131: Layout of the microplate used for the inhibitory enzyme kinetic assay.

Since a transport-protein is involved in this method, the measured fluorescence must be adjusted to fit an inhibitory enzymatic kinetic. A typical concentration-response curve of compound **54** after subtraction of the background-fluorescence of the substrate Hoechst 33342 in KHB (row A) from the other rows is illustrated in Figure 132.

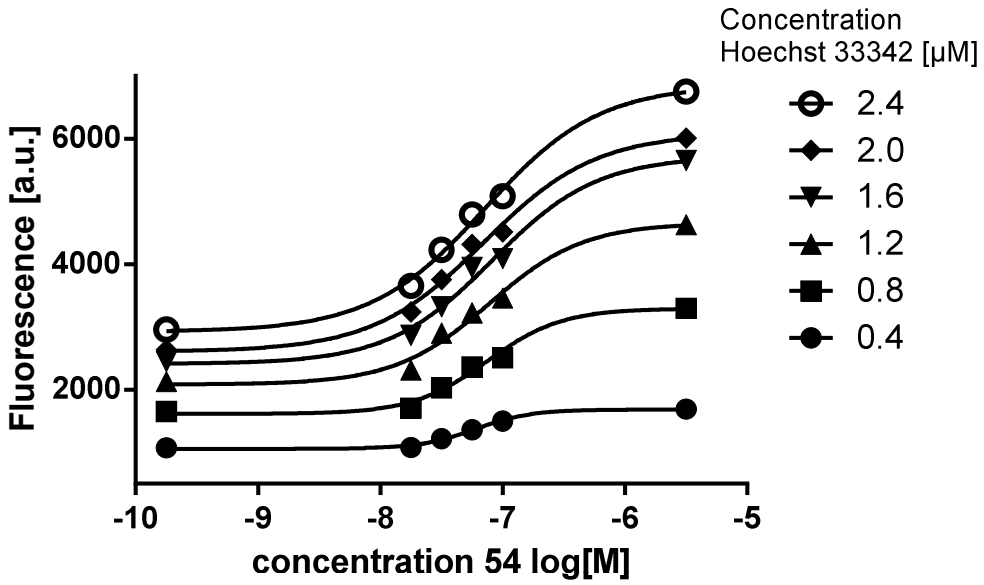

*Figure 132: concentration-response curve of compound **54** with different concentrations of Hoechst 33342.*

Fluorescence increases as increasing compound concentrations restrict the efflux of the substrate giving a sigmoidal concentration-response curve. Likewise, increased Hoechst 33342 concentrations lead to an increase of the fluorescence. The top and bottom values to each Hoechst 33342 concentration are then plotted against each other and lines generated by linear regression which should intersect with the origin of the coordinate system. Since the enzyme kinetic method requires fluorescence values that are proportional to the transport velocity v they had to be adjusted according to Equation 4.

$$v = k_{BCRP} = Top - Fluorescence\ value$$

Equation 4: Adjustment of the transport velocity to the enzyme kinetic method.

The efflux velocity is dependent on the concentration of the inhibitor which restricts the transport activity of the transport protein. Calculation of the intracellular concentration of the substrate is then carried out according to Equation 5.

$$c_{in} = S = \frac{[S] \cdot Fluo}{Top}$$

Equation 5: Calculation of the intracellular substrate concentration.

The transport velocity v, it can be derived from the fluorescence data by relating the top value to the substrate concentration and the fluorescence to the intracellular concentration giving Equation 6.

$$v = [S] - c_{in}$$

Equation 6: Reaction velocity calculated from the experimental data.

Thereby, v and S could be calculated and used for the double reciprocal Lineweaver-Burk plot. The transformation was carried out with the GraphPad® 5.01 Lineweaver-Burk implementation to obtain straight lines as presented in Figure 129 and to evaluate the underlying kinetic interaction between an inhibitor and the substrate Hoechst 33342.

10.2.2.9 Conformation sensitive 5D3 antibody binding assay

Conformation-sensitive binding assay was carried out with the monoclonal antibody PerCP-Cy™5.5 Mouse Anti-Human CD338. This conjugated primary antibody specifically binds to an epitope of ABCG2, the human CD338 antigen and exhibits an excitation maximum of 482 nm and an emission maximum of 695 nm. With ABCG2 expressing cells the 5D3 antibody exhibited a saturable labelling, inhibiting ABCG2 transport and ATPase function at high concentration. At low concentration the labelling correlated with the conformational change of the protein.[200] Non-specific staining was determined with PerCP-Cy™5.5 Mouse IgG2b κ Isotype Control. The assay was carried out with the mammalian PLB-985 acute myeloid leukemia cell line with an overexpression of ABCG2 using flow cytometry. Previous studies had shown, that this cell line expresses a relatively small amount of ABCG2 in comparison to other cell lines but led to the best results with the 5D3 antibody in the presence of Ko143.[201] Moreover,

the monoclonal antibody can serve as a sensitive tool to study intramolecular changes, reflects ATP binding and provides information about the formation of a catalytic intermediate, or substrate inhibition within the transport cycle of the ABCG2 protein.[200] Also, it was found that substrates often induced a smaller shift than inhibitors.[201]

Procedure: For the assay, cells were centrifuged and washed with a solution of DPBS containing 0.25% BSA. Subsequently, the cell density was adjusted with further DPBS/BSA solution to 2.5 million cells per mL and added in 98 µL portions to 1.5 mL Eppendorf reaction tubes. Then, 1 µL of a solution prepared from a compound in DMSO in the desired concentration was added to the tube, followed by a 5 minute pre-incubation period at 37 °C with shaking at 500 rpm. After pre-incubation, 1 µL of the antibody solution (PerCP-Cy™5.5 Mouse Anti-Human CD338 antibody, BD Bioscience) was added to the tube to a final volume of 100 µL and the mixture incubated with shaking (500 rpm) at 37 °C for another 30 min. Cells were then centrifuged, the supernatants removed and the cell-pellet re-suspended in 1 mL DPBS for immediate measurement at the FACSCalibur. The measurement was performed using an excitation wavelength of 488 nm and the fluorescence detected in the FL3 channel (red spectrum). Additionally, a control containing the same amount of DMSO as the test samples but without compound was established. Thereby, a shift of the fluorescence between cells without compound and cells with compound could be observed in most cases. The corrected fluorescence was obtained by subtraction of the geometric mean of the obtained fluorescence by the isotype-control from the geometric mean of the obtained fluorescence by the 5D3 antibody. The shift was then calculated for every test compound by subtracting the corrected fluorescence obtained in the absence of a compound from the corrected fluorescence obtained in the presence of a compound.

10.2.2.10 ATPase activity assay with ABCG2 membranes

ABC transport proteins rely on the hydrolysis of ATP to generate the necessary energy for an active efflux of molecules out of cells. The ATPase assay is a colorimetric method to detect inorganic phosphate (Pi) which is formed by cleavage of ATP. Hence, the formation of Pi is directly linked to the activity of the transporter. For a more accurate

correlation of the ATP hydrolysis to the transport activity, few other factors have to be taken into account. On the one hand, a basal activity can be measured which is not dependent on the transport activity of the protein. On the other hand, a vanadate-insensitive ATPase can be detected from other unspecific processes, which is obtained by adding orthovanadate. It is known that orthovanadate inhibits the ATPase activity of ABC transport proteins (vanadate-sensitive ATPase activity) and thus, the specific ATPase activity originating from the transport protein can be calculated by subtracting the insensitive vanadate ATPase activity from the total ATPase activity. Ko143 was used as standard for ATPase inhibition and quercetin was used as positive control with high stimulation of ABCG2 transport activity.

Procedure: High Five ™ insect cells were seeded in culture flasks with Express Five® medium and were incubated at 27°C. After a few passages when cells were healthy and homogenous, cells were counted and about 20 million cells per flask were seeded for baculovirus infection with Autographa californica multicapsid nuclear polyhedrosis virus (AcMNPV). Cells were harvested 72 hours after infection, centrifuged and afterwards membrane preparation was performed.[226] Two mL of membrane preparation homogenization buffer (50 mM Tris pH 7.5, 2 mM EGTA pH 7.0, 50 mM Mannitol, 2 mM DTT, 1 mM PMSF, 2 µM pepstatin, 1 µM leupeptin, 1 mM benzamidine) was used for 20 million cells. Cells were disrupted by a dounce homogenizer. Cellular debris was pelleted by centrifugation at 500 × g for 10 min at 4 °C and discarded. The supernatant was centrifuged at 300,000 × g for 30 min at 4 °C to obtain a pellet of enriched plasma membranes. Finally membranes were resuspended in 100 µL re-suspension buffer (50 mM Tris pH 7.5, 1 mM EGTA at pH 7.0, 10% (v/v) glycerol, 0.3 M mannitol, 1 mM DTT, 1 mM PMSF, 2 µM pepstatin, 1 µM leupeptin, 1 mM benzamidine) per flask and were frozen and stored at −80 °C. ATPase activity measurements of selected compounds was performed by a colorimetric ascorbic acid ammonia molybdate reaction.[247] Vanadate-sensitive basal ATPase activity was compared to vanadate-sensitive drug-stimulated or inhibited activity. Ko143 was used as standard for ATPase inhibition, quercetin was used as positive control with high stimulation of ABCG2 transport activity. Investigated compounds were dissolved in DMSO, final concentration of DMSO was 1%, which showed no observable effect on basal ATPase activity. All measurements were

repeated at least three times. All experiments were carried out by Jennifer Gallus and will be reviewed in her PhD thesis.

10.2.3 Calculation of concentration-effect curves with GraphPad Prism

Calculation of the IC_{50} and GI_{50} values were performed with GraphPad® 5.01 software. For this purpose the concentration dependent effect values from different experiments were transferred to the software and concentration-effect curves calculated with the four parameter logistic equation with variable slope or the three parameter logistic equation with a fixed slope = 1 (Equation 7: Four parameter logistic equation.). Both models were evaluated and chosen depending on the best curve-fit.

$$Y = \frac{Top - Bottom}{1 + 10^{n_H \cdot (\log EC_{50} - logX)}} + Bottom$$

*Equation 7: Four parameter logistic equation. With the response (**Y**), compound concentration (**X**), maximum response (**Top**), minimum baseline response (**Bottom**), slope of the curve ($\boldsymbol{n_H}$) and the concentration where the half-maximal effect is achieved.*

Experiments were carried out at least as three independent runs. To evaluate the quality of the data, the arithmetic mean was calculated and the corresponding standard deviation SD determined as the root of the variance (expected value of the squared deviation from the mean) using Equation 8.

$$s = \sqrt{s^2} = \sqrt{\frac{\sum_{i=1}^{n} x_i - \bar{x}}{n - 1}}$$

Equation 8: Formula used for the standard deviation (SD) calculated from the root of the variance. With $\boldsymbol{n}$ = number of measured values; $\boldsymbol{x_i}$ = corresponding measured value; $\boldsymbol{\bar{x}}$ = arithmetic mean value.

10.2.4 Materials

10.2.4.1 Chemicals

Chemicals	Manufacturer	Article number
Bovine serum albumin (BSA)	Sigma	A 7906
Calcein AM	Sigma	17783
Calcium chloride dihydrate	Merck	P 4901
Cyclosporine A	Sigma	C 3662
D-glucosemonohydrate	Merck	1040740500
Dimethylsulfoxid (DMSO)	Acros	AC19773
Disodium phosphate	Applichem	A4732
Erlotinib	LC Laboratories	E 4007
Gefitinib	LC Laboratories	G 4408
HEPES (free acid)	Applichem	A 3707
Hoechst 33342	Sigma	B 2261
Hydrochloric acid (0.5 M)	Grüssing	23204
Ko143	Tocris	3241
Magnesium sulfate heptahydrate	Applichem	A4101
Melsept SF	Braun	18907
Methanol	Merck	107018
Mitoxanthron	Sigma	M 6545
PerCP-Cy™5.5 Mouse Anti-Human CD338 antibody	BD Biosciences	561460
PerCP-Cy™5.5 Mouse IgG2b, κ Isotype Control	BD Biosciences	558304
Pheophorbide A	Fontier Scientic Inc.	15664296
Potassium chloride	Merck	104936
Potassium phosphate	Applichem	A 3095
SN-38	TCI Europe N.V.	E0748
Sodium bicarbonate	Merck	106329
Sodium chloride	Merck	106404
Sodium hydroxide solution (1 M)	Grüssing	22195

10.2.4.2 Materials for cell culture and assays

Materials	Manufacturer	Article number
Amber microtubes with attached pp cap, 1.5 mL	Sarstedt	72690004
CASYton solution	Schärfe System	43001
Conical test tube PP 15 ml, sterile	Nerbeplus GmbH	25027001
Conical test tube PP 50 ml, sterile	Nerbeplus GmbH	25707001
Cryos PP with screw cap, sterile	Greiner bio-one	123263
FACSClean	Becton Dickinson	340345
FACSFlow	Becton Dickinson	342003
FACSRinse	Becton Dickinson	340346
FACS-testtubes	Sarstedt	551579
Fetal bovine serum	Sigma	F 7524
Glass pasteur pipettes (230 mm)	VWR international	612-1702
Growth medium D-MEM 5671	Sigma	M 5650
Growth medium RPMI-1640	PAN Biotech GmbH	P0416500
L-Glutamine 200 mmol/l	Sigma	G 7513
MaxyClear microtubes, 2.0 mL	Axygen scientic	MCT-200-C
Membrane filter 0.2 µm, sterile	Whatman	10462200
Microplate clear PS, 96-Well, flat bottom	Greiner bio-one	655098
Microplate clear PS, 96-Well, U-shape bottom	Greiner bio-one	650101
Microwell SH plate, untreated black, 96F	Nunc	237108
Neutral microtubes with attached pp cap, 1.5 mL	Sarstedt	7269001
Natural pipette tips, 1.0-5.0 mL Bulk	Starlab	I1009-5000
Norm-Ject 10 mL syringe	Henke Sass Wolf	4100-000V0
Norm-Ject 20 mL syringe	Henke Sass Wolf	4200-000V0
Penicillin-Streptomycin solution	Sigma	P0781
Serological pipette 10 mL, sterile	Sarstedt	86.1254.001
Serological pipette 25 mL, sterile	Sarstedt	86.1685.001
TipOne 0.1-10.0 µL natural pipette tips	Starlab	S1111-3000
TipOne 101-1000 µL natural pipette tips	Starlab	S1111-2020
TipOne 1-200 µL yellow pipette tips	Starlab	S1111-0006
Tissue culture flasks, 175 cm², sterile, filter cap	Greiner bio-one	660175
Tissue culture flasks, 25 cm², sterile, filter cap	Greiner bio-one	690175
Tissue culture flasks, 75 cm², sterile, filter cap	Greiner bio-one	658175

Tissue culture plate, 96-Well, flat bottom with lid, sterile	Sarstedt	831835
Trypsin-EDTA solution	PAN Biotech GmbH	P100231SP

10.2.4.3 Instruments

Instruments	Manufacturer	Serial number
Accu-Jet suction pump	Brand	441938
Avanti centrifuge J-25	Beckman	JHY97G35
Axiovert 25 microscope	Zeiss	660197
CASY1 model TT	Schaerfe System	SC1 TT
CO_2 cell	MMM Group	-
Discover-SP W/Activent	CEM	DC8032
FACSCalibur	Becton Dickinson	E3231
FLUOstar Optima fluorescence	BMG Lab Technologies	4131164
FLUOstar Optima fluorescence	BMG Lab Technologies	4132279
Laminar flow cabinet (model: Antares 48)	Steril S.p.A.	10155/1996
Luminescence Spectrometer LS55	Perkin Elmer	69542
pH-Meter 744	Metrohm	20506
Pipette 0.1-2.5 µL	Eppendorf	3638475
Pipette 100-1000 µL	Eppendorf	4741196
Pipette 20-200 µL	Eppendorf	3534296
Pipette 2-20 µL	Eppendorf	3407866
Pipette 500-5000 µL	Eppendorf	3615095
POLARstar Galaxy fluorescence plate reader	BMG Lab Technologies	4030639
RH basic magnetic stirrer	IKA Labortechnik	3061661
Vacuum pump BVC21	Brand	08E12592
Vortex stirrer Minishaker	Vacuubrand	2.88069E+13
Waterbath type 1083	GFL	11530203

11 Appendix

11.1 List of Abbreviations

ABC transporter	ATP binding cassette transporter
ALD	adrenoleukodystrophy
ATCC	American Type Culture Collection
ATP	adenosine-5´-triphosphate
APT	attached proton test
BBB	blood-brain barrier
BCRP	breast cancer resistance protein, ABCG2
BSA	bovine serum albumin
Calcein AM	calcein acetoxymethyl ester
$CDCl_3$	deuterated chloroform
CsA	cyclosporine A
d	doublet
dd	doublet of doublets
DEPT	distorsionless enhancement by polarisation transfer
DMEM	Dulbecco's modified Eagle medium
DMF	dimethylformamide
DMSO	dimethylsulfoxide
DNA	deoxyribonucleic acid
DPBS	Dulbecco's phosphate buffered saline
dt	doublet of triplets
EC_{50}	half-maximal effective concentration
ECACC	European Collection of Authenticated Cell Cultures
EGFR	epidermal growth factor receptor
ER	endoplasmic reticulum
FACS	fluorescence-activated cell scanning
FBS	fetal bovine serum

FRET	fluorescence resonance energy transfer
FSC	forward scatter
FTC	Fumitremorgin C
GI_{50}	compound concentration leading to a cell survival of 50%
GFP	green fluorescent protein
GSH	glutathione
HBA	hydrogen bond acceptor
HBD	hydrogen bond donor
HCl	hydrochloric acid
HEPES	4-(2-hydroxyethyl)-1-piperazineethanesulfonic acid
HIV	human immunodeficiency virus
IC_{50}	compound concentration leading to 50% inhibition
IAAP	[I^{125}]iodoarylazidoprazosine
KHB	krebs-HEPES buffer
KOH	potassium Hydroxide
LTC4	Leukotriene C4
m	multiplet
MDR	multidrug resistance
MRP1	Multidrug Resistance related Protein 1
MTT	3-(4,5-dimethylthiazol-2-yl)-2,5-diphenyltetrazolium bromide
MTX	methotrexate
MX	mitoxantrone
MXR	mitoxantrone resistance protein
n.a.	not active
NADH	nicotineamide adenine dinucleotide (reduced form)
NaOH	sodium hydroxide
n.d.	not determined
n.d.a.	no data available
n.t.	not tested
NBD	nucleotide binding domain
NMR	nuclear magnetic resonance

PBS	phosphate buffered saline
PDT	photodynamic therapy
P-gp	permeability glycoprotein, ABCB1
PhA	pheophorbide A
PhIP	2-amino-1-methyl-6-phenylimidazo[4,5-b]pyridine
ppm	parts per million
q	quartet
RT	room temperature
s	singlet
SAR	structure-activity relationship
SD	standard deviation
SNP	single-nucleotide polymorphism
SSC	side scatter
t	triplet
td	triplet of doublets
TKI	tyrosine kinase inhibitor
TLC	thin layer chromatography
TMD	transmembrane domain
TR	therapeutic ratio
wt	wild type

11.2 List of tables

11.3 List of figures

11.4 List of schemes and equations

12 Index of publications

12.1 Publications

[1] Krapf, M. K.; Wiese, M. Synthesis and Biological Evaluation of 4-Anilino-quinazolines and -quinolines as Inhibitors of Breast Cancer Resistance Protein (ABCG2). *J. Med. Chem.* **2016**, *59*, 5449-5461.

[2] Krapf, M. K.; Gallus, J.; Wiese, M. 4-Anilino-2-pyridylquinazolines and -pyrimidines as Highly Potent and Nontoxic Inhibitors of Breast Cancer Resistance Protein (ABCG2). *J. Med. Chem.* **2017**, *60*, 4474-4495.

[3] Krapf, M. K.; Gallus, J.; Wiese, M. Synthesis and Biological Investigation of 2,4-Substituted Quinazolines as Highly Potent Inhibitors of Breast Cancer Resistance Protein (ABCG2). *Eur. J. Med. Chem.* **2017**. (just accepted)

[4] Krapf, M. K.; Gallus, J.; Wiese, M. New Selective, Non-toxic and Highly Potent Inhibitors of Breast Cancer Resistance Protein (ABCG2) containing a 2,4-Substituted Pyridopyrimidine Scaffold. *J. Med. Chem.* (submitted to journal)

[5] Krapf, M. K.; Gallus, J.; Wiese, M. 2,4,6-Substituted Quinazolines Display a Significant Inhibitory Potency and Selectivity Toward ABCG2. *J. Med. Chem.* (submitted to journal)

[6] Krapf, M. K.; Gallus, J.; Wiese, M. Synthesis and Biological Evaluation of Quinazoline Derivatives – A SAR Study of Novel Inhibitors of ABCG2. (under review)

12.2 Congress-contributions (Poster)

[1] Krapf, M. K.; Willmes, T.; Wiese, M. Development and 3D-QSAR Study of Quinazoline Derivatives as Potent Inhibitors of ABCG2. FEBS (Federation of European Biochemical Societies) special meeting, Innsbruck, **2014**.

[2] Krapf, M. K.; Willmes, T.; Wiese, M. Investigation of Quinazoline Derivatives as Potent Inhibitors of ABCG2. 7th SFB35 Symposium, Vienna, **2014**.

[3] Willmes, T.; Krapf, M. K.; Wiese, M. QSAR Studies of Quinazoline Derivatives as Potent Inhibitors of ABCG2. 7th SFB35 Symposium, Vienna, **2014**.

[4] Krapf, M. K.; Gallus, J.; Wiese, M. New Potent Inhibitors of ABCG2 Based on the Structure of Gefitinib. TTMC (Therapeutic Targets and Medicinal Chemistry), Münster, **2015**.

[5] Krapf, M. K.; Gallus, J.; Wiese, M. Investigation of 4-Substituted-2-phenylquinazolines as Inhibitors of ABCG2. AAPS (American Association of Pharmaceutical Scientists), Orlando, **2015**.

13 References

[1] Siegel, R.; Miller, K.; Jemal, A. Cancer statistics, 2016. *Ca-Cancer J. Clin.* **2016**, *66*, 7-30.

[2] Polgar, O.; Robey, R. W.; Bates S.E. ABCG2: structure, function and role in drug response. *Expert Opin. Drug Metab. Toxicol.* **2008***, 4*, 1-15.

[3] Fojo, A. T.; Ueda, K.; Slamon, D. J.; Poplack, D. G.; Gottesman, M. M.; Pastan, I. Expression of a multidrug-resistance gene in human tumors and tissues. *Proc. Natl. Acad. Sci. USA* **1987***, 84*, 265-269.

[4] Robey, R. W.; To, K. K.; Polgar, O.; Dohse, M.; Fetsch, P.; Dean, M.; Bates, S. E. ABCG2: A Perspective. *Adv. Drug. Deliv. Rev.* **2009***, 61*), 3-13.

[5] Cancer multidrug resistance. *Nature Biotechnology* **2000***, 18*, IT18-IT20.

[6] Mo, W.; Zhang, J.-T. Human ABCG2: structure, function, and its role in multidrug resistance. *Int. J. Biochem. Mol. Biol.* **2012***, 1*, 1-27.

[7] Lippert, T. H.; Ruoff, H. J.: Volm, M. Current status of methods to assess cancer drug resistance. *Int. J. Med. Sci.* **2011***, 8*, 245-53.

[8] Gottesman, M. M.; Fojo, T.; Bates, S. E. Multidrug Resistance in Cancer: Role of ATP-Dependent Transporters. *Nat. Rev. Cancer* **2002***, 2*, 48–58.

[9] Dassa, E.; Bouige, P. The ABC of ABCS: a phylogenetic and functional classification of ABC systems in living organisms. *Res. Microbiol.* **2001***, 152*, 211-29.

[10] Higgins, C. F. ABC Transporters: From Microorganisms to Man. *Annu. Rev. Cell Biol.* **1992***, 8*, 67-113.

[11] Rees, D. C.; Johnson, E.; Lewinson, O. ABC transporters: the power to change. *Nat. Rev. Mol. Cell Biol.* **2009***, 10*, 218-227.

[12] Wilkens, S. Structure and Mechanism of ABC Transporters. *F1000Prime Rep.* **2015***, 7*, 14.

[13] Vasiliou, V.; Vasiliou, K.: Nebert, D. W. Human ATP-binding cassette (ABC) transporter family. *Hum. Genomics* **2009***, 3*, 281-90.

[14] ter Beek, J.; Guskov, A.; Slotboom, D. J. Structural diversity of ABC transporters. *J. Gen. Physiol.* **2014***, 143*, 419-435.

[15] Szakács, G.; Váradi, A.; Özvegy-Laczka, C.; Sarkadi, B. The role of ABC transporters in drug absorption, distribution, metabolism, excretion and toxicity (ADME–Tox). *Drug Discovery Today* **2008***, 13*, 379-393.

[16] Albrecht, C.; Viturro, E. The ABCA subfamily—gene and protein structures, functions and associated hereditary diseases. *Pfluegers Archiv - European Journal of Physiology* **2007***, 453*, 581-589.

[17] Chen, Z.; Vulevic, B.; Ile, K.; Soulika, A.; Davis Jr., W.; Reiner, P. B.; Connop, B. P.; Nathwani, P.; Trojanowski, J. Q.; Tew, K. D. Association of ABCA2 expression with determinants of Alzheimer's disease. *FASEB J.* **2004***, 18*, 1129-31.

[18] Kelsell, D.; Norgett, E.; Unsworth, H.; Teh, M.; Cullup, T.; Mein, C. A.; Dopping-Hepenstal, P. J.; Dale, B. A.; Tadini, G.; Fleckman, P.; Stephens, K. G.; Sybert, V. P.; Mallory, S. B.; North, Bernard V.; Witt, David R.; Sprecher, Eli; Taylor, Aileen E M; Ilchyshyn, Andrew; Kennedy, Cameron T; Goodyear, H.; Moss, C.; Paige, D.; Harper, J. I.; Leigh, I. M.; Eady, R. A. J.; O'Toole, E. A. Mutations in ABCA12 underlie the severe congenital skin disease harlequin ichthyosis. *Am. J. Hum. Genet.* **2005***, 76*, 794-803.

[19] Dean, M.; Rzhetsky, A.; Allikmets, R. The human ATP-binding cassette (ABC) transporter superfamily. *Genome Res.* **2001***, 42*, 1007-1017.

[20] Mosser, J.; Douar, A. M.; Sarde, C. O.; Kioschis, P.; Feil, R.; Moser, H.; Poustka, A. M.; Mandel, J. L.; Aubourg, P. Putative X-linked adrenoleukodystrophy gene shares unexpected homology with ABC transporters. *Nature* **1993***, 361*, 726-730.

[21] Tian, Y.; Han, X.; Tian, D. The biological regulation of ABCE1. *IUBMB Life* **2012***, 64*, 795-800.

[22] Wu, C. P.; Calcagno, A. M.; Ambudkar, S. V. Reversal of ABC drug transporter-mediated multidrug resistance in cancer cells: evaluation of current strategies. *Curr. Mol. Pharmacol.* **2008***, 1*, 93-105.

[23] Higgins, C. F.; Linton, K. J. The ATP switch model for ABC transporters. *Nat. Struct. Mol. Biol.* **2004***, 11*, 918-926.

[24] Dawson, R. J. P.; Locher, K. P. Structure of a bacterial multidrug ABC transporter. *Nature* **2006***, 443*, 180-185.

[25] Higgins, C. F.; Haag, P. D.; Nikaido, K.; Ardeshir, F.; Garcia, G.; Ames, G. F. Complete nucleotide sequence and identification of membrane components of the histidine transport operon of S. typhimurium. *Nature* **1982***, 298*, 723-727.

[26] Seeger, M. A.; van Veen, H. Molecular basis of multidrug transport by ABC transporters. *Biochim. Biophys. Acta, Proteins Proteomics* **2009***, 1794*, 725-737.

[27] Choudhury, H. G.; Tong, Z.; Mathavan, I.; Li, Y.; Iwata, S.; Zirah, S.; Rebuffat, S.; van Heen, H. W.; Beis, K. Structure of an antibacterial peptide ATP-binding cassette transporter in a novel outward occluded state. *Proc. Natl. Acad. Sci. U. S. A.* **2014***, 111*, 9145-9150.

[28] Senior, A. E.; al-Shawi, M. K.; Urbatsch, I. L. The catalytic cycle of P-glycoprotein. *FEBS Letters* **1995***, 377*, 285-289.

[29] Timachi, M. H.; Hutter, C. A. J.; Hohl, M.; Assafa, T.; Böhm, S.; Mittal, A.; Seeger, M. A.; Bordignon, E. Exploring conformational equilibria of a heterodimeric ABC transporter. *eLife* **2017***, 6*, 586-597.

[30] Juliano, R. L.; Ling, V. A Surface Glycoprotein Modulating Drug Permeability in Chinese Hamster Ovary Cell Mutants. *Biochim. Biophys. Acta* **1976***, 455*, 152–162.

[31] Katayama, K.; Noguchi, K.; Sugimoto, Y. Regulations of P-Glycoprotein/ABCB1/MDR1 in Human Cancer Cells. *New J. Sci.* **2014***, 2014*, 1-10.

[32] Gupta, S.; Gollapudi, S. P-glycoprotein (MDR 1 gene product) in cells of the immune system: its possible physiologic role and alteration in aging and human immunodeficiency virus-1 (HIV-1) infection. *J. Clin. Immunol.* **1993***, 13*, 289-301.

[33] Leslie, E. M.; Deeley, R. G.; Cole, S. P. Multidrug resistance proteins: role of P-glycoprotein, MRP1, MRP2, and BCRP (ABCG2) in tissue defense. *Toxicol. Appl. Pharmacol.* **2005***, 204*, 216-237.

[34] Loo, T. W.; Clarke, D. M. Recent Progress in Understanding the Mechanism of P-Glycoprotein-mediated Drug Efflux. *J. Membr. Biol.* **2005***, 206*, 173-185.

[35] Rosenberg, M. F.; Callaghan, R.; Modok, S.; Higgins, C. F.; Ford, R. C. Three-dimensional structure of P-glycoprotein: the transmembrane regions adopt an asymmetric configuration in the nucleotide-bound state. *J. Biol. Chem.* **2005***, 280*, 2857-2862.

[36] Schinkel, A. H.; Jonker, J. W. Mammalian drug efflux transporters of the ATP binding cassette (ABC) family: an overview. *Adv. Drug Delivery Rev.* **2012***, 64*, 138-153.

[37] Raviv, Y.; Pollard, H. B.; Bruggemann, E. P.; Pastany, I.; Gottesman, M. M. Photosensitized Labeling of a Functional Multidrug Transporter in Living Drug-resistant Tumor Cells. *J. Biol. Chem.* **1990***, 265*, 3975-3980.

[38] Sharom, F. J. Complex Interplay between the P-Glycoprotein Multidrug Efflux Pump and the Membrane: Its Role in Modulating Protein Function. *Front. Oncol.* **2014***, 4*, 1-19.

[39] Sharom, F. J. ABC multidrug transporters: structure, function and role in chemoresistance. *Pharmacogenomics* **2008***, 9*, 105-127.

[40] Siarheyeva, A.; Lopez, J. J.; Glaubitz, C. Localization of Multidrug Transporter Substrates within Model Membranes. *Biochemistry* **2006***, 45*, 6203-6211.

[41] Seelig, A.; Landwojtowicz, E. Structure-activity relationship of P-glycoprotein substrates and modifiers. *Eur. J. Pharm. Sci.* **2000***, 12*, 31-40.

[42] Dantzig, A. H.; de Alwis, D. P.; Burgess, M. Considerations in the design and development of transport inhibitors as adjuncts to drug therapy. *Adv. Drug Delivery Rev.* **2003***, 55*, 133-50.

[43] Tamaki, A.; Ierano, C.; Szakacs, G.; Robey, R. W.; Bates, S. E. The controversial role of ABC transporters in clinical oncology. *Essays Biochem.* **2011***, 50*, 209-232.

[44] Sharom, F. J. The P-glycoprotein multidrug transporter. *Essays Biochem.* **2011***, 50*, 161-178.

[45] Amin, M. L. P-glycoprotein Inhibition for Optimal Drug Delivery. *Drug target insights* **2013***, 7*, 27-34.

[46] Darby, R. A.; Callaghan, R.; McMahon, R. M. P-glycoprotein inhibition: the past, the present and the future. *Curr. Drug Metab.* **2011***, 12*, 722-31.

[47] Pusztai, L.; Wagner, P.; Ibrahim, N.; Rivera, E.; Theriault, R.; Booser, D.; Symmans, F. W.; Wong, F.; Blumenschein, G.; Fleming, D. R.; Rouzier, R.; Boniface, G.; Hortobagyi, G. N. Phase II study of tariquidar, a selective P-glycoprotein inhibitor, in patients with chemotherapy-resistant, advanced breast carcinoma. *Cancer* **2005***, 104*, 682-691.

[48] Malingré, M. M.; Beijnen, J. H.; Rosing, H.; Koopman, F. J.; Jewell, R. C.; Paul, E. M.; Ten, W. W.; Bokkel, H.; Schellens, J. H. M. Co-administration of GF120918 significantly increases the systemic exposure to oral paclitaxel in cancer patients. *Br. J. Cancer* **2001***, 84*, 42-7.

[49] Kuppens, I. E.; Witteveen, E. O.; Jewell, R. C.; Radema, S. A.; Paul, E. M.; Magnum, S. G.; Beijnen, J. H.; Voest, E. E.; Schellens, J. H. A Phase I, Randomized, Open-Label, Parallel-Cohort, Dose-Finding Study of Elacridar (GF120918) and Oral Topotecan in Cancer Patients. *Clin. Cancer Res.* **2007***, 13*, 3276-3285.

[50] Cole, S. P.; Bhardwaj, G.; Gerlach, J. H.; Mackie, J. E.; Grant, C. E.; Almquist, K. C.; Stewart, A. J.; Kurz, E. U.; Duncan, A. M.; Deeley, R. G. Overexpression of a Transporter Gene in a Multidrug-Resistant Human Lung Cancer Cell Line. *Science* **1992***, 258*, 1650-1654.

[51] Wijnholds, J.; de Lange, E. C. M.; Scheffer, G. L.; van den Berg, D.-J.; Mol, C. A. A. M.; van der Valk, M.; Schinkel, A. H.; Scheper, R. J.; Breimer, D. D.; Borst, P. Multidrug resistance protein 1 protects the choroid plexus epithelium and contributes to the blood-cerebrospinal fluid barrier. *J. Clin. Invest.* **2000***, 105*, 279-85.

[52] Johnson, D. R.; Finch, R. A.; Lin, Z. P.; Zeiss, C. J.; Sartorelli, A. C. The pharmacological phenotype of combined multidrug-resistance mdr1a/1b- and mrp1-deficient mice. *Cancer Res.* **2001***, 61*, 1469-76.

[53] Chang, X. B. A molecular understanding of ATP-dependent solute transport by multidrug resistance-associated protein MRP1. *Cancer Metastasis Rev.* **2007***, 26*, 15-37.

[54] Yin, J.; Zhang, J. Multidrug resistance-associated protein 1 (MRP1/ABCC1) polymorphism: from discovery to clinical application. *J. Cent. South Univ., Med. Sci.* **2011***, 36*, 927-38.

[55] Cole, S. P. Targeting Multidrug Resistance Protein 1 (MRP1, ABCC1): Past, Present, and Future. *Annu. Rev. Pharmacol. Toxicol* **2014***, 54*, 95-117.

[56] Deeley, R. G; Westlake, C.; Cole, S. P. Transmembrane Transport of Endo- and Xenobiotics by Mammalian ATP-Binding Cassette Multidrug Resistance Proteins. *Physiol. Rev.* **2006***, 86*, 849-899.

[57] Rosenberg, M. F.; Oleschuk, C. J.; Wu, P.; Mao, Q.; Deeley, R. G.; Cole, S. P.; Ford, R. C. Structure of a human multidrug transporter in an inward-facing conformation. *J. Struct. Biol.* **2010***, 170*, 540-7.

[58] Yang, Y.; Mo, W.; Zhang, J.-T. Role of transmembrane segment 5 and extracellular loop 3 in the homodimerization of human ABCC1. *Biochemistry* **2010***, 49*, 10854-61.

[59] Bakos, E.; Evers, R.; Szakacs, G.; Tusnady, G. E.; Welker, E.; Szabo, K.; de Haas, M.; van Deemter, L.; Borst, P.; Vàradi, A.; Sarkadi, B. Functional Multidrug Resistance Protein (MRP1) Lacking the N-terminal Transmembrane Domain. *J. Biol. Chem.* **1998***, 273*, 32167-32175.

[60] Renes, J.; de Vries, E. G. E.; Nienhuis, E. F.; Jansen, P. L. M.; Müller, M. ATP- and glutathione-dependent transport of chemotherapeutic drugs by the multidrug resistance protein MRP1. *Br. J. Pharmacol.* **1999***, 126*, 681-8.

[61] Leslie, E., Deeley, R., & Cole, S. (2001). Toxicological relevance of the multidrug resistance protein 1, MRP1 (ABCC1) and related transporters. *Toxicology, 167*, 3-23.

[62] Zaman, G. J.; Lankelma, J.; van Tellingen, O.; Beijnen, J.; Dekker, H.; Paulusma, C.; Elferink, R. P. O.; Baas, F.; Borst, P. Role of glutathione in the export of compounds from cells by the multidrug-resistance-associated protein. *Proc. Natl. Acad. Sci. U. S. A.* **1995***, 92*, 7690-4.

[63] Prince, L.; Korbas, M.; Davidson, P.; Broberg, K.; Rand, M. D. Target organ specific activity of drosophila MRP (ABCC1) moderates developmental toxicity of methylmercury. *Toxicol. Sci.* **2014***, 140*, 425-435.

[64] Boumendjel, A.; Baubichon-Cortay, H.; Trompier, D.; Perrotton, T.; Di Pietro, A. Anticancer multidrug resistance mediated by MRP1: Recent advances in the discovery of reversal agents. *Med. Res. Rev.* **2005***, 25*, 453-472.

[65] Leier, I.; Jedlitschky, G.; Buchholz, U.; Cole, S. P.; Deeley, R. G.; Keppler, D. The MRP gene encodes an ATP-dependent export pump for leukotriene C4 and structurally related conjugates. *J. Biol. Chemistry* **1994**, *269*, 27807-10.

[66] Ni, Z.; Bikadi, Z.; Rosenberg, M. F.; Mao, Q. Structure and Function of the Human Breast Cancer Resistance Protein (BCRP/ABCG2). *Curr. Drug Metab.* **2010**, *11*, 603-617.

[67] Doyle, L. A.; Yang, W.; Abruzzo, L. V.; Krogmann, T.; Gao, Y.; Rishi, A. K.; Ross, D. D. A multidrug resistance transporter from human MCF-7 breast cancer cells. *Proc. Natl. Acad. Sci.* **1998**, *95*, 15665-15670.

[68] Allikmets, R.; Schriml, L. M.; Hutchinson, A.; Romano-Spica, V.; Dean, M. A human placenta-specific ATP-binding cassette gene (ABCP) on chromosome 4q22 that is involved in multidrug resistance. *Cancer Res.* **1998**, *58*, 5337-9.

[69] Miyake, K.; Mickley, L.; Litman, T.; Zhan, Z.; Robey, R.; Cristensen, B.; Brangi, M.; Greenberger, L.; Dean, M.; Fojo, T.; Bates, S. E. Molecular Cloning of cDNAs Which Are Highly Overexpressed in Mitoxantrone resistant Cells: Demonstration of Homology to ABC Transport Genes. *Cancer Res.* **1999**, *59*, 8-13.

[70] Kim, M.; Turnquist, H.; Jackson, J.; Sgagias, M.; Yan, Y.; Gong, M.; Dean, M.; Sharp, J. G.; Cowan, K. The Multidrug Resistance Transporter ABCG2 (Breast Cancer Resistance Protein 1) Effluxes Hoechst 33342 and Is Overexpressed in Hematopoietic Stem Cells. *Clin. Cancer Res.* **2002**, *8*, 22-28.

[71] Moitra, K.; Silverton, L.; Limpert, K.; Im, K.; Dean, M. Moving out: from sterol transport to drug resistance – the ABCG subfamily of efflux pumps. *Drug Metabolism and Drug Interactions* **2011**, *26*, 105-11.

[72] Kusuhara, H.; Sugiyama, Y. ATP-binding cassette, subfamily G (ABCG family). *Eur. J. Physicol.* **2007**, *453*, 735-744.

[73] Doyle, L.; Ross, D. D. Multidrug resistance mediated by the breast cancer resistance protein BCRP (ABCG2). *Oncogene* **2003**, *22*, 7340–7358.

[74] Ding, X.; Wu, J.; Jiang, C. ABCG2: A potential marker of stem cellsand novel target in stem cell and cancer therapy. *Life Sciences* **2010***, 86*, 631-637.

[75] Litman, T.; Jensen, U.; Hansen, A.; Covitz, K.-M.; Zhan, Z.; Fetsch, P.; Use of peptide antibodies to probe for the mitoxantrone resistance-associated protein MXR/BCRP/ABCP/ABCG2. *Biochim. Biophys. Acta, Biomembr.* **2002***, 1565*, 6-16.

[76] Jonker, J. W.; Smit, J. W.; Brinkhuis, R. F.; Maliepaard, M.; Beijnen, J. H; Schellens, J. H.; Schinkel, A. H. Role of breast cancer resistance protein in the bioavailability and fetal penetration of topotecan. *J. Natl. Cancer Inst.* **2000***, 92*, 1651-6.

[77] Zhang, Y.; Wang, H.; Unadkat, J.; Mao, Q. Breast Cancer Resistance Protein 1 Limits Fetal Distribution of Nitrofurantoin in the Pregnant Mouse. *Drug Metab. Dispos.* **2007***, 35*, 2154-2158.

[78] Staud, F.; Vackova, Z.; Pospechova, K.; Pavek, P.; Ceckova, M.; Libra, A.; Cygalova, L.; Nachtigal, P.; Fedrich, Z. Expression and Transport Activity of Breast Cancer Resistance Protein (Bcrp/Abcg2) in Dually Perfused Rat Placenta and HRP-1 Cell Line. *J. Pharmacol. Exp. Ther.* **2006***, 319*, 53-62.

[79] Myllynen, P.; Kummu, M.; Kangas, T.; Ilves, M.; Immonen, E.; Rysä, J.; Pirilä, R.; Lastumäki, A.; Vähäkangas, K. H. ABCG2/BCRP decreases the transfer of a food-born chemical carcinogen, 2-amino-1-methyl-6-phenylimidazo[4,5-b]pyridine (PhIP) in perfused term human placenta. *Toxicol. Appl. Pharmacol.* **2008***, 232*, 210-217.

[80] van Herwaarden, A. E.; Wagenaar, E.; Merino, G.; Jonker, J. W.; Rosing, H.; Beijnen, J. H.; Schinkel, A. H. Multidrug transporter ABCG2/breast cancer resistance protein secretes riboflavin (vitamin B2) into milk. *Mol. Cell. Biol.* **2007***, 27*, 1247-53.

[81] Jonker, J. W.; Merino, G.; Musters, S.; van Herwaarden, A. E.; Bolscher, E.; Wagenaar, E.; Mesman, E.; Dale, T. C.; Schinkel, A. H. The breast cancer

resistance protein BCRP (ABCG2) concentrates drugs and carcinogenic xenotoxins into milk. *Nat. Med.* **2005***, 11*, 127-129.

[82] Herwaarden, A. E.; Wagenaar, E.; Karnekamp, B.; Merino, G.; Jonker, J. W.; Schinkel, A. H. Breast cancer resistance protein (Bcrp1/Abcg2) reduces systemic exposure of the dietary carcinogens aflatoxin B1, IQ and Trp-P-1 but also mediates their secretion into breast milk. *Carcinogenesis* **2005***, 27*, 123-130.

[83] The Breast Cancer Resistance Protein (BCRP/ABCG2) Affects Pharmacokinetics, Hepatobiliary Excretion, and Milk Secretion of the Antibiotic Nitrofurantoin. *Mol. Pharmacol.* **2005***, 67*, 1758-1764.

[84] Xia, C. Q.; Liu, N.; Yang, D.; Miwa, G.; Gan, L. S. (2005). Expression, localization, and functional characteristics of breast cancer resistance protein in Caco-2 cells. *Drug Metab. Dispos.* **2005***, 33*, 637-43.

[85] Cooray, H. C.; Blackmore, C. G.; Maskell, L.; Barrand, M. A. Localisation of breast cancer resistance protein in microvessel endothelium of human brain. *Neuroreport* **2002***, 13*, 2059-63.

[86] Zhang, W.; Petrovic, J.-M.; Andrade, M. F.; Zhang, H.; Ball, M.; Stanimirovic, D. B. The expression and functional characterization of ABCG2 in brain endothelial cells and vessels. *FASEB* **2003***, 17*, 2085-7.

[87] Aronica, E.; Gorter, J.; Redeker, S.; van Vliet, E. A.; Ramkema, M.; Scheffer, G. L.; Scheper, R. J.; van der Valk, P.; Leenstra, S.; Baayen, J. C.; Spliet, W. G.; Troost, D. Localization of Breast Cancer Resistance Protein (BCRP) in Microvessel Endothelium of Human Control and Epileptic Brain. *Epilepsia* **2005***, 46*, 849-857.

[88] Pardridge, W. M. The blood-brain barrier: bottleneck in brain drug development. *NeuroRx* **2005***, 2*, 3-14.

[89] Agarwal, S. H.; Hartz, A. M.; Elmquist, W. F.; Bauer, B. Breast Cancer Resistance Protein and P-glycoprotein in Brain Cancer: Two Gatekeepers Team Up. *Curr. Pharm. Des.* **2011***, 17*, 2793-2802.

[90] Stacy, A. E.; Jansson, P. J.; Richardson, D. R. Molecular pharmacology of ABCG2 and its role in chemoresistance. *Mol. Pharmacol.* **2013***, 84*, 655-669.

[91] McDevitt, C. A.; Collins, R.; Kerr, I. D.; Callaghan, R. Purification and structural analyses of ABCG2. *Adv. Drug Deliv. Rev.* **2009***, 61*, 57-65.

[92] Wang, H.; Lee, E. W.; Cai, X.; Ni, Z.; Zhou, L.; Mao, Q. Membrane Topology of the Human Breast Cancer Resistance Protein (BCRP/ABCG2) Determined by Epitope Insertion and Immunofluorescence. *Biochemistry* **2008***, 47*, 13778-87.

[93] Horsey, A. C.; Cox, M. H.; Sarwat, S.; Kerr, I. D. The Multidrug Transporter ABCG2: Still More Questions Than Answers Multidrug Transporters in Biology. *Biochem. Soc. Trans.* **2016***, 44,* 824-830.

[94] Kerr, I. D. Structure and association of ATP-binding cassette transporter nucleotide-binding domains. *Biochim. Biophys. Acta, Biomembr.* **2002***, 1561*, 47-64.

[95] Kerr, I. D.; Haider, A. J.; Gelissen, I. C. The ABCG family of membrane-associated transporters: you don't have to be big to be mighty. *Br. J. Pharmacol.* **2011***, 164*, 1767-1779.

[96] Wong, K.; Briddon, S. J.; Holliday, N. D.; Kerr, I. D. Plasma membrane dynamics and tetrameric organisation of ABCG2transporters in mammalian cells revealed by single particle imaging techniques. *Biochim. Biophys. Acta* **2016** *1863*, 19-29.

[97] Rosenberg, M. F.; Bikadi, Z.; Chan, J.; Liu, X.; Ni, Z.; Cai, X.; Ford, R. C.; Mao, Q. The Human Breast Cancer Resistance Protein (BCRP/ABCG2) shows conformational changes with mitoxantrone. *Structure* **2010***, 18*, 482-493.

[98] Natarajan, K.; Xie, Y.; Baer, M. R.; Ross, D. D. Role of Breast Cancer Resistance Protein (BCRP/ABCG2) in Cancer Drug Resistance. *Biochem. Pharmacol.* **2012***, 83*, 1084-1103.

[99] Henriksen, U.; Fog, J. U.; Litman, T.; Gether, U. Identification of Intra- and Intermolecular Disulfide Bridges in the Multidrug Resistance Transporter ABCG2. *J. Biol. Chem.* **2005***, 280*, 36926-36934.

[100] Wakabayashi, K.; Nakagawa, H.; Tamura, A.; Koshiba, S.; Hoshijima, K.; Komada, M.; Ishikawa, T. (2007). Intramolecular Disulfide Bond Is a Critical Check Point Determining Degradative Fates of ATP-binding Cassette (ABC) Transporter ABCG2 Protein. *J. Biol. Chem.* **2007***, 282*, 27841-27846.

[101] Liu, Y.; Yang, Y.; Qi, J.; Peng, H.; Zhang, J. T. Effect of cysteine mutagenesis on the function and disulfide bond formation of human ABCG2. *J. Pharmacol. Exp. Ther.* **2008***, 326*, 33-40.

[102] Kage, K.; Fujita, T.; Sugimoto, Y. (2005). Role of Cys-603 in dimer/oligomer formation of the breast cancer resistance protein BCRP/ABCG2. *Cancer Sci.* **2005***, 96*, 866-872.

[103] Polgar, O.; Ierano, C.; Tamaki, A.; Stanley, B.; Ward, Y.; Xia, D.; Tarasova, N.; Robey, R. R.; Bates, S. E. Mutational analysis of threonine 402 adjacent to the GXXXG dimerization motif in transmembrane segment 1 of ABCG2. *Biochemistry* **2010***, 49*, 2235-45.

[104] Wakabayashi, K.; Nakagawa, H.; Adachi, T.; Kii, I.; Kobatake, E.; Kudo, A.; Ishikawa, T. Identification of cysteine residues critically involved in homodimer formation and protein expression of human ATP-binding cassette transporter ABCG2: a new approach using the flp recombinase system. *J. Exp. Ther. Oncol.* **2006***, 5*, 205-22.

[105] Wakabayashi-Nakao, K.; Tamura, A.; Furukawa, T.; Nakagawa, H.; Ishikawa, T. Quality control of human ABCG2 protein in the endoplasmic reticulum: Ubiquitination and proteasomal degradation. *Adv. Drug Delivery Rev.* **2009***, 61*, 66-72.

[106] Diop, N. K.; Hrycyna, C. A. N-Linked Glycosylation of the Human ABC Transporter ABCG2 on Asparagine 596 Is Not Essential for Expression,

Transport Activity, or Trafficking to the Plasma Membrane. *Biochemistry* **2005**, *44*, 5420-5429.

[107] Honjo, Y.; Hrycyna, C. A.; Yan, Q. W.; Medina-Pérez, W. Y.; Robey, R. W.; van de Laar, A.; Litman, T.; Dean, M.; Bates, S. E. Acquired Mutations in the MXR/BCRP/ABCP Gene Alter Substrate Specificity in MXR/BCRP/ABCP-overexpressing Cells. *Cancer Res.***2001**, *61*, 6635-6639.

[108] Honjo, Y.; Morisaki, K.; Huff, L. M.; Robey, R. W.; Hung, J.; Dean, M.; Bates, S. E. Single-nucleotide polymorphism (SNP) analysis in the ABC half-transporter ABCG2 (MXR/BCRP/ABCP1). *Cancer Biol. Ther.* **2002**, *1*, 696-702.

[109] Ejendal, K. F.; Diop, N. K.; Schweiger, L. C.; Hrycyna, C. A. The nature of amino acid 482 of human ABCG2 affects substrate transport and ATP hydrolysis but not substrate binding. *Protein Sci.* **2006**, *15*, 1597-1607.

[110] Pozza, A.; Perez-Victoria, J. M.; Sardo, A.; Ahmed-Belkacem, A.; Di Pietro, A. Purification of breast cancer resistance protein ABCG2 and role of arginine-482. *Cell. Mol. Life Sci.* **2006**, *63*, 1912-1922.

[111] Ni, Z.; Bikadi, Z.; Shuster, D. L.; Zhao, C.; Rosenberg, M. F.; Mao, Q. Identification of proline residues in or near the transmembrane helices of the human breast cancer resistance protein (BCRP/ABCG2) that are important for transport activity and substrate specificity. *Biochemistry* **2011**, *50*, 8057-66.

[112] Mao, Q.; Unadkat, J. D. Role of the Breast Cancer Resistance Protein (BCRP/ABCG2) in drug transport - an update. *AAPS J.* **2014**, *17*, 65-82.

[113] Sarkadi, B.; Özvegy-Laczka, C.; Nemet, K.; Varadi, A. ABCG2 - a Transporter for All Seasons. *FEBS Lett.* **2004**, *567*, 116-120.

[114] Morisaki, K.; Robey, R. W.; Özvegy-Laczka, C.; Honjo, Y.; Polgar, O.; Steadman, K.; Sarkadi, B.; Bates, S. E. Single nucleotide polymorphisms modify the transporter activity of ABCG2. *Cancer Chemother. Pharmacol.* **2005**, *56*, 161-172.

[115] Zhou, S.; Schuetz, J. D.; Bunting, K. D.; Colapietro, A. M.; Sampath, J.; Morris, J. J.; Lagutina, I.; Grosveld, G. C.; Osawa, M.; Nakauchi, H.; Sorrentino, B. P. (2001). The ABC transporter Bcrp1/ABCG2 is expressed in a wide variety of stem cells and is a molecular determinant of the side-population phenotype. *Nat. Med.* **2001***, 7*, 1028-1034.

[116] Robey, R. W.; Steadman, K.; Polgar, O.; Bates, S. E. ABCG2-mediated transport of photosensitizers: potential impact on photodynamic therapy. *Cancer Biol. Ther.* **2005***, 4*, 187-94.

[117] Chen, Z. S.; Robey, R. W.; Belinsky, M. G.; Shchaveleva, I.; Ren, X. Q.; Sugimoto, Y.; Ross, D. D.; Bates, S. E.; Kruh, G. D. Transport of methotrexate, methotrexate polyglutamates, and 17beta-estradiol 17-(beta-D-glucuronide) by ABCG2: effects of acquired mutations at R482 on methotrexate transport. *Cancer Res.* **2003***, 63*, 4048-54.

[118] Volk, E.; Farley, K. M.; Wu, Y.; Li, F.; Robey, R. W.; Schneider, E. Overexpression of Wild-Type Breast Cancer Resistance Protein Mediates Methotrexate Resistance. *Cancer Res.* **2002***, 62*, 5035-5040.

[119] Shafran, A.; Ifergan, I.; Bram, E.; Jansen, G.; Kathmann, I.; Peters, G. J.; Robey, R. W.; Bates, S. E.; Assaraf, Y. G. ABCG2 Harboring the Gly482 Mutation Confers High-Level Resistance to Various Hydrophilic Antifolates. *Cancer Res.* **2005***, 65*, 8414-8422.

[120] Robey, R. W.; Honjo, Y.; Morisaki, K.; Nadjem, T. A.; Runge, S.; Risbood, M.; Poruchynsky, M. S.; Bates, S. E. Mutations at amino-acid 482 in the ABCG2 gene affect substrate and antagonist specificity. *Br. J. Cancer* **2003***, 89*, 1971-1978.

[121] Litman, T.; Brangi, M.; Hudson, E.; Fetsch, P.; Abati, A.; Ross, D. D.; Miyake, K.; Resau, J. H.; Bates, S. E. The multidrug-resistant phenotype associated with overexpression of the new ABC half-transporter, MXR (ABCG2). *J. Cell Sci.* **2000***, 113*, 2011-21.

[122] Hazlehurst, L. A.; Foley, N. E.; Gleason-Guzman, M. C.; Hacker, M. P.; Cress, A. E.; Greenberger, L. W.; De Jong, M. C.; Dalton, W. S. Multiple mechanisms confer drug resistance to mitoxantrone in the human 8226 myeloma cell line. *Cancer Res.* **1999**, *59*, 1021-8.

[123] Rabindran, S. K.; Ross, D. D.; Doyle, L. A.; Yang, W.; Greenberger, L. M. Fumitremorgin C reverses multidrug resistance in cells transfected with the breast cancer resistance protein. *Cancer Res.* **2000**, *60*, 47-50.

[124] Robey, R. W.; Medina-Pérez, W. Y.; Nishiyama, K.; Lahusen, T.; Miyake, K.; Litman, T.; Senderowicz, A. M.; Ross, D. D.; Bates, S. E. Overexpression of the ATP-binding cassette half-transporter, ABCG2 (Mxr/BCrp/ABCP1), in flavopiridol-resistant human breast cancer cells. *Clin. Cancer Res.* **2001**, *7*, 145-52.

[125] Nakatomi, K.; Yoshikawa, M.; Oka, M.; Ikegami, Y.; Hayasaka, S.; Sano, K.; Shiozawa, K.; Kawabata, S.; Soda, H.; Ishikawa, T.; Tanabe, S.; Kohno, S. Transport of 7-Ethyl-10-hydroxycamptothecin (SN-38) by Breast Cancer Resistance Protein ABCG2 in Human Lung Cancer Cells. *Biochem. Biophys. Res. Commun.* **2001**, *288*, 827-832.

[126] Rabindran, S. K.; He, H.; Singh, M.; Brown, E.; Collins, K. I.; Annable, T.; Greenberger, L. M. Reversal of a novel multidrug resistance mechanism in human colon carcinoma cells by fumitremorgin C. *Cancer Res.* **1998**, *58*, 5850-5858.

[127] Maliepaard, M.; van Gastelen, M. A.; Tohgo, A.; Hausheer, F. H.; van Waardenburg, R. C.; de Jong, L. A.; Pluim, D.; Benijnen, J. H.; Schellens, J. H. Circumvention of breast cancer resistance protein (BCRP)-mediated resistance to camptothecins in vitro using non-substrate drugs or the BCRP inhibitor GF120918. *Clin. Cancer Res.* **2001**, *7*, 935-41.

[128] Nezasa, K., Tian, X., Zamek-Gliszczynski, M., Patel, N., Raub, T., & al., e. (2006). Altered hepatobiliary disposition of 5 (and 6)-carboxy-2',7'-dichlorofluorescein in Abcg2 (Bcrp1) and Abcc2 (Mrp2) knockout mice. *Drug Metabolism and Disposition* **2006**, *34*, 718-723.

[129] Robey, R. W.; Steadman, K.; Polgar, O.; Morisaki, K.; Blayney, M.; Mistry, P.; Bates, S. E. Pheophorbide a is a specific probe for ABCG2 function and inhibition. *Cancer Res.* **2004**, *64*, 1242-6.

[130] Robey, R. W.; Fetsch, P. A.; Polgar, O.; Dean, M.; Bates, S. E. The livestock photosensitizer, phytoporphyrin (phylloerythrin), is a substrate of the ATP-binding cassette transporter ABCG2. *Res. Vet. Sci.* **2006**, *81*, 345-349.

[131] Imai, Y.; Tsukahara, S.; Asada, S.; Sugimoto, Y. Phytoestrogens/Flavonoids Reverse Breast Cancer Resistance Protein/ABCG2-Mediated Multidrug Resistance. *Cancer Res.* **2004**, *64*, 4346-4352.

[132] Youdim, K. A.; Qaiser, M. Z.; Begley, D. J.; Rice-Evans, C. A.; Abbott, N. Flavonoid permeability across an in situ model of the blood–brain barrier. *Free Radic. Biol. Med.* **2004**, *36*, 592-604.

[133] Mao, Q.; Unadkat, J. D. (2005). Role of the breast cancer resistance protein (ABCG2) in drug transport. *AAPS J.* **2005**, *7*, E118-E133.

[134] Breedveld, P.; Zelcer, N.; Pluim, D.; Sönmezer, O.; Tibben, M. M.; Beijnen, J. H.; Schinkel, A. H.; van Tellingen, O.; Borst, P.; Schellens, J. H. Mechanism of the Pharmacokinetic Interaction between Methotrexate and Benzimidazoles: Potential Role for Breast Cancer Resistance Protein in Clinical Drug-Drug Interactions. *Cancer Res.* **2004**, *64*, 5804-5811.

[135] Nakagawa, R.; Hara, Y.; Arakawa, H.; Nishimura, S.; Komatani, H. ABCG2 confers resistance to indolocarbazole compounds by ATP-dependent transport. *Biochem Biophys. Res. Commun.* **2002**, *299*, 669-75.

[136] van der Heijden, J.; de Jong, M. C.; Dijkmans, B.; Lems, W.; Oerlemans, R.; Kathmann, I.; Schalkwijk, C.; Scheffer, G.; Scheper, R.; Jansen, G. Development of sulfasalazine resistance in human T cells induces expression of the multidrug resistance transporter ABCG2 (BCRP) and augmented production of TNFα. *Ann. Rheum. Dis.* **2004**, *63*, 138-143.

[137] Pan, G.; Giri, N.; Elmquist, W. F. Abcg2/Bcrp1 Mediates the Polarized Transport of Antiretroviral Nucleosides Abacavir and Zidovudine. *Drug Metab. Dispos.* **2007***, 35*, 1165-1173.

[138] Szakács, G.; Hall, M. D.; Gottesman, M. M.; Boumendjel, A.; Kachadourian, R.; Day, B. J.; Baubichon-Cortay, H.; Di Pietro, A. Targeting the Achilles Heel of Multidrug-Resistant Cancer by Exploiting the Fitness Cost of Resistance. *Chem. Rev.* **2014***, 114*, 5753-5774.

[139] Allen, J. D.; van Loevezijn, A.; Lakhai, J. M.; van der Valk, M.; van Tellingen, O.; Reid, G.; Schellens, J. H.; Koomen, G. J. Schinkel, A. H. Potent and Specific Inhibition of the Breast Cancer Resistance Protein Multidrug Transporter in Vitro and in Mouse Intestine by a Novel Analogue of Fumitremorgin C. *Mol. Cancer Ther.* **2002***, 1*, 417–425.

[140] van Loevezijn, A.; Allen, J. D.; Schinkel, A. H.; Koomen, G. J. Inhibition of BCRP-mediated drug efflux by fumitremorgin-type indolyl diketopiperazines. *Bioorg. Med. Chem. Lett.* **2001***, 11*, 29-32.

[141] Pavek, P.; Merino, G.; Wagenaar, E.; Bolscher, E.; Novotna, M.; Jonker, J. W.; Schinkel, A. H. Human Breast Cancer Resistance Protein: Interactions with Steroid Drugs, Hormones, the Dietary Carcinogen 2-Amino-1-methyl-6-phenylimidazo(4,5-b)pyridine, and Transport of Cimetidine. *J. Pharmacol. Exp. Ther.* **2005***, 312*, 144-152.

[142] Cooray, H. C.; Janvilisri, T.; van Veen, H. W.; Hladky, S. B.; Barrand, M. A. Interaction of the breast cancer resistance protein with plant polyphenols. *Biochem. Biophys. Res. Commun.* **2004***, 317*, 269-275.

[143] Gupta, A.; Dai, Y.; Vethanayagam, R.; Hebert, M. F.; Thummel, K. E.; Undekat, J. D.; Ross, D. D.; Mao, Q. Cyclosporin A, tacrolimus and sirolimus are potent inhibitors of the human breast cancer resistance protein (ABCG2) and reverse resistance to mitoxantrone and topotecan. *Cancer Chemother. Pharmacol.* **2006***, 58*, 374-83.

[144] Ozvegy-Laczka, C.; Hegedus, T.; Varady, G.; Ujhelly, O.; Schuetz, J. D.; Varadi, A.; Keri, G.; Orfi, L.; Nemet, K.; Sarkadi, B.; High-affinity Interaction of Tyrosine Kinase Inhibitors with the ABCG2 Multidrug Transporter. *Mol. Pharmacol.* **2004***, 65*, 1485-95.

[145] de Bruin, M.; Miyake, K.; Litman, T.; Robey, R.; Bates, S. E. Reversal of resistance by GF120918 in cell lines expressing the ABC half-transporter, MXR. *Cancer Lett.* **1999***, 146*, 117-126.

[146] Jekerle, V.; Klinkhammer, W.; Reilly, R. M.; Piquette-Miller, M.; Wiese, M. Novel tetrahydroisoquinolin-ethyl-phenylamine based multidrug resistance inhibitors with broad-spectrum modulating properties. *Cancer Chemother. Pharmacol.* **2006***, 59*, 61-69.

[147] Zhang, S.; Yang, X.; Morris, M. E. Flavonoids Are Inhibitors of Breast Cancer Resistance Protein (ABCG2)-Mediated Transport. *Mol. Pharmacol.* **2004***, 65*, 1208-1216.

[148] Zhang, S.; Wang, X.; Sagawa, K.; Morris, M. E. Flavonoids chrysin and benzoflavone, potent breast cancer resistance protein inhibitors, have no significant effect on topotecan pharmacokinetics in rats or mdr1a/1b (-/-) mice. *Drug Metab. Dispos.* **2005***, 33*, 341-348.

[149] Pulido, M. M.; Molina, A. J.; Merino, G.; Mendoza, G.; Prieto, J. G.; Alvarez, A. I. Interaction of enrofloxacin with breast cancer resistance protein (BCRP/ABCG2): influence of flavonoids and role in milk secretion in sheep. *J. Vet. Pharmacol. Ther.* **2006***, 29*, 279-287.

[150] Zhang, Y.; Gupta, A.; Wang, H.; Zhou, L.; Vethanayagam, R. R.; Undekat, J. D.; Mao, Q. BCRP Transports Dipyridamole and is Inhibited by Calcium Channel Blockers. *Pharm. Res.* **2005***, 22*, 2023-2034.

[151] Peng, H.; Dong, Z.; Qi, J.; Yang, Y.; Liu, Y.; Li, Y.; Xu, J.; Zhang, J. T. A Novel Two Mode-Acting Inhibitor of ABCG2-Mediated Multidrug Transport and Resistance in Cancer Chemotherapy. *PLoS ONE* **2009***, 4*, e5676.

[152] Peng, H.; Qi, J.; Dong, Z.; Zhang, J.; Peng, H. Dynamic vs Static ABCG2 Inhibitors to Sensitize Drug Resistant Cancer Cells. *PLoS ONE* **2010***, 5*, e15276.

[153] Chearwae, W.; Shukla, S.; Limtrakul, P.; Ambudkar, S. V. Modulation of the function of the multidrug resistance-linked ATP-binding cassette transporter ABCG2 by the cancer chemopreventive agent curcumin. *Mol. Cancer Ther.* **2006** *5*, 1995-2006.

[154] Limtrakul, P.; Chearwae, W.; Shukla, S.; Phisalphong, C.; Ambudkar, S. V. Modulation of function of three ABC drug transporters, P-glycoprotein (ABCB1), mitoxantrone resistance protein (ABCG2) and multidrug resistance protein 1 (ABCC1) by tetrahydrocurcumin, a major metabolite of curcumin. *Mol. Cell. Biochem.* **2007***, 296*, 85-95.

[155] Ding, R.; Shi, J.; Pabon, K.; Scotto, K. W. Xanthines Down-Regulate the Drug Transporter ABCG2 and Reverse Multidrug Resistance. *Mol. Pharmacol.* **2012***, 81*, 328-337.

[156] Weidner, L. D.; Zoghbi, S. S.; Lu, S.; Shukla, S.; Ambudkar, S. V.; Pike, V. W.; Mulder, J.; Gottesmann, M. M.; Innis, R. B.; Hall, M. D. The Inhibitor Ko143 Is Not Specific for ABCG2. *J. Pharmacol. Exp. Ther.* **2015***, 354*, 384-393.

[157] Hegedus, T.; Orfi, L.; Seprodi, A.; Váradi, A.; Sarkadi, B.; Keri, G. Interaction of tyrosine kinase inhibitors with the human multidrug transporter proteins, MDR1 and MRP1. *Biochim. Biophys. Acta* **2002***, 1587*, 318-25.

[158] Tiwari, A. K.; Sodani, K.; Wang, S.-R.; Kuang, Y.-H..; Ashby, C. R. Jr.; Chen, X.; Chen, Z.-S. Nilotinib (AMN107, Tasigna®) reverses multidrug resistance by inhibiting the activity of the ABCB1/Pgp and ABCG2/BCRP/MXR transporters. *Biochem. Pharmacol.* **2009***, 78*, 153-161.

[159] Mahon, F. X.; Réa, D.; Guilhot, J.; Guilhot, F.; Huguet, F.; Nicolini, F.; Legros, L.; Charbonnier, A.; Guerci, A.; Varet, B.; Etienne, G.; Reiffers, J.; Rousselot, P. Discontinuation of imatinib in patients with chronic myeloid leukaemia who have

maintained complete molecular remission for at least 2 years: the prospective, multicentre Stop Imatinib (STIM) trial. *Lancet Oncol.* **2010***, 11*, 1029-1035.

[160] Jia, Y.; Yun, C. H.; Park, E.; Ercan, D.; Manuia, M.; Juarez, J.; Xu, C.; Rhee, K.; Chen, T.; Zhang, H.; Palakurthi, S.; Jang, J.; Lelais, G.; Di Donato, M.; Bursulaya, B.; Michellys, P.Y.; Epple, R.; Marsilje, T. H.; Mc Neill, M.; Lu, W.; Harris, J.; Bender, S.; Wong, K. K.; Jänne, P. A.; Eck, M. J. Overcoming EGFR(T790M) and EGFR(C797S) resistance with mutant-selective allosteric inhibitors. *Nature* **2016***, 534*, 129-132.

[161] Yu, H. A.; Pao, W. Targeted therapies: Afatinib—new therapy option for EGFR-mutant lung cancer. *Nat. Rev. Clin. Oncol.* **2013***, 10*, 551-552.

[162] Durmus, S.; Sparidans, R. W.; Wagenaar, E.; Beijnen, J. H.; Schinkel, A. H. Oral Availability and Brain Penetration of the B-RAF^{V600E} Inhibitor Vemurafenib Can Be Enhanced by the P-Glycoprotein (ABCB1) and Breast Cancer Resistance Protein (ABCG2) Inhibitor Elacridar. *Mol. Pharmaceutics* **2012***, 9*, 3236-3245.

[163] Kruijtzer, C. M.; Beijnen, J. H.; Rosing, H.; ten Bokkel Huinink, W. W.; Schot, M.; Jewell, R. C.; Paul, E. M.; Schellens, J. H. Increased Oral Bioavailability of Topotecan in Combination With the Breast Cancer Resistance Protein and P-Glycoprotein Inhibitor GF120918. *J. Clin. Oncol.* **2002***, 20*, 2943-2950.

[164] Shukla, S.; Robey, R. W.; Bates, S. E.; Ambudkar, S. V. The Calcium Channel Blockers, 1,4-Dihydropyridines, Are Substrates of the Multidrug Resistance-Linked ABC Drug Transporter, ABCG2. *Biochemistry* **2006***, 45*, 8940-8951.

[165] Clark, R. K.; Kerr, I. D.; Callaghan, R. Multiple Drugbinding Sites on the R482G Isoform of the ABCG2 Transporter. *Br. J. Pharmacol.* **2006***, 149*, 506-515.

[166] Takenaka, K.; Morgan, J. A.; Scheffer, G. L.; Adachi, M.; Stewart, C. F.; Sun, D.; Leggas, M.; Ejendal, K. F.; Hrycyna, C. A.; Schuetz, J. D. Substrate Overlap between Mrp4 and Abcg2/Bcrp Affects Purine Analogue Drug Cytotoxicity and Tissue Distribution. *Cancer Res.* **2007***, 67*, 6965-6972.

[167] Giri, N.; Agarwal, S.; Shaik, N.; Pan, G.; Chen, Y.; Elmquist, W. F. Substrate-Dependent Breast Cancer Resistance Protein (Bcrp1/Abcg2)-Mediated Interactions: Consideration of Multiple Binding Sites in in Vitro Assay Design. *Drug Metab. Dispos.* **2009***, 37*, 560-570.

[168] Li, J.; Jaimes, K. F.; Aller, S. G. Refined structures of mouse P-glycoprotein. *Prot. Sci.* **2014***, 23*, 34-46.

[169] Lee, J.-Y.; Kinch, L. N.; Borek, D. M.; Wang, J.; Wang, J.; Urbatsch, I. L.; Xie, X.-S.; Grishin, N. V.; Cohen, J. C.; Otwinowski, Z.; Hobbs, H. H.; Rosenbaum, D. M. Crystal structure of the human sterol transporter ABCG5/ABCG8. *Nature* **2016***, 533*, 561-4.

[170] László, L.; Sarkadi, B.; Hegedűs, T. Jump into a New Fold—A Homology Based Model for the ABCG2/BCRP Multidrug Transporter. *PLoS One* **2016***, 11*, 1-22.

[171] Choi, C.-H. ABC transporters as multidrug resistance mechanisms and the development of chemosensitizers for their reversal. *Cancer Cell Int.* **2005***, 5*, 30.

[172] Ricci, J. W.; Lovato, D.; Larson, R. S. ABCG2 inhibitors: Will they find clinical relevance? *J. Dev. Drugs* **2015***, 4*, 1-6.

[173] Rijavec, M.; Šilar, M.; Triller, N.; Kern, I.; Čegovnik, U.; Kosnik, M.; Korosec, P. Expressions of Topoisomerase IIα and BCRP in Metastatic Cells are Associated with Overall Survival in Small Cell Lung Cancer Patients. *Pathol. Oncol. Res.* **2011***, 17*, 691-696.

[174] Yoh, K.; Ishii, G.; Yokose, T.; Minegishi, Y.; Tsuta, K.; Goto, K.; Nishiwaki, Y.; Kodama, T.; Suga, M.; Ochiai, A. Breast cancer resistance protein impacts clinical outcome in platinum-based chemotherapy for advanced non-small cell lung cancer. *Clin. Cancer Res.* **2004***, 10*, 1691-7.

[175] Tian, C.; Ambrosone, C. B.; Darcy, K. M.; Krivak, T. C.; Armstrong, D. K.; Bookman, M. A.; Davis, W.; Zhao, H.; Moysich, K.; Gallion, H.; De Loia, J. A. Common variants in ABCB1, ABCC2 and ABCG2 genes and clinical outcomes among women with advanced stage ovarian cancer treated with platinum and

taxane-based chemotherapy: A Gynecologic Oncology Group study. *Gynecol. Oncol.* **2012***, 124*, 575-581.

[176] Kovalev, A. A.; Tsvetaeva, D. A.; Grudinskaja, T. V. Role of ABC-cassette transporters (MDR1, MRP1, BCRP) in the development of primary and acquired multiple drug resistance in patients with early and metastatic breast cancer. *Exp. Oncol.* **2013***, 35*, 287-290.

[177] Maciejczyk, A. (2013). New Prognostic Factors in Breast Cancer. *Adv. Clin. Exp. Med.* **2013***, 22*, 5-15.

[178] Lee, S.; Kim, H.; Hwang, J. H.; Lee, H.; Cho, J. Y.; Yoon, Y. S.; Han, H. S. Breast cancer resistance protein expression is associated with early recurrence and decreased survival in resectable pancreatic cancer patients. *Pathol. Int.* **2012***, 62*, 167-175.

[179] Kim, Y. H.; Ishii, G.; Goto, K.; Ota, S.; Kubota, K.; Murata, Y.; Mishima, M.; Saijo, N.; Nishiwaki, Y.; Ochiai, A. Expression of breast cancer resistance protein is associated with a poor clinical outcome in patients with small-cell lung cancer. *Lung Cancer* **2009***, 65*, 105-111.

[180] Galimberti, S.; Nagy, B.; Benedetti, E.; Pacini, S.; Brizzi, S.; Caracciolo, F.; Papineschi, F.; Ciabatti, E.; Guerrini, F.; Fazzi, R.; Canestraro, M.; Petrini, M. Evaluation of the MDR1, ABCG2, Topoisomerases IIalpha and GSTpi gene expression in patients affected by aggressive mantle cell lymphoma treated by the R-Hyper-CVAD regimen. *Leuk. Lymphoma* **2007***, 48*, 1502-1509.

[181] Uggla, B.; Ståhl, E.; Wågsäter, D.; Paul, C.; Karlsson, M. G.; Sirsjö, A.; Tidefelt, U. BCRP mRNA expression v. clinical outcome in 40 adult AML patients. *Leuk. Res.* **2005***, 29*, 141-146.

[182] Lheureux, S.; Krieger, S.; Weber, B.; Pautier, P.; Fabbro, M.; Selle, F.; Bourgeois, H.; Petit, T.; Lortholary, A.; Plantade, A.; Briand, M.; Leconte, A.; Richard, N.; Vilquin, P.; Clarisse, B.; Blanc-Fournier, C.; Joly, F. (2012). Expected Benefits

of Topotecan Combined With Lapatinib in Recurrent Ovarian Cancer According to Biological Profile. *Int. J. Gynecol. Cancer* **2012***, 22*, 1483–1488.

[183] Molina, J. R.; Kaufmann, S. H.; Reid, J. M.; Rubin, S. D.; Galvez-Peralta, M.; Friedman, R.; Flatten, K. S.; Koch, K. M.; Gilmer, T. M.; Mullin, R. J.; Jewell, R. C.; Felten, S. J.; Mandrekar, S.; Adjei, A. A.; Erlichman, C. Evaluation of Lapatinib and Topotecan Combination Therapy: Tissue Culture, Murine Xenograft, and Phase I Clinical Trial Data. *Clin. Cancer Res.* **2008***, 14*, 7900-7908.

[184] Stewart, C. F.; Tagen, M.; Schwartzberg, L. S.; Blakely, L. J.; Tauer, K. W.; Smiley, L. M. Phase I dosage finding and pharmacokinetic study of intravenous topotecan and oral erlotinib in adults with refractory solid tumors. *Cancer Chemother. Pharmacol.* **2014***, 73*, 561-8.

[185] Weroha, S. J.; Oberg, A. L.; Ziegler, K. L.; Dakhilm, S. R.; Rowland, K. M.; Hartmann, L.C.; Moore, D. F.; Keeney, G. L.; Peethambaram, P. P.; Haluska, P. Phase II trial of lapatinib and topotecan (LapTop) in patients with platinum-refractory/resistant ovarian and primary peritoneal carcinoma. *Gynecol. Oncol.* **2011***, 122*, 116-120.

[186] Westover, D. L.; Li, F. NewTrends for Overcoming ABCG2/BCRP-mediated Resistance to Cancer Therapies. *J. Exp. Clin. Canc. Res.* **2015***, 34*, 3-9.

[187] Lewis, C. W.; Anderson, J. G.; Smith, J. E. Health-Related Aspects of the Genus Aspergillus. Plenum Press, New York **1994**, 219-261.

[188] Shukla, S.; Zaher, H.; Hartz, A.; Bauer, B.; Ware, J. A.; Ambudkar, S. V. Curcumin Inhibits the Activity of ABCG2/BCRP1, a Multidrug Resistance-Linked ABC Drug Transporter in Mice. *Pharm. Res. 2009, 26*, 480-487.

[189] Hyafil, F.; Vergely, C.; Du Vignaud, P.; Grand-Perret, T. In vitro and in vivo reversal of multidrug resistance by GF120918, an acridonecarboxamide derivative. *Cancer Res.* **1993***, 53*, 4595-602.

[190] Houghton, P. J.; Germain, G. S.; Harwood, F. C.; Schuetz, J. D.; Stewart, C. F.; Buchdunger, E.; Traxler, P. Imatinib mesylate is a potent inhibitor of the ABCG2 (BCRP) transporter and reverses resistance to topotecan and SN-38 in vitro. *Cancer Res.* **2004***, 64*, 2333-7.

[191] Shukla, S.; Robey, R. W.; Bates, S. E.; Ambudkar, S. V. Sunitinib (Sutent, SU11248), a Small-Molecule Receptor Tyrosine Kinase Inhibitor, Blocks Function of the ATP-Binding Cassette (ABC) Transporters P-Glycoprotein (ABCB1) and ABCG2. *Drug Metab. Dispos.* **2009***, 37*, 359-365.

[192] Eadie, L. N.; Hughes, T. P.; White, D. L. Interaction of the Efflux Transporters ABCB1 and ABCG2 With Imatinib, Nilotinib, and Dasatinib. *Clinic. Pharmacol. Ther.* **2014***, 95*, 294-306.

[193] Shi, Z.; Parmar, S.; Peng, X. X.; Shen, T.; Robey, R. W.; Bates, S. E.; Fu, L. W.; Shao, Y.; Chen, Y. M.; Zang, F.; Chen, Z. S. The epidermal growth factor tyrosine kinase inhibitor AG1478 and erlotinib reverse ABCG2-mediated drug resistance. *Oncol. Rep.* **2009***, 21*, 483-9.

[194] Takada, T.; Suzuki, H.; Gotoh, Y.; Sugiyama, Y. Regulation of the cell surface expression of human BCRP/ABCG2 by the phosphorylation state of Akt in polarized cells. *Drug Metabol. Dispos.* **2005***, 33*, 905-9.

[195] Liu, W.; Baer, M. R.; Bowman, M. J.; Pera, P.; Zheng, X.; Morgan, J.; Pandey, R. A.; Oseroff, A. R. The Tyrosine Kinase Inhibitor Imatinib Mesylate Enhances the Efficacy of Photodynamic Therapy by Inhibiting ABCG2. *Clin. Cancer Res.* **2007***, 13*, 2463-2470.

[196] Juvale, K.; Wiese, M. 4-Substituted-2-phenylquinazolines as inhibitors of BCRP. *Bioorg. Med. Chem. Lett.* **2012***, 22*, 6766–6769.

[197] Juvale, K. (2013). Development of New Breast Cancer Resistance Protein Inhibitors. Ph.D. thesis, University of Bonn, **2013.**

[198] Juvale, K.; Gallus, J.; Wiese, M. Investigation of quinazolines as inhibitors of breast cancer resistance protein (ABCG2). *Bioorg. Med. Chem.* **2013***, 21*, 7858-7873.

[199] FlowJo X 10.0.7r2, Tree star, USA.

[200] Özvegy-Laczka, C.; Várady, G.; Köblös, G.; Ujhelly, O.; Cervenak, J.; Schuetz, J. D.; Sorrentino, B. P.; Koomen, G. J.; Varadi, A.; Nemet, A.; Sarkadi, B. Function-dependent Conformational Changes of the ABCG2 Multidrug Transporter Modify Its Interaction with a Monoclonal Antibody on the Cell Surface. *J. Biol. Chem.* **2005***, 280*, 4219-4227.

[201] Telbisz, Á.; Hegedüs, C.; Özvegy-Laczka, C.; Goda, K.; Váradym, G.; Takáts, Z.; Szabo, E.; Sorrentino, B. P.; Varadi, A.; Sarkadi, B. Antibody binding shift assay for rapid screening of drug interactions with the human ABCG2 multidrug transporter. *Eur. J. Pharm. Sci.* **2012***, 45*, 101-109.

[202] Litman, T.; Zeuthen, T.; Skovsgaard, T.; Stein, W. D. Structure-activity relationships of P-glycoprotein interacting drugs: kinetic characterization of their effects on ATPase activity. *Biochim. Biophys. Acta* **1997***, 1361*, 159-168.

[203] An, G.; Gallegos, J.; Morris, M. The Bioflavonoid Kaempferol Is an Abcg2 Substrate and Inhibits Abcg2-Mediated Quercetin Efflux. *Drug Metabol. Dispos.* **2011***, 39*, 426-32.

[204] Sesink, A. L.; Arts, I. C.; de Boer, V. C.; Breedveld, P.; Schellens, J. H.; Hollman, P. C.; Russel, F. G. Breast Cancer Resistance Protein (Bcrp1/Abcg2) Limits Net Intestinal Uptake of Quercetin in Rats by Facilitating Apical Efflux of Glucuronides. *Mol. Pharmacol.* **2005***, 67*, 1999-2006.

[205] Krapf, M. K., Wiese, M. Synthesis and Biological Evaluation of 4-Anilino-quinazolines and -quinolines as Inhibitors of Breast Cancer Resistance Protein (ABCG2). *J. Med. Chem.* **2016***, 59*, 5449-5461.

[206] Glavinas, H.; Kis, E.; Pal, A.; Kovacs, R.; Jani, M.; Vagi, E.; Molnar, E.; Bansaghi, S.; Kele, Z.; Janaky, T.; Bathori, G.; von Richter, O.; Koomen, G. J.;

Krajcsi, P. ABCG2 (Breast Cancer Resistance Protein/MitoxantroneResistance-Associated Protein) ATPase Assay: A Useful Tool to Detect Drug-Transporter Interactions. *Drug Metabolism and Disposition* **2007***, 35*, 1533-1542.

[207] Spindler, A. Synthese und Untersuchung neuer ABCG2 Inhibitoren. Ph.D. thesis, University of Bonn, **2017**.

[208] Pick, A.-K. Funktionelle Untersuchungen des ABC-Transporters Breast Cancer Resistance Protein (BCRP). Ph.D. thesis, University of Bonn, **2011**.

[209] Gozzi, G. J.; Bouaziz, Z.; Winter, E.; Daflon-Yunes, N.; Honorat, M.; Guragossian, N.; Marminon, C.; Valdameri, G.; Bollacke, A.; Guillon, J.; Pinaud, N.; Marchivie, M.; Cadena, S. M.; Jose, J.; Le Borgne, M.; Di Pietro, A. Phenolic indeno[1,2-b]indoles as ABCG2-selective potent and non-toxic inhibitors stimulating basal ATPase activity. *Drug Des. Devel. Ther.* **2015***, 9*, 3481-3495.

[210] Tournier, N.; Goutal, S.; Auvity, S.; Traxl, A.; Mairinger, S.; Wanek, T.; Helal, O.-B.; Buvat, I.; Soussan, M.; Caille, F.; Langer, O. Strategies to Inhibit ABCB1- and ABCG2-Mediated Efflux Transport of Erlotinib at the Blood–Brain Barrier: A PET Study on Nonhuman Primates. *J. Nucl. Med.* **2016***, 58*, 117-122.

[211] Xu, Y.; Egido, E.; Li-Blatter, X.; Müller, R.; Merino, G.; Bernèche, S.; Seelig, A. Allocrite Sensing and Binding by the Breast Cancer Resistance Protein (ABCG2) and P-Glycoprotein (ABCB1). *Biochemistry* **2015***, 54*, 6195-6206.

[212] Boumendjel, A.; Macalou, S.; Valdameri, G.; Pozza, A.; Gauthier, C.; Arnaud, O.; Nicolle, E.; Magnard, S.; Falson, P.; Terreux, R.; Carrupt, P. A.; Payen, L.; Di Pietro, A. Targeting the multidrug ABCG2 transporter with flavonoidic inhibitors: in vitro optimization and in vivo validation. *Curr. Med. Chem.* **2011***, 18*, 3387-401.

[213] Mc Devitt, C. A.; Collins, R. F.; Conway, M.; Modok, S.; Storm, J.; Kerr, I. D.; Ford, R. C.; Callaghan, R. Purification and 3D Structural Analysis of Oligomeric Human Multidrug Transporter ABCG2. *Structure* **2006***, 14*, 1623–1632.

[214] Bircsak, K. M.; Richardson, J. R.; Aleksunes, L. M. Inhibition of human MDR1 and BCRP transporter ATPase activity by organochlorine and pyrethroid insecticides. *J. Biochem. Mol. Toxicol.* **2013***, 27*, 157-64.

[215] Kraege, S.; Stefan, K.; Juvale, K.; Ross, T.; Willmes, T.; Wiese, M. The combination of quinazoline and chalcone moieties leads to novel potent heterodimeric modulators of breast cancer resistance protein (BCRP/ABCG2). *Eur. J. Med. Chem.* **2011***, 117*, 212-229.

[216] Egido, E.; Müller, R.; Li-Blatter, X.; Merino, G.; Seelig, A. Predicting Activators and Inhibitors of the Breast Cancer Resistance Protein (ABCG2) and P-Glycoprotein (ABCB1) Based on Mechanistic Considerations. M*ol. Pharm.* **2015***, 12*, 4026-4037.

[217] Krapf M., Gallus, J.; Wiese, M. 4-Anilino-2-pyridylquinazolines and -pyrimidines as Highly Potent and Nontoxic Inhibitors of Breast Cancer Resistance Protein (ABCG2). *J. Med. Chem.* **2017***, 60*, 4474-4495.

[218] Sirisoma, N.; Pervin, A.; Zhang, H.; Jiang, S.; Willardsen, J. A.; Anderson, M. B.; Mather, G.; Pleiman, C. M.; Kasibhatla, S.; Tseng, B.; Drewe, J.; Cai, S. X. Discovery of N-(4-methoxyphenyl)-N,2-dimethylquinazolin-4-amine, a potent apoptosis inducer and efficacious anticancer agent with high blood brain barrier penetration. *J. Med. Chem.* **2009***, 52*, 2341-51.

[219] Parish, C. R. (1999). Fluorescent dyes for lymphocyte migrat ion and proliferation studies. *Immunol. Cell Biol.* **1999***, 77*, 499-508.

[220] Pick A.; Müller, H.; Wiese, M. Structure-activity Relationships of New Inhibitors of Breast Cancer Resistance Protein (ABCG2). *Bioorg. Med. Chem.* **2008**, *16*, 8224–8236.

[221] Pick, A.; Klinkhammer, W.; Wiese, M. Specific Inhibitors of the Breast Cancer Resistance Protein (BCRP). *Chem. Med. Chem.* **2010**, *5*, 1498–1505.

[222] Marighetti, F.; Steggemann, K.; Hanl, M.; Wiese, M. Synthesis and Quantitative Structure-activity Relationships of Selective BCRP Inhibitors. *Chem. Med. Chem.* **2013**, *8*, 125–135.

[223] Pick, A.; Müller, H.; Mayer, R.; Haenisch, B.; Pajeva, I. K.; Weigt, M.; Bonisch, H.; Müller, C. E.; Wiese, M. Structure-activity Relationships of Flavonoids as Inhibitors of Breast Cancer Resistance Protein (BCRP). *Bioorg. Med. Chem.* **2011**, *19*, 2090–2102.

[224] Müller, H.; Klinkhammer, W.; Globisch, C.; Kassack, M. U.; Pajeva, I. K.; Wiese, M. New Functional Assay of P-glycoprotein Activity Using Hoechst 33342. *Bioorg. Med. Chem.* **2007**, *15*, 7470–7479.

[225] Juvale, K.; Pape, V. F.; Wiese, M. Investigation of Chalcones and Benzochalcones as Inhibitors of Breast Cancer Resistance Protein. *Bioorg. Med. Chem.* **2012**, *20*, 346-355.

[226] Gallus, J.; Juvale, K.; Wiese, M. Characterization of 3-Methoxy Flavones for their Interaction with ABCG2 as Suggested by ATPase Activity. *Biochim. Biophys. Acta* **2014**, *1838*, 2929-2938.

[227] Singh, M. S.; Juvale, K.; Wiese, M.; Lamprecht, A. Evaluation of Dual P-gp-BCRP Inhibitors as Nanoparticle Formulation. *Eur. J. Pharm. Sci.* **2015**, *77*, 1-8.

[228] Juvale, K.; Stefan, K.; Wiese, M. Synthesis and Biological Evaluation of Flavones and Benzoflavones as Inhibitors of BCRP/ABCG2. *Eur. J. Med. Chem.* **2013**, *67*, 115–126.

[229] Müller, H.; Pajeva, I. K.; Globisch, C.; Wiese, M. Functional Assay and Structure-activity Relationships of New Third-generation P-glycoprotein Inhibitors. *Bioorg. Med. Chem.* **2008**, *16*, 2456–2470.

[230] Pick, A.; Müller, H.; Wiese, M. Structure-activity Relationship of New Inhibitors of Breast Cancer Resistance Protein (ABCG2). *Bioorg. Med. Chem. Lett.* **2010**, *20*, 180–183.

[231] Köhler, S.; Wiese, M. HM30181 Derivatives as Novel Potent and Selective Inhibitors of the Breast Cancer Resistance Protein (BCRP/ABCG2). *J. Med. Chem.* **2015**, *58*, 3910–3921.

[232] https://en.wikipedia.org/wiki/Log-normal_distribution, last accessed on 3.10.2016.

[233] http://de.mathworks.com/help/stats/lognstat.html, last accessed on 3.10.2016.

[234] Jonker, J. W.; Buitelaar, M.; Wagenaar, E.; Van Der Valk, M. A; Scheffer, G. L.; Scheper, R. J.; Plosch, T.; Kuipers, F.; Elferink, R. P.; Rosing, H.; Beijnen, J. H.; Schinkel, A. H. The breast cancer resistance protein protects against a major chlorophyll-derived dietary phototoxin and protoporphyria. *Proc. Natl. Acad. Sci. U. S. A.* **2002***, 99*, 15649-15654.

[235] Henrich, C. B.; Bokesch H. R.; Dean, M.; Bates, S. E.; Robey, R. W.; Goncharova, E. I.; Wilson, J. A.; Mc Mahon, J. B. Cell-Based Assay for Inhibitors of ABCG2 Activity A High-Throughput Cell-Based Assay for Inhibitors of ABCG2 Activity. *J. Biomol. Screen.* **2006***, 11*, 176-183.

[236] Lebedeva, I. V.; Pande, P.; Patton, W. F. Sensitive and Specific Fluorescent Probes for Functional Analysis of the Three Major Types of Mammalian ABC Transporters. *PLoS ONE* **2011***, 6*, e22429.

[237] Feller, N.; Broxterman, H. J.; Wahrer, D. C.; Pinedo, H. M. TP-dependent efflux of calcein by the multidrug resist ance protein (MRP): no inhibition by intracellular glutathione depletion. *FEBS Lett.* **1995***, 368*, 385-88.

[238] Olson, D. P.; Taylor, B. J.; Ivy, S. P. Detection of MR P functional activity: calcein AM but not BCECF AM as a Multidrug Resistance-related Protein (MRP1) substrate. *Cytometry* **2001***, 46*, 105-113.

[239] Tiberghien, F.; Loor, F. Ranking of P-glycoprotein substrates and inhibitors by a calcein-AM fluorometry screening assay. *Anticancer Drugs* **1996***, 7*, 568-578.

[240] Essodaigui, M.; Broxterman, H. J.; Garnier-Suillerot, A. Kinetic analysis of calcein and calcein-acetoxymethylester efflux mediated by the multidrug resistance protein and P-glycoprotein. *Biochemistry* **1998***, 37*, 2243-2250.

[241] Berridge, M.; Herst, P. M.; Tan, A. S. Tetrazolium dyes as tools in cell biology: new insights into their cellular reduction. *Biotechnol. Annu. Rev.* **2005***, 11*, 127-52.

[242] Mosmann, T. Rapid colorimetric assay for cellular growth and survival: Application to proliferation and cytotoxicity assays. *J. Immunol. Methods* **1983***, 65*, 55-63.

[243] Marighetti, F.; Steggemann, K.; Karbaum, M.; Wiese, M. Scaffold Identification of a New Class of Potent and Selective BCRP-inhibitors. *Chem. Med. Chem.* **2015**, *10*, 742–751.

[244] De Leoz, M. L. A.; Chua, M. T.; Endoma-Arias, M. A. A.; Concepcion, G. P.; Cruz, L. J. A Modified Procedure for the Preparation of Mitoxantrone. *Philipp. J. Sci.* **2006***, 135*, 83-92.

[245] Lineweaver, H.; Burk, D. The Determination of Enzyme Dissociation Constants. *J. Am. Chem. Soc.* **1934***, 56*, 658-666.

[246] Eisenthal, R.; Cornish-Bowden, A. The Direct Linear Plot: A New Graphical Procedure for Estimating Enzyme Kinetic Parameters. *Biochem. J.* **1974***, 139*, 715-720.

[247] Sarkadi, B.; Price, E.M.; Boucher R.C.; Germann U.A.; Scarborough G.A. Expression of the human multidrug resistance cDNA in insect cells generates a high activity drug-stimulated membrane ATPase. *J. Biol. Chem.* **1992**, *267*, 4854-4858.